CHARACTERIZATION OF CREEP DEFORMATION AND DAMAGE OF METALLIC MATERIALS AT HIGH TEMPERATURE

by

Baoku Sun

A thesis

Submitted to
the Faculty of Graduate Studies of the University of Manitoba
in Partial Fulfillment of the Requirements
for the Degree of Doctor of Philosophy

Department of Mechanical and Industrial Engineering
University of Manitoba
Winnipeg, Manitoba, Canada

ISBN 0-315-99069-4

Name Baoko Sun

Dissertation Abstracts International is arranged by broad, general subject categories. Please select the one subject which most nearly describes the content of your dissertation. Enter the corresponding four-digit code in the spaces provided.

Mechanical Engineering
SUBJECT TERM

0548
SUBJECT CODE

U·M·I

Subject Categories

THE HUMANITIES AND SOCIAL SCIENCES

COMMUNICATIONS AND THE ARTS
- Architecture 0729
- Art History 0377
- Cinema 0900
- Dance 0378
- Fine Arts 0357
- Information Science 0723
- Journalism 0391
- Library Science 0399
- Mass Communications 0708
- Music 0413
- Speech Communication 0459
- Theater 0465

EDUCATION
- General 0515
- Administration 0514
- Adult and Continuing 0516
- Agricultural 0517
- Art 0273
- Bilingual and Multicultural 0282
- Business 0688
- Community College 0275
- Curriculum and Instruction 0727
- Early Childhood 0518
- Elementary 0524
- Finance 0277
- Guidance and Counseling 0519
- Health 0680
- Higher 0745
- History of 0520
- Home Economics 0278
- Industrial 0521
- Language and Literature 0279
- Mathematics 0280
- Music 0522
- Philosophy of 0998
- Physical 0523
- Psychology 0525
- Reading 0535
- Religious 0527
- Sciences 0714
- Secondary 0533
- Social Sciences 0534
- Sociology of 0340
- Special 0529
- Teacher Training 0530
- Technology 0710
- Tests and Measurements 0288
- Vocational 0747

LANGUAGE, LITERATURE AND LINGUISTICS
- Language
  - General 0679
  - Ancient 0289
  - Linguistics 0290
  - Modern 0291
- Literature
  - General 0401
  - Classical 0294
  - Comparative 0295
  - Medieval 0297
  - Modern 0298
  - African 0316
  - American 0591
  - Asian 0305
  - Canadian (English) 0352
  - Canadian (French) 0355
  - English 0593
  - Germanic 0311
  - Latin American 0312
  - Middle Eastern 0315
  - Romance 0313
  - Slavic and East European 0314

PHILOSOPHY, RELIGION AND THEOLOGY
- Philosophy 0422
- Religion
  - General 0318
  - Biblical Studies 0321
  - Clergy 0319
  - History of 0320
  - Philosophy of 0322
- Theology 0469

SOCIAL SCIENCES
- American Studies 0323
- Anthropology
  - Archaeology 0324
  - Cultural 0326
  - Physical 0327
- Business Administration
  - General 0310
  - Accounting 0272
  - Banking 0770
  - Management 0454
  - Marketing 0338
- Canadian Studies 0385
- Economics
  - General 0501
  - Agricultural 0503
  - Commerce-Business 0505
  - Finance 0508
  - History 0509
  - Labor 0510
  - Theory 0511
- Folklore 0358
- Geography 0366
- Gerontology 0351
- History
  - General 0578
  - Ancient 0579
  - Medieval 0581
  - Modern 0582
  - Black 0328
  - African 0331
  - Asia, Australia and Oceania 0332
  - Canadian 0334
  - European 0335
  - Latin American 0336
  - Middle Eastern 0333
  - United States 0337
- History of Science 0585
- Law 0398
- Political Science
  - General 0615
  - International Law and Relations 0616
  - Public Administration 0617
- Recreation 0814
- Social Work 0452
- Sociology
  - General 0626
  - Criminology and Penology 0627
  - Demography 0938
  - Ethnic and Racial Studies 0631
  - Individual and Family Studies 0628
  - Industrial and Labor Relations 0629
  - Public and Social Welfare 0630
  - Social Structure and Development 0700
  - Theory and Methods 0344
- Transportation 0709
- Urban and Regional Planning 0999
- Women's Studies 0453

THE SCIENCES AND ENGINEERING

BIOLOGICAL SCIENCES
- Agriculture
  - General 0473
  - Agronomy 0285
  - Animal Culture and Nutrition 0475
  - Animal Pathology 0476
  - Food Science and Technology 0359
  - Forestry and Wildlife 0478
  - Plant Culture 0479
  - Plant Pathology 0480
  - Plant Physiology 0817
  - Range Management 0777
  - Wood Technology 0746
- Biology
  - General 0306
  - Anatomy 0287
  - Biostatistics 0308
  - Botany 0309
  - Cell 0379
  - Ecology 0329
  - Entomology 0353
  - Genetics 0369
  - Limnology 0793
  - Microbiology 0410
  - Molecular 0307
  - Neuroscience 0317
  - Oceanography 0416
  - Physiology 0433
  - Radiation 0821
  - Veterinary Science 0778
  - Zoology 0472
- Biophysics
  - General 0786
  - Medical 0760

EARTH SCIENCES
- Biogeochemistry 0425
- Geochemistry 0996
- Geodesy 0370
- Geology 0372
- Geophysics 0373
- Hydrology 0388
- Mineralogy 0411
- Paleobotany 0345
- Paleoecology 0426
- Paleontology 0418
- Paleozoology 0985
- Palynology 0427
- Physical Geography 0368
- Physical Oceanography 0415

HEALTH AND ENVIRONMENTAL SCIENCES
- Environmental Sciences 0768
- Health Sciences
  - General 0566
  - Audiology 0300
  - Chemotherapy 0992
  - Dentistry 0567
  - Education 0350
  - Hospital Management 0769
  - Human Development 0758
  - Immunology 0982
  - Medicine and Surgery 0564
  - Mental Health 0347
  - Nursing 0569
  - Nutrition 0570
  - Obstetrics and Gynecology 0380
  - Occupational Health and Therapy 0354
  - Ophthalmology 0381
  - Pathology 0571
  - Pharmacology 0419
  - Pharmacy 0572
  - Physical Therapy 0382
  - Public Health 0573
  - Radiology 0574
  - Recreation 0575
  - Speech Pathology 0460
  - Toxicology 0383
- Home Economics 0386

PHYSICAL SCIENCES

Pure Sciences
- Chemistry
  - General 0485
  - Agricultural 0749
  - Analytical 0486
  - Biochemistry 0487
  - Inorganic 0488
  - Nuclear 0738
  - Organic 0490
  - Pharmaceutical 0491
  - Physical 0494
  - Polymer 0495
  - Radiation 0754
- Mathematics 0405
- Physics
  - General 0605
  - Acoustics 0986
  - Astronomy and Astrophysics 0606
  - Atmospheric Science 0608
  - Atomic 0748
  - Electronics and Electricity 0607
  - Elementary Particles and High Energy 0798
  - Fluid and Plasma 0759
  - Molecular 0609
  - Nuclear 0610
  - Optics 0752
  - Radiation 0756
  - Solid State 0611
- Statistics 0463

Applied Sciences
- Applied Mechanics 0346
- Computer Science 0984
- Engineering
  - General 0537
  - Aerospace 0538
  - Agricultural 0539
  - Automotive 0540
  - Biomedical 0541
  - Chemical 0542
  - Civil 0543
  - Electronics and Electrical 0544
  - Heat and Thermodynamics 0348
  - Hydraulic 0545
  - Industrial 0546
  - Marine 0547
  - Materials Science 0794
  - Mechanical 0548
  - Metallurgy 0743
  - Mining 0551
  - Nuclear 0552
  - Packaging 0549
  - Petroleum 0765
  - Sanitary and Municipal 0554
  - System Science 0790
- Geotechnology 0428
- Operations Research 0796
- Plastics Technology 0795
- Textile Technology 0994

PSYCHOLOGY
- General 0621
- Behavioral 0384
- Clinical 0622
- Developmental 0620
- Experimental 0623
- Industrial 0624
- Personality 0625
- Physiological 0989
- Psychobiology 0349
- Psychometrics 0632
- Social 0451

Nom _____

Dissertation Abstracts International est organisé en catégories de sujets. Veuillez s.v.p. choisir le sujet qui décrit le mieux votre thèse et inscrivez le code numérique approprié dans l'espace réservé ci-dessous.

_____ ☐☐☐ U·M·I

SUJET — CODE DE SUJET

Catégories par sujets

HUMANITÉS ET SCIENCES SOCIALES

COMMUNICATIONS ET LES ARTS
Architecture 0729
Beaux-arts 0357
Bibliothéconomie 0399
Cinéma 0900
Communication verbale 0459
Communications 0708
Danse 0378
Histoire de l'art 0377
Journalisme 0391
Musique 0413
Sciences de l'information 0723
Théâtre 0465

ÉDUCATION
Généralités 515
Administration 0514
Art 0273
Collèges communautaires 0275
Commerce 0688
Économie domestique 0278
Éducation permanente 0516
Éducation préscolaire 0518
Éducation sanitaire 0680
Enseignement agricole 0517
Enseignement bilingue et multiculturel 0282
Enseignement industriel 0521
Enseignement primaire. 0524
Enseignement professionnel 0747
Enseignement religieux 0527
Enseignement secondaire 0533
Enseignement spécial 0529
Enseignement supérieur 0745
Évaluation 0288
Finances 0277
Formation des enseignants 0530
Histoire de l'éducation 0520
Langues et littérature 0279
Lecture 0535
Mathématiques 0280
Musique 0522
Orientation et consultation 0519
Philosophie de l'éducation 0998
Physique 0523
Programmes d'études et enseignement 0727
Psychologie 0525
Sciences 0714
Sciences sociales 0534
Sociologie de l'éducation 0340
Technologie 0710

LANGUE, LITTÉRATURE ET LINGUISTIQUE
Langues
- Généralités 0679
- Anciennes 0289
- Linguistique 0290
- Modernes 0291

Littérature
- Généralités 0401
- Anciennes 0294
- Comparée 0295
- Médiévale 0297
- Moderne 0298
- Africaine 0316
- Américaine 0591
- Anglaise 0593
- Asiatique 0305
- Canadienne (Anglaise) 0352
- Canadienne (Française) 0355
- Germanique 0311
- Latino-américaine 0312
- Moyen-orientale 0315
- Romane 0313
- Slave et est-européenne 0314

PHILOSOPHIE, RELIGION ET THÉOLOGIE
Philosophie 0422
Religion
- Généralités 0318
- Clergé 0319
- Études bibliques 0321
- Histoire des religions 0320
- Philosophie de la religion 0322

Théologie 0469

SCIENCES SOCIALES
Anthropologie
- Archéologie 0324
- Culturelle 0326
- Physique 0327

Droit 0398
Économie
- Généralités 0501
- Commerce-Affaires 0505
- Économie agricole 0503
- Économie du travail 0510
- Finances 0508
- Histoire 0509
- Théorie 0511

Études américaines 0323
Études canadiennes 0385
Études féministes 0453
Folklore 0358
Géographie 0366
Gérontologie 0351
Gestion des affaires
- Généralités 0310
- Administration 0454
- Banques 0770
- Comptabilité 0272
- Marketing 0338

Histoire
- Histoire générale 0578
- Ancienne 0579
- Médiévale 0581
- Moderne 0582
- Histoire des noirs 0328
- Africaine 0331
- Canadienne 0334
- États-Unis 0337
- Européenne 0335
- Moyen-orientale 0333
- Latino-américaine 0336
- Asie, Australie et Océanie 0332

Histoire des sciences 0585
Loisirs 0814
Planification urbaine et régionale 0999
Science politique
- Généralités 0615
- Administration publique 0617
- Droit et relations internationales 0616

Sociologie
- Généralités 0626
- Aide et bien-être social 0630
- Criminologie et établissements pénitentiaires 0627
- Démographie 0938
- Études de l' individu et de la famille 0628
- Études des relations interethniques et des relations raciales 0631
- Structure et développement social 0700
- Théorie et méthodes. 0344
- Travail et relations industrielles 0629

Transports 0709
Travail social 0452

SCIENCES ET INGÉNIERIE

SCIENCES BIOLOGIQUES
Agriculture
- Généralités 0473
- Agronomie. 0285
- Alimentation et technologie alimentaire 0359
- Culture 0479
- Élevage et alimentation 0475
- Exploitation des pâturages 0777
- Pathologie animale 0476
- Pathologie végétale 0480
- Physiologie végétale 0817
- Sylviculture et faune 0478
- Technologie du bois 0746

Biologie
- Généralités 0306
- Anatomie 0287
- Biologie (Statistiques) 0308
- Biologie moléculaire 0307
- Botanique 0309
- Cellule 0379
- Écologie 0329
- Entomologie 0353
- Génétique 0369
- Limnologie 0793
- Microbiologie 0410
- Neurologie 0317
- Océanographie 0416
- Physiologie 0433
- Radiation 0821
- Science vétérinaire 0778
- Zoologie 0472

Biophysique
- Généralités 0786
- Medicale 0760

SCIENCES DE LA TERRE
Biogéochimie 0425
Géochimie 0996
Géodésie 0370
Géographie physique 0368
Géologie 0372
Géophysique 0373
Hydrologie 0388
Minéralogie 0411
Océanographie physique 0415
Paléobotanique 0345
Paléoécologie 0426
Paléontologie 0418
Paléozoologie 0985
Palynologie 0427

SCIENCES DE LA SANTÉ ET DE L'ENVIRONNEMENT
Économie domestique 0386
Sciences de l'environnement 0768
Sciences de la santé
- Généralités 0566
- Administration des hôpitaux 0769
- Alimentation et nutrition 0570
- Audiologie 0300
- Chimiothérapie 0992
- Dentisterie 0567
- Développement humain 0758
- Enseignement 0350
- Immunologie 0982
- Loisirs 0575
- Médecine du travail et thérapie 0354
- Médecine et chirurgie 0564
- Obstétrique et gynécologie 0380
- Ophtalmologie 0381
- Orthophonie 0460
- Pathologie 0571
- Pharmacie 0572
- Pharmacologie 0419
- Physiothérapie 0382
- Radiologie 0574
- Santé mentale 0347
- Santé publique 0573
- Soins infirmiers 0569
- Toxicologie 0383

SCIENCES PHYSIQUES
Sciences Pures
Chimie
- Généralités 0485
- Biochimie 487
- Chimie agricole 0749
- Chimie analytique 0486
- Chimie minérale 0488
- Chimie nucléaire 0738
- Chimie organique 0490
- Chimie pharmaceutique 0491
- Physique 0494
- PolymÈres 0495
- Radiation 0754

Mathématiques 0405
Physique
- Généralités 0605
- Acoustique 0986
- Astronomie et astrophysique 0606
- Électronique et électricité 0607
- Fluides et plasma 0759
- Météorologie 0608
- Optique 0752
- Particules (Physique nucléaire) 0798
- Physique atomique 0748
- Physique de l'état solide 0611
- Physique moléculaire 0609
- Physique nucléaire 0610
- Radiation 0756

Statistiques 0463

Sciences Appliqués Et Technologie
Informatique 0984
Ingénierie
- Généralités 0537
- Agricole 0539
- Automobile 0540
- Biomédicale 0541
- Chaleur et thermodynamique 0348
- Conditionnement (Emballage) 0549
- Génie aérospatial 0538
- Génie chimique 0542
- Génie civil 0543
- Génie électronique et électrique 0544
- Génie industriel 0546
- Génie mécanique 0548
- Génie nucléaire 0552
- Ingénierie des systèmes 0790
- Mécanique navale 0547
- Métallurgie 0743
- Science des matériaux 0794
- Technique du pétrole 0765
- Technique minière 0551
- Techniques sanitaires et municipales 0554
- Technologie hydraulique 0545

Mécanique appliquée 0346
Géotechnologie 0428
Matières plastiques (Technologie) 0795
Recherche opérationnelle 0796
Textiles et tissus (Technologie) 0794

PSYCHOLOGIE
Généralités 0621
Personnalité 0625
Psychobiologie 0349
Psychologie clinique 0622
Psychologie du comportement 0384
Psychologie du développement 0620
Psychologie expérimentale 0623
Psychologie industrielle 0624
Psychologie physiologique 0989
Psychologie sociale 0451
Psychométrie 0632

CHARACTERIZATION OF CREEP DEFORMATION AND DAMAGE OF METALLIC MATERIALS AT HIGH TEMPERATURE

BY

BAOKU SUN

A Thesis submitted to the Faculty of Graduate Studies of the University of Manitoba in partial fulfillment of the requirements for the degree of

DOCTOR OF PHILOSOPHY

Dedicated to

My parents, my wife and my daughter

Abstract

Investigations of cyclic creep fracture are reviewed, from both microscopic mechanisms of creep deformation and creep damage and from macroscopic response of materials under a specified stress and temperature history. Various models and methods describing macroscopic cyclic creep response and various influencing factors are catalogued.

A continuum damage mechanics based constitutive model for describing cyclic creep response of commonly used engineering materials is proposed. The model can take into account the load cycling effect, the load dwell time effect and the interaction between creep damage and high temperature low cycle fatigue damage in cyclic creep fracture analysis. The model is incorporated into an existing finite element program for numerical analyses. Mixed implicit-explicit algorithm is adopted for integrating the rate form equations. The strain localization analysis is employed for simulating crack extension. Finite element equations incorporating the new model and the strain localization analysis are derived based on variational principles.

The effect of loading history on creep response and crack behavior, i.e., the incubation time for a crack to propagate and the subsequent crack growth rate, is studied systematically. Effects of the various influencing factors for cyclic creep fracture, such as load cycling effect, load dwell time effect and interaction between creep damage and high temperature low cycle fatigue damage, etc., are evaluated respectively.

Acknowledgements

I would like to thank both my advisors, Dr. M.L. Ayari and Dr. T.R. Hsu for their consistent guidance and generous support with neverending patience during all my years as a graduate student at the University of Manitoba. Sincere appreciation is also due to Dr. E.Z. Lajtai, Dr. J. Shewchuk and Dr. S. Sheppard for their valuable suggestions.

As well, thanks are due to Mr. D. Kuss, Mr. M. DeCaire and Mr. R. Hurtle for being fantastic people to work and learn with. Thanks extends to Drs. G. Chen, Z. Gong, N. Sun, P. Zhang, H. Li, and Mr. D. Young for the useful discussions with them. Thanks also extends to Dr. N. Popplewell for his guidance at the beginning of this study.

The financial support by the National Science and Engineering Research Council of Canada (NSERC) is gratefully appreciated. The computation facility provided by the University of Manitoba is also appreciated.

Last but not least, I would like to sincerely thank my wife, Yuxiang, my parents, and my brothers and sisters for their love and support through thick and thin during all my years as a student.

Contents

List of Figures

Nomenclature and Abbreviations

K, ΔK: stress intensity factor and its range

J: J integral

C^*: C^* parameter

Q^*: Q^* parameter

σ_{net}: net section stress

σ_{ij}: stress tensor component

T: absolute temperature

T_m: melting temperature

D: damage parameter

R_{ij}: internal stress tensor

R: Boltzmann constant

$\varepsilon^c, \varepsilon^c_{ij}$: creep strain, creep strain tensor

$(\dot{\cdot})$: time derivative operator

t: time

S_{ij}: deviatoric stress component

$\tilde{\sigma}$: damage equivalent stress

$\bar{R}$: effective internal stress in von Mises sense

$\bar{\sigma}$: effective stress in von Mises sense

R_s: current maximum internal stress

R^o_s: initial maximum internal stress

R^u, R^u_{ij}: internal stress and internal stress component during unloading

R^r, R^r_{ij}: residual internal stress and its component before unloading

$\dot{D}_c$: creep damage rate

ΔD_f: fatigue damage increment in one load cycle

Δt_d: length of dwell time

σ_H: hydrostatic stress

$\Delta \varepsilon_p$: plastic strain range in the load cycling process

E: Young's modulus

ν: Poisson's ratio, loading frequency

Q: activation energy

N: number of load cycles

σ_n: creep stress threshold value

$\frac{\partial D_f}{\partial N}$: fatigue damage rate

A,n,m,B_1,p,C_1,C_2,r_o,α,β,B_2, k,c_o,B:

material constants dependent upon temperature

A_1,A_2,B_3,B_4: material constants

γ: constant in numerical one step integration formulae

CTOD: Crack Tip Opening Displacement

LEFM: Linear Elastic Fracture Mechanics

CDM: Continuum Damage Mechanics

EI: Explicit-Implicit

HTLCF: High Temperature Low Cycle Fatigue

HRR: Hutchinson-Rosengren-Rice

M-C: Manson-Coffin Relation

ICF: Interaction between Creep and Fatigue

SRP: Strain Range Partitioning

SEP: Strain Energy Partitioning

SEN: Single Edge Notch

MEOS: Mechanical Equations Of State

NASA: The National Aeronautics and Space Administration (U.S.)

IUTAM: International Union of Theoretical and Applied Mechanics

ASME: The American Society of Mechanical Engineers

Other signs and terms used are defined in the text.

Chapter 1

Introduction

1.1 Background

Modern machinery such as jet engines, airframes of high-speed aircraft, steam and gas turbines and nuclear reactors are required to perform complex patterns of operating schedules. A common service load cycle is one which begins with an initial 'start-up', an 'operation' period and then, 'shutdown' followed by a long 'rest' time. Fig. 1.1 shows a sketch of a typical flight cycle of an airplane. The loading history of the airplane engine has such typical service load cycle. Also shown in the figure are the corresponding profiles of temperature and speed of the turbine blade of the engine.

Although different time scales are involved in the various types of machinery, common problems arise due to the required operating schemes. Start-up and shut-down are short in time in comparison with the prolonged operation and rest periods. The rapid change of loads usually cause local plastic deformation in certain locations of the components and consequently creep deformation occurs during the operation time and stresses are redistributed within the material. After the long rest time, certain kind of microstructural changes could be observed and the material's resistance to further creep deformation is changed. During the lifetime of such a machine, the 'start-up – operation – shutdown – rest' cycle repeats itself from a few hundred to several thousand times. In such applications, components are required to function

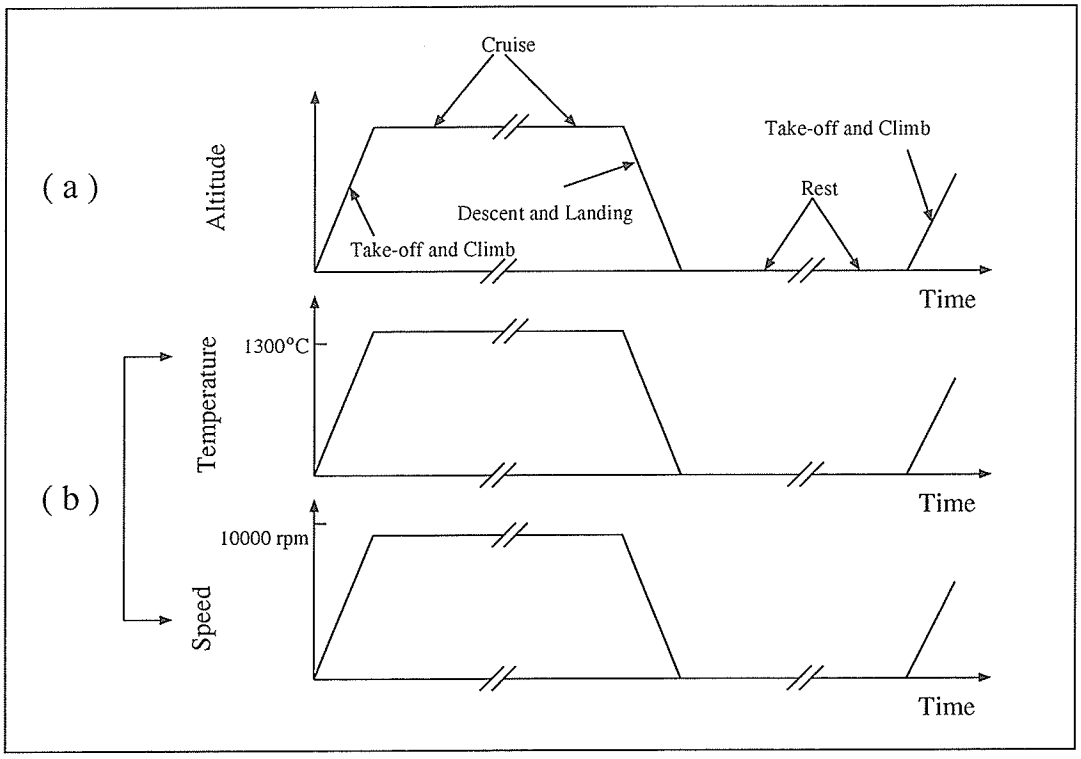

Figure 1.1: (a) A typical flight cycle of an airplane, (b) Profiles of temperature and speed of the turbine blade[342]

well and to maintain strength within the operating life.

In engineering applications, nearly all mechanical engineering components contain flaws, such as voids, inclusions, microcracks, etc., albeit if only at the microscopic level. In service, these flaws can nucleate and grow into small but visible cracks. Voids can also nucleate and grow at the grain boundaries in materials during the processes of creep deformation and creep damage. Under the combined cyclic thermo-mechanical loading and creep deformation conditions, these distributed voids and microcracks can be coalesced to form macroscopic cracks whose growth would cause the final fracture of the structure. A crack may reduce the load-carrying capacity or the lifetime of a component considerably.

Creep fracture is a major cause of failure of many key components in industrial applications, such as turbine blades and disks of gas propulsion engines. If creep crack growth is a potential failure mode, design codes and inspection standards should provide means to assess the relevance of creep damage in high temperature

components. Such an assessment should include crack-like defects which could be detected by nondestructive evaluation. In some critical applications, one must assume that cracks of a certain significant size, which might have escaped detection, are present. A lifetime prediction should then be based on the expected growth rates of such defects in future service. Design codes, such as those based on the 'safe-life' philosophy, usually rely on the unrealistic requirement that high temperature components should not contain any crack-like defects at all[225, 314]. A better understanding of the mechanics and the mechanisms of creep damage and creep crack growth would help to improve the situation.

In the past, design against creep failure is usually based on unnotched, uniaxial laboratory test data to ensure that creep deformation is kept within acceptable limits and that creep damage accumulation does not cause premature fracture during the service life of the component[261]. This, however, has caused too conservative designs and a considerable amount of waste. For example, in the past, the US Air Force removed an airplane component (especially that working in the hot section) from service when it reached its cyclic creep fracture design life which was based on very conservative statistical analyses[225-227]. This has resulted in the early retirement of many useful components. Gas propulsion engine disks, for example, were regarded as having reached their design life when 1 in 1000 was expected to develop a $0.1mm$ crack. Once the design life was met, all parts were removed from service even though a large percentage of the parts could have at least 10 more times of the useful lifetimes. This proved to be a necessary but uneconomical way to avert potential disasters. New design criterion based on the 'fail-safe' philosophy, e.g., the Engine Structural Integrity Program (ENSIP), now requires a damage tolerant design approach for all new engines. Accurate crack growth predictions are part of this design approach. In addition, the 'Retirement For Cause (RFC)' program was adopted. The purpose of the RFC program is to periodically inspect components for cracks and replace them only if the part is found to be unsafe for further use.

To implement the damage tolerant design and to design for higher structural reliability of components under the above stated working conditions, an accurate method to describe the initiation and growth behavior of a crack is essential. It is therefore necessary to develop reliable crack growth models. A successful model should accurately predict crack initiation and simulate its growth, or at the very least, conservatively. It is necessary to know how and when macroscopic cracks might be formed, grow further and run, and the ultimate breaking of the component. The microstructural changes of the material in the process of creep deformation and creep damage and their influence upon the macroscopic deformation response and fracture characteristics under such working conditions should also be known and reflected. Because creep deformation is the main cause of damage of materials under such operating condition, this kind of material failure is usually referred to as cyclic creep fracture in the literatures. It includes the macroscopic crack initiation process and the macroscopic crack propagation process.

Significant research effort has been devoted in the last three decades to the study of cyclic creep fracture behavior of materials. This research is not only theoretical important; but is also practical for high temperature technology. An interdisciplinary research effort among material scientists, engineering designers and researchers of solid mechanics had been involved in the study of cyclic creep fracture[10-12,14,21-22,190,261,291,327]. Different methods and models, based on conventional continuum mechanics, fracture mechanics, material science, micromechanics and continuum damage mechanics (CDM) have been proposed. Many factors, such as load dwell time, cyclic loading, interaction between creep damage and high temperature low cycle fatigue (HTLCF) damage and environmental attack, etc., have been indentified as having significant influence upon cyclic creep fracture behavior of many common materials. This work has led to significant understanding and modelling of the cyclic creep fracture behavior of structures.

However, in spite of all the advances in the study of cyclic creep fracture, a widely accepted and adequate theoretical framework for fracture at high temperature has

not been made available yet. As being pointed out by Halford[125], a senior scientific technologist of the National Aeronautics and Space Administration (NASA) of the United States, that we are still actively developing more descriptive, more accurate and more efficient tools for describing the cyclic creep fracture behavior. These include thermal-structural finite element analysis programs, advanced constitutive stress-strain-temperature-time relations and the creep-fatigue-environmental models for crack initiation and propagation.

In real applications, many of the factors mentioned above act on the material at the same time, such as the loading of gas propulsion engine turbine blades and disks in which both cyclic thermal and mechanical loads are involved, both load holding time and load dwell time are included in one load cycle and the high temperature low cycle fatigue damage and the creep damage are in an interactive mode. To the best of the author's knowledge, models incorporating all these factors in cyclic creep fracture analysis are not available yet. Also, in most of the stress analysis of components and structures working under the above-stated loading conditions, the loading pattern used is not based on the real working path, but rather a simplified one. For instance, in most of the analyses, the load dwell time effect is not considered, even though it has been known that long dwell time has significant influences on the creep response and crack behavior of the material upon reloading[119-120, 218]. The creep response and the crack behavior of materials under different loading histories was not reported.

For accurate structural integrity evaluations of components under the above stated working condition, a reliable methodology for creep deformation and creep damage analysis should reflect the loading history effect since creep deformation is highly dependent upon loading paths[43,115,180]. All effects that can change the creep response and crack behavior of materials, such as the load cycling effect, the load dwell time effect and the interaction between HTLCF damage and the creep damage, etc., should also be reflected.

1.2 Research objective

The objective of this thesis study is to propose a new constitutive model in describing the creep deformation and creep damage behavior of metallic materials at high temperature. The model should incorporates all stages of creep deformation into consideration. Also, the load cycling effect, the load dwell time effect and the interaction between creep damage and HTLCF damage on creep deformation response, creep damage evolution, incubation time for a crack to propagate and crack propagation rate have to be accounted for.

The effect of loading history on cyclic creep response and crack behavior of simple engineering structures, such as a cracked panel is to be investigated. The crack behavior includes the incubation time for a crack to propagate and its subsequent propagation rate. The loading history is simulated in this study by different combinations of load holding time and load dwell time during the cyclic creep deformation process. The effects of load cycling, load dwell time and interaction between creep damage and HTLCF damage on cyclic creep fracture behavior are evaluated respectively.

1.3 Scope of thesis

This thesis is divided into the following chapters:

Chapter 1 presents the general introduction to this thesis research work. This includes a statement on the background of research, a description of the research objective and an outline of the scope of this thesis.

Chapter 2 contains a comprehensive review of the investigations of cyclic creep fracture. Different models and methods used to describe the cyclic creep fracture behavior and relevant factors that influence the cyclic creep deformation, creep damage and fracture are catalogued.

A new CDM-based constitutive model is presented in Chapter 3 for describing the cyclic creep deformation response and creep damage of commonly used engineering

materials. The model has the capacity of reflecting the load cycling effect, the load dwell time effect and the interaction between creep damage and HTLCF damage on cyclic creep response and fracture behavior. The thermodynamic foundation of the model is discussed.

Chapter 4 contains the description of the finite element algorithm of cyclic creep fracture with the CDM-based constitutive model. The derivation of the finite element equations, the algorithm for integrating the rate form equations, the strain localization analysis as used for simulating crack extension and the critical damage condition, etc., are also described in this chapter.

Chapter 5 describes case studies for verification of the proposed CDM-based constitutive model in describing the cyclic creep fracture behavior. Both one-dimensional and two-dimensional cases are included.

In Chapter 6, a systematic study of the effect of loading history on cyclic creep response and crack behavior is presented. The effects of load cycling, load dwell time and interaction between creep damage and HTLCF damage on creep response and crack behavior are evaluated respectively.

Chapter 7 presents a summary, conclusions and contributions of this study and recommendations for further research.

Appendix A contains a summary of the micromechanisms of creep deformation, creep damage and fracture of metallic materials at high temperature. The detailed derivations of finite element equations are included in Appendices B-D. This includes both strain localization concepts for simulating crack extension and the cyclic creep fracture analysis with the proposed CDM-based constitutive model. Figures showing details of the analyses are attached in Appendices E-S.

Chapter 2

Review of the Investigations of Cyclic Creep Fracture

2.1 Introduction

In this chapter, investigations of cyclic creep fracture are reviewed. Particular attention is focused on the methods and models describing the cyclic creep fracture behavior and the relevant factors that influence cyclic creep deformation response and the evolution of creep damage of materials.

Because of its complex nature, an interdisciplinary research effort among material scientists, engineering designers and researchers in solid mechanics was witnessed in the study of cyclic creep fracture[99,190,224,272]. A vast amount of knowledge on the material's behavior under cyclic creep deformation conditions in the microscopic aspects[291,327]. Different theories and models have been put forward to explain the mechanisms of creep deformation, creep damage and fracture. From the viewpoint of macro-mechanics, there are generally two schools of thought in tackling creep fracture problems, the parametric approach[298-300] and the continuum damage mechanics (CDM) approach[168,203-205]. The two types of descriptions are integral parts of a unified research effort for the modelling of creep deformation, creep damage and fracture. They are complementary to each other[204]. In the problems fracture mechanics is used to solve, usually a macrocrack has been developed. CDM is used to describe material deterioration before and after a macrocrack is formed.

Many factors have been identified as having significant influence upon creep response and fracture behavior. These factors include:

- Cyclic load;
- Load dwell time;
- Interaction between creep damage and high temperature low cycle fatigue (HTLCF) damage;
- Environmental attack

2.2 The phenomenon of creep deformation and research on creep

According to the definition given in the latest version of the Encyclopedia of Science and Technology[101], the time-dependent strain occurring when solids are subjected to an applied stress is called creep. Creep becomes of particular importance at elevated temperature (greater than around $0.3T_m$, where T_m is the melting point of the material in degrees Kelvin). Generally speaking, for metallic materials, creep deformation is dependent upon the applied stress, temperature, loading history (or the microstructure of materials) and time. The essential feature of creep is that it is a process that involves significant time-dependent deformation. The elementary test to study creep deformation and creep failure is the uniaxial creep test in which a smooth bar is subjected to a constant tensile load (or stress, σ), and the elongation (or strain, ε) is measured as a function of time. A typical creep curve is shown in Fig. 2.1, with the corresponding creep strain rate curve shown in Fig. 2.2. By examining the creep strain rate curve, the whole creep deformation process could usually be divided into three stages, i.e., the primary stage, the secondary or the steady stage and the tertiary stage which corresponds to the cases where the creep strain rate is less than, equal to and larger than zero. The shapes of the

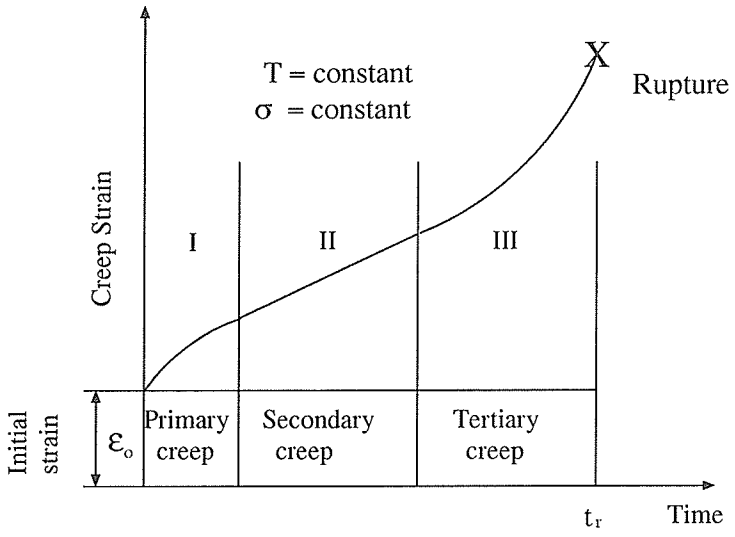

Figure 2.1: Typical creep curve[43]

creep curves vary from material to material. Pure metals often have a pronounced primary stage, whereas in many structural alloys, the tertiary stage predominates. The temperature and stress dependence of the creep deformation are shown in Fig. 2.3 and Fig. 2.4, respectively.

Many physical phenomena related to creep deformation of solids have been known for centuries. For example, usual occurrences such as the 'natural elongation' of a fine wire by its dead weight, sinking of heavy structures into ground, etc., are common knowledge[149]. Over the times, people must have taken these happenings for granted, because only until over 150 years ago research on creep was reported.

Although the phenomenon of creep has been the subject of extensive theoretical and experimental investigations since the beginning of this century[261], a detailed understanding of creep deformation and damage mechanisms as well as the description and modelling of them emerged at a much later time. This understanding arose through the use of a semi-empirical, or phenomenological, approach, whereby experiments were conducted to separately isolate the dependence of creep rate on external variables such as stress and temperature.

The particular significance of creep deformation and creep damage of compo-

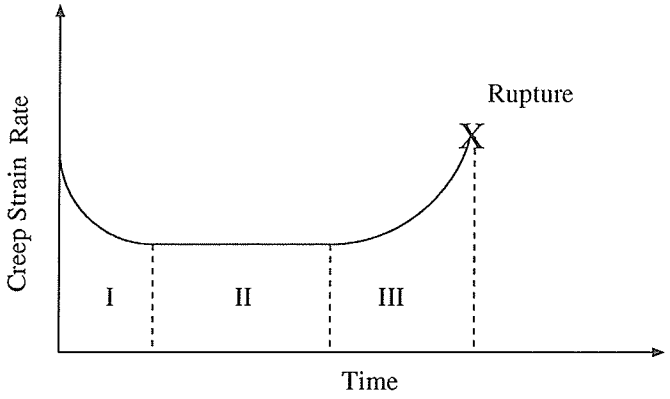

Figure 2.2: Typical creep strain rate curve[43]

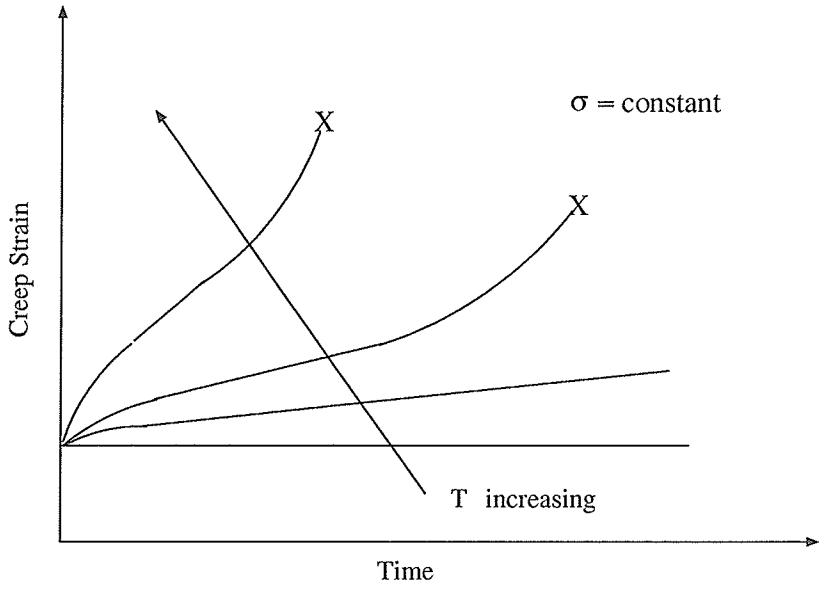

Figure 2.3: Temperature dependence of the creep strain[43]

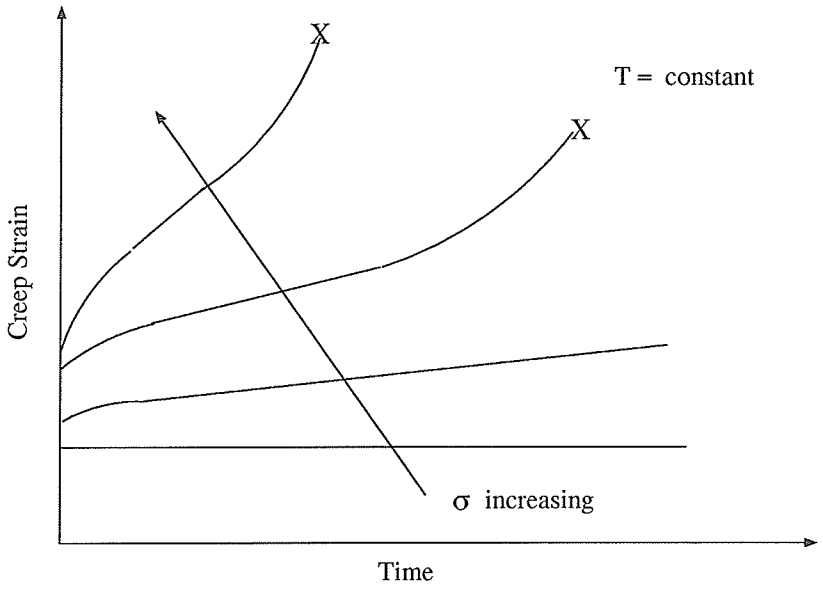

Figure 2.4: Stress dependence of the creep strain[43]

nents and structures in practical engineering applications was not recognized until the time during the World War Two. In the 1950's, creep mechanics and creep fracture mechanics were widely discussed and research in both theoretical and experimental aspects was initiated[293]. With the invention and rapid improvement of the digital computers, much progress had been made in these areas in the past fifty years[190,224]. As a result, a number of different deformation mechanisms occurring during creep process have been identified, and models developed, either theoretically or empirically based on the evaluation of experimental data, to describe creep deformation of common engineering materials.

It is worth noting that during the past 20 years, continuum damage mechanics (CDM), based on the concept proposed first by Kachanov[168-169], has made much progress in describing the creep deformation, creep damage and creep fracture of materials. It provides a realistic tool for modelling the progressive deterioration of materials due to creep deformation and creep damage. Much deeper understanding and effective modelling of creep deformation and creep damage and fracture behavior has been obtained by CDM methods. These progresses had been documented by Lemaitre[200-207], Chaboche[48-53], Chow[63-69]1, Leckie[189-193], Hayhurst[135-

140] and Krajcinovic[175-179], and others.

2.3 The parametric approach

The parametric approach is an extension of fracture mechanics concepts and models to account for creep fracture problems. Many researchers used this approach to treat creep-related problems.

2.3.1 Extension of fracture mechanics parameters for creep fracture modelling

Both linear and nonlinear fracture mechanics theories are useful in describing crack initiation, crack propagation of different components and structures under various loading conditions. In many cases, it constitutes a practical tool to predict material failure, especially in situations in which both material and loading conditions involve only small scale yielding in the bulk material and around the crack tip zone, and the final failure of the material is caused by the formation and growth of one major macroscopic crack.

Many researchers extended fracture mechanics parameters to creep fracture analyses [38,45,81,103,108,110,160,187,195-196,234,262,318]. One common feature of the parametric approach persists in correlating creep deformation and creep fracture data with one of the many fracture mechanics parameters. The commonly used fracture mechanics parameters are:

- the stress intensity factor, K[167,255,257];
- the stress intensity factor range, ΔK[255,257];
- the strain energy release rate, G[311];
- the J integral[283-284,287,323];
- the C^* parameter[298-301] and its extensions[291];

- the Q^* parameter[343-345];
- the crack tip opening displacement, $CTOD$[255];
- the nominal stress or the net section stress, σ_{net}[132].

In general, good correlation is achieved by means of certain forms of function relation between creep crack growth rate and one of the fracture mechanics parameters. The following expression is a typical such relation:

$$\frac{da}{dt} = A * P^n \tag{2.1}$$

where da/dt is the crack growth rate, P is one of the fracture mechanics parameters, A and n are material constants.

In these models, the effect of damage on the stress and strain distribution ahead of the crack tip was ignored. It has been pointed out that as long as damage is confined to a sufficiently small 'process zone' near the crack tip, the deformation field encompasses and controls the evolution of damage and therefore the respective load parameters should control crack growth[291,298-301]. In many real applications, it is indeed true that such calculated crack-tip fields control the crack growth rates. These fracture mechanics parameters are used to correlate creep fracture data of particular materials under various conditions and have achieved different degrees of success.

2.3.2 The limitations of typical fracture mechanics parameter in creep analysis

Despite the advantage of being simple in the forms, extension of correlations of the type given by Eq. 2.1 to the situations involving cyclic creep fracture does not appear to be sound. This is not surprising because the yield stress drops with increased temperature and the stress around the crack tip region redistributes during creep deformation process. This suggests that yielding is not confined to a small

zone around the crack tip and hence linear elastic fracture mechanics (LEFM) and elastic-plastic fracture mechanics conditions are violated. Actually, the absence of a unique relationship between fracture mechanics parameters and creep deformation and creep fracture data is natural because creep fracture behavior exhibits high dependence upon loading history, as supported by a number of researchers, which these fracture mechanics parameters have no means of description.

2.3.2.1 The K, ΔK and the net section stress

In the early contributions on creep crack growth, the stress intensity factor, K and the net section stress were considered as favorable candidates for appropriate load parameters for correlating creep fracture data. While K turned out to have its range of validity, the net section stress has no sound theoretical basis, but was occasionally successfully applied[132]. Nevertheless, the processes of creep deformation, creep damage, crack initiation, crack propagation and the final fracture, etc., are all related to the underlying stress field within the material, especially in the vicinity of the crack tip region. The crack tip fields change with the development of deformation and evolution of damage. The crack tip fields are also influenced by the cyclic loading. The stress intensity factor or its range are all based on a purely singular stress distribution around the crack tip region (i.e., the HRR fields in fracture mechanics) which is priori inexistent in high temperature creep fracture problems of metallic materials[56,136,139,191,291]. The net section stress also ignores the underlying stress distribution and its evolution which is fundamentally the driving force behind cyclic creep fracture. As such, these methods which can be characterized as indirect, had performed with a relative degree of success.

The stress intensity factor K and its range ΔK were used to characterize the condition at the start of the test when stress redistribution due to creep deformation has insufficient time to take place. Application of σ_{net} assumes full redistribution to a practically uniform level. Actually, the stress intensity factor or its range and the

net section stress describe two extremes of stress distribution in a solid under creep condition. The true stress distribution probably lies between these two extremes[56].

2.3.2.2 The C^* parameter and its extension

It is generally accepted that the C^* parameter is a good correlating parameter for creep crack growth behavior under steady state conditions in creeping materials[291,298-301,318]. Steady state conditions exist in a cracked body when widespread creep deformation characterized by power law creep occurs. Under these conditions, C^* becomes path independent, it equals the energy release rate. In most of the creep fracture analyses using the C^* parameter, it was usually assumed that the material obeys a power-law viscous stress-strain rate relation and that the development of cavities or the material damage do not modify the HRR-fields. The power-law constitutive equation simplifies the description of stress and strain rate fields. All stress components at any point of the solid body increase in proportion to the n^{th} power of the load, where n is the stress exponent in the creep rate equation. While the calculation of the whole stress field in a finite body usually requires numerical techniques, the asymptotic field near a crack tip can be obtained analytically. These are the so-called HRR-fields.

It is important to note that the C^*-integral, which can be measured far from the crack tip, at the same time determines the crack tip stress field certain distance away from the crack tip, i.e., outside the process zone. Load and specimen geometry affect the crack tip field only through the C^*-integral. Therefore, in viscous materials, creep crack growth will be described macroscopically by C^*. It is argued that[298-301] this remains true even if a sufficiently small zone near the crack tip behaves arbitrarily differently, say, due to grain boundary cavitation or other processes which offset the validity of a nonlinear viscous description. In other words, in analyses involving the C^* parameter, it is assumed that the cavities do not modify the HRR-fields. C^* is valid for general viscous behavior, even though most of the explicit

expression of the C^* parameter was derived for power-law materials. The power-law is especially convenient in that the near-tip fields can be given in closed analytical form.

However, the application of C^* is limited because of the restriction to steady state creep[298-301]. Most elevated temperature components are designed to resist widespread creep deformation. As a result, the creep strains are expected to be in the primary creep regime for a significant portion of the lifetime. Because of the stress and temperature gradients and periodic start-ups and shutdowns in thick section components, there is also a good likelihood of the presence of the small-scale creep conditions during most of the service lifetime. The presence of crack growth also promotes transient stress conditions near the crack tip and so does the occurrence of tertiary creep. Thus, in several practical situations, the consideration of transient stress field is important and, for these applications, C^* is no longer a valid crack tip parameter.

Also, the proposal of the C^* parameter is based on mathematical analogy of creep flow law and the constitutive relation of materials assumed in the J-integral analysis. There is no mechanic basis other than mathematical convenience.

In reality, before a crack starts growing, for example by coalescence of grain boundary cavities, its tip is blunted by creep flow of the surrounding material. And the microstructures, and hence the material properties of the material at the crack tip are changed. In the derivation of the HRR-field, on the other hand, the crack is treated as being mathematically sharp. Therefore, strictly speaking, the validity of the HRR-field is restricted to distances from the crack tip which are large compared to the crack-tip opening displacement, δ_t[291]. It has been found that blunting disturbs the stress field over distances 3 to 5 times δ_t, whereas outside that zone the analysis which neglects blunting becomes increasingly accurate. Thus, the range of validity of the HRR-field is limited by blunting towards small distances from the crack tip, and by the outer specimen geometry towards large distances. It is important to realize that the existence of a unique asymptotic field is essential for

C^*-testing since it guarantees a unique behavior of crack tips in differently shaped specimens.

The J-integral and the C^*-integral are both path-independent because the stress-strain and the stress-strain rate relations are all independent of the spatial variables. The J and the C^* parameters generally depend on the prior loading history and are time-dependent even for constant load (note that the time dependances are given by $J \propto \sigma\varepsilon$, and $C^* \propto \sigma\dot{\varepsilon}$). In order to remove the dependence of C^* on the prior loading history, Riedel[291] defined the following parameter C_h^*:

$$C_h^* = C^*(1+p)\left(\int P(t')^{m(1+p)}dt'\right)^{\frac{p}{1+p}} \frac{1}{p(t)^{mp}} \tag{2.2}$$

where the subscript h indicates the suitability of C_h^* for hardening creep. $P(t)$ is the time-dependent load and p and m are material parameters.

Obviously, C_h^* is time-independent since it differs from J or C^* only by time-dependent factors. It reduces to C^* if $p = 0.$ and it has the desired property of depending on the current load only. This is an improvement of the C^* parameter in treating creep fracture problems. A similar parameter C_t, was proposed by Saxena[299]. This parameter was proposed to account for creep crack growth under transient conditions. According to Saxena, there is no inherent limitations in the use of C_t for transient results from stress relaxation, primary and tertiary creep deformation, cyclic loading and crack growth[299]. However, much work remains to be done in developing accurate expressions to estimate C_t in components in the presence of primary creep deformation and crack growth. Hence, these parameters all have limited range of application[291].

Therefore, it can be safely stated that all these load parameters have certain limitations in correlating the creep deformation and creep fracture data. The relevance of these characterizing fracture mechanics parameters in correlating with creep crack growth rates is not fully established.

2.3.3 The load parameter map

Riedel[291] developed a load parameter map which is a diagram with time on the vertical axis and the net section stress, σ_{net}, on the horizontal axis showing the dominant area of these controlling parameters on creep deformation and creep damage. In this map, four types of deformation, namely, elastic, plastic, primary creep and secondary creep, were considered. In the time-stress plane, the areas are indicated in which each of the four deformation mechanisms determines the specimen behavior. Associated with each deformation mechanism is a fracture mechanics parameter which describes creep crack growth macroscopically in the respective regime. The regimes are separated by characteristic times. Fig. 2.5 schematically shows an example of such map. In the low stress/short time regime, the elastic response dominates and therefore K_I is applicable. At higher stresses, the specimen becomes fully plastic, which requires the use of the $J-$integral, until, at very high stresses crack tip blunting bounds the regime of $J-$controlled crack growth. The primary creep regime, which is labelled by C_h^*, is separated from the elastic regime by $t_1 \propto \sigma_{net}^A$, while after the time $t_2 \propto \sigma_{net}^B$, steady-state creep starts to dominate. At higher stresses, where no primary-creep regime exists, the secondary-creep zone catches up with the primary-creep zone while both are still small, and the further evolution of the secondary-creep zone ensues effectively in an elastic surrounding. The transition to steady-state creep then occurs with the characteristic time $t_3 \propto \sigma_{net}^C$. At even higher stresses, the transition from instantaneous plasticity to secondary creep occurs at around $t_4 \propto \sigma_{net}^D$. At longer times, crack tip blunting bounds the range of validity of C^* unless fracture of the specimen intervenes. The limitation on C^* set by blunting varies as $t_b \propto \sigma_{net}^E$. It is also shown in this map that the various fracture mechanics parameters have limited applications.

The load parameter map is a deformation map of cracked bodies, but is not in any sense related to the fracture mechanism map or the deformation mechanism map described in the proceeding chapter. The precise position of the lines representing

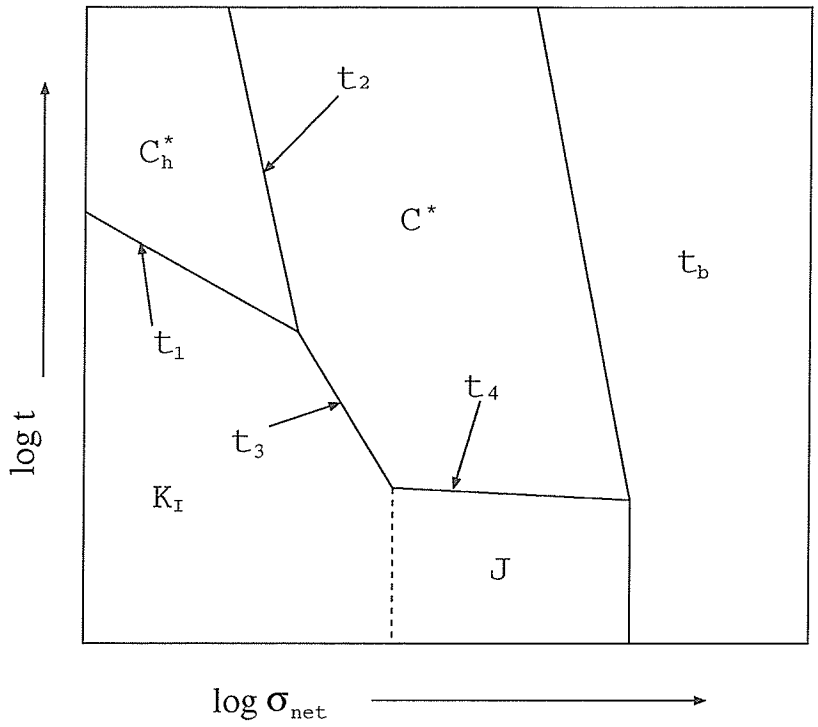

Figure 2.5: Typical load parameter maps[291]

the characteristic times depends on the material parameters, A, B, C, D, E, and on the geometrical parameters, such as crack length and specimen thickness and width, etc., but not on the absolute specimen size. For example, the regime dominated by C_h^* will be larger in a material with pronounced primary creep.

2.3.4 Limitations of the parametric approach

In summary, the limitations of the parametric approach in treating creep deformation and creep fracture problems are as follows:

- They are basically empirical correlations extended based on the applicability of these parameters in describing the elastic-plasticity deformation. There is no rigorous physical and mathematical foundations;

- They did not incorporate the governing physical mechanisms and processes of creep damage in the correlations. In most of the models, the material properties were assumed unchanged during the deformation process. The analyses

were based on the information at the beginning of the creep deformation, i.e., the undamaged material.

- The effect of stress redistribution caused by the creep deformation and creep damage was not reflected. The parametric method constitutes a 'black-box' approach. The effects of the evolutions of the crack tip fields are ignored in the correlations.

- The parametric approach relies on small-scale yielding and small-scale damage assumption. This means that the effect of damage (in the form of cavities, for example) on the stress fields is neglected. The approach is therefore not valid once intense damage spreads across the whole ligament rather than being confined to a small process zone.

- They cannot model the changes of the behavior of components and structures induced by prior loading or temperature change, i.e., the loading history effect because these fracture mechanics parameters are not of additive nature.

- The influence of the various effects on cyclic creep fracture cannot be sequentially accounted for through one of these parameters. The typical influencing factors on cyclic creep fractures are load cycling effect, load dwell time effect, interaction between creep damage and HTLCF damage and environmental attack.

- Because of the reasons stated above, these models can not describe the cyclic creep fracture behavior under an irregular loading pattern, e.g., loading cycles with various load holding time and various load dwell time.

Hence, the parametric approach has limited applicability for cyclic creep fracture analysis. Even though the parametric approach is being improved steadily to characterize cyclic creep crack growth, fracture mechanics parameters for general usage is not available yet[291].

2.4 The micromechanics approach

In the micromechanics approach, attempts are made to determine the thermo-mechanical behavior of grains and the effect of the distribution, density and shape of specified defects on some important physical properties of the material, such as the stiffness, by the methods of the mechanics of solids. At the microscale of grains, good representation of physical mechanisms of creep deformation and creep damage can be introduced. No macroscopic assumptions, such as homogeneity and isotropy are needed. Material scientists have proposed many phenomenological theories to account for these changes[291].

However, difficulties arise when these analyses have to be included in large scale structures to predict ductile failures. The main reason is the lack of accuracy of local stress calculations at the microstructural level. As pointed out by Krajcinovic[175-179], the exact description of the actual evolution of micro-defects would not only defy our computational capability but would also represent a meaningless task in view of the fact that the details of the crack and defect pattern would, to a significant degree, differ from one experiment to the other. For example, the theory of slip in a single crystal is reasonably well developed, the extension of such theory to a polycrystalline solid involving averaging in conjunction with substantial simplications is too complicated for practical usage. Also, accurate modelling of the various defects and their statistical presentation are not easy to be realized. In addition, it is not easy to relate the overall material deterioration to a particular microstructural change. Wilsdorf[339] has made the following statement on this issue: '...The numerous combinations and variations of microstructures have a significant influence on fracture, and it is clear that the annealing and deformation histories must lead to different mechanisms in regard to microcrack initiation, their propagation and the final separation. Point defects and their aggregates will interact with volume defects. It can be seen immediately that there exists a profound difficulty in developing a one-parameter criterion for ductile fracture based entirely on the microstructural

regime'.

Hence, to reflect the changes of the material properties (i.e., with the development and accumulation of damage) and the damage pattern of the material, a promising strategy is to establish a macro-model which will broadly mirror the salient trends of the microstructural kinetics with more or less distortion and blurring of detail. The goal is to represent a discontinuous state (micro-cracks, micro-cavities) by a continuous variable, thus allowing to construct the macroscopic theory from microscopic considerations. If the geometrical nature of the defects is simple and known, micro-mechanics and homogenization techniques are the tools to do it. But most often, the mechanisms are not well known and a simple mean value of a defect characteristic is the only way to represent the effect.

So, instead of trying to reproduce the fine details of the micro-defect pattern and its evolution, it appears reasonable to introduce a set of kinetic variables reflecting the degree of deterioration and other forms of microstructural changes of the material in an appropriately chosen smoothed sense. Towards this goal, the continuum damage mechanics (CDM) was developed. CDM is the micro-mechanisms approach which relates the strain state, the damage evolution and the stress state and the material behavior at the crack tip to the state variables, such as the damage parameter and the internal stress. It requires an understanding of the physical process of creep deformation and damage growth and an abstraction and generalization of such process. The micromechanics analyses and models resemble those of the CDM (see later), and can be thought of as a mechanistically-based extension of CDM methods and models in describing a specific damage mechanism.

Attempts were undertaken to develop constitutive models for cavitating materials based on the physical laws for cavity growth[159,332-333]. Models of this type were based on the results of material scientists for the particular forms of creep strain. However, these model-based descriptions are not yet in a shape to replace the empirical description of CDM proposed first by Kachanov[168-169] which is

described in the next section.

2.5 The CDM approach

2.5.1 The fundamental notion of CDM

Proper understanding and description of the damage process of materials brought about by the internal defects and their growth with the development of creep deformation is important. It would help in discussing the macroscopic behavior of materials, as well as in elucidating the process leading from these defects to the final occurrence of fracture. As stated above, creep deformation causes creep damage of materials in the form of grain boundary cavitation and creep damage in turn accelerates creep deformation. Conversely, the nucleation, growth and coalescence of cavities on the grain boundaries influences the macroscopic stress/creep strain-rate response of the material. The fundamental notion of CDM is to represent the damage state of materials in terms of appropriate internal state variables, such as the damage parameter and the internal stress. Mechanical equations can then be established to describe the evolution of the internal variables and the mechanical behavior of the damaged materials. The coupling effects between damage processes and the stress-strain behavior of materials can thus be described. In this theory, the damage field and other internal variables implicitly account for the evolution of creep strains and internal damage. This is essentially the basic idea of the CDM in treating creep fracture problems. CDM relies on simple phenomenological definitions so that the required material constants can be determined from conventional creep tests. For creep deformation of metallic materials at high temperature, at least part of the accelerating creep rate must be ascribed to grain boundary cavities and micro-cracks and to other changes of material microstructures. Creep damage equations takes into account the evolution of microstructural defects in an indirect manner. Fundamental conceptual descriptions of CDM and its application are reflected in the works by Chaboche[48-53], Chow[63-69], Hayhurst[135-140], Hult[158],

Krajcinovic[175-179], Leckie[189-193], Lemaitre[200-207] and Murakami[248-251], to name a few.

2.5.2 Applicability and limitation of CDM

CDM is a rapidly developing branch of mechanics based on the conceptual idea first proposed by Kachanov and Rabotnov for uniaxial creep rupture characterization[168-169,293]. At that stage of development, damage was purely an empirical quantity used to account for the deviation of material behavior from the creep curve predicted by the power law. Damage under the present concept of CDM is generally considered as a collection of permanent microstructural changes in material elements brought about by some irreversible processes resulting from thermomechanical loadings. It is often reflected in the deterioration of the mechanical/service properties such as stiffness and residual life of a material entity. CDM is the modelling of these microscopic quantities through homogenization so that their aggregated effects in material service behavior can be considered at the continuum level. Instead of taking the crack tip fields as a black box or as approximated by the HRR fields in the fracture mechanics methods, the CDM considers the local stress and strain fields near a crack tip and the corresponding deterioration of material with time and the evolution of these fields. Local failure criterion incorporated with CDM analyses allows a crack increment to be predicted, and eventually a smooth crack extension could be described.

CDM is also classified as a local approach of fracture since only local field variables are considered necessary in order to determine the onset of cracking, failure, etc. It does not have the limitation due to different modes of failure (e.g., G_I, G_{II}, G_{III}, K_I, K_{II}, K_{III}, etc.)[63-64], or due to the scale of yielding and finite deformation such as required by the fracture mechanics parameters. Intuitively, it is a more versatile tool than the traditional fracture mechanics which is, strictly speaking, limited to fracture in brittle materials or with the limitation of small scale yielding or small scale damage.

According to CDM, the deformation (especially the permanent deformation, such as creep deformation and plastic deformation) process is at the same time a damage process[55,313,338]. Damage accumulates within the material with the development of permanent deformation, and ultimately causes failure of the material. In this theory, it is assumed that besides the external loads (i.e., the stress and temperature), the creep response of a material depends on its current microstructural state, which can be described by a set of internal variables, such as the damage parameter and the internal stress. One prominent advantage of this approach is that it can represent material behavior under different loading histories. This is because the damage parameter is a quantity of additive nature. Also, this approach incorporates the inherent mechanisms (loosely speaking, the progressive deterioration of material properties due to creep damage and other forms of damage) in the description of the current macroscopic deformation responses.

While simplicity is a very attractive feature of this theory, CDM has been criticized for treating materials without appropriate regard for metallurgical processes associated with creep damage. Although this criticism has been mounting, micromechanical modelling of creep deformation and fracture remains too complicated and unreliable for routine engineering applications. As pointed out by S.R. Bonder and Z. Hashin[41], the co-chairmen of the 2^{nd} International Conference on Continuum Damage Mechanics, 1986, Israel, that the sponsorship (of international conferences on continuum damage mechanics) by the International Union of Theoretical and Applied Mechanics (IUTAM) indicated that the field of continuum damage mechanics has reached a level of scientific maturity and activity that warrants recognition by the mechanics community.

2.5.3 Relationship between fracture mechanics and CDM

Both fracture mechanics and CDM are tools to deal with problems of material failure. In fracture mechanics problems, material failure is usually caused by the

initiation and propagation of one major crack in the specimen. It is usually assumed that only the material at the crack tip experience damage or degradation, and the material in other parts of the specimen is not influenced. In CDM, it is regarded that final failure is caused by progressive degradation of the material. The damage is distributed unevenly throughout the material and therefore influences its properties at every point depending upon the degree of damage. The final failure of the material is caused by the evolution and accumulation of the damage. For example, when the accumulated damage at a particular point reaches a critical value, the material at the point is regarded as having lost its load-carrying capability and damage is 'complete'. The locus of such damaged points forms a macrocrack and its progressive propagation leads to the final failure of the component or the structure. Fig. 2.6 shows the relationship between fracture mechanics and CDM as complementary sciences[51].

Damage develops rapidly near a crack tip forming an area which is referred to as the 'process zone' in which the material properties change drastically because of the damage. This is described more specifically in the next section. As long as the growing process zone is small enough, the boundary value problem can be formulated by prescribing the nonlinear viscous HRR-fields (without damage) as the initial condition at $t = 0$ and the remote boundary condition for the solution of the damage mechanics equations. This is because the HRR field describe the material state outside the process zone[291]. The limitation of small-scale damage of the fracture mechanics parameters has important practical consequences. Only when this limitation is met, the fracture mechanics approach based on C^* and C_h^* parameters remains valid. If the small-scale damage limitation is not met, the process zone becomes large enough to perturb the singular fields which validate the use of the respective fracture mechanics parameters. Therefore, no fracture mechanics description of creep crack growth based on macroscopic load parameters appears to be possible if the small-scale damage limitation is not met. Nearly all the fracture mechanics parameters related to the HRR fields assume that the cavities or

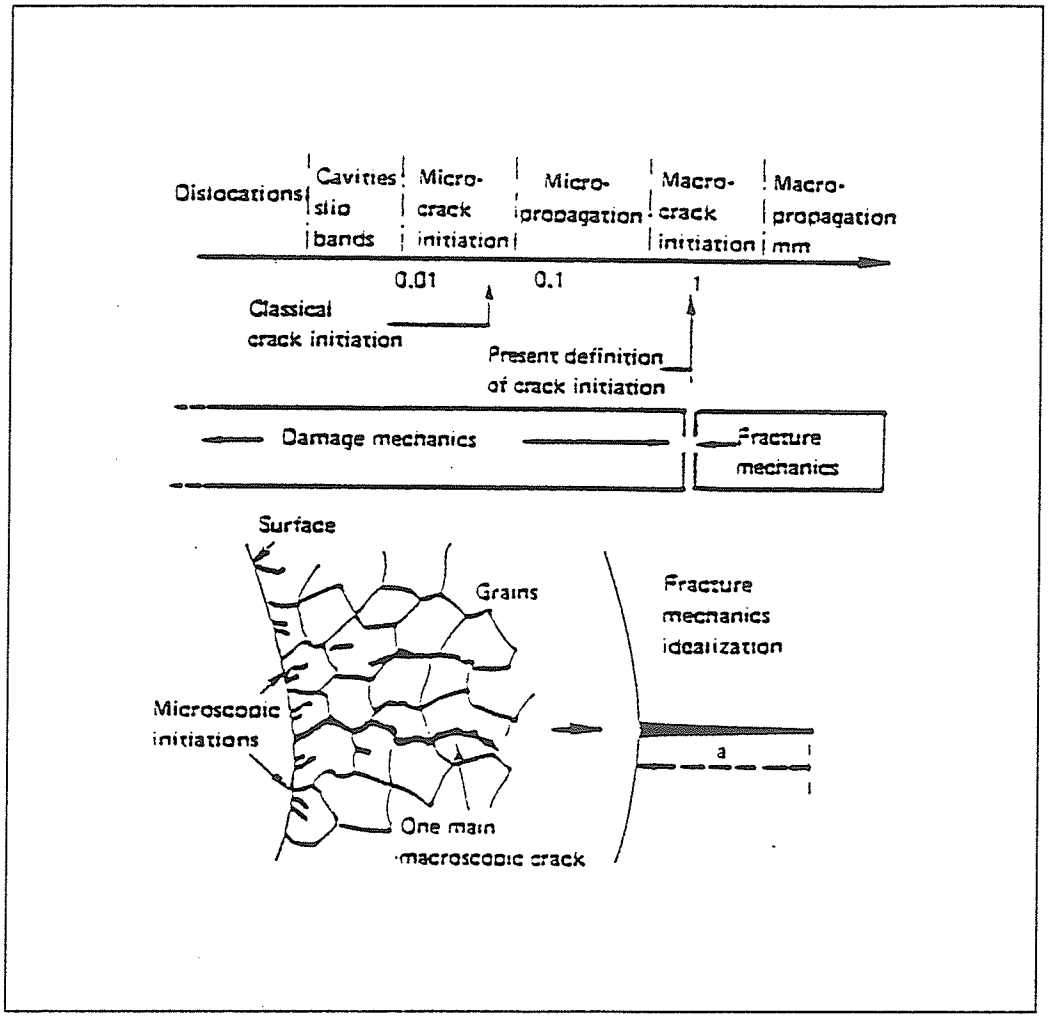

Figure 2.6: Fracture mechanics and continuum damage mechanics as complementary sciences[51]

damage in the crack tip area do not modify the HRR fields. But it is found that as long as the damage is confined to a sufficiently small process zone near the crack tip, i.e., if the small-scale damage limitation is met, the continuum deformation fields based on the HRR solutions encompass and control the evolution of damage and therefore the respective fracture mechanics parameters should control crack growth. In many cases, it is the crack tip fields that control the crack growth rates[298-301].

2.5.4 The concept of process zone

The crack tip area usually experiences high stress concentration. In the creep deformation process, higher stress produces higher rate of creep strain and higher rate of damage. Therefore, the small area surrounding the crack tip experiences severe damage or has higher degree of material deterioration as compared to other parts of the material during creep deformation process prior to crack growth. The material properties within this small area change drastically with the development of creep strains. This small area is referred to as the process zone[291]. There is no generally accepted definition of the size of the process zone. Somewhat arbitrarily, in one case, the process zone is defined as the zone within which the equivalent strain rate is at least doubled by damage in comparison with the undamaged viscous materials. An estimate for the size of the so-defined process zone is obtained by calculating the creep strain rate coupled with damage and the creep strain rate using the undisturbed HRR-field centered at the original crack tip.

As shown by Riedel[291], Fig. 2.7 illustrates that this definition of the process zone is reasonable. In this figure, normalized units are used. The process zone size, r_p as shown on the horizontal coordinate is normalized by the crack growth increment. This figure shows results of the stress evolution ahead of the crack in the normalized units based on the CDM analysis and the theoretical calculations with the HRR-fields. According to stress analysis based on CDM models, the stress in the small zone surrounding the crack tip is relaxed progressively towards the crack tip in

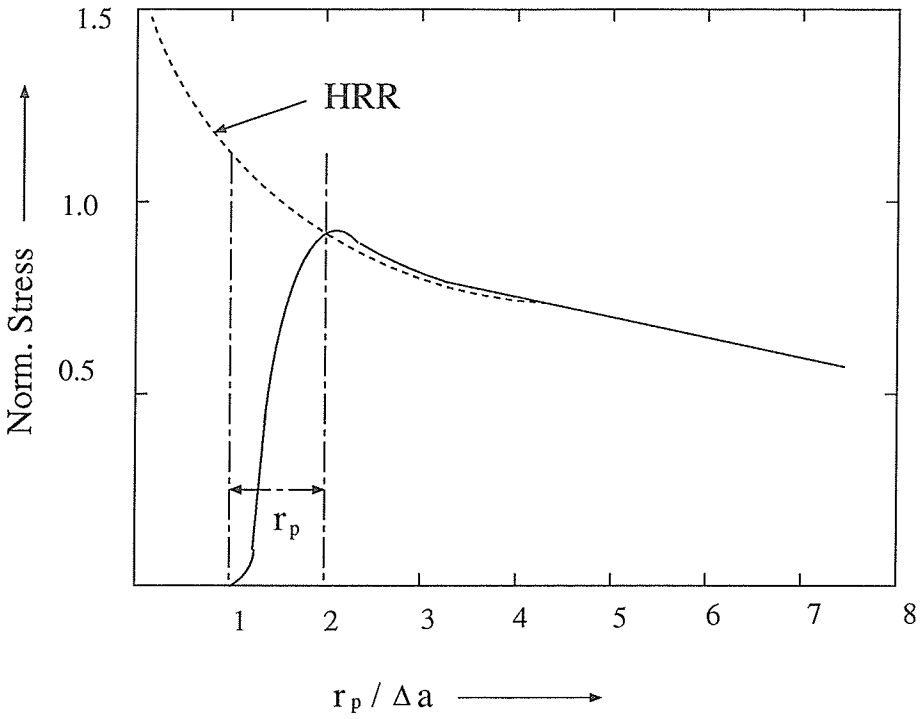

Figure 2.7: Stress distribution in the process zone ahead of a growing crack[291]

the creep deformation process. And with the evolution of creep deformation and the accumulation of damage, the stress at the crack tip is relaxed progressively to zero. Shown in the figure, the process zone size is a measure of the zone within which the stress calculated from CDM models deviates markedly from the undisturbed HRR-field.

CDM provides a realistic and easy way to describe the material behavior within the process zone which is difficult to describe by using the conventional fracture mechanics method. But outside the process zone, CDM and fracture mechanics are equally widely used tools to describe the thermomechanical behavior of materials and similar results are found[291]. This is natural because outside the process zone, the damage value of the material is small, its effect on the creep evolution could be neglected. And the CDM analysis is reduced to the conventional mechanics analysis without considering the material deterioration.

2.6 CDM models for creep fracture analysis

2.6.1 Kachanov-Robertnov's model

Kachanov[168-169] first proposed a phenomenological theory which reflects material deterioration due to creep deformation and creep damage. It was originally intended to describe the tertiary stage of creep deformation and creep fracture. In this theory, a new variable, the damage parameter, was incorporated into the well-known equation, the Norton's law, describing high temperature creep response of materials.

$$\dot{\varepsilon}^c = A(\frac{\sigma}{1-D})^n \tag{2.3}$$

The damage parameter as used in this model is an abstract description of material deterioration due to creep deformation. It is not meant to be a physically identifiable quantity, although it is somehow related to the cavitated area fraction of the grain boundary. The damage caused by creep strain was represented by the damage parameter D. It is an internal variable which is assumed to be not directly measurable. It is further assumed that damage evolution obeys the following kinetic law:

$$\dot{D} = B(\frac{\sigma}{1-D})^m \tag{2.4}$$

When the material is in a virgin state, D=0.0, Eq. 2.3 reduces to the Norton's law of steady state creep deformation. D=1.0 characterizes total material failure. Kachanov[168] regarded the parameter D as quantifying the degree of microcracking or a macroscopic expression of the degree of deterioration of the material. Over the fraction D of the cross sectional area, the cohesion of the material is taken as zero and over the remaining fraction $(1-D)$, it is taken as normal. A consequence is that creep strain rate $\dot{\varepsilon^c}$ depends on $\frac{1}{1-D}$, with the result that ε^c and D become auto-catalytic or coupled with each other. Hence, the deterioration of the material

is taken into account in the macroscopic description of the material response.

Robertnov[293] improved Kachanov's model to include the primary stage of creep deformation. The improved model has the following form:

$$\dot{\varepsilon}^c = A(\frac{\sigma}{1-D})^n t^\phi \tag{2.5}$$

$$\dot{D} = B(\frac{\sigma}{1-D})^m \tag{2.6}$$

Kachanov and Robertnov's model is a significant step towards the simulation of material deterioration due to creep deformation and creep rupture. Subsequently, many improved and extended models were proposed[190]. Following are two typical such models.

2.6.2 Leckie and Hayhurst's model

Leckie and Hayhurst[192-193] improved and extended Kachanov-Robertnov's model to the three-dimensional case. Their model has the following form:

$$\dot{\varepsilon}^c_{ij} = \frac{3}{2}A(\frac{\bar{\sigma}}{1-c_o D})^n \frac{S_{ij}}{\bar{\sigma}} t^m \tag{2.7}$$

$$\dot{D} = B\left[\frac{(1-\alpha)\bar{\sigma} + \alpha\sigma_I}{1-D}\right]^\phi \tag{2.8}$$

Many contributions followed based on this model. According to the results from this model, the effects of damage produced in creep deformation is to blunt the sharpness of the crack tip, to nullify the stress singularity around the crack tip region and to cause the stress to redistribute. Such stress redistribution has profound influence upon the subsequent creep and damage evolutions, the incubation time for a crack to propagate and the subsequent crack propagation rate[56-59].

Leckie and Hayhurst were probably the first to study creep fracture problems using the method of CDM in three-dimensional domains. Their derivation of the constitutive equations are based on constant multiaxial stress tests and on uniaxial

tensile notched bar. Though creep fracture problems are also studied, the loading was static.

2.6.3 Gong and Hsu's model

Gong and Hsu[120] proposed another set of constitutive equations to describe creep behavior of selected engineering materials under cyclic mechanical loading (with both load holding time and load dwell time) with a set of constant temperatures. Their model takes the following form:

$$\dot{\varepsilon}^c = A(\frac{\sigma - R}{1 - D})^n Sign(\sigma - R) \tag{2.9}$$

$$\dot{R} = B_1(R_s - R)^p \dot{\varepsilon}^c \tag{2.10}$$

$$\dot{D} = C_1 \frac{\sigma}{1 - D} + C_2(\frac{\sigma - R}{1 - D})^{r_o n}(\frac{\sigma}{1 - D})^{r_o} \tag{2.11}$$

and:

$$R_s = R_s^o[1 + \beta(\frac{\sigma - \sigma_n}{\sigma})\Delta t_d]^\alpha \tag{2.12}$$

For unloading:

$$\dot{R}^u = B_2(R^r - R^u)^k \tag{2.13}$$

In this model, besides the damage parameter, another state variable, the internal stress, R, was introduced. The internal stress is introduced to reflect the microstructural changes not reflected by the damage parameter within the creeping material[2-3,77,113-114,317], such as the creep hardening due to the multiplication of the dislocation movement.

Uniaxial isothermal high temperature tension tests were carried out to verify the validity of the model (Eqs. 2.9-2.13) for describing creep behavior of selected engineering materials. Good results in favour of the model were obtained[119-120]. This model takes all stages of creep deformation into consideration. It can also reflect the effect of the rest (or dwell) time on subsequent creep development. The

effect of dwell periods in the cyclic creep deformation of solids was accounted for by considering variations of the internal stresses during the deformation. Actually, just because of this, this model is termed as 'generalized creep damage model' because it was the first attempt to describe the creep deformation response and creep damage of a material according to real loading path, with the load dwell time effect reflected through the change of the state variables. Experimental tests showed cyclic creep acceleration behavior of 316L stainless steel under the loading condition which was also predicted by theoretical calculation using this model[119-120].

2.6.4 Other CDM-based models

Many other CDM-based models were proposed to describe creep deformation, creep damage and fracture behavior. Among these, the typical ones are:

- Lemaitre and Chaboche's model[205];
- Miller's model[142,219-220,241,325];
- Chow-Wang's model[65];
- Murakami-Ohno's model[248];
- Krajcinovic-Fonseka's model[178]

Numerous contributions followed these models in the understanding of the mechanical behavior of cyclic creep deformation and micromechanisms of creep damage and fracture, to predict the operation life of components under the condition of the interaction between creep damage and HTLCF damage and in the modelling of these features.

2.6.5 Limitations of CDM models

CDM models suffer from limitations which are of various degrees of importance. It can be stated that:

- Some of these models are too complicated to implement. They are thus unsuitable for practical uses;
- A large number of material parameters are involved in some of the models. Some of these parameters are difficult to obtain;
- Most of the models are applicable only for static loading conditions. When extended and used for cyclic loading cases, the load cycling effect on the creep deformation and creep damage process is ignored by nearly all models;
- Many influencing effects are not reflected in these models. For example, the load dwell time effect was ignored by most models.

Hence, there is a need to develop new models to describe the development of creep strain and damage of materials when they are subjected to complex histories of stress and temperature. Ideally, such models should adequately represent the material behavior as observed experimentally on one hand and should, on the other hand, be sufficiently simple in form and suitable for mathematical manipulation and numerical computation. Also, such a model should be easier to be understood and make full use of available material constants. The various influencing factors on cyclic creep fracture of the materials should be reflected. The major influencing factors for cyclic creep fracture are the load cycling effect, the load dwell time effect and the interaction between creep damage and the HTLCF damage. This is the guideline for the proposal of a new CDM-based constitutive model in this thesis study.

2.7 State variables

As stated above, in CDM, certain state variables are introduced on the basis of conventional mechanics in describing the material response with various stress and temperature histories. These state variables are used to reflect the microstructural

changes of the material or the material texture in the deformation process. The commonly used variables are the damage parameter and the internal stress.

2.7.1 The damage parameter

The damage parameter is the most commonly used state variable in CDM. It generally describes the degree of material deterioration with the accumulation of permanent deformation.

2.7.1.1 Conceptual understanding

An exact and universal definition of 'damage' is difficult to formulate and is not available yet[206]. This is mainly because different mechanisms are involved in the damage process for different materials under different loading conditions. What can be done now is to give a general description of the understanding of the term of damage as used in practice.

In CDM sense, damage of materials is such a property of material deterioration that diminishes the strength, rigidity, toughness, stability and residual life. It mainly consists of the creation and development of the discontinuity in the solid media, such as the cavities in metals. The damage of a material is associated with the internal structural changes during creep deformation process. The distributed defects in materials not only lead to crack initiation and ultimate fracture, but it also gradually induces deterioration and reduction of load-carrying capacity of the material. The acceleration of creep in the tertiary stage and in the final fracture are usually ascribed to the progressive accumulation of damage (e.g., in the form of shapes, densities and distribution of cavities) in the material during creep. In many applications, damage as used in many CDM models is not meant to be identified with a particular form of microstructural change of the material. Geometrically, this corresponds to the reduction of the effective cross sectional area that actually bear the external load.

From the viewpoint of practical application, any load that exceeds the initial

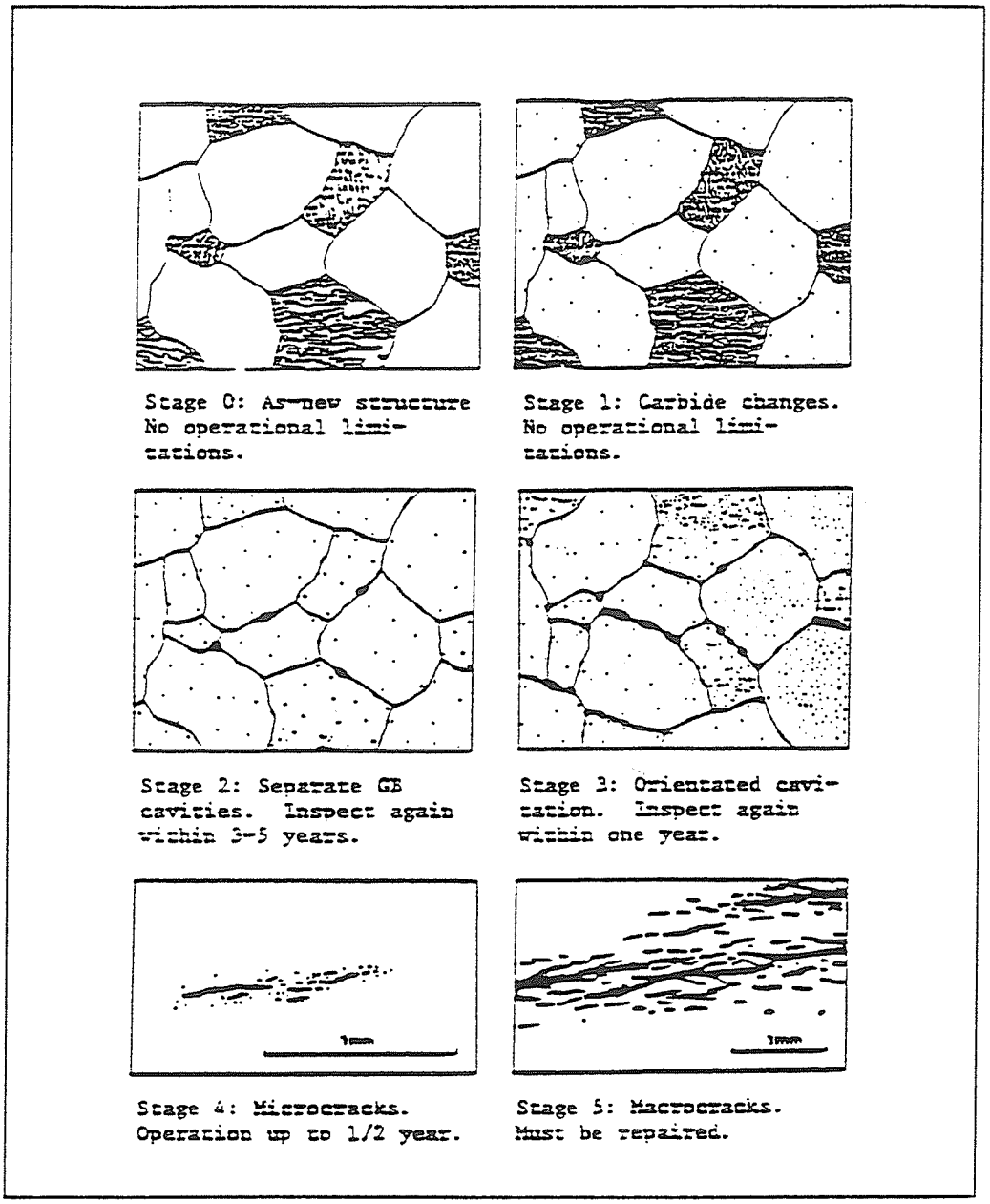

Figure 2.8: Classification of creep damage of steam pipings made of low alloy steels: Stage 0: a new structure; Stage 1: Carbide changes; Stage 2: Separate grain boundary cavities; Stage 3: Oriented cavitation: Stage 4: Formation of microcracks; Stage 5: Formation of macrocracks[15]

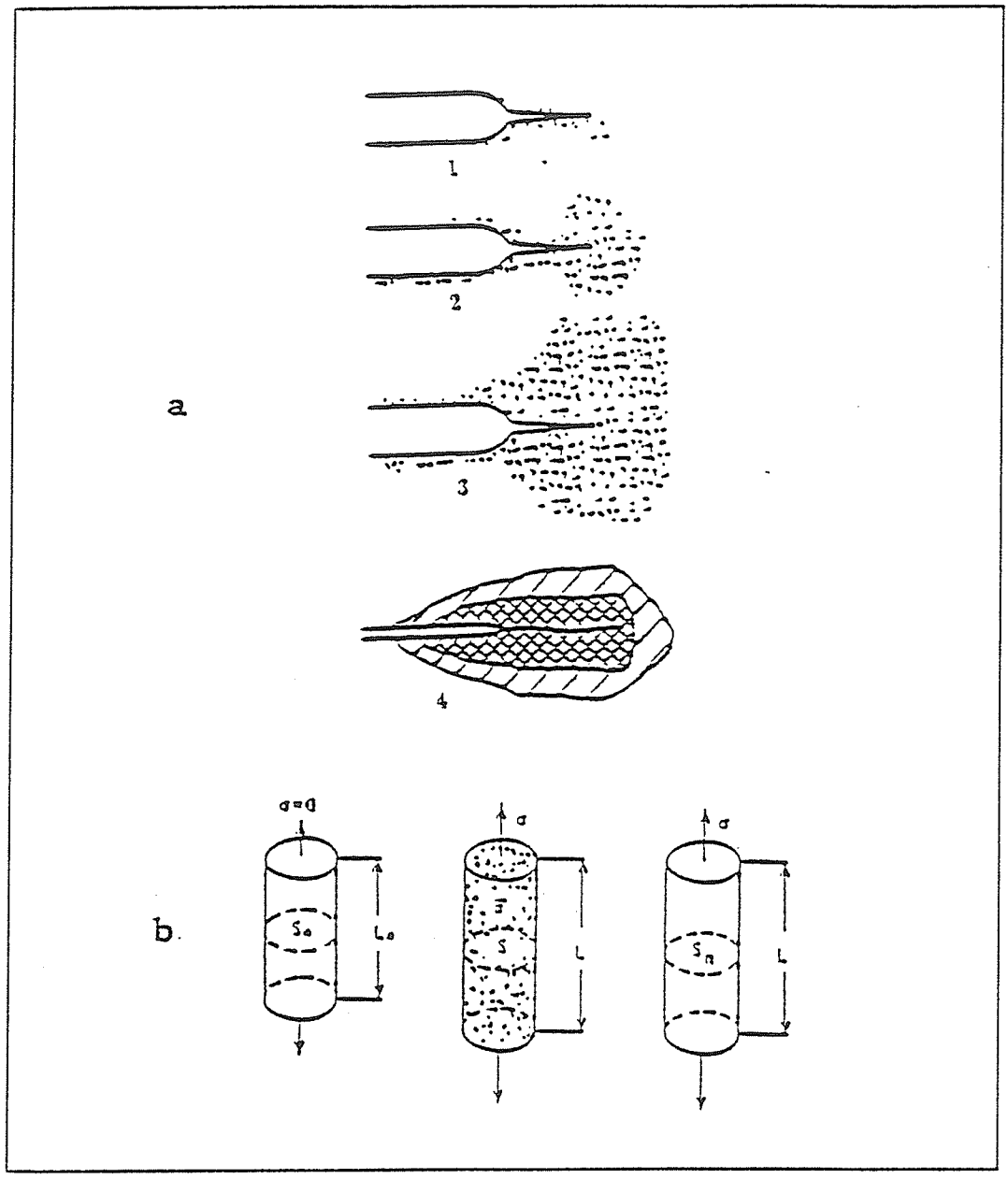

Figure 2.9: Illustration of damage, (a) Schematic representation of damage and cracking process at an notch end[55]; (b) Deformation and damage of bar under tension[248]

yield stress of the material would cause certain permanent deformation and certain damage to the material. The damage parameter is an indication of the degree of such material deterioration. The development of damage is a prelude to failure and hence three regions in the state of a solid body can be distinguished throughout the loading process:

- The virgin state with no damage;
- The evolution of damage and the solid is in a damaged state;
- Failure, which corresponds to fracture of an element of the material into two parts.

The concept of damage initiated a new branch of mechanics, the CDM. The CDM is supported by the general framework of thermodynamics of irreversible process and offers complementary possibilities to the conventional fracture mechanics for describing material's response when it experiences larger permanent deformation under complex thermomechanical loads.

Since creep damage is mainly caused by nucleation and growth of grain boundary voids, it seems that the area fraction of voids on grain boundary provide a natural measurement of damage. Many researchers used this concept to be the definition of damage of materials. But it is not the case for all the loading conditions and all the materials. As stated before, there exist other forms of damage caused by creep deformation. According to the study by Johnson[165], it was found that in the case of aluminum alloys, there is no evidence of voids during creep deformation process, in spite of the fact that the creep curves of this material also have a pronounced tertiary portion which suggests evidence of some forms of damage instead of cavitation. the classification of the creep damage of steam pipings made of low alloy steels[15]. Based on such classification, certain checkup and repair cycle was recommended[15]. Fig. 2.9 is an illustration of the damage within the material. Fig. 2.9(a) shows the damage process in a crack tip area. The dots represent the damaged points of the

material. From state 1 to state 4, the degree of deterioration of the crack tip material increases. Fig. 2.9(b) is a geometrical illustration of the deformation and damage of a bar under tension. In this figure, S_o and L_o denote the initial cross sectional area and initial length of the bar, while S and L denote the current cross sectional area and current length of the bar. σ is the applied stress. $\bar{\sigma}$ is the net stress and S_n is the net cross sectional area.

2.7.1.2 Measurement

Partly for obtaining a commonly acceptable definition of the damage parameter, many researchers proposed different methods for measuring the damage parameter. Some of the methods are related to a particular way for defining the damage of materials before failure[206].

The most widely used approach and the classical way of defining and measuring the damage parameter is due to Kachanov[168-169], who used simple ideas from the one-dimensional tensile test to define a quantity called continuity as

$$\psi(t) = \frac{A_e(t)}{A_o} \tag{2.14}$$

where A_o is the initial cross sectional area of the test specimen, and $A_e(t)$ is the effective undamaged cross sectional area bearing the load at any instant. The damage $D(t)$ is then introduced in terms of the continuity as

$$D(t) = 1 - \psi(t) = \frac{A_o - A_e(t)}{A_o} \tag{2.15}$$

which is defined as running from 0 to 1 as the material undergoes transition from the initial undamaged state ($A_e(t) = A_o$) to the final state of critical damage and rupture ($A_e(t) = 0$). Many methods for measuring the damage parameter are based on this definition.

Lemaitre and co-workers[206] summarized over ten different methods developed for measuring the damage parameter employed by different researchers. These

methods include direct measurement of the damage, such as observation of micrographic pictures, count of the grain boundary voids and measurement of variation of density of the material, etc. Many other methods were related to indirect measurements, such as the measurement of the variation of elasticity modulus, ultrasonic waves propagation, variation of the cyclic plasticity response, variation of the tertiary creep response, variation of the microhardness, variation of the electrical potential, acoustic emission, Hydrogen absorption; X-Ray diffusion and small angle X-ray diffraction, etc.

Due to the fact that different mechanisms are involved in the damage process of different materials with different extents of deformation, it is difficult to ensure one basic definition of damage. As being pointed out by Lemaitre[206]: 'If about ten methods may be applied to measure damage, it means that no one is perfect with excellent results. This is mainly due to the fact that they depend on the definition of damage and on the scale of the phenomenon'. Fig. 2.10 shows the comparison between damage measurements by four different methods[206]. As can be seen, the fundamental trend of measured data by the four different methods are identical. The value of the damage parameter reflects the material's deterioration due to permanent deformation.

Take the measurement of the Young's modulus as an example. The law of elasticity coupled with damage through the thermodynamic potential allows to evaluate the damage by means of its influence on the elasticity modulus. For one dimensional case, for the initial loading, we have:

$$\varepsilon_e = \frac{\sigma}{E} \tag{2.16}$$

where E is the initial Young's modulus corresponding to non-damaged material. For subsequent loadings, we have:

$$\varepsilon_e = \frac{\sigma}{E'} \tag{2.17}$$

where E' is the current Young's modulus corresponding to a damaged material.

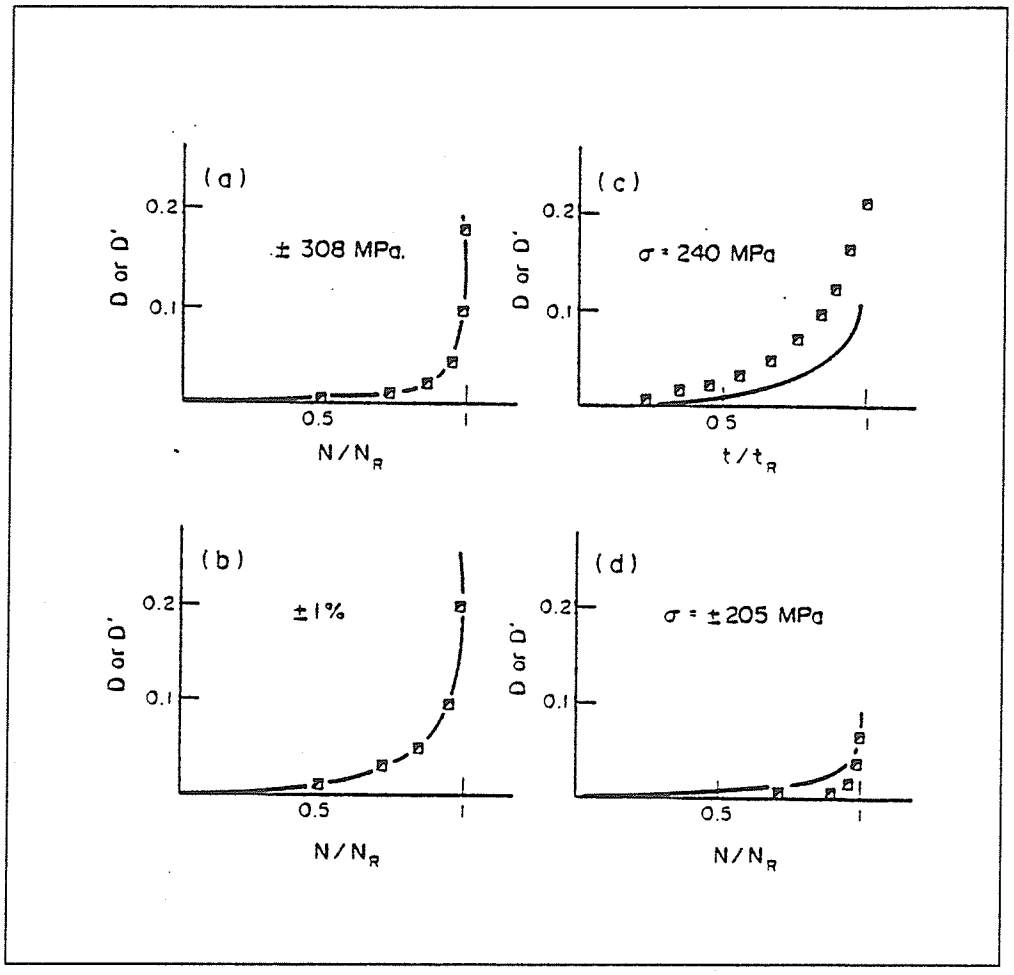

Figure 2.10: Comparison between damage measurements by variation of the electrical potential and by (a) the elasticity modulus change on stress controlled fatigue of 316 stainless steel; (b) the elasticity modulus change on strain controlled fatigue of 316 stainless steel; (c) the tertiary creep method on creep damage of IN 100 superalloy at $1000^{o}C$; (d) the cyclic plasticity response on stress controlled fatigue of IN 100 superalloy at $1000^{o}C$[206]

Damage is then defined as:

$$D = 1 - \frac{E'}{E} \tag{2.18}$$

And the current Young's modulus is expressed as $E' = E(1 - D)$. It is found that the current Young's modulus decreases as the damage increases, which is in agreement with experimental observations. Hence, if the initial Young's modulus is known, and the current Young's modulus is measured in the damaged material, the corresponding damage state of the material is known. Shown in Fig. 2.11 is the results of the measurement of the ductile plastic damage for 99.9 percent purity copper by the measurement of the change of the Young's modulus[206].

This method has been extensively used in many laboratories since it was first developed in 1977. But many argued that the variations of the Young's modulus do not represent the damage of the material because the Young's modulus is an inherent material parameter and does not change under external loadings.

For example, material scientists pointed out that Young's modulus E of a material is dependent particularly upon the radius of atom and the kind of crystal lattice. It can be expressed approximately as:

$$E = \frac{K}{r^m} \tag{2.19}$$

where r be the radius of the atom, K and m are material constants. It is thus obvious that E is an inherent material parameter and only the factors that have influence over the constants of the crystal lattice, can change the Young's modulus of the metal. Precisely because of this, the Young's modulus is the most stable mechanical behavior of metal. Alloying, heat treatment and hot working or cold-working hardly change the value of the Young's modulus E. For this, the following seems a reasonable explanation[62]:

For a specimen (e.g., metal bar) subjected to a tensile load P, assume the apparent area of the cross section be A_a, the effective cross section area be A_e, in a

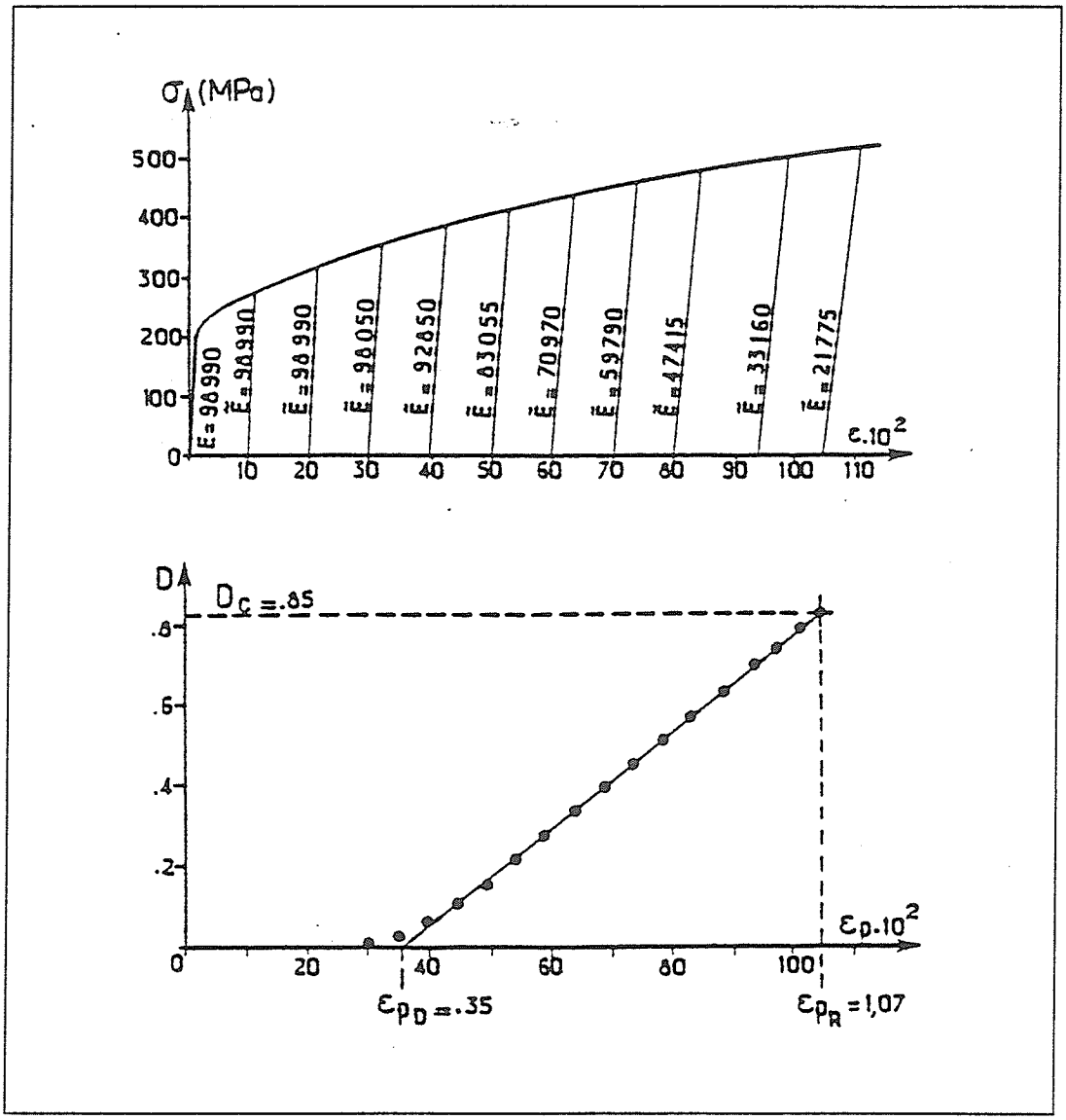

Figure 2.11: The damage measurement by Young's modulus method[206]

damage state when the specimen experiences the damage of D. Then, we have:

$$A_e = A_a(1 - D) \tag{2.20}$$

according to the general definition of the damage parameter. After material becomes deteriorated, reload the specimen with a tensile load of P', which causes the specimen an elastic deformation. We treat it according to material scientists' idea, i.e., the Young's modulus E does not change, i.e.,

$$(P'/A_e) = E\varepsilon \tag{2.21}$$

Substitute Eq. 2.20 into Eq. 2.21, we obtain:

$$P'/[A_a(1 - D)] = E\varepsilon \tag{2.22}$$

that is:

$$(P'/A_a)(1/\varepsilon) = E(1 - D) \tag{2.23}$$

P', A_a and ε in the left side of the above equation all can be measured. We denote purely manmade data measured $(P'/A_a)(1/\varepsilon)$ by the sign E', i.e.:

$$(P'/A_a)(1/\varepsilon) = E' \tag{2.24}$$

We call $(P'/A_a)(1/\varepsilon)$ the Young's modulus of the damaged specimen. Here, one quotes only the term of Young's modulus used in metal physics, but this term does not possess such an implication of the Young's modulus defined in metal physics (imply $E = 1/r^m$). From Eqs. 2.23 and 2.24, we obtain:

$$E(1 - D) = E' \tag{2.25}$$

that is:

$$D = 1 - \frac{E'}{E} \tag{2.26}$$

Another explanation is proposed by Hult[158]. One can consider the damaged material as a composite material in which the second phase is microcavities. According to the rule of mixture for the law of Young's modulus of the composite

material, the Young's modulus of the damaged material is:

$$E' = E\frac{V - V_d}{V} + E_d\frac{V_d}{V} \tag{2.27}$$

where, E is the Young's modulus of the undamaged material, V is the apparent total volume of the specimen, V_d is the volume occupied by microcavities within the specimen and E_d is the Young's modulus of the second phase 'microcavities'. Because $E_d = 0.$, then from Eq. 2.27 we obtain:

$$E' = E\frac{V - V_d}{V} \tag{2.28}$$

and:

$$V = LA_a \tag{2.29}$$

therefore:

$$A_d = A_a - A_e \tag{2.30}$$

Where A_d is the area occupied by microcavities in the cross section, and L equals the length of the specimen. Suppose it is in the strain-controlled test, the length of the specimen does not change. Hence:

$$V_d = LA_d \tag{2.31}$$

and:

$$V - V_d = LA_e \tag{2.32}$$

Once more, we obtain:

$$D = 1 - \frac{E'}{E} \tag{2.33}$$

This is exactly the same expression of damage derived before.

2.7.2 Internal stress

In some CDM models, the internal stress is used as an additional state variable to describe the material's microstructural changes related to the dislocation movement.

2.7.2.1 Definition

In the past two decades, there has been a rather widespread acceptance of the idea that the mechanical deformation of materials at elevated temperature is not driven by the full applied stress but rather a reduced stress[11,113-114,183,258,317]. This reduced stress which could be regarded as the driving stress for the mechanical deformation reflects the resistance of the material to deformation and invariably calculated by subtracting a term from the applied stress[2-3,12,77,219-220]. The subtracted term is called internal stress. Its quantity may depend on temperature, strain, current microstructural composition of the material, the thermomechanical loading history and the imposed stress or strain rates. Thus in the process of creep deformation, the creep strain rate is attributed not just to the applied stress, σ, but to the effective stress:

$$\sigma_e = \sigma - R \tag{2.34}$$

where R denotes the internal stress. Fig. 2.12 schematically represents the concept of internal stress.

The internal stress is related to the dislocation movement, such as dislocation climb and interactions during the deformation process. It accounts for a significant portion of the applied stress. The internal stress R does not need to be a constant threshold stress, but it may vary as a function of the microstructure of the material. Gibeling and Nix[114] have prepared a review on observations and models pertaining to the concept of internal stress. The idea of a variable internal stress is employed in the description of primary creep and in the proposed constitutive model of this thesis research.

In general, the internal stress developed in a dislocation network is very complicated and position dependent. A rigorous analysis would, if necessary, treat this as the complex statistical problem. The phenomenological treatment usually neglects the position dependence. The internal and effective stress are considered in an average sense in this research for simplicity.

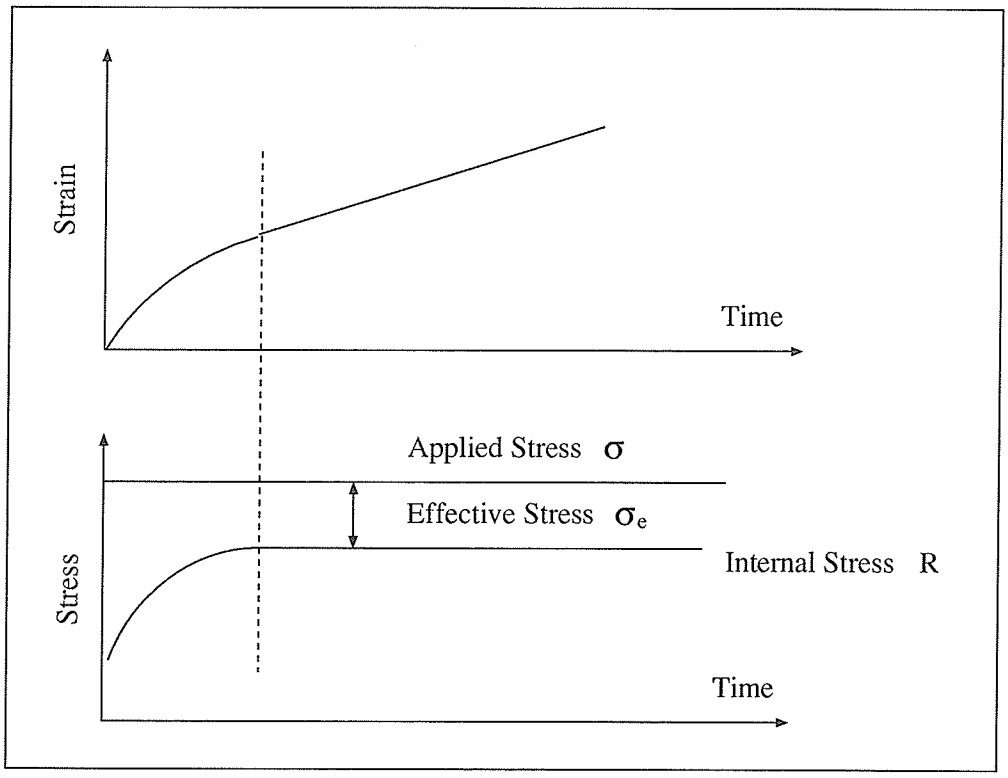

Figure 2.12: Conceptual understanding of internal stress[2-3]

2.7.2.2 Measurement

Experimental methods have been proposed to determine the internal stress in a deforming solid for various materials. The commonly used methods is the so-called dip tests[3,40,80,275].

This method involves a kind of decremental relaxation. The specimen is first creep-tested under constant stress into the steady state, whereupon a small portion of the load is removed. Typically $\Delta\sigma$ is around 5% of the applied stress. After an instantaneous contraction, which appears to be entirely elastic within the limits of resolution, a delay time of zero creep rate is observed, followed eventually by the recommence of forward creep at the lowered stress. As soon as creep deformation is again detectable, a further stress decrease is made. A sequence of delay times is produced by repeating these steps as shown in Fig. 2.13. These delay times have been attributed to the time required for small changes in the dislocation network which must occur before further creep can begin at the reduced stress. Eventually

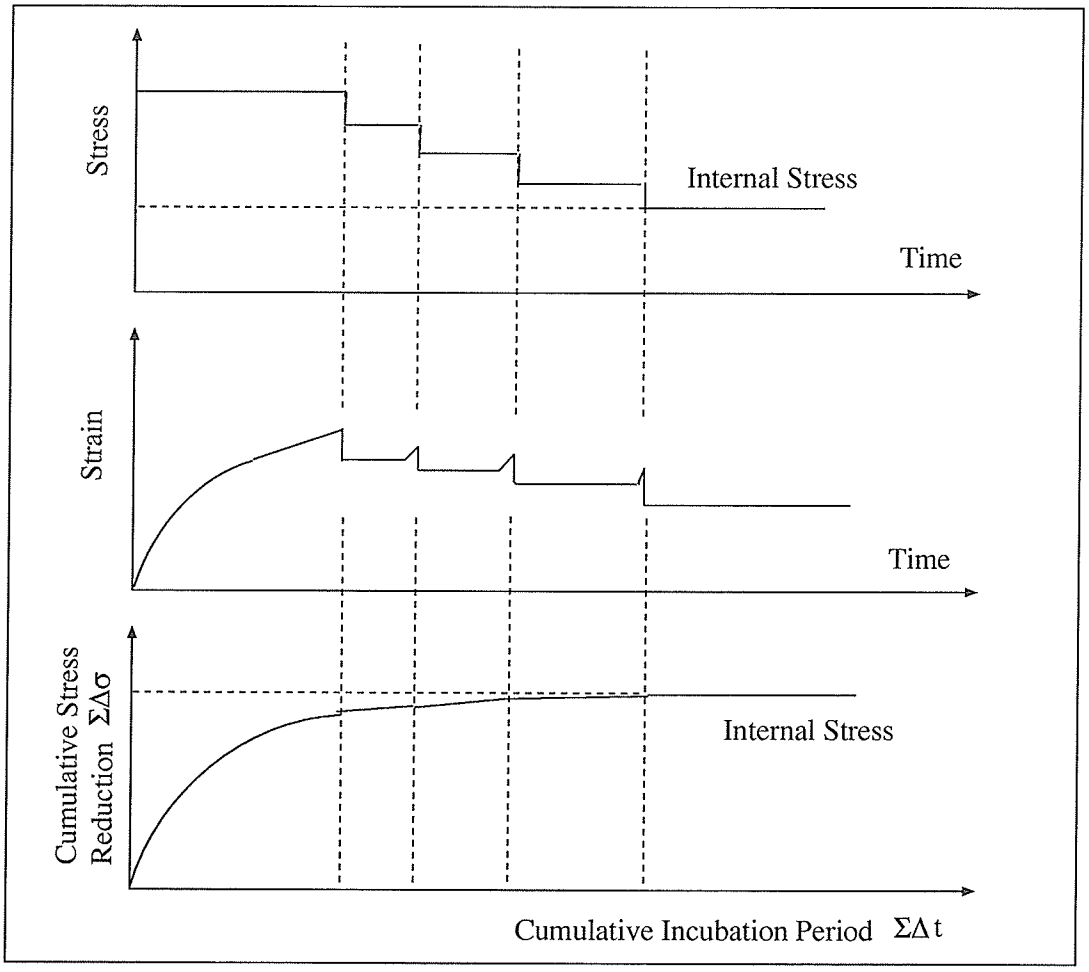

Figure 2.13: Illustrative measurement of the internal stress[2-3]

the incubation periods become very long and it is assumed that any further creep must be associated with the recovery of the internal stress via subgrain growth. It is regarded then the microstructure has reached certain force equilibrium. The effective impetus for further creep deformation is zero.

In order to determine the internal stress, the data is plotted as cumulative incubation period ($\sum \Delta t$) versus cumulative stress reduction ($\sum \Delta \sigma$) on a linear scale as shown in Fig. 2.13. Such a graph appears to indicate an asymptotic value of ($\sum \Delta \sigma$). And the internal stress is the remaining stress when the cumulative incubation period is apparently infinite, that is:

$$R = \sigma - \sum \Delta \sigma \tag{2.35}$$

The internal stress measured by this means is the average value over the whole cross sectional area which is used in this study.

2.8 Major factors influencing cyclic creep

Besides the load, time and temperature which are the external controlling parameters for describing static creep deformation, many other factors have shown great influence upon cyclic creep response. These factors may include the load dwell time effect, load cycling effect, the interaction between creep damage and HTLCF damage and environmental attack.

2.8.1 The load dwell time effect

In the early 1950's, Lubahn tested Cr-Mo-V steel at 1000 °F for a two-step loading case[221]. He observed that after 96 hours of recovery at zero stress, the material became less creep resistant. This phenomenon was termed as cyclic creep acceleration. Cyclic creep retardation is defined in the same fashion, but for the opposite effect[218]. Cyclic creep acceleration has been observed in Aluminum, Copper, Lead,

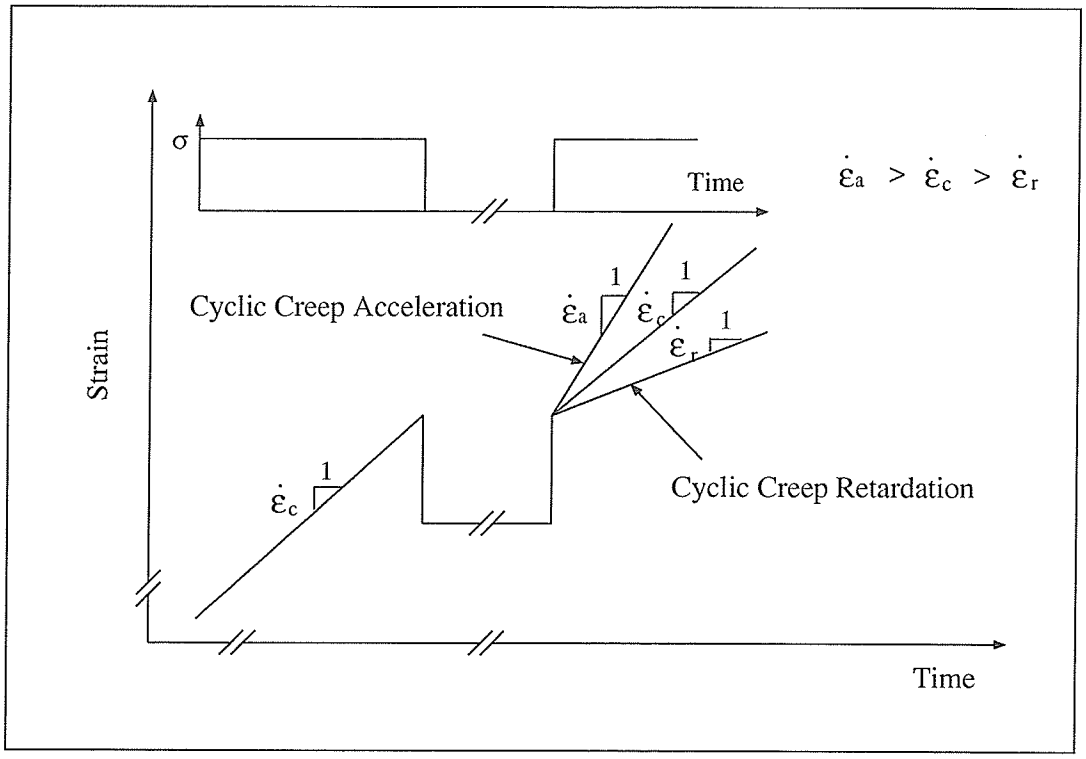

Figure 2.14: The phenomenon of cyclic creep acceleration and cyclic creep retardation[218]

and high temperature alloys. Cyclic creep retardation has been reported for Cadmium, Zinc, Nickel alloys and Copper alloys. Cases of acceleration and retardation of creep for the same material has also been reported. Several investigators regard cyclic creep acceleration and cyclic creep retardation as characteristics of different materials. Other researchers hold the opinions that cyclic creep acceleration and cyclic creep retardation can occur in the same material[218]. They believe that cyclic creep retardation occurs for low stress in cyclic creep, and cyclic creep acceleration happens at high stress. It is further believed that for any testing temperature, there exists a stress threshold for cyclic creep acceleration. This threshold can be determined by experimental tests[119-120].

The mechanisms of cyclic creep acceleration and cyclic creep retardation have yet to be clarified. But it is sure by now that the dwell time effect can be observed only when the dwell time is long enough. And load dwell time has significant effect upon further creep deformation. However, only a few modellings of the load dwell

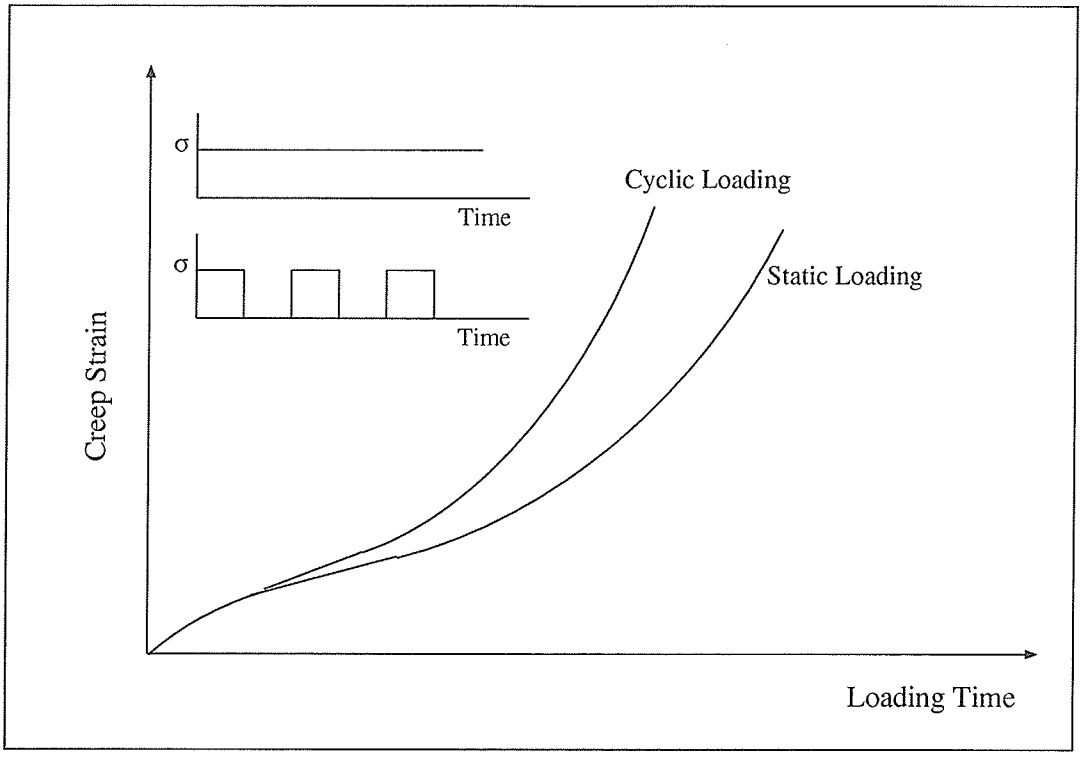

Figure 2.15: Effect of cyclic loading on creep strains[307-308]

time effect are available in literatures. Fig. 2.14 illustrates the phenomenon of cyclic creep acceleration and cyclic creep retardation.

2.8.2 The load cycling effect

Engineering structures are often subjected to variable, rather than merely constant loads. Cyclic loading causes degradation of materials which is called fatigue damage. In the process of creep deformation, if the loads are cyclic, the damage and fracture of the components are attributed to both creep deformation and fatigue damage[18,36,72-73,106,147,302-304,307-308,331,342], and sometimes also to the interaction between them (see next section). Static and cyclic creep tests were carried out to show the effect of prior high-strain fatigue on subsequent creep, and vice versa[1,116-118,172,326]. It is found that the material softens by the cyclic plastic strain and evidence was obtained to suggest that the fatigue damage and the creep damage interacted to give shortened cyclic creep lifes. This is probably

because of the fact that the effects of cyclic softening altered the creep strength of the material so that predictions based on the virgin material were seriously in error. Fig. 2.15 shows schematically the effect of cyclic loading in the creep deformation process, which is the case of cyclic creep acceleration.

There are roughly three basic methods which describe low cycle fatigue. These are the strain method, the damage method and the energy method.

2.8.2.1 Methods based on inelastic strain

The well-known Manson-Coffin relationship (M-C law)[74-75, 230] has been used by numerous researchers to describe low cycle fatigue.

$$\Delta\varepsilon_t = \Delta\varepsilon_e + \Delta\varepsilon_p = C_e N_f^{-b} + C_p N_f^{-c} \tag{2.36}$$

where $\Delta\varepsilon_t, \Delta\varepsilon_e$ and $\Delta\varepsilon_p$ are the total strain increment, elastic strain increment and plastic strain increment in an average loading cycle.

This law forms the basis of a large group of methods in describing low cycle fatigue (LCF). According to the M-C law, the controlling parameter for fatigue is the strain range. In low cycle fatigue cases, the controlling parameter is the plastic strain range. The M-C relationship has sustained continual improvement over the years[37,42,82-84,163,239,279,294,296]. The Degallaix's thermal activation model[82-84] is a typical one in this group.

Degallaix et al[82-84] proposed a model for combined thermal and mechanical cycling fatigue analysis. It was found that for total strain range value of less than or equal to 0.02, the fatigue damage is controlled by two types of mechanisms depending upon the plastic strain range: mechanisms which are thermally activated and mechanisms which are not thermally activated. The contribution from the thermally activated mechanisms increases when the plastic strain range decreases. This model has the following form:

$$\frac{1}{N_f} = A_1 \Delta\varepsilon_p^{B_3} e^{-\frac{Q}{RT}} + A_2 \Delta\varepsilon_p^{B_4} \tag{2.37}$$

Measurements of material constants under cyclic thermal and mechanical loads for the material 316L stainless steel were conducted. This model gave good prediction of the low cycle fatigue life[82-84].

2.8.2.2 Damage models

The damage concept proposed by Kachanov to describe creep fracture was used by many researchers in fatigue life analysis. The damage parameter used here has the same meaning as in creep analysis, i.e., an abstract description of the material deterioration under cyclic loading even though the micromechanisms of deformation and damage could be different type. Followings are two typical models:

- Lemaitre and Chaboche[51,205] proposed a fatigue damage model, which has the following form:

$$dD = D^{\alpha(\sigma_M,\bar{\sigma})}\left[\frac{\sigma_M - \bar{\sigma}}{M(\bar{\sigma})}\right]^{\beta} dN \tag{2.38}$$

  Different choice of α can lead to the rules by other researchers. The function $M(\bar{\sigma})$ is deduced from a linear dependence between $\bar{\sigma}$, the von Mises effective stress and the fatigue limit.

- Ostergren[267-268] proposed a damage model which associates the tensile part of the plastic strain hysteresis energy with the fatigue life. Ostergren assumed that an M-C type relationship exists between the tensile part of hysteresis strain energy and the fatigue life. His model has the following form:

$$\sigma_M \Delta\varepsilon_p N_f^{\beta} \nu^{\beta(k-1)} = C \tag{2.39}$$

2.8.2.3 Energy methods

Some researchers[100,105,107,124,197-199,244] analyzed the fatigue life using an energy method. The fatigue life is related to the plastic strain hysteresis energy per cycle. In this method, the following assumptions are made:

- The plastic strain hysteresis energy is a measure of the fatigue damage;
- The total damaging energy required to cause fatigue fracture is constant which is equal to the area under the static true stress-true strain curve, i.e., the static strain energy up to rupture.

The model has the following form:

$$W_f = \Delta W N_f = \left(\frac{1-n'}{1+n'}\right) \sigma_f' \varepsilon_f' (2N_f)^{1+b+c} \tag{2.40}$$

It should be noted that the division among the different methods and models in describing the low cycle fatigue problems is just for simplicity. There is no physical reasoning behind this. For example, the Degallaix's model can also be classified as a damage model. The damage per load cycle is expressed as:

$$\Delta D = \frac{1}{N_f} = A_1 \Delta \varepsilon_p^{B_3} e^{-\frac{Q}{RT}} + A_2 \Delta \varepsilon_p^{B_4} \tag{2.41}$$

2.8.3 Interaction between creep and fatigue (ICF)

When metallic components are subjected to periodic or varying loading at high temperature ($T > \frac{1}{3}T_m$), creep damage and fatigue damage occur simultaneously in the material. A difficult problem is that these two phenomena interact with each other in a nonlinear manner. This fact is well known to engineers and scientists as the interaction between creep and fatigue[13,30,32,34,60,123,125-130,205,329]. It is one of the main concerns in designing structural components operating at elevated temperature.

Probably because of its tremendous engineering significance, a vast amount of research was conducted on the high-temperature creep-fatigue prediction methods which could be traced back to the late 1940s. An interdisciplinary research effort was witnessed. According to the summary by Halford[128] on the evolution of creep-fatigue life prediction models, nearly one hundred approaches and their variations

have been proposed to date which have been identified as being combinations of fourteen different classifications.

The vast majority of the methods, once proposed, had little or no follow-up. From the standpoint of effort put-forth toward their development, three basic methods stand out:

- The time- and cycle-fraction rule as used in ASME Nuclear Code Case N-47;
- The CDM method, as proposed by Lemaitre and Chaboche[205];
- The strain-range partitioning method (SRP), as proposed by Halford and Manson[231-232].

Each of the three methods has sustained continual refinement. The latter two have received much attention during the last two decades.

2.8.3.1 The time- and cycle-fraction rule

The simplest form of this rule can be expressed as:

$$\sum \frac{n_i}{N_{fi}} + \sum \frac{t_j}{t_{fj}} = D \tag{2.42}$$

That is to say that after n cycles of loading and a total creep time of t, the creep-fatigue damage at certain stress amplitude is calculated by referencing to the expected life under equivalent purely time-independent (fatigue) and purely time-dependent (creep) conditions. This is actually a linear summation of the separate effects of creep and fatigue. There is no term corresponding to their interaction. This rule is still widely used because of its simplicity even though the results obtained from using it are far from being satisfactory. Most often, this rule leads to errors by a factor of 2 to 10 or more[276].

2.8.3.2 The CDM method

Lemaitre and Chaboche[205] proposed a damage summation model for analysis of the ICF. The general form is:

$$dD = \dot{D}_c dt + \frac{\partial D_f}{\partial N} dN \tag{2.43}$$

This is a model of nonlinear summation of the creep damage and fatigue damage. In this model, the interaction between creep damage and the HTLCF damage is reflected because the accumulated damage is used in the calculation of the creep response and the low cycle fatigue behavior. Both fatigue damage and creep damage contribute to the current total accumulated damage which in turn affects the calculation of both the creep damage and the fatigue damage. The two damage mechanisms become mutually reinforcing, until the accumulated total damage reaches a critical value. The application of the damage theory gives a much better prediction of operation lifes of engineering structures, i.e., within a factor of 2, as shown by Lemaitre and Chaboche[205].

One of the advantages of the CDM approach in creep and fatigue analysis is to allow a natural way to predict creep-fatigue interaction[205,250-251,274]. Most of the cumulative damage theories are based on a hypothesis that damage variables (creep damage and fatigue damage) are of similar nature and that their interactions are additive. The model may be used by assuming that creep damage increment dD_C and fatigue increment dD_F are functions of the summation of the two damages such that:

$$dD_C = f_c(\sigma, R, D_C + D_F) \tag{2.44}$$

$$dD_F = f_F(\sigma, R, D_F + D_C) \tag{2.45}$$

And the total damage increment introduced by in one load cycle is calculated by the addition of the two damage incremental components:

$$dD = dD_C + dD_F = f_C(\sigma, R, D) + f_F(\sigma, R, D) \tag{2.46}$$

As shown in several applications, the nonlinearities of interaction processes can be effectively described, in spite of the different nonlinearities of functions describing creep damage and fatigue damage. Under this hypothesis, only one damage variable has to be considered for the general case, i.e., the total accumulated damage increment in one load cycle. This makes the evaluation of the deterioration of the material under complex loading conditions an easy task.

It should be noted that the additive hypothesis does not correspond to the direct addition of physical damages of different natures. For instance, the microcracks and cavities are not additive. Only their mechanical effects are added. The mechanical effects are obtained by the investigations of the relationship between the physical damage (microcracks or cavities) and the corresponding macroscopic damage parameters.

2.8.3.3 The strain-range partition method

The strain range partition method as proposed by Manson and Halford[128-130,231-232] is widely used for predicting the operation life of components under the working conditions of creep-fatigue interaction.

This method divides the imposed strain into four basic ranges involving time-dependent and time-independent components. The expected lifetime of a component is obtained by weighting each of the basic lifes which are related to a fraction of the inelastic strain range, i.e., one of the basic ranges of the imposed strain. There exists an M-C type relation between one of the basic ranges of the imposed strain and the corresponding basic life. The constants in these relations could be obtained by specially designed tests. Hence, this model uses linear summation for life prediction in situations in which creep and fatigue are occurring simultaneously. In this model, the creep-fatigue damage is related to the strain amplitudes.

The model has the following expressions:

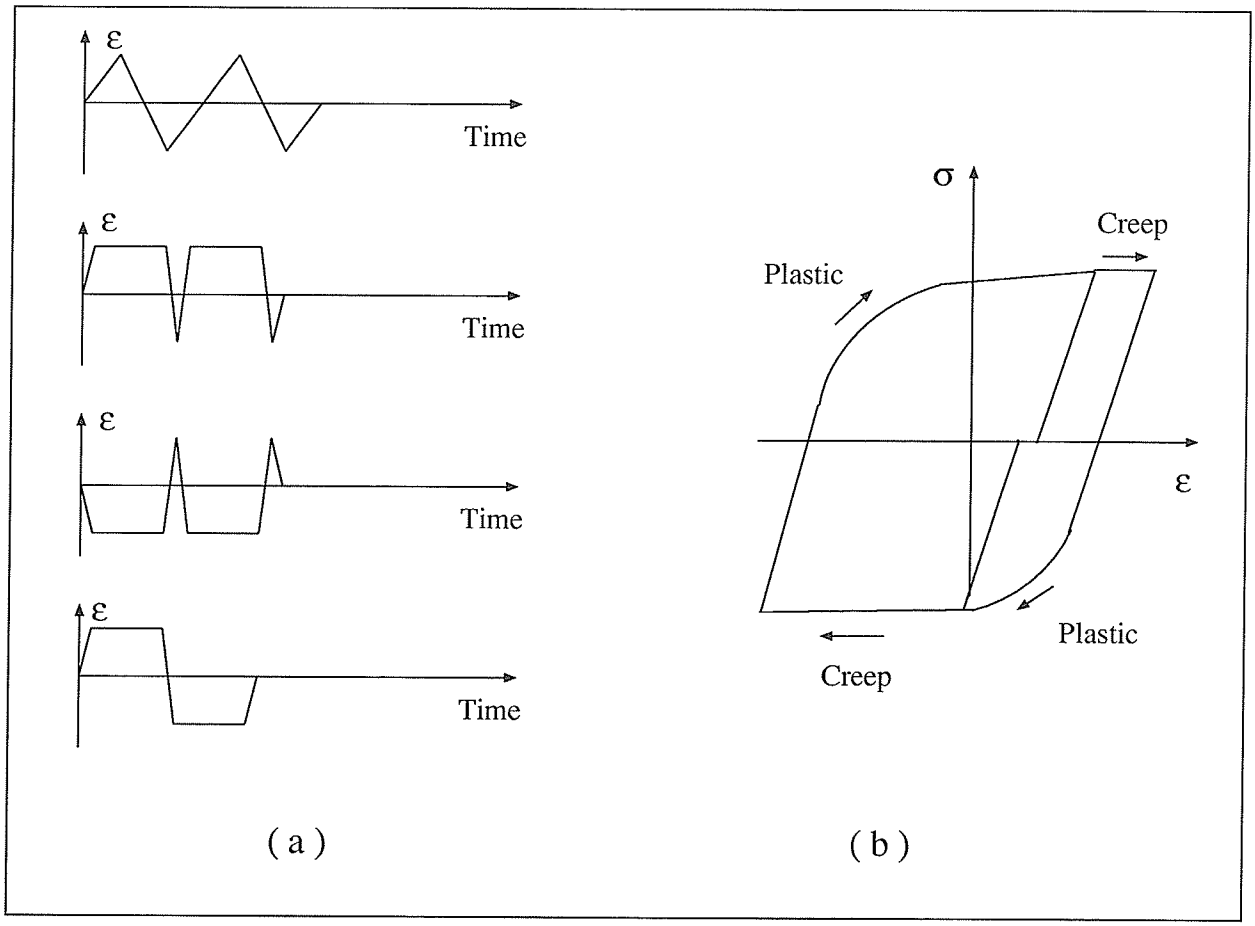

Figure 2.16: The schematic illustration of the stain-range partition method, (a) Typical loading pattern of the strain-controlled low cycle fatigue, (b) Evaluation of strain components from a given hysteresis loop for SRP analysis[231]

$$\frac{1}{N_f} = \frac{F_{pp}}{N_{pp}} + \frac{F_{pc}}{N_{pc}} + \frac{F_{cp}}{N_{cp}} + \frac{F_{cc}}{N_{cc}} \tag{2.47}$$

$$\Delta\varepsilon_{pp} = C_1 N_{pp}^{n_1} \tag{2.48}$$

$$\Delta\varepsilon_{pc} = C_2 N_{pc}^{n_2} \tag{2.49}$$

$$\Delta\varepsilon_{cp} = C_3 N_{cp}^{n_3} \tag{2.50}$$

$$\Delta\varepsilon_{cc} = C_4 N_{cc}^{n_4} \tag{2.51}$$

where the subscripts p and c mean plastic component creep component respectively. Fig. 2.16 is a schematic illustration of the SRP method.

The strain-range partitioning method gives better accuracy than most of other models do. But they are difficult to apply for a three-dimensional state of stress and when the stress or strain are not periodic or when the loading pattern is not regular, e.g., a loading pattern with various load holding time and load dwell times. Also, certain basic experimental tests have to be conducted to determine the material constants involved in this model.

The SRP method has sustained continual improvement over the years[130,140,236]. For example, He et al[140] improved the SRP method by replacing the inelastic s-train range with the tensile part of the strain energy as used in the Ostergren model in the SRP formulations. This improved model is referred to as the strain energy partition (SEP) method in literatures.

2.8.4 The environmental effect

At high temperature, the influence of time is often increased by the superposition of corrosive process[89,112,166,242,254,281-282,302-304,346].

2.8.4.1 Damage mechanisms due to corrosion

The environmental damage contributes to the cyclic creep fracture of materials at high temperature, as does by the HTLCF damage. One environmental effect,

corrosion may complicate both fatigue and creep damage mechanisms. It contributes to both damage nucleation (in the form of surface cracks, preferential grain boundary oxidation, or internal voids) and damage growth (crack tip material deterioration and void growth from particles). A number of corrosive damage mechanisms have been identified. These include[254,302-304,346]:

- Enhanced crack nucleation and crack growth by brittle cracking of the oxide skin;
- Grain boundary oxidation which results in or promotes intergranular cracking;
- Preferential oxidation of second-phase particles.

The interaction of oxidation and fatigue can result in shorter lifetime of the structure as compared to the cases where either of them acts alone. The corrosive damage at or below the surface, such as internal oxidation, sometimes occurs selectively along grain boundaries, and subsequent crack formation constitutes another possible cause for accelerating creep rate in the tertiary stage of creep deformation. Crack initiation by corrosion alone has been observed. Also, some materials fail by the growth of oxidized surface cracks. At a stressed crack tip, however, the layer ruptures continuously and oxygen atoms can penetrate into the material, especially along the grain boundaries. It is not yet known precisely as how oxygen accelerates creep crack growth. Possibly, it reacts with constituents of the alloy to form brittle oxides which fracture more readily. Oxygen may also attack carbides at the carbide/matrix interface which leads to decohesion of the carbides. Further, the oxide spikes formed along grain boundaries usually have a greater volume than the metal had before oxidation and therefore they exert an opening force on the crack faces. Finally, the grain boundaries can be embrittled by segregation of oxygen. It should be mentioned that an atmosphere environment does not always accelerate creep crack growth compared to vacuum. It was found that ferritic and austenitic steels and even some of the cast superalloys appear to be relatively insensitive to

the air. The diverse behavior of superalloys might result from their microstructure, which varies from material to material and has a pronounced effect on creep crack growth rates[302-304].

2.8.4.2 Mechanical behavior of surface oxide

At elevated temperatures, an oxide layer may form on the surface of the specimen. This layer experiences a mechanical strain which can result from anyone or a combination of the following mechanisms:

- Mismatch in thermal expansion coefficients of the oxide and substrate;
- Geometry effects (convexity of surface, etc.);
- Relative creep behavior between the oxide and substrate;
- Viscous sliding of the oxide segments over the metal substrate;
- The strain due to diffusion of oxygen into the substrate preferentially at grain boundaries depending on the crystal orientation and grain size.

Grain boundary oxides may generate stresses (and strains) in their vicinity and in neighboring grains. These mechanisms could affect the morphology of the surface oxide as well as the growing oxide-induced crack.

2.8.4.3 The corrosive damage mechanisms of cyclic loading

It has been noted that under cyclic loading in the creep deformation process, just as during static creep deformation process, crack growth rates are often much larger in atmosphere containing oxygen or sulfur than in vacuum or in an inert gas environment. According to Riedel[291], in steels and Ni-base alloys, the enhancement factor for the growth rate is typically 10 times higher in the sensitive temperature range. But smaller and larger factors have been observed as well. This variability is not

surprising considering the multitude of possible mechanisms and their interactions with other mechanisms of cyclic creep fracture.

In general, an oxygen-containing atmosphere is detrimental for the high temperature cyclic creep lifetime. Following are several causes:

- Surface cracks in initially smooth specimen are easily nucleated in the presence of oxygen.
- In the absence of oxygen, cyclic creep crack growth may be impeded by full or partial rewelding of the crack surfaces during unloading. A layer of oxygen, which quickly adheres to the freshly exposed metal surface, or a layer of oxide can prevent such rewelding. Consequently, oxidation enhances transgranular crack growth by crack tip blunting mechanism.
- Since no stable protective oxide layer can be formed at the continually deforming crack tip, oxygen can penetrate into the material. Usually, this occurs along grain boundaries and hence could enhance intergranular crack growth.

2.8.4.4 Study of damage due to corrosion

In spite of these understanding about the environmental effects on cyclic creep fracture process, very few tests in inert atmospheres have been conducted under cyclic creep fracture conditions, hence no comparisons of air and nonoxidizing environment results have been reported[291,302-304]. The problem of oxidation in creep crack growth has received a limited amount of systematic study although significant results of the effect of oxidation on crack growth at elevated temperature have been carried out under fatigue conditions. These results, however, are basically of qualitative nature. Little work has been done to model the corrosive effects on creep crack growth rates quantitatively. Before a more detailed understanding of the corrosive processes at crack tips emerges, this will remain an area dominated by metallurgical empiricism.

Chapter 3

Development of a Constitutive Model for Creep Deformation and Damage

As has been pointed out in the Introduction of this thesis, a well-accepted theoretical framework for high temperature creep fracture has been elusive even though significant understanding of creep deformation, creep damage and creep fracture mechanisms have been achieved and various modellings of the phenomena had been made in the last three decades[291]. Phenomenological methods and models have been used by many researchers in treating creep fracture problems. They provided a powerful engineering approach that has permitted the economical life assessment of countless structural components over the years.

This chapter contains the proposal of a constitutive model for creep deformation and damage of metallic materials at high temperature. This model is based on the CDM concept. Two state variables are introduced to describe the microstructural variation of materials in the creep deformation and damage process. The influencing factors on creep response, such as load cycling effect, load dwell time effect and interaction between creep damage and HTLCF damage could be reflected by the model.

3.1 Requirements for phenomenological models

In the absence of detailed knowledge of the internal structure of a material and its evolution in time, the representation of its mechanical behavior under cyclic creep deformation condition involves a series of choices made in light of experimental evidence of phenomenological and microscopic kind. For example, one must decide on the number and type of variables used. In proposing a phenomenological constitutive model, certain principles have to be adhered to, even though it appears to be somehow arbitrary[6-7,11,36,86,134,146,162,179,213,297,306]. Examples of this process of choice could be found in the works of Onat and Leckie[263-264], Lemaitre[200-204], Hayhurst[135-140] and Murakami[248-249], etc. Following are common opinion on the essential requirements for a phenomenological model:

- The constitutive model has to be verifiable experimentally;
- The model should be suitable for use in structural analysis, e.g., the model should contain only limited number of state variables and simple in form and in implementation;
- Major factors influencing cyclic creep fracture behavior should be reflected;
- The main trend of the phenomenon as observed in experimental tests should be shown;
- The general physical principles, such as thermodynamic laws and the axioms of continuum mechanics have to be satisfied;

These are also the principle of guidance in proposing the CDM-based constitutive model in this thesis research.

3.2 Representation of the 3-D stress level

As stated above, the controlling parameters for creep fracture are temperature, stress, material microstructural state and time, etc. While temperature and time

can be determined easily, the material microstructural state can be described approximately by the evolutions of state variables, such as the damage parameter and the internal stress. The controlling stress parameter, however, is not so easy to determine[90]. This is because when metallic materials are subjected to creep in an engineering service, a multiaxial stress state is usually imposed. For example, as being pointed out by Leckie[191-193], even for a uniaxial specimen, the introduction of a notch creates multiaxial state of stress. Geometrical and physical irregularities unavoidably involve stress concentrations at these points.

Various stress functions had been identified to have different effects on the creep deformation and creep damage behavior of a material under certain conditions. Experiments have shown that an error of 10:1[193] is quite possible If a wrong stress component or stress function is used in forecasting fracture life. This explains why the influence of stress system had been widely studied with the objective of evolving predictive rules usable in design.

3.2.1 Johnson's findings

One of the early contributions to the multiaxial stress creep of metals was made by Johnson[165]. The essential result is that, as far as the lifetime t_f in creep under steady load is concerned, metals and alloys fall into three categories. For those in the first category, such as commercially pure copper, t_f depends only on the maximum principal stress σ_1. For those in the second category, such as the aluminium alloy, t_f depends only on the von Mises effective stress $\bar{\sigma}$. There is also an intermediate category of metals and alloys whose behavior lies between these limits where the relative importance of the maximum principal stress σ_1 and the von Mises effective stress $\bar{\sigma}$ depends on the material and the loading conditions.

3.2.2 The relevant influence of stress functions

It is of interest to consider the physical bases of the various multiaxial stress functions in describing creep deformation and creep damage.

It is well known that the growth of intergranular cavities is driven by the tensile stresses acting on the grain boundaries[191,258]. Since intergranular fracture usually occurs first on those grain boundaries perpendicular to the maximum principal stress, it is reasonable to assume that this component of the stress plays a central role in creep rupture[291]. Cavity growth at high temperatures can be driven also by the hydrostatic tension component of the multiaxial stress state, in the same way as it is in ductile rupture. Thus, the first stress invariant, $J_1 = 3\sigma_H$ should, in principle, appear in the generalized creep rupture expression. The nucleation of cavities is also required for creep rupture. This process requires very high stress concentrations that are produced only by inhomogeneous plastic and creep deformation such as grain boundary sliding and slip band formation. Because these deformation processes are driven by shear stresses, it follows that some form of shear stress should also enter the equation for creep rupture. Also, diffusive cavity growth on a grain boundary facet is often constrained by creep of the surrounding matrix. Even though the constrained diffusive growth process is driven by the normal stress acting on the grain boundaries, the overall rate of the process is governed by the creep rate of the surroundings and this includes the effect of shear stresses. This too, suggests that a shear stress should be included in the creep rupture equation.

So, in general, the octahedral shear stress is related to the effects of shear; the hydrostatic stress greatly affects the growth of the cavities; and the maximum principal stress opens the microcracks and causes them to grow. Based on these findings, different models to represent the comprehensive stress level of a material under creep deformation conditions have been proposed. Following are three typical such models:

3.2.3 Leckie-Hayhurst's model

Leckie and Hayhurst[192-193] showed that for a smooth round bar subjected to uniaxial tension, the rupture lifetime at a given temperature can be expressed as:

$$t_f = M\sigma^{-\chi} \tag{3.1}$$

where σ is the uniaxial stress and M and χ are parameters that characterize the evolution of damage at the temperature in question. They argued that the creep rupture life of a specimen subjected to multiaxial stress is controlled by the linear combinations of different multiaxial stress functions, such as the maximum principal stress, the first stress invariant and the second stress invariant. Their idea is expressed by the following equation.

$$t_f = M(\alpha\sigma_1 + \beta J_1 + \gamma J_2)^{-\chi} \tag{3.2}$$

where t_f is the rupture time, σ_1 is the maximum principal stress, i.e., $\sigma_1 > \sigma_2 > \sigma_3$. J_1 is the first stress invariant defined by:

$$J_1 = \sigma_1 + \sigma_2 + \sigma_3 = 3\sigma_H \tag{3.3}$$

where σ_H is the hydrostatic stress and J_2 is the second stress invariant defined by:

$$J_2 = \frac{1}{\sqrt{2}}[(\sigma_1 - \sigma_2)^2 + (\sigma_2 - \sigma_3)^2 + (\sigma_3 - \sigma_1)^2]^{\frac{1}{2}} = \bar{\sigma} \tag{3.4}$$

where $\bar{\sigma}$ is the von Mises effective stress.

The first stress invariant is related to the hydrostatic stress through $J_1 = 3\sigma_H$ and the second invariant is the von Mises equivalent stress or the effective stress, $J_2 = \bar{\sigma}$. The coefficients, α, β, and γ, dependent upon the material and temperature, describe the relative contributions of the different multiaxial stress components to the rupture life. The material constants M and χ again characterize the evolution of damage. Their values are assumed to be independent of stress state. In order to make Eq. 3.2 consistent with Eq. 3.1 for the case of uniaxial tension, the coefficients

α, β and γ must be chosen such that $\alpha + \beta + \gamma = 1$. Then for the case of uniaxial tension (i.e., $J_1 = \sigma_1, J_2 = \sigma_1$), Eq. 3.2 reduces to Eq. 3.1 ($\sigma_1 = \sigma$).

Leckie and Hayhurst have reviewed the multiaxial creep rupture data for several metals (e.g., the Johnson's findings) and found that the maximum principal stress, σ_1, and the effective stress $\bar{\sigma}$ are much more important than the hydrostatic stress σ_H in determining creep rupture lifes of these materials. Thus they let $\beta = 0$ in Eq. 3.2 as an approximation and rewrote the equation as:

$$t_f = M[\alpha\sigma_1 + (1 - \alpha)\bar{\sigma}]^{-\chi} \tag{3.5}$$

when α is a single parameter that describes the relative importance of σ_1 and $\bar{\sigma}$ in determining the creep rupture. It is evident that the parameter α cannot be determined from uniaxial creep rupture tests alone. Multiaxial tests in which σ_1 and $\bar{\sigma}$ can be changed independently are needed to determine α.

3.2.4 Nix's model

Nix et al[259] proposed the principal facet stress as a parameter for predicting creep rupture of metallic materials under multiaxial stresses. Their model was based on micromechanical considerations and observations.

Because grain boundary sliding and the associated stress redistribution are expected to occur under creep conditions, it is reasonable to assume that the stress directly influencing the cavitation which leads failure is not the applied stress, but the concentrated normal stress acting on the transverse or nearly transverse grain boundaries. This is the principal facet stress according to Nix et al and was used as a parameter for describing creep rupture of materials under multiaxial stress conditions. Analytical results reported by Anderson and Rice[9] have been used by Nix et al[259] to show that, prior to cavitation, the average tensile stress on grain boundary facets perpendicular to the maximum principal stress can be approximately expressed by:

$$\sigma_F = 2.24\sigma_1 - 0.62(\sigma_2 + \sigma_3) \tag{3.6}$$

where $\sigma_1 > \sigma_2 > \sigma_3$ are the principal stresses.

This model is also an empirical one. It was proposed based on microstructural observations. According to the results using this model, for four different materials, the principal facet stress predicts the multiaxial creep rupture better than other models do. This correlation was proved to be quite useful because it allows a prediction of the rupture time of materials under multiaxial stresses from uniaxial creep rupture data. Of course, this prediction requires a knowledge of the multiaxial stress state imposed. It was found that there is also cases for which this parameter does not accurately predict multiaxial creep rupture, such as the cases of Aluminium alloy and commercially pure copper.

3.2.5 Lemaitre's model

Both the Leckie and Hayhurst's model and the Nix's model correlated the creep fracture data in triaxial loading conditions well. But they are basically empirical models. Lemaitre[200-204], based on a thermodynamic analysis, proposed another model related to 'damage equivalent stress' for characterizing the three-dimensional stress level. The damage equivalent stress has the following expression:

$$\tilde{\sigma} = \bar{\sigma}[\frac{2}{3}(1+\nu) + 3(1-2\nu)(\frac{\sigma_H}{\bar{\sigma}})^2]^{\frac{1}{2}} \tag{3.7}$$

By analogy to the von Mises effective stress for plasticity, the damage equivalent stress can act as a criterion for damage just as $\bar{\sigma}$ acts as a criterion for plasticity.

It is interesting to note that $\tilde{\sigma}$ is equal to the von Mises effective stress multiplied by a factor function of the triaxiality ratio, $\sigma_H/\bar{\sigma}$, which is very important for damage evolution as shown by many experimental and theoretical studies. According to Lemaitre[200-204], the damage equivalent stress could be used to write any three-dimensional damage constitutive equation (isotropic) in the same way as for the one-

dimensional case. Lemaitre's continuum damage mechanics model with the damage equivalent stress characterizing the three-dimensional stress level has yielded a lot of contributions. This model characterizing the three dimensional stress level was adopted in the proposed CDM-based constitutive model in this thesis research.

3.3 Proposal of a constitutive model of creep deformation and damage

In this thesis study, a new CDM-based constitutive model was proposed for describing the cyclic creep fracture behavior of selected engineering materials, such as the 316L stainless steel. Microstructural changes within the material in the creep deformation process are reflected through the evolution of the internal state variables. Internal state variables describe the material state on which the macroscopic response of the material depends. Therefore, the material microscopic variations could be reflected in the description of macroscopic response.

3.3.1 Background

As stated in Chapter 2 and in Appendix A, ever since the 1950's, an interdisciplinary research effort has been witnessed in the study of cyclic creep deformation, damage and fracture, and much progress has since been made. Many CDM-based models were proposed to describe the cyclic creep fracture behavior of materials. However, for some reasons, none of the models or theories can be used to make structural analyses under creep deformation conditions based on a real loading trace. For example, virtually no model or analysis reflected the load dwell time effect. Long load dwell time has shown significant effect upon the material's creep response upon reloading[218,221]. Such cyclic creep acceleration and cyclic creep retardation have been reported in the published literatures. Omission of such effect unavoidably would lead to erroneous results in the prediction of deformation response and the fracture behavior of structural components under cyclic creep deformation condi-

tions. Creep deformation as an irreversible permanent deformation shows a strong dependence upon loading paths[43]. With different loading paths or different loading histories, the creep response of materials would be different even when the same amount of creep deformation is accumulated within the material. Also, the various influencing factors for cyclic creep fracture were neglected by most of the models and analyses. Besides the load dwell time effect, the salient influencing factors on cyclic creep fracture are the load cycling effect, the interaction between creep damage and the HTLCF damage and the environmental attack.

3.3.2 The new CDM-based constitutive model

A new CDM-based constitutive model for describing the cyclic creep deformation and damage was proposed in this thesis study. The creep deformation and damage analyses could be conducted based on the real loading pattern of components with a load cycle including the loading, load holding, unloading and load resting time. The major influencing factors on the cyclic creep fracture behavior of components and materials, such as the load dwell time effect, load cycling effect and the interaction between creep damage and HTLCF damage could be reflected in the model.

The new model was based on the works of Gong and Hsu[119-120], Degallaix et al[82-84], Lemaitre[200-207], Chaboche[48-531], Plumtree[274], etc. The model has the following mathematical formulations:

$$\dot{\varepsilon}^c_{ij} = A\left(\frac{\tilde{\sigma}-\bar{R}}{1-c_oD}\right)^n \frac{S_{ij}}{\bar{\sigma}} \tag{3.8}$$

$$\dot{R}_{ij} = B_1(R_s-\bar{R})^p\dot{\varepsilon}^c_{ij} \tag{3.9}$$

$$\dot{D}_c = C_1\frac{\tilde{\sigma}}{1-D} + C_2\left(\frac{\tilde{\sigma}-\bar{R}}{1-D}\right)^{r_o n}\left(\frac{\tilde{\sigma}}{1-D}\right)^{r_o} \tag{3.10}$$

$$R_s = R^o_s[1+\beta(\frac{\tilde{\sigma}-\sigma_n}{\tilde{\sigma}})\Delta t_d]^\alpha \tag{3.11}$$

$$\dot{R}^u_{ij} = B_2(R^r_{ij}-R^u_{ij})^k \tag{3.12}$$

$$\tilde{\sigma} = \bar{\sigma}[\frac{2}{3}(1+\nu)+3(1-2\nu)(\frac{\sigma_H}{\bar{\sigma}})^2]^{\frac{1}{2}} \tag{3.13}$$

$$\Delta D_f = A_1(\Delta\varepsilon_p)^{B_3}e^{-\frac{Q}{RT}}+A_2(\Delta\varepsilon_p)^{B_4} \tag{3.14}$$

$$\Delta D = \dot{D}_c dt+\frac{\partial D_f}{\partial N}dN \tag{3.15}$$

In these equations, $\dot{\varepsilon}_{ij}^c$ is the tensor of creep strain rate. $\tilde{\sigma}$ is the damage equivalent stress. $\bar{R}$ is the effective internal stress. S_{ij} is the tensor of deviatoric stress. $\bar{\sigma}$ is the von Mises effective stress. D is the damage parameter. R_{ij} is the internal stress tensor. R_{ij}^u is the internal stress developed in the unloading process. R_{ij}^r is the internal stress developed before the unloading process. ν is the Poisson's ratio. σ_H is the hydrostatic stress. ΔD_f is the fatigue damage increment. $\Delta\varepsilon_p$ is the plastic strain range in one load cycle. Q is the activation energy. R is the Boltzmann constant. T is the absolute temperature. ΔD is the damage increment in one load cycle. $\dot{D}_c$ is the creep damage rate. $\frac{\partial D_f}{\partial N}$ is the fatigue damage rate. And $A, c_o, n, B_1, p, C_1, C_2, r_o, \beta, \alpha, B_2, k, A_1, A_2, B_3, B_4$ are material constants.

In this model, the first six equations (Eqs. 3.8–3.13) are used to describe creep deformation response. These include the evolution of damage parameter and the development of internal stress in the creep deformation process. They are basically extension of Gong and Hsu's model in the multiaxial stress state. Certain modifications were made in the extension. The sixth equation shows the characterization of the 3-D stress level in CDM analysis. The seventh equation (Eq. 3.14) is the extension of the Degallaix's thermal activation model in CDM's form describing the HTLCF damage in the cyclic creep deformation process. The eighth equation (Eq. 3.15) represents the nonlinear summation of the damage produced by the HTLCF and the creep deformation respectively.

Descriptions of state variables used and these equations are presented in the subsequent sections.

3.3.3 The two internal state variables used

As being pointed out in Chapter 2 and in Appendix A, in the creep deformation process, the microstructure of the material changes. By abstractation and generalization, these changes could be described by the evolution of a set of internal state variables.

In the proposed model, two state variables, the damage parameter and the internal stress, were introduced to represent the damage due to various microstructural changes of the creeping material. The damage parameter, which was chosen to be a scalar here, was used to represent the degree of material deterioration due to the various kinds of microstructural changes. The damage of the metallic materials at high temperature could be (but not necessarily) related to the nucleation and growth of the grain boundary cavities. But it is not meant to be a physically directly identifiable quantity. It is an abstract description of material's degradation which includes the formation and growth of creep damage as a field quantity. The other state variable, the internal stress, was used to describe the microstructural changes related to the dislocation movement in the creep deformation process. The incorporation of the two internal state variables in this CDM-based constitutive model is based on the observations of the physical processes underlying the creep curve. Creep damage and fracture analyses based on models with two state variables have been tried by other researchers[176,341]. It was found that models with two state variables contained much more information and hence provided deeper insight into the process of creep deformation and creep damage.

The primary and secondary stages of the creep curve are determined by the combined action of strain hardening and thermally activated recovery of the dislocation structure[2-3,11-12,77,285]. In the primary stage, strain hardening by the formation of dislocation tangles or a dislocation substructure predominates, whilst the secondary stage is characterized by a balance between strain hardening and recovery. Changes in microstructures during creep play an important rule in the final

failure of a material. In metallic materials, the usage of the internal stress, R, is to provide information about the distribution of dislocations and their evolutions. The difference between the current stress state and the internal stress are the controlling parameter of the creep strain rate, especially during the early stages of the creep deformation.

The tertiary stage of creep deformation is characterized by the rapid nucleation, growth and coalescence of the grain boundary voids. The damage parameter is used here as an indication of the degree of deterioration of the material properties because of such happenings. Internal damage has a more local character. It may be confined to grain boundaries in the form of voids, to the vicinity of precipitates as zones of decohesion or local cracking, to intense pileups of dislocations that act as nuclei to explosive void growth during the final stages of tertiary creep. The damage parameter is used here to describe these events.

During the creep deformation process, the evolution of the internal stress and the damage parameter may not take place simultaneously. Usually, the internal stress may grow first. The combined results of the applied stress and the internal stress then initiates the microstructural changes described by the damage parameter. The damage parameter and the internal stress constitute the building blocks for the representation of the internal structure and the texture (or the damage state) of materials in the creep deformation process.

3.3.4 The creep flow rule

The first equation is the creep flow rule. This is actually the extension of the well-known Norton's law for steady creep. But the creep strain described by this equation is not restricted only to the steady creep. The whole creep deformation process could be reflected. This is achieved through the evolutions of the two internal state variables. The primary creep stage may be described as the period during which the internal stress increases from zero to a peak value, R_s, reached at the beginning of the secondary stage of the creep deformation. The creep strain rate

decreases as the internal stress increases which is the characteristic of the primary creep stage. The damage is assumed to be very small during the primary stage and at the beginning of the steady creep stage. The fast increase of creep rate typifying the tertiary stage of creep deformation is mainly caused by the accumulated damage. This description is consistent with experimental observations. Hence, even though the form of the creep flow rule appears to be suitable only for steady state creep development, it can actually describe the whole process of creep deformation.

To account for the incompressibility of creep flow, this model assumes that the creep strain rate component is proportional to the corresponding deviatoric stress component, and depends otherwise only on the current effective creep deformation driving stress: $\frac{\tilde{\sigma}-\bar{R}}{1-c_o D}$. This is in agreement with the behavior of real materials, because the trace of the creep strain rate is zero, i.e., $\dot{\varepsilon}^c_{ii} \propto S_{ii} = 0$. by the definition of the deviatoric stress. The term $\frac{\tilde{\sigma}-\bar{R}}{1-c_o D}$ is a comprehensive effective stress, taking into account the weakness of the material due to the presence of voids or microcracks and the presence of other forms of microstructural changes, such as the movements of dislocations. The normal stress as calculated based on the material properties with no creep deformation and damage is no longer the only controlling parameter. The material has developed certain degree of resistance for further creep deformation, as indicated by the internal stress. Also, the material becomes damaged, whose degree is measured by the damage parameter. With the microstructural changes and damage developed within the material, the stress redistributes within the material, especially in the crack tip area. As compared to the virgin material, the material with certain degree of damage has a lower capacity of load-bearing. This is because that while the load on the cavitated lattice is kept constant, the effective cross sectional area for carrying the load is reduced because of the damage. From the viewpoint of thermodynamics, the damage parameter, D, and the internal stress, R, are two internal variables of an irreversible micro-rupture process.

According to Eq. 3.8, the creep strain rate increase sharply if the damage pa-

rameter approaches unity. When the damage parameter is small, its effect on creep deformation evolution is negligible.

In this model, developments are restricted to isotropic damage. Any loading should result in same amount of damaging effect in all directions. In other words, all the effective stress components are modified by the same value $\frac{1}{1-c_o D}$ to define the effective creep deformation driving stress, $\frac{\tilde{\sigma}-\bar{R}}{1-c_o D}$.

3.3.5 The creep hardening rule

Eqs. 3.9, 3.11 and 3.12 constitute the law for the evolution of the internal stress. The internal stress, as being pointed out by material scientists, is dependent upon the inelastic deformation and the viscous recovery process. The proposal of the evolution law of the internal stress, i.e., Eq. 3.9 was just based on such observations[247]. In this equation, R_s is the maximum value of the internal stress reached during the steady state of creep deformation under the applied stress, σ; B_1 and p are material constants dependent upon temperature. During the primary creep deformation process, the internal stress, R_{ij}, increases from its initial value and gradually approaches the maximum value R_s. If the material is loaded for the first time, the initial value of the internal stress is zero. Once a maximum value is reached, it remains unchanged unless the applied load is altered. The maximum value of the internal stress, R_s is kept in the material memory as a new creep process commences. It indicates the material's resistance to further creep deformation with current microstructural state.

Eq. 3.12 describes the evolution of the internal stress R_{ij} during the unloading process. It was based on the same microstructural observations as the loading process. In this equation, $\dot{R}^u_{ij}$ is the internal stress recovery rate; R^r_{ij} is the internal stress developed during the active creep deformation process; b_2 and k are material constants dependent upon temperature. Once the magnitude of R^u_{ij} reaches a value equivalent to the fraction of the recoverable internal stress developed during active

creep, R_{ij}^u ceases increasing. At this moment, the residual internal stress has a value of $(R_{ij}^r - R_{ij}^u)$, where R_{ij}^r is the internal stress develped in the creep deformation process before unloading.

The evolution of the internal stress also specifies the hardening or softening behavior of materials due to load dwell effect. When a material is reloaded after a period of load dwell time, Δt_d, the evolution rule of the internal stress, i.e., Eq. 3.9 is valid for the subsequent active creep process, but the maximum internal stress is modified by the rule expressed by Eq. 3.11. The active loading process after reloading, creates a dislocation structure which is slightly modified by the motions of the mobile dislocations during the unloading events. This modifications affects the internal stress upon reloading and its subsequent evolution. Eq. 3.11 just accounts for such modifications. In Eq. 3.11, $R_s = R_s^o f(\Delta t_d)$ is the maximum internal stress reached in the steady creep state after reloading. The function $f(\Delta t_d)$ accounts for the hardening or softening behavior of materials due to the load dwell time. In fact, for the first loading process, $f(\Delta t_d) = 1$. R_s is only dependent upon the applied stress level. After a load dwell time, there is an additional variation of the maximum internal stress, as expressed by $f(\Delta t_d)$. The change of the maximum internal stress depends on the length of the dwell time exponentially within a limit. In other words, the duration of the dwell time is regarded as a hardening or softening measure. In this equation, $R_s^{(o)}$ is the peak value of the internal stress reached in the previous load cycle; σ_n is the threshold stress for cyclic softening; β and α are material constants. If $\beta < 0$, material softening occurs; if $\beta > 0$, material hardening takes place.

It should be noted that the damage parameter D is not present in the rules of the evolution of the internal stress in the unloading and the load dwell periods, as expressed by Eqs. 3.11 and 3.12, respectively. This is because it was assumed that the damage process in terms of the void nucleation and void growth would not influence the motion of the mobile dislocations. However, the inverse influences are

reflected as stated in the next section.

The absence of a stress term in the right hand side of Eq. 3.9 merits attention and comment. This absence implies that a sudden change in the stress level will leave the internal stress unchanged. In other words, the microstructural changes described by the internal stress need time to develop. This, however, would not be the case, for instance, if the sudden closure or extension of cracks plays an important role in the mechanical behavior. Nevertheless, we shall be interested only in materials for which this equation holds.

3.3.6 The damage evolution law

Eq. 3.10 specifies the kinetic law for the evolution of damage in the creep deformation process. Physically, the damage parameter represents the degree or state of degradation of a material. In this model, the damage parameter itself is not meant to be measurable, only its effect on the stress-strain rate relation is detectable. From the viewpoint of energy, the process of the degradation of a material was accompanied by energy dissipation. In other words, the variation of energy dissipation reflects the creep damage process. The damage law, i.e., Eq. 3.10, was derived based on these observations[119-120].

The first term on the right hand side of Eq. 3.10 represents the brittle damage due to diffusion controlled cavity growth and grain boundary cavities occurred in materials crept at low temperature and low stress. The second term on the right hand side of Eq. 3.10 represents ductile damage induced by the accumulation of mobile dislocations and cavitations induced by plastic sliding, etc.[247,321-322].

The introduction of the internal stress in the damage rule is to accommodate the damage of a material generated by mechanisms other than void nucleation and growth on grain boundaries, such as the accumulations of the mobile dislocation density during cyclic loadings.

3.3.7 The damage law for the HTLCF

Eq. 3.14 specifies the development of the high temperature low cycle fatigue in the load cycling process. This is an extension of Degallaix's model which is expressed in a CDM form. In this way, the damage caused by the HTLCF process is calculated cycle by cycle, rather than calculated in a statistical way, e.g., calculated at half life time. Hence the results are expected to take account of the instantaneous response like work hardening and strain softening, etc., and hence is expected to be more accurate and more reasonable.

3.3.8 The evolution law for the interaction between creep damage and HTLCF damage

The damage produced by HTLCF and by creep deformation is added in a mutually reinforcing manner as shown in the eighth equation. With the hypothesis that creep damage and fatigue damage are of similar nature and interact additively, it was postulated in accordance with Lemaitre and Chaboche's methodology[205] that the damage increment in one load cycle under cyclic creep condition be of the form as shown in Eq. 3.15. The hypothesis is made that the creep damage parameter related with the proportion of intercrystalline microcracks and the fatigue damage parameter related with the proportion of transcrystalline microcracks can be added together to give the total creep-fatigue damage, each of them being related to the total damage of both inter- plus transcrystalline microcracks in order to represent the effect of creep-fatigue damage coupling. The first term in Eq. 3.15 accounts for the damage rendered from creep deformation (the creep damage) and the second term gives the damage accumulation due to the load cycling effects (the fatigue damage). It is observed that a complete coupling exists between creep damage and fatigue damage.

3.3.9 Other features of the model

The model also expresses a two way coupling between material damage and creep strain. In the creep law, the term of damage is included to show the reduction of the material's capacity of load-bearing. But it is noted that the damage term in this model in the creep rate equation is not completely the same as in Kachanov's sense. A weighted coefficients c_o which is less than unity is used to discount the effect of damage on the development of the creep strain rate. This is based on the observation of better correlation of the test results by using such a constant[248].

The influence of creep strain on damage evolution is expressed through the evolution of the internal stress whose rate of growth is a function of the creep strain. The consequence is that the creep strain rate $\dot{\varepsilon}$ depends on $\frac{1}{1-c_o D}$, with the result that creep strain ε^c and the damage parameter D become autocatalytic.

According to this model, at the initial state, the damage is zero while the damage rate is high. The damage rate becomes infinite theoretically at failure which occurs in this law when the damage parameter equals unity. The creep strain rate will be high but remain finite according to this model when the material fails.

3.4 Thermodynamic constraints

3.4.1 General statement

As stated before, the phenomenological theories of creep have allowed engineers to predict successfully the mechanical behavior of a variety of structures working under creep conditions. However, such theories are often criticized for lacking rigorous physical and mathematical foundations. Furthermore, such theories rely on a variety of more-or-less *ad hoc* constitutive laws related to the history of loading. They are seldom derived from or verified by broader principles.

As being pointed out by J. Kestin[170-171], the shortcomings of the phenomenological theories can be eliminated by embedding the description of creep deformation

and creep damage in the wider discipline of thermodynamics with due attention paid to the results provided by crystallography and material science. A more widespread use of conventional thermodynamics in the study of problems of solid mechanics will lead to simplicity of presentation and agreement with experimental results. A well-known fact is that creep is an irreversible deformation process. A solid experiencing creep deformation should be considered as a thermodynamic system. The purpose of the study of thermodynamics of continuum solids is to determine the constraints on the real irreversible processes, such as creep deformation.

The subject of conventional thermodynamics and the subject of solid mechanics have developed largely independently to each other. The marriage between thermodynamics and continuum mechanics was neither simple nor straightforward. However, much progress has been made in this research field in the past three decades[23,71,104,170-171,175-179,200-204,263-264,286,335-336].

There are basically two approaches in the study of the thermodynamics of solids. They are the one which takes the Helmholtz free energy as the basic thermodynamic system and the one which takes the Gibbs free energy as basic thermodynamics system. The Helmholtz free energy takes the strains as independent variables while the Gibbs free energy takes the stresses as independent variables. In this thesis research, the derivations of the thermodynamic foundations of the proposed CDM-based constitutive model was based on the Gibbs free energy and the procedures of Cozarelli et al[46,146,194] were followed.

3.4.2 The first and second laws of thermodynamics

The fundamental principles of the thermodynamics is the first and second laws[228]. To derive the expression of the two laws as used in the solid mechanics, consider a continuum solid subjected to work input W and heat input Q on its surface and throughout its volume. This energy input is converted into change of the internal kinetic and potential energy U, associated not only with the velocity v_i, strain ε_{ij}

and temperature T fields, but also with the damage field D due to the creation of new internal surface area at voids and the other microstructural changes described by the internal stress R as stated above.

The global form of the first law of thermodynamics is expresses as:

$$\dot{W} + \dot{Q} = \dot{U} \tag{3.16}$$

where a dot indicates time rate of change. Introducing the Gibbs free energy:

$$G = (\sigma_{ij}\varepsilon_{ij}/\rho) - u + Ts \tag{3.17}$$

where ρ is the mass density of the material and thus assumed constant, u is the specific internal potential energy and s is the entropy per unit mass. Thus, based on the global form, the local form of the first law of thermodynamics is obtained as:

$$-\varepsilon_{ij}\frac{\partial \sigma_{ij}}{\partial t} - \frac{\partial q_i}{\partial x_i} + \rho r = \rho(-\frac{\partial G}{\partial t} + s\frac{\partial T}{\partial t} + T\frac{\partial s}{\partial t}) \tag{3.18}$$

where $\partial q_i/\partial x_i$ is the divergence of the rate of heat efflux vector q_i, r is the strength of a distributed rate of heat source. The second law of thermodynamics is expressed as the usual Duhem-Clausius inequality:

$$\rho T\frac{\partial s}{\partial t} - \rho r + \frac{\partial q_i}{\partial x_i} - \frac{q_i}{T}\frac{\partial T}{\partial x_i} \geq 0. \tag{3.19}$$

Combining the first and second laws of thermodynamics, we get:

$$-\varepsilon_{ij}\frac{\partial \sigma_{ij}}{\partial t} + \rho\frac{\partial G}{\partial t} - \rho s\frac{\partial T}{\partial t} - \frac{q_i}{T}\frac{\partial T}{\partial x_i} \geq 0. \tag{3.20}$$

For brevity, we consider only the situation of isothermal, uniaxial and static loading case. According to the isothermal assumption, the second law of thermodynamics could be expressed as:

$$-\varepsilon_{ij}\frac{\partial \sigma_{ij}}{\partial t} + \rho\frac{\partial G}{\partial t} \geq 0. \tag{3.21}$$

By the uniaxial assumption, the inequality is further simplified to:

$$-\varepsilon\frac{\partial\sigma}{\partial t}+\rho\frac{\partial G}{\partial t}\geq 0. \tag{3.22}$$

In this thesis research, the derivation of the thermodynamic constraints on the model was based on the above inequality, i.e., the condition of isothermal, uniaxial and static loading.

3.4.3 Derivations of the constitutive equations in general form based on the thermodynamic laws

According to the proposed model, at any moment in the loading history, the response of the material could be described by the current condition of the stress, the internal stress and the damage state of the material. Hence, in this analysis, the stress, σ, the internal stress, R, and the damage parameter D are considered as the basic thermodynamic variables.

We postulate the Gibbs free energy functional in the following general expression:

$$G=\sum_{k}[f_k(\sigma,R,D)+g_k(\sigma,R,D)\{\sigma,R,D\}_k] \tag{3.23}$$

where f_k and g_k are scalar and tensor functions respectively involving σ, R and D, and the notion $\{\sigma,R,D\}_k$ represents products of powers of time integrals which are functions of σ, R and D.

By postulating G in this general form, one may obtain via thermodynamics the constitutive equations in a general form.

Differentiating Eq. 3.23, we obtain:

$$\begin{aligned}\frac{\partial G}{\partial t} &= \sum_{k}([\frac{\partial f_k}{\partial\sigma}\dot{\sigma}+\frac{\partial f_k}{\partial R}\dot{R}+\frac{\partial f_k}{\partial D}\dot{D}] \\ &+ [\frac{\partial g_k}{\partial\sigma}\dot{\sigma}+\frac{\partial g_k}{\partial R}\dot{R}+\frac{\partial g_k}{\partial D}\dot{D}]\{\sigma,R,D\}_k\end{aligned} \tag{3.24}$$

$$+ \quad g_k \dot{\overline{\{\sigma, R, D\}_k}})$$

Substitute Eq. 3.24 into the second law of thermodynamics, i.e. Eq. 3.22, we could obtain:

$$\begin{aligned} -\varepsilon\dot{\sigma} \quad &+ \quad \rho(\sum_k (\frac{\partial f_k}{\partial \sigma} + \frac{\partial g_k}{\partial \sigma}\{\sigma, R, D\}_k)\dot{\sigma} \\ &+ \quad \sum_k (\frac{\partial f_k}{\partial R} + \frac{\partial g_k}{\partial R}\{\sigma, R, D\}_k)\dot{R} \\ &+ \quad \sum_k (\frac{\partial f_k}{\partial D} + \frac{\partial g_k}{\partial D}\{\sigma, R, D\}_k)\dot{D}) \\ &+ \quad \rho g_k \dot{\overline{\{\sigma, R, D\}_k}} \geq 0. \end{aligned} \tag{3.25}$$

That is:

$$\begin{aligned} [-\varepsilon \quad &+ \quad \rho \sum_k (\frac{\partial f_k}{\partial \sigma} + \frac{\partial g_k}{\partial \sigma}\{\sigma, R, D\}_k)]\dot{\sigma} \\ &+ \quad \rho \sum_k (\frac{\partial f_k}{\partial R} + \frac{\partial g_k}{\partial R}\{\sigma, R, D\}_k)\dot{R} \\ &+ \quad \rho \sum_k (\frac{\partial f_k}{\partial D} + \frac{\partial g_k}{\partial D}\{\sigma, R, D\}_k)\dot{D} \\ &+ \quad \rho \sum_k g_k \dot{\overline{\{\sigma, R, D\}_k}} \geq 0. \end{aligned} \tag{3.26}$$

This inequality is satisfied with any increment of the basic thermodynamic variables, σ, R and D. Hence, we could set the coefficients of these basic thermodynamic variables equal to zero, and thereby obtain the general constitutive relations:

$$\varepsilon = \rho \sum_k (\frac{\partial f_k}{\partial \sigma} + \frac{\partial g_k}{\partial \sigma}\{\sigma, R, D\}_k) \tag{3.27}$$

$$0 = \sum_k (\frac{\partial f_k}{\partial R} + \frac{\partial g_k}{\partial R}\{\sigma, R, D\}_k) \tag{3.28}$$

$$0 = \sum_k (\frac{\partial f_k}{\partial D} + \frac{\partial g_k}{\partial D}\{\sigma, R, D\}_k) \tag{3.29}$$

This is the general form of the constitutive equation with the stress, the internal stress and the damage parameter as the basic thermodynamic variables. The internal state variables, such as the damage parameter and the internal stress, are incorporated in the description of the mechanical response of materials on the bases of conventional continuum mechanics. Eq. 3.27 is the equation for the evolution of creep strain. Eqs. 3.28 and 3.29 in general yield implicit relations of the evolution and development of the internal stress, R, and the damage parameter, D. It then follows that for the inequality to be satisfied, it is necessary that:

$$\rho \sum_k g_k \dot{\overline{\{\sigma, R, D\}_k}} \geq 0. \tag{3.30}$$

Define the rate of energy dissipation as:

$$\Lambda = \rho \sum_k g_k \dot{\overline{\{\sigma, R, D\}_k}} \tag{3.31}$$

Then the inequality becomes:

$$\Lambda \geq 0. \tag{3.32}$$

3.4.4 Thermodynamic foundation of the proposed CDM-based model

For the particular case of this thesis research, the Gibbs free energy functional expressions were chosen as:

$$f_1 = \frac{1}{\rho}(\frac{\sigma^2}{2E} + \varepsilon^{(P+T)}\sigma) \tag{3.33}$$

$$g_1 = \sigma \tag{3.34}$$

$$\{\sigma, R, D\}_1 = \frac{1}{\rho}\int_0^t A(\frac{\sigma - R}{1 - c_o D})^n dt \tag{3.35}$$

$$f_2 = -\frac{R^2}{2} \tag{3.36}$$

$$g_2 = R \tag{3.37}$$

$$\{\sigma, R, D\}_2 = \int_0^t B_1(R_s - R)^p \dot{\varepsilon^c} \tag{3.38}$$

$$f_3 = -\frac{D^2}{2} \tag{3.39}$$

$$g_3 = D \tag{3.40}$$

$$\{\sigma, R, D\}_3 = \int_o^t [c_1 \frac{\sigma}{1-D} + c_2 (\frac{\sigma - R}{1-D})^{r_o n} (\frac{\sigma}{1-D})^{r_o}] dt \tag{3.41}$$

Hence, we have:

$$\frac{\partial f_1}{\partial \sigma} = \frac{1}{\rho}(\frac{\sigma}{E} + \varepsilon^{(P+T)}) \tag{3.42}$$

$$\frac{\partial f_1}{\partial R} = 0. \tag{3.43}$$

$$\frac{\partial f_1}{\partial D} = 0. \tag{3.44}$$

$$\frac{\partial g_1}{\partial \sigma} = 1. \tag{3.45}$$

$$\frac{\partial g_1}{\partial R} = 0. \tag{3.46}$$

$$\frac{\partial g_1}{\partial D} = 0. \tag{3.47}$$

$$\overline{\dot{\{\sigma, R, D\}}}_1 = \frac{1}{\rho} A (\frac{\sigma - R}{1 - c_o D})^n \tag{3.48}$$

$$\frac{\partial f_2}{\partial \sigma} = 0. \tag{3.49}$$

$$\frac{\partial f_2}{\partial R} = -R \tag{3.50}$$

$$\frac{\partial f_2}{\partial D} = 0. \tag{3.51}$$

$$\frac{\partial g_2}{\partial \sigma} = 0. \tag{3.52}$$

$$\frac{\partial g_2}{\partial R} = 1. \tag{3.53}$$

$$\frac{\partial g_2}{\partial D} = 0. \tag{3.54}$$

$$\overline{\{\sigma, \dot{R}, D\}}_2 = B_1(R_s - R)^p \dot{\varepsilon^c} \tag{3.55}$$

$$\frac{\partial f_3}{\partial \sigma} = 0. \tag{3.56}$$

$$\frac{\partial f_3}{\partial R} = 0. \tag{3.57}$$

$$\frac{\partial f_3}{\partial D} = -D \tag{3.58}$$

$$\frac{\partial g_3}{\partial \sigma} = 0. \tag{3.59}$$

$$\frac{\partial g_3}{\partial R} = 0. \tag{3.60}$$

$$\frac{\partial g_3}{\partial D} = 1. \tag{3.61}$$

$$\overline{\{\sigma, \dot{R}, D\}}_3 = C_1 \frac{\sigma}{1-D} + C_2 (\frac{\sigma - R}{1-D})^{r_o n} (\frac{\sigma}{1-D})^{r_o} \tag{3.62}$$

Substitute these derivatives into the derived constitutive equations expressed in the general form, the proposed model could be derived.

According to Eq. 3.27, we have:

$$\varepsilon = \frac{\sigma}{E} + \varepsilon^{(P+T)} + \int_0^t A(\frac{\sigma - R}{1 - c_o D})^n dt \tag{3.63}$$

put in the rate form, we obtain:

$$\dot{\varepsilon} = \frac{\dot{\sigma}}{E} + \dot{\varepsilon}^{(P+T)} + A(\frac{\sigma - R}{1 - c_o D})^n \tag{3.64}$$

where $A(\frac{\sigma-R}{1-c_o D})^n$ is the creep strain rate component of the total strain rate. According to Eq. 3.28, we have:

$$-R + \int_o^t B_1(R_s - R)^p \dot{\varepsilon^c} dt = 0. \tag{3.65}$$

Expressed in the rate form, we obtain:

$$\dot{R} = B_1(R_s - R)^p \dot{\varepsilon^c} \tag{3.66}$$

This is the equation of the evolution of the internal stress. According to Eq. 3.29, we obtain:

$$-D + \int_0^t [C_1 \frac{\sigma}{1-D} + C_2(\frac{\sigma - R}{1-D})^{r_o n}(\frac{\sigma}{1-D})^{r_o}]dt = 0. \tag{3.67}$$

Expressed in the rate form, we obtain:

$$\dot{D} = C_1 \frac{\sigma}{1-D} + C_2(\frac{\sigma - R}{1-D})^{r_o n}(\frac{\sigma}{1-D})^{r_o} \tag{3.68}$$

This is the equation of the development of the creep damage. The energy dissipation equation, i.e., Eq. 3.32, is then expressed as:

$$\begin{aligned} \Lambda &= g_1 \overline{\{\sigma, R, D\}}_1 + g_2 \overline{\{\sigma, R, D\}}_2 + g_3 \overline{\{\sigma, R, D\}}_3 \\ &= \sigma \dot{\varepsilon^c} + R\dot{R} + D\dot{D} \end{aligned} \tag{3.69}$$

The first term of this equation is due to the creep strain, the second term is due to the internal stress and the third term is due to the damage. Since all material constants are assumed to be positive, and all the terms in this equation are non-negative. Accordingly, $\Lambda \geq 0$. Thus the present formulation is consistent with the second law of the thermodynamics.

Chapter 4

Finite Element Analysis of Cyclic Creep Fracture with the Proposed CDM-based Model

The proposed model has been incorporated to an existed finite element code, TEPSAC (stands for Thermal-Elastic-Plastic Stress Analysis with Creep)[149-155]. A series of case studies have been conducted using the proposed model by the finite element analysis. In this chapter, the details of the finite element analyses and the numerical implementations are described. This includes the following features:

- The finite element algorithm when creep is included for structural analysis;
- The adoption of the proposed model into finite element code;
- The finite element algorithm for time invariant thermal-elastic-plastic stress analysis;
- The simulation of crack extension.

4.1 Basic finite element equations

In finite element analysis of the thermal-elastic-plastic response with creep, the following assumption is made:

$$\{\Delta\varepsilon\} = \{\Delta\varepsilon^e\} + \{\Delta\varepsilon^p\} + \{\Delta\varepsilon^T\} + \{\Delta\varepsilon^c\} \tag{4.1}$$

where $\{\Delta\varepsilon\}, \{\Delta\varepsilon^e\}, \{\Delta\varepsilon^p\}, \{\Delta\varepsilon^T\}$ and $\{\Delta\varepsilon^c\}$ are the respective total, elastic, plastic, thermal and creep strain increments. The creep strain increment and the plastic strain increment are treated separately. Researches have shown that this assumption is a convenient and reasonable one[5,214] since at elevated temperature, plastic strain increment is usually associated with high rates of loading while creep strain increment is time-dependent.

In this research, the thermal strain and creep strain are treated as decoupled. This is because that the temperature change is assumed to change rapidly in comparison with the long load holding time and long load dwell time. So, it is reasonable to treat the thermal effects as instantaneous and to assume that no creep occur during the thermal cycling process. The well developed thermal-elastic-plasticity theory[149] is used for the analysis of the instantaneous response.

So, according to the above stated assumption, when creep is included in the thermal elastic-plasticity finite element analysis, the following equations could be obtained:

$$\{\Delta\sigma\} = [C_{ep}](\{\Delta\varepsilon\} - \{\Delta\varepsilon^c\}) \tag{4.2}$$

that is:

$$\{\Delta\sigma\} = [C_{ep}]([B]\{\Delta u\} - \{\Delta\varepsilon^c\}) \tag{4.3}$$

where $[C_{ep}]$ is the thermal elastic-plasticity matrix in the finite element analysis, $\{\Delta\varepsilon\}$ is the total strain increment, $\{\Delta\varepsilon^c\}$ is the creep strain increment. the $[B]$ matrix relates the element strains and the nodal displacements. The governing finite element equation for the analysis is then expressed as:

$$\int_v [B]^T\{\Delta\sigma\}dv = \{\Delta F\} \tag{4.4}$$

4.2 Finite element analysis of creep

According to the assumption and the basic finite element equations described in section 4.1, when creep is included in finite element analysis, the solution procedures

are not changed[20,28,55,110,245,273,316]. As long as the creep strain increment is obtained and substituted into the incremental constitutive equation, i.e., Eq. 4.2, the solution procedure of the finite element analysis can proceed as in the conventional elastic-plastic finite element analysis. Hence, it is the first step to obtain the creep strain increment in the thermal-elastic plastic stress analysis with creep by the finite element method. Because creep deformation is time-dependent, the evolution law of creep is usually expressed in rate form. In the finite element analysis of creep, integration over time is involved. Hence, it is logical to start with the integration algorithms for the finite element analysis involving creep.

4.2.1 Integration algorithm

For simplicity, in this thesis research, only one-step integration algorithm is used. Generally speaking, there are two classes of commonly used one-step integration algorithms for creep stress analysis, i.e., the explicit algorithm and the implicit algorithm. Implicit algorithms tend to be numerically stable, permitting large time step, but the computational effort per time step is high and the computer storage requirement tends to increase dramatically with the size of the mesh. On the other hand, explicit algorithms tend to be inexpensive per time step and require less storage than implicit algorithms, but numerical stability requires that small time step be employed. There are some problems for which implicit algorithms are very efficient and others for which explicit algorithms are very efficient. However, in large scale engineering problems, the many different finite element types and local mesh refinements often result in neither class being very efficient by itself[16-17,19,76,185].

To circumvent these difficulties, methods have been developed in which it is attempted to simultaneously achieve the attributes of both classes of algorithms. The mixed explicit-implicit (EI) algorithm as proposed by Belystchko et al[29], Hughes and Liu[156-157], Liu et al[215-216] for structural dynamics and nonlinearity problems was applied to creep stress analysis by Chen and Hsu[57], and significant

computational advantage was obtained by the algorithm[56-59].

The main idea of the mixed EI algorithm is to make full use of the advantages of both the implicit algorithm and the explicit algorithm at the same time. In the implementation of the finite element analysis, the finite element mesh is partitioned into the implicit element group and the explicit element group. Within each group, corresponding integration algorithm is adopted. Different time step can be used at the same time in the two element groups. In the implicit group, a limited Taylor series expansion technique is introduced to obtain the creep strain increment[57].

4.2.2 Adoption of the proposed CDM-based constitutive model

The proposed CDM-based constitutive model describes the evolution of creep deformation and the microstructural changes of the material in the creep deformation process through two state variables. The adoption of the proposed CDM-based constitutive model involves the calculation of the rate of the creep strain and the rates of the evolution of the state variables. These calculations will require the evolution of the damage parameter and the internal stress, and then integrate the rates to obtain the relevant increments of these variables. Physically, creep deformation follows with the elapse of time once an instantaneous thermal elastic-plastic load is exerted on a solid. In the implementation of the finite element analysis, the same procedure is followed.

In creep analysis, the major external input is time increment. Whenever an incremental time is introduced in the creep analysis at any instant in the creep deformation process, the creep rate, the evolution rates of the internal state variables could be obtained from the constitutive model based on the information obtained just before this time instant. Then the increment of the creep strain and the increments of the internal state variables could be obtained through the mixed EI integration algorithm.

Then, these variables, that is the creep strain, the damage parameter and the

internal stress are updated by incorporating these newly calculated increments to the corresponding accumulated values. Certain kinds of logical judgements could be made about the newly reached material state, such as the damage state of the material or whether the accumulated creep strain exceeds the critical value, etc. Based on the concept of the mixed EI integration algorithm, the finite element mesh is partitioned into two groups: the explicit element group and the implicit element group. The corresponding integration formula for the two groups of elements are presented as follows:

4.2.2.1 Integration algorithm for the explicit element group

With the integration algorithm for the explicit group of elements, the increments of the creep strain $\{\Delta\varepsilon^c\}$, the damage parameter ΔD and the internal stress $\{\Delta R\}$ in a time interval $\Delta t = t_{n+1} - t_n$ are calculated as:

$$\{\Delta\varepsilon_c\} = \{\dot{\varepsilon}_n^c\}\Delta t \tag{4.5}$$

$$\Delta D = \dot{D}_n \Delta t \tag{4.6}$$

$$\{\Delta R\} = \{\dot{R}_n\}\Delta t \tag{4.7}$$

where n denotes the number of time step. The stress increment can then be expressed by substituting Eq. 4.5 into Eq. 4.2 as follows:

$$\{\Delta\sigma\} = [C_{ep}]([B]\{\Delta u\} - \{\dot{\varepsilon}_n^c\}\Delta t) \tag{4.8}$$

The governing finite element equation in Eq. 4.4 now becomes:

$$(\int_v [B]^T[C_{ep}][B]dv)\{\Delta u\} = \int_v [B]^T[C_{ep}]\{\dot{\varepsilon}_n^c\}\Delta t dv + \{\Delta F\} \tag{4.9}$$

4.2.2.2 Integration algorithm for the implicit element group

For the group of implicit elements, the integration formula for the increments of the creep strain, the damage parameter and the internal stress is as follows:

$$\{\Delta\varepsilon_c\} = [(1-\gamma)\{\dot{\varepsilon}_n^c\} + \gamma\{\dot{\varepsilon}_{n+1}^c\}]\Delta t \tag{4.10}$$

$$\Delta D = [(1-\gamma)\dot{D}_n + \gamma\dot{D}_{n+1}]\Delta t \tag{4.11}$$

$$\{\Delta R\} = [(1-\gamma)\{\dot{R}_n\} + \gamma\{\dot{R}_{n+1}\}]\Delta t \tag{4.12}$$

This equation is a general integration algorithm because it can be reduced to different kinds of integration modes by setting the parameter γ to different values. For example, when $\gamma = 0.0$, the equation reduces to the explicit integration mode; when $\gamma = 1$, the equation reduces to the pure implicit integration mode; when $\gamma = 0.5$, the equation reduces to the well-known Crank-Nicolson integration mode.

According to the proposed model (Eqs. 4.8–4.15), we have:

$$\{\dot{\varepsilon}^c\} = f_1(\{\sigma\}, \{R\}, D) \tag{4.13}$$

$$\{\dot{R}\} = f_2(\{\sigma\}, \{R\}, D) \tag{4.14}$$

$$\dot{D} = f_3(\{\sigma\}, \{R\}, D) \tag{4.15}$$

The incremental creep strain rate $\{\dot{\varepsilon}^c_{n+1}\}$ and the two state variables: $\dot{D}_{n+1}$ and $\{\dot{R}_{n+1}\}$ can be approximated by a limited Taylor series expansion as:

$$\{\dot{\varepsilon}^c_{n+1}\} = \{\dot{\varepsilon}^c_n\} + [H_1]\{\Delta\sigma\} + [H_2]\{\Delta R\} + \{H_3\}\Delta D \tag{4.16}$$

$$\dot{D}_{n+1} = \dot{D}_n + \{G_1\}\{\Delta\sigma\} + \{G_2\}\{\Delta R\} + G_3\Delta D \tag{4.17}$$

$$\{\dot{R}_{n+1}\} = \{\dot{R}_n\} + [E_1]\{\Delta\sigma\} + [E_2]\{\Delta R\} + \{E_3\}\Delta D \tag{4.18}$$

where:

$$[H_1] = \frac{\partial\{\dot{\varepsilon}^c\}}{\partial\{\sigma\}} \tag{4.19}$$

$$[H_2] = \frac{\partial\{\dot{\varepsilon}^c\}}{\partial\{R\}} \tag{4.20}$$

$$\{H_3\} = \frac{\partial\{\dot{\varepsilon}^c\}}{\partial D} \tag{4.21}$$

$$[E_1] = \frac{\partial\{\dot{R}\}}{\partial\{\sigma\}} \tag{4.22}$$

$$[E_2] = \frac{\partial\{\dot{R}\}}{\partial\{R\}} \tag{4.23}$$

$$\{E_3\} = \frac{\partial\{\dot{R}\}}{\partial D} \tag{4.24}$$

$$\{G_1\} = \frac{\partial\dot{D}}{\partial\{\sigma\}} \tag{4.25}$$

$$\{G_2\} = \frac{\partial\dot{D}}{\partial\{R\}} \tag{4.26}$$

$$G_3 = \frac{\partial\dot{D}}{\partial D} \tag{4.27}$$

Thus, by substituting Eq. 4.16 into Eq. 4.10, the creep strain increment could be obtained. The increments of the internal stress and the damage parameter could be obtained by substituting Eqs. 4.17 and 4.18 into Eqs. 4.11 and 4.12 respectively. Then, by substituting Eq. 4.10 into Eq. 4.2, the stress increment in the time step is obtained. Substitute the stress increment into Eq. 4.4, the governing finite element equation is obtained which has the following form:

$$\int_v [B]^T [C^*_{ep}][B] dv \{\Delta u\} = \{\Delta F\} + \int_v [B]^T [C^*_{ep}]\{A_{12}\} dv \tag{4.28}$$

where $[C^*_{ep}] = (I + [C_{ep}][A_8])^{-1}[C_{ep}]$ is the modified thermal elastic-plastic matrix. The expressions of the process parameters $[A_8]$ and $\{A_{12}\}$ are given in the appendices. These matrices and arrays should be updated at every time step.

4.2.2.3 Self-adjusting element partition

In the implementation of the mixed EI integration algorithm in creep stress analysis by the finite element method, the partition of the two element groups is self-adjusted based on the current rates of the creep strain, the damage parameter and the internal stress in the elements. Before every computation step, the division

of explicit and implicit element groups is carried out according to the following criteria:

$$(\dot{\overline{\varepsilon^c}})_e \geq (\dot{\overline{\varepsilon^c}})_s \tag{4.29}$$

$$(\dot{D})_e \geq (\dot{D})_s \tag{4.30}$$

$$(\dot{\overline{R}})_e \geq (\dot{\overline{R}})_s \tag{4.31}$$

in which the subscripts e and s denote respectively the current values in the element and the specified values. These specified values are selected by the user. If any of these conditions is satisfied in a particular element, that element is treated as an implicit element and all the other elements are treated as explicit elements. If the parameters $(\dot{\overline{\varepsilon^c}})_s$, $(\dot{D})_s$ and $(\dot{\overline{R}})_s$ are properly chosen, implicit elements would take up a relative large portion of the total elements in the early stage due to high rates of the creep strain, the damage parameter and the internal stress of the material during the primary creep deformation or upon reloading or when the material is near being broken. The number of the implicit elements would be automatically reduced with time as the creep deformation proceeds beyond the primary stage and the creep strain rate reduces. During such time, only a small number of elements in the crack tip region remains to be treated as implicit. Since implicit elements require much more operations than those required for the explicit elements, this self-adjusted element partition algorithm results in a significant saving in the computational effort.

4.2.2.4 Automatic time step selection

Both constant and variable time increments are allowed in the current mixed EI integration algorithm. For the variable time step scheme, the selection of the time increment is based on the following considerations:

1. Restriction on the increment of the creep strain. The magnitude of the time step is restricted by the ratio of the incremental effective creep strain to the

current effective creep strain rate as shown by the following expression:

$$\Delta t_1 = \tau_1 \frac{\Delta \overline{\varepsilon}}{\dot{\overline{\varepsilon}}} \tag{4.32}$$

where τ_1 is an input parameter controlling the time steps on the basis of the change of the creep strain.

2. Restriction on the increase of the damage parameter. The following relation is employed:

$$\Delta t_2 = \tau_2 \frac{\Delta D}{\dot{D}} \tag{4.33}$$

where τ_2 is an input parameter controlling the time steps on the basis of the change of the damage parameter.

3. Restriction on the change of the internal stress. This is implemented by the following expression:

$$\Delta t_3 = \tau_3 \frac{\Delta \overline{R}}{\dot{\overline{R}}} \tag{4.34}$$

where τ_3 is an input parameter controlling the time steps on the basis of the change of the internal stress.

τ_1, τ_2 and τ_3 are all constants less than unity.

These conditions are applied to all the elements of the structure. The time increment for the next step of calculation is selected by the following criterion which is obvious:

$$\Delta t = Min[\Delta t_1, \Delta t_2, \Delta t_3] \tag{4.35}$$

Since oscillations may result from abrupt changes of the time step size, a limit of the time step change to one and half of the previous time step length is adopted in this analysis.

4.2.3 Influencing factors on the cyclic creep fracture

In this section, the implementation in the finite element analysis of the influencing factors on cyclic creep fracture is introduced. Since the implementation is difficult to describe without a statement of the unique features of the program used, only a brief description is given. The influencing factors of cyclic creep fracture considered in this study are the HTLCF damage or the load cycling effect, the load dwell time effect and the interaction between creep damage and the HTLCF damage.

4.2.3.1 The effect of HTLCF damage

When the load is cyclic in creep deformation process, the effect of HTLCF damage should be taken into account in the cyclic creep fracture analysis. In the implementation of the finite element analysis, this is achieved by calculating the HTLCF damage according to the plastic strain range of a load cycle[82-84], and then adding this amount of damage to the current total accumulated damage. This part of the damage accounts partly for the effect of the HTLCF in the cyclic creep fracture process.

Another important effect of the cyclic load on creep deformation and damage development is to redistribute the stress field within the material. Since the damage development and the creep evolution are all based on the current stress level, the stress redistribution hence would alter the development of damage and creep strain evolution, and eventually the failure of the material.

4.2.3.2 The effect of load dwell time

During the load dwell time, the material experiences certain microstructural changes. In the proposed CDM-based constitutive model, this phenomenon is described by the evolution of the internal stress. In the implementation of finite element analysis of this research, this is reflected through the change of the maximum internal stress which is the indication of the material's resistance to further creep de-

formation. The maximum internal stress is an exponential function of the duration of the load dwell time. The change of the maximum internal stress would change the evolution rate of the internal stress accordingly, which would alter the development of the internal stress, the damage parameter and the evolution of the creep deformation. And hence, even the final failure of the material would be influenced by the dwell time.

4.2.3.3 The interaction between creep and HTLCF

In the finite element analysis, the interaction between creep damage and the high temperature low cycle fatigue damage is achieved through the addition of the damage caused in the creep deformation process and the damage caused in the HTLCF process within a load cycle, and then the accumulated damage within this load cycle enters the calculation of the creep damage and the HTLCF damage in the next load cycle. The two parts of the damage parameter are added together in a nonlinear way. The creep damage and the HTLCF damage are mutually reinforcing.

4.3 Factors for complete creep analysis

In this thesis research, the calculation of the creep deformation follows the analysis of the time-invariant thermal elastic-plastic response. For the analysis of the instantaneous thermal-elastic-plasticity, the finite element method and the implementation were very well developed and documented[5,24,35,181-183,214,233,237-238,328]. In this thesis research, the thermal-elastic-plastic stress analysis is based on the works of Hsu[149-155]. Since a lot of work had been done and published by the thermal-elastic-plasticity theory and the finite element method, only a brief description of the highlights of this study is made in this section.

4.3.1 Yield criterion

The von Mises yield criterion is used in this analysis. According to the von Mises criterion for an isotropic material, the yield surface F is expressed:

$$F = J_2 - \frac{1}{3}\sigma_Y^2 \tag{4.36}$$

in which

$$J_2 = \frac{1}{2}S_{ij}S_{ij} \tag{4.37}$$

is the second deviatoric stress invariant, S_{ij} is the deviatoric stress tensor and σ_Y denotes the initial yield strength of the material. The function F in Eq. 4.36 represents the plastic yielding at current stress state during plastic deformation. Obviously, a plastic state is attained when $F = 0$, while the material is in the elastic region if $F < 0$.

4.3.2 Plastic flow law

The Prandtl-Reuss flow law is used in this study. This theory assumes that the plastic strain increment is at any instant of loading proportional to the instantaneous stress deviation. Mathematically, this can be expressed as:

$$d\varepsilon_{ij}^p = S_{ij}d\lambda \tag{4.38}$$

in which $d\varepsilon_{ij}^p$ is the components of the plastic strain increment, S_{ij} is the deviatoric stress tensor and $d\lambda$ is a constant.

4.3.3 Hardening rules

One of the major problems in the theory of plasticity is to describe the behavior of hardening of materials in the plastic range for complex loading histories. Besides the flow law and the yield law, the hardening rule is needed to complete the description of the material's response. When the initial yield is reached, the hardening rule defines its modification during the process of plastic flow.

There are two rules of hardening widely used. These are the isotropic and kinematic hardening rules. Isotropic hardening occurs when the initial yield surface (representing the initial yield condition in the stress space) expands uniformly in all stress directions during plastic flow. According to the kinematic hardening rule, however, the yield surface not only changes its initial form and orientation but also translates in the stress space like a rigid body. These are the basic hardening rules. In reality, the hardening behavior is much more complicated than the cases described by the two hardening rules. Hence, advanced hardening rules are proposed to account for the hardening phenomenon expressed by materials with different loading histories. One of the examples is the combined kinematic and isotropic hardening rule. A combination of kinematic and isotropic hardening would lead to the following relation:

$$f(\sigma_{ij} - \alpha_{ij}) - F(\lambda) = 0 \tag{4.39}$$

where α_{ij} denotes the translation of the initial yield surface and $F(\lambda)$ is a measure of its expansion, λ is a scalar parameter monotonically increasing during the deformation process. When $F(\lambda)$ equals a constant, we obtain the case of kinematic hardening; if there is no translation, $\alpha_{ij} = 0$, and $F(\lambda)$ is a monotonically increasing function, isotropic hardening occurs.

In this research, however, the Mroz's hardening rule coupled with the several yield surfaces[246] is adopted. This is because that though the model of combined kinematic and isotropic hardening is more realistic, some difficulty appears when it is applied to complex loading histories involving unloading and subsequent loading along a different stress path. Since during plastic deformation process, especially when the load is cyclic, the stress and strain is no longer one-to-one correspondent as in the elastic case. In the domain of several yield surfaces theory, Mroz's hardening rule assumes that the translation of the current yield surface is in the direction of the same outward normal with its adjacent yield surface after it reaches the adjacent yield surface, instead of translating in the direction of the vector connecting

the center of the surface with the stress point. Mroz's law had been shown to be reasonable in practical analysis when complex loading is involved[56-59].

4.4 The critical damage criterion

In this research, it is assumed that when $D = 0$, the material is in a virgin state; when $0 < D < D_c$, the material is in a damage state but still has the capability of bearing load, and when $D = D_c$, the material be damaged completely. That is to say, $D = D_c$ is the critical damage criterion. D_c as used here is the critical value of the damage parameter which characterizes the material failure. Few books and papers give this characteristic. Many experiments have shown that $0.2 \leq D_c \leq 0.8$, depending upon the materials and experimental methods. Followed the suggestions of Lemaitre[200-204], $D_c = 0.5$ was used in this study.

According to the author's experience, the value of the critical damage parameter D_c does not make very much difference on the final failure of the material. This is because when the accumulated damage reaches around 0.4, the evolution rate of the damage parameter increases drastically and quickly leads to the final failure of the material. The period between the damage parameter $D = 0.4$ and the final failure, i.e., $D = D_c$ is very short, and does not account much to the lifetime of the material.

4.5 Simulation of crack extension

Since crack propagation was involved in fracture problems, numerical algorithms are needed for simulating crack extension in the finite element analysis.

4.5.1 The conventional methods

In terms of finite element simulation, crack growth is commonly achieved by successive relaxation of the nodal forces at the node representing the crack tip. The released node represents the movement of the crack tip. Once a criterion for crack growth is satisfied, the relaxation is performed by applying negative nodal force

at the crack tip node until the original crack tip nodal force is relaxed and a free crack surface is developed to one element ahead. The physical quantity working as the criteria for crack growth can be an equivalent stress or strain, energy, or some measure of local damage. The original crack tip nodal force is divided into small increments and applied so that it can be relaxed in such a way that the stress in the area surrounding the crack tip can redistribute smoothly. This nodal force relaxation technique for simulating crack growth was once widely used[8,88,271]. One shortcoming is that once the nodal force is relaxed, the crack tip 'jumps' to the next element and hence fails to produce a smooth crack extension, even though very small elements were used in the crack tip region. In other words, these methods produce a discrete crack increment. In some commercial program package, such as ADINA[310], similar procedures are adopted in simulating crack extension.

Hsu and co-workers[56-59,150,154] improved such methods for simulating the crack growth by finite element analysis and proposed the 'breakable element' method. The concept of the breakable element method is based on the fact of the successive reduction of the stiffness matrix of the crack tip element during a simulated crack growth. This was based on the physical observations of the progressive deterioration and the corresponding stiffness reduction of materials due to permanent deformation and damage. In the initial development of this method, the breakable element skipped during crack growth. Later, this method was improved by creating a pseudo-point in the breakable element used in the stiffness reduction scheme. This pseudo-nodal point moves through the breakable element as the crack tip extends, producing smoother crack growth. A lot of contributions followed this method[56-59,149-155].

However, certain limitations exist within these methods for simulating crack extension. These methods are basically direct simulation of crack extension. Another shortcoming of these methods is that the direction of crack propagation has to be determined by some other means. These methods themselves do not have the abili-

ty to predict the direction of crack propagation under creep deformation conditions which is not easy to attain.

4.5.2 The strain localization analysis for simulating crack extension

In this research, a new method, the strain localization analysis, is used to simulate crack growth under creep deformation conditions. In this method, the phenomenon of crack extension was associated with a more rigorous framework of the continuum solid mechanics.

There is considerable physical evidence that, if a homogeneous body is subjected to homogeneous boundary conditions, it may under some circumstances undergo an inhomogeneous deformation accompanied with which is the formation of localized bands of intense straining[144-145,188,208,210-211,266,269-270,285,334]. This phenomenon of localization occurs in a widely variety of solids: in structural metals, in ductile single crystal, in rocks and in concretes. The physical mechanisms responsible for triggering localization vary widely. Localization also occurs in metals at low rates of loading. Once localization takes place, large strains can accumulate inside the band and lead to fracture. There is a large and growing literature on such effects. Similar phenomena may occur in materials which may undergo damage. Consequently, an inhomogeneous damage field which may or may not be coupled to an inhomogeneous strain field, may arise as a result of homogeneous loading[25,143,204]. This problem was relevantly stated by Lemaitre[204] as follows: 'Damage, as a softening process, may induce localization of strain, as it is the case for plastic shear bands in plasticity. This is the beginning of the process of failure by mesocrack which transforms a volume phenomenon into a surface of separation'

Finite element algorithms have been developed in which an element has the capability of incorporating embedded localization lines[91-92]. Such an algorithm is adopted in this thesis study. Attached in appendixes are the derivations of the finite element equations for strain localization analysis based on the general variational

principle. The algorithm was extended to incorporate with the CDM analysis. One of the features of the strain localization analysis is to incorporate a damaged line of material within an element. The resulting effect of such damaged line of materials is to reduced the stiffness of materials and hence reduce the capability of load bearing of the material. And the locus of such damaged lines is the extended crack.

4.5.3 The direction of crack extension

The direction of crack extension can be determined automatically using the damage mechanics method in finite element analysis for cyclic creep fracture. This is possible due to the fact that the critical damage criterion was checked at every time step. Once the critical damage criterion was met at a point or an element of the material, this particular point or element was declared to be damaged and hence lost the capability of load bearing. The locus of such material points or elements specifies the place of damaged material and hence the direction of the crack extension.

4.6 The computer code TEPSAC

The computer program TEPSAC (stands for Thermal Elastic-Plastic Stress Analysis with Creep) was used in this thesis research. This finite element code was originally developed by Hsu and his co-workers to analyze thermal elastic-plastic-creep stress problems[56-59,149-155]. The code, although limited to two-dimensional plane or three dimensional axisymmetrical structures, can handle large classes of thermomechanical problems using a simplex element algorithm.

In this research, the CDM-based constitutive model for describing creep response and damage, the strain localization analysis for simulating crack extension and the various influencing factors on cyclic creep fracture, such as the high temperature low cycle fatigue or the load cycling effect, the load dwell time effect and the interaction between creep damage and the high temperature low cycle fatigue damage, were incorporated to this program for numerical results.

Chapter 5

Verification of the Proposed CDM-based Model

In this chapter, numerical results verifying the proposed model are presented. A series of case studies have been conducted to verify the solidity of the proposed CDM-based constitutive model in describing creep deformation, creep damage and fracture behavior of selected engineering materials (e.g., the 316L stainless steel) and in representing the various influencing factors on creep response and crack behavior. Part of the results are compared with available experimental data obtained in the open literatures. Other part of the results are compared with similar analyses reported by other researchers. These case studies include:

- One-dimensional analyses

    1. Static creep analysis;
    2. Cyclic creep fracture analysis
        (a) Load cycling effect;
        (b) Load dwell time effect;
        (c) Interaction between creep damage and HTLCF damage;
        (d) Cyclic creep fracture analysis with complete load path

- Two dimensional case studies

1. Central cracked plate specimen

2. Single edge notch (SEN) plate specimen;

In the one-dimensional analyses, the loading conditions for the case studies are shown in Fig. 5.1. The loading conditions correspond to static creep deformation, cyclic creep deformation with and without load dwell time respectively. The computational domain, as shown in Fig. 5.2, is a tensile bar having the same size as the one used in Gong's experimental tests[119-120]. In the two dimensional case studies, the analysis focuses on studying creep deformation response and crack behavior of single edge notch plate, as shown in Fig. 5.12, and of central cracked thin panel, as shown in Fig. 5.6. In all the case studies, it is assumed that creep deformation happens only during the load holding period. The loading and unloading processes are short in comparison with the load holding time and the load dwell time. The loading and unloading are hence regarded as instantaneous thermal elastic-plastic deformation process. The creep deformations occurred in these instantaneous processes are assumed to be negligibly small.

In these case studies, the material is treated as a continuum under load and the constitutive equations are used to describe how the stress, strain and damage (or strain rate and damage rate) are inter-related. Different points in the solid body experience different stress levels and are at different stages of material deterioration. The constitutive equations remain valid until the specified fracture criterion is reached. At this time, the material point under consideration can no longer sustain the applied load and, the material is deemed to have failed. Ultimately a region of failed material will progress through the body until the applied load can no longer be sustained and the solid body fails by a global collapse mechanism.

The numerical procedure used to solve the boundary value problem for creep deformation and creep damage is based on the finite element method and employs constant strain elements, which have been extensively used to model the behavior of cracked creep components. The procedure takes the elastic solution as its starting

point and integrates creep strain, the creep damage parameter and the internal stress with respect to time. The integration is carried out over a series of discrete time steps using the mixed explicit-implicit one-step integration algorithm. The deterioration of the material, as represented by the damage parameter, develops monotonically with time throughout the structure, and failure of an element is deemed to have occurred when the damage parameter attains the prescribed value of 0.5. The material element is then unable to transmit or sustain load. The boundary value problem is then redefined to allow either a crack or damage zone to develop and spread. Once the boundary value problem is redefined, the time integration is continued by taking the field variables just before the local failure occurred as the new starting point. The procedure is then repeated until complete failure of the cracked member occurs.

5.1 Identification of material constants

In all the case studies, the material is 316L stainless steel. The constants used in the proposed CDM-based model are obtained from experimental measurements as reported in the open literatures.

Constants used in the first six equations of the model (Eqs. 3.8-3.13) were obtained from test results conducted in the Thermomechanics Laboratory of the University of Manitoba[119-120]. Special tests were conducted for measuring these constants.

The constants used in the seventh equation (Eq. 3.14) were obtained from the results of G. Degallaix[82-84]. The Manson-Coffin type equation used by Degallaix properly described the high temperature low cycle fatigue behavior of 316 stainless steel. The agreement between theoretical predictions and experimental measurements was good.

The physical constants, such as the Young's modulus, initial yield stress and ultimate tensile strength of 316L stainless steel at high temperature (650^o) were

measured in the Thermomechanics Laboratory of the University of Manitoba[56]. Other constants are from the paper by Maas and Pineau[222] and from commonly used Metals Handbooks.

Table 1, Input material parameters for 316L stainless steel[82-84,119-120]

A	4.36×10^{-15}
C_1	2.15×10^{-14}
C_2	1.18×10^{-12}
n	5.84
r_o	0.711
B_1	1.32×10^{2}
α	3.0×10^{-2}
β	-1.80×10^{-2}
p	0.88
σ_n	1.00×10^{2}
A_1	0.6445
A_2	0.69×10^{-3}
B_3	1.624
B_4	1.792
Q	$4.80(Kcal/Mol)$

The material parameters used in the analyses are tabulated above.

5.2 One-dimensional case studies

5.2.1 Static creep analysis

The purpose of this group of case studies is to verify the validity of the proposed model in describing static creep behavior. For creep evolution, good correlations are found between the case study results and the test results reported in the open literatures[119-120], as shown in Fig. 5.3. The basic features of the experimental measurements are reflected by the finite element results. The response of the uniaxial bar under tension is examined under four levels of mechanical load, $234, 221, 193$ and 165 MPa, are applied respectively. The highest temperature is 650^o. The finite element results of creep evolution agree well with the experimental test results.

The three stages of creep deformation are clearly shown by the evolution and development of the variables with time. These variables include the creep strain, the creep strain rate, the damage parameter, the damage rate, the internal stress, the difference between the damage equivalent stress and the internal stress and the effective creep deformation driving stress, etc. Figs. 5.4–5.5 are two typical figures showing the three stages of creep deformation. They correspond to the development of the creep strain rate and the effective creep deformation driving stress $\frac{\tilde{\sigma}-\bar{R}}{1-c_o D}$ respectively for the applied load of 193 MPa.

Attached in Appendix E (Figs. E1-E6) are the results of the evolution of the various variables in this group of case studies. They include the creep strain rate, the damage parameter, the internal stress, the damage rate, the difference between damage equivalent stress and internal stress $(\tilde{\sigma}-\bar{R})$ and the effective creep deformation driving stress $\frac{\tilde{\sigma}-\bar{R}}{1-c_o D}$. As can be seen from these figures, the various features of creep deformation can be described by the model through the change of the various variables. In the primary stage of the creep deformation, the creep strain develops rapidly while the creep strain rate drops quickly to a relative constant value. This is because the microstructure of the material changes quickly upon the application of the load. The material's resistance to further creep deformation which is expressed in this model by the internal stress increases rapidly with the development of creep deformation until a steady state is reached. Corresponding to this, the damage rate is very high at the beginning of the creep deformation when the material is relative 'pure' or 'virgin' because the internal stress is not yet developed, and hence the driving force for creep deformation is high. With the rapid development of the internal stress, the driving force for creep deformation decreases, so are the damage rate and the creep strain rate. At the primary stage of creep deformation, the damage value of the material is relative low, the driving force for creep deformation and for the development of the damage can be regarded as the difference between the damage equivalent stress and the internal stress $(\tilde{\sigma}-\bar{R})$. The relative durations of the pri-

mary creep deformation stages depend on the stress level as shown in these figures. This is because the evolution of the internal stress is dependent upon the creep deformation which is function of the applied load. When the internal stress reaches its maximum value, the material enters a relative steady deformation process, i.e., the secondary stage of the creep deformation.

In the secondary stage of creep deformation process, the internal stress has reached its maximum value and will remain at this value until the applied load changes or until fracture occurs. Because of this, the driving force for creep deformation and for damage development is at a relatively constant value because the applied load is kept constant and the damage parameter is so low that it could not affect the creep strain rate and the damage rate significantly. Correspondingly, the creep strain rate and the damage rate are all at relatively constant levels, even though the creep strain evolves and the damage grows with time. The duration of the steady creep process depends upon the applied loading levels as shown in these figures.

When the accumulated damage reaches a certain value, e.g., larger than 0.1, its effect upon the material's mechanical behavior can no longer be ignored. The material's effective resistance to further creep deformation is reduced because of the damage development. For example, it could be explained by the fact that the effective cross sectional area of the material to bear the load is reduced with the nucleation and growth of the grain boundary voids. Hence, in a relative sense, the effective driving force of the material for creep deformation and for damage development, $\frac{\tilde{\sigma}-\bar{R}}{1-c_o D}$, increases rapidly in the damaged material and causes further development of damage within the material. Consequently, the creep strain rate and the damage rate of the material increase rapidly which result in a fast development of creep deformation and the associated damage until the material fails (when the damage parameter reaches a critical value, 0.5 in the case studies). At the time the material fails, the internal stress, the material's resistance to creep deformation,

drops to zero.

It is worth noting that the shape of the curves of the effective creep deformation driving stress as shown in Fig. E6 and the shape of the curves of the development of the creep strain rate as shown in Fig. E1 are similar. The shapes of these curves are different from that of the applied stress which is a horizontal straight line and that of the curves of the development of the difference between the damage equivalent stress and the internal stress $(\tilde{\sigma} - \bar{R})$ as shown in Fig. E5 for the same four different loading levels. This illustrates the purpose of the model in making the effective creep deformation driving stress $\frac{\tilde{\sigma}-\bar{R}}{1-c_o D}$ to be the controlling parameter for the development of creep strain. However, by the conventional mechanics methods, such as the Norton's law, it is difficult to explain why the creep strain rate changes drastically as observed experimentally and shown in Fig. 2.2 during the whole creep deformation process while the applied loads are kept constant at all times. This shows one of the advantages of the proposed CDM-based constitutive model over the conventional mechanics methods in treating creep fracture problems.

The dependence of the creep deformation upon the stress level is also shown in these figures. At different loading levels, the relative portion of the three creep deformation stages are also different. Another phenomenon worth commenting is that the creep strain to failure of a specimen under different stress levels is different. It is noted in Fig. 5.3 that the creep strain to failure increases at lower applied stresses, which corresponds to longer durability. This same trend was observed by other researchers[135-140,189-193,248-251]. As stated in Appendix A, the loss of durability of metallic materials under creep deformation is usually caused by inter-granular cavities. A plausible crack growth criterion is assumed by some researchers that the crack starts growing and continues to grow at such a rate that the condition for cavity coalescence is met[291] at a distance X_c ahead of the crack tip. Usually X_c is equal to the cavity spacing. In other words, the critical creep strain criterion is related to the material reaching the critical strain ε_f. at a distance X_C ahead of

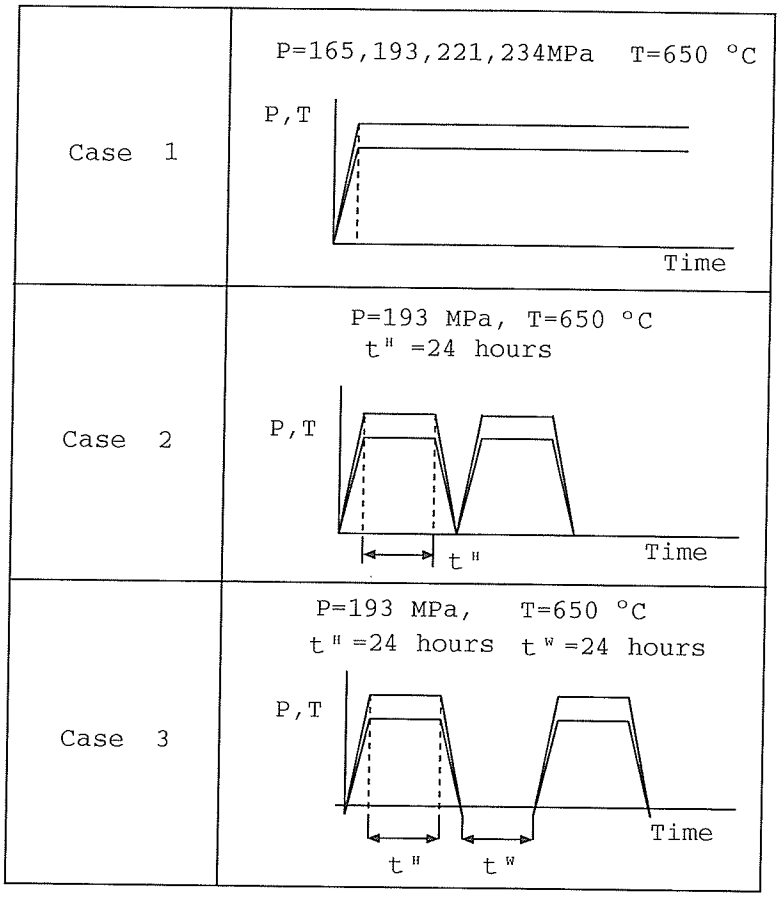

Figure 5.1: The loading conditions for the three groups of case studies

current crack tip. This leads to an equation of motion for the crack tip. The results of this group of case studies show that the criterion of the local critical creep strain in predicting crack initiation and propagation is to be improved. This is because the critical creep strain is not a constant but is rather dependent upon the loading level.

All the trends and features in these figures agree well with the experimental observations reported in the open literatures[119-120], which reinforces the validity of the model in describing the static creep behavior.

5.2.2 Cyclic creep fracture analysis

This group of case studies was conducted to demonstrate the importance of the mechanical load cycling effect and the load dwell time effect on creep response and

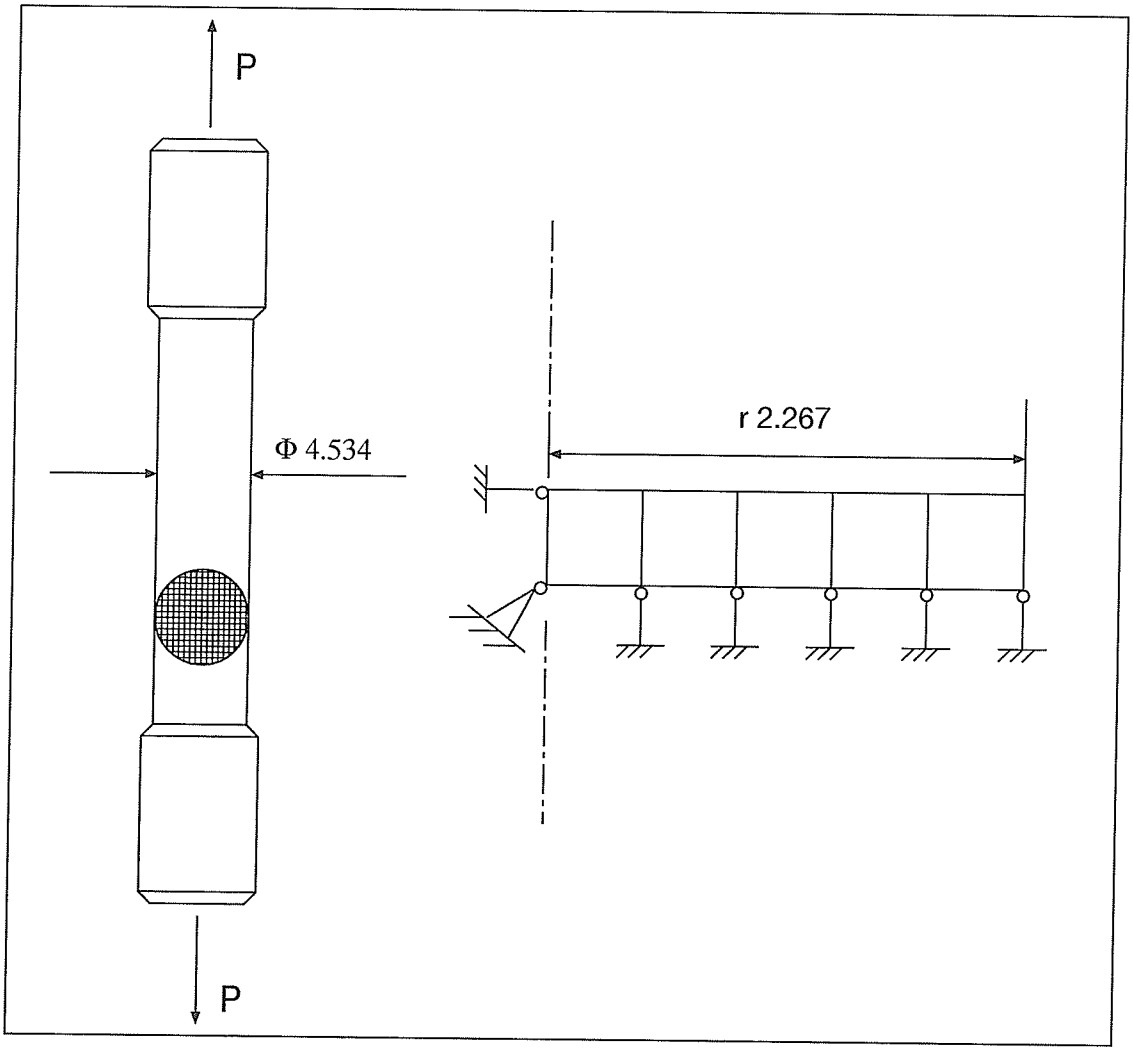

Figure 5.2: The computational domain and the finite element mesh for one dimensional case studies

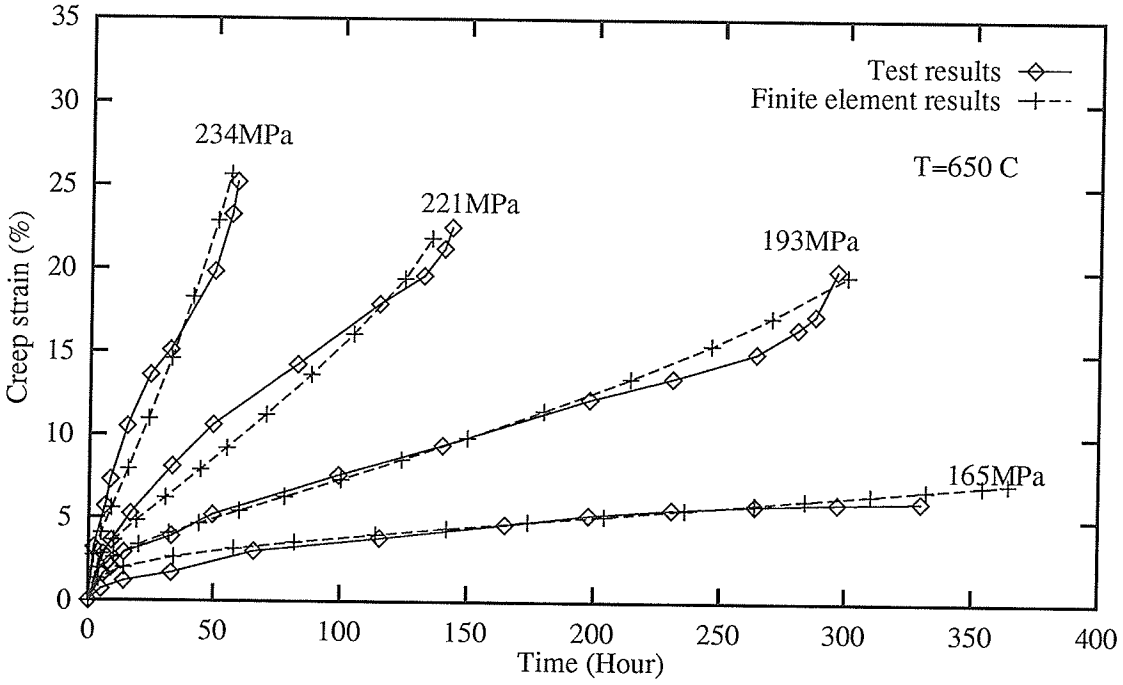

Figure 5.3: Creep strain by test[119-120] and by finite element calculation

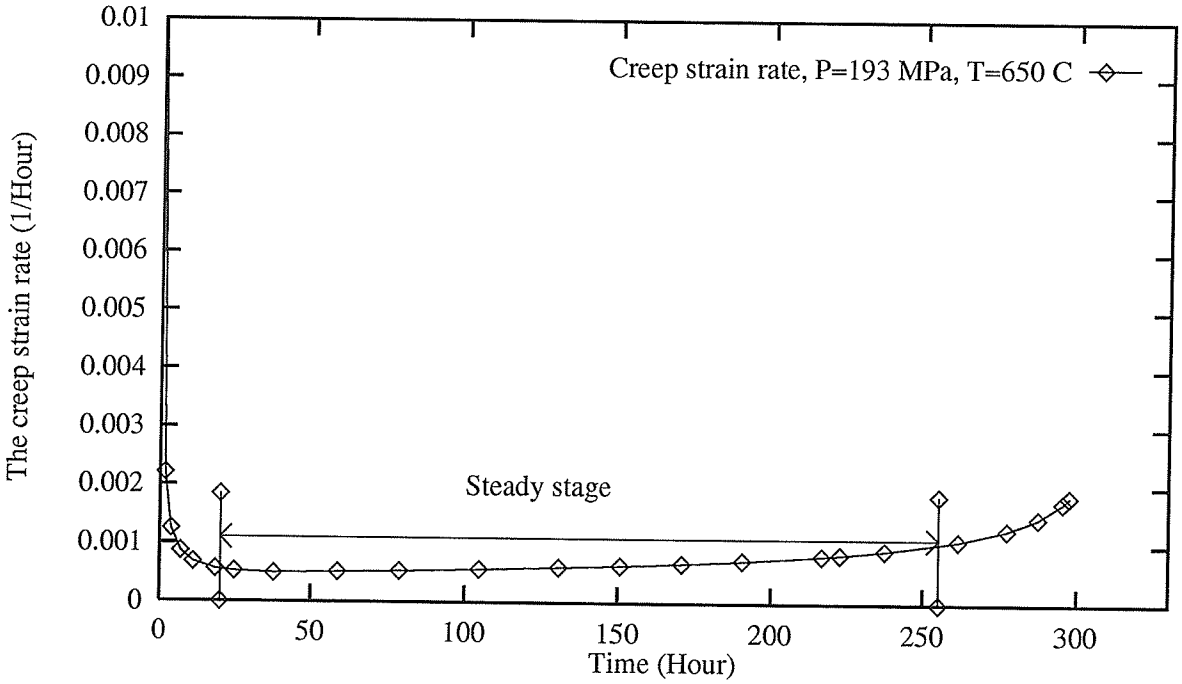

Figure 5.4: The development of the creep strain rate under the static load of 193 MPa and 650°C

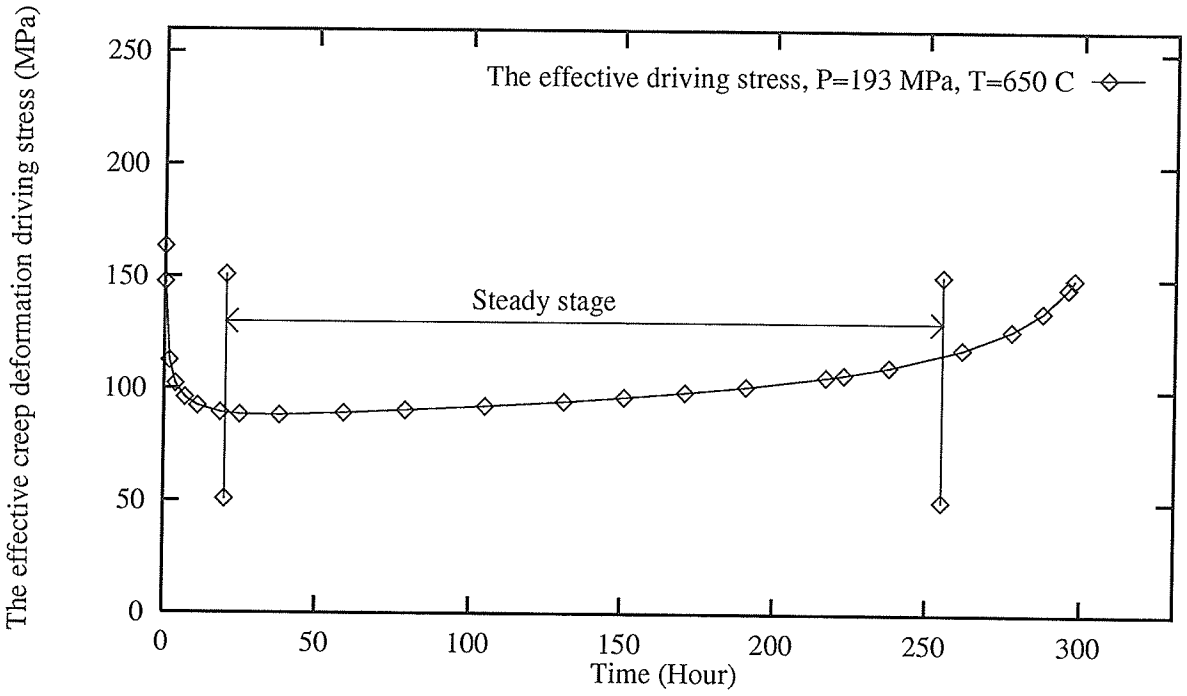

Figure 5.5: The development of the effective creep deformation driving stress $\frac{\tilde{\sigma}-\bar{R}}{1-c_o D}$ under the static load of 193 MPa and 650°C

damage development. This corresponds to two cases: cyclic load with and without load dwell time, i.e., Case 2 and Case 3 respectively in Fig. 5.1.

5.2.2.1 The importance of load cycling effect in the cyclic creep deformation process

In the proposed model, the equation for describing the load cycling effect in the cyclic creep deformation process (Eq. 3.14), or the so-called HTLCF behavior, was basically an extension of the Degallaix's model in the CDM form. There are numerous reports and experimental data showing good agreement of the HTLCF analysis results on 316L stainless steel between experimental measurements and the theoretical prediction made through the model[82-84].

In the case studies, the mechanical load is 193 MPa. The temperature changes from 30^oC to 650^oC. The mechanical load and the temperature change are in phase with each other. As indicated by the results of the case studies, the load cycling effect has significant influence upon the cyclic creep fracture behavior. For emphasizing

the load cycling effect, the results of the case studies are plotted together with those corresponding results of the static creep deformation. These are shown in the figures attached in Appendix F (Figs. F1-F7). There are no experimental data under the same loading condition of the case studies in the literatures to compare with the case study results. But in Fig. F4, the results of the development of the creep strain measured experimentally under the condition of isothermal cyclic mechanical loading with load dwell time are plotted together with the finite element results of this group of case studies. As can be seen, the finite element results basically reflects the trend of the experimental measurements even though there are some gaps between them. This, however, exactly shows the importance of the load dwell time effect which would be checked in the next section.

According to the case study results, the load cycling process has obvious influence upon the material's creep response and the damage development, especially with the increase of load cycles. As shown in these figures, the load cycling process enhances the creep strain rate and the damage rate by introducing certain amount of damage to the material directly, even though the amount of damage thus introduced is small. The enhanced creep strain rate and the damage rate dictate faster development of creep strain and faster deterioration of the material than those under monotonic loading conditions and hence change the creep response and damage development of the material. In other words, creep damage is reinforced by the HTLCF process. The operation life of the specimen is therefore shortened by the load cycling process. Hence, the load cycling process, or the HTLCF process is detrimental to the evolution of the material properties and its performance.

It should be noted that in the one-dimensional case studies, the mechanical load is kept constant all the time. Even in the cyclic loading case the damage equivalent stress is the same during the load holding times. Because the stress is kept constant, and there is no dwell time involved in one load cycle, the internal stress is not affected. Only the damage pattern is changed after the load cycling event. This change affects the effective creep deformation driving stress $\frac{\tilde{\sigma}-\bar{R}}{1-c_o D}$, and

hence the creep strain rate and the damage rate. But since the HTLCF damage is not large in one load cycle, the influence of the load cycling effect after one load cycling event is not obvious. However, with the increase of the number of loading cycles, the accumulated HTLCF damage becomes large enough, and its effect on the creep response and the damage development is obviously shown. This is just the trends of Figs. F5-F7. In two dimensional case, the load cycling process probably appears to be more important because it not only would change the creep strain rate, damage rate and the internal stress rate, etc., but also would change the stress distribution in the crack tip area which in turn influence the creep response and the crack behavior of the material.

It is also observed from the results of this group of case studies that the higher the loading level, the more pronounced the load cycling effect on the creep response and the damage development would be. It is the same trends as observed in engineering applications. For example, at lower level of stress while other conditions are the same, it takes many more load cycles to make a specimen 'fatigue'. Hence, the low cycle fatigue life of a specimen increases as the loading level is reduced. This is also the trend of the experimental observations as shown in Fig. H8. This characteristic of high temperature low cycle fatigue is expressed by the model through the finite element analysis, as shown in Fig. H9.

5.2.2.2 The importance of the load dwell time effect in the cyclic creep deformation process

To show the importance of the load dwell time effect on cyclic creep fracture, the results corresponding to the cyclic loading with and without load dwell time are plotted together. These are shown in the figures attached in Appendix G (Figs. G1-G7). From these figures, it is clearly seen that the load dwell time has significant influence upon the development of the variables, such as the creep strain rate, creep strain, the damage parameter, the damage rate, the internal stress, the difference between the damage equivalent stress and the internal stress and the effective creep

deformation driving stress, etc.

The load dwell time has a detrimental effect on the creep response. The damage development due to load dwell time is similar to that of the load cycling effect, i.e., to reduce the material's resistance to further creep deformation. But unlike the damage mechanisms of the load cycling effect on the cyclic creep deformation, which introduces certain amount of damage to the material directly during the load cycling event and to cause stress redistribution around the crack tip region in the two dimensional case, the load dwell time effect manifests itself through the change of the maximum internal stress which is an indicator of the material's resistance to further creep deformation. Even though the amplitude of the change of the maximum internal stress is not significant, its influence on the creep response is too significant to be ignored. This is due to the fact that a decrease of the internal stress increases the difference between the damage equivalent stress and the internal stress $(\tilde{\sigma} - \bar{R})$ and the effective creep deformation driving stress $\frac{\tilde{\sigma}-\bar{R}}{1-c_o D}$. The increased effective creep deformation driving stress and the difference between the damage equivalent stress and the internal stress dictate higher rates of creep strain and higher values of the damage parameter. Consequently, the change of internal stress results in a faster development of creep strains and faster deterioration of the material than those under cyclic loading without load dwell time. Hence, the cyclic loading with load dwell time is more detrimental than the cyclic loading without load dwell time. But the difference between the two loading conditions is not obvious after only one load cycling event. With the increase of load cycles, the difference becomes significant. This trend is shown in Figs. G1-G7 for all the variables checked in this group of case studies. Therefore, for complete cyclic creep fracture analysis, the load dwell time effect should not be ignored.

5.2.2.3 Interaction between creep damage and HTLCF damage

There are many reports on the interactions between creep and HTLCF, which is still an active research topic in various industrial applications[128]. In the proposed model, the description of the interaction between creep damage and the HTLCF damage was based on Lemaitre and Chaboche's work[205]. It is assumed that the HTLCF damage and the creep damage are of similar and additive nature. Because there are many reports about the validity of the damage summation model in describing the interaction between creep damage and HTLCF damage, no particular case studies are designed to study its effect on the creep response and damage development in the one-dimensional case in this thesis research.

5.2.2.4 Cyclic creep fracture analysis with complete loading path

This group of case studies are designed to conduct cyclic creep fracture analysis using the proposed model. The mechanical loading pattern is made of complete load cycles. Each load cycle includes loading, load holding, unloading and load dwell periods. The load holding time, t_H, and the load dwell time, t_W, are all selected to be 24 hours and the mechanical load level is 193 MPa. The temperature change is from 30°C to 650°C in one load cycle. The test results under the condition of isothermal and cyclic mechanical loading of 193 MPa is available in the literatures[119-120]. The results of this group of case studies are plotted together with the corresponding results under monotonic loading conditions as shown in the figures attached in Appendix H (Figs. H1-H9).

The results of this group of case studies show a cyclic creep acceleration behavior of the material. This trend has been observed and reported in the literatures[119-120]. The incorporation of the load cycling process and the load dwell time makes the load more detrimental than the case involves monotonic load. As a result, the creep strain rate and the damage rate are enhanced and the effective creep deformation driving stress is also enhanced by the introduction of certain amount

of damage in the load cycling process and the reduction of the maximum internal stress during the load dwell time. The enhanced creep strain rate, the damage rate and the effective creep deformation driving stress causes faster evolution of the creep strain and faster development of the damage of the material. The operation life of the material is hence shortened as compared with those under static loading conditions. Fig. H8 shows the comparison of the experimental measurements of the creep strains under static and cyclic loading conditions under the cyclic loading of 193 MPa and constant temperature of 650°C as reported in the literatures[119-120]. It is also observed from these experimental data that the creep strain develops faster under cyclic loading.

Shown in Fig. H4 is the evolution of the creep strain under the cyclic loading of 193MPa with load dwell time and constant temperature of 650°C obtained from experimental observations and from the finite element analysis conducted in this thesis study. For comparison, the finite element results corresponding to cyclic loading without load dwell time is also plotted in these figures. As shown in these figures, the finite element analysis results and those of experimental measurements agree well. And the finite element analysis results under cyclic loading with load dwell time agree better with experimental data than those of the finite element analysis results under cyclic loading without load dwell time. This also shows the importance of the load dwell time effect in the process of cyclic creep deformation and the damage development. Again, it is noted that the differences between the variables under static loading and cyclic loading become progressively significant with the increase of the load cycles. After just one load cycle, the differences are not obvious. These are the trends for all the variables checked in this group of case studies for both finite element analysis results and the experimental measurements.

Shown in Fig. H9 is the result of the finite element analysis of the creep strain under similar loading conditions of the experiments. As can be seen from these figures, all the features of the cyclic creep strain development are expressed by the proposed model through the finite element analysis and the analysis results agree

well with the available experimental measurements. This verifies the validity of the proposed model in describing cyclic creep fracture behavior.

5.3 Two dimensional case studies

In the open literatures, static creep fracture research is well documented[298-301]. In this group of case studies, the creep fracture behavior of single edge notch (SEN) plate and central cracked panel are analysed. The results on SEN specimens are compared with the test results as reported in the literature[222]. For the ease of collecting data, a layer of fine elements are placed along the anticipated crack propagation path, with numbering starts from the crack tip element. In the following statements, the elements refer to these elements along the anticipated crack extension line, unless otherwise stated. The objective of this group of case studies is to show the validity of the proposed CDM-based constitutive model in simulating creep crack extension through the finite element analysis. The load used in this case study is static.

5.3.1 Creep fracture analysis of central cracked panel

A case study of central cracked thin panel under uniaxial loading of 90 MPa and 650°C is conducted. The geometrical size of the thin panel, the computational domain and the loading conditions are shown in Figs. 5.6–5.7. The finite element mesh and the fine mesh in the crack tip area are shown in Figs. 5.8 and 5.9 respectively. The crack tip fields, the evolution of the crack tip fields, the evolution of the damage pattern around the crack tip area are all checked and recorded, as shown in in the figures attached in Appendices I,J,K,L.

5.3.1.1 Crack extension history

The crack extension history of the plate problem shown in Fig. 5.6 is illustrated in Fig. 5.10. According to the case study results, it takes about 130 Hours for the

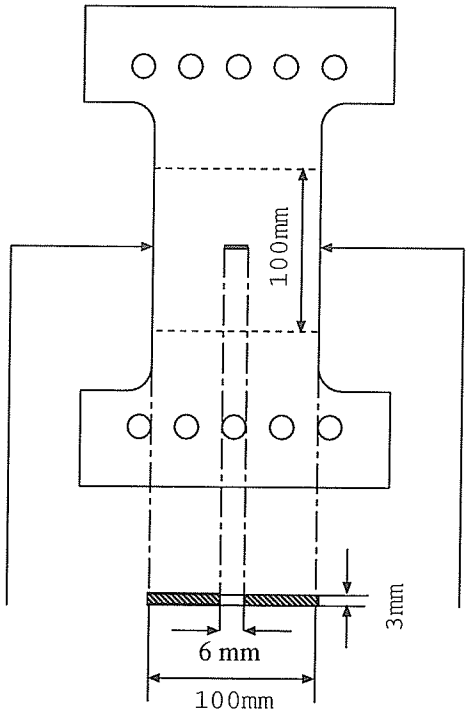

Figure 5.6: The central cracked specimen for the finite element analysis

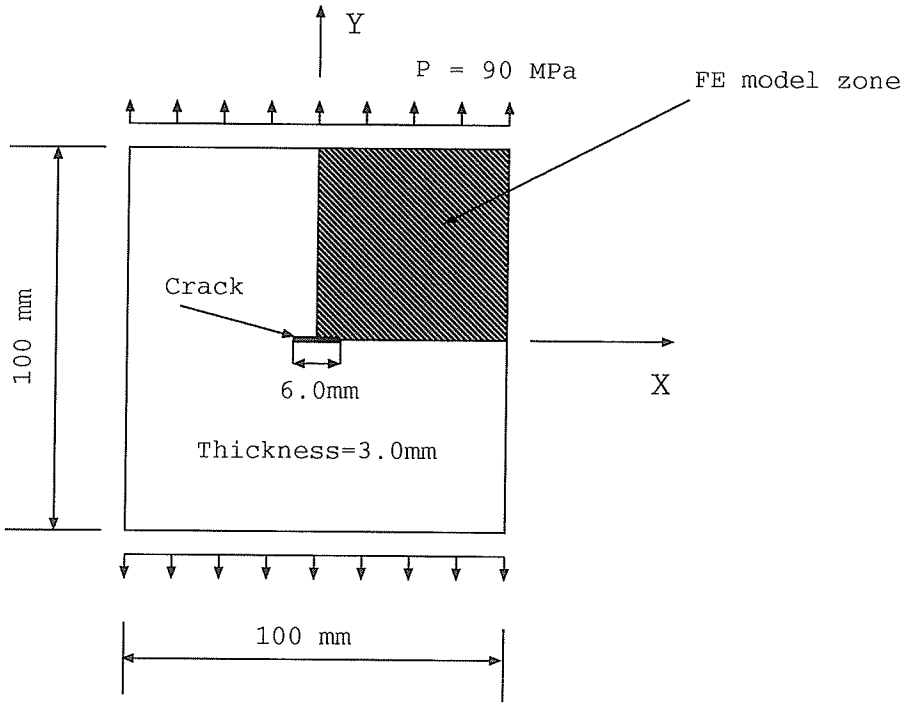

Figure 5.7: Computational domain and mechanical loading pattern for the case study of central cracked panel

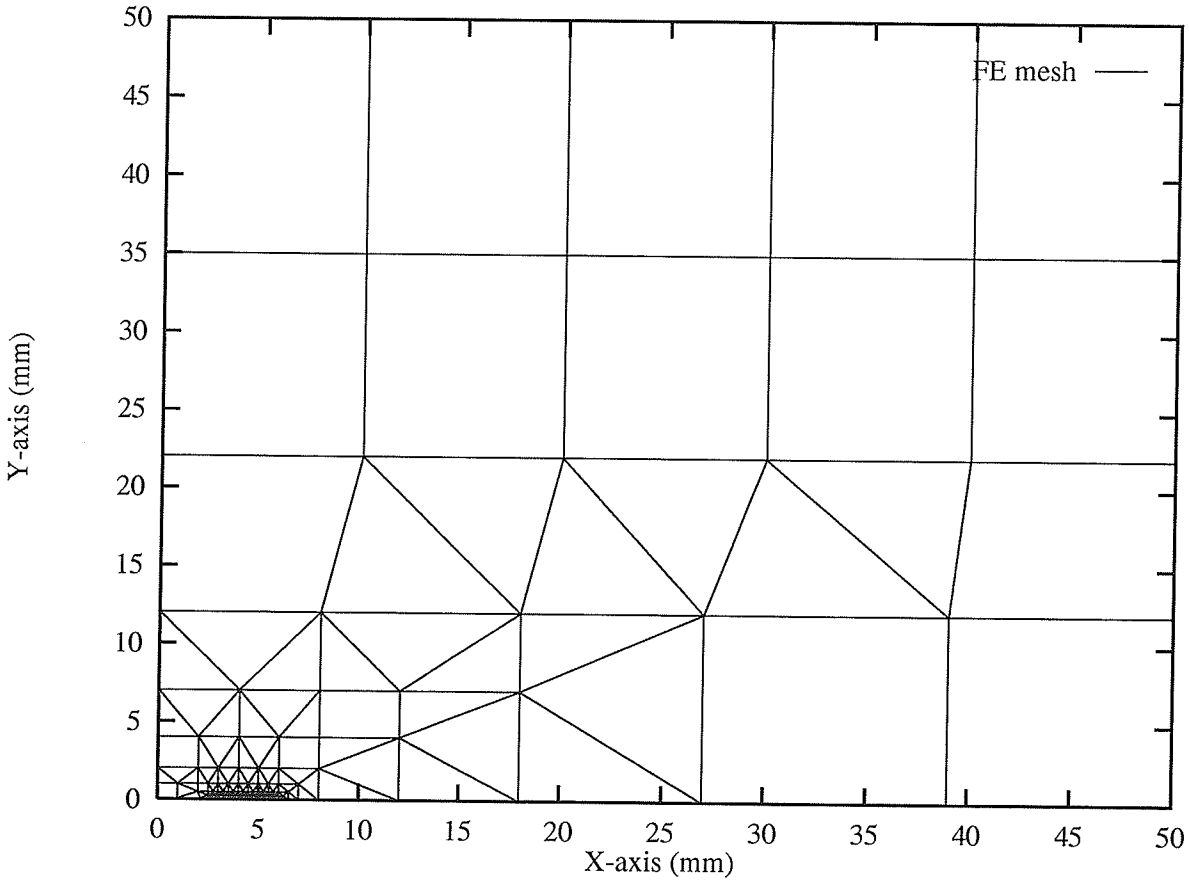

Figure 5.8: FE mesh for the case study of central cracked panel

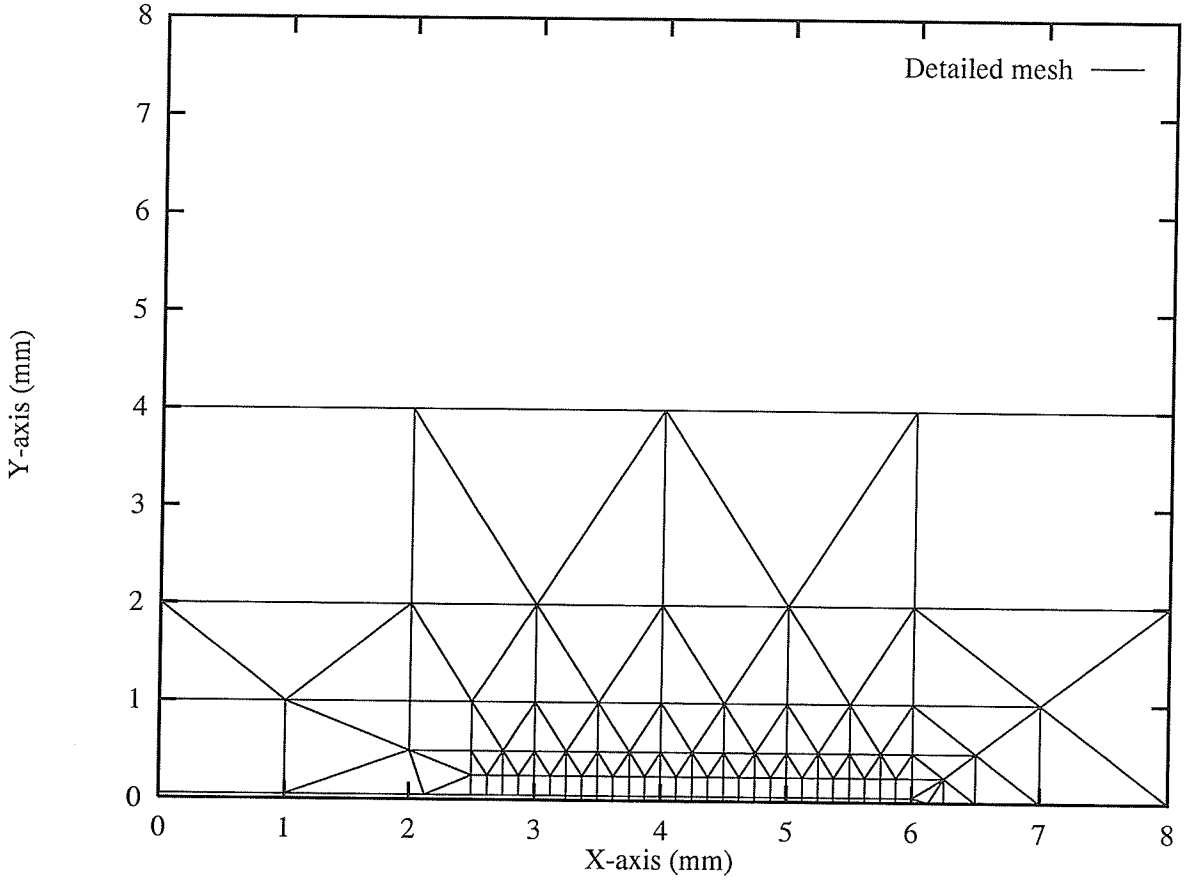

Figure 5.9: Detailed FE mesh in the crack tip region for the case study of central cracked panel

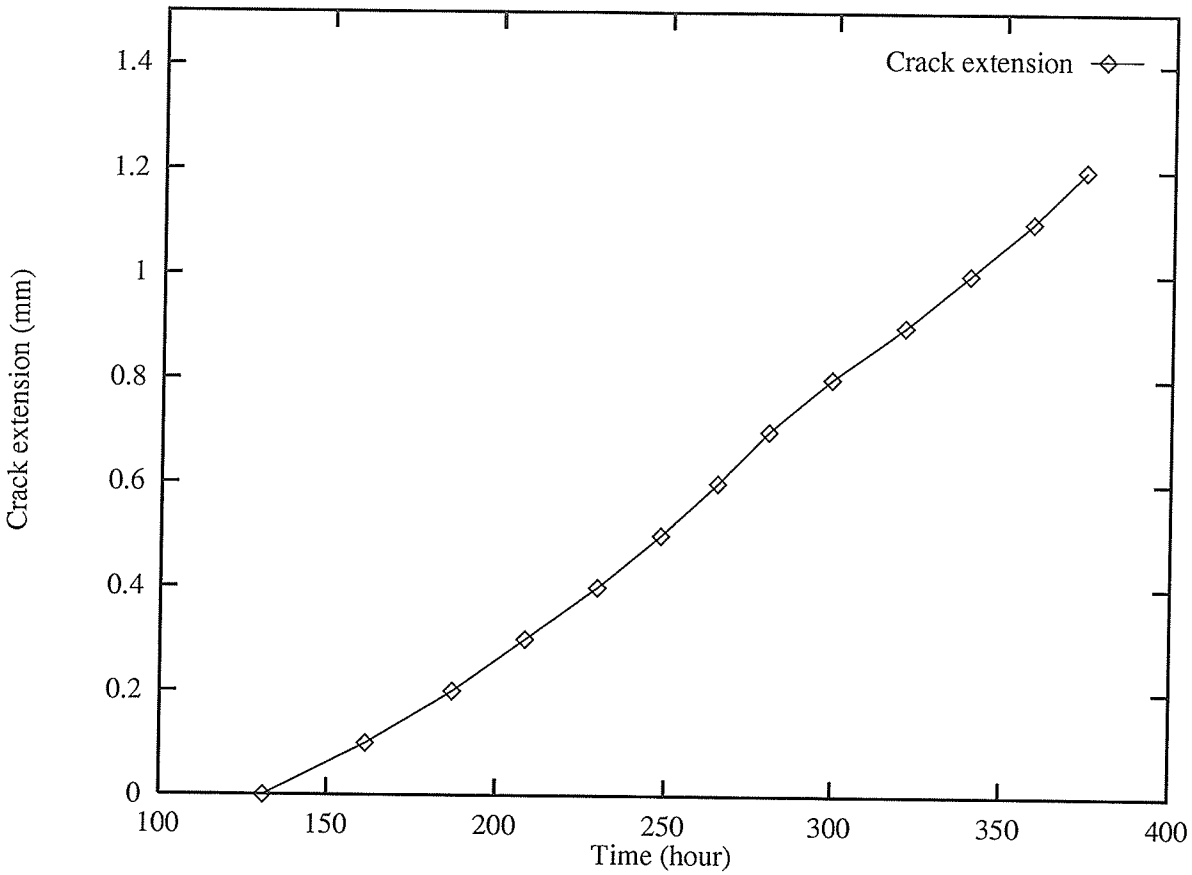

Figure 5.10: The crack extension history

notched thin panel to initiate a crack at the notch end and to begin propagation. It takes another 200 Hours of continuous creep deformation for the crack to extend 1mm in length in one direction. Experimental data are needed to verify the validity of this prediction.

5.3.1.2 The crack tip fields

The creep response and the fracture behavior of a specimen is inherently related to the crack tip fields. The distributions and evolution of the crack tip field variables with time play an important role in the deformation response of the specimen. Hence, the crack tip fields are particularly checked and recorded in this case study. The distributions of these variables around the crack tip area are shown in the figures attached in Appendix I (Figs. I1-I9).

As shown in these figures, when all the thermal and mechanical loads are applied to the panel, there is a large stress concentration in the crack tip region. Correspondingly, the creep strain rate, the damage rate and the effective creep deformation driving stress, etc. are all higher in this region than those in other parts of the material. The creep strain and the damage parameter, as in other points, are not yet developed. However, this situation does not last long. When creep deformation develops, the stress concentration in the crack tip area becomes less severe because of stress relaxation in the crack tip region. Such relaxation is caused by the faster creep deformation in this region than those in the less stressed region of the specimen, i.e., the area away from the crack tip, the deformation in the crack tip region will be restrained by the surrounding area where the creep strain is much less. Consequently, as a result of the condition of compatibility, creep deformation relax the initial stress concentration at the crack tip. The load across the cavitated facet is then shed to the surrounding material, locally reducing the stress until the creep strain becomes compatible with that of the surrounding area. Stress relaxation in the crack tip region causes the damage equivalent stress in the first few elements ahead of the crack tip to drop, and the creep strain and damage to develop rapidly near the crack tip.

The higher damage equivalent stress and the larger effective internal stress can also cause larger creep strain rate and larger damage rate at the same time. So damage in the first few elements which is in the crack tip area develops faster than those in other elements. As the damage develops, the material becomes softer and less creep resistant. When the damage accumulates to certain degree, the material becomes too soft to withstand the damage equivalent stress any more, the damage equivalent stress in these elements will drop fast and the damage will develop in these elements rapidly, and finally cause the elements to break.

As a result of stress relaxation in the crack tip area, the variables, such as the von Mises effective stress, the damage equivalent stress, the internal stress and the difference between the damage equivalent stress and the internal stress all have a

peak value away from the crack tip as shown in the curve corresponding creep time of 161 hours in Figs. I1-I4. This appears contradictory to the fact that the crack tip area has always the highest values of the creep strain rate and damage rate and the largest creep strain and accumulated damage as shown in Figs. I5-I8. But by checking the distribution of the effective creep deformation driving stress $\frac{\tilde{\sigma}-\bar{R}}{1-c_o D}$ (Fig. I9), it is found that the characteristic of the distribution of the effective creep deformation driving stress and those of the creep strain rate and damage rate are same. A peak value of the effective creep deformation driving stress at the crack tip appears reasonable. The fact that the crack tip area has the highest values of the creep strain rate and damage rate and largest creep strain and accumulated damage implies that the impetus for the development of creep strain and damage there is locally higher. Even though the variables have a peak value away from the crack tip, the actual stress exerted on the effective load-bearing cross sectional area of the material, as indicated by the effective creep deformation driving stress is still highest at the crack tip. Here again, it is shown that the effective creep deformation driving stress $\frac{\tilde{\sigma}-\bar{R}}{1-c_o D}$ is the controlling parameter for creep deformation.

Similar results had been found by Chen and Hsu in their analysis of creep fracture using the extended Kachanov-Rabortov model[58-59]. Similar finding was also reported in the area of brittle failure in the Potash Rock. The trend of the distribution of the stress ahead of the crack tip is also the same as found in similar analyses[51,295,341]. According to the results of creep fracture by parameter approach, such as those in which the C^* parameter was used[298-301], there is a stress singularity at the crack tip, characterized by the C^* parameter. The present study indicates that this is not true. Also, the C^* approach suggests that after an initial transient period, the near tip stress field reaches a stable state characterized by the C^* parameter. The stress distribution and its evolution with time which is described in the following section shows that no such stable state can be found when the damage is the material was taken into account.

5.3.1.3 The evolution of the crack tip fields

The evolution of the crack tip field variables at certain points near the crack tip are also checked and recorded. Because of the compatibility, all the variables in the crack tip area change with time. And as a matter of fact, it is these variables in evolution that actually control the creep response and the crack behavior of the material at the crack tip and the whole specimen. The evolution of these crack tip variables at different points in the vicinity of the crack tip show many common features as illustrated in the figures attached in Appendix J (Figs. J1-J9).

As the thermal and mechanical loads are applied to the specimen, the point nearest to the crack tip experiences the highest stress concentration. Hence, the points near the crack tip has a higher creep strain rate and damage rate. They also have the highest rate of development of internal stress. As a result, the internal stress at these points develop quickly towards their respective maximum values. Hence, the effective creep deformation driving stress $\frac{\tilde{\sigma}-\bar{R}}{1-c_o D}$ drops quickly. The damage takes time to develop, and at the beginning of the creep deformation, its effect on creep response and damage development could be ignored. So, by the condition of compatibility of the crack tip area with the surrounding materials, the variables, e.g., the damage equivalent stress at these points are increased so that the trend that the crack tip area has the highest creep strain rate and the damage rate is kept until the material at that point is damaged completely and loses the load-carrying capability. On the other hand, the difference between the damage equivalent stress and the internal stress $(\tilde{\sigma} - \bar{R})$ and the effective creep deformation driving stress $\frac{\tilde{\sigma}-\bar{R}}{1-c_o D}$ in the crack tip area all relax steadily, as shown in Figs. J4 and J9. And again, it is found that the shapes of the creep strain rates and the shapes of the effective creep deformation driving stress are similar, but are different from those of the variables, such as the von Mises effective stress, the damage equivalent stress, the internal stress, etc. This shows the dependence of creep strain rate on the effective creep deformation driving stress.

Another characteristic worth of comment is what happens to the surrounding material when a point of material is broken. When a point of material is in a damage state, its load-carrying capability is reduced. But when it is completely damaged, i.e., the accumulated damage at this particular material point reaches the critical value, it loses its load-carrying capability completely. The load previously carried by this point is then shed to the surrounding material. And for the surrounding materials, it is like an exertion of load on the point of the damaged material. The surrounding materials hence experience a sudden increase of stress, which in turn causes sudden increase of creep strain rate and damage rate, too. This effect is also reflected in the development of the creep strain and the damage parameter. To show this characteristic more clearly, the results of the evolution of these variables for the sixth element are plotted separately, as shown in the figures attached in Appendix K (Figs. k1-k2). There is one feature to be noted from these figures, i.e., the failure of an element is a local phenomenon. Only the material very close to it is affected. For instance, when the first element is broken, there are no significant changes in the states of the variables in the sixth element. But when the fifth element is broken, the variables in the sixth element change drastically. Also, the crack tip element has a faster rate of stress relaxation than other elements. The creep strain rate and the damage rate are all higher near the crack tip than in other parts of the specimen.

5.3.1.4 The evolution of the crack face profile

The evolution of the crack face profile with creep time is also checked and illustrated in Fig. 5.11. The shapes of the crack profile are very similar to the results published by Hsu and Zhai[155] and Nakagaki and Atluri[253]. Before the crack extension, the crack tip is blunted. The crack tip blunting is clearly shown in the figure. This is the case before and after the crack first propagates. It could also be observed that the growing crack is sharper than the stationary crack before the crack propagation. These results confirm the observation made by Taira et al[323] and by Hsu et al[154-155]. These curves also show that both COD and CTOA (Crack

Tip Opening Angle) are not constant before the crack propagation. Hence, when damage is included in the analysis, the COD and CTOA criteria in predicting crack growth could not be used.

5.3.1.5 The evolution of damage pattern of the crack tip area

The damage pattern of the crack tip area evolves with time. This is shown in the figures attached in Appendix L (Figs. L1-L4). It can been seen from these figures that damage of the material develops and accumulates progressively. And the damage is confined only to small area around the crack tip, or the damage process zone. This is reasonable because the crack tip region is the highly stressed area which in turn produces larger creep strain and damage. As indicated in the proceeding sections, this area also has the highest creep strain rate and damage rate. In the regions away from this small area, the damage is so low (e.g., less than 0.02) that its effect on creep response and the damage development can be neglected.

5.3.2 Creep fracture analysis on single edge notch (SEN) specimen[222]

The SEN specimen as used in the literature[222] is analysed. Two case studies are conducted. The loading and the notch size of the specimen correspond to those of the specimen No. 4 and No. 10, respectively, in the literature, i.e., $a/W = 0.38, 0.34$ and $P = 9189, 12070(N)$ were used in the analysis[222]. Shown in Figs. 5.13 and 5.14 are the finite element discretization and its details around the crack tip area for the finite element analysis. For the two case studies, the meshes are identical except a small shift of the detailed mesh which corresponds to the slight difference in the specimen shape and size. The load is static and is applied by concentrated force.

Shown in Figs. 5.15 and 5.16 are the calculated crack extension histories and experimental measurements[222] of the specimen No. 10 and No. 4 respectively. As

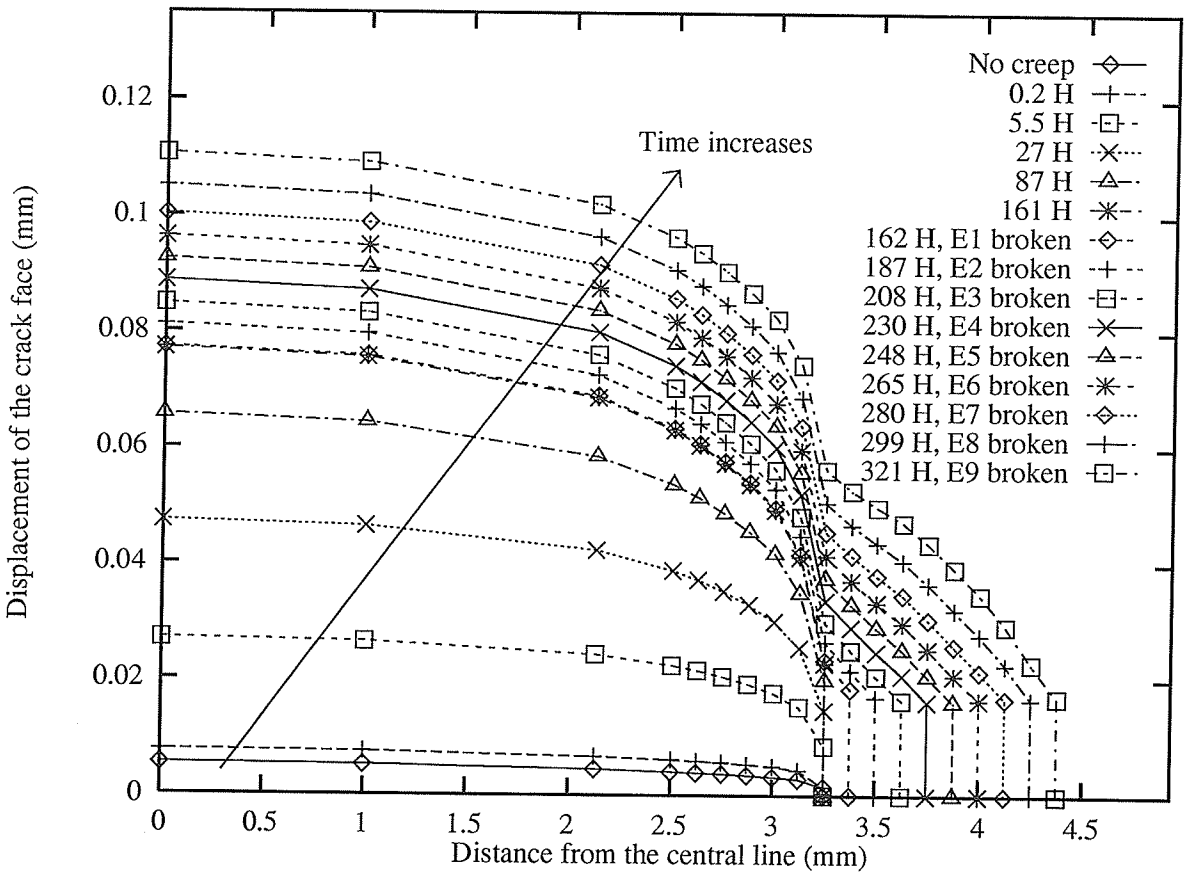

Figure 5.11: The evolution of the crack face profile

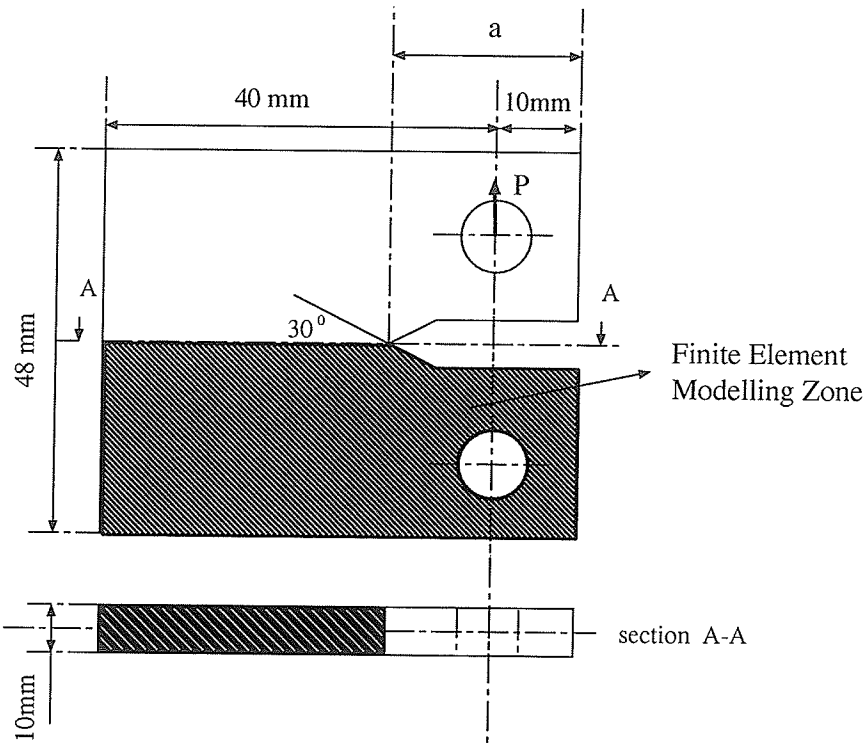

Figure 5.12: The SEN specimen for the finite element analysis[222]

can be seen, there is a gap between the experimental measurement and the finite element prediction using the proposed CDM-based constitutive model in the case of specimen No. 10. But the crack extension rate, i.e., the slopes of the curves match well. In the case of specimen No. 4, the agreement is better. And the theoretical prediction based on the CDM model is much better in comparison with those calculated results based on load parameters no matter it was based on the primary creep or stationary creep laws[222].

Possible reasons for the discrepancies in the results for the theoretical prediction and the experimental measurements may be attributed to the following: In the finite element analysis, the physical parameters, such as the Young's modulus, the initial yield stress, etc., are based on the measured value at $650°C$, while the experiments were conducted at $600°C$. This may have introduced certain errors in the results. The selection of the critical damage value, D_c to be 0.5 is an arbitrary one based on what is suggested by some researchers[200-204]. For different materials, different

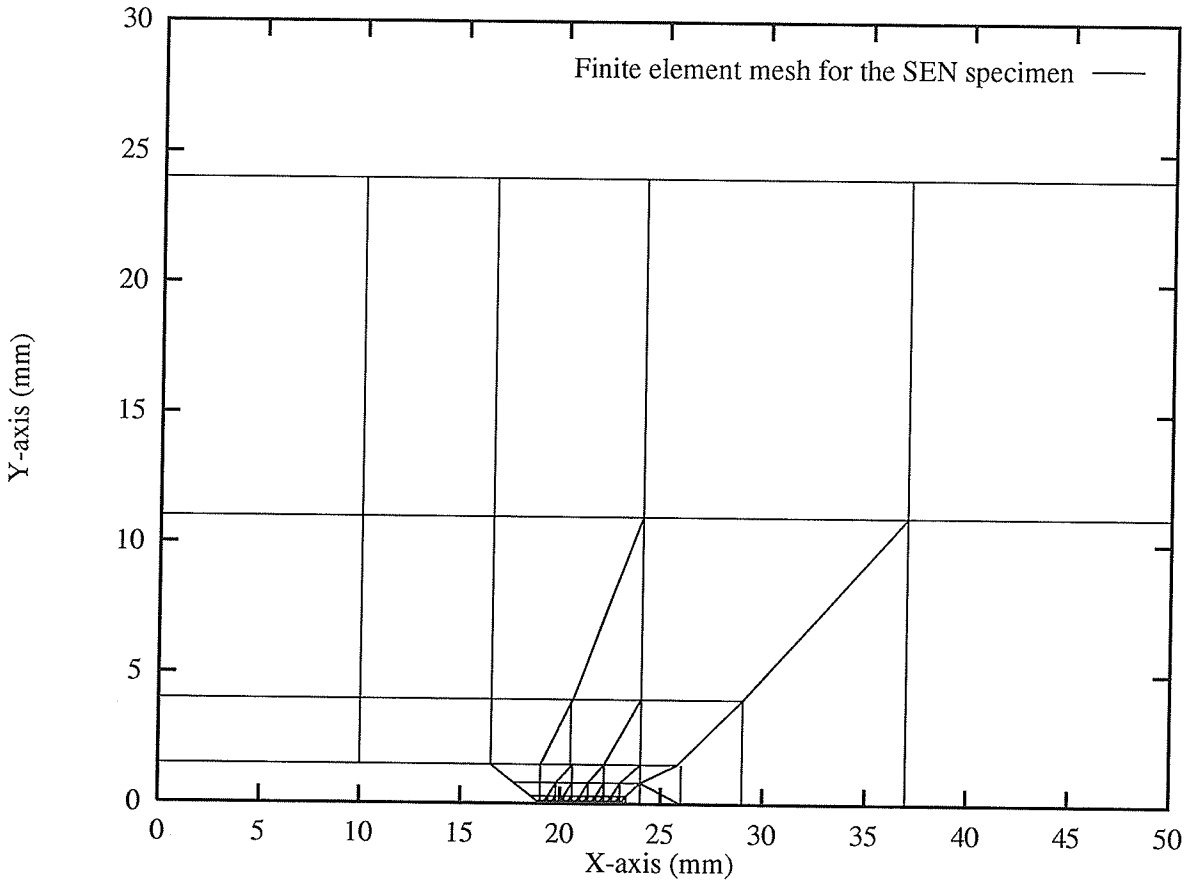

Figure 5.13: The finite element mesh for the SEN specimen

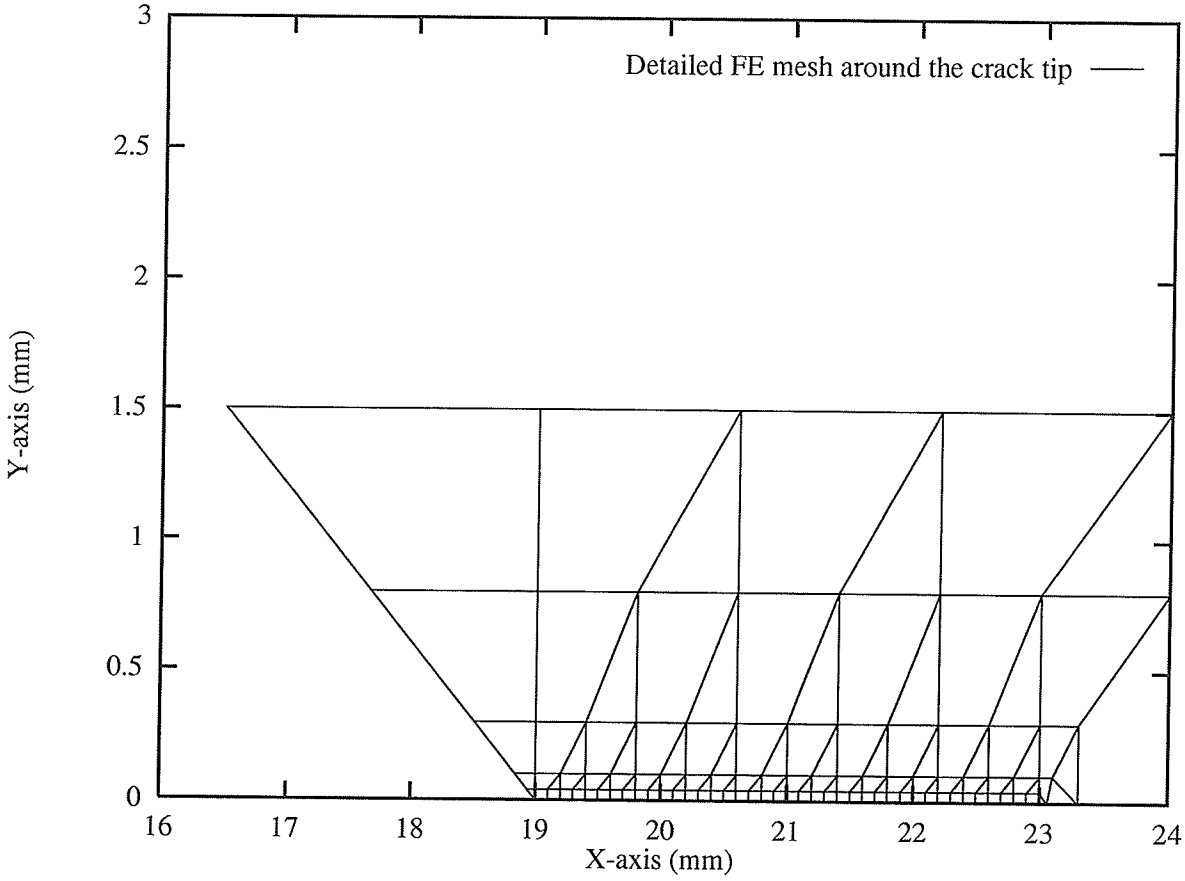

Figure 5.14: The detailed finite element mesh around the crack tip area for the SEN specimen

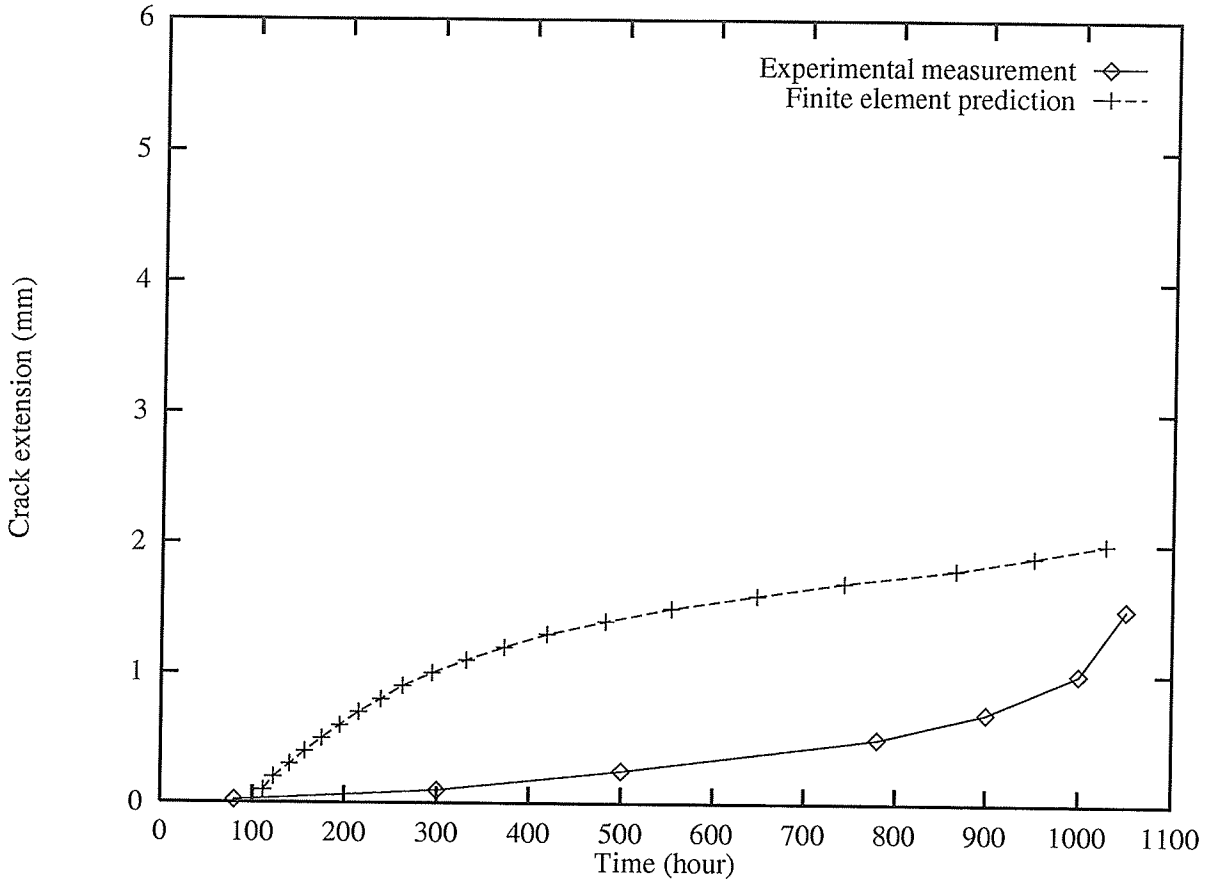

Figure 5.15: The crack extension history of specimen No. 10[222]

specimen geometries and different loading conditions, this critical damage value needs to be further evaluated. In the analysis, the plane stress assumption was used. According to the geometries of the specimen as shown in Fig. 5.12, the problem in consideration is certainly not an 'ideal' plane stress one.

The results of this group of case studies show that the proposed CDM-based constitutive model is suitable for creep crack extension analysis.

5.4 Summary

According to the case studies, it could be concluded that the proposed CDM-based constitutive model reflects the major features of the creep deformation. The various influencing factors, such as load cycling effect, load dwell time effect and interaction between creep damage and HTLCF damage could be reflected by the

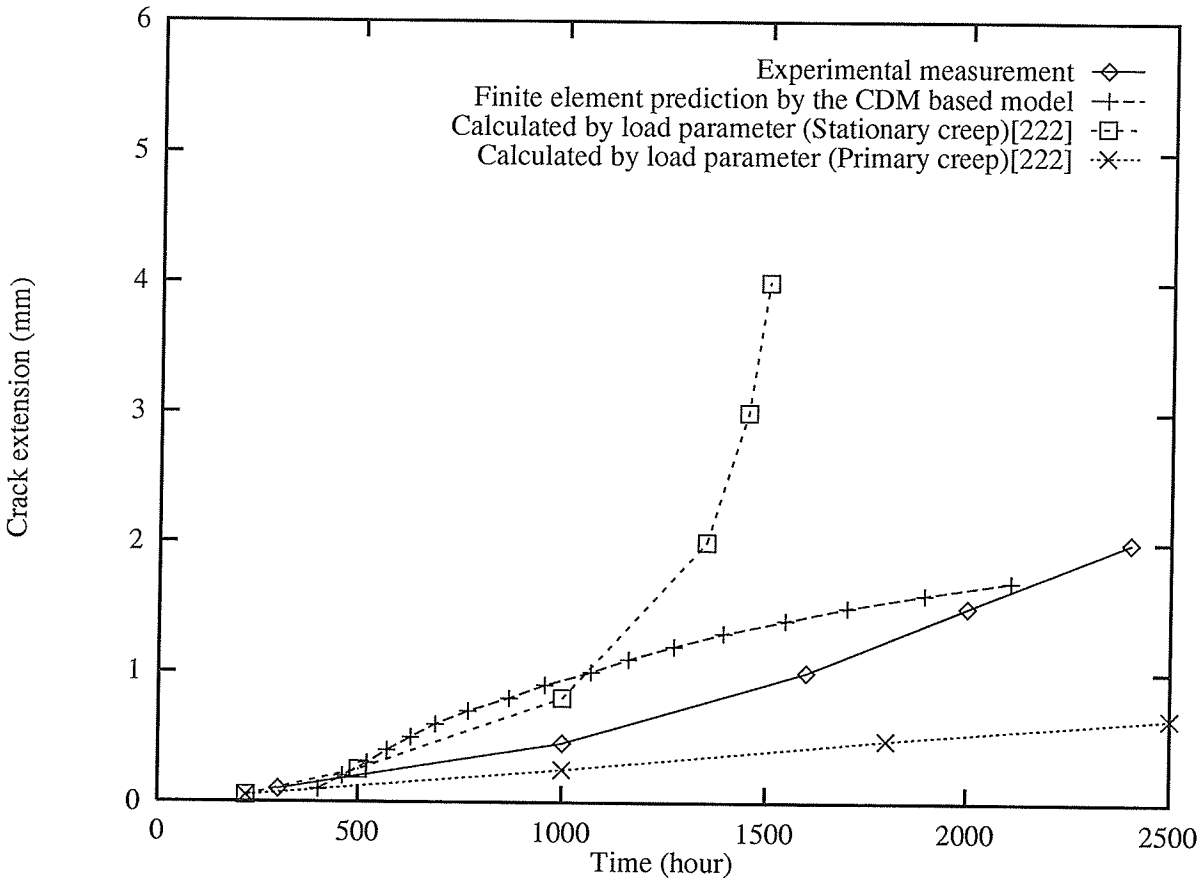

Figure 5.16: The crack extension history of specimen No. 4[222]

model. The trends of the distribution and evolution of the variables, such as the damage equivalent stress in the crack tip region is consistent with the finding of other researchers. Therefore, it is appropriate to use the proposed CDM-based model to describe the creep response and crack behavior.

Chapter 6

The effect of loading history on cyclic creep fracture

As having been pointed out earlier, the nonlinear response of materials such as creep deformation can be different under different loading pattern. For example, the HTLCF response of a material with pre-exposure to creep deformation is different from those of virgin materials[116-118] and vice versa[161]. If different loading processes such as load holding time, load dwell time and load cycling process are involved within one load cycle, the damage caused by different loading processes accumulates within a load cycle. And the damage further amasses due to the succession of these loading cycles. Consequently, the stresses in the crack tip area are continuously being redistributed in these process or by these factors. Hence, the sequential creep response and the fracture behavior of the solid with different loading histories would be different and the operation lifetime of the component is affected.

Attempts have been made in establishing a multiaxial Mechanical Equation Of States (MEOS), analogous to the Equation of State for a perfect gas[115]. Material constants in the MEOS would be calculated from the creep behavior of the material in comparatively simple laboratory experiments. Once calibrated for a specific material, the MEOS could then be used to predict the amount of deformation which is produced in an engineering component by the anticipated service stress versus time and temperature versus time history. However, such attempts had not

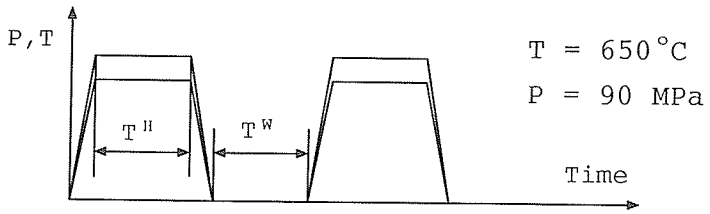

		Holding time T^H (Hours)		
		24	40	infinite
Dwell time T^W (Hours)	0			X
	40	X	X	
	70	X	X	

Figure 6.1: The thermal and mechanical loading patterns and the simulation of loading histories in the case studies

yielded the desired results. At least part of the reason is due to the nature of the problem itself. The laws of thermodynamics are expressed in terms of quantities that depend only upon the thermodynamic state of a system and not upon the processes by which that state is reached. The rate of transient creep of a metal, however, depends not only upon the values of the stress, strain and temperature at the moment the creep rate is measured, but also on all the past histories of these quantities, i.e., upon the entire history of loading and deformation. This shows that it is very important to investigate the loading history effect upon material's creep response and crack behavior and its influence upon the operation lifetime of a component[32,54,85,97,109,172-173,184,305,326,330,327,349].

In this chapter, a research effort is presented to reveal the loading history effect on creep response and crack behavior and its influence upon the operation lifetime of a component. The loading history is simulated in this thesis study by the different combinations of the load holding time and the load dwell time, as shown in Fig. 6.1. The specimen size and the finite element mesh are those of the central cracked panel used in the two-dimensional case study reported in the proceeding chapter.

There is considerable interest in the high temperature mechanical performance of 316 stainless steel because of its application in several high temperature structural components of advanced reactors[44,78,131,174,186,212,217,222,229,346-348]. Therefore, extensive mechanical testing of this material has been conducted in the temperature range of 427^oC to 650^oC (800^oF to 1200^oF) and reported in open literatures. In that temperature range, the microstructure of the material changes, e.g., the carbides had been coarsened and the creep resistance of the material had dropped accordingly. However, only limited data is available on the creep crack growth behavior of this material. In this thesis research, creep deformation and crack behavior of a cracked thin panel made of 316 stainless steel with temperature reaching 650^oC is studied through case studies.

6.1 Influencing factors on cyclic creep fracture

As being pointed out in the proceeding chapter, the cyclic loading, load dwell time and interaction between creep damage and HTLCF damage have important influence upon the cyclic creep fracture behavior. When crack is involved, the creep fracture behavior becomes complicated because the crack tip area has severe stress concentration. The stress distribution in the crack tip area evolves as the creep deformation proceeds. There is also redistribution of stress by influencing processes or factors. Because creep response and damage development of the cracked thin panel are all attributed to the stress state around the crack tip area, these influencing factors are expected to change the creep deformation response, damage development and hence the fracture behavior of the cracked thin panel significantly.

To show the importance of these factors, the static creep deformation is interrupted at different times (e.g., when the static creep time is 30 hours and 150 hours, respectively) which correspond to different stages of creep deformation and different degrees of damage of the crack tip material (the damage of the crack tip element is 0.18 and 0.45, respectively and there is no crack extension yet). Changes of the

crack tip field variables are checked after each of such influencing processes, and their influence are hence determined by analyzing these changes. The long term effect of these processes or factors are also determined by checking the evolution of the crack tip field variables certain time after the load cycling event, e.g., 10 hours later.

The crack tip field variables checked in this group of case studies include von Mises effective stress, damage equivalent stress, internal stress, difference between damage equivalent stress and internal stress ($\tilde{\sigma} - \bar{R}$), creep strain rate, creep strain, damage parameter, damage rate and effective creep deformation driving stress $\frac{\tilde{\sigma}-\bar{R}}{1-c_o D}$.

6.1.1 Load cycling effect on cyclic creep fracture

As a comparison, results of crack tip field variables after a load cycling event without load dwell time and the evolution of these variables 10 hours later are plotted together with corresponding results of static creep deformation. These are shown in the figures attached in Appendix M (Figs. M1-M18). As can be seen from these figures, the load cycling process has significant influence upon the crack tip fields and their evolution.

Just after the load cycling event, the relaxed stresses at the crack tip elements are 'rejuvenated' by the load cycling process. But the changes of the stresses are confined to a very small area around the crack tip. The stresses away from this area are not influenced (Figs. M1-M4 and M10-M13). The enhanced stresses of the crack tip elements dictate higher creep strain rates (Figs. M5 and M14) and higher damage rates (Figs. M8 and M17) of the crack tip material. Also, the load cycling process introduces certain amount of damage to the material directly. The higher the stress, the more damage introduced to the material in the load cycling process. This is because the HTLCF damage is highly dependent upon the loading level. Higher stress produces higher strain increment in one load cycling event which implies more damage to the material. Hence, after one load cycling event,

the damage distribution around the crack tip is changed which are shown in Figs. M7 and M16. However, it takes time for the creep strain to develop. Therefore, the creep strain distribution at the crack tip is not immediately changed by the load cycling process.

The long term effect of the load cycling process is also checked by comparing the distributions of the crack tip field variables 10 hours after the load cycling event without load dwell time and the corresponding results of static creep deformation at that time. It is found that even though the stress redistribution is significant immediately after the load cycling event without load dwell time, the distributions of these variables are almost back to the same as the results of the static creep deformation except small difference in the crack tip area after 10 hours of creep deformation. The effective creep deformation driving stress $\frac{\tilde{\sigma}-\bar{R}}{1-c_o\bar{D}}$ with the load cycling event is still higher in the crack tip area than the corresponding values of the static creep deformation. But the difference of damage distribution around the crack tip area is still there and the difference is becoming larger because the damage rate with the load cycling event is higher than the corresponding value of the static creep deformation ever since the load cycling event. The creep strain is also higher 10 hours after the load cycling event than the corresponding static creep strain. This is more obvious in the case when the load cycling event happens at the creep time of 150 hours. This is because in the case when the load cycling event happens at the creep time of 150 hours, the material (especially in the crack tip area) is highly damaged already (the damage parameter of the crack tip element is 0.45). A load cycling event introduces more damage to the material directly which in turn produces higher damage rate and higher creep strain rate. Hence, it can be concluded that the long term effect of the load cycling event without load dwell time is an introduction of certain amount of damage to the material directly, enhancement of damage rate and creep strain rate, and therefore higher damage value and higher creep strain in the crack tip area.

There are several points which need to be emphasized about the stress distribution around the crack tip area just before and after the load cycling event. These are illustrated in Figs. M1-M4, M9-M14 and M18. It is seen in these figures that after the load cycling event, there are still higher stress in the crack tip elements as if the relaxed crack tip stresses are rejuvenated. But the amplitude of the stresses at the crack tip is lower than the concentrated stresses experienced by these elements when the material is in a virgin state, i.e., when the creep time is zero and the damage parameter of the crack tip elements are zero (Refer Figs. I1-I4 and I9). This is because the material has experienced creep deformation and certain degree of damage have been accumulated within the material before the load cycling event happens. The material has become softer and less creep resistant. Therefore, the stress concentration is less severe in the damaged crack tip material than the virgin material. And the higher the damage of the crack tip material, the flatter the crack tip stress distributions, as shown in these figures. These figures correspond to two damage stages of the crack tip material (Figs. M7 and M16) before the load cycling event happens.

Another reason for the flatter crack tip stress distribution after a load cycling event as compared to the corresponding stress distribution of the virgin material is the residual stress experienced by the crack tip material during the load cycling event. As shown in the figures attached in Appendix N (Figs. N1-N8), when the load is removed from the specimen completely, the crack tip area is actually under compression. This is reasonable because the stress of the bulk material away from the crack tip is actually in elastic range while the material around the crack tip has experienced plastic and creep deformation. When the load is removed, the bulk material would contract and deform by the Hooke's law and the deformation can be recovered completely. But the crack tip material has experienced large scale permanent deformation and could not be completely recovered. The contraction of the surrounding bulk material exerts certain stress on the crack tip material. Hence, the crack tip material is under compression when the load is removed completely

from the specimen. This is the case for the two normal stress components parallel and perpendicular to the direction of the applied load and for the two damage stages of the material as shown in these figures.

This also accounts for the shapes of the stress distributions after the load cycling event. While the stresses in the crack tip elements increase, the stresses a little away from the crack tip drop and the stresses in the elements further away from the crack tip are slightly affected. This is the situation for the two load cycling events. The explanations for such a phenomenon are as follows: When the load is applied again, the stress distribution at the crack tip region is based on the residual stress state when the load is removed completely but not based on a plain stress state. Hence, the new stress state is a superposition of the residual stress and the stress of the damaged material under reloading. In the crack tip area of the damaged material, there is still stress concentration after reloading. So, even though there is compressive residual stress there, a resultant higher stress at the crack tip is still obtained. This stress is higher than the stress value of the crack tip material before the load cycling event but lower than the initial concentrated stress. So the crack tip stress is 'rejuvenated'. For the material a little away from the crack tip, the residual stress is higher and the stress caused by reloading is lower than those at the crack tip. Hence, a resultant lower stress is obtained. This stress is lower than its corresponding stress before the load cycling event. For the material further away from the crack tip, the residual stress is positive and small, the resultant stress is very close to the corresponding stress before the load cycling event. Hence, the load cycling event changes the stress distribution of the crack tip material significantly.

Another phenomenon to be noted is that after certain time of creep deformation, the plastic zone is actually away from the crack tip. And the damaged crack tip material is actually in an elastic stressing state. The initially concentrated stress in the crack tip area has been relaxed progressively if not interrupted by the load cycling event. This is the same trend observed by other researchers[56-59,135-140,189-193]. But if the load is cyclic, the crack tip is again surrounded by a plastic zone after

the load cycling event, as seen in these figures. And the 'rejuvenated' stress in the crack tip area dictates higher creep strain rate and higher damage rate which result in an earlier failure of the crack tip material and shorter operation lifetime. It can be seen from these figures that in the static loading case, the crack tip stresses continually decrease due to stress relaxation. In the cyclic loading cases, however, the stress relaxation at the vicinity of the crack tip is frequently interrupted by the unloading and reloading. After each load cycling event, the crack tip stress increases significantly and then the stress relaxation restarts from a new stress level. As a consequence, the crack tip stresses in the cyclic loading cases are always higher than those under static loading. This is actually the reason why cyclic loading is more detrimental to the material than static loading.

6.1.2 The dwell time effect on cyclic creep fracture

To show the importance of load dwell time effect on cyclic creep fracture, results of crack tip field variables after one load cycling event with and without load dwell time are plotted together. These are shown in the figures attached in Appendix O (Figs. O1-O18). The length of the load dwell period is 60 hours in these case studies. The load dwell time also shows important influence upon the distribution of crack tip field variables after the load cycling event. But unlike the load cycling effect, which is confined only to a few elements in the crack tip area, load dwell time effect is shown in a wider range. Again, the stress at the crack tip is rejuvenated in the case of cyclic loading with load dwell time, but the extent is not as high as the one under cyclic loading without load dwell time (Figs. O1-O4, O9-O13 and O18). Such observations are more obvious in the case when the load cycling event happens at the creep time of 150 hours. This is because the material at the crack tip becomes softer during the load dwell time which is indicated by a decrease of the maximum internal stress (Figs. O3 and O12). Hence, the stresses in the crack tip area have a lower extent of rejuvenation after a load cycling event with dwell time

because of the decrease in material's load-carrying capability. And by equilibrium of forces at the crack tip, the stress a little away from the crack tip is increased. Hence, the stress ahead of the crack tip is also redistributed by the load dwell time effect. The creep strain rate and the damage rate change accordingly. But the creep strain and the damage parameter are unchanged during the load dwell time. This is reasonable because during the load dwell period, the impetus for the development of creep strain and the damage parameter are removed. The only change to the material is some kind of microstructural rearrangement which is reflected by the change of the maximum internal stress after the load cycling event. So, even though the crack tip field variables, such as stress, damage rate and the creep strain rate are changed during the dwell period, the creep strain and the damage parameter are not affected (Figs. O6-O6 and O15-O16).

The long term effect of the load dwell time is also checked. This is done by comparing the distribution of the crack tip field variables immediately after the load cycling event and the results after 10 hours into the creep deformation and their corresponding results without load dwell time. The crack tip field variables of cyclic loading with load dwell time is again plotted together with the corresponding results of cyclic load without load dwell time, which are also shown in Figs. O1-O18. It is seen in these figures that after 10 hours of creep deformation following the load cycling event, the stress distributions induced by cyclic loadings with and without load dwell time are different. This shows the importance of the load dwell time effect. The stresses with load dwell time are lower than those without load dwell time (Figs. O1-O3 and O10-O12). However, the difference between damage equivalent stress and internal stress $(\tilde{\sigma} - \bar{R})$ and the effective creep deformation driving stress $\frac{\tilde{\sigma}-\bar{R}}{1-c_o D}$ at the crack tip are all higher than the corresponding results of cyclic loading without load dwell time (Figs. O4, O9, O13 and O18). This is also the situation of the creep strain rate and the damage rate (Figs. O5, O8, O14 and O17). The creep strain and damage parameter also show different distribution

even though the difference is small. As shown in Figs. O6-O7 and O15-O16, the creep strain and the damage parameter of cyclic loading with dwell time are higher than those corresponding results of the cyclic loading without load dwell time. This shows that the load dwell time effect appears to be detrimental to the material, just as the load cycling effect. Hence, the load dwell time effect should be considered for complete cyclic creep fracture analysis. According to the results of the one dimensional case studies presented in the proceeding chapter, the significance of the load dwell time effect is more obviously shown after several load cycles. Also, the load dwell time effect is shown only after a long dwell time. Short dwell time does not provide enough time for the material to experience microstructural changes.

6.1.3 Importance of interaction between creep damage and HTLCF damage on cyclic creep fracture

To show the importance of interaction between creep damage and HTLCF damage on creep response and fracture behavior, results of the distribution of crack tip field variables after one load cycling event with and without consideration of the interaction in the calculation, and the evolution of these variables after 10 hours of creep deformation are plotted together. These are shown in the figures attached in Appendix P (Figs. P1-P18). Through these figures it is observed that the interaction between creep damage and HTLCF damage does not change the crack tip stress fields after the load cycling event. But by considering the interaction between creep damage and HTLCF damage in the calculation, creep strain rate and damage rate are increased immediately after the load cycling event, and damage pattern around the crack tip is updated just after the load cycling event. This is because that the interaction between creep damage and the HTLCF damage tends to weaken the material and to increase the total accumulated damage. Though the interaction between creep damage and HTLCF damage does not change the distributions of the crack tip field variables very much, its effect on creep response and the fracture

behavior should not be underestimated, because its significance could be shown with the elapse of time. For checking this, the results of the crack tip variables with and without consideration of the interaction after 10 hours of creep deformation after the load cycling event are recorded and plotted together as seen in these figures.

As shown in these figures, the long term effect of the interaction between creep damage and HTLCF damage on creep response is significant. By considering the interaction, not only the damage pattern around the crack tip area is updated, but also the stress fields and the damage rate are changed in the crack tip area after 10 hours of creep deformation following the load cycling event. The effective creep deformation driving stress is higher in the case considering the interaction than those without considering the interaction. In other words, the impetus for creep deformation is higher by considering the interaction. This is because the introduction of the interaction increases the accumulated damage of the crack tip material, and hence the stress on the remaining lattice of the cavitated material is higher. It is noted that the difference of the accumulated damage in the crack tip area is significant with and without considering the interaction. The trend is more obvious in the case when the load cycling event happens at the creep time of 150 hours. Therefore, for complete cyclic creep fracture analysis, the interaction between creep damage and HTLCF damage should not be ignored.

6.2 Evolution of the crack face profile during the unloading process

The evolution of the crack face profile during the unloading process in a load cycle is also checked. Shown in Figs. 6.2-6.3 are the results of the crack face displacement during an unloading process when the creep time is 87 hours and 327 hours respectively, which correspond to the cases when the crack tip element has the accumulated damage of 0.28 without crack extension and the case with the crack tip has extended near 1 mm. Two features could be observed from these figures:

- There is no crack closure when the load is completely removed. This is probably because that the permanent strain in the crack tip area is so high that the displaced crack face could not recover to its original place by the removal of load;

- The crack tip blunting is reduced but not eliminated when the load is removed. This is the case before and after the crack has propagated.

Similar results on crack extension analysis were obtained by Nakagaki and Atluri[253].

6.3 Direction of crack extension

Another finding of the case studies is that with the CDM model and the finite element analysis, the direction of crack extension is automatically determined. This is an advantage of the CDM method in creep fracture analysis. Because under creep deformation condition, there is no existing theories to predict accurately the direction of the crack extension. And the conventional fracture mechanics methods provide no feasible and accurate approach for such analysis.

It is found that the crack initiates and grows in the element with the fastest rate of damage accumulation. Once the accumulated damage in an element reaches the critical value, it is assumed that the element is broken and the crack tip moves one element ahead. The extended crack length is the locus of the damaged elements. These are special case of the criteria developed by Chow et al[68] for predicting crack growth direction using the CDM theory and the finite element method, which is stated as follows:

Two fracture criteria are required to determine the threshold conditions of crack initiation and postulated:

1. A crack propagates in the direction of maximum effective damage equivalent stress $\tilde{\sigma}$ around the crack tip, and

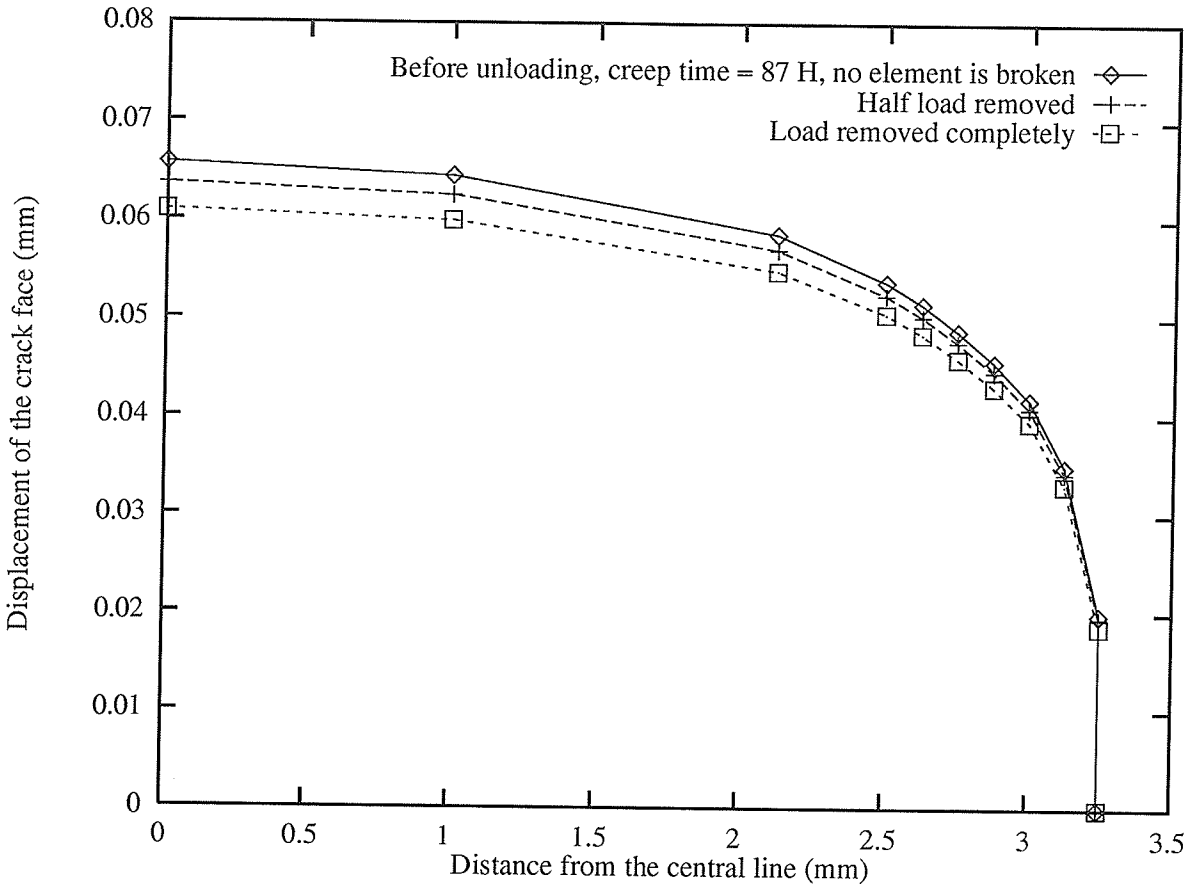

Figure 6.2: The evolution of crack face profile during a unloading process when the creep time is 87 hours

2. The threshold condition for ductile fracture is satisfied when the overall damage D in an element at the prospective direction of fracture reaches its critical value, D_c.

6.4 The loading history effect on cyclic creep fracture

Case studies corresponding to different loading histories as shown in Fig. 6.1 are conducted to show the importance of the loading history effect upon cyclic creep fracture behavior. According to the case study results, with different loading histories, the creep response and the crack behavior (the incubation time for a crack to propagate and the subsequent crack extension rate) of the cracked thin panel are

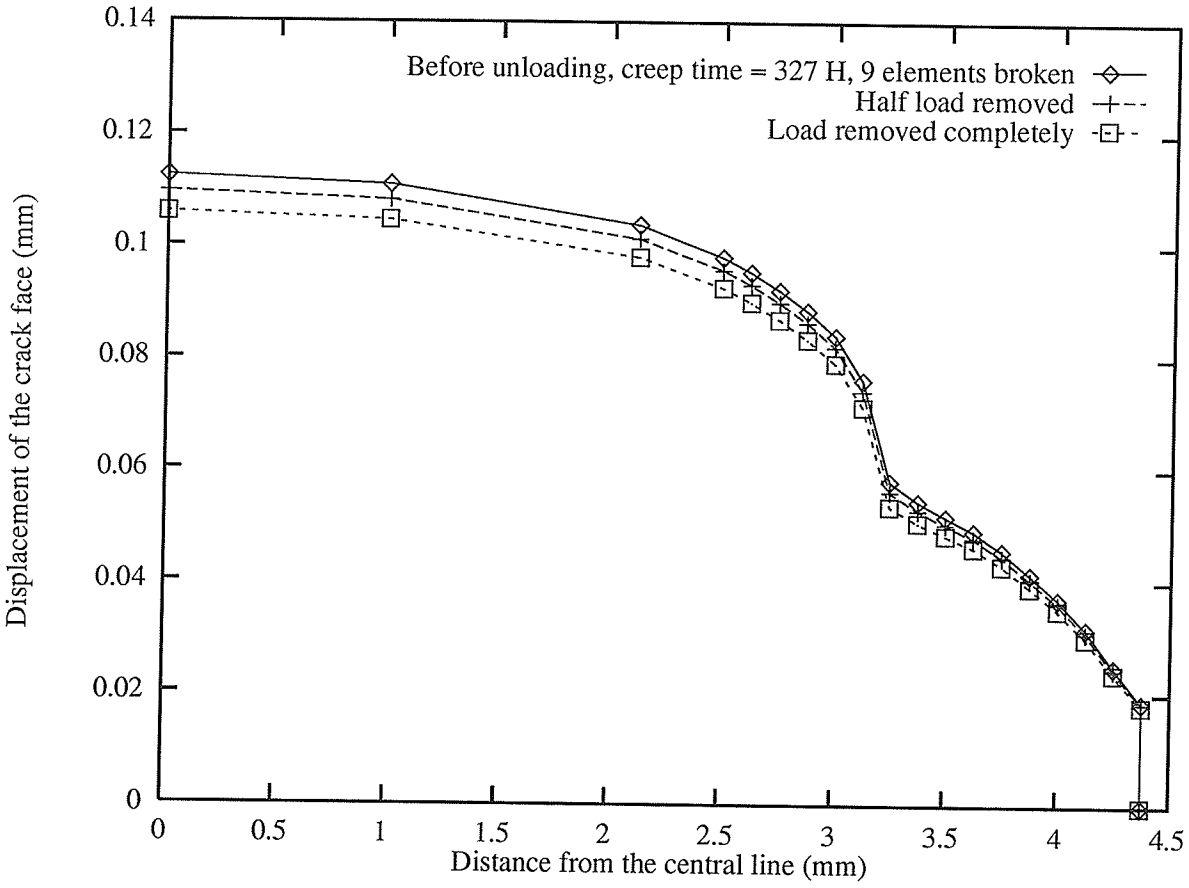

Figure 6.3: The evolution of crack face profile during a unloading process when the creep time is 327 hours and the crack extension is around 1 mm

different.

6.4.1 Crack behavior under different loading histories

Under different loading histories, the crack behavior of a central cracked thin panel is different. Shown in Figs. 6.4-6.7 are the crack extension histories corresponding to four different combinations of loading patterns as shown in Fig. 6.1. Figs. 6.4 and 6.5 correspond to the cases with different load dwell time while the load holding time is kept the same of 24 hours and 40 hours respectively. In each case, the load dwell times of the two cyclic loading curves are 40 and 70 hours respectively. Figs. 6.6 and 6.7 correspond to the cases with different load holding time while the load dwell time is kept the same of 40 hours and 70 hours respectively. In each case, the load holding times of the two cyclic loading curves are 24 and 40 hours respectively. For the ease of comparison, the crack extension history under static loading condition is also plotted with the crack extension results under these cyclic loading conditions. From these figures, it is shown that even though the incubation time of crack propagation change slightly between the different loading histories, the subsequent crack propagation change significantly from case to case. Following are the explanations.

6.4.2 Effect of the duration of load holding time

From Figs. 6.6 and 6.7 it is observed that with different load holding time in one load cycle while other conditions are the same, the crack extension histories are different. The duration of the load holding time actually determines the frequency of the load cycling event. With more load cycling event, the relaxed crack tip stresses have more opportunities of 'rejuvenation' as shown in the proceeding chapter and by other researchers[58-59]. Hence the crack tip stresses under cyclic loading with more frequent load cycling events always have higher values than the loading patterns corresponding to less load cycling events. This is like the comparison between cycling loading and static loading. The static loading could be conceived as cyclic loading

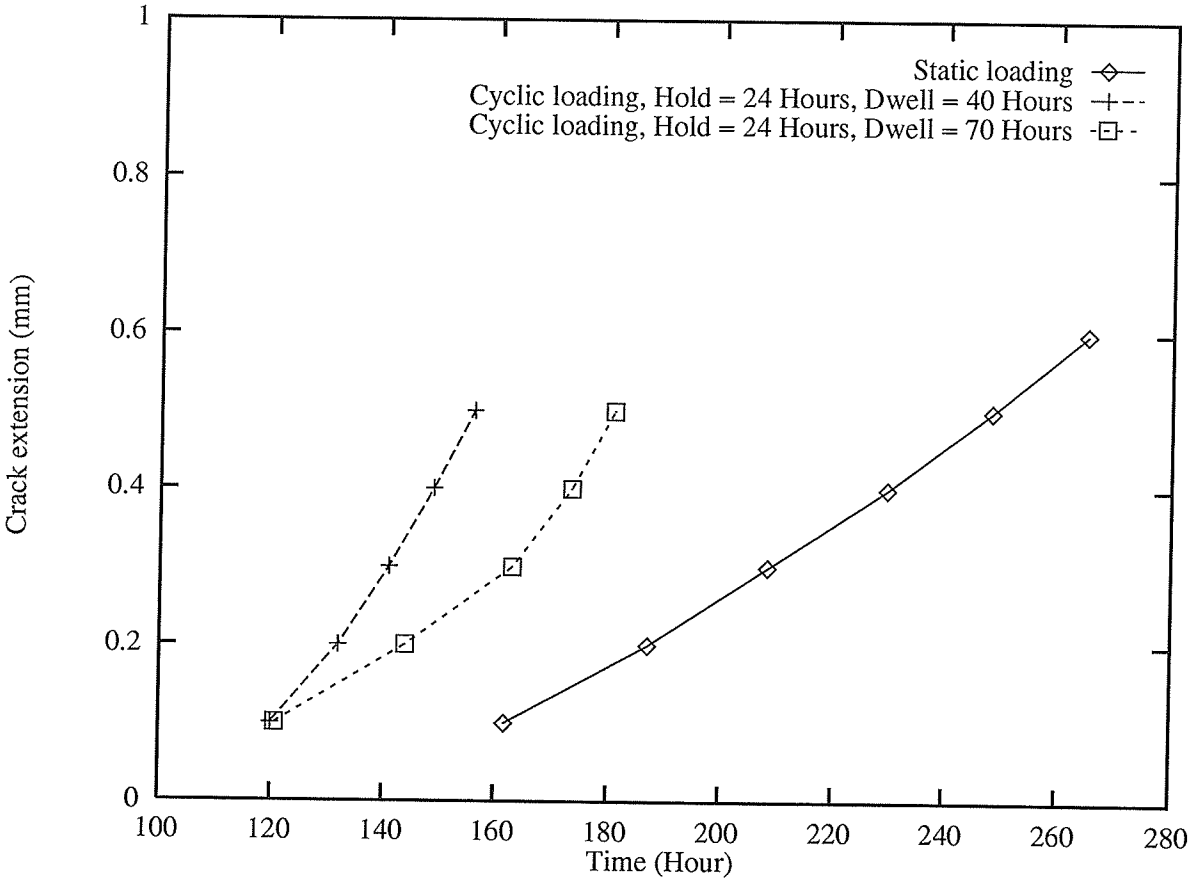

Figure 6.4: The crack extension history under static loading and cyclic loading which load holding time equals 24 hours and dwell times equal 40 and 70 hours

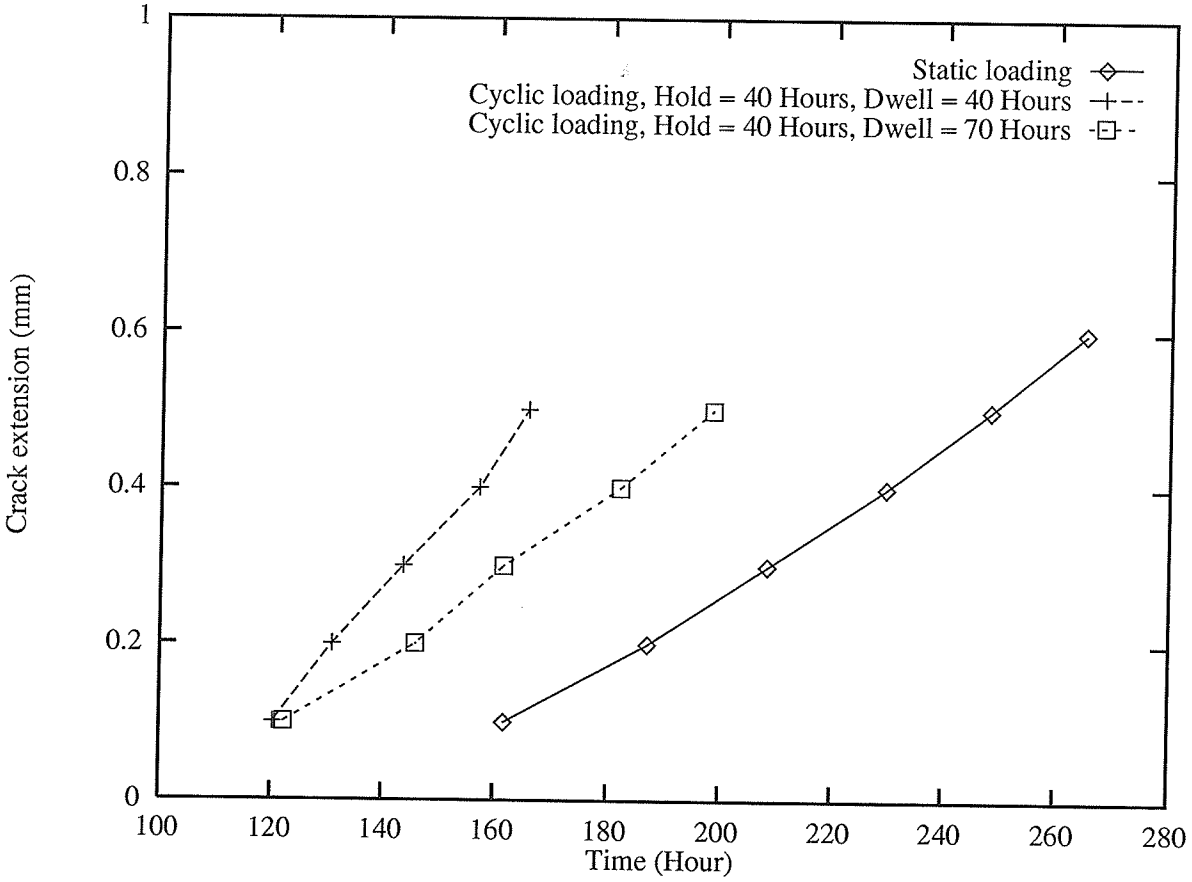

Figure 6.5: The crack extension history under static loading and cyclic loading which load holding time equals 40 hours and dwell times equal 40 and 70 hours

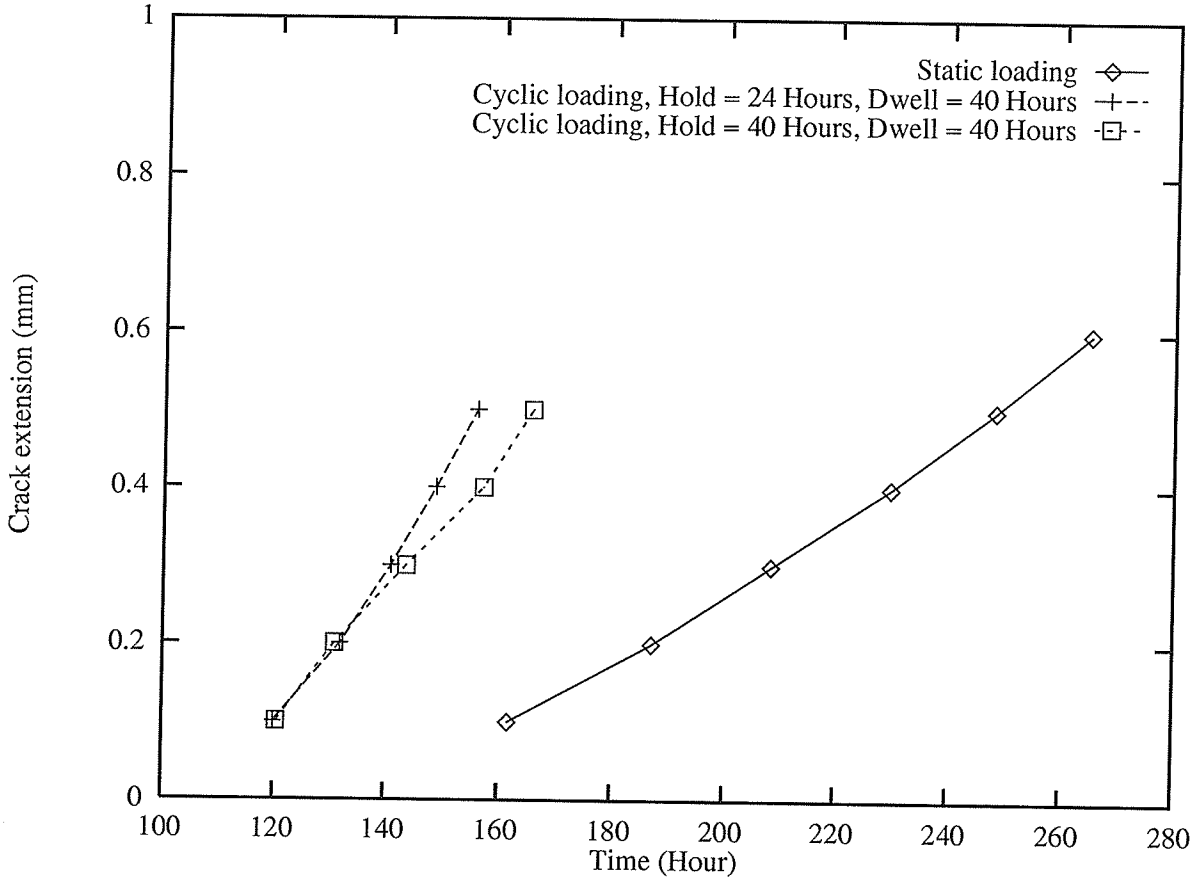

Figure 6.6: The crack extension history under static loading and cyclic loading which load dwell time equals 40 hours and load holding times equal 24 and 40 hours

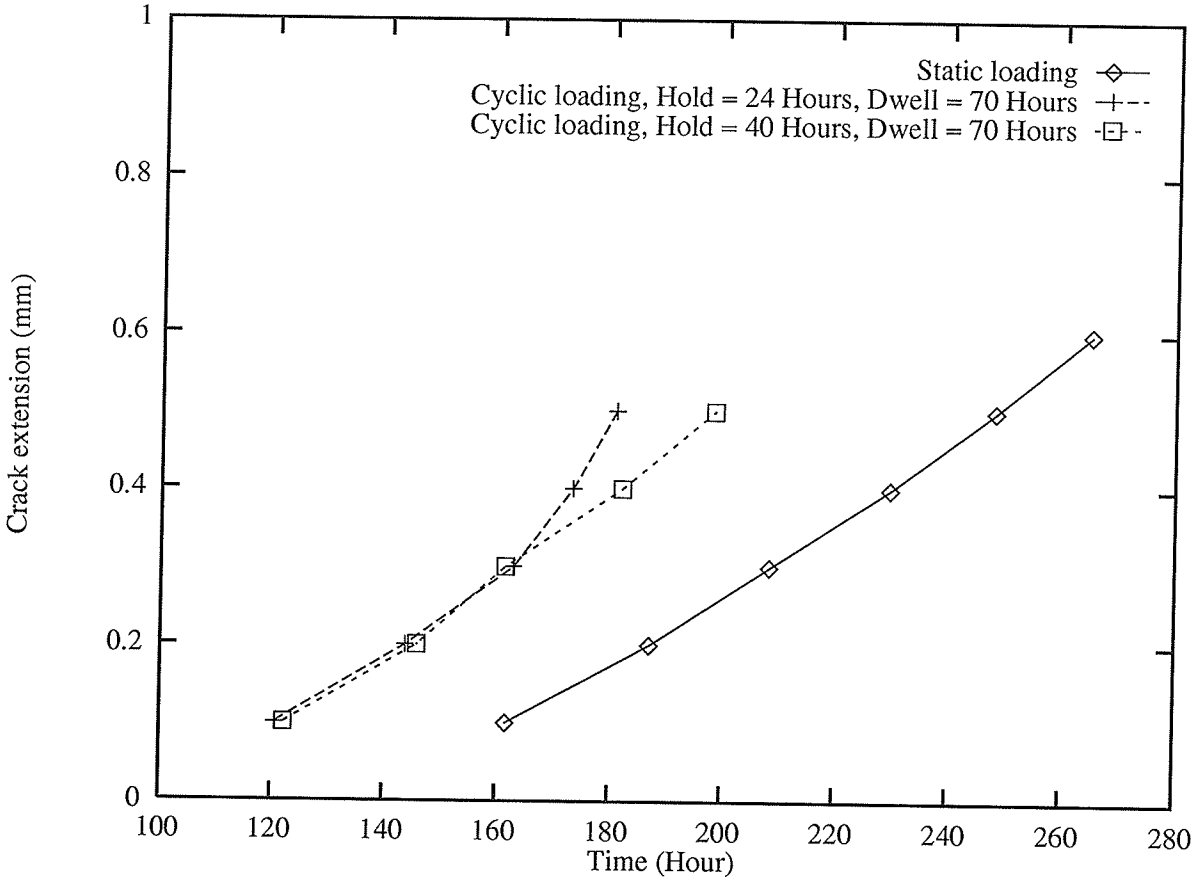

Figure 6.7: The crack extension history under static loading and cyclic loading which load dwell time equals 70 hours and load holding times equal 24 and 40 hours

with no load cycling event.

6.4.3 Effect of the duration of load dwell time

From Figs. 6.4-6.5 it is observed that with different load dwell time in one load cycle while other conditions are the same, the crack extension histories are different. While the incubation time for a crack to propagate is slightly different, the subsequent crack extension are significantly different. Such observed phenomena are inherently related to the distributions of the variables which determine the state of the material, especially those around the crack tip area. To check the effect of the duration of load dwell time, the variables of the material before and after the first element is broken are recorded. Distributions of these variables in the crack tip area just before the first element is broken indicate the difference of the incubation time for a crack to propagate. The differences of the distributions of these variables in the crack tip area just after the first element is broken control the difference of the crack propagation rate. In addition, the distributions and the evolutions of such variables are the reasons for the observed phenomena of the creep response and the fracture behavior. The results corresponding to the same amount of load holding time but different amount of load dwell time are plotted together to show the difference.

6.4.3.1 Distribution of variables before crack propagation

Obviously, the difference in the incubation time for a crack to propagate is caused by the different accumulation of damage around the crack tip under different loading histories. The damage rate is inherently related to the distribution of variables around the crack tip area. It is found that the difference between the distribution of variables after one load cycling event corresponding to different load dwell time are not significant. However, such difference accumulates with the further load cycling events. Before the first element is broken, the material state variables corresponding to different loading histories are evaluated as shown in the figures attached in Appendix Q (Figs. Q1-Q9). These loading histories correspond to the load holding

time of 40 hours, and two durations of load dwell time (40 and 70 hours).

As shown in Figs. Q1-Q4, and Q9, the stress variables (such as von Mises effective stress, damage equivalent stress, internal stress and the difference between damage equivalent stress and internal stress ($\tilde{\sigma} - \bar{R}$), etc.) and effective creep deformation driving stress $\frac{\tilde{\sigma}-\bar{R}}{1-c_o D}$ around the crack tip area are all higher in the case with 40 hours of load dwell time than in the case with 70 hours of load dwell time. In other words, it appears that after longer load dwell time, the material becomes softer and more ductile. The capability of the crack tip material in carrying load is reduced. This is reflected by smoother stress distributions around the crack tip area in the case with longer load dwell time. The effect of the residual stress on the distribution of the stress is less in the case with longer load dwell time. Just as the blunting of the crack tip by plastic deformation retards further crack growth in plasticity analysis, the softening of the crack tip material by the change of the maximum internal stress during the load dwell time also retards the incubation time for a crack to propagate. Corresponding to this, creep strain rate and damage rate in the crack tip area are all lower and smoother in the case with longer load dwell time. The effect of residual stress on creep strain rate and damage rate are less severe in the case with longer load dwell time. This is also an indication of the softening of materials during the load dwell period.

Another observation is that the highest stress variables are actually not at the crack tip element, but rather at a point away from the crack tip just before the first element is broken. This is the trend under all the loading histories in this group of case studies which is the same phenomenon as observed in the static creep fracture analysis presented in the proceeding chapter. Such an observation has also been reported by other researchers[56,58-59,137,189]. In spite of this, the effective creep deformation driving stress $\frac{\tilde{\sigma}-\bar{R}}{1-c_o D}$ finds the highest value in the crack tip element just before the first element is broken. That is to say, at the moment just before the first element is broken, the actual stress of the cavitated lattice of the crack tip material

is still highest among all the points of the material. This explains why the crack tip element experiences the highest creep strain rate and the highest damage rate just before the first element is broken.

Corresponding to the difference of the distribution of the variables in the crack tip area, the creep strain has higher value in the crack tip area in the case with longer load dwell time under different loading histories (Fig. Q6). That is, in order to achieve the critical damage value for the material to be broken, the material underwent longer load dwell time requires more ductile flow to rupture than the material underwent shorter load dwell time. The same trend is observed for the material further away from the crack tip. This is another indication of softening of materials during long load dwell time.

In spite of the difference of the distribution of creep strain under different loading histories, the case with longer load dwell time has lower value of damage for the material points away from the crack tip (Fig. Q7). This trend is more obvious in the case with shorter load holding time as shown in the two figures. This is because that with shorter load holding time, the creep strain and the creep damage is less dominant in the whole damage and fracture process. Other damage mechanisms, such as HTLCF damage in the load cycling process and the softening of material during the load dwell time have more opportunities to show their effects. Therefore, the load dwell time effect is thus more obviously exposed with shorter load holding time in a load cycle while other conditions are kept the same. This also shows that the softer the material becomes, the more ductile strain is needed for the material to be damaged. This is the same trend as observed in engineering applications. Hence, the degree of material deterioration could not be assessed merely by the ductile strain it has experienced, but it also depends on the material state that is characterized by other state variables, such as the internal stress which indicates the material's resistance to further creep deformation.

The difference of in distribution of the damage parameter under different loading histories results in the material having different incubation time for crack propaga-

tion. Shown in Fig. Q7 is the crack tip elements that have the same amount of damage. Such distributions of damage correspond to the time just before the first element is broken. Such time is different under different loading histories, as shown in Figs. 6.4-6.7. Under cyclic loading, while other conditions are kept the same, the longer the load dwell time in one load cycle is, the longer is the incubation time for crack propagation. However, such a trend is not obvious in this group of case studies as shown in these figures. In the case without sufficient numerical or experimental data, the author surmises that this is because the case studies involved too few cycles of loading. With only limited loading cycles to failure, the creep strain and creep damage play dominant roles for the final damage and fracture of the material. The load dwell time and the load cycling event has less opportunities to be shown of their effects. If the load holding time is shortened or if the loading level is reduced while other conditions are kept the same, the load dwell time effect is probably more obviously shown by the difference of the incubation time for a crack to propagate under different loading histories. More experimental and numerical work are needed in this regard.

6.4.3.2 Distribution of variables after the first element is broken

Obviously, the difference in crack propagation rate is caused by the different accumulation of the damage around the crack tip under different loading histories once the crack begins to propagate. The damage pattern and the damage rate are inherently related to the distributions of the material state variables around the crack tip area, which are shown in the figures attached in Appendix R (Figs. R1-R9).

As shown in Figs. R1-R4 and R9, immediately after the first element is broken, the crack tip area has higher stress variables and higher effective creep deformation driving stress $\frac{\tilde{\sigma}-\bar{R}}{1-c_o D}$ in the case with shorter load dwell time than in the case with longer load dwell time. This is probably the reason why the case with longer load

dwell time results in a lower rate of crack extension. As shown in the proceeding section, the longer the load dwell time, while other conditions are kept the same, the softer the material becomes after the load dwell time. For the softer material, the stress concentration is less severe than that of the harder material. This is the reason for the trends of the curves in these figures. Also, softer material has lower load carrying capacity. Hence, the distribution of stresses with longer load dwell time is smoother and the effect of residual stress is less severe. This is the same trend of distribution of stress corresponding to different loading histories, as shown in these figures. Also, the new crack tip element does not have the highest value of stress variables (Figs. R1-R4).

Corresponding to the stress distributions, the new crack tip element has the highest creep strain rate and the highest damage rate (Figs. R5 and R8). The distributions of creep strains and damage parameter around the crack tip do not change just before and after the first element is broken (Figs. Q6-Q7 and R6-R7). Hence, the case with longer load dwell time always has lower rate of damage development in the crack tip area, and hence a slower crack propagation.

6.4.4 Material states corresponding to different loading histories

The damage patterns and the distribution of the variables corresponding to different loading histories, including those of the static loading case are checked after the first element is broken. The distribution of representative variables are shown in in the figures attached in Appendix S (Figs. S1-S2). As shown in these figures, the material states as characterized by these variables are different under different loading histories at the time when the same amount of crack extension is achieved. One feature to be noted from these figures is that under static loading, the stress variables always has a higher value in the crack tip element, while under cyclic loading conditions, the highest stress variables occur some place away from the crack tip. This is the reflection of the effect of the residual stress involved in the

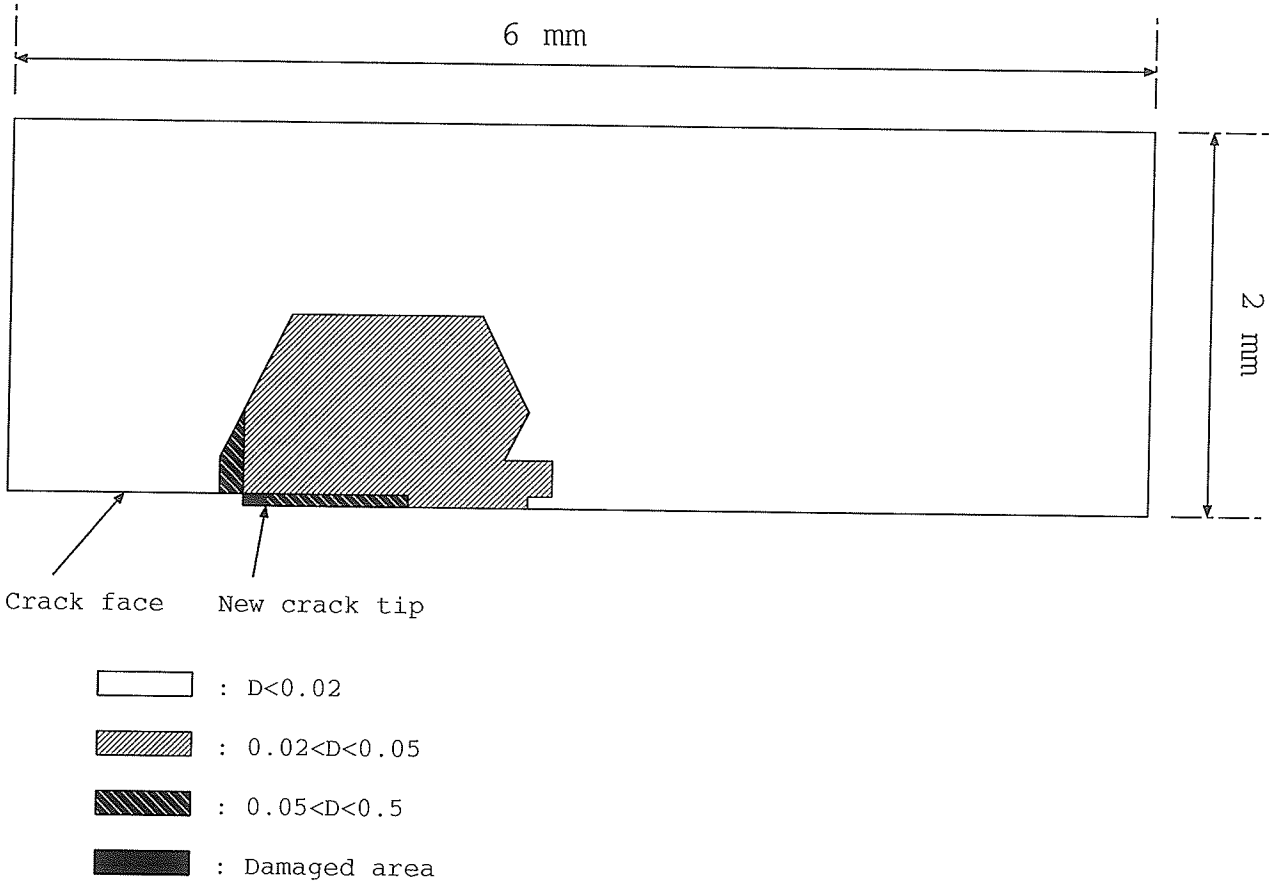

Figure 6.8: The damage pattern of the crack tip area just after the first element is broken. The load is static

load cycling process.

As compared to the damage pattern around the crack tip area produced by static loading (Fig. 6.8), the damage pattern of the material in the crack tip area under cyclic loading (holding time equals 24 hours and dwell time is 40 hours) is also changed. This is shown by the change of shape and distribution of the shaded area (Fig. 6.9). This is the comprehensive expression of the effect of loading history on the damage development around the crack tip area.

6.4.5 Summary

In conclusion, the loading history effect on creep response and fracture behavior of metallic materials at high temperature is important. The material states indicated

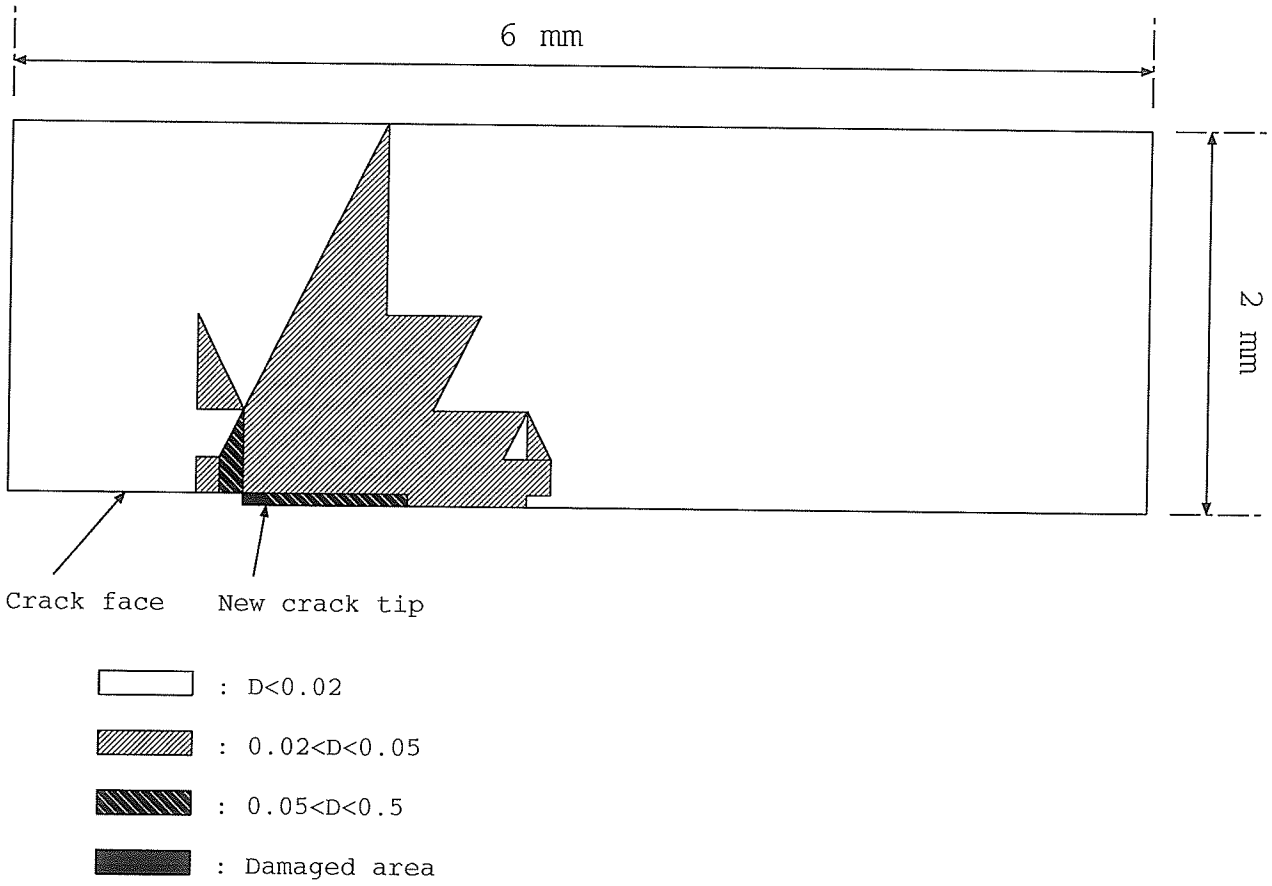

Figure 6.9: The damage pattern of the crack tip area just after the first element is broken. The load is cyclic with 24 hours of load holding time and 40 hours of load dwell time

by the material variables, such as stress, strain, damage and the internal stress, etc., are different, especially around the crack tip area under different loading histories. This is the reason why the creep response and the crack behavior of the material under different loading histories are different.

The load dwell time effect is shown in the softening of material during the load dwell time period. Such material softening has an important effect upon the material's creep response and crack behavior. It lowers the levels of stress variables of the material at the crack tip area upon reloading. In other words, the degree of the severity of the stress concentration in the case with load dwell time is not as high as the case without load dwell time. The stress distribution in the crack tip area becomes smoother. The effect of residual stress on the distribution of stress upon reloading is not as severe as in the case without load dwell time. Hence, the incubation time for a crack to propagate is longer when the load dwell time is longer and the subsequent crack growth rate is lower while other conditions are kept the same.

Chapter 7

Summary, conclusions, contributions and recommendations

7.1 Summary

Continuum damage mechanics has emerged as a viable tool to describe the damage and fracture behavior of solid materials in cases where global fracture mechanics analysis fails. An improved CDM-based constitutive model in which the strain and damage are coupled is proposed to describe creep response and fracture behavior of selected engineering materials such as 316 stainless steel under complex histories of stress and temperature. The proposal of the model is based on the abstraction and generalization of the microstructural changes of metallic materials at high temperature. Major influencing factor of cyclic creep fracture, such as load cycling effect, load dwell time effect and interaction between creep damage and HTLCF damage could be reflected by the model. The model was incorporated into an existing finite element computer program, TEPSAC, for numerical analysis of cyclic creep fracture. A series of case studies were conducted to predict the creep response of uniaxial tension bar and cracked thin panel. The material 316L stainless steel is used. The loads involved are both static and cyclic, thermal and mechanical. The cyclic load includes both load holding time and load dwell time. The mechanical load and the thermal load are in-phase with each other.

Parts of the numerical results calculated using the proposed model by finite element analysis are compared with the available experimental results in the open literatures. Good correlations between them are found.

The effect of loading history on creep response and crack behavior (the incubation time for a crack to propagate and the subsequent crack propagation rate) is systematically studied. The load cycling effect, load dwell time effect and interaction between creep damage and HTLCF damage on cyclic creep fracture and the crack tip field variables are evaluated respectively.

7.2 Conclusions

The following conclusions could be drawn from this thesis study:

1. The CDM method is a viable way for creep damage and fracture analysis.

2. The proposed CDM-based constitutive model provides a realistic and convenient tool in treating cyclic creep fracture of metallic materials at high temperature. Major effects influencing cyclic creep fracture behavior, such as load cycling effect, load dwell time effect and interaction between creep damage and HTLCF damage could be reflected by the model.

3. The load cycling effect, load dwell time effect and interaction between creep damage and HTLCF damage are all found to have significant influence upon the cyclic creep fracture behavior of metallic materials at high temperature. For complete cyclic creep fracture analysis, these effects should be included. The following specific points worth mentioning:

   (a) The load cycling process tends to rejuvenate the stress concentration at the relaxed crack tip and hence to enhance the creep strain rate and the damage rate there. The load cycling process itself introduces certain amount of damage to the material directly. So, after one load cycling event, the damage pattern at the crack tip is updated. The load cycling

event is detrimental to the material. The long term effect of the load cycling event is shown in the fact that the damage pattern around the crack tip area is changed and this area has higher rates of creep strain and damage development thereafter than the corresponding static creep deformation case.

(b) The stress distribution around the crack tip area is also changed after a period of load dwell time. The extent of the stress redistribution caused by the load dwell time is not as high as those caused by the load cycling process. However, it has a wider range of influence than the load cycling process. The stress distribution becomes flatter and smoother in the case of cyclic loading with load dwell time than that of the case of cyclic loading without load dwell time. The material becomes ductile and softer after long load dwell time. The long term effect of the load dwell time lies in a reduced stress variables and a higher effective creep deformation driving stress $\frac{\tilde{\sigma}-\tilde{R}}{1-c_o D}$ at the crack tip than the corresponding case of cyclic loading without load dwell time. Correspondingly, the creep strain rate and the damage rate of the crack tip material are higher under cyclic loading with load dwell time than those under cyclic loading without load dwell time. The accumulated damage and the creep strain at the crack tip area are also enhanced. The load dwell time is also detrimental to the material in terms of load carrying capacity. But it takes longer time for a crack to propagate and the crack propagation rate is lower in the case of cyclic loading with longer load dwell time.

(c) The interaction between creep damage and HTLCF damage tends to enhance rates of creep strain and damage development, and hence the creep strain and the damage degree there. It has long term effect on creep response and on crack behavior. It also changes the stress distribution in the crack tip area, but the extent of this change is not high. The

creep strain and the damage parameter change after the load cycling event. The damage distribution considering the interaction between creep damage and HTLCF damage is higher than that without considering such interaction. Hence, the interaction between creep damage and HTLCF damage is also detrimental to the material.

4. With different loading histories, creep response and crack behavior (the incubation time for a crack to propagate and the subsequent crack propagation rate) are different. For accurate structural analysis and lifetime prediction, the analysis should be based on real loading paths.

5. The long load dwell time effect in cyclic loadings causes the softening of material. Such material softening has an important effect upon creep response and crack behavior. It lowers the levels of the stress variables of the crack tip material upon reloading. The degree of the severity of stress concentration is not as high as that in the case of cyclic loading without load dwell time. The longer the dwell time the material experiences in one load cycling event, the softer the material becomes. The stress distribution becomes flatter and smoother after long load dwell time. The effect of residual stress on the distribution of stress upon reloading is not as severe as the case of cyclic loading without load dwell time. Hence, the incubation time for a crack to propagate is longer in the case with longer load dwell time and the subsequent crack growth rate is slower.

7.3 Original contributions

The original contributions of this thesis study lie in two aspects: the proposal of an improved CDM-based constitutive model for describing creep deformation and creep damage and a systematic study of the effect of loading history on creep response and fracture behavior of metallic materials at high temperature.

- Proposal of an improved CDM-based constitutive model;

  1. The improved model is based on the extension of Gong and Hsu's model to 3-D. Certain modifications are made;
  2. The model could reflect the load dwell time effect through the evolution of the internal state variables which describe the material microstructural changes in the creep deformation and creep damage process;
  3. The model could reflect the load cycling effect on creep response. This is achieved by incorporating Degallaix's model;
  4. The capacity of reflecting the interaction of creep damage and HTLCF damage on creep response and crack behavior is built in the model;
  5. The thermodynamics foundation of the model is checked and found that the model is consistent with the second law of thermodynamics;
  6. Finite element equations incorporating the improved constitutive model in creep analysis are derived and implemented into an existing finite element computer program, TEPSAC;
  7. The strain localization analysis is adopted in couple with the model for treating creep damage problem;
  8. Numerical verifications of the model are conducted;
  9. Reasonable results are obtained through the finite element analysis incorporating the model.

- Systematic study of the effect of loading history on creep response and fracture behavior:

  1. The individual effects of cyclic load, load dwell time and the interaction between creep damage and HTLCF damage on creep response and fracture behavior of the central cracked panel are quantitatively evaluated. It is found that these effects all influence the creep response and crack behavior.

2. The effect of loading history on cyclic creep fracture behavior is checked. The focus is on the crack behavior and the load dwell time effect. It was found that the effect of loading history on creep response and crack behavior is important. For complete and accurate creep fracture analysis, the calculation should base on real loading trace of the specimen. Material states under different loading histories are shown numerically to be different.

7.4 Recommendations for further research

The following recommendations with regard to further researches are in order:

- Experimental investigations are recommended to verify the theoretical analysis of the loading history effects on the creep response and the fracture behavior. The load dwell time effect on cyclic creep fracture should be emphasized in the experimental study because of limited references available on this topic. Research for measuring the damage parameters of a material at failure is also recommended.

- Environmental attacks on the material during the creep-fatigue damage process should be included in further research. The creep-fatigue-environment interaction is relevant to the real working conditions of most machine components.

- The damage caused by instantaneous plastic deformation is recommended to be considered in further modelling of the damage of materials. And the creep deformation and creep damage occurred in the load cycling process is recommended to be considered too.

- Further theoretical study of the convergence, stability and accuracy of the finite element analysis of creep deformation is recommended. Mesh dependence, time step dependence and the improvement of numerical integration algorithm are also recommended for further study.

Bibliography

[1] Abuelfoutouh, N.M. (1992) 'Evaluation of the effect of creep and mean stress on fatigue life using a damage mechanics approach', Advances in Fatigue Lifetime Predictive Techniques, ASTM STP 1122, Mitchell, M.R. and Landgraf, R.W. (Editors) pp. 77–83

[2] Ahlquist,G.N., Gasga-Neri, R and Nix, W.D. (1970) 'A phenomenological theory of steady state creep based on average internal and effective stresses', Acta. Metall., Vol. 18, Jun. pp. 663–671

[3] Ahlquist, C.N. and Nix, W.D. (1971) 'The measurement of internal stresses during creep of Al and Al-Mg alloys', Acta. Metall. Vol. 19, pp. 373–385

[4] Ahmad, Z.B. and Ashby, M.F. (1988) 'Failure-mechanism maps for engineering polymers', J. Mater. Sci., Vol. 23, No. 6, Jun., pp. 2037–2050

[5] Allen, D.H. (1982) 'Computational aspects of the nonisothermal classical plasticity', Computers and Structures, Vol. 15, No. 5, pp. 589–599

[6] Allen, D.H., Harris, C.E. and Groves, S.E. (1987) 'A thermomechanical constitutive theory for elastic composites with distributed damage, Part 1 and Part 2', Int. J. Solids Structures, Vol 23, No. 9, pp. 1301–1318

[7] Anand, L. (1982) 'Constitutive equations for the rate-dependent deformation of metals at elevated temperatures', J. Engng. Mater. Tech., Vol. 104, pp. 12–17

[8] Anderson, H. (1973) 'A finite-element representation of stable crack-growth', J. Mech. Phys. Solids, Vol. 21, pp. 337–356

[9] Anderson, P.M. and Rice, J.R. (1985) 'Constrained creep cavitation of grain boundary facets', Acta. Metall., Vol. 33, No. 3, pp. 409–422

[10] Argon, A.S. (1983) 'Intergranular cavitation in creeping alloys', Scripta Metall., Vol. 17, pp. 5-12

[11] Argon, A.S. (1982) 'Physical basis of constitutive equations for inelastic deformation', Constitutative Equations for Engineering Materials, Chen, W.f. (Editor) pp. 1–23

[12] Argon, A.S. and Takeuchi, S. (1981) 'Internal stresses in power-law creep', Acta. Metall., Vol. 29, pp. 1877–1884

[13] Asada, Y., Okamoto, Y. and Hashimoto, T. (1991) 'Creep-fatigue evaluation based on the overstress', J. Pressure Vessel Tech., Vol. 113, May, pp. 187–193

[14] Ashby, M.F., Gandhi, C. and Taplin, D.M.R. (1979) 'Overview No. 3, Fracture mechanism maps and their construction for F.C.C. metals and alloys', Acta. Metall., Vol. 27, pp. 699-729

[15] Auerkari, P (1983) 'Remanent creep life estimates of old power plant steam piping systems', Proceedings of the ASME International Conference on Advances in Life Prediction methods, pp. 353–356

[16] Ayari, M.L. (1988) 'Static and dynamic fracture mechanics of concrete gravity dams', Ph.D thesis, University of Colorado

[17] Ayari, M.L. and Saouma, V.E. (1991) 'Static and dynamic contact/impact problems using fictitious forces', Int. J. Num. Methods Engng., Vol. 32, No. 3, pp. 623–643

[18] Bannantine, J.A. and Socie, D.F. (1992) 'A multiaxial fatigue life estimation technique', Advances in Fatigue Lifetime Predictive Techniques, ASTM STP 1122, Mitchell, M.R. and Landgraf, R.W. (Editors) pp. 249–275

[19] Banthia, V. and Mukherjee, S. (1985) 'On an improved time integration scheme for stiff constitutive models of inelastic deformation', J. Engng. Mater. Tech., Vol. 107, Oct., pp. 282–285

[20] Barnby, J.T. (1975) 'Crack propagation during steady state creep', Engng. Fract. Mech., Vol. 7, pp. 299-304

[21] Bassani, J.L. (1988) 'Mechanics of damage, crack growth and life prediction under creep conditions', Mater. Sci. Engng., A103, pp. 115–123

[22] Bassani, J.L. (1988) 'High temperature creep', Mater. Sci. Engng., A103, pp. 95–95

[23] Bataille, J. and Kestin, J. (1976) 'Irreversible processes and physical interpretation of rational thermodynamics', J. Non-Equilib. Thermodyn., Vol. 4, pp. 229–258

[24] Bathe, K. and Dvorkin, E.N. (1983) 'On the automatic solution of nonlinear finite element equations', Computers Structures, Vol. 17, No. 5-6, pp. 871–879

[25] Bazant, Z.P. (1988) 'Softening instability: part 1 and part 2', J. App. Mech., Vol. 55, pp. 517–529

[26] Beere, W. (1983) 'Models of creep cavitation and their interrelationships', Scripta Metall., Vol. 17, pp. 13–16

[27] Beere, W. and Speight, M.V. (1978) 'Creep cavitation by vacancy diffusion in plastically deforming solids', Metal Sci., Apr., pp. 172–176

[28] Belloni, G., Bernasconi, G. and Piatti, G. (1977) 'Creep damage and rupture in AISI 310 austenitic steel', Mechanica, Jun. pp. 84–96

[29] Belytschko, T., Smolinski, P. and Liu, W.K. (1985) 'Stability of multi-time step partitioned integrators for first-order finite element systems', Computer Methods App. Mech. Engng., Vol. 49, pp. 281–279

[30] Ben-Amoz, M. (1991) 'A cumulative damage theory for creep and creep-fatigue interaction', Engng. Fract. Mech., Vol. 39, No. 2, pp. 309–314

[31] Benci, J.E. and Pope, D.P. (1988) 'Creep damage nucleation sites in Ferrous alloys', Mater. Sci. Engng., Vol. A103, pp. 97–102

[32] Bennett, P.S.G. and Evans, J.T. (1979) 'Creep stimulated by interrupted loading in Copper and Copper-1% Cadmium', Mater. Sci. Engng., Vol. 38, pp. 111-122

[33] Beremin, F.M. (1981) 'Cavity formation from inclusions in ductile fracture of A508 steel', Metall. Trans., A Vol. 12A, May, pp. 723–731

[34] Berkovits, A. and Nadiv, S. (1990) 'Relationship between fatigue life in the creep-fatigue region and stress-strain response', Experimental Mech., Sep. pp. 303–308

[35] Bernstein, H.L. and Allen, J.M. (1992) 'Analysis of cracked gas turbine blades', J. Engng. Gas Turbines Power, Vol. 114, Apr., pp. 293–301

[36] Betten, J. (1986) 'Application of tensor functions to the formulation of constitutive equations involving damage and initial anisotropy', Engng. Fract. Mech., Vol. 25, Nos 5/6, pp. 573–584

[37] Bicego, V. (1989) 'Low cycle fatigue life predictions in terms of an EPFM small crack model', Engng. Fract. Mech., Vol. 32, No. 3, pp. 339–349

[38] Biner, S.B., Wilkinson, D.S. and Watt, D. (1985) 'On the stress and strain fields ahead of a stationary crack in creeping solids', Engng. Fract. Mech., Vol. 21, No. 2, pp. 315–328

[39] Bizon, P.T. and Spera, D.A. (1976) 'Thermal-stress fatigue behavior of twenty-six superalloys', Thermal fatigue of Materials and Components, ASTM STP 612, Spera, D.A. and Mowbray, D.F. (Editors), pp. 106–122

[40] Blum, W., Hausselt, J. and Konig, G. (1976) 'Transient creep and recovery after stress reduction during steady state creep of AlZn', Acta. Metall., Vol. 24, pp. 293–297

[41] Bodner, S.R. and Hashin, Z. (1986) 'Preface', Engng. Fract. Mech., Vol. 25, No. 5/6, pp. 503–504

[42] Boismier, D.A. and Sehitoglu, H. (1990) 'Thermal-mechanical fatigue of Mar-M247: Part 1 – Experiments, Part 2 – Life prediction', J. Engng. Mater. Tech., Vol. 112, pp. 68–79

[43] Boyle, J.T. and Spence, J. (1983) 'Stress Analysis for Creep', Butterworths (Publisher)

[44] Brookfield, D.J., Moreton, D.N. and Moffat, D.G. (1986) 'Shakedown and cold creep of stainless steel type 316 torispherical drumheads subjected to internal pressure', J. Pressure Vessel Tech., Vol. 108, pp. 289–296

[45] Brust, F.W., Nakagaki, M. and Springfield, C. (1988) 'Integral parameters for thermal fracture', Engng. Fract. Mech., Vol. 33, No. 4, pp. 561–579

[46] Burke, K. and Cozzarelli, F.A. (1984) 'On the thermodynamic foundations of strain-dependent damage and rupture in three dimensions', Int. J. Solids Structures, Vol. 20, No. 5, pp. 487–497

[47] Cadek, J. (1988) 'Creep in metallic materials', Elsevier (publisher)

[48] Chaboche, J.L. (1981) 'Continuous damage mechanics – a tool to describe phenomena before crack initiation', Nuclear Engng. Design, Vol. 64, pp. 233–247

[49] Chaboche, J.L. (1983) 'Constitutive equations in creep-fracture damage', Recent Advances in Creep and Fracture of Engineering Materials and Structures, Vol. 2, Pineridge Press (publisher), pp. 177–235

[50] Chaboche, J.L. (1986) 'Time-dependent constitutive theories for cyclic plasticity', Int. J. Plasticity, Vol. 2, No. 2, pp. 149–188

[51] Chaboche, J.L. (1988) 'Continuum damage mechanics, part 1 and part 2', J. App. Mech., Mar., Vol. 55, pp. 59–72

[52] Chaboche, J.L., Lemaitre, J. et al, (1980) 'Discussion on problems of models identification', IUTAM Symposium, Senlis, France, pp. 37–51

[53] Chaboche, J.L. and Nouailhas, D. (1989) 'A unified constitutive model for cyclic viscoplasticity and its applications to various stainless steels', J. Engng. Mater. Tech., Vol. 111 pp. 424–430

[54] Challenger, K.D., Miller, A.K. and Brinkman, C.R. (1981) 'An explanation for the effects of hold periods on the elevated temperature fatigue behavior of $2\frac{1}{4}Cr - 1$Mo steel', J. Engng. Mater. Tech., Vol. 103, pp. 7–14

[55] Chen, E.P. (1992) 'Continuum damage response of a center-cracked plain concrete panel in tension', Engng. Fract. Mech., Vol. 39, No. 3, pp. 553–560

[56] Chen, G.G. (1988) 'Creep Crack Growth under Cyclic Loading Conditions — A Continuum Damage Approach', Ph.D Thesis, University of Manitoba

[57] Chen, G.G. and Hsu, T.R. (1988) 'A mixed explicit-implicit (EI) algorithm for creep stress analysis', Int. J. Num. Meth. Engng., Vol. 26, pp. 511-524

[58] Chen, G.G. and Hsu, T.R. (1991) 'Effects of cyclic plasticity on creep crack growth', Engng. Fract. Mech., Vol. 39, No. 3, pp. 509–524

[59] Chen, G.G. and Hsu, T.R. (1991) 'The role of plastic strains in creep crack growth', Engng. Fract. Mech., Vol. 39, No. 3, pp. 493–508

[60] Chen, G.L. et al (1988) 'A maximum stress modified life equation on the basis of a fatigue-creep interaction map', Low Cycle Fatigue, ASTM STP 942, pp. 531–542

[61] Chen, I.W. (1983) 'Mechanisms of cavity growth in creep', Scripta Metall., Vol. 17, pp. 17-22

[62] Cheng, Y.S. and Huang, Y.B. (1988) 'Measurement of continuous damage parameter', Engng. Fract. Mech., Vol. 31, No. 6, pp. 985–992

[63] Chow, C.L. and Lu, T.J. (1989) 'On evolution laws of anisotropic damage', Engng. Fract. Mech., Vol. 34, No. 3, pp. 679–701

[64] Chow, C.L. and Sze, K.Y. (1990) 'Characteriztion of notched ductile failure with continuum damage mechanics', J. Engng. Mater. Tech., Vol. 112, Oct., pp. 412–421

[65] Chow, C.L. and Wang, J. (1987) 'An anisotropic theory of continuum damage mechanics for ductile fracture', Engng. Fract. Mech., Vol. 27, No. 5, pp. 547–558

[66] Chow, C.L. and Wang, J. (1988) 'A finite element analysis of continuum damage mechanics for ductile fracture', Int. J. Fract., Vol. 38, pp. 83–102

[67] Chow, C.L. and Wang, J. (1988) 'Ductile fracture characterization with an anisotropic continuum damage theory', Engng. Fract. Mech., Vol. 30, No. 5, pp. 547–563

[68] Chow, C.L. and Wang, J. (1989) 'On crack initiation angle of mixed mode ductile fracture with continuum damage mechanics', Engng. Fract. Mech., Vol. 32, No. 4, pp. 601–612

[69] Chow, C.L. and Xu, J. (1985) 'Ductile crack propagation with the strain energy density criterion', Engng. Fract. Mech., Vol. 21. No. 3, pp. 537–545

[70] Cocks, A.C.F. and Ashby, M.F. (1982) 'On creep fracture by void growth', Mater. Sci., Vol. 27, pp. 189-244

[71] Cocks, A.C.F. and Leckie, F.A. (1987) 'The thermodynamics of creep damage', Thermomechanical Couplings in Solids, Bui, H.D. and Nguyen, Q.S. (Editors), Elsevier Science Publishers B.V. (North-Holland) pp. 207-221

[72] Cocks, A.C.F. and Ponter, A.R.S. (1985) 'Cyclic thermal loading in the creep range, part 1 and part 2', Int. J. Solids Struct., Vol. 21, No. 2, pp. 187–206

[73] Cocks, A.C.F. and Ponter, A.R.S. (1987) 'Creep deformation and failure under cyclic thermal loading', Preprints of the Sixth International Seminar on Inelastic Analysis and Life Prediction in High-Temperature Environment, Paris, France, Aug. 24-25, pp. c5.1-c5.55

[74] Coffin, L.F. (1976) 'Instability effects in thermal fatigue', Thermal Fatigue of Materials and Components, ASTM STP 612, Spera, D.A. and Mowbray, D.F. (Editors), pp. 227–238

[75] Coffin, L.F. (1979) 'Review of fatigue predictive methods in the regime where inelastic strains dominate', Methods for predicting material life in fatigue, Presented at ASME Winter Annu. Meet., New York, NY, Dec. 2-7, pp. 1-24

[76] Cormeau, I. (1975) 'Numerical stability in quasi-static elasto/visco-plasticity', Int. J. Num. Methods Engng., Vol. 9, pp. 109–127

[77] Cuddy, L.J. (1970) 'Internal stresses and structures developed during creep', Metall. Trans., Vol. 1, Feb., pp. 395–401

[78] Curbishley, I. et al (1986), 'Macroscopic creep crack growth in type 316 stainless steel part 1, part 2 and part 3', Engng. Fract. Mech., Vol. 23, No. 2, pp. 359–422

[79] Davanas, K. and Solomon, A.A. (1990) 'Theory of intergranular creep cavity nucleation, growth and interaction', Acta. Metall. Mater., Vol. 38, No. 10, pp. 1905–1916

[80] Davies, P.W., Nelmes, G., Williams, K.R. and Wilshire, B. (1973) 'Stress-change experiments during high-temperature creep of Copper, Iron, and Zinc', Metal Sci. J., Vol. 7, pp. 87–92

[81] Dean, R.H. and Hutchinson, J.W. (1980) 'Quasi-static steady crack growth in small-scale yielding', Fracture Mechanics: Twelfth Conference, ASTM STP 700, pp. 383–405

[82] Degallaix, G. and Fict, J. (1982) 'High-temperature low-cycle fatigue of a Martensitic stainless steel, New damage model, applied to thermal fatigue', Proceedings of the 4th E.C.F. Conference, pp. 672–679

[83] Degallaix, G., Degallaix, S. and Foct, J. (1983) 'A damage law for predicting the elevated temperature low cycle fatigue life of a Martensitic stainless steel', Mater. Sci. Engng., Vol. 58, pp. 55–62

[84] Degallaix, G., Korn, C. and Pluvinage, G. (1990) 'lifetime prediction on Cr-Mo-V and 316L steels under thermal and mechanical cycling', Fatigue Fract. Engng. Mater. Struct., Vol. 13 No. 5, pp. 473–485

[85] Delobelle, P. and Lachat, R. (1993) 'Viscoplastic behavior and modelization of an austenitic stainless steel (17-12 SPH) at high temperature ($T = 600°C$), under in and out of phase cyclic tension-torsion loading', J. Engng. Mater. Tech., Vol. 115, Jan. pp. 68–76

[86] Delph, T.J. (1980) 'A comparative study of two state-variable constitutive theories', J. Engng. Mater. Tech., Oct. Vol. 102, pp. 327–336

[87] Dib, M.W. and Rodin, G.J. (1993) 'Continuum damage mechanics of constrained intergranular cavitation', Acta. Metall. Mater. Vol. 41, No. 5, pp. 1567–1575

[88] Dougill, J.W. (1976) 'On stable progressively fracturing solids', J. App. Mathematics Phys. (ZAMP), Vol. 27, pp. 423–437

[89] Driver. J.H. et al (1988) 'Influence of temperature and environment on the fatigue mechanisms of single-crystal and polycrystal 316L', Low Cycle Fatigue, ASTM STP 942, pp. 438–455

[90] Dunne, F.P.E., Othman, A.M., Hall. F.R. and Hayhurst, D.R. (1990) 'Representation of uniaxial creep curves using continuum damage mechanics', Int. J. Mech. Sci., Vol. 32, No. 11, pp. 945–957

[91] Dvorkin, E.N. and Assanelli, A.P. (1991) '2D finite elements with displacement interpolated embedded localization lines: The analysis of fracture in frictional materials', Computer Methods App. Mech. Engng., Vol. 90, pp. 829–844

[92] Dvorkin, E.N., Cuitino, A.M. and Gioia, G. (1990) 'Finite elements with displacement interpolated embedded localization lines insensitive to mesh size and distortions', Int. J. Num. Methods Engng., Vol. 30, pp. 541–564

[93] Dyson, B.F. (1983) 'Continuous cavity nucleation and creep fracture', Scripta Metall. Vol. 17, pp. 31–37

[94] Dyson, B.F. and Leckie, F.A. (1988) 'Physically based modelling of remanent creep life', Mater. Sci. Engng., Vol. A103, pp. 111–114

[95] Dyson, B.F., Loveday, M.S. and Rodgers, M.J. (1976) 'Grain boundary cavitation under various states of applied stress', Proc. R. Soc. Lond. A. 349, pp. 245–259

[96] Dyson, B.F. and McLean, D. (1977) 'Creep of Nimonic 80A in torsion and tension', Metal Sci., February, pp. 37-45

[97] Earthman, J.C. and Nix, W.D. (1987) 'Characterizations of high temperature crack growth in copper and Cu+1wt%Sb under different loading conditions', Acta. Metall., Vol. 35, No. 2, pp. 463–472

[98] Edward, G.H. and Ashby, M.F. (1979) 'Intergranular fracture during power-law creep', Acta. Metall., Vol. 27, pp. 1505–1518

[99] Ellison, E.G. and Harper, M.P. (1978) 'Creep behavior of components containing cracks – a critical review', J. Strain Analysis, Vol. 13, No. 1, pp. 35–51

[100] Ellyin, F. and Kujawski, D. (1984) 'Plastic strain energy in fatigue failure', J. Pressure Vessel Tech., Vol. 106, pp. 342–347

[101] 'Encyclopedia of Science and Technology', Book 4, CLI-CYT, 7th edition, McGraw-Hill (publisher) pp. 506–507

[102] Evans, J.T. and Parkins, R.N. (1976) 'Creep induced by load cycling in a C-Mn steel', Acta. Metall., Vol. 24, pp. 511–515

[103] Evans, W.J. and Harrison, G.F. (1976) 'The development of a universal equation for secondary creep rates in pure metals and engineering alloys', Metal Sci., Sept., pp. 307–313

[104] Fan, J. (1987) 'On a thermomechanical constitutive theory and its application to CDM, fatigue, fracture and composites', Thermomechanical Couplings in Solids, Bui, H.D. and Nguyen, Q.S. (Editors), Elsevier Science Publishers B.V. (North-Holland), pp. 223–237

[105] Feltner, C.E. and Morrow, J.D. (1961) 'Microplastic strain hysteresis energy as a criterion for fatigue fracture', J. Basic Engng., Mar., pp. 15–22

[106] Fischer, F.D. et al, (1990) 'Fatigue and fracture of high-alloyed steel specimens subjected to purely thermal cycling', Metall. Trans., Vol. 21, A, Apr., pp. 935–948

[107] Fong, J.T. (1975) 'Energy approach for creep-fatigue interactions in metals at high temperatures', J. Pressure Vessel Tech., Aug., pp. 214–222

[108] Foo, W.P. and Castillo, R. (1992) 'Fracture mechanics approach to creep growth in welded IN738LC gas turbine blades', J. Engng. Gas Turbines Power, Vol. 114, pp. 275–283

[109] Foth, J., Nowack, H. and Lutjering, G. (1982) 'Crack initiation and microcrack propagation under constant amplitude and program loading histories', Proceedings of the 4th E.C.F. Conference, pp. 391–397

[110] Freeman, B.L. and Neate, G.J. (1978) 'An approach to the prediction of failure of cracked bodies operating in the creep range', Mater. Sci. Engng., Vol. 36, pp. 241–251

[111] Gandhi, C. and Ashby, M.F. (1979) 'Overview No. 5, Fracture-mechanism maps for materials which cleave: F.C.C., B.C.C. and H.C.P. metals and ceramics', Acta. Metall., Vol. 27, pp. 1565–1602

[112] Garud, Y.S. (1991) 'Quantitative evaluation of environmentally assisted cracking: a survey of developments and application of modeling concepts', J. Pressure Vessel Tech., Vol. 113, Feb., pp. 1–9

[113] Gibeling, J.C. and Nix, W.D. (1977) 'The existence of a friction stress for high-temperature creep', Metal Sci., Oct., pp. 453–457

[114] Gibeling, J.C. and Nix, W.D. (1980) 'The description of elevated temperature deformation in terms of threshold stresses and back stress: A review', Mater. Sci. Engng., Vol. 45, pp. 123–135

[115] Gittus, J. (1975) 'Creep, viscoelasticity and creep fracture in solids', Applied Science Publishers Ltd. (publisher)

[116] Gomuc, R. and Bui-Quoc, T. (1986) 'An analysis of the fatigue/creep behavior of 304 stainless steel using a continuous damage approach', J. Pressure Vessel Tech., Vol. 108, pp. 280–288

[117] Gomuc, R., Bui-Quoc, T. and Biron, A. (1987) 'Evaluation of the creep-fatigue behavior of $2\frac{1}{4}Cr - 1$Mo steel by a continuous damage approach', Res. Mechanica, Vol. 21, pp. 135–154

[118] Gomuc, R., Bui-Quoc, T., Biron, A. and Bernard, M. (1990) 'Analysis of type 316 stainless steel behavior under fatigue, creep and combined fatigue-creep loading', J. Pressure Vessel Tech., Vol. 112, Aug., pp. 240–250

[119] Gong, Z.L. (1990) 'On the Constitutive Equations for Selected Engineering Metals Subjected to Cyclic Creep', Ph.D Thesis, University of Manitoba

[120] Gong, Z.L. and Hsu, T.R. (1991) 'A constitutive model for metals subjected to cyclic creep', J. Engng. Mater. Tech., Vol. 113, pp. 419–424

[121] Goods, S.H. and Brown, L.M. (1979) 'The nucleation of cavities by plastic deformation', Acta. Metall., Vol. 27, pp. 1–15

[122] Goods, S.H. and Nieh, T.G. (1983) 'Mechanisms of intergranular cavity nucleation and growth during creep', Scripta Metall., Vol. 17, pp. 23–30

[123] Hales, R. (1983) 'A method of creep damage summation based on accumulated strain for the assessment of creep-fatigue endurance', Fatigue Engng. Mater. Struct., Vol. 6, No. 2, pp. 121-135

[124] Halford, G.R. (1966) 'The energy required for fatigue', J. Mater., Vol. 1, No. 1, Mar., pp. 3–18

[125] Halford, G.R. (1991) 'Evolution of creep-fatigue life prediction models', ASME report, AD-Vol. 21, pp. 43–57

[126] Halford, G.R. et al (1988) 'Fatigue life prediction modeling for turbine hot section materials', Towards Improved Durability in Advanced Aircraft Engine Hot Sections, ASME report IGTI-Vol. 2, pp. 97–107

[127] Halford, G.R, et al (1989) 'Fatigue life prediction modeling for turbine hot section materials', J. Engng. Gas Turbines Power, Vol. 111, pp. 279–285

[128] Halford, G.R. (1991) 'Evolution of creep-fatigue life prediction models', ASME report, AD-Vol. 21, pp. 43–57

[129] Halford, G.R. and Manson, S.S. (1976) 'Life prediction of thermal-mechanical fatigue using strainrange partitioning', Thermal Fatigue of Materials and Components, ASTM STP 612, Spera, D.A. and Mowbray, D.F. (Editors), pp. 239–254

[130] Halford, G.R. and Saltsman, J.F. (1983) 'Strainrange partitioning – a total strain range version', Proceedings of the ASME International Conference on Advances in Life Predictive Methods, New York, pp. 17–26

[131] Hannula, S.P. and Li, C.Y. (1984) 'Repeated load relaxations of type 316 austenitic stainless steel', Scripta Metall., Vol. 18, pp. 225–229

[132] Harrison, C.B. and Sandor, G.N. (1971) 'High-temperature crack growth in low-cycle fatigue', Engng. Fract. Mech., Vol. 3, pp. 403–420

[133] Hart, E.W. (1976) 'Constitutive relations for the nonelastic deformation of metals', J. Engng. Mater. Tech., Jul., pp. 193–202

[134] Hart, E.W. (1984) 'A micromechanical basis for constitutive equations with internal state variables', J. Engng. Mater. Tech., Vol. 106, Oct., pp. 322–325

[135] Hayhurst, D.R. (1983) 'On the role of creep continuum damage in structural mechanics', Recent Advances in Creep and Fracture of Engineering Materials and Structures, Pineridg Press (publisher), pp. 85–175

[136] Hayhurst, D.R., Brown, P.R. and Morrison, C.J. (1984) 'The role of continuum damage in creep crack growth', Phil. Trans. R. Soc. Lond., A 311, pp. 131–158

[137] Hayhurst, D.R., Dimmer, P.R. and Chernuka, M.W. (1975) 'Estimates of the creep rupture lifetime of structures using the finite element method', J. Mech. Phys. Solids, Vol. 23, pp. 335–355

[138] Hayhurst, D.R. and Felce, I.D. (1986) 'Creep rupture under tri-axial tension', Engng. Fract. Mech., Vol. 25, Nos. 5/6, pp. 645–664

[139] Hayhurst, D.R., Leckie, F.A. and Morrison, C.J. (1978) 'Creep rupture of notched bars', Proc. R. Soc. Lond., A. 360 pp. 243–264

[140] Hayhurst, D.R., Trampczynski and Leckie, F.A. (1983) 'On the role of cavity nucleation in creep deformation and fracture', Acta. Metall., Vol. 31, No. 10, pp. 1537–1542

[141] He, J. et al (1983) 'Strain energy partitioning and its application to GH33A Nickel-base superalloy and $1Cr18Ni9Ti$ stainless steel', Proceedings of the ASME International Conference on Advances in Life Predictive Methods, New York, pp. 27-32

[142] Henshall, G.A. and Miller, A.K. (1990) 'Simplifications and improvements in unified constitutive equations for creep and plasticity, Part 1 and Part 2', Acta. Metall. Mater., Vol. 38, No. 11, pp. 2101–2115

[143] Hild, F., Larsson, P. and Leckie, F.A. (1992) 'Localization due to damage in fober-reinforced composites', Int. J. Solids Structures, Vol. 29, No. 24, pp. 3221–3238

[144] Hill, R. (1957) 'On uniqueness and stability in the theory of finite elastic strain', J. Mech. Physics Solids, Vol. 5, pp. 229–241

[145] Hill, R. and Hutchinson, J.W. (1975) 'Bifurcation phenemena in the plane tension test', J. Mech. Phys. Solids, Vol. 23, pp. 239–264

[146] Hosseini, A., Cozzarelli, F.A. and Gu, R.J. (1989) 'Rupture analysis of a nonlinear viscous tube under creep-fatigue interactive environments', Engng. Fract. Mech., Vol. 34, No. 2, pp. 295–303

[147] Howes, M.A.H. (1976) 'A study of thermal fatigue mechanisms', Thermal Fatigue of Materials and Components, ASTM STP 612, Spera, D.A. and Mowbray, D.F. (Editors), pp. 86-105

[148] Hsia, K.J., Argon, A.S. and Parks, D.M. (1992) 'Dominant creep failure process in tensile components', J. Engng. Mater. Tech., Vol. 114, pp. 255–264

[149] Hsu, T.R. (1986) 'The Finite Element Method in Thermomechanics', Allen and Unwin (publishers), Boston

[150] Hsu, T.R. (1980) 'On behavior of fuel elements subject to combined cyclic thermo-mechanical loads', Nuclear Engng. Design, Vol. 56, pp. 279–287

[151] Hsu, T.R. and Bertels, A.W.M. (1974) 'An improved approximation of constitutive elasto-plastic stress-strain relationship for finite element analysis', J. AIAA, Vol. 12, pp. 1450–1452

[152] Hsu, T.R. and Bertels, A.W.M. (1976) 'Propagation and opening of a through crack in a pipe subjected to combined cyclic thermo-mechanical loading', J. Pressure Vessel Tech., Vol. 98, pp. 17–25

[153] Hsu, T.R. et al (1976) 'Theoretical basis for a transient thermal elasto-plastic stress analysis of nuclear reactor fuel element', Atomic Energy of Canada Ltd., Report AECL-5233

[154] Hsu, T.R. and Kim, Y.J. (1979) 'On slow crack growth in fuel cladding by finite element analysis', 5th Int. Conf. on Struct. Mech. in Reactor Tech., C3/12

[155] Hsu, T.R. and Zhai, Z.H. (1984) 'A finite element algorithm for creep crack growth', Engng. Fract. Mech., Vol. 20, pp. 521–533

[156] Hughes, T.J.R. and Liu, W.K. (1978) 'Implicit-explicit finite elements in transient analysis: stability theory', J. App. Mech., Vol. 45, Jun. pp. 371–378

[157] Hughes, T.J.R. and Taylor, R.L. (1978) 'Unconditionally stable algorithms for quasi-static elasto/visco-plastic finite element analysis', Computers Structures, Vol. 8, pp. 169–173

[158] Hult, J. (1978) 'CDM – capabilities, limitations and problems', Mechanisms of Deformation and Fracture, Easterling, K.E. (Editor), pp. 233–247

[159] Hutchinson, J.W. (1983) 'Constitutive behavior and crack tip fields for materials undergoing creep-constrained grain boundary cavitation', Acta. Metall., Vol. 31, No. 7, pp. 1079–0188

[160] Hutchinson, J.W. and Paris, P.C. (1979) 'Stability analysis of J-controlled crack growth', Elastic-Plastic Fracture, ASTM STP 668, Landes, J.D., Begley, J.A. and Clarke, G.A. (Editors) pp. 37–64

[161] Ishikawa, H. and Sasaki, K. (1989) 'Stress-strain relations of SUS304 stainless steel after cyclic preloading', J. Engng. Mater. Tech., Vol. 111, Oct., pp. 417–423

[162] Jackson, M.S. et al (1981) 'A phenomenological model for transient deformation based on state variables', J. Engng. Mater. Tech., Vol. 103, Oct., pp. 314–325

[163] Jaske, C.E. (1976) 'Thermal-mechanical, low-cycle fatigue of AISI 1010 steel', Thermal Fatigue of Materials and Components, ASTM STP 612, Spera, D.A. and Morbray, D.F. (Editors) pp. 170–198

[164] Jiang, X., Cui, J. and Ma, L. (1993) 'A cavity nucleation model during high temeprature creep deformation of metals', Acta. Metall., Vol. 41, No. 2, pp. 539–542

[165] Johnson, A.E. (1941) 'The creep recovery of a 0.17 per cent Carbon steel', J. Institute Mech. Engng., Vol. 145, pp. 210–220

[166] Jones, R.H. (1988) 'Environmentally assisted crack growth', Mater. Sci. Engng., A103, pp. 141–141

[167] Jordan, E.H. and Meyers, G.J. (1986) 'Fracture mechanics applied to nonisothermal fatigue crack growth', Engng. Fract. Mech., Vol. 23, No. 2, pp. 345–358

[168] Kachanov, L.M. (1958) 'On the creep fracture time', Izu, AN SSR, Otd. Tekhn. Nauk, 8, pp. 26–31 (in Russian)

[169] Kachanov, M. (1980) 'Crack growth under conditions of creep and damage', IUTAM Symposium, Leicester, UK, pp. 520-524

[170] Kestin, J. (1987) 'Metal plasticity as problem in thermodynamics', Thermomechanical Couplings in Solids, Bui, H.D. and Nguyen, Q.S. (Editors), Elsevier Science Publishers B.V. (North-Holland), pp. 23–36

[171] Kestin, J. (1992) 'Local-equilibrium formalism applied to mechanics of solids', Int. J. Solids Structures, Vol. 29, No. 14/15, pp. 1827–1836

[172] Kikuchi, K. et al, (1987) 'Stress-holding time effects on creep-fracture cracking in a notched specimen', Engng. Fract. Mech., Vol. 28, No. 3, pp. 345–360

[173] Kikuchi, K. and Kaji, Y. (1991) 'Relaxation behavior of Hastelloy XR in LCF tests', Engng. Fract. Mech., Vol. 40, No. 4/5, pp. 749–755

[174] Korn, C. and Pluvinage, G. (1989) 'Isothermal and thermal mechanical low cycle fatigue of 316L steel', Advances in Fract. Research, Proc. 7th Inter. Conf. Fract. (ICF7), Houston, Texas, pp. 1221–1228

[175] Krajcinovic, D. (1983) 'Constitutive equations for damaging materials', J. App. Mech., Vol. 50, pp. 355-360

[176] Krajcinovic, D. (1985) 'Continuous damage mechanics revisited: basic concepts and definitions', J. App. Mech., Vol. 52, pp. 829–834

[177] Krajcinovic, D. and Fanella, D. (1986) 'A micromechanical damage model for concrete', Engng. Fract. Mech., Vol. 25, Nos 5/6, pp. 585–596

[178] Krajcinovic, D. and Fonseka, G.U. (1981) 'The continuous damage theory of brittle materials, part 1 and part 2', J. App. Mech., Dec., Vol. 48, pp. 809–824

[179] Krajcinovic, D. and Selvaraj, S. (1984) 'Creep rupture of metals – An analytical model', J. Engng. Mater. Tech., Oct., Vol. 106, pp. 405–409

[180] Kraus, H. (1976) 'Creep analysis', John Wiley and Sons (publisher)

[181] Krempl, E. (1979) 'Viscoplasticity based on total strain, the modeling of creep with special considerations of initial strain and aging', J. Engng. Mater. Tech., Vol. 101, Oct. pp. 380–386

[182] Krempl, E. (1979) 'An experimental study of room-temperature rate-sensitivity, creep and relaxation of AISI type 304 stainless steel', J. Mech. Phys. Solids, Vol. 27, pp. 363–375

[183] Krempl, E. (1987) 'Models of viscoplasticity, some comments on equilibrium (back) stress and drag stress', Acta. Mechanica, Vol. 69, pp. 25–42

[184] Kumar, R. and Garg, S.B.L. (1989) 'Influence of stress ratio and material properties on effective stress range ratio and crack growth', Engng. Fract. Mech., Vol. 32, No. 2, pp. 195-202

[185] Kumar, V., Morjaria, M. and Mukherjee, S. (1980) 'Numerical integration of some stiff constitutive models of inelastic deformation', J. Engng. Mater. Tech., Vol. 102, Jan. pp. 92–96

[186] Lai, J.K. and Wickens, A. (1979) 'Microstructural changes and variations in creep ductility of 3 casts of type 316 stainless steel', Acta. Metall., Vol. 27, pp. 217–230

[187] Landes, J.D. and Begley, J.A. (1976) 'A fracture mechanics approach to creep crack growth', Mechanics of Crack Growth, ASTM STP 590, pp. 128–148

[188] Larsson, R. and Runesson, K. (1993) 'Discontinuous displacement approximation for capturing plastic localization', Int. J. Num. Methods Engng., Vol. 36, pp. 2087–2105

[189] Leckie, F.A. (1978) 'The constitutive equations of continuum creep damage mechanics', Phil. Trans. R. Soc. Lond., A 288, pp. 27–47

[190] Leckie, F.A. (1980) 'Advance in creep mechanics', IUTAM Symposium, Leicester, UK, pp. 13-65.

[191] Leckie, F.A. (1986) 'The micro- and macromechanics of creep rupture', Engng. Fract. Mech., Vol. 25, Nos 5/6. pp. 505–521

[192] Leckie, F.A. and Hayhurst, D.R. (1974) 'Creep rupture of structures', Proc. R. Soc. Lond., A 340, pp. 323–347

[193] Leckie, F.A. and Hayhurst, D.R. (1977) 'Constitutive equations for creep rupture', Acta. Metall., Vol. 25, pp. 1059–1070

[194] Lee, C., Cozzarelli, F.A. and Burke, K. (1986) 'One-dimensional strain-dependent creep damage in inhomogeneous materials', Int. J. Non-Linear Mechanics, Vol. 21, No. 4, pp. 303–314

[195] Leeuwen, H.P.V. (1977) 'The application of fracture mechanics to creep crack growth', Engng. Fract. Mech., Vol. 9, pp. 951–974

[196] Leeuwen, H.P.V. and Schra, L. (1987) 'Fracture mechanics and creep crack growth of $1\%Cr - \frac{1}{2}\%Mo$ steel with and without prior exposure to creep conditions', Engng. Fract. Mech., Vol. 27, pp. 483–499

[197] Lefebvre, D. and Ellyin, F. (1984) 'Cyclic response and inelastic strain energy in low cycle fatigue', Int. J. Fatigue, Vol. 6, No. 1, pp. 9-15

[198] Lefebvre, D., Neale, K.W. and Ellyin, F. (1981) 'A criterion for low-cycle fatigue failure under biaxial states of stress', J. Engng. Mater. Tech., Vol. 103, Jan., pp. 1–6

[199] Leis, B.N. (1977) 'An energy-based fatigue and creep-fatigue damage parameter', J. Pressure Vessel Tech., Nov., pp. 524–533

[200] Lemaitre, J. (1984) 'How to use damage mechanics', Nuclear Engng. Design, Vol. 80, pp. 233–245

[201] Lemaitre, J. (1985) 'A continuous damage mechanics model for ductile fracture', J. Engng. Mater. Tech., Jan. Vol. 107 pp. 83–89

[202] Lemaitre, J. (1985) 'Coupled elasto-plasticity and damage constitutive equations', Computer Methods App. Mech. Engng., Vol. 51, pp. 31–49

[203] Lemaitre, J. (1986) 'Local approach of fracture', Engng. Fract. Mech., Vol. 25, Nos 5/6, pp. 523–537

[204] Lemaitre, J. (1992) 'A course on damage mechanics', Springer-Verlag (publisher)

[205] Lemaitre, J. and Chaboche, J.L. (1974) 'A non-linear model of creep-fatigue damage cumulation and interaction', IUTAM Symposium, Gothenburg, Sweden, pp. 291–301

[206] Lemaitre, J. and Dufailly, J. (1987) 'Damage measurements', Engng. Fract. Mech., Vol. 28, Nos. 5/6, pp. 643–661

[207] Lemaitre, J. and Plumtree, A. (1979) 'Application of damage concepts to predict creep-fatigue failures', J. Engng. Mater. Tech., Vol. 101, pp. 284–292

[208] Leroy, Y.M. and Chapuis, O. (1991) 'Localization in strain-rate-dependent solids', Computer Methods App. Mech. Engng., Vol. 90, pp. 969–986

[209] Le Roy, G., Embury, J.D., Edward, G. and Ashby, M.F. (1981) 'A model of ductile fracture based on the nucleation and growth of voids', Acta. Metall., Vol. 29, pp. 1509–1522

[210] Leroy, Y. and Ortiz, M. (1989) 'Finite element analysis of strain localization in frictional materials', Int. J. Num. Ana. Methods Geomech., Vol. 13, pp. 53-74

[211] Leroy, Y. and Ortiz, M. (1990) 'Finite element analysis of transient strain localization phenomena in frictional solids', Int. J. Num. Ana. Methods Geomech., Vol. 14, pp. 93–124

[212] Levaillant, C., Grattier, J., Mottot, M. and Pineau, A. (1988) 'Creep and creep-fatigue intergranular damage in austenitic stainless steels: discussion of the creep-dominated regime', Low Cycle Fatigue, ASTM STP 942, pp. 414–437

[213] Levy, A.J. (1985) 'A physically based constitutive equation for creep-damaging solids', J. App. Mech., Vol. 52, pp. 615–620

[214] Levy, A. and Pifko, A.B. (1981) 'On computational strategies for problems involving plasticity and creep', Int. J. Num. Methods Engng., Vol. 17, pp. 747–771

[215] Liu, W.K. (1983) 'Development of mixed time partition procedures for thermal analysis of structures', Inter. J. Num. Methods Engng., Vol. 19, pp. 125–140

[216] Liu, W.K., Zhang, Y.F. and Belytschko, T. (1985) 'Implementation of mixed-time partition algorithms for nonlinear thermal analysis of structures', Computer Methods App. Mech. Engng., Vol. 48, pp. 245–263

[217] Lloyd, G.J. (1986) 'Macroscopic creep crack growth in type 316 stainless steel', Engng. Fract. Mech., Vol. 23, No. 2, pp. 359–382

[218] Lorenzo, F. and Laird, C. (1984) 'Cyclic creep acceleration and retardation in polycrystalline copper tested at ambient temperature', Acta. Metall., Vol. 32, No. 5, pp. 681–692

[219] Lowe, T.C. and Miller, A.K. (1984) 'Improved constitutive equations for modeling strain softening -Part 1 and part 2', J. Engng. Mater. Tech., Vol. 106, Oct. pp. 337–348

[220] Lowe, T.C. and Miller, A.K. (1986) 'Modeling internal stresses in the nonelastic deformation of metals', J. Engng. Mater. Tech., Vol. 108, Oct. pp. 365–373

[221] Lubahn, J.D. (1953) 'The role of anelasticity in creep, tension, and relaxation behavior', Trans. American Society for Metal, Vol. 45, pp. 787-838

[222] Maas, E. and Pineau, A. (1985) 'Creep crack growth behavior of type 316L steel', Engng. Fract. Mech., Vol. 22, No. 2, pp. 307–325

[223] Magnusen, P.E., Srolovitz, D.J. and Koss, D.A. (1990) 'A simulation of void linking during ductile microvoid fracture', Acta. Metall., Vol. 38, No. 6, pp. 1013–1022

[224] Malik, S.N. (1982) 'Elevated temperature creep crack growth: state-of-art review and recommendations', Nuclear Engng. Design, Vol. 72, pp. 359–371

[225] Mall, S. et al, (1991) 'Crack growth in a Titanium Aluminide alloy under thermal mechanical cycling', Fatigue Fract. Engng. Mater. Struct., Vol. 14, No. 1, pp. 79–87

[226] Mall, S., Perez, J.A. and Nicholas, T. (1990) 'Influence of loading history on fatigue threshold behavior in a Titanium alloy', Engng. Fract. Mech., Vol. 37, No. 1, pp. 15–26

[227] Mall, S., Staubs, E.A. and Nicholas, T. (1990) 'Investigation of creep/fatigue interaction on crack growth in a Titanium Aluminide alloy', J. Engng. Mater. Tech., Oct., Vol. 112, pp. 435–441

[228] Malvern, L.E. (1969) 'Introduction to the Mechanics of a Continuous Medium', Prentice-Hall (publisher)

[229] Manfredi, E. and Vitale, E. (1989) 'Elevated temperature low-cycle fatigue strength of butt welded AISI 316 steel pipes', J. Engng. Mater. Tech., Vol. 111, pp. 354–362

[230] Manson, S.S. (1966) 'Thermal Stress and Low Cycle Fatigue', McGraw-Hill Book Company (publisher)

[231] Manson, S.S., Halford, G.R. and Hirschberg, M.H. (1971) 'Creep-fatigue analysis by strain-range partitioning', ASME Symp. Elevated Temp. Environ., First Nal. Congr, San Francisso, Calif, May 10-12, pp. 12-24

[232] Manson, S.S. and Halford, G.R. (1986) 'Re-examination of cumulative fatigue damage analysis – An engineering perspective', Engng. Fract. Mech., Vol. 25, Nos 5/6, pp. 539–571

[233] Marchand, N.J., Pelloux, R.M. and Ilschner, B. (1988) 'A fracture mechanics criterion for thermal-mechanical fatigue crack growth of gas turbine materials', Engng. Fract. Mech., Vol. 31, No. 3, pp. 535–551

[234] May, I.L. (1979) 'Developments in parametric methods for handling creep and creep-rupture data', J. Engng. Mater. Tech., Vol. 101, Oct. pp. 326–330

[235] May, Le and Silverira, T.L. da, (1984) 'Creep damage assessment and remaining life prediction', Creep and Fracture, pp. 1117–1133

[236] McGaw, M.A. (1992) 'Cumulative creep-fatigue damage evolution in an austenitic steel', Advances in Fatigue Lifetime Predictive Techniques, ASTM STP 1122, pp. 84–106

[237] McKnight, R.L. et al (1983) 'Turbine blade nonlinear structural and life analysis', J. Aircraft, Vol. 20, No. 5, pp. 475–480

[238] McKnight, R.L. (1989) 'Structural analysis applications', J. Engng. Gas Turbines Power, Vol. 111, pp. 271–278

[239] Melton, K.N. (1982) 'Strain wave shape and frequency effects on the high temperature, low cycle fatigue behaviour of a 1Cr-Mo-V Ferritic steel', Mater. Sci. Engng., Vol. 55, pp. 21–28

[240] Meshii, M., Shetty, D.K. and Ochiai, Y. (1974) 'Cyclic creep of metals', Proceedings of the Symposium on Mechanical Behavior of Materials, Kyato, Japan, pp. 179–192

[241] Miller, A. (1976) 'An inelastic constitutive model for monotonic, cyclic and creep deformation, part 1 and part 2', J. Engng. Mater. Tech., Apr. pp. 97–113

[242] Miller, M.P., McDowell, D.L. and Oehmke, R.L.T. (1992) 'A creep-fatigue-oxidation microcrack propagation model for thermo-mechanical fatigue', J. Engng. Mater. Tech., Vol. 114, pp. 282-288

[243] Mohamed, F.A. and Langdon, T.G. (1976) 'Deformation mechanism maps: their use in predicting creep bahavior', J. Engng. Mater. Tech., Apr. pp. 125–131

[244] Morrow, J.D. and Tuler, F.R. (1965) 'Low cycle fatigue evaluation of Inconel 713C and Waspaloy', J. Basic Engng., Jun. pp. 275–289

[245] Moyer, E.T., Jr and Liebowitz, H. (1987) 'Creep crack growth modelling and near tip stress fields', Engng. Fract. Mech., Vol. 28, No. 5/6, pp. 601–621

[246] Mroz, Z. (1967) 'On the description of anisotropic work-hardening', J. Mech. Phys. Solids, Vol. 15, pp. 163–175

[247] Mroz, Z. and Trampzcynski, W.A. (1984) 'On the creep-hardening rule for metals with a memory of maximum prestress', Int. J. Solids Structures, Vol. 20, No. 5, pp. 467–486

[248] Murakami, S. and Ohno, N. (1981) 'A continuum theory of creep and creep damage', Creep in Structures, 3rd IUTAM Symposium, Leichester, UK, pp. 422-444

[249] Murakami, S. (1988) 'Mechanical modeling of material damage', J. App. Mech., Vol. 55, pp. 280–286

[250] Murakami, S. and Sanomura, Y. (1986) 'Analysis of the coupled effect of plastic damage and creep damage in Nimonic 80A at finite deformation', Engng. Fract. Mech., Vol. 25, Nos 5/6, pp. 693–704

[251] Murakami, S., Sanomura, Y. and Hattori, M. (1986) 'Modelling of the coupled effect of plastic damage and creep damage in Nimonic 80A', Int. J. Solids Structures, Vol. 22, No. 4, pp. 373–386

[252] Needleman, A. and Rice, J.R. (1980) 'Plastic creep flow effects in the diffusive cavitation of grain boundaries', Acta. Metall., Vol. 28, pp. 1315–1332

[253] Nakagaki, M. and Atluri, S.N. (1982) 'Analysis of fatigue cracks in center cracked panels and cold-worked fastener holes', ASME report, No. 82-pvp-24, pp. 1-11

[254] Neu, R.W. and Sehitoglu, H. (1989) 'Thermalmechanical fatigue, oxidation and creep: Part 1. damage mechanisms, Part 2. life prediction', Metall. Trans., A Vol. 20, pp. 1755–1783

[255] Nicholson, R.D. and Formby, C.L. (1975) 'The validity of various fracture mechanics methods at creep temperatures', Int. J. Fract., Vol. 11, No. 4, Aug. pp. 595–604

[256] Nikbin, K.M. and Webster, G.A. (1988) 'Prediction of crack growth under creep-fatigue loading conditions', ASTM STP 942 pp. 281–292

[257] Nikbin, K.M., Webster, G.A. and Turner, C.E. (1976) 'Relevance of nonlinear fracture mechanics to creep cracking', Cracks and Fracture, ASTM STP 601, pp. 47–62

[258] Nix, W.D. (1988) 'Mechanisms and controlling factors in creep fracture', Mater. Sci. Engng., Vol. A103, pp. 103–110

[259] Nix, W.D., Earthman, J.C., Eggeler, G. and Ilschner, B. (1989) 'The principal facet stress as a parameter for predicting creep rupture under multiaxial stresses', Acta. Metall., Vol. 37, No. 4, pp. 1067–1077

[260] Nix, W.D., Matlock, D.K. and Dimelfi, R.J. (1977) 'A model for creep fracture based on the plastic growth of cavities at the tips of grain boundary wedge cracks', Acta. Metall., Vol. 25, pp. 495–503

[261] Odqvist, F.K.G. (1980) 'Historical survey of the development of creep mechanics from its beginnings in the last century to 1970', IUTAM Symposium, Leicester, UK, pp. 1-12.

[262] Ohtani, R. and Taira, S. (1979) 'Effects of nonlinear stress-strain rate relation on deformation and fracture of materials in creep range', J. Engng. Mater. Tech., Vol. 101, Oct. pp. 369–373

[263] Onat, E.T. (1986) 'Representation of mechanical behavior in the presence of internal damage', Engng. Fract. Mech., Vol. 25, Nos 5/6, pp. 605–614

[264] Onat, E.T. and Leckie, F.A. (1988) 'Representation of mechanical behavior in the presence of changing internal structure', J. App. Mech., Vol. 55, pp. 1–10

[265] Ortiz, M. (1988) 'Microcrack coalescence and microscopic crack growth initiation in brittle solids', Int. J. Solids Structures, Vol. 24, No. 3, pp. 231–250

[266] Ortiz, M., Leroy, Y. and Needleman, A. (1987) 'A finite element method for localized failure analysis, Computer Methods App. Mech. Engng., Vol. 61 pp. 189-214

[267] Ostergren, W.J. (1976) 'A damage function and associated failure equations for predicting hold time and frequency effects in elevated temperature, low cycle fatigue', J. Testing and Evaluation, Vol. 4, No. 5, Sep., pp. 327–339

[268] Ostergren, W.J. and Krempl, E. (1979) 'A uniaxial damage accumulation law for time-varying loading including creep-fatigue interaction', J. Pressure Vessel Tech., Vol. 101, May, pp. 118–124

[269] Passman, S.L. and Trucano, T.G. (1986) 'A theory of localization of damage in creep', Engng. Fract. Mech., Vol. 25, Nos 5/6. pp. 597–603

[270] Peric, D., Mitchell, G.P. and Owen, D.R.J. (1991) 'Some computational issues in strain localization problems for rate independent solids', Int. J. Num. Methods Engng., Vol. 32, pp. 79–101

[271] Perl, M. et al, (1986) 'Numerical simulation of fatigue creep crack growth in a visco-elasto-plastic material, part 1 and part 2', Engng. Fract. Mech., Vol. 23, No. 2, pp. 321–331

[272] Pilkington, R. (1979) 'Critical assessment, Creep crack growth in low-alloy steels', Metal Sci., Oct., pp. 555–564

[273] Pizzo, P.P. (1979) 'Rate equations for elevated temperature creep', J. Engng. Mater. Tech., Vol. 101, Oct., pp. 396–402

[274] Plumtree, A. (1977) 'Creep/fatigue interaction in type 304 stainless steel at elevated temperature', Metal Sci., Aug./Sep., pp. 425-431

[275] Poirier, J.P. (1977) 'Microscopic creep models and the interpretation of stress-drop tests during creep', Acta. Metall., Vol. 25, pp. 913–917

[276] Puglia, A.D. and Manfredi, E. (1978) 'High-temperature low cycle fatigue damage', Creep of Engineering Materials and Structures, Applied Science publishers Ltd., London, Bernasconi, G. and Piatti, G. (Editors), pp. 229–265

[277] Raj, R. (1983) 'Correlations between cavitation, creep and dilation for multiaxial loading', Acta. Metall., Vol. 31, pp. 29–36

[278] Raj, R. and Ashby, M.F. (1975) 'Intergranular fracture at elevated temperature', Acta. Metall., Vol. 23, Jun. pp. 653–666

[279] Rao, K.B.S., Valsan, M. and Mannan, S.L. (1990) 'Strain-controlled low cycle fatigue behaviour of type 304 stainless steel base material, type 308 stainless steel weld metal and 304-308 stainless steel weldments', Mater. Sci. Engng., A130, pp. 67–82

[280] Rees, D.W. and Dyson, B.F. (1986) 'Deformation and fracture behavior under combined creep and fatigue', Int. J. Plasticity, Vol. 2, pp. 1-19

[281] Reger, M. and Remy, L. (1982) 'Influence of environment on microcrack propagation in high temperature low cycle fatigue', Proceedings 4th E.C.F. Conference, pp. 531–539

[282] Rezai-Aria, F. and Remy, L. (1989) 'An oxidation fatigue interaction damage model for thermal fatigue crack growth', Engng. Fract. Mech., Vol. 34, No. 2, pp. 283–294

[283] Rice, J.R. (1968) 'A path independent integral and the approximate analysis of strain concentration by notches and cracks', J. App. Mech., Jun. pp. 379–386

[284] Rice, J.R. (1971) 'Inelastic constitutive relations for solids: an internal-variable theory and its application to metal plasticity', J. Mech. Phys. Solids, Vol. 19, pp. 433–455

[285] Rice, J.R. (1976) 'The localization of plastic deformation', Theoretical and Applied Mechanics, Koiter, W.T. (Editor), North-Holland Publishing Company, pp. 207–220

[286] Rice, J.R. (1982) 'Continuum mechanics and thermodynamics of plasticity in relation to microscale deformation mechanisms', Constitutive Equations for Engineering Materials, Chen, W.F. (Editor), pp. 23–56

[287] Rice, J.R., Paris, P.C. and Merkle, J.G. (1973) 'Some further results of J-Integral analysis and estimates', Progress in Flaw Growth and Fracture Toughness Testing, ASTM STP 536, pp. 231–245

[288] Rice, J.R. and Tracey, D.M. (1969) 'On the ductile enlargement of voids in triaxial stress fields', J. Mech. Phys. Solids, Vol. 17, pp. 201–217

[289] Riedel, H. (1981) 'Creep deformation at crack tips in elastic-viscoplastic solids', J. Mech. Phys. Solids, Vol. 29, pp. 35–49

[290] Riedel, H. (1984) 'A continuum damage approach to creep crack growth', Fundamentals of Deformation and Fracture, Baily, B.A., Miller, K.J. and Willis, J.R. (Editors), pp. 293–309

[291] Riedel, H. (1986) 'Fracture at High Temperature', Springer-Verlag (publisher)

[292] Riedel, H. and Rice, J.R. (1980) 'Tensile cracks in creeping solids', Fracture Mechanics: Twelfth Conference, ASTM STP 700, pp. 112–130

[293] Rabortnov, Yu.N. (1969) 'Creep Problems in Structural Members', North-Holland (publisher), New York

[294] Rubiolo, G.H. (1991) 'Temperature and strain rate superposition properties of low cycle fatigue failure curves in the Coffin-Manson representation', Acta. Metall. Mater., Vol. 39, No. 4, pp. 619–626

[295] Saanouni, K., Chaboche, J.L. and Bathias, C. (1986) 'On the creep crack growth prediction by a local approach', Engng. Fract. Mech., Vol. 25, Nos 5/6. pp. 677–691

[296] Sakane, M. et al (1989) 'Frequency and hold-time effects on low cycle fatigue life of notched specimens at elevated temperature', J. Engng. Mater. Tech., Vol. 111, Jan., pp. 54–60

[297] Sarfarazi, M. (1988) 'An overview of the constitutive behavior of crystalline solids', Engng. Fract. Mech., Vol. 31, No. 6, pp. 1035–1046

[298] Saxena, A. (1980) 'Evaluation of C^* for the characterization of creep-crack-growth behavior in 304 stainless steel', Fracture Mechanics: Twelfth Conference, ASTM STP 700, pp. 131–151

[299] Saxena, A. (1988) 'Creep crack growth under transient conditions', Mater. Sci. Engng., Vol. A103, pp. 125–129

[300] Saxena, A. (1991) 'Creep crack growth in high temperature ductile materials', Engng. Fract. Mech., Vol. 40, No. 4/5, pp. 721–736

[301] Saxena, A., Ernst, H.A. and Landes, J.D. (1983) 'Creep crack growth behavior in 316 stainless steel at 594^oC (1100^oF)', Int. J. Fract., Vol. 23, pp. 245–257

[302] Sehitoglu, H. (1986) 'Material behavior under thermal loading', J. Pressure Vessel Tech., Feb. Vol. 108, pp. 113–119

[303] Sehitoglu, H. (1992) 'Thermo-mechanical fatigue life prediction methods', Advances in Fatigue Lifetime Predictive Techniques, ASTM STP 1122, Mitchell, M.R. and Landgraf, R.W. (Editors) pp. 47–76

[304] Sehitoglu, H. and Karasek, M. (1986) 'Observations of material behavior under isothermal and thermo-mechanical loading', J. Engng. Mater. Tech., Vol. 108, Apr., pp. 192–198

[305] Shaninian, P. and Sadananda, K. (1979) 'Effects of stress ratio and hold-time on fatigue crack growth in alloy 718', J. Engng. Mater. Tech., Vol. 101, Jul. pp. 224–230

[306] Sherby, O.D. and Miller, A.K. (1979) 'Combining phenomenology and physics in describing the high temperature mechanical behavior of crystalline solids', J. Engng. Mater. Tech., Vol. 101, Oct., pp. 387–395

[307] Shetty, D.K. and Meshii, M. (1975) 'Plastic deformation of aluminium under repeated loading', Metall. Trans., A, Vol. 6, Feb. pp. 349–358

[308] Shetty, D.K., Mura, T. and Meshii, M. (1975) 'Analysis of creep daformation under cyclic loading conditions', Mater. Sci. Engng., Vol. 20, pp. 261–266

[309] Sidey, D. and Coffin, L.F. Jr. (1979) 'Low-cycle fatigue damage mechanisms at high temperature', ASTM STP 675, Symp On Fatigue Mech, Kansas city, Mo, May 22-24 1978, Publ. by ASTM, Philadelphia, Pa. pp. 528-568.

[310] Siegele, D. and Schmitt, W. (1983) 'Determination and simulation of stable crack growth in ADINA', Computers Structures, Vol. 17, No. 5-6, pp. 697–703

[311] Sih, G.C. and Kiefer, B.V. (1979) 'Nonlinear response of solids due to crack growth and plastic deformation', Nonlinear and Dynamic Fracture Mechanics, Perrone, N. and Atluri, S.N. (Editors) Vol. 35, pp. 135–156

[312] Simbeya, K.W. and Shrive, N.G. (1990) 'A discussion of continuum damage mechanics', Research Report No. CE90-3, Dept. of Civil Engineering, The University of Calgary

[313] Simo, J.C. and Ju, J.W. (1987) 'Strain- and stress-based continuum damage models – Part 1 and Part 2', Int. J. Solids Structures, Vol. 23, No. 7, pp. 821–840

[314] Sinclair, G. (1993) 'Structural reliability through fracture mechanics', Mechanical Engng., Jun., pp. 79–84

[315] Smith, S.D., Webster, J.J. and Hyde, T.H. (1989) 'Finite element investigation of creep crack growth from surface thumbnail cracks', Engng. Fract. Mech., Vol. 34, No. 3, pp. 625–635

[316] Snowden, K.U., Stathers, P.A. and Hughes, D.S. (1982) 'The elevated temperature creep behaviour of type 321 and 310 stainless steel', Res. Mechanica, Vol. 4, pp. 115–126

[317] Solomon, A.A. and Nix, W.D. (1970) 'Interpretation of high temperature plastic deformation in terms of measured effective stresses', Acta. Metall., Vol. 18, Aug., pp. 863–876

[318] Staley, J.T., Jr and Saxena, A. (1990) 'Mechanisms of creep crack growth in $1wt\%$ ANTIMONY-COPPER: implications for fracture parameters', Acta. Metall. Mater., Vol. 38, No. 6, pp. 897–908

[319] Stigh, U. (1986) 'Effects of interacting cavities on damage parameter', J. App. Mech., Vol. 53, Sept., pp. 485–490

[320] Svoboda, J. and Sklenicka, V. (1990) 'Thermal cavity nucleation at intergranular inclusions in high temperature creep', Acta. Metall. Mater., Vol. 38, No. 6, pp. 1141–1149

[321] Tai, W. (1990) 'Plastic damage and ductile fracture in mild steels', Engng. Fract. Mech., Vol. 37, No. 4, pp. 853–880

[322] Tai, W. and Yang, B. (1986) 'A new microvoid-damage model for ductile fracture', Engng. Fract. Mech., Vol. 25, No. 3, pp. 377–384

[323] Taira, S., Ohtani, R. and Kitamura, T. (1979) 'Application of J-Integral to high-temperature crack propagation, Part 1 – creep crack propagation, Part 2 – fatigue crack propagation', J. Engng. Mater. Tech., Vol. 101, Apr. pp. 154–167

[324] Takeuchi, S. and Argon, A.S. (1976) 'Review, Steady-state creep of single-phase crystalline matter at high temperature', J. Mater. Sci., Vol. 11, pp. 1542–1566

[325] Tanaka, T.G. and Miller, A.K. (1988) 'Development of a method for integrating time-dependent constitutive equations with large, small or negative strain rate sensitivity', Int. J. Num. Methods Engng., Vol. 26, pp. 2457–2485

[326] Tanimura, S. and Duffy, J. (1986) 'Strain rate and temperature history effects for three different tempers of 4340 Var steel', Int. J. Plasticity, Vol. 2, pp. 21–35

[327] Thomason, P.F. (1990) 'Ductile fracture of metals', Pergamon Press (publisher)

[328] Thompson, R.L. (1989) 'Structural analysis method development for turbine hot section components', J. Engng. Gas Turbines Power, Vol. 111, Apr., pp. 286–300

[329] Tomkins, B. and Wareing, J. (1977) 'Elevated-temperature fatigue interactions in engineering materials', Metal Sci., August/September, pp. 414–424

[330] Trampczynski, W.A., Hayhurst, D.R. and Leckie, F.A. (1981) 'Creep rupture of Copper and Aluminium under non-proportional loading', J. Mech. Phys. Solids, Vol. 29, No. 5/6, pp. 353–374

[331] Tsuji, K. et al, (1991) 'Thermal fatigue characteristics of Ni-Ti-Cu alloy coils', Mater. Sci. Engng., A136, pp. L1-L4

[332] Tvergaard, V. (1982) 'Ductile fracture by cavity nucleation between larger voids', J. Mech. Phys. Solids, Vol. 30, No. 4, pp. 265–186

[333] Tvergaard, V. (1984) 'Constitutive relations for creep in polycrystals with grain boundary cavitation', Acta. Metall., Vol. 32, No. 11, pp. 1977–1990

[334] Tvergaard, V., Needleman, A. and Lo, K.K. (1981) 'Flow localization in the plane strain tensile test', J. Mech. Phys. Solids, Vol. 29, No. 2, pp. 115–142

[335] Valanis, K.C. (1971) 'Irreversibility and existence of entropy', Int. J. Non-Linear Mechanics, Vol. 6, pp. 337–360

[336] Valanis, K.C. (1990) 'A theory of damage in brittle materials', Engng. Fract. Mech., Vol. 36, No. 3, pp. 403–416

[337] Wareing, J. (1988) 'Influence of material microstructure on low cycle fatigue failure, with particular reference to austenitic steel', Low Cycle Fatigue, ASTM STP 942, pp. 711–727

[338] Weitsman, Y. (1988) 'A continuum damage model for viscoelastic materials', J. App. Mech., Vol. 55, Dec. pp. 773–780

[339] Wilsdorf, H.G.F. (1983) 'The ductile fracture of metals: a microstructural viewpoint', Mater. Sci. Engng., Vol. 59, pp. 1–39

[340] Woodford, D.A. (1979) 'Creep damage and the remaining life concept', J. Engng. Mater. Tech., Oct., Vol. 101, pp. 311-315

[341] Wu, K.H. and Leckie, F.A. (1990) 'Static and cyclic loading of notched 304 stainless steel bars at 650^oC', Fatigue Fract. Engng. Mater. Struct., Vol. 13, No. 2, pp. 155-169

[342] Xiong, C. (1986) 'The research and development on the life prediction of high temperature structures', Teaching notes, Beijing University of Aeronautics and Astronautics, P.R. China, Jun.

[343] Yokobori, A.T. Jr et at (1987) 'Representation of the displacement rate between the loading points in terms of applied stress and temperature and its relation to creep crack growth rate, C^*, P and Q^* parameters', Engng. Fract. Mech., Vol. 28, No. 5/6, pp. 805–816

[344] Yokobori, A.T. Jr, Yokobori, T. and Kuriyama, T. (1988) 'Life of crack initiation, propagation, and final fracture under high-temperature creep, fatigue, and creep-fatigue multiplication conditions', ASTM STP 942, pp. 236–256

[345] Yokobori, A.T., Jr. and Yokobori, T. (1988) 'The crack initiation and growth under high temperature creep, fatigue and creep-fatigue multiplication', Engng. Fract. Mech., Vol. 31, No. 6, pp. 931–945

[346] Yuen, J.L. and Copeland, J.F. (1979) 'Fatigue crack growth bahavior of stainless steel type 316 plate and 16-8-2 weldments in air and high-carbon liquid sodium', J. Engng. Mater. Tech., Vol. 101, pp. 214–223

[347] Zamrik, S.Y. (1990) 'An interpretation of axial creep-fatigue damage interaction in type 316 stainless steel', J. Pressure Vessel Tech., Vol. 112, Feb. pp. 4–19

[348] Zamrik, S.Y., Davis, D.C. and Kulowitch, P.J. (1992) 'Failure modes in a type 316 stainless steel under biaxial strain cycling', Advances in Fatigue Lifetime Predictive Techniques, ASTM STP 1122, Mitchell, M.R. and Landgraf, R.W. (Editors) pp. 299-318

[349] Zhang, A., Bui-Quoc, T. an d Gomuc, R. (1990) 'A procedure for low cycle fatigue life prediction for various temperatures and strain rates', J. Engng. Mater. Tech., Vol. 112, Oct. pp. 422–428

APPENDICES

Appendix A

Micromechanisms of Creep Deformation, Creep Damage and Fracture

A.1 Introduction

Fracture of a structural component by creep is the result of monotonic creep damage accumulation within it. Creep damage development is intimately related to the creep deformation the component has experienced. Creep damage is partially the result of creep deformation, but it also contributes to the evolution of creep deformation.

The nonlinear creep deformation behavior of engineering solids arises in general as a consequence of the irreversible changes of the material microstructure. The observed change of creep strain with time is the macroscopic reflection of the kinetics of several different modes of microstructural rearrangements of the polycrystalline lattices. A majority of these modes (such as dislocation glides and climbs) are viscous in nature. For example, the three stages of a typical creep deformation curve are nothing but the macroscopic manifestation of the dominant mode in which the microstructure of the material changes[176].

In contrast, the nucleation and growth of cavities and microcracks on the grain boundaries which also contributes to creep deformation is of different nature. In

the whole process of creep deformation, after the protracted initial period dominated by viscous deformation (primary and secondary stages), the rapid increase of the creep strain rate which typifies the tertiary stage is directly traced to the accelerated microcrack growth proceeding coalescence or linkage leading to the final creep fracture[10,21-22,25-26]. The discovery in some materials that the period of accelerating creep is also a period of accelerating growth of cavity volume[28,96] suggests, as a reasonable hypothesis. The idea that cavities accelerate creep, and cavities, their distributions, densities and shapes indicate creep damage to some extent[48-52,248-251].

The full complexity of the mechanisms of creep deformation, creep damage and fracture has become more and more apparent in the past three decades[47,93-96,280,289-292]. What was once thought to be a simple mechanism has now revealed itself as a hierarchy of interacting mechanisms, each dominant over a certain ranges of stress, temperature and microstructure[98,102,319,327]. We are still some distance from a full understanding of these processes, and from modelling them in a way that is useful to a design engineer. But enormous advance has been made, both in identifying the mechanisms and in the modelling of the response[10,87,258]. In this section, only qualitative description of the mechanisms of creep deformation, creep damage and fracture is presented. The modelling of these mechanisms could be found in open literatures[9,79,159,209,235,252,260,265,288].

It should be pointed out that some of the creep deformation mechanisms and the creep damage and fracture mechanisms are identical in nature. For example, grain boundary sliding not only cause creep deformation, but it also cause nucleation and growth of voids along the grain boundaries[47,327]. Generally speaking, for metallic materials at high temperature, the creep damage is the process of nucleation, growth and coalescence of voids and microcracks along grain boundaries. It contributes to the creep deformation, while the creep deformation also contributes to the creep damage. The creep damage and fracture are usually intimately related to the defor-

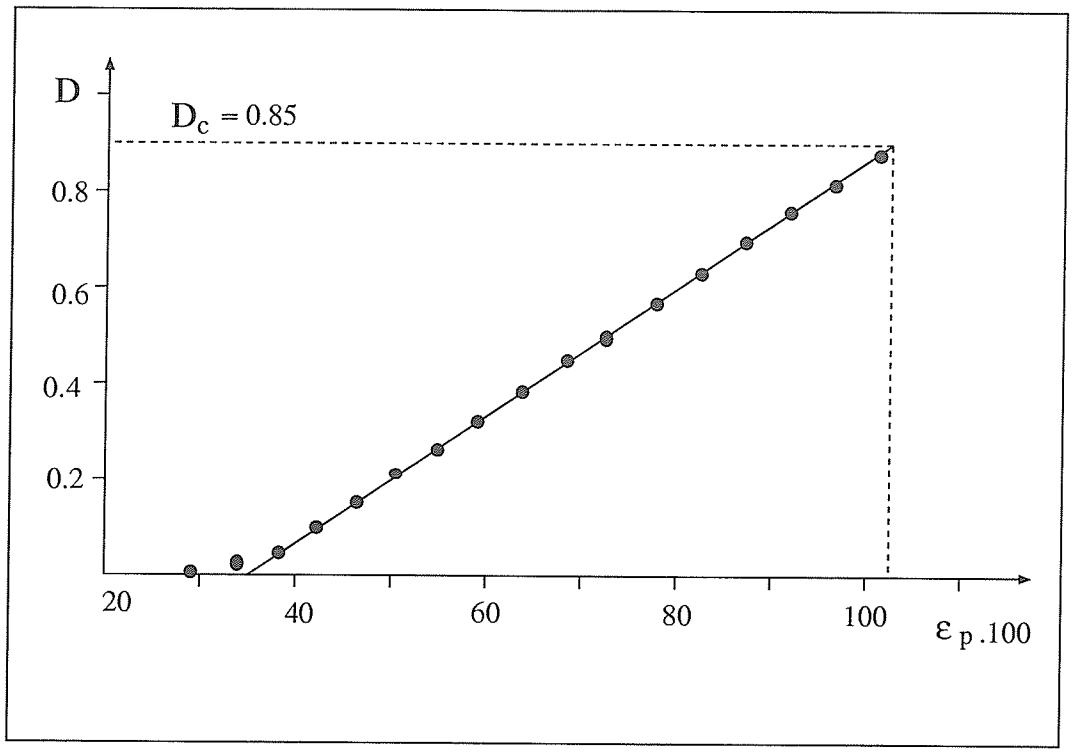

Figure A.1: The relations between ductile strain and ductile damage[204]

mation processes. It is difficult to separate the creep damage process from the creep deformation process, and vice versa. There is actually certain function relations between damage and ductile strain as reported in the literatures. Fig. A.1 shows the evaluation of ductile damage based on ductile strain as reported by Lemaitre[200-204]. In the following sections, the micromechanisms of creep deformation, creep damage and fracture are described.

A.2 Micromechanisms of creep deformation

The inherent controlling mechanisms of creep deformation of a material vary due to the different external loading pattern (the amplitude of temperature and stress and rates of loading) and the microstructural state of the material[324]. For 'virgin' material, i.e., the material with no previous history of creep deformation, the main controlling parameters of creep deformation are basically the stress and temperature.

The deformation mechanism maps which show the various controlling mechanisms in meso-mechanics sense of deformation in the stress-temperature plane were developed by material scientists, in which the normalized normal σ/G or shear stress τ/G, are plotted as a function of the homologous temperature, T/T_m, at constant grain size[4,14,224,243,278], as shown in Fig. A.2. The figure shows normalized system of coordinates which is used so that different materials may be directly compared on the same map. The idea is that different mechanisms operate independently and the fastest one determines the deformation behavior and occupies the respective regime in the stress-temperature plane. The boundaries between different regimes are usually calculated (rather than measured) by comparing the strain rate equations for the different mechanisms. In this map, the creep deformation corresponds to the high stress and high temperature region. Also shown in Fig. A.3 is an illustrative creep deformation mechanism map[224].

At low stress and very high temperature (above 0.7 T_m, where creep strain rate varies with applied stress), the creep-controlling mechanism is the stress-directed atomic diffusion process. This 'bulk-diffusional' creep (Nabarro/Hering type) involves the flow of vacancies from tensile to compressive grain boundaries and corresponding reverse flow of atoms leading to grain elongation. However, at intermediate temperatures and low stresses, the governing mechanisms is the so-called 'grain-boundary-diffusional' creep (Coble type). It requires atomic diffusion along grain boundaries. In the regime of intermediate to high stress level and temperatures above $0.5T_m$, the process is controlled by the 'diffusion-controlled-dislocation' creep mechanism, which involves the climb of edge dislocations away from the dislocation barrier. Hart[133-134] has subdivided the diffusion process in this dislocation climb region into additive contributions of 'lattice-diffusion' at the higher end of the temperature range and 'core-diffusion' at the lower end. The final creep deformation mechanism involves 'grain-boundary-sliding'. This is not an independent deformation mode. It has to be accommodated by other mechanisms[291,327], such

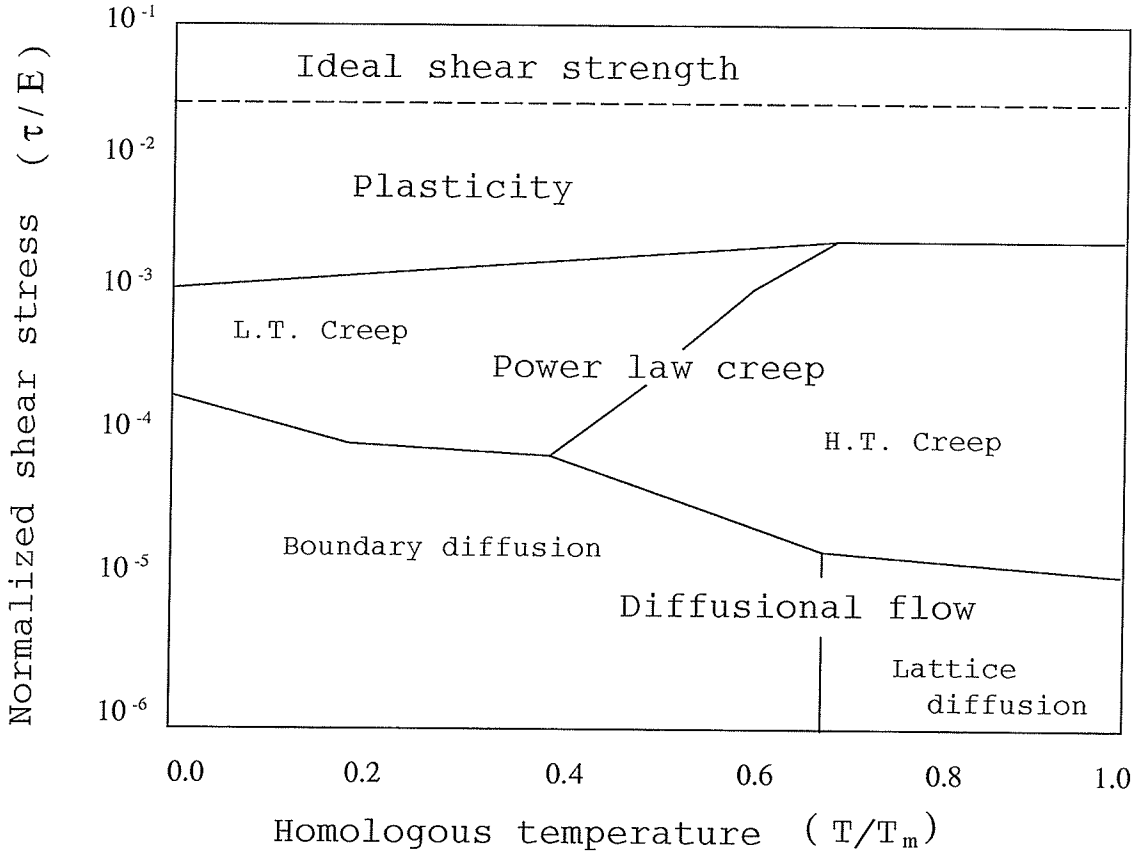

Figure A.2: Illustrative deformation mechanism map[70]

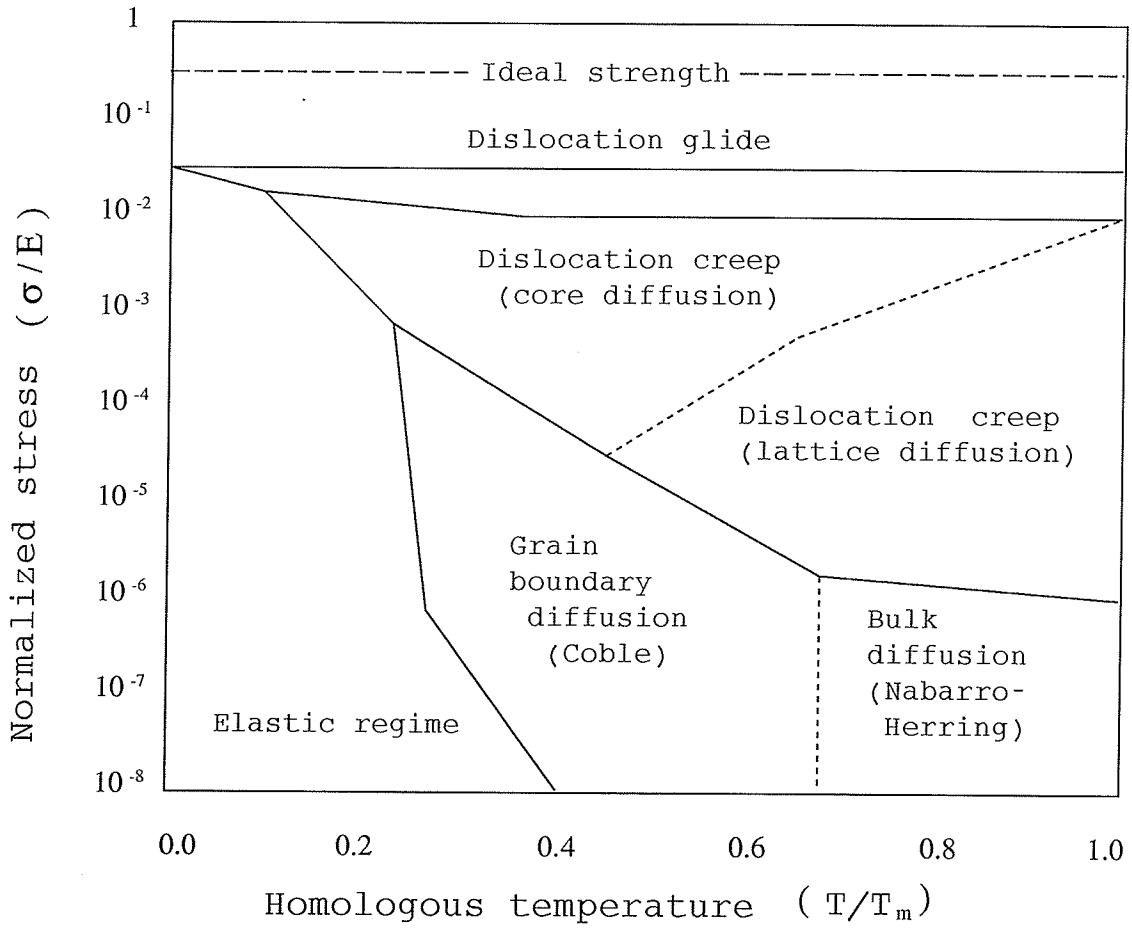

Figure A.3: Illustrative creep deformation mechanism map[224]

as diffusional flow of vacancies or dislocation climb, etc.

These creep mechanisms can be identified on the deformation mechanism maps for various grain sizes of a material as plotted in terms of stress and temperature. For a complicated cyclic thermomechanical loading process, all kinds of controlling mechanisms of creep deformation can be encountered. Sometimes, a combination of these mechanisms can be found active at the same time. Deformation mechanism maps provide an overall presentation of the creep deformation behavior and a useful tool in the prediction of creep behavior with a given thermomechanical loading history. They are also very useful for the designers in identifying the testing domain of creep specimens for simulating the actual service conditions of the material, and in choosing the proper constitutive law for the stress analysis of a given part. The greatest practical advantage of the deformation maps probably lies in the guidance which they provide in the extrapolation of creep data. Most creep tests in the laboratory are done within a year or less, sometimes within a few years, whereas engineering structures like electric power-generating plants are designed to last for at least 25 years[19]. The laboratory data can be extrapolated to the in-service conditions with some confidence only if both lie in the same regime of the deformation mechanisms map.

A.3 Micromechanisms of creep damage and fracture

A.3.1 The nature of creep damage and fracture

When a solid deforms at high temperature, its internal structure changes. Holes, voids or microcracks may nucleate at certain sites along the grain boundaries and within the grains and, grow inside the solid as the material creeps; its grain size may increase (because of grain growth) or decrease (because of dynamic recrystallisation); precipitates within it may coarsen or dissolve; a dominant dislocation structure introduced by prior working may be destroyed; or the microstructure may, in some

other sense, be altered. All these changes are referred to as 'creep damage'[175-176,291,327]. But the dominant creep damage mechanism characterizing the tertiary stage of creep deformation for most metallic materials is the formation and growth of the micro-cavities on grain boundaries[148]. Creep fracture is therefore generally intergranular[116-118]. The cavities may be nucleated early in the creep life, possibly even during the primary stage of creep deformation. But their effects on the creep rate are initially negligibly small. As their number and size increase, they weaken the material progressively. And finally, these voids and microcracks are coalesced to give an intergranular fracture path. The creep damage usually accelerates the creep-rate, which in turn accelerates the rate of the appearance of damage, until the material or component fails. The shape of the tertiary part of the creep curve is a direct result of this coupling between creep-rate and damage-rate. In this section, the micro-flaws such as holes, voids or cavities, microcracks, etc., are collectively termed 'cavity' unless stated elsewhere.

The systematic study of cavitation was probably motivated by the need for the understanding of long-term performance of aircraft engines in the 1930's. Another impetus to the study of intergranular cavitation came from failures of nuclear reactor fuel rods in the 1950's. From these studies it was found that the loss of ductility at high temperatures and slow strain rate was a consequence of grain boundary cavitation. Although cavitation is a widespread failure mechanism, it is by no means a universal fracture mode of high temperature creep. For example, it was reported that pure aluminum, lead and titanium do not exhibit cavitation nor do some of the low-alloy creep-resistant steels and some austenitic steels. For example, certain materials fail by the growth of oxidized surface cracks at high temperature[291,327].

A.3.2 Micromechanisms of fracture

In the same context of the creep deformation mechanism maps, the fracture mechanism maps were also developed, in which phenomenologically different types of

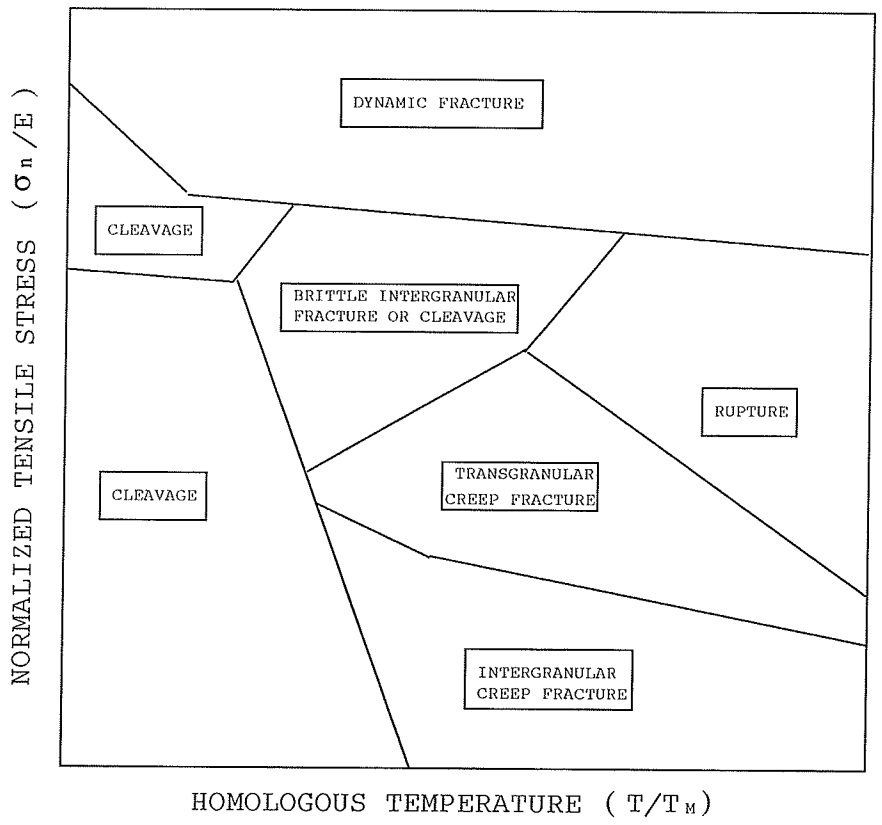

Figure A.4: Illustrative map of the fracture mechanisms[14]

fracture in many metals and a number of important engineering creep resistant alloys have been catalogued[4,14,111,278,291,327]. Shown in Fig. A.4 is a typical fracture mechanism map. As shown in Fig. A.4, there are many mechanisms controlling the fracture process. Crystalline solids can fracture by one of the several mechanisms or a combination of these mechanisms. Although the subject of this thesis research is only on high temperature creep fracture at low strain rates, it is worth to know which alternative mechanisms exist and in which stress and temperature regime they predominate for the final failure of the material. In a somewhat simplified picture, many of the important mechanisms can be displayed on the fracture mechanism map. In analogy to the deformation mechanism maps, fracture mechanism maps have tensile stress on one axis and temperature on the other. In the stress-temperature plane, the regions are indicated within which the different fracture modes are found to prevail. The fields outlined by the contours characterize the regions of conditions in which different types of fracture dominate. This form of presentation of fracture data, when taken together with the corresponding deformation mechanism map for the same material, relates the fracture mechanism to the deformation process that preceded it, and provides guidance in selecting materials for high temperature use and in the extrapolation of fracture data.

Fracture at high temperature in structural alloys can be of several forms as shown in Fig. A.4. Of these, the only one of interest in this thesis research is the intergranular form of creep fracture that occurs under usual service stresses at high temperature and takes a relatively long time to develop. This kind of fracture goes through several stages. It starts with nucleation of cavities along grain boundaries. It is then followed by cavity growth and the increase of the cavity density. With the development of creep deformation, coalescence or linkage of these cavities happens, leading to the development of grain boundary cracks, with or without eventual macro-crack evolution before final fracture[291,327]. It is generally agreed that the intergranular creep fracture of metallic materials is dominated by the formation, growth and coalescence of grain boundary cavities. It is these

intergranular damage processes that are most frequently met in service conditions. A number of material scientists have investigated the damage of materials or the growth of micro-cracks under creep conditions. In these studies, it was emphasized that creep crack extension takes place along the grain boundaries. For instance, it has been reported that under cyclic loading conditions, crack propagation was essentially transgranular[111,116-118]. On the other hand, with an extended load holding time introduced in the cyclicity so that creep deformation can develop, the fracture mode becomes practically intergranular. In addition, mixed modes of fracture under creep deformation conditions were also noted, depending upon the imposed strain level[111,116-118]. Even though voids may nucleate within grains at second phase particles, the intergranular nature of creep fracture indicates that the most damaging cavities are those which exist at grain boundaries. For this reason creep damage as stated in this chapter and in the next chapter is limited only to the grain boundary cavity formation, growth and coalescence. These grain boundary voids then assist both intergranular crack initiation and growth. In certain sense, creep damage in the commonly used engineering metallic materials is manifested by the grain boundary voids. In engineering alloys, cavity nucleation usually occurs continuously, so that the rupture time is affected by the nucleation and growth kinetics in a rather more complicated manner.

A.3.3 Cavity nucleation sites

The nucleation of cavities is of a heterogeneous nature but not a random one[10, 31, 33, 291,327]. Cavity nucleation occurs at distinct nucleation sites along the grain boundaries, rather than homogeneously in the crystal lattice. One of the reasons behind this is that special cavity shapes which can be accommodated at these locations may greatly reduce the nucleation barrier. It has been found that cavity nucleation is prone to occur at the following particular points within the material:

- slip band;
- grain boundary ledge;
- triple grain junctions;
- grain boundary particles

This is due to the fact that these locations within the material have built-in advantages as potential nucleation sites. These geometrical and structural irregularities on grain boundaries, where high stress concentrations could develop, can make use of four special properties of the grain boundary to favour them as potential void nucleation sites[10]. These are:

- A surface energy which favours the nucleation of voids in the grain boundary, or at inclusions contained in it;
- A capacity to act as high diffusivity path, which accelerates the growth of grain boundary voids;
- The ability to act as a sink for matter, which favours rapid void growth;
- The ability of certain boundaries to slide, concentrating stress which favours the nucleation of voids, and creating sliding displacements which may contribute to their growth.

According to these advantage, voids nucleate and grow predominantly on the grain boundary surfaces within the creeping solid. For example, there are several reasons why grain boundary particles act as preferred cavity nucleation sites:

- They resist grain boundary sliding and hence experience stress concentrations;
- They may be weakly bonded to the matrix;
- Cavity nucleation at particle/matrix interfaces may be relatively easy via vacancy condensation even if the interface has a high strength.

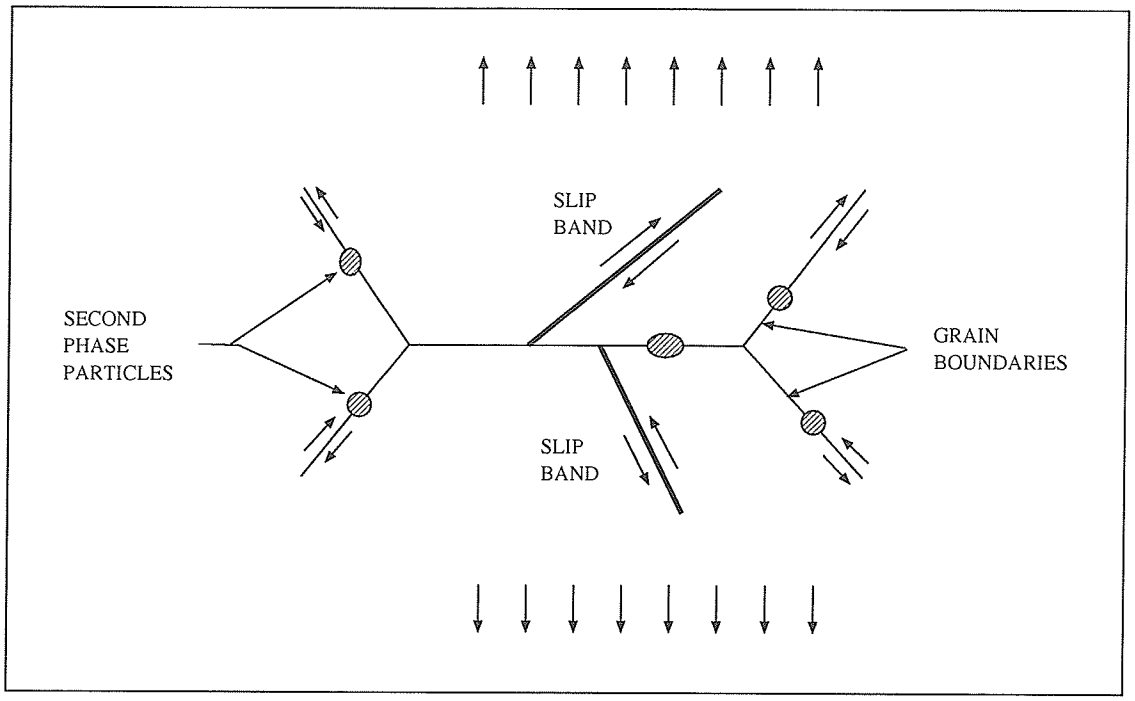

Figure A.5: Intergranular cavity nucleation processes[122]

A.3.4 The observed nucleation kinetics

It was observed that cavity nucleation starts early and continues over an appreciable fraction of, or over the whole, creep life time. Voids can nucleate in many different ways[93,121-122,164,277-278,320].

In a single crystal or where nucleated within grains in polycrystals, cavities are usually associated with inclusions or second phase particles. Their formation occurs either by particle fracture or by separation of the particle-matrix interface.

In polycrystalline solids, nucleation invariably occurs in regions where deformation is nonuniform. It is precisely for this reason that cavity nucleation and creep fracture are localized in grain boundaries. Some of the basic process involved in creep cavity nucleation are illustrated in Fig. A.5. For example, the intersection of a slip band and a grain boundary is a likely site for cavity nucleation. In tests conducted by material scientists, one important common observation was that the cavities were not all nucleated immediately upon the application of load or even after an incubation period, but rather their number was found to increase progres-

sively during the test. Nucleation was either continuous until fracture intervened or the number of cavity reached an approximate saturation value before fracture. As Dyson[93] further noticed, a common result of many experimental studies was that the number of cavities per unit grain boundary area increased approximately in proportion to creep strain with a factor which, to a first approximation, was independent of stress. The proportionality of the cavity density to strain sometimes holds until the very late stage close to final failure. Another equally important deduction from some of the researches is that strain was the parameter controlling the number of cavities and not time. Furthermore, in the early stage of deformation, the cavity number increased linearly with strain and the rate of cavity accumulation varied greatly with different materials. It was also found that the material with the lowest cavity densities exhibit the highest ductilities[291,327].

A.3.5 Basic theories of creep cavity nucleation

There are two basic theories on the mechanisms of creep cavity nucleation: the rupturing of atomic bonds by high local stresses and the condensation of atomic vacancies[291].

A.3.5.1 Cavity nucleation by rupturing of atomic bonds

The ideal cohesive strength of solids is determined by the forces between neighboring planes of atoms. According to the analysis of material scientists, the ideal strength of metallic materials is of the order of 10,000 MPa, whereas typical stresses applied under creep rupture conditions are 100 times lower. Hence, it is clear that the rupturing of atomic bonds in the perfect crystal lattice cannot be expected to occur unless very high stress concentrations are built up locally.

However, in most metallic materials, certain inclusions are weakly bonded to the matrix. The particle/matrix interface has lower cohesion than other parts of the solid. Usually cavities are nucleated at interfaces, where the bonding strength are

much weaker than those of the lattices and, possibly, have other properties that favor cavity nucleation.

On the other hand, in creep tests, the applied stresses are usually much lower than the ideal strength, but the stress concentrations at grain boundaries are much higher. Hence, it cannot be excluded that a local stress higher than the stress at the weakly bonded particle/matrix interface can be achieved under creep conditions. And at that point, the bonding of the particle and the matrix is broken by the local stress, and form a cavity.

A.3.5.2 Cavity nucleation by vacancy condensation

As we have seen in the proceeding section, the rupturing of atomic bonds requires rather high stresses. At elevated temperatures, it was found that the creep deformation processes might nucleate cavities at lower stresses[27,327]. Early in the history of research on creep cavity, it was proposed (first in the 1950's) that voids could be nucleated by the condensation of atomic vacancies. According to this theory, lattice vacancies were condensed under the action of an applied tensile stress to form voids on grain boundaries oriented normally to the tensile axis. But this theory was challenged by some researchers. For example, it was argued that while excess vacancies can be generated by dislocation motion, it is hard to visualize how they can agglomerate on grain boundaries which act as sinks for point defects. It has been shown theoretically[291] that in the presence of high grain boundary stresses, a supersaturation of vacancies may produce voids but the required vacancy concentrations (or local stress) are higher than what might be realistically expected. It was concluded that at high temperatures the local stresses never achieve values that exceed the grain boundary cohesive strength. The models which predict nucleation are possible only at applied stresses approximately 100 times higher than the stresses usually present in engineering applications. Therefore, the idea that stress driven vacancy condensation alone can account for cavity nucleation seems unrea-

sonable. The idea was first dismissed soon after it was proposed, since theoretical arguments seemed to indicate that vacancy condensation into voids was unlikely under creep-rupture conditions.

The idea of cavity nucleation by vacancy condensation was revived in the 1970s. In the revived theory, it was emphasized that the driving force for vacancy condensation is the mechanical stress, whereas earlier workers had considered the supersaturation of vacancies caused by dislocation reactions to be the driving force for vacancy condensation.

A.3.6 Discussion of cavity nucleation theories

In many cases, the basic theories of cavity nucleation as described in the proceeding section are not directly compatible with the observed phenomenon of cavity nucleation. For example, theory predicts that nucleation occurs more or less instantaneously once the nucleation stress is applied, whereas in reality nucleation are found to occur continuously throughout the creep process, and the nucleation rate is controlled by the creep strain rate rather than by the applied stress. Hence, the basic cavity nucleation theories have been criticized for being too primitive. More advanced models have been worked out[291,327]. Some of the models are based on thermodynamics analysis. However, despite the considerable efforts made in order to understand the physical mechanisms of creep cavitation, the cause and mechanisms of cavity nucleation have not been unambiguously determined yet. The solution of this problem could significantly contribute to the improvement of creep life prediction methods and to the design of creep resistant materials with better creep strength and ductility.

A.3.7 Cavity growth and coalescence

According to the results of researches by material scientists, it is generally accepted that the growth of voids on grain boundaries are controlled by the following

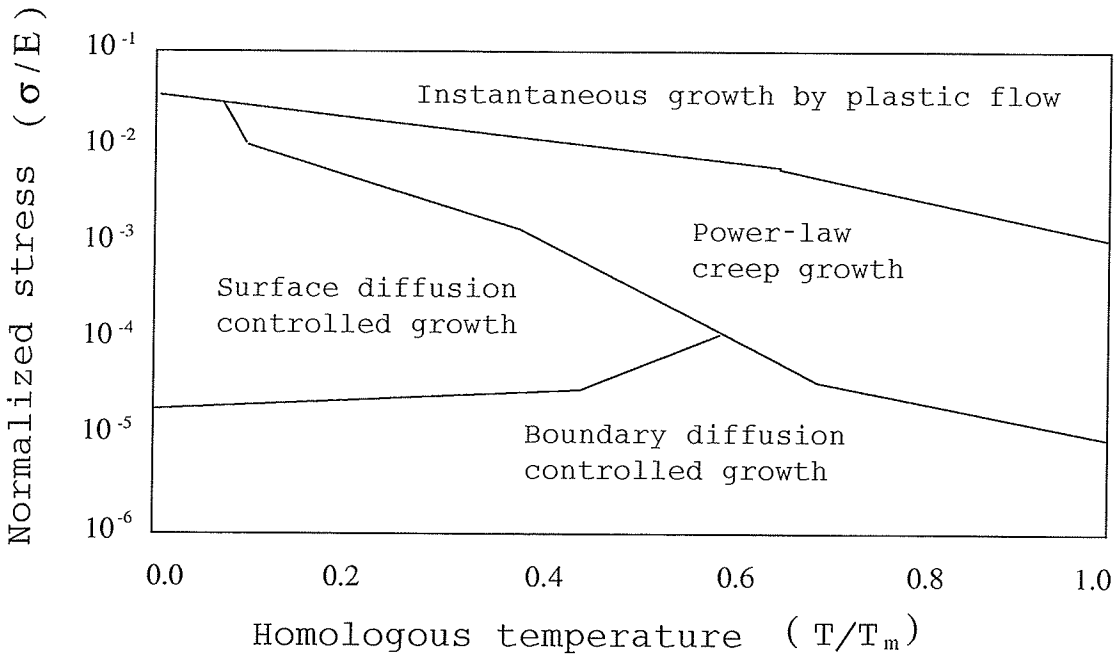

Figure A.6: Illustrative voids growth map[70]

mechanisms[61,70,223]:

- Boundary diffusion;
- Surface diffusion;
- Power-law creep;
- Combinations of these mechanisms

Each mechanism alone or in various combinations may contribute to void growth. The voids grow on grain-boundaries when diffusion is involved. They may grow within the grains when power-law creep is dominant.

The results are conveniently displayed as void growth maps[70] as shown in Fig. A.6. The axes are the local tensile stress, normalized by Young's modulus, σ/E, and temperature, T/T_m, where T_m is the melting temperature. The map is divided into fields in which a single cavity growth mechanism is dominant.

It is well-known that the coalescence of voids occur either by void enlargement (i.e., the material between the voids is reduced by void growth followed by subse-

quent internal necking to a local reduction in area of 100%) or by linkage where the connection between voids is made by shear on a set of glide planes, often parallel to each other. The conditions and mechanisms for void coalescence or linkage are not well understood. In a model of ductile fracture, Le Roy et al[209] adopted a geometrical condition for cavity linkage. He proposed that linkage occurs when the longest void length of an ellipsoid is of the order of the mean planar nearest neighbour spacing. The modelling of void linkage is rarely mentioned in literatures.

A.3.8 Effect of grain boundary sliding

Grain-boundary sliding has an important effect on the void nucleation and subsequent growth[70,291,327]. Such sliding is essential to accommodate diffusional void growth; without it, the voids cannot grow. Also, it has the effect of concentrating stress onto some boundaries and induces a local triaxial stress field as well. Furthermore, it relaxes the shearing stress at the grain boundaries. It is clear that a polycrystalline array generally can not be deformed by grain boundary sliding alone without deforming the grains, i.e., sliding is constrained by the surrounding material. Associated with sliding are stress concentrations at obstacles like second-phase particles or triple grain junctions. This may enhance cavity nucleation. In spite of these effects, grain boundary sliding is usually found not to be the overriding factor for the cavity nucleation and growth processes in engineering materials[291]. For example, in polycrystals, grain boundaries which are oriented normal to the applied tensile stress, and therefore slide the least, cavitate preferentially.

Grain boundary sliding contributes to cavity growth in two different ways[291]. The first is that sliding sheds load on a cavitating boundary. Under normal tensile stresses, this only means that cavity growth rates are enhanced, but under a transverse compressive stress, the cavities would not grow at all unless sliding took place. Sliding transposes the transverse stress into a wedging force pushing the grains adjacent to the cavitation facet apart. The second mechanism by which sliding con-

tributes to cavity growth is that a cavity located at a tensile ledge is pulled out by grain boundary sliding. This mechanism is expected to predominate on boundaries which are inclined to the tensile direction[291].

It has been observed that grain boundary cavitation appears more readily under those conditions which favour a change in deformation mode from bulk deformation to grain boundary sliding. Usually triple points or ledges give rise to sufficient stress concentration to nucleate cavities in grain boundaries by blocking sliding. The presence of particles in a boundary will have much the same effect. It was found that the number of cavities produced increases with an increasing degree of sliding. Alternatively, it has been shown in certain cases that by inhibiting grain boundary sliding, cavity nucleation can be suppressed. Grain boundary sliding against an obstacle such as an underformable particle or a grain boundary ledge seems to be the reasonable source of cavity nucleation.

A.4 Micromechanisms of cyclic creep fracture

In the process of creep deformation, if the load is cyclic, the creep damage and fracture mechanisms become complicated. Generally, the damage to materials during the load cycling process can be described by the following two theories: the theory of the blunting and resharpening of the crack tip and the theory of cavitation on grain boundaries[32,143,240,291].

A.4.1 Crack-tip blunting model

The common mode of cyclic creep crack growth up to moderately high temperatures and moderate hold times is a direct consequence of the cyclic blunting and resharpening of the crack tip. The new crack surface created during the opening mode is not removed reversibly during the subsequent closure of the crack tip. This irreversibility can be caused, for example, by oxygen atoms which quickly adhere to a freshly exposed metal surface. It prevents rewelding of the crack surfaces. There-

fore, the crack advances in each cycle by an increment which, ideally, should be of the order of the cyclic crack-tip opening displacement. Often the opening and closing events leave a microscopically visible striation marking on the fracture surfaces, but seldom does the total number of striations on a fracture surface correspond to the number of loading cycles.

However, the cyclic opening and closing of the crack tip is not the whole truth of the cyclic creep crack growth. There are several complicated factors which could not be explained by this model. One of these factors is the phenomenon of crack closure. In some cases, as the crack grows it leaves behind a wake of plastically stretched material, which leads to crack closure well behind the crack tip during unloading even when the applied load is still tensile. The mechanical contact of the crack faces reduces the cyclic stress intensity experienced by the crack tip region.

A.4.2 Grain boundary cavitation model

The mechanisms of grain boundary cavitation in the creep deformation and creep damage process were described in the previous section. Damage caused by the load cycling process occurs by more or less homogeneous cavitation on grain boundaries over the whole cross sectional area of a specimen[102]. At high temperatures and low loading frequencies or long tensile hold times, cracks may propagate by coalescence of grain boundary cavities. The crack tip blunting mechanism and the cavitation mechanism act in parallel on cyclic creep fracture of the material, and the one which gives higher growth rate predominates[291].

A.4.3 Discussion on cyclic creep fracture

From the viewpoint of continuum damage mechanics, no matter which process dominates, load cycling is a process of damage in which the material's properties become degraded, and so is the macroscopic performance of the material. This finding of the load cycling damage mechanism provides the physical foundation of

the hypothesis that creep damage and high temperature low cycle fatigue damage are of similar physical phenomena and hence of additive nature (addressed in detail in the next two chapters), especially under the loading conditions in this research[205].

A special way in which cyclic creep crack growth may interact with cavitation damage was described[291]. Under cyclic loading conditions, cracks in stainless steel usually grow transgranularly with cyclic loads by the crack tip blunting mechanism. If, however, a long tensile hold time precedes the cyclic loading, the crack path of the cyclic creep fracture changes to intergranular, and this change is accompanied by a large increase in crack growth rate. An explanation is that the hold time causes grain boundary cavitation ahead of the main crack. The subsequent cyclic creep crack growth can occur by fracturing the pre-cavitated grain boundaries by the cavity growth and coalescence mechanism. This mode is preferred only at very high crack growth increments per cycle. Otherwise the transgranular mode of crack growth remains active despite the presence of grain boundary damage.

A.5 Summary

Creep deformation occurs in materials in different modes. In a particular region of the stress-temperature plane, one of these modes dominates. For metallic materials, the creep damage and fracture are generally caused by the nucleation, growth and coalescence of cavities on the grain boundaries. Cavities are not randomly nucleated, their nucleation is prone to occur at certain particular locations within the material. The mechanisms of cavity nucleation need to be further clarified. Grain boundary sliding plays an important role in the creep damage process. Under cyclic loading, the crack tip blunting mechanism and the cavitation mechanism act concurrently to produce cyclic creep fracture of the material, and ultimately, the one which gives higher growth rate dominates. Finally, creep fracture of metallic material is usually in an intergranular form.

Appendix B

Derivation of the finite element equations for creep stress analysis using the proposed CDM based model

For using the proposed CDM based model for cyclic creep fracture analysis, finite element equations had been derived as stated in Chapter 4. In this appendix, details of the derivations are presented.

B.1 Derivation of the derivatives

In chapter 4, only the definitions of the derivatives are given. Followings are the explicit forms of these derivatives:

$$[H_1] = \frac{At^m(\tilde{\sigma} - \bar{R})^{n-1}}{(1 - c_o D)^n}[\frac{n}{\bar{\sigma}}\frac{\partial \tilde{\sigma}}{\partial\{\sigma\}}\{S\} + \frac{\tilde{\sigma} - \bar{R}}{\bar{\sigma}}\frac{\partial\{S\}}{\partial\{\sigma\}} - \frac{(\tilde{\sigma} - \bar{R})\{S\}}{\bar{\sigma}^2}\frac{\partial\bar{\sigma}}{\partial\{\sigma\}}] \quad \text{(B.1)}$$

$$[H_2] = -\frac{n}{\tilde{\sigma} - \bar{R}}\{\dot{\varepsilon}^c\}\frac{\partial\bar{R}}{\partial\{R\}} \quad \text{(B.2)}$$

$$\{H_3\} = \frac{c_o n}{1 - c_o D}\{\dot{\varepsilon}^c\} \quad \text{(B.3)}$$

$$[E_1] = \quad B_1 A(R_s - \bar{R})^p t^m (\frac{\tilde{\sigma} - \bar{R}}{1 - c_0 D})^n \frac{1}{\bar{\sigma}^2}$$

$$[\frac{n\bar{\sigma}}{\tilde{\sigma}-\bar{R}}\{S\}\frac{\partial\tilde{\sigma}}{\partial\{\sigma\}}+\bar{\sigma}\frac{\partial\{S\}}{\partial\{\sigma\}}-\{S\}\frac{\partial\bar{\sigma}}{\partial\{\sigma\}}] \tag{B.4}$$

$$[E_2]=-\{\dot{R}\}\frac{\partial\bar{R}}{\partial\{R\}}[\frac{p}{R_s-\bar{R}}+\frac{n}{\tilde{\sigma}-\bar{R}}] \tag{B.5}$$

$$\{E_3\}=(\frac{nc_0}{1-c_0D})\{\dot{R}\} \tag{B.6}$$

$$\begin{aligned}\{G_1\}= \quad & \{\frac{C_1}{1-D}+\frac{C_2}{(1-D)^{(n+1)r_0}} \\ & [r_0n(\tilde{\sigma}-\bar{R})^{(r_0n-1)}\tilde{\sigma}^{r_0}+(\tilde{\sigma}-\bar{R})^{r_0n}r_0\tilde{\sigma}^{r_0-1}]\}\frac{\partial\tilde{\sigma}}{\partial\{\sigma\}}\end{aligned} \tag{B.7}$$

$$\{G_2\}=-\frac{C_2r_0n}{\tilde{\sigma}-\bar{R}}(\frac{\tilde{\sigma}}{1-D})^{r_0}(\frac{\tilde{\sigma}-\bar{R}}{1-D})^{r_0n}(\frac{1}{\tilde{\sigma}-\bar{R}})\frac{\partial\bar{R}}{\partial\{R\}} \tag{B.8}$$

$$G_3=\frac{C_1\tilde{\sigma}}{(1-D)^2}+C_2r_0(n+1)(\frac{\tilde{\sigma}-\bar{R}}{1-D})^{r_0n}(\frac{1}{1-D})(\frac{\tilde{\sigma}}{1-D})^{r_0} \tag{B.9}$$

B.2 Derivation of the governing equation and the definitions of the process matrices, vectors and constants

Substitute Eq. 4.16 into Eq. 4.10, we have:

$$\begin{aligned}\{\Delta\varepsilon^c\}= \quad & (1-\gamma)\{\dot{\varepsilon}_n^c\}\Delta t+\gamma\Delta t(\{\dot{\varepsilon}_n^c\} \\ & +[H_1]\{\Delta\sigma\}+[H_2]\{\Delta R\}+\{H_3\}\Delta D)\end{aligned} \tag{B.10}$$

that is:

$$\{\Delta\varepsilon^c\}=\{\dot{\varepsilon}_n^c\}\Delta t+\gamma\Delta t[H_1]\{\Delta\sigma\}+\gamma\Delta t[H_2]\{\Delta R\}+\gamma\Delta t\{H_3\}\Delta D \tag{B.11}$$

Substitute Eq. 4.18 into Eq. 4.12, get:

$$\{\Delta R\}=(1-\gamma)\{\dot{R}_n\}\Delta t+\gamma\Delta t(\{\dot{R}_n\}+[E_1]\{\Delta\sigma\}+[E_2]\{\Delta R\}+\{E_3\}\Delta D) \tag{B.12}$$

that is:

$$\{\Delta R\} = \{\dot{R}_n\}\Delta t + \gamma\Delta t[E_1]\{\Delta\sigma\} + \gamma\Delta t[E_2]\{\Delta R\} + \gamma\Delta t\{E_3\}\Delta D \tag{B.13}$$

In concise form, we get:

$$(I - \gamma\Delta t[E_2])\{\Delta R\} = \{\dot{R}_n\}\Delta t + \gamma\Delta t[E_1]\{\Delta\sigma\} + \gamma\Delta t\{E_3\}\Delta D \tag{B.14}$$

Assume:

$$[A_1] = I - \gamma\Delta t[E_2] \tag{B.15}$$

the above equation becomes:

$$\{\Delta R\} = [A_1]^{-1}\Delta t\{\dot{R}_n\} + \gamma\Delta t[A_1]^{-1}[E_1]\{\Delta\sigma\} + \gamma\Delta t[A_1]^{-1}\{E_3\}\Delta D \tag{B.16}$$

Substitute Eq. 4.17 into Eq. 4.11, get:

$$\Delta D = (1-\gamma)\Delta t\dot{D}_n + \gamma\Delta t(\dot{D}_n + \{G_1\}\{\Delta\sigma\} + \{G_2\}\{\Delta R\} + G_3\Delta D) \tag{B.17}$$

that is:

$$\Delta D = \Delta t\dot{D}_n + \gamma\Delta t\{G_1\}\{\Delta\sigma\} + \gamma\Delta t\{G_2\}\{\Delta R\} + \gamma\Delta t G_3\Delta D \tag{B.18}$$

Substitute Eq. B.16 into Eq. B.18, get:

$$\begin{aligned}(1-\gamma\Delta t G_3)\Delta D = \quad & \Delta t\dot{D}_n + \gamma\Delta t\{G_1\}\{\Delta\sigma\} + \gamma\Delta t\{G_2\}[A_1]^{-1}\Delta t\{\dot{R}_n\} \\ & +\gamma\Delta t\{G_2\}\gamma\Delta t[A_1]^{-1}[E_1]\{\Delta\sigma\} \\ & +\gamma\Delta t\{G_2\}\gamma\Delta t[A_1]^{-1}\{E_3\}\Delta D \end{aligned} \tag{B.19}$$

Make it simpler by algebraic manipulation, get:

$$\begin{aligned} & (1-\gamma\Delta t G_3 - (\gamma\Delta t)^2\{G_2\}[A_1]^{-1}\{E_3\})\Delta D \\ = \quad & \Delta t\dot{D}_n + \gamma(\Delta t)^2\{G_2\}[A_1]^{-1}\{\dot{R}_n\} \\ & +((\gamma\Delta t)^2\{G_2\}[A_1]^{-1}[E_1] + \gamma\Delta t\{G_1\})\{\Delta\sigma\} \end{aligned} \tag{B.20}$$

To make it even simpler, assume:

$$A_2 = 1 - \gamma\Delta t G_3 - (\gamma\Delta t)^2\{G_2\}[A_1]^{-1}\{E_3\} \tag{B.21}$$

and:

$$\{A_3\} = \gamma\Delta t\{G_1\} + (\gamma\Delta t)^2\{G_2\}[A_1]^{-1}[E_1] \tag{B.22}$$

Then, Eq. B. 20 is reduced to the following form:

$$\Delta D = \Delta t A_2^{-1}\dot{D}_n + \gamma(\Delta t)^2 A_2^{-1}\{G_2\}[A_1]^{-1}\{\dot{R}_n\} + A_2^{-1}\{A_3\}\{\Delta\sigma\} \tag{B.23}$$

Substitute Eq. B. 23 into Eq. B. 16, we get:

$$\begin{aligned}\{\Delta R\} &= \Delta t[A_1]^{-1}\{\dot{R}_n\} + \gamma\Delta t[A_1]^{-1}[E_1]\{\Delta\sigma\} \\ &\quad +\gamma\Delta t[A_1]^{-1}\{E_3\}\Delta t A_2^{-1}\dot{D}_n \\ &\quad +\gamma\Delta t[A_1]^{-1}\{E_3\}\gamma(\Delta t)^2 A_2^{-1}\{G_2\}[A_1]^{-1}\{\dot{R}_n\} \\ &\quad +\gamma\Delta t[A_1]^{-1}\{E_3\}A_2^{-1}\{A_3\}\{\Delta\sigma\}\end{aligned} \tag{B.24}$$

After some rearrangement, we get:

$$\begin{aligned}\{\Delta R\} &= (\Delta t[A_1]^{-1} + (\gamma\Delta t)^2\Delta t[A_1]^{-1}\{E_3\}A_2^{-1}\{G_2\}[A_1]^{-1})\{\dot{R}_n\} \\ &\quad +\gamma(\Delta t)^2[A_1]^{-1}\{E_3\}A_2^{-1}\dot{D}_n \\ &\quad +(\gamma\Delta t[A_1]^{-1}[E_1] + \gamma\Delta t[A_1]^{-1}\{E_3\}A_2^{-1}\{A_3\})\{\Delta\sigma\}\end{aligned} \tag{B.25}$$

To make it in concise form, assume:

$$[A_4] = \Delta t[A_1]^{-1} + (\gamma\Delta t)^2\Delta t[A_1]^{-1}\{E_3\}A_2^{-1}\{G_2\}[A_1]^{-1} \tag{B.26}$$

$$\{A_5\} = \gamma(\Delta t)^2[A_1]^{-1}\{E_3\}A_2^{-1} \tag{B.27}$$

$$\{A_6\} = \gamma\Delta t[A_1]^{-1}[E_1] + \gamma\Delta t[A_1]^{-1}\{E_3\}A_2^{-1}\{A_3\} \tag{B.28}$$

and:

$$\{A_7\} = 0 \tag{B.29}$$

Eq. B. 25 is now reduced to:

$$\{\Delta R\} = [A_4]\{\dot{R}_n\} + \{A_5\}\dot{D}_n + [A_6]\{\Delta\sigma\} + \{A_7\} \tag{B.30}$$

Substitute Eqs. B. 23 and B. 30 into Eq. B. 11, get:

$$\begin{aligned}\{\Delta\varepsilon^c\} &= \{\dot{\varepsilon}^c_n\}\Delta t + \gamma\Delta t[H_1]\{\Delta\sigma\} \\ &\quad +\gamma\Delta t[H_2][A_4]\{\dot{R}_n\} + \gamma\Delta t[H_2]\{A_5\}\dot{D}_n \\ &\quad +\gamma\Delta t[H_2][A_6]\{\Delta\sigma\} + \gamma\Delta t[H_2]\{A_7\} \\ &\quad +\gamma\Delta t\{H_3\}\Delta t A_2^{-1}\dot{D}_n \\ &\quad +\gamma\Delta t\{H_3\}\gamma(\Delta t)^2 A_2^{-1}\{G_2\}[A_1]^{-1}\{\dot{R}_n\} \\ &\quad +\gamma\Delta t\{H_3\}A_2^{-1}\{A_3\}\{\Delta\sigma\}\end{aligned} \tag{B.31}$$

that is:

$$\begin{aligned}\{\Delta\varepsilon^c\} &= \{\dot{\varepsilon}^c_n\}\Delta t \\ &\quad +(\gamma\Delta t[H_1] + \gamma\Delta t[H_2][A_6] + \gamma\Delta t\{H_3\}A_2^{-1}\{A_3\})\{\Delta\sigma\} \\ &\quad +(\gamma\Delta t[H_2][A_4] + \gamma\Delta t\{H_3\}\gamma(\Delta t)^2 A_2^{-1}\{G_2\}[A_1]^{-1})\{\dot{R}_n\} \\ &\quad +(\gamma\Delta t[H_2]\{A_5\} + \gamma\Delta t\{H_3\}\Delta t A_2^{-1})\dot{D}_n \\ &\quad +\gamma\Delta t[H_2]\{A_7\}\end{aligned} \tag{B.32}$$

Assume:

$$[A_8] = \gamma\Delta t[H_1] + \gamma\Delta t[H_2][A_6] + \gamma\Delta t\{H_3\}A_2^{-1}\{A_3\} \tag{B.33}$$

$$[A_9] = \gamma\Delta t[H_2][A_4] + (\gamma\Delta t)^2\Delta t\{H_3\}A_2^{-1}\{G_2\}[A_1]^{-1} \tag{B.34}$$

$$\{A_{10}\} = \gamma\Delta t[H_2]\{A_5\} + \gamma(\Delta t)^2\{H_3\}A_2^{-1} \tag{B.35}$$

and:

$$\{A_{11}\} = \gamma\Delta t[A_7] \tag{B.36}$$

Then, Eq. B. 32 is reduced to:

$$\{\Delta\varepsilon^c\} = \Delta t\{\dot{\varepsilon}^c_n\} + [A_8]\{\Delta\sigma\} + [A_9]\{\dot{R}_n\} + \{A_{10}\}\dot{D}_n + \{A_{11}\} \tag{B.37}$$

Substitute Eq. B. 37 into Eq. 4.2, get:

$$\begin{aligned}\{\Delta\sigma\} &= [C_{ep}](\{\Delta\varepsilon\} - \Delta t\{\dot{\varepsilon}_n^c\} - [A_8]\{\Delta\sigma\} - [A_9]\{\dot{R}_n\} \\ &\quad -\{A_{10}\}\dot{D}_n - \{A_{11}\}) \end{aligned} \tag{B.38}$$

Assume:

$$\{A_{12}\} = \Delta t\{\dot{\varepsilon}_n^c\} + [A_9]\{\dot{R}_n\} + \{A_{10}\}\dot{D}_n + \{A_{11}\} \tag{B.39}$$

Then, Eq. B. 37 is reduced to:

$$(I + [C_{ep}][A_8])\{\Delta\sigma\} = [C_{ep}](\{\Delta\varepsilon\} - \{A_{12}\}) \tag{B.40}$$

Assume:

$$[C_{ep}^*] = (I + [C_{ep}][A_8])^{-1}[C_{ep}] \tag{B.41}$$

the we derive:

$$\{\Delta\sigma\} = [C_{ep}^*][[B]\{\Delta U\} - \{A_{12}\}] \tag{B.42}$$

Substitute this equation into Eq. 4.4, get:

$$(\int_V [B]^T[C_{ep}^*][B]dV)\{\Delta U\} = \{\Delta F\} + \int_V [B]^T[C_{ep}^*]\{A_{12}\}dV \tag{B.43}$$

This is the governing equation for creep stress analysis using the proposed CDM based model by the finite element method.

Appendix C

Derivation of the finite element equations with strain localization line embedded for creep stress analysis using the proposed CDM based constitutive model

In finite element analysis, some of the basic equations are:

The governing equation (or the equilibrium equation):

$$\int_V [B]^T \{\Delta\sigma\} dV = \{\Delta F\} \tag{C.1}$$

The constitutive equation:

$$\{\Delta\sigma\} = [C_{ep}](\{\Delta\varepsilon\} - \{\Delta\varepsilon^c\}) \tag{C.2}$$

The compatibility equation:

$$\{\Delta\varepsilon\} = [B]\{\Delta U\} \tag{C.3}$$

Once localization is triggered within an element, according to the derivations in Appendix D, we have in the particular element:

$$\{\Delta\varepsilon\} = [B](\{\Delta U\} - \phi R\hat{U}^c) \tag{C.4}$$

and:

$$\hat{U^c} = S_{CC}^{-1} S_{UU} \{\Delta U\} \tag{C.5}$$

that is:

$$\{\Delta\varepsilon\} = [B](\{\Delta U\} - \phi R S_{CC}^{-1} S_{UU} \{\Delta U\}) \tag{C.6}$$

or:

$$\{\Delta\varepsilon\} = [B][I - \phi R S_{CC}^{-1} S_{UU}]\{\Delta U\} \tag{C.7}$$

According to the derivation in the previous section, for creep stress analysis using the proposed CDM based model, we have:

$$\{\Delta\varepsilon^c\} = \Delta t\{\dot{\varepsilon}_n^c\} + [A_8]\{\Delta\sigma\} + [A_9]\{\dot{R}_n\} + \{A_{10}\}\dot{D}_n + \{A_{11}\} \tag{C.8}$$

Substitute Eqs. C.7 and C.8 into Eq. C.2, one could obtain:

$$\begin{aligned}\{\Delta\sigma\} \;=\; & [C_{ep}]([B][I - \phi R S_{CC}^{-1} S_{UU}\{\Delta U\} - [\Delta t\{\dot{\varepsilon}_n^c\} + [A_8]\{\Delta\sigma\} \\ & + [A_9]\{\dot{R}_n\} + \{A_{10}\}\dot{D}_n + \{A_{11}\}])\end{aligned} \tag{C.9}$$

that is:

$$(I + [C_{ep}][A_8])\{\Delta\sigma\} = [C_{ep}]([B][I - \phi R S_{CC}^{-1} S_{UU}]\{\Delta U\} - \{A_{12}\}) \tag{C.10}$$

where:

$$\{A_{12}\} = \Delta t\{\dot{\varepsilon}_n^c\} + [A_9]\{\dot{R}_n\} + \{A_{10}\}\dot{D}_n + \{A_{11}\} \tag{C.11}$$

Hence, we could get:

$$\{\Delta\sigma\} = [C_{ep}^*]([B][I - \phi R S_{CC}^{-1} S_{UU}]\{\Delta U\} - \{A_{12}\}) \tag{C.12}$$

where:

$$[C_{ep}^*] = (I + [C_{ep}][A_8])^{-1}[C_{ep}] \tag{C.13}$$

Substitute Eq. C.12 into Eq. C.1, the equilibrium equation derived based on the variational principle, we get:

$$\int_V [B]^T [C_{ep}^*]([B][I - \phi R S_{CC}^{-1} S_{UU}]\{\Delta U\} - \{A_{12}\}) dV = \{\Delta F\} \tag{C.14}$$

To make it in simpler form, we get:

$$\int_V [B]^T [C^*_{ep}][B][I - \phi R S^{-1}_{CC} S_{UU}] dV \{\Delta U\} = \{\Delta F\} + \int_V [B]^T [C^*_{ep}]\{A_{12}\} dV \quad \text{(C.15)}$$

That is:

$$[K^*]\{\Delta U\} = \{\Delta F\} + \{\Delta F_1\} \quad \text{(C.16)}$$

where:

$$[K^*] = \int_V [B]^T [C^*_{ep}][B][I - \phi R S^{-1}_{CC} S_{UU}] dV \quad \text{(C.17)}$$

$$\{\Delta F_1\} = \int_V [B]^T [C^*_{ep}]\{A_{12}\} dV \quad \text{(C.18)}$$

Other parameters, such as S_{CC} and S_{UU} are defined in the subsequent appendix. Eq. C.16 is the governing finite element equation with strain localization line embedded for creep fracture analysis. The strain localization line is used here to simulate the damaged material or the extended crack length.

Appendix D

Derivation of the finite element equations with localization line embedded

D.1 Finite element equations

In this appendix, derivation of the finite element equations with localization line embedded is presented. These derivations are based on the works of Bathe and Dvorkin[91-92]. They are provided here for the ease of reading the other related derivations. Suppose there is an element within the global finite element mesh with an embedded localization line (crack or the locus of damaged material) running through, and it is in equilibrium at time step (load level) t. Now, we seek the equilibrium configuration of the element at time $t + \Delta t$ as shown in Fig. D.1. The principle of virtual work must be satisfied in the domain of the element. This leads to the following equation:

$$\int_{V_1} \delta\Delta\varepsilon^T \sigma dV_1 + \int_{V_2} \delta\Delta\varepsilon^T \sigma dV_2 = \int_{S_1} \delta U^T P_1 dS_1 + \int_{S_2} \delta U^T P_2 dS_2 + \int_{A_1} \delta U^T r_1 dA_1 + \int_{A_2} \delta U^T r_2 dA_2 \quad \text{(D.1)}$$

where:

$\Delta\varepsilon$ is the incremental infinitesimal strain vector

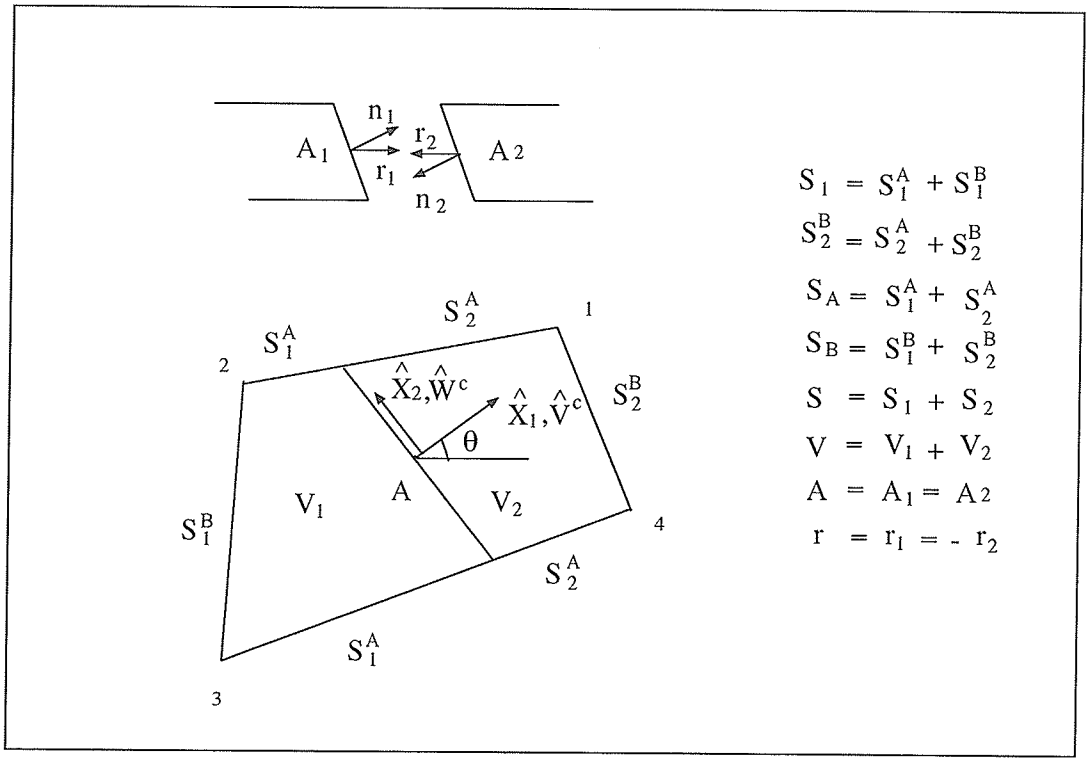

Figure D.1: Element with a strain localization line embedded[91-92]

σ is the stress vector at time $t + \Delta t$

u is the incremental displacement vector

P_1 is the traction acting upon the edges of element of portion V_1

P_2 is the traction acting upon the edges of element of portion V_2

Other terms in the above equations should be self-explanatory.

Assume:

$$\hat{U}^c = \left\{ \begin{array}{c} \hat{v}^c \\ \hat{w}^c \end{array} \right\}$$

and prior to localization occurs in the element:

$$u = HU \tag{D.2}$$

where $\hat{U}^c$ is the vector of the rigid incremental displacement of the localization line in a local $CCS(\hat{x}_1, \hat{x}_2)$. R is the matrix that rotates local $CCS(\hat{x}_1, \hat{x}_2)$ to the global

CCS. ϕ is a matrix:

$$\phi = \begin{bmatrix} \phi_1 \\ \cdot \\ \cdot \\ \cdot \\ \phi_N \end{bmatrix}$$

where N is the number of nodes, the submatrix $\phi_{i2\times 2}$ depends on the position of node i relative to the localization line, according to the following rule:

$$\phi_i = \begin{cases} 0 & \text{when node } i \in V_1 \\ I & \text{when node } i \in V_2 \end{cases}$$

H is the displacement interpolation matrix, U is the vector of incremental nodal displacement, u is the displacement field within the domain of V. Hence, the displacement interpolation for the subdomain V_1 is:

$$u_1 = H(U - \phi R\hat{U}^c) \tag{D.3}$$

for the right subdomain V_2:

$$u_2 = HU + (H\phi - I)R\hat{u}^c \tag{D.4}$$

That is, for two neighboring points on either side of the localization line, the incremental displacement discontuity is:

$$u^+ - u^- = R\hat{U}^c \tag{D.5}$$

And the strain interpolation is:

$$\Delta\varepsilon = B(U - \phi R\hat{U}^c) \tag{D.6}$$

Substitute Eqs. D.3, D.4 and D.6 into Eq. D.1, and take into account that δU and $\delta\hat{U}^c$ are independent variations, after some simple mathematical manipulations, the following two sets of equations are derived:

$$\int_V B^T \sigma dV = \int_S H^T P dS \tag{D.7}$$

Or in incremental form:

$$\int_V B^T \Delta\sigma dV = \int_S H^T \Delta P dS \tag{D.8}$$

and:

$$R^T\phi^T \int_V B^T \sigma dV = R^T\phi^T \int_{S_A} H_{S_A}^T P dS - \int_{S_2^A} R^T P_2 dS_2^A - \int_A R^T r dA \tag{D.9}$$

Eq. D.8 is the standard set of global equilibrium equation. Eq. D.9 is an additional condition for the global equilibrium which is derived due to the existence of the strain localization line within an element and is dealt with here in detail. After some algebraic manipulation, Eq. D.9 can be expressed as:

$$\int_{S_2} R^T P_2 dS = \int_A (-R)^T r dA \tag{D.10}$$

Also, according to the equilibrium of subdomain V_2, one gets:

$$\int_{S_2} R^T P_2 dS = \int_A \underline{\sigma} n_A dA \tag{D.11}$$

where $\underline{\sigma}$ is a second order tensor of stress, n_A is the direction vector of the localization line. By properly defining a matrix ψ, we can get:

$$\underline{\sigma} n_A = \psi\sigma \tag{D.12}$$

According to Eqs. D. 10, D. 11 and D. 12, one can get:

$$\int_A \psi\sigma dA = \int_A (-R)^T r dA \tag{D.13}$$

Expressed in incremental form, the above equation can be expressed as:

$$\int_A \psi\Delta\sigma dA = \int_A (-R)^T \Delta r dA \tag{D.14}$$

For the linearized incremental step, we have:

$$\sigma^{t+\Delta t} - \sigma^t = D_t \Delta\varepsilon \tag{D.15}$$

where D_t is the elasto-plastic stiffness matrix, σ^t is the stress vector at time step (load level) t. Substitute Eqs. D. 6, D. 14 and D. 15 into Eq. D. 8, we could obtain:

$$\int_V B^T D_t B(U - \phi R\hat{U}^c)dA = \int_S H^T \Delta P dS \tag{D.16}$$

Assume the stress–displacement incremental relationship of the localization line is:

$$\Delta r = \hat{C}^c \hat{U}^c \tag{D.17}$$

Substitute Eqs. D. 6, D. 15 and D. 17 into Eq. D.14, get:

$$(\int_A \psi D_t B dA)U = (\int_A (\psi D_t B \phi R - R^T \hat{C}^c)dA)\hat{U}^c \tag{D.18}$$

Calling:

$$S_{UU} = \int_A \psi D_t B dA \tag{D.19}$$

$$S_{CC} = \int_A (\psi D_t B \phi R - R^T \hat{C}^c)dA \tag{D.20}$$

Eq. D. 18 is then simplified to the following form:

$$\hat{U}^c = S_{CC}^{-1} S_{UU} U \tag{D.21}$$

Bring Eq. D.21 to Eq. D. 16, we could get:

$$[\int_V B^T D_t B(I - \phi R S_{cc}^{-1} S_{UU})dV]U = \int_s H^T \Delta P dS \tag{D.22}$$

This is the governing equation of the element with localization line embedded.

D.2 Direction of the strain localization line embedded in an element

When strain localization is triggered within an element, there is a jump of strain field across the plane of discontinuity (localization line), i.e.:

$$[U_{i,j}] = U_{i,j}^+ - U_{i,j}^- \tag{D.23}$$

and $[U_{i,j}] \neq 0$ And the jump may be expressed as follows with an arbitrary vector g:

$$[U_{i,j}] = g_i n_i \tag{D.24}$$

Assume:

$$m_i = g_i / g \tag{D.25}$$

and:

$$g = \mid g \mid \tag{D.26}$$

The pair of unit vectors m and n entirely defines the nature of the discontinuity. The corresponding strain jump is given by:

$$[\varepsilon_{ij}] = \frac{1}{2}(g_i n_j + g_j n_i) \tag{D.27}$$

that is:

$$[\varepsilon_{ij}] = \frac{\dot{g}}{2}(m_i n_j + m_j n_i) \tag{D.28}$$

Assuming the incremental stress-strain relations take the following form:

$$\dot{\sigma}_{ij} = D_{ijkl}\dot{\varepsilon}_{kl} \tag{D.29}$$

where D is the tangent stiffness tensor for the material. We restrict actually attention to the cases where D is piece wise independent of $\dot{\varepsilon}$. For elastic-plastic-creep stress analysis, the localization bifurcation analysis is carried out using the same D across the incipient planes of discontinuity. Hence, taking jumps in Eq. D.29 leads to:

$$[\dot{\sigma}_{ij}] = D_{ijkl}[\dot{\varepsilon}_{ij}] \tag{D.30}$$

Equilibrium across the discontinuity planes requires that the tractions r be continuous, i.e.:

$$[\dot{r}_j] = 0 \tag{D.31}$$

and:

$$[\dot{r}_j] = n_i[\dot{\sigma}_{ij}] \tag{D.32}$$

Combine Eqs. D.29 and D.32, it follows that:

$$n_i D_{ijkl}[\dot{\varepsilon}_{kl}] = 0 \tag{D.33}$$

Finally, using the kinematic relation as expressed in Eq. D.27 and the definition in Eq. D.25, one can get:

$$A_{jk}(n)m_k = 0 \tag{D.34}$$

where:

$$A_{jk}(n) = n_i D_{ijkl} n_l \tag{D.35}$$

This condition has to be satisfied by m and n for the localized mode to be possible. The onset of the localization occurs at the first point in the deformation history for which a nontrivial solution of the above equation exists. For localization to occur along the direction n, the localization matrix $A(n)$ has to have at least one nonzero eigenvalue. This in turn necessitates:

$$det(A(n)) = 0 \tag{D.36}$$

Now, the problem turns to calculating the direction $n = (cos\theta, sin\theta)$ which will satisfy the above equation. Such direction corresponds to the direction of the localization line.

In the literatures, detailed formula was presented to calculate the direction of the localization line embedded in an element in two dimensional cases[265-266].

Appendix E

Static creep results of the bar under tension

This appendix contains the figures of static creep of the uniaxial bar under tension.

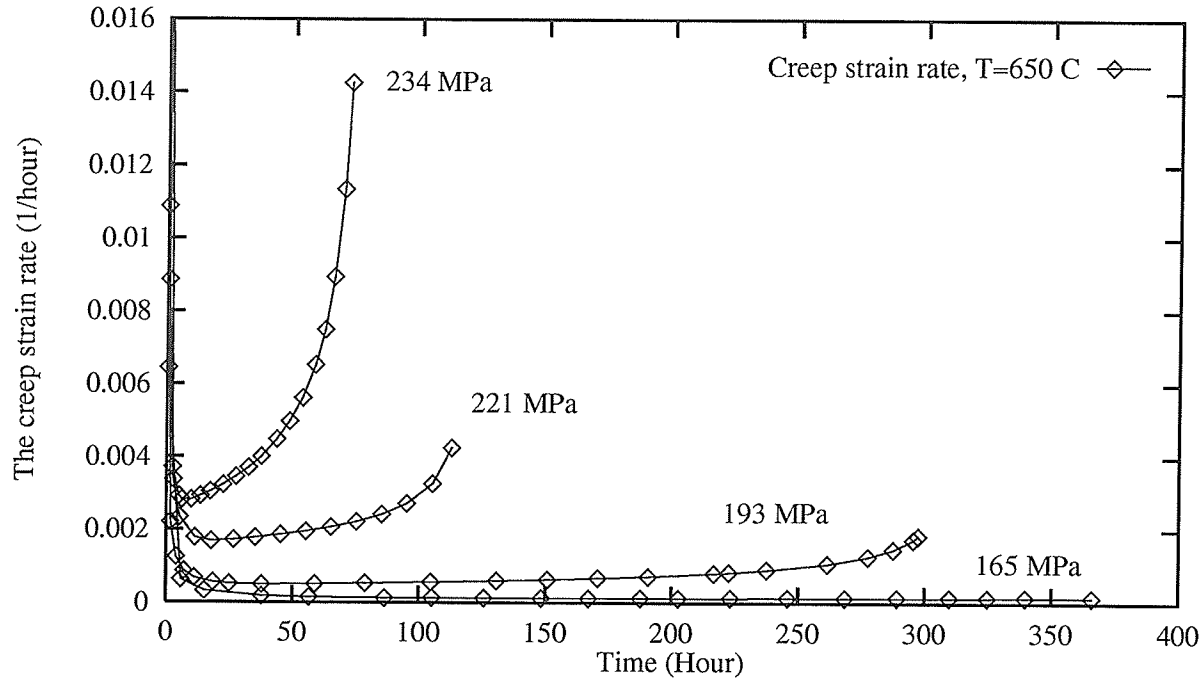

Figure E.1: The development of the creep strain rate

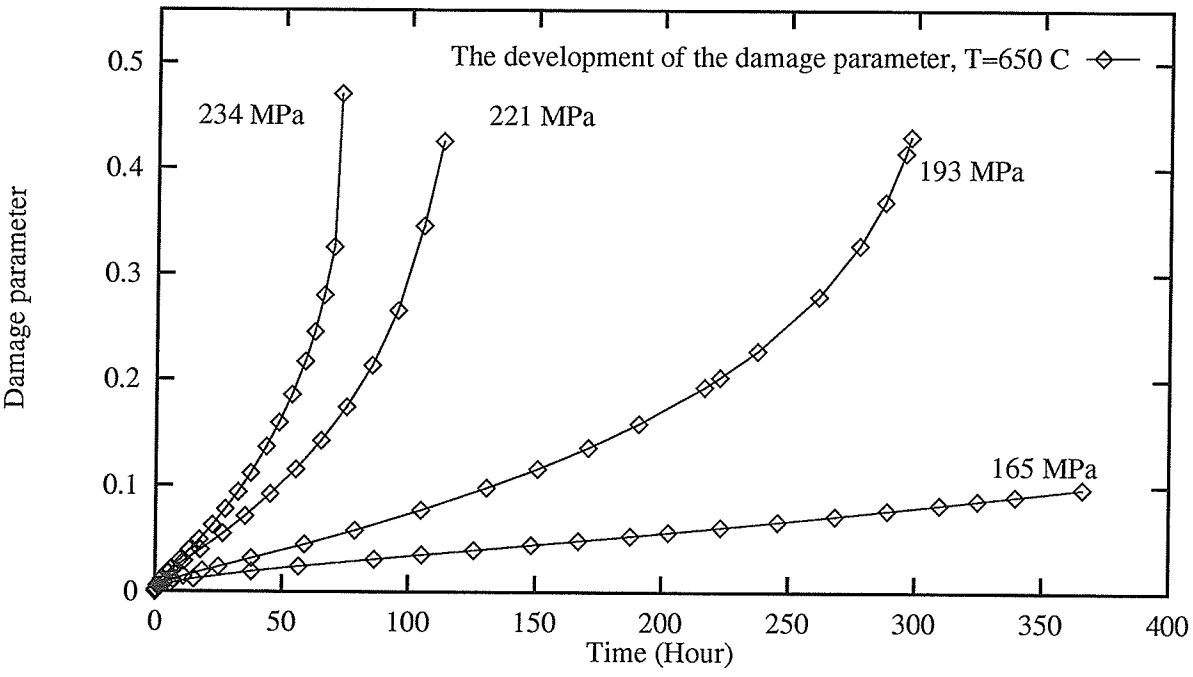

Figure E.2: The development of the damage parameter

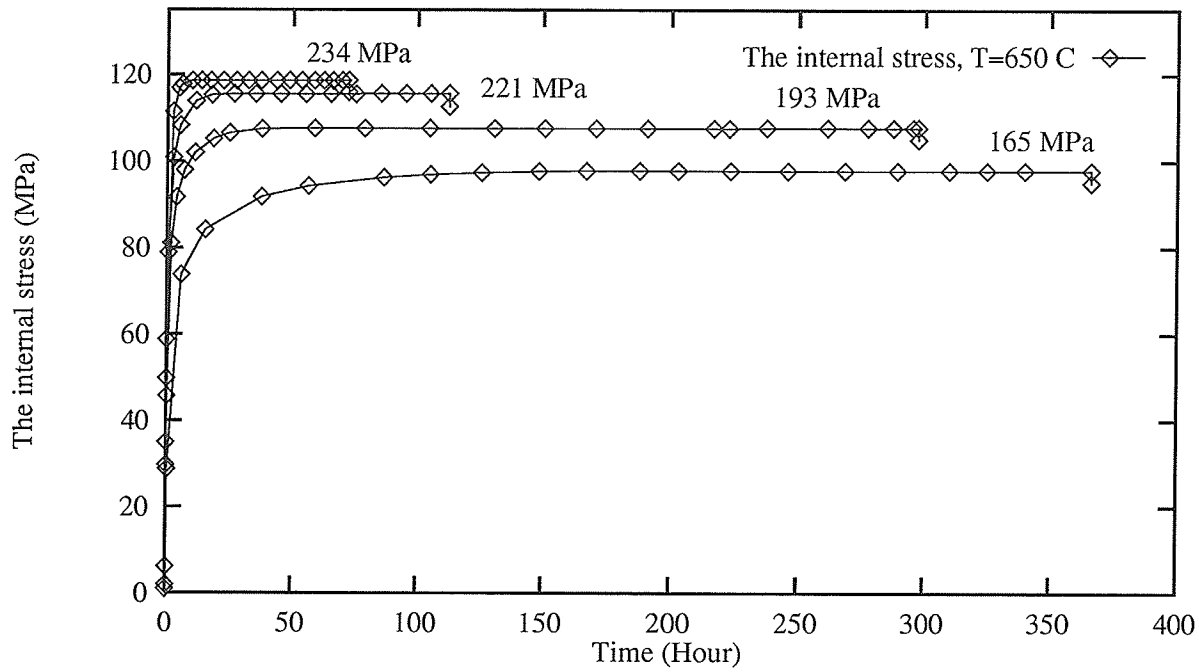

Figure E.3: The development of the internal stress

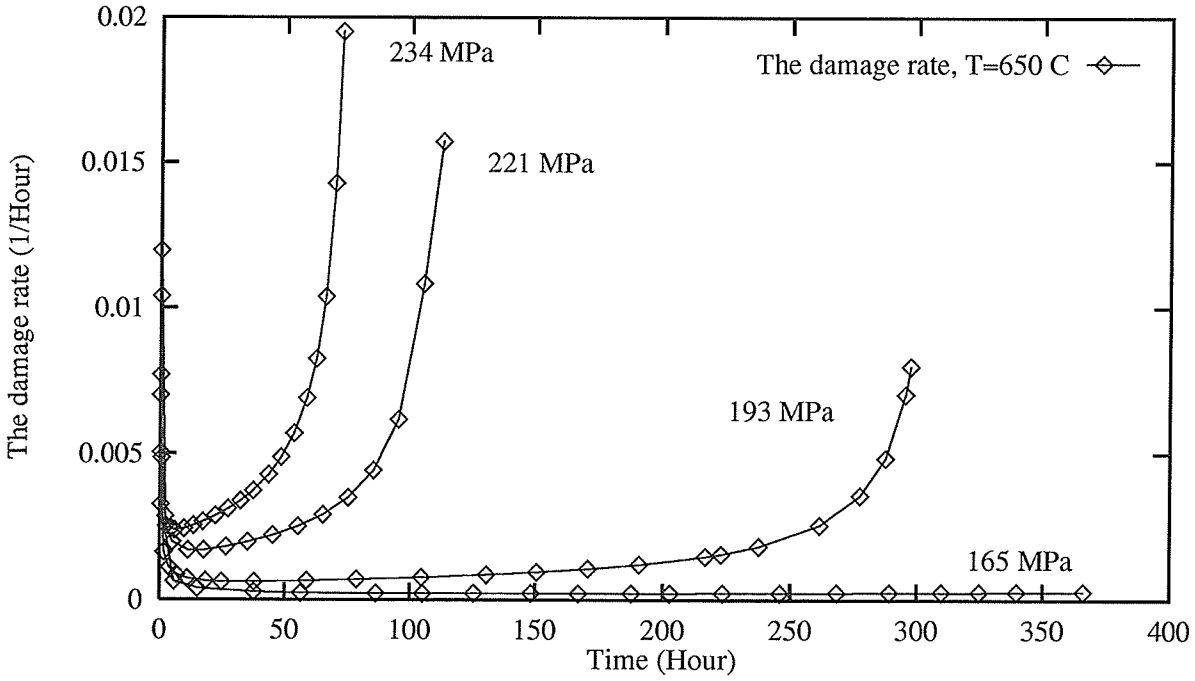

Figure E.4: The development of the damage rate

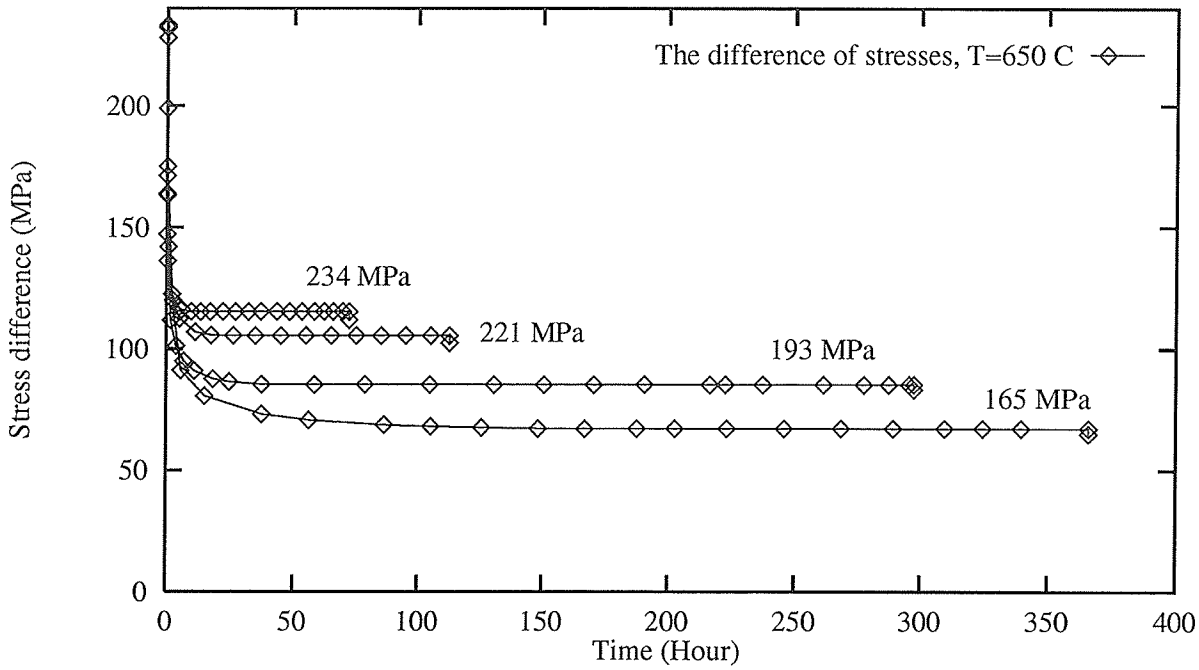

Figure E.5: The evolution of the difference between the damage equivalent stress and the internal stress $(\tilde{\sigma} - \bar{R})$

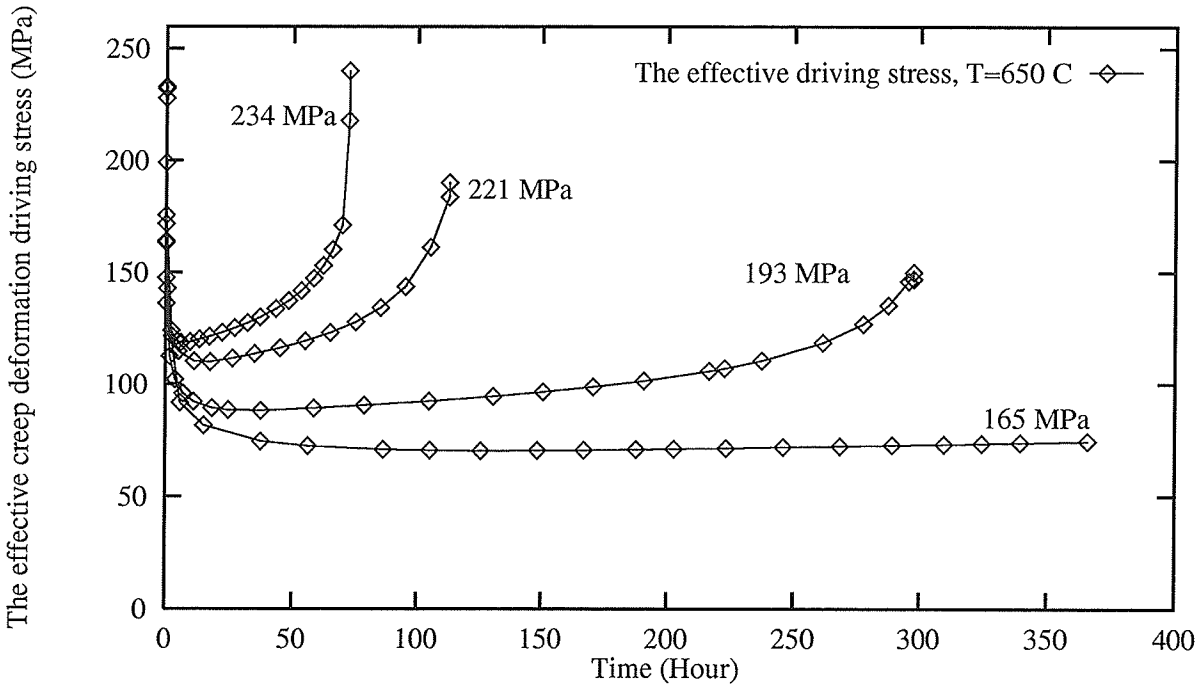

Figure E.6: The evolution of the effective creep deformation driving stress $\frac{\tilde{\sigma}-\bar{R}}{1-c_o D}$

Appendix F

Cyclic creep results of the bar under tension – load cycling effect

This appendix contains the figures which show the importance of load cycling effect in the creep deformation process. As a comparison, results of the uniaxial bar under cyclic loading without load dwell time are plotted together with the corresponding results under static loading condition.

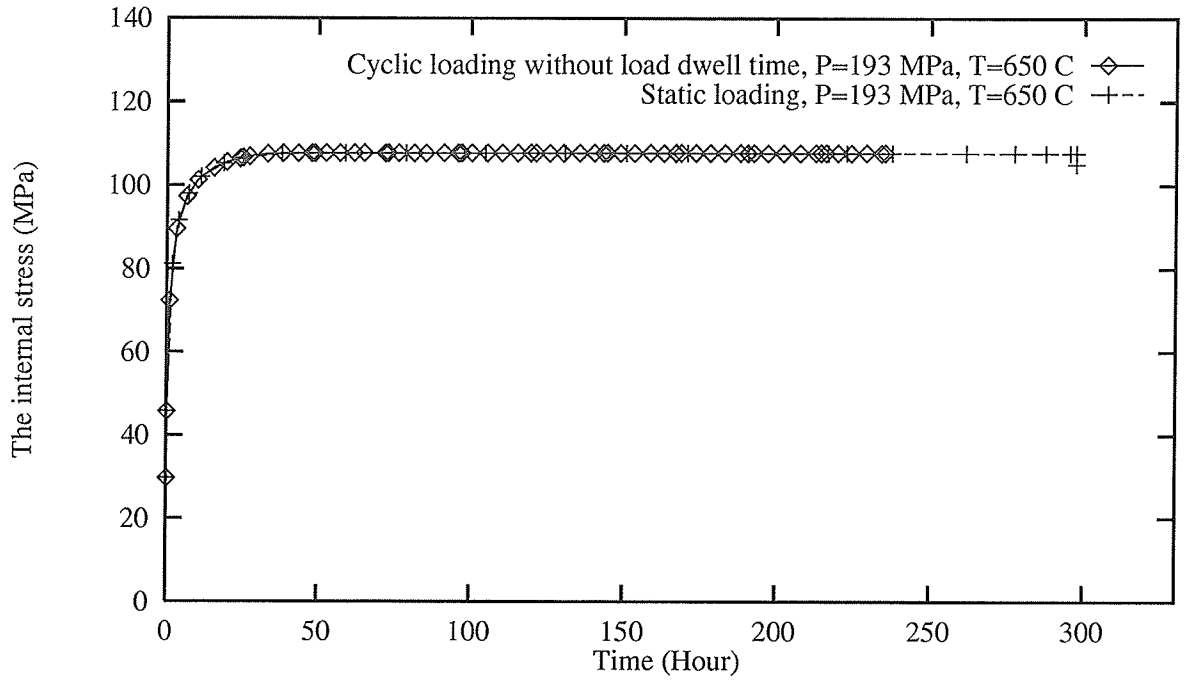

Figure F.1: The development of the internal stress under the static and cyclic load of 193 MPa and 650°C without load dwell time

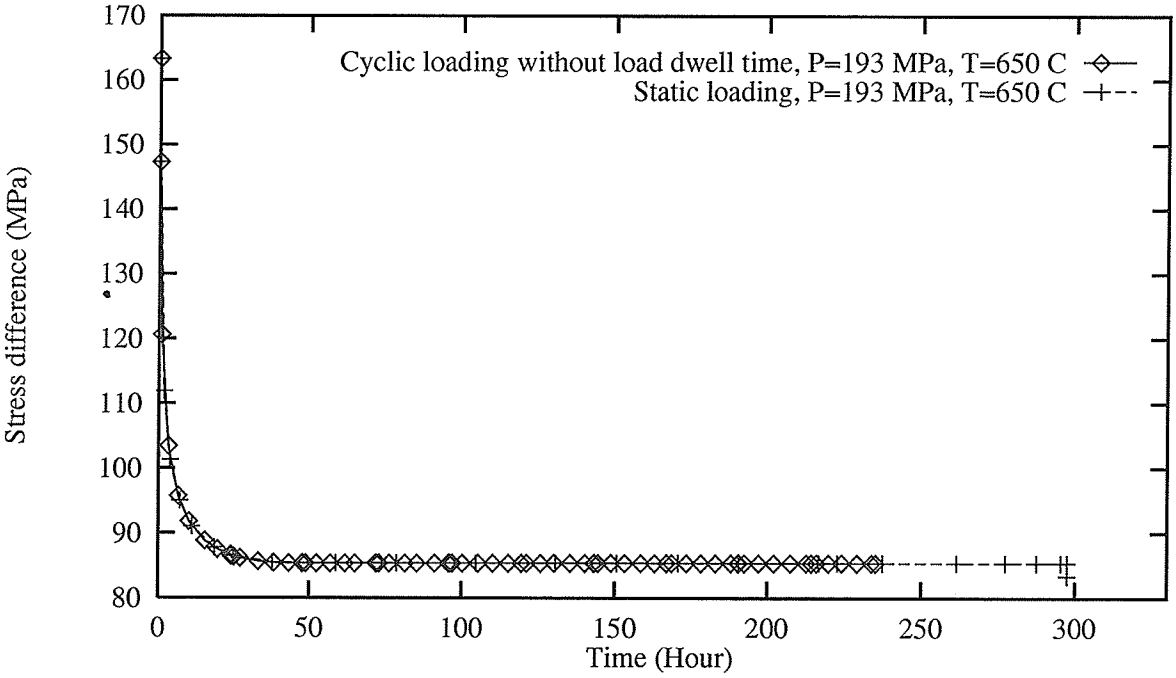

Figure F.2: The development of the difference between the damage equivalent stress and the internal stress $(\tilde{\sigma} - \bar{R})$ under the static and cyclic load of 193 MPa and 650°C without load dwell time

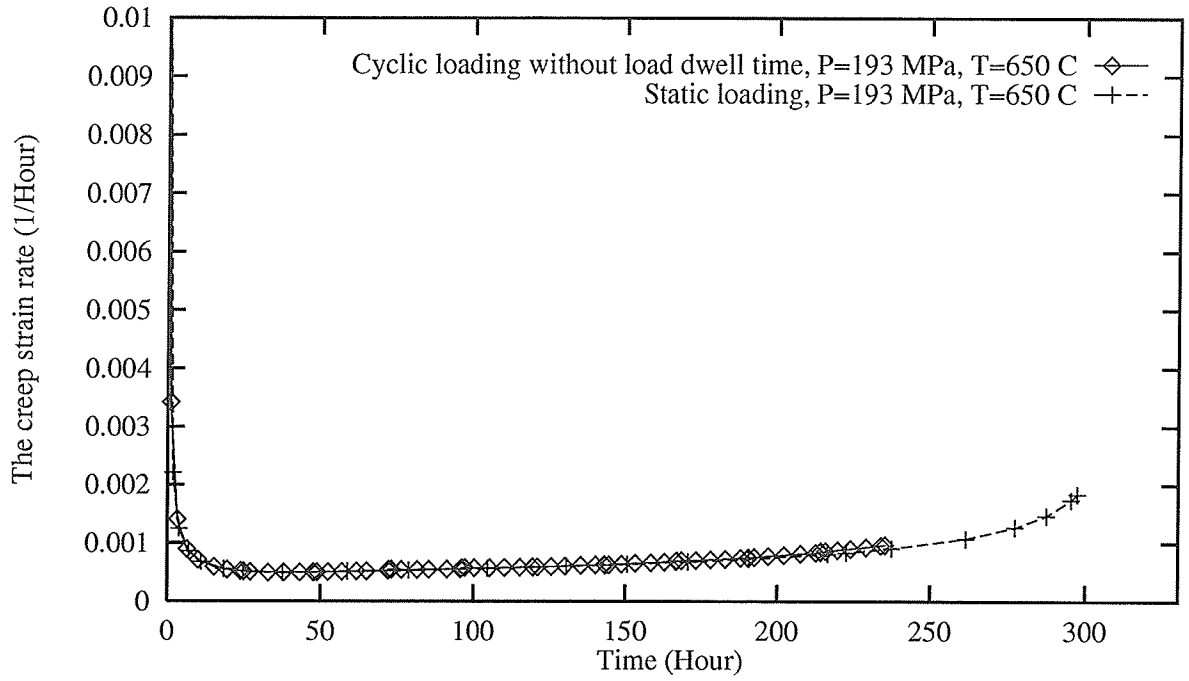

Figure F.3: The development of the creep strain rate under the static and cyclic load of 193 MPa and 650°C without load dwell time

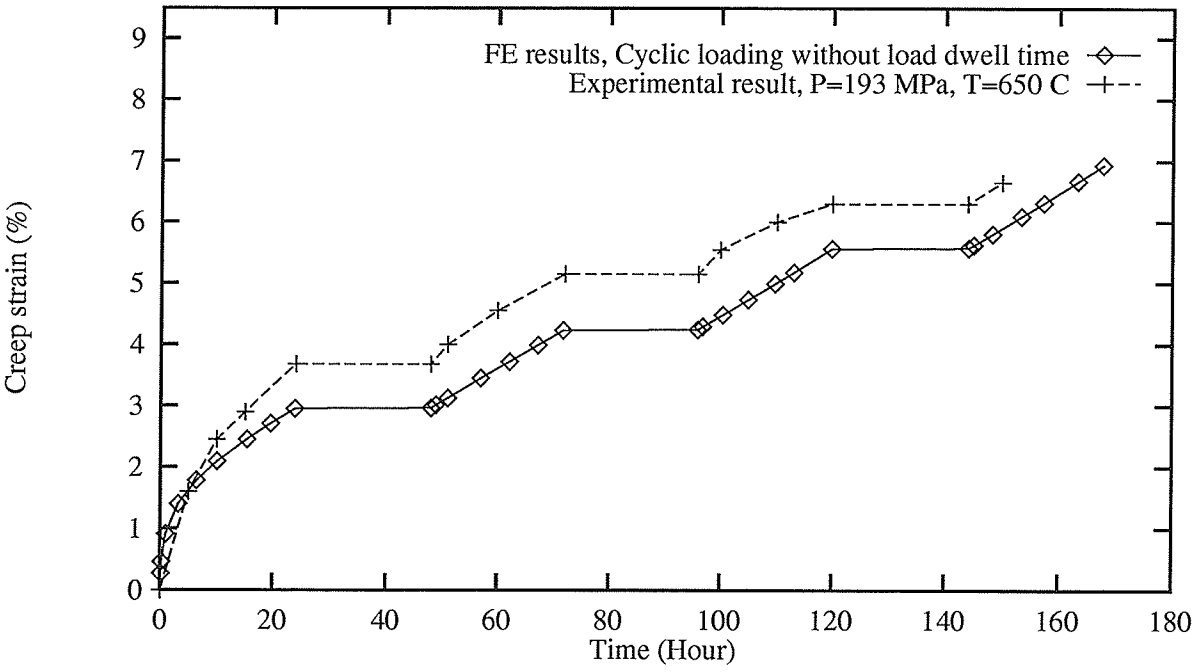

Figure F.4: The development of the creep strain under the static and cyclic load of 193 MPa and 650°C without load dwell time[119-120]

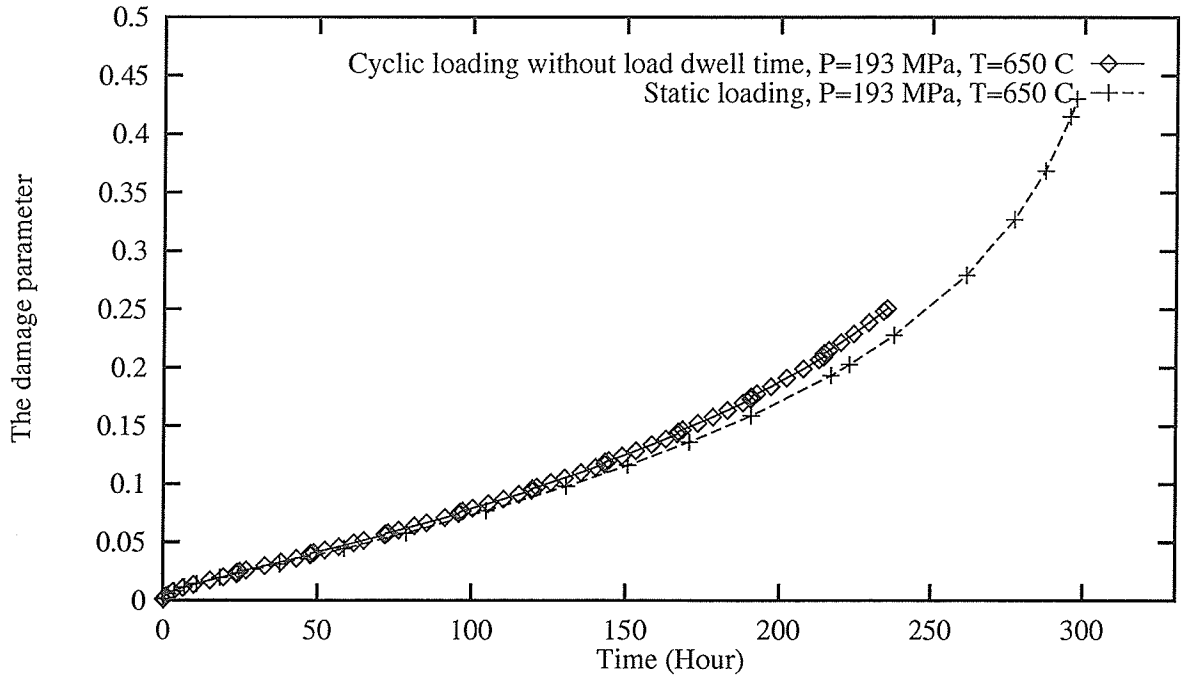

Figure F.5: The development of the damage parameter under the static and cyclic load of 193 MPa and 650°C without load dwell time

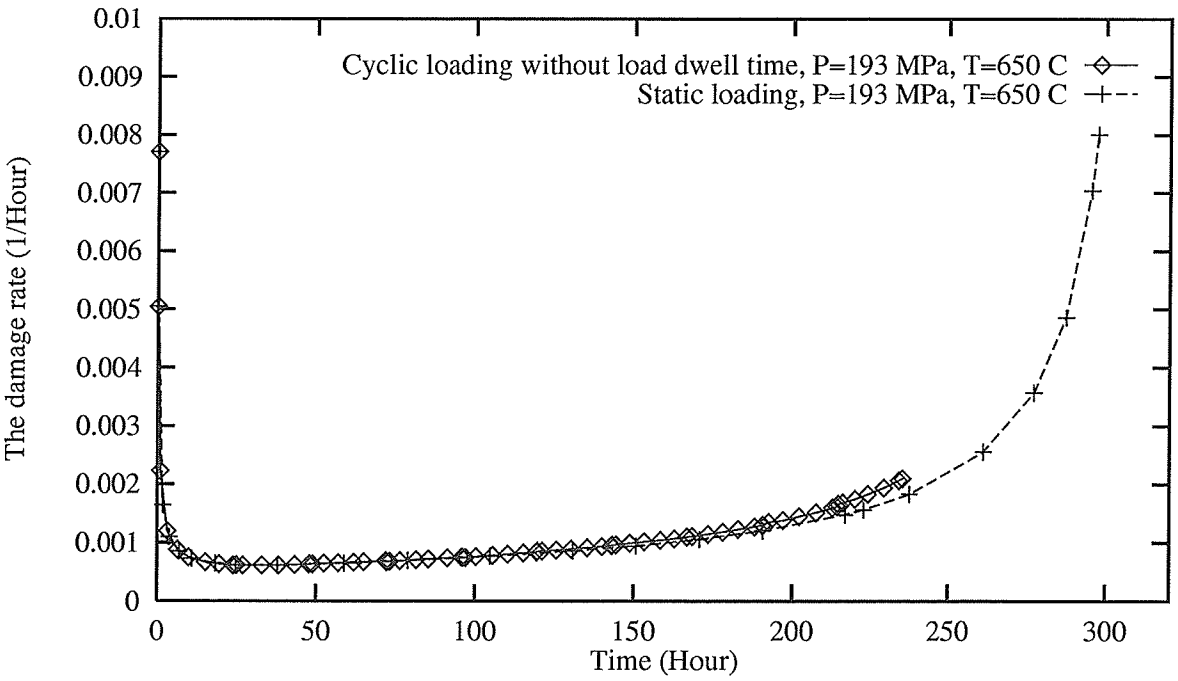

Figure F.6: The development of the damage rate under the static and cyclic load of 193 MPa and 650°C without load dwell time

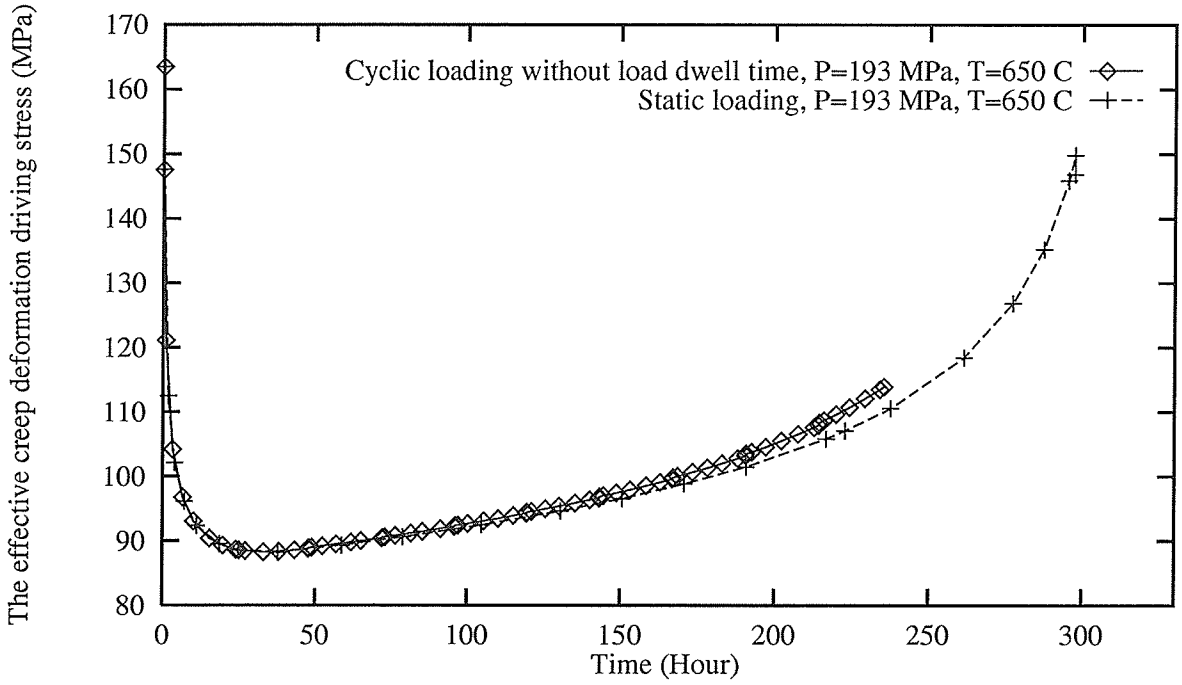

Figure F.7: The development of the effective creep deformation driving stress $\frac{\tilde{\sigma}-\bar{R}}{1-c_o D}$ under the static and cyclic load of 193 MPa and 650°C without load dwell time

Appendix G

Cyclic creep results of the bar under tension – load dwell time effect

This appendix contains the figures which show the importance of load dwell time effect on creep response. As a comparison, results of the uniaxial bar under cyclic loading with and without load dwell time are plotted together.

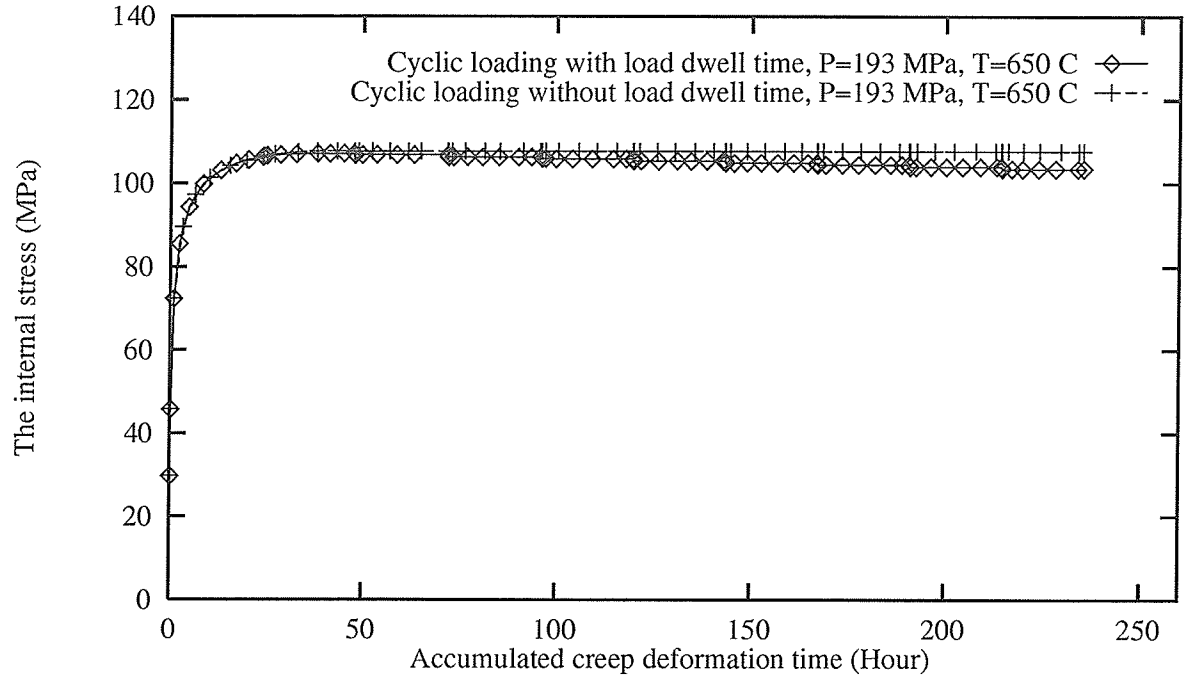

Figure G.1: Comparison of the development of the internal stress under the cyclic load of 193 MPa and 650°C with and without load dwell time

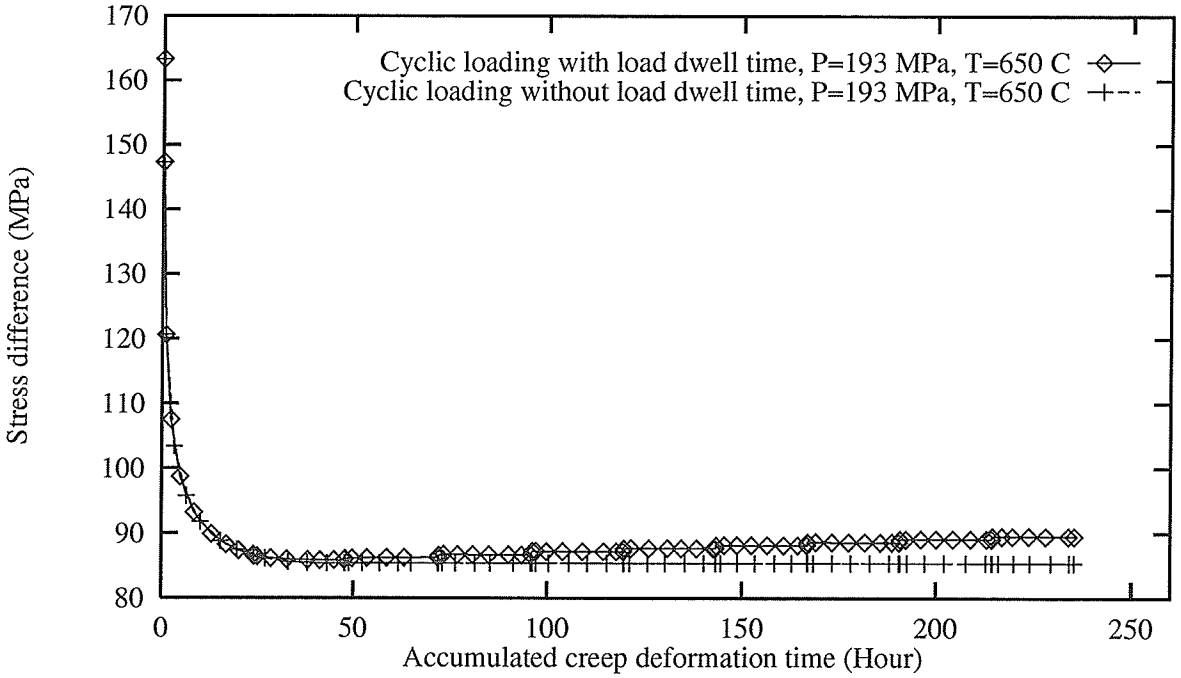

Figure G.2: Comaprison of the development of the difference between the damage equivalent stress and the internal stress $(\tilde{\sigma} - \bar{R})$ under the cyclic load of 193 MPa and 650°C with and without load dwell time

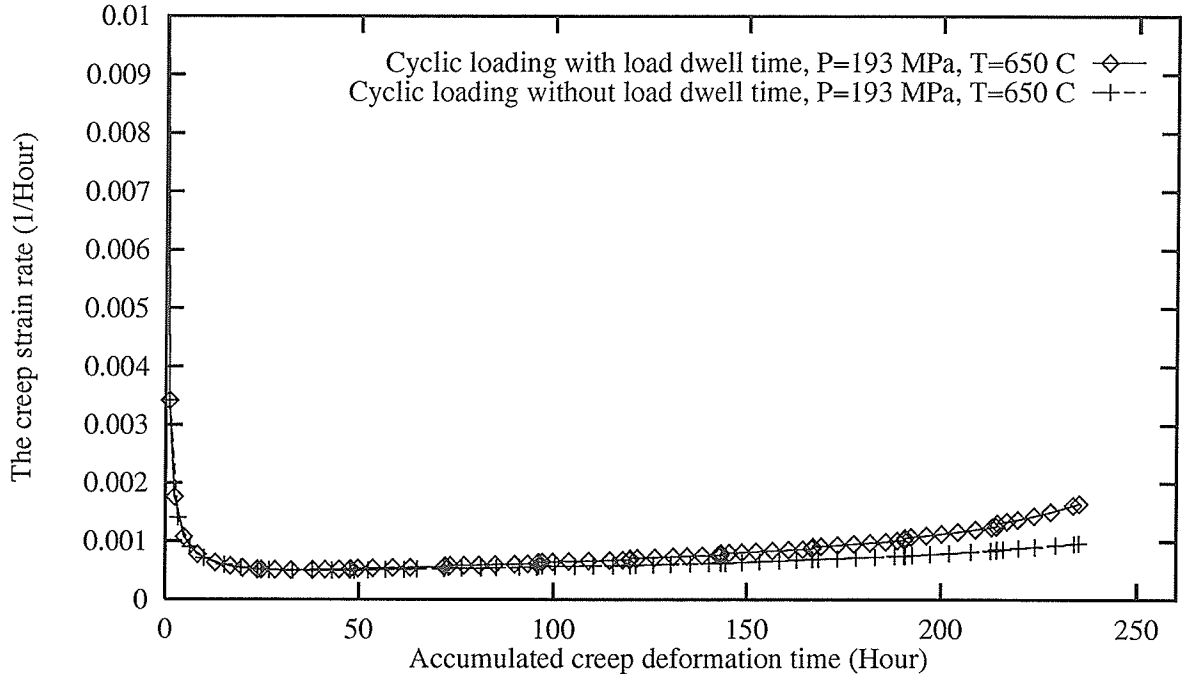

Figure G.3: Comparison of the development of the creep strain rate under the cyclic load of 193 MPa and 650°C with and without load dwell time

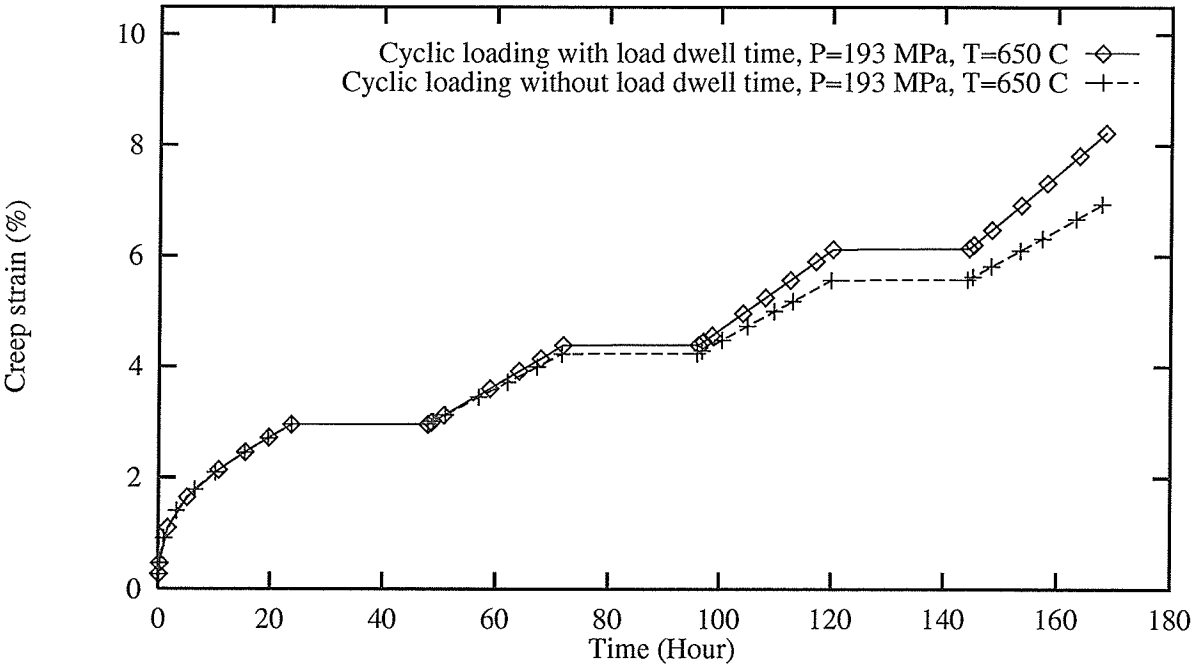

Figure G.4: Comparison of the development of the creep strain under the cyclic load of 193 MPa and 650°C with and without load dwell time

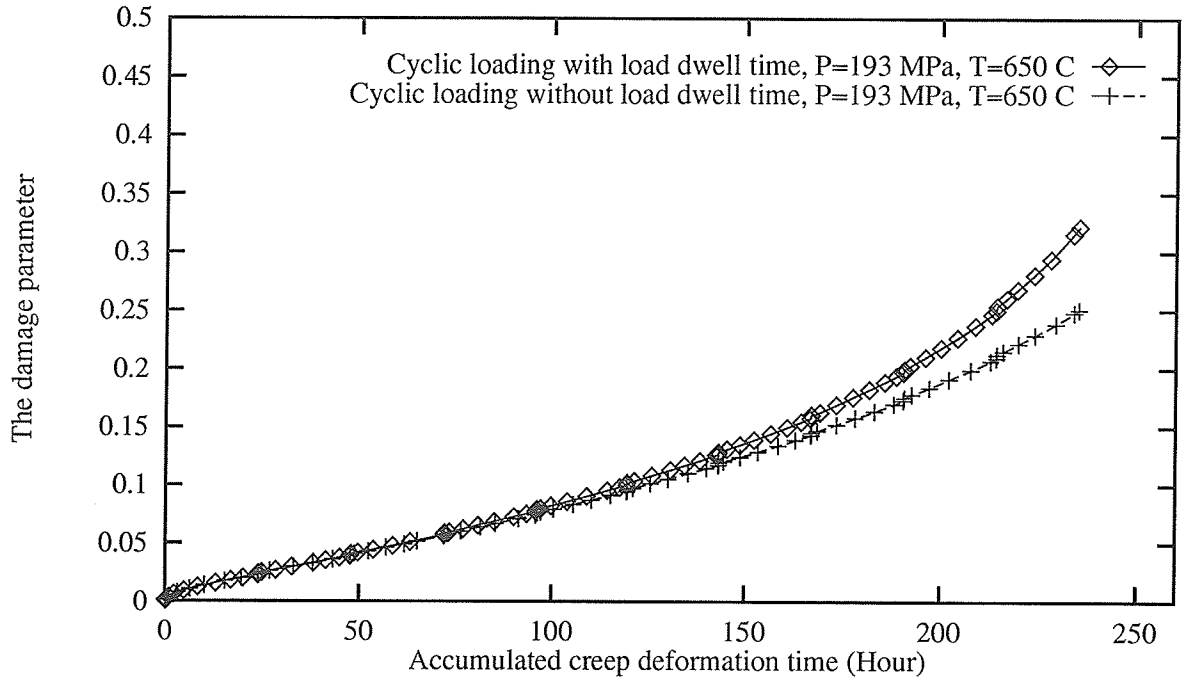

Figure G.5: Comparison of the development of the damage parameter under the cyclic load of 193 MPa and 650°C with and without load dwell time

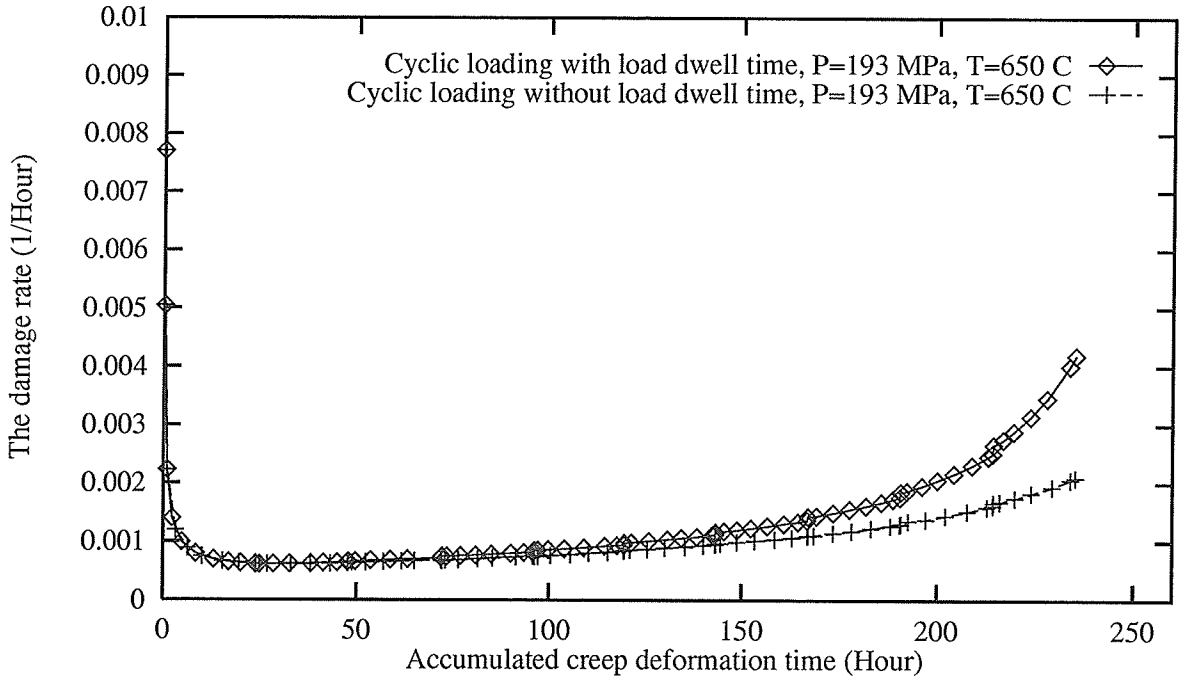

Figure G.6: Comparison of the development of the damage rate under the cyclic load of 193 MPa and 650°C with and without load dwell time

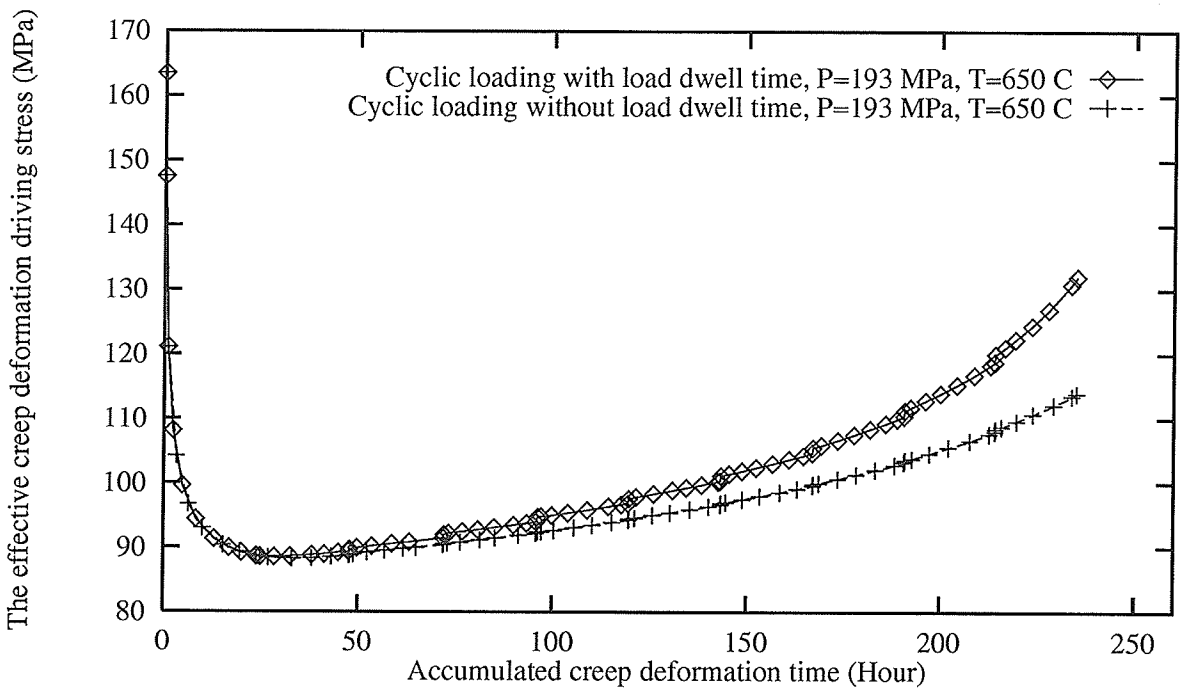

Figure G.7: Comparison of the development of the effective creep deformation driving stress $\frac{\tilde{\sigma}-\bar{R}}{1-c_o D}$ under the cyclic load of 193 MPa and 650^{o}C with and without load dwell time

Appendix H

Cyclic creep results of the bar under complete loading pattern

This appendix contains the figures which show the creep response of the uniaxial bar under a complete cyclic loading pattern. As a comparison, results of the uniaxial bar under complete cyclic loading pattern are plotted together with the corresponding results under static loading.

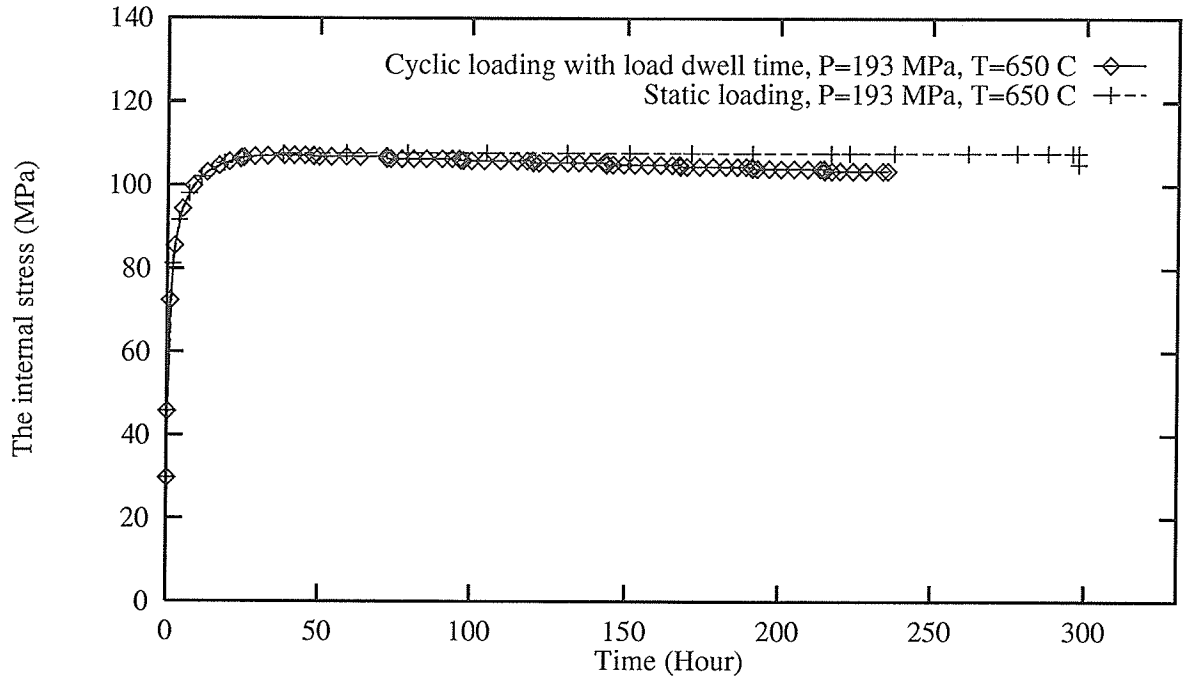

Figure H.1: The development of the internal stress under the static and cyclic load of 193 MPa and 650°C with load dwell time

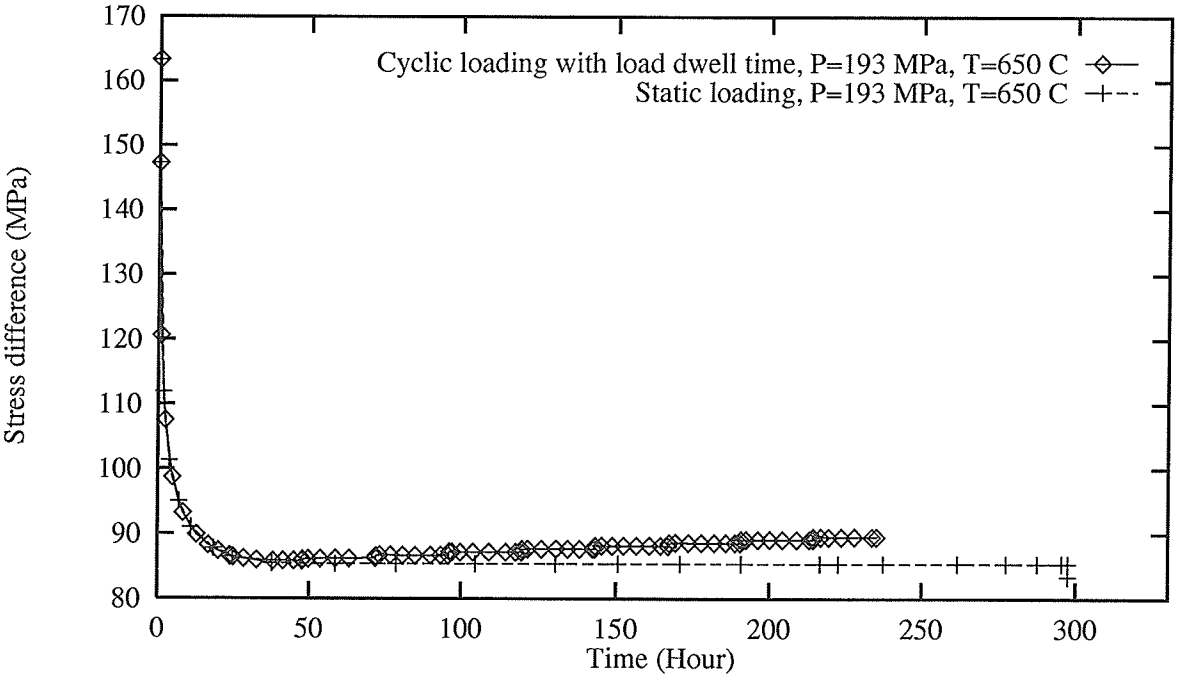

Figure H.2: The development of the difference between the damage equivalent stress and the internal stress $(\tilde{\sigma} - \bar{R})$ under the static and cyclic load of 193 MPa and 650°C with load dwell time

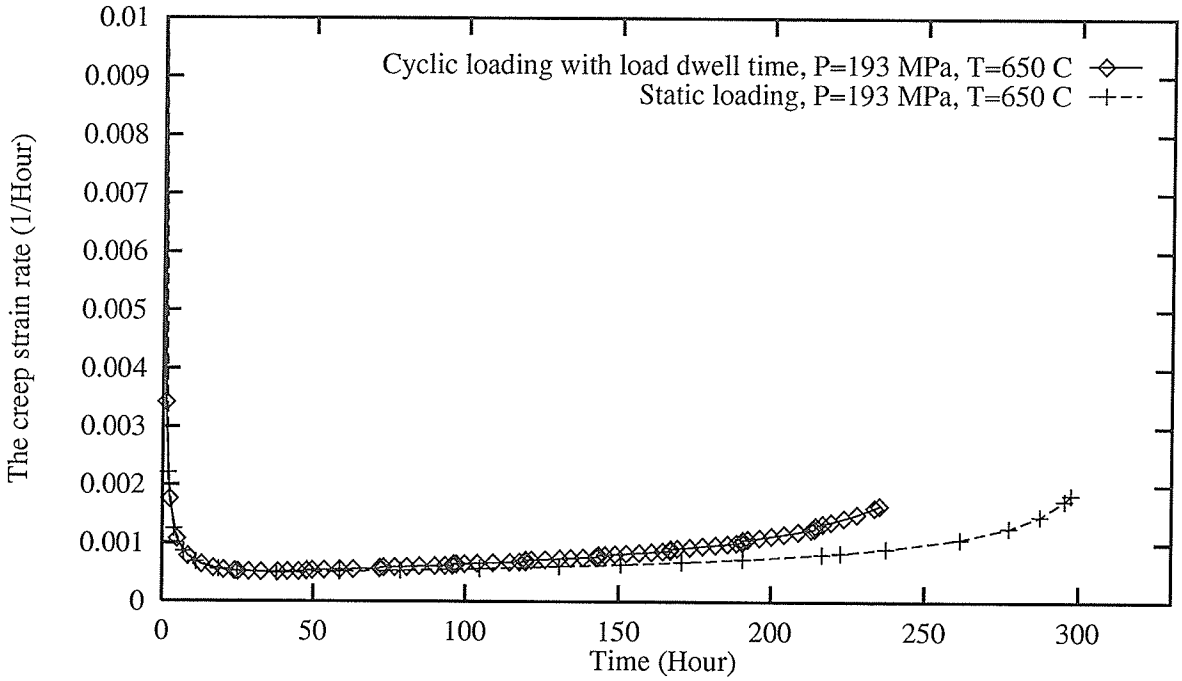

Figure H.3: The development of the creep strain rate under the static and cyclic load of 193 MPa and 650°C with load dwell time

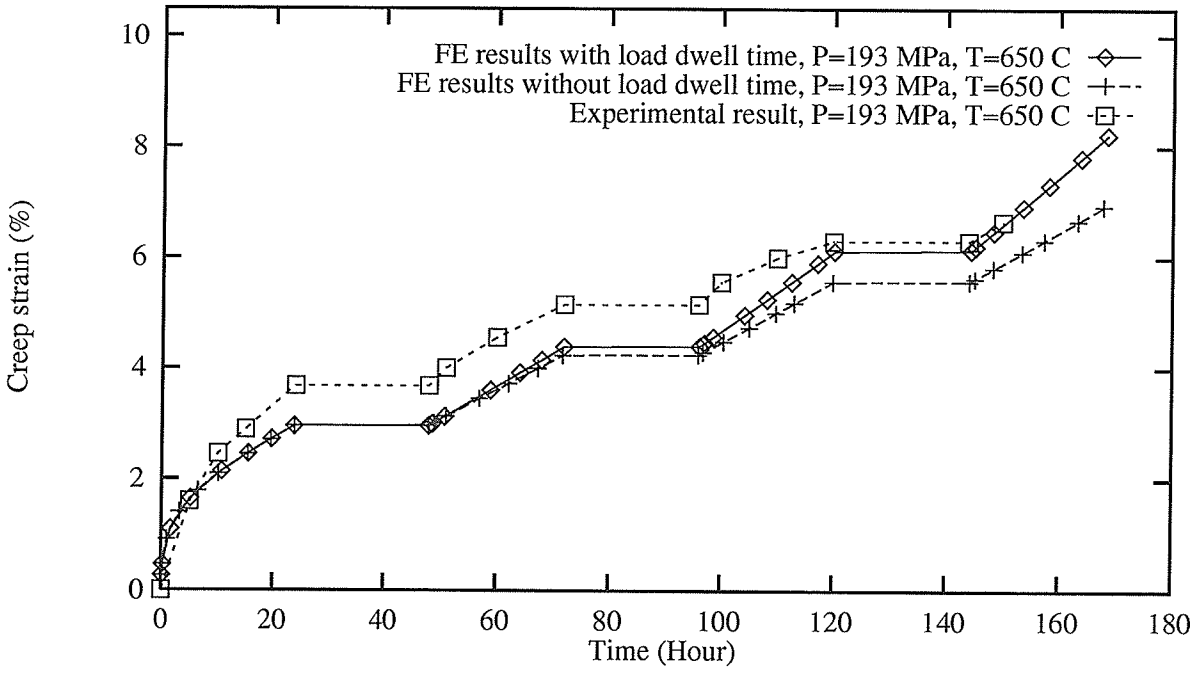

Figure H.4: The development of the creep strain under the static and cyclic load of 193 MPa and 650°C with and without load dwell time[119-120]

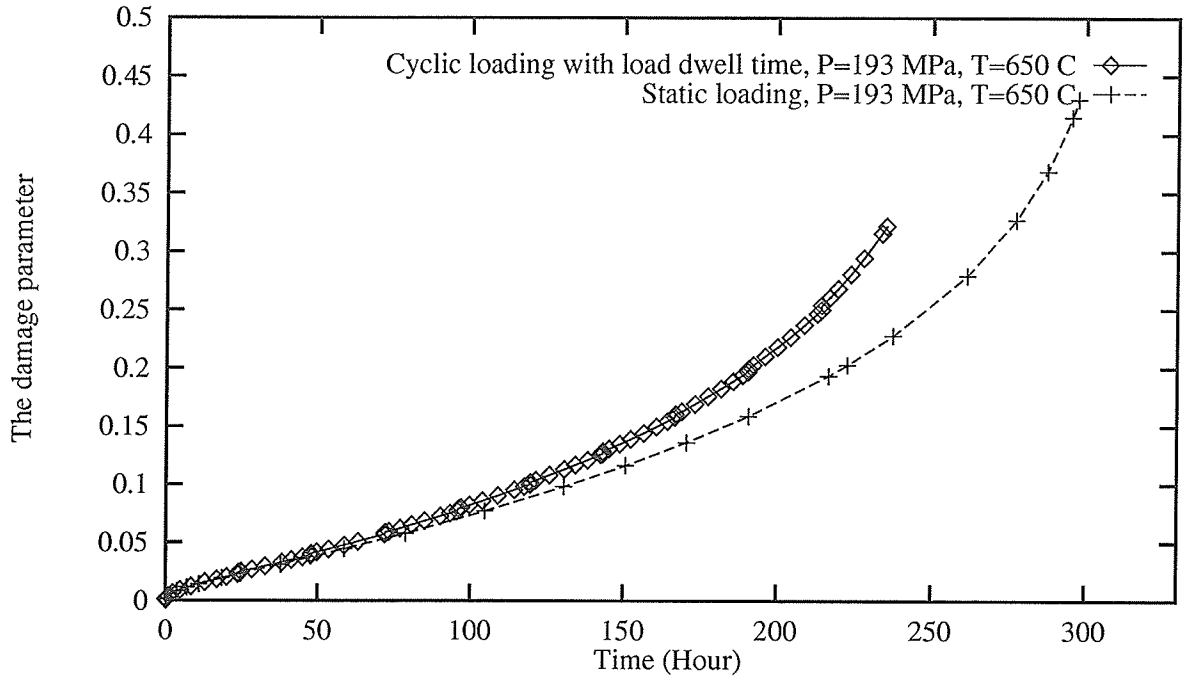

Figure H.5: The development of the damage parameter under the static and cyclic load of 193 MPa and 650°C with load dwell time

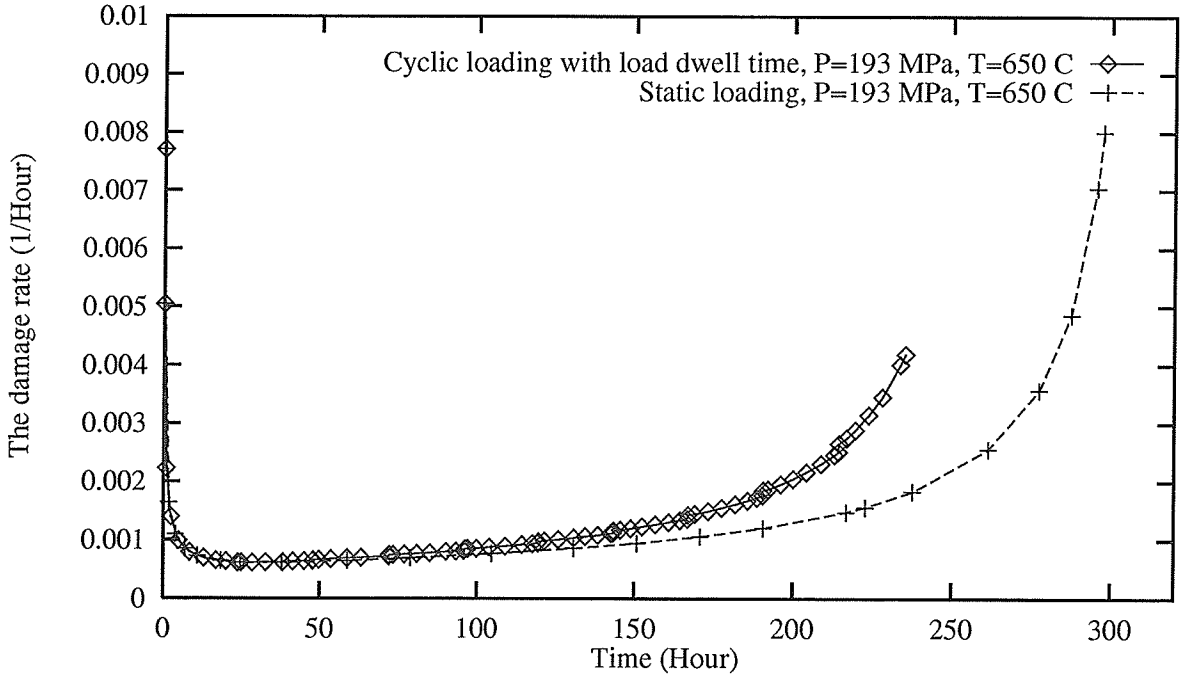

Figure H.6: The development of the damage rate under the static and cyclic load of 193 MPa and 650°C with load dwell time

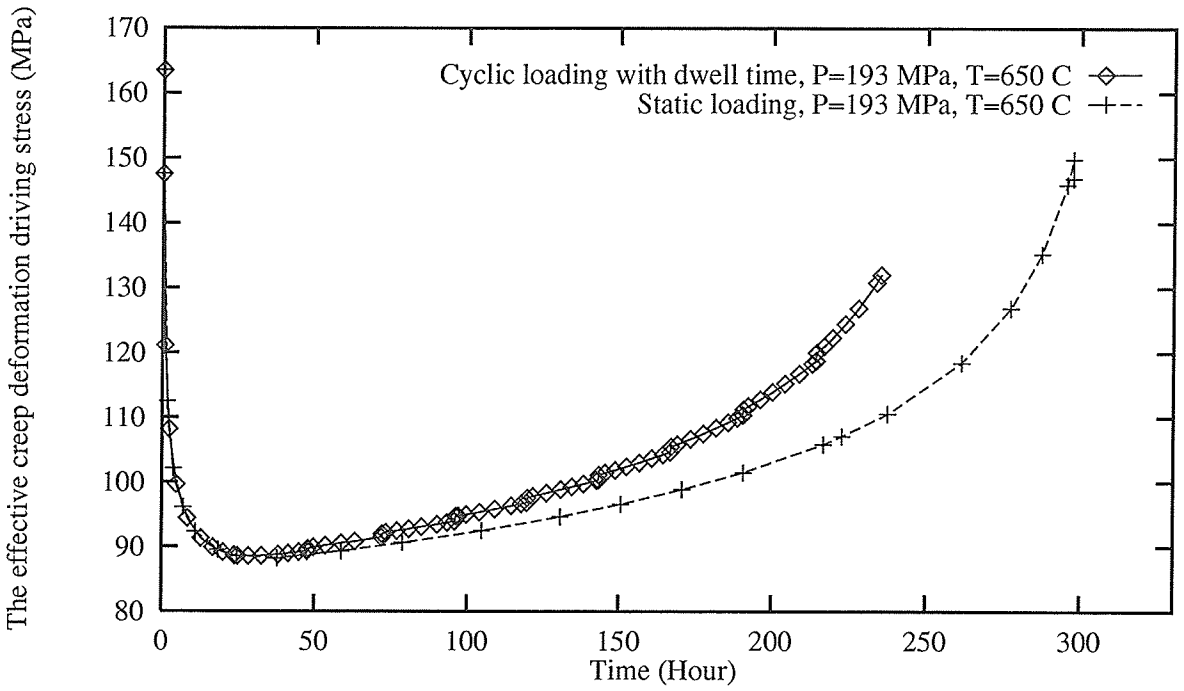

Figure H.7: The development of the effective creep deformation driving stress $\frac{\tilde{\sigma}-\bar{R}}{1-c_o D}$ under the static and cyclic load of 193 MPa and 650°C with load dwell time

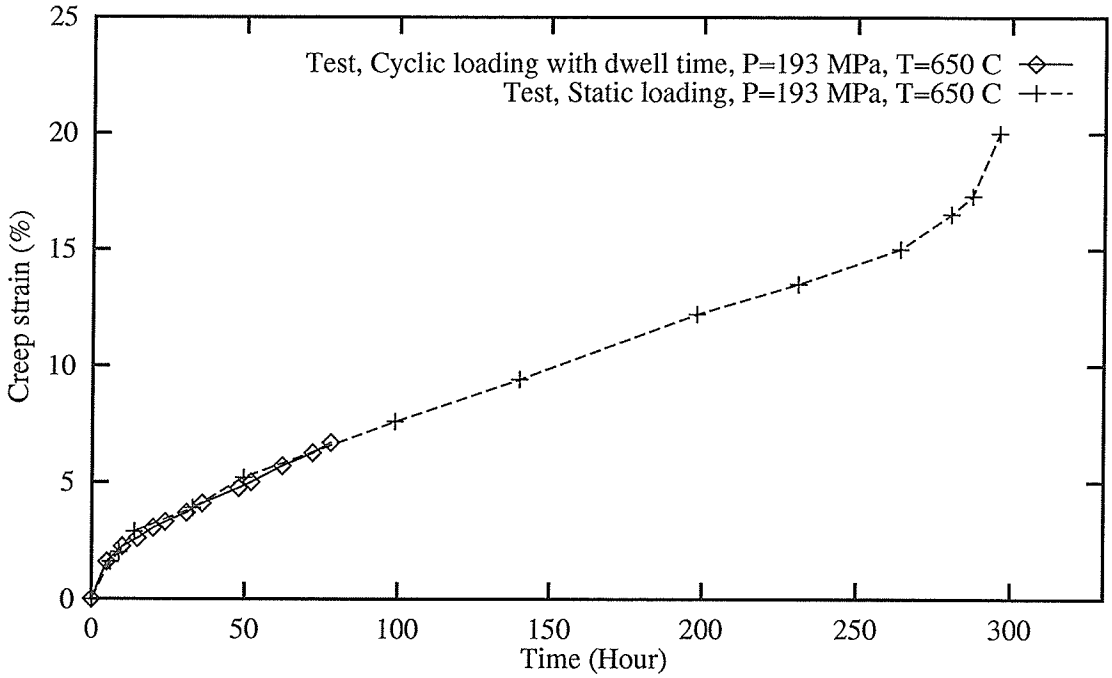

Figure H.8: Experimental measurements of the creep strain under the static and cyclic load of 193 MPa with load dwell time. The temperature is constant at 650°C

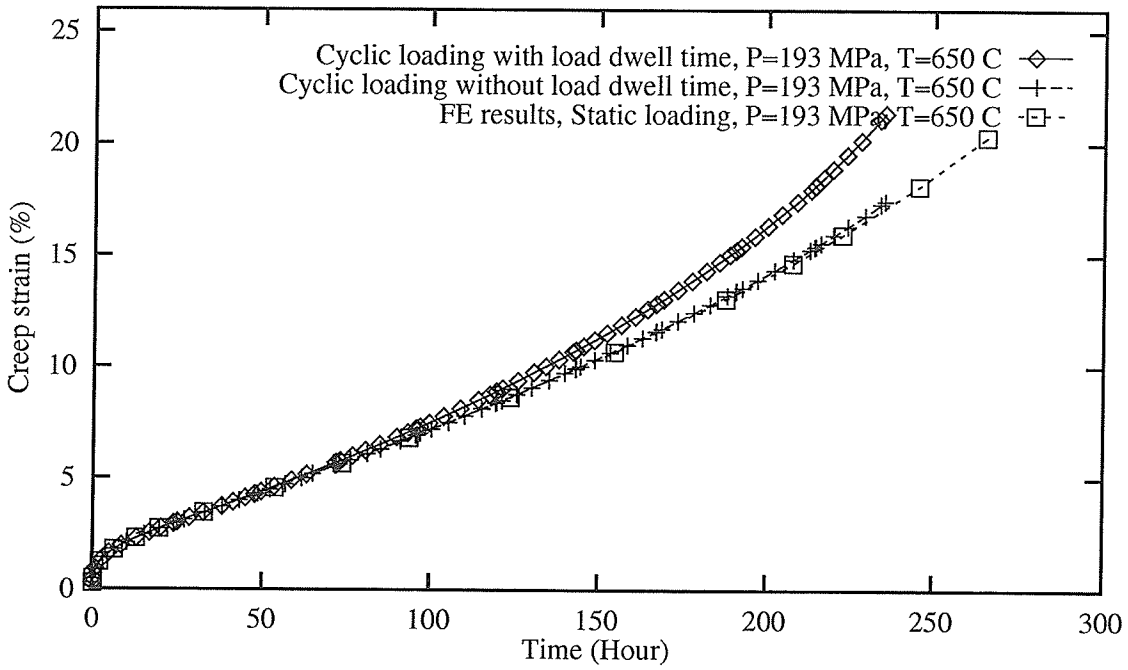

Figure H.9: Finite element calculation of the creep strain under the static and cyclic load of 193 MPa and 650°C with and without load dwell time

Appendix I

Distribution of the crack tip variables

This appendix contains the figures which show the distribution of the crack tip variables of the central cracked thin panel under static loading.

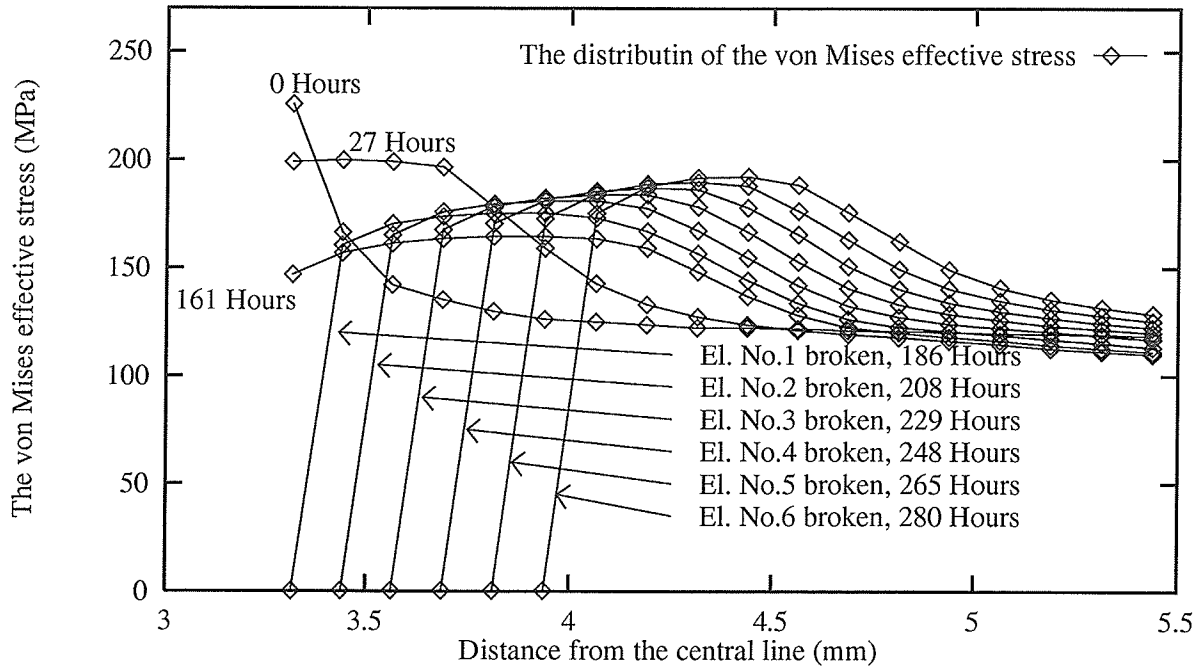

Figure I.1: The distribution of the von Mises effective stress around the crack tip area

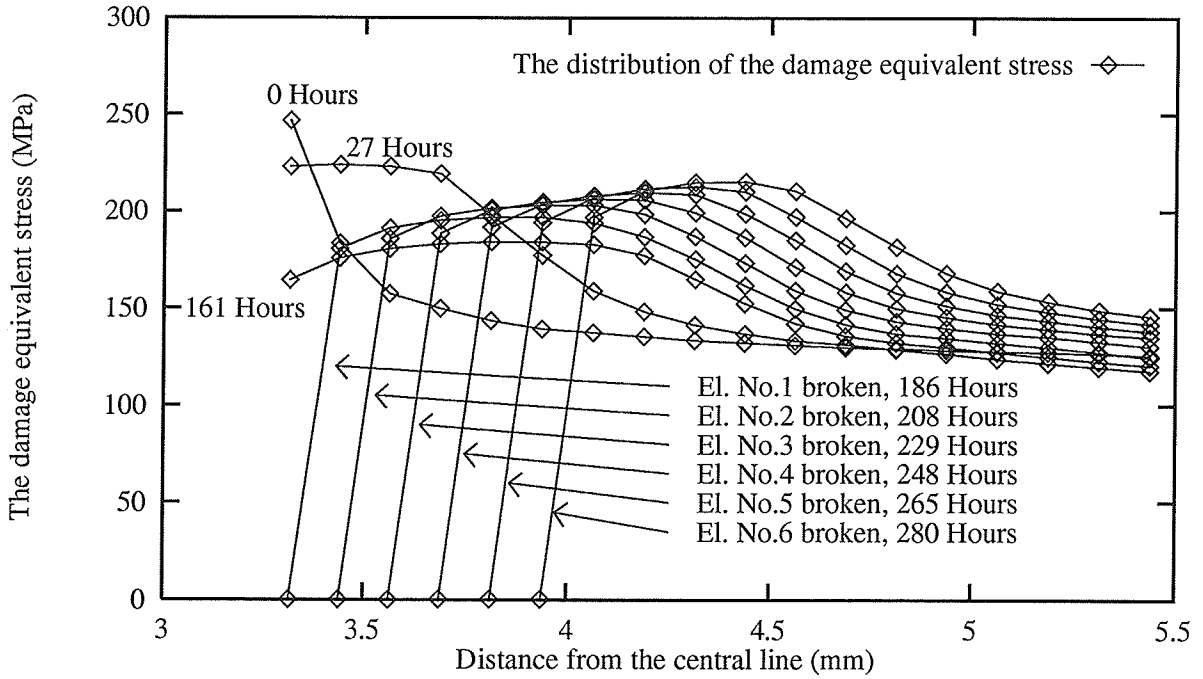

Figure I.2: The distribution of the damage equivalent stress around the crack tip area

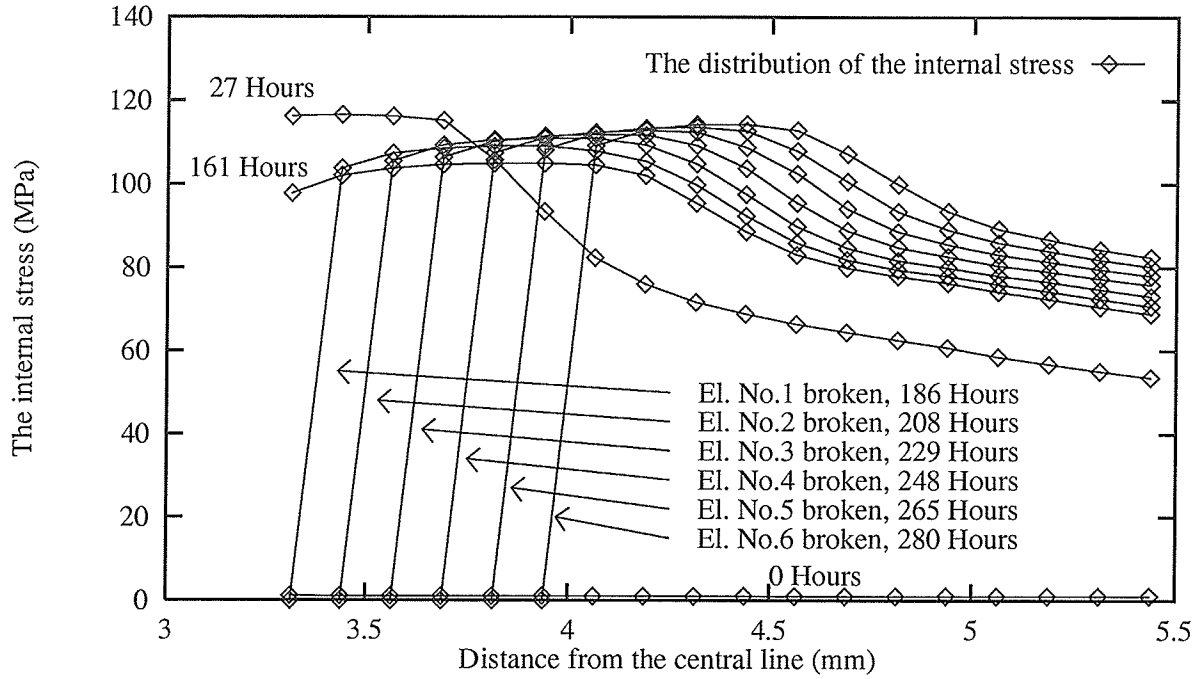

Figure I.3: The distribution of the internal stress around the crack tip area

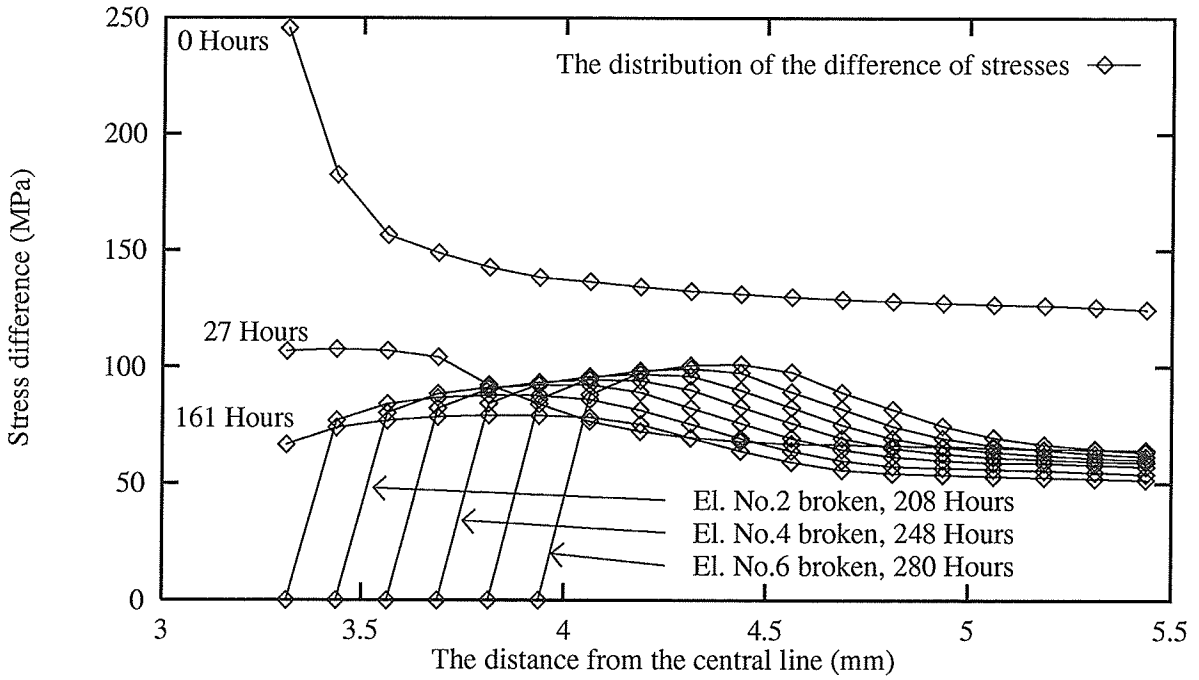

Figure I.4: The distribution of the difference between the damage equivalent stress and the internal stress $(\tilde{\sigma} - \bar{R})$ around the crack tip area

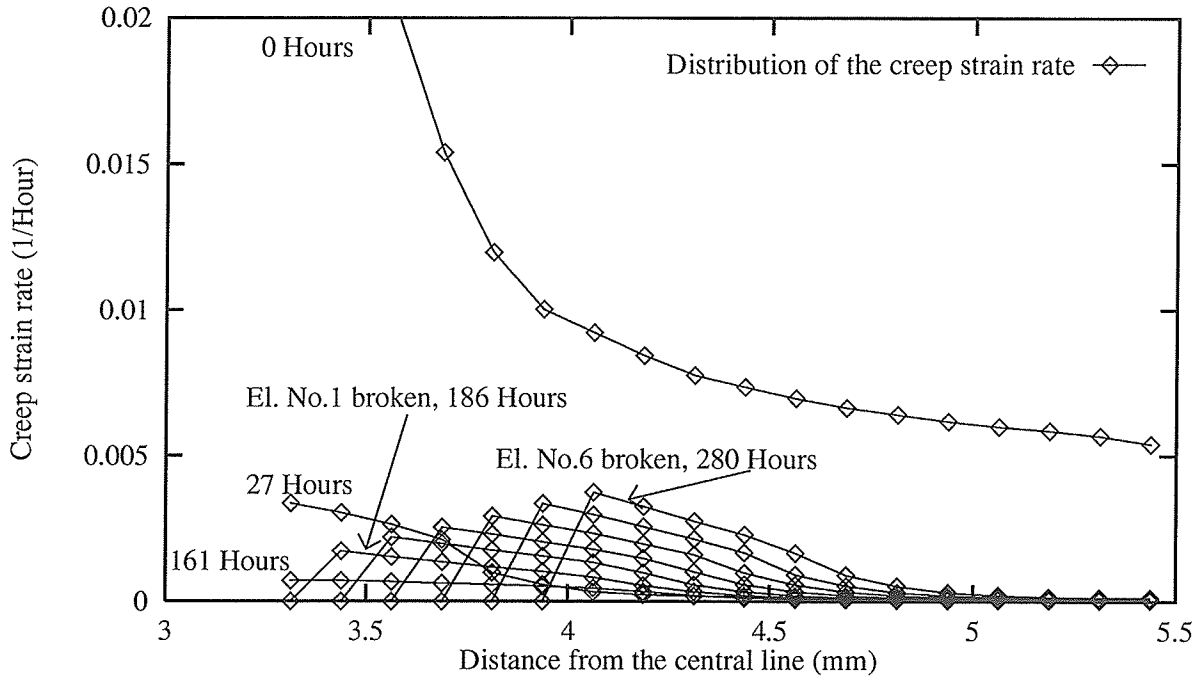

Figure I.5: The distribution of the creep strain rate around the crack tip area

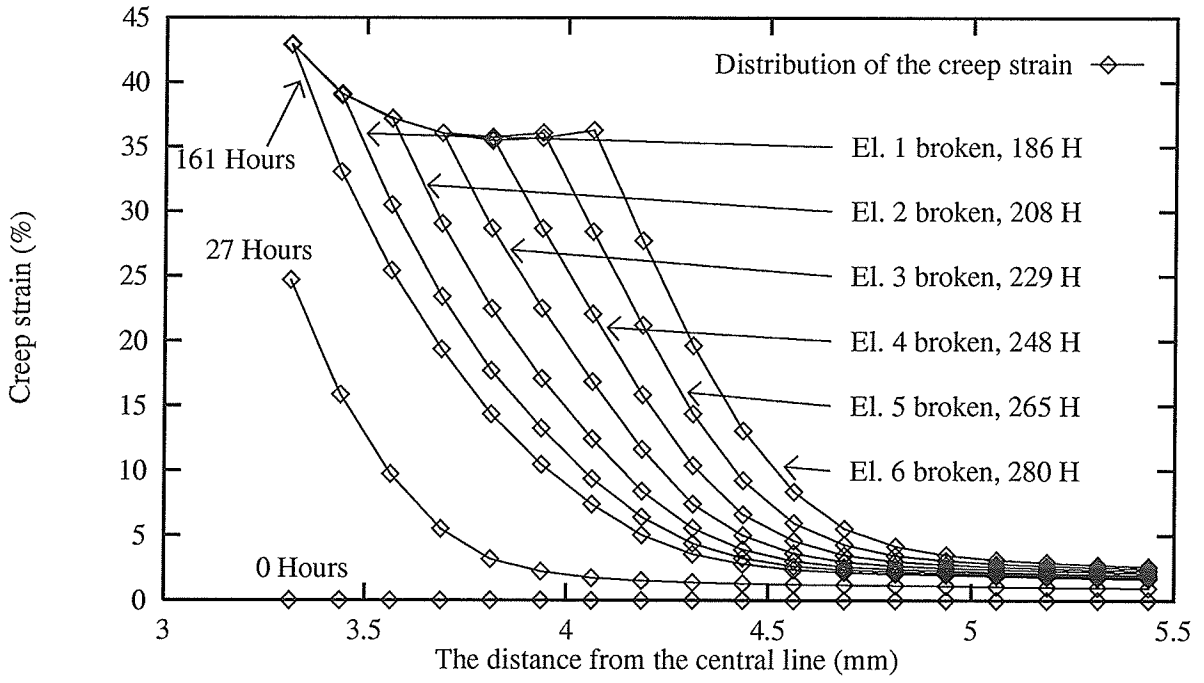

Figure I.6: The distribution of the creep strain around the crack tip area

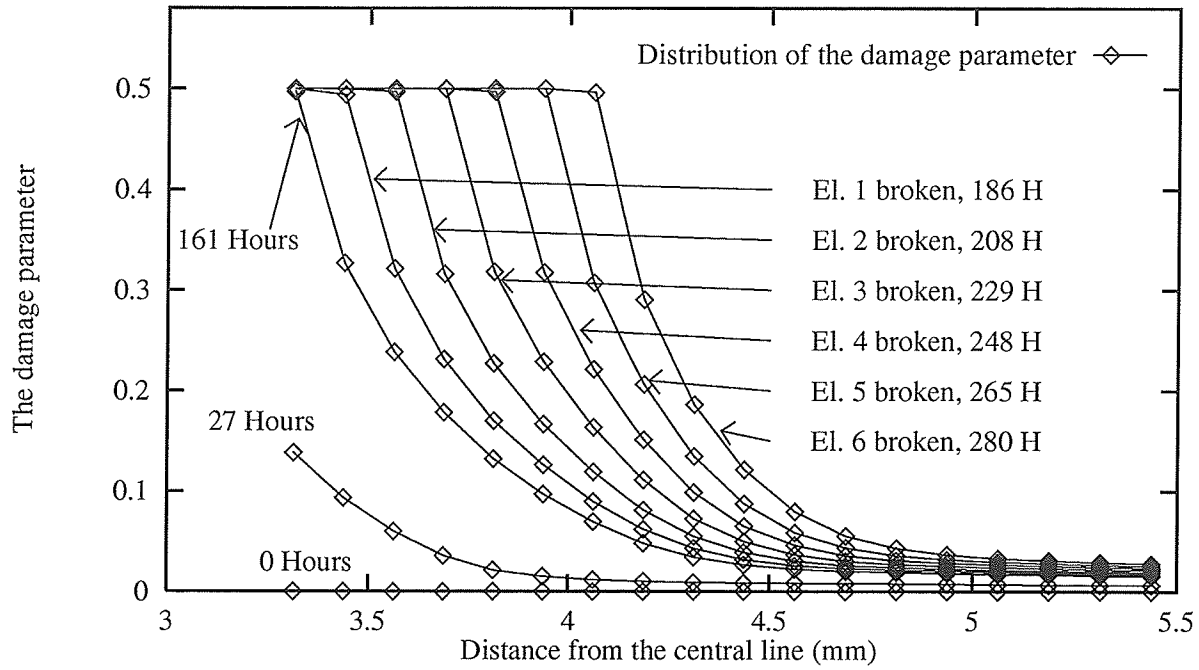

Figure I.7: The distribution of the damage parameter around the crack tip area

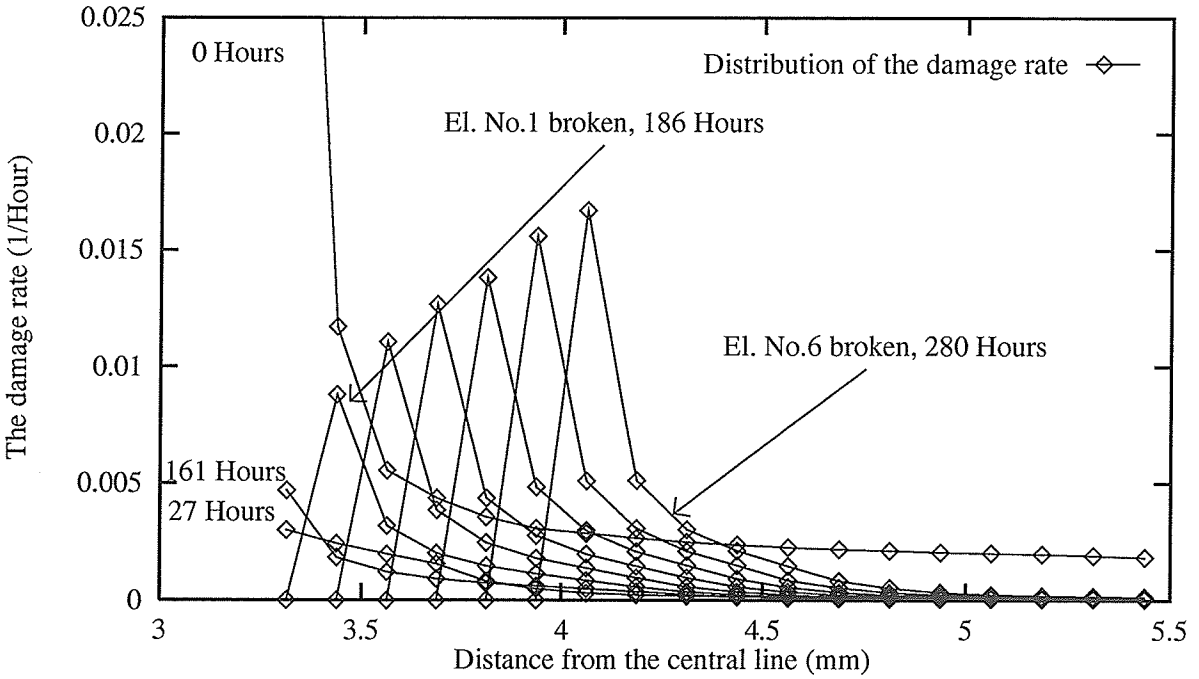

Figure I.8: The distribution of the damage rate around the crack tip area

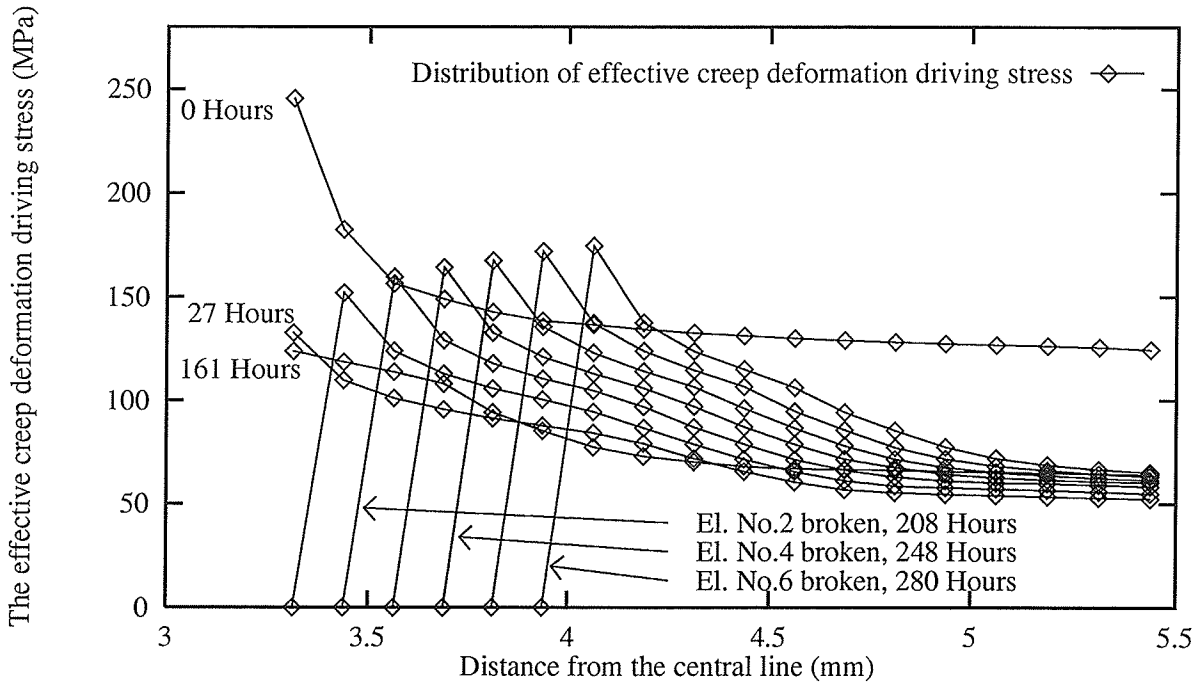

Figure I.9: The distribution of the effective creep deformation driving stress $\frac{\tilde{\sigma}-\tilde{R}}{1-c_o D}$ around the crack tip area

Appendix J

Evolution of the crack tip variables

This appendix contains the figures which show the evolution of the crack tip variables.

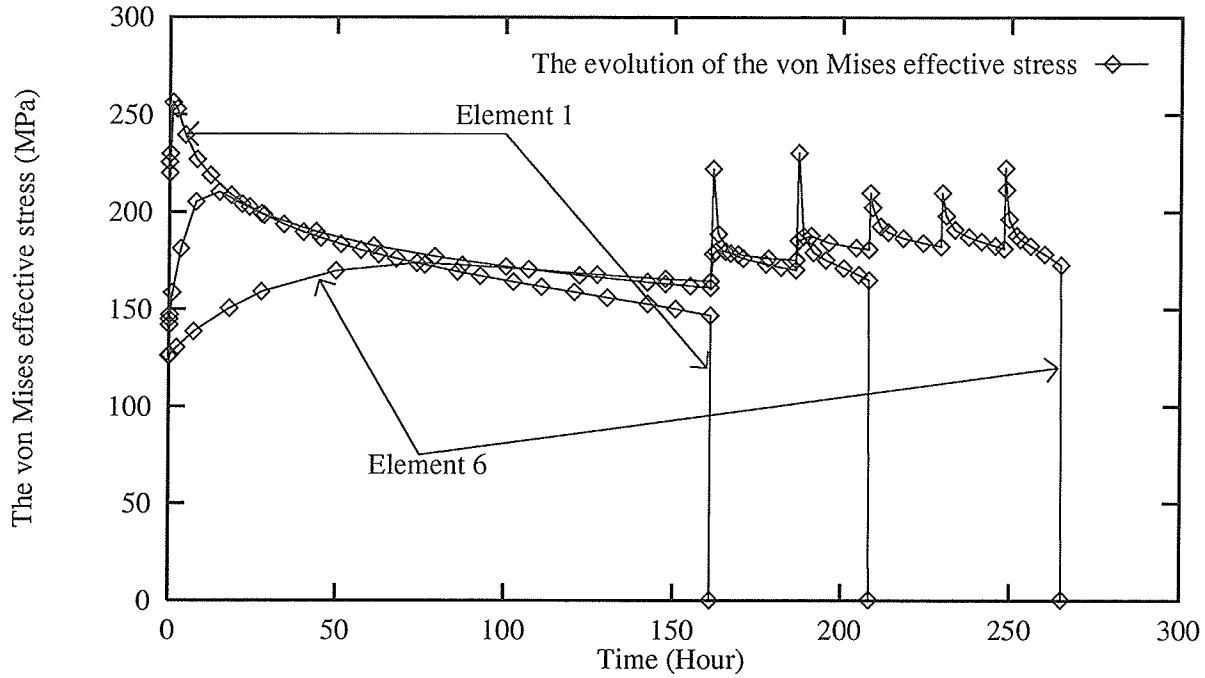

Figure J.1: The evolution of the von Mises effective stress in the crack tip area

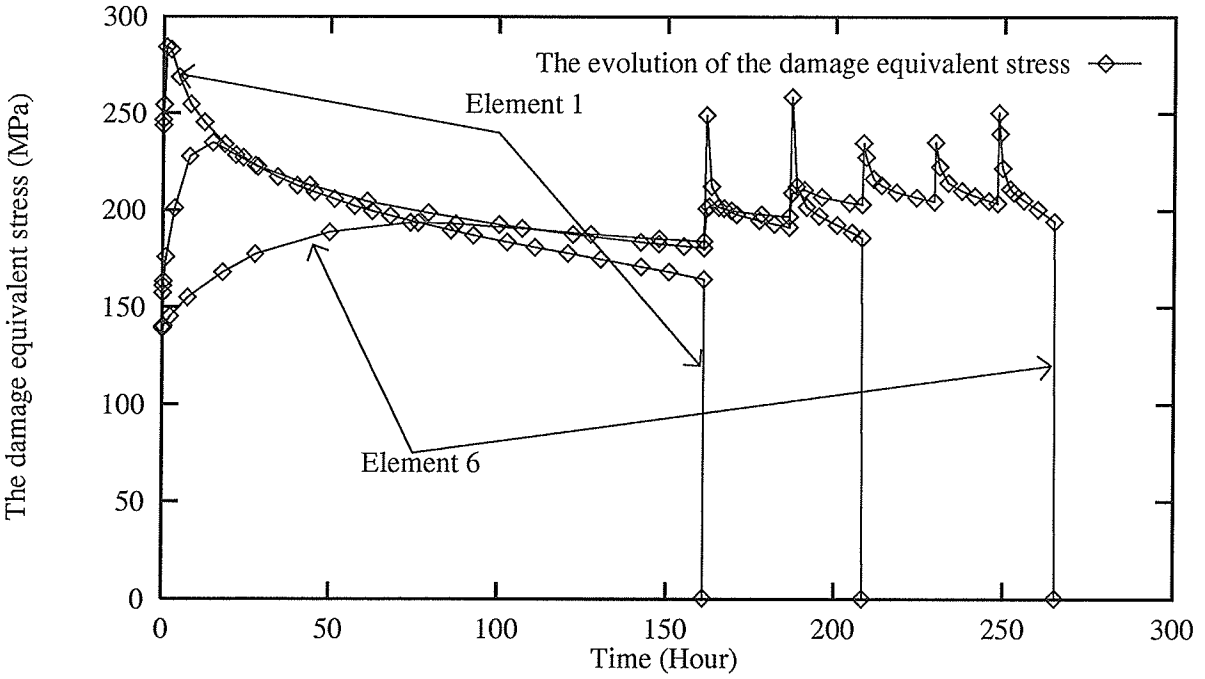

Figure J.2: The evolution of the damage equivalent stress in the crack tip area

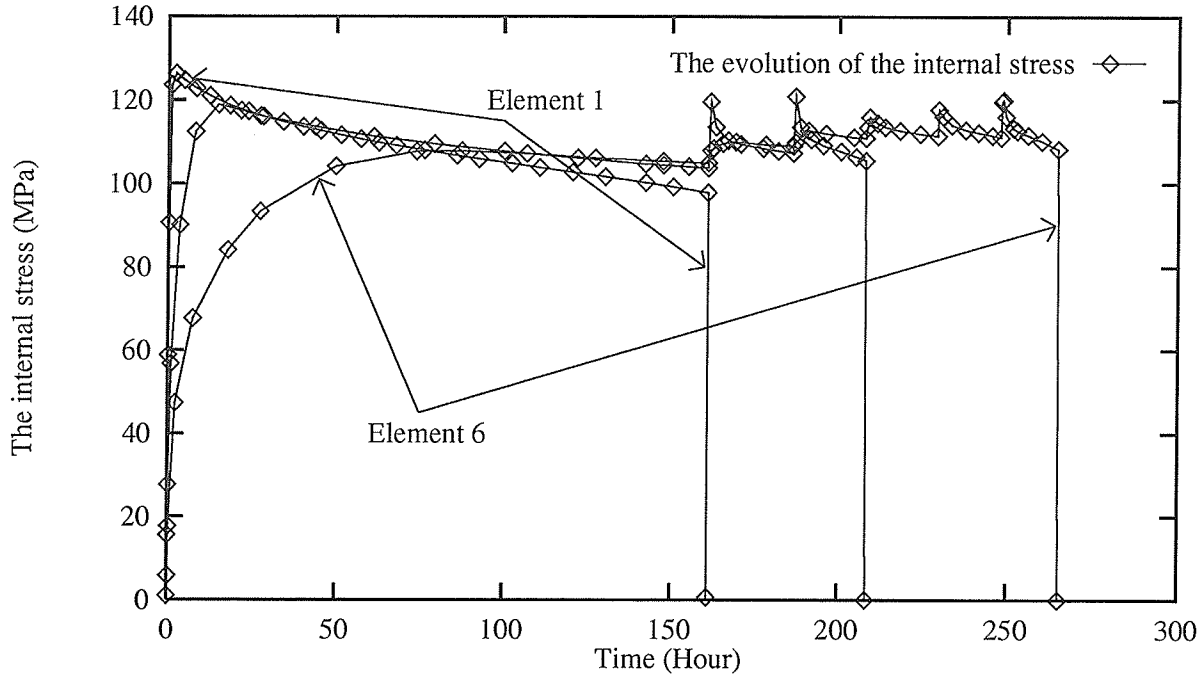

Figure J.3: The evolution of the internal stress in the crack tip area

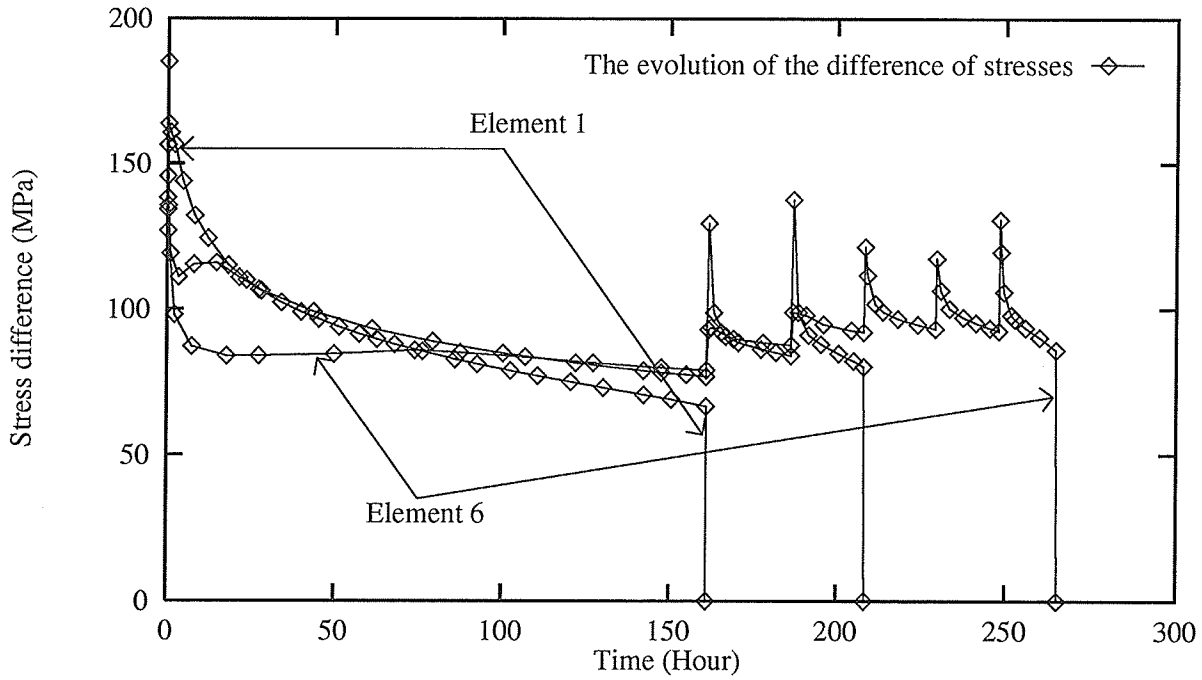

Figure J.4: The evolution of the difference between the damage equivalent stress and the internal stress $(\tilde{\sigma} - \bar{R})$ in the crack tip area

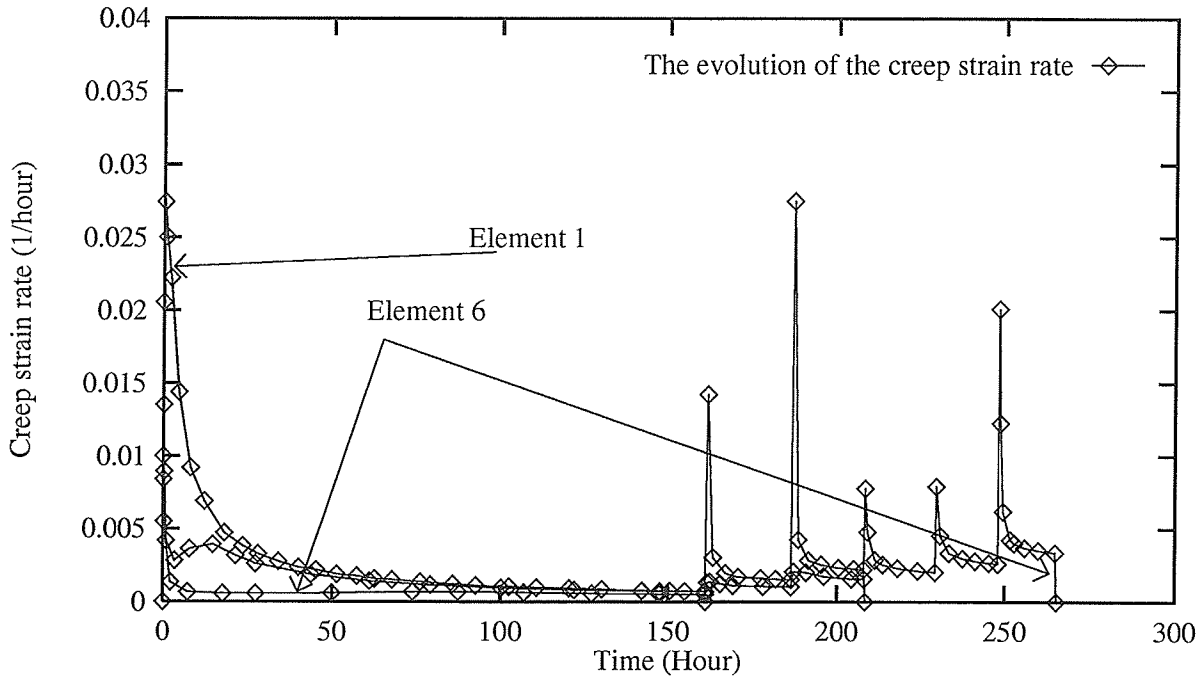

Figure J.5: The evolution of the creep strain rate in the crack tip area

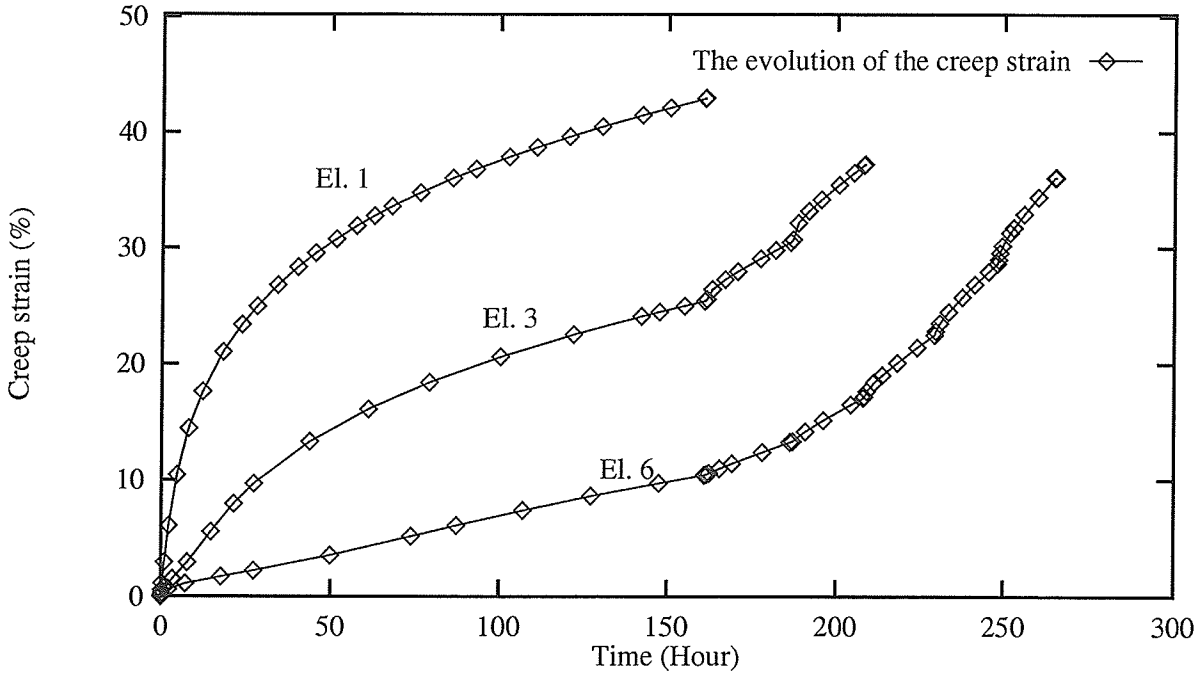

Figure J.6: The evolution of the creep strain in the crack tip area

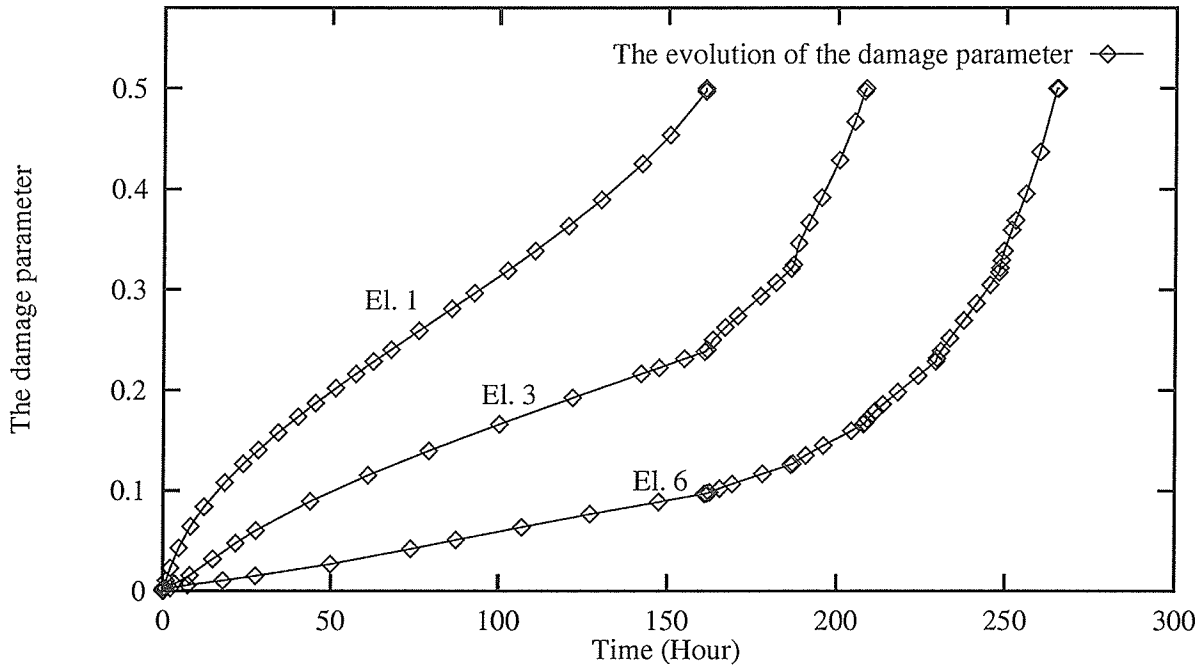

Figure J.7: The evolution of the damage parameter in the crack tip area

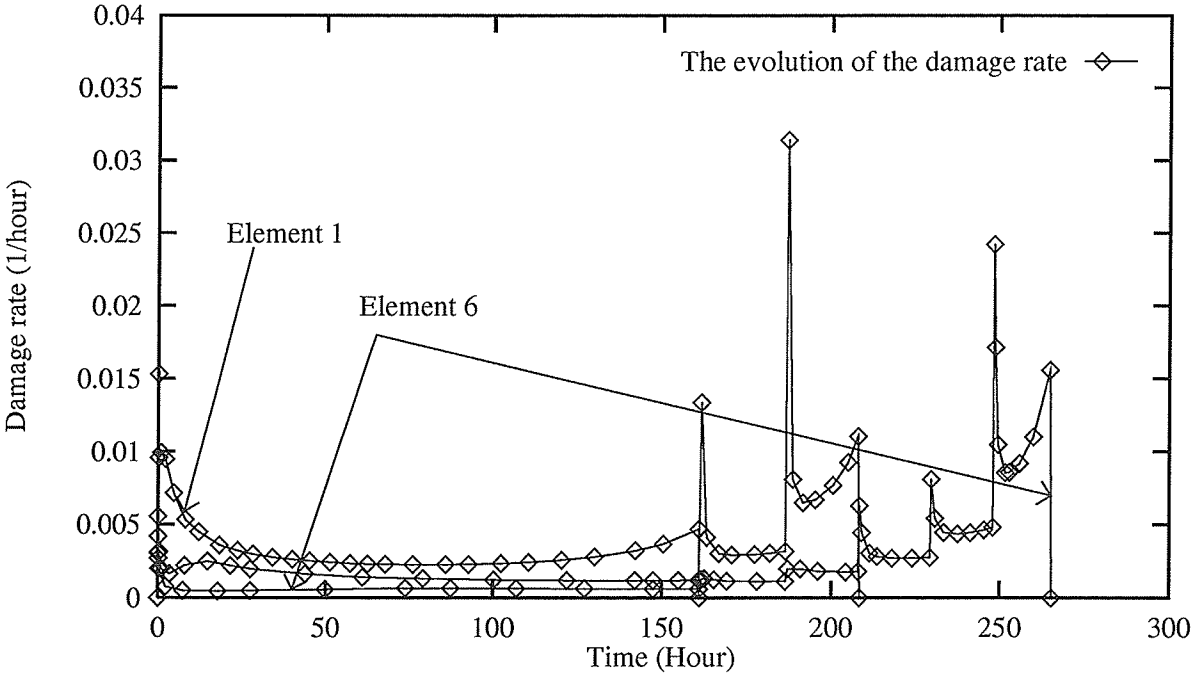

Figure J.8: The evolution of the damage rate in the crack tip area

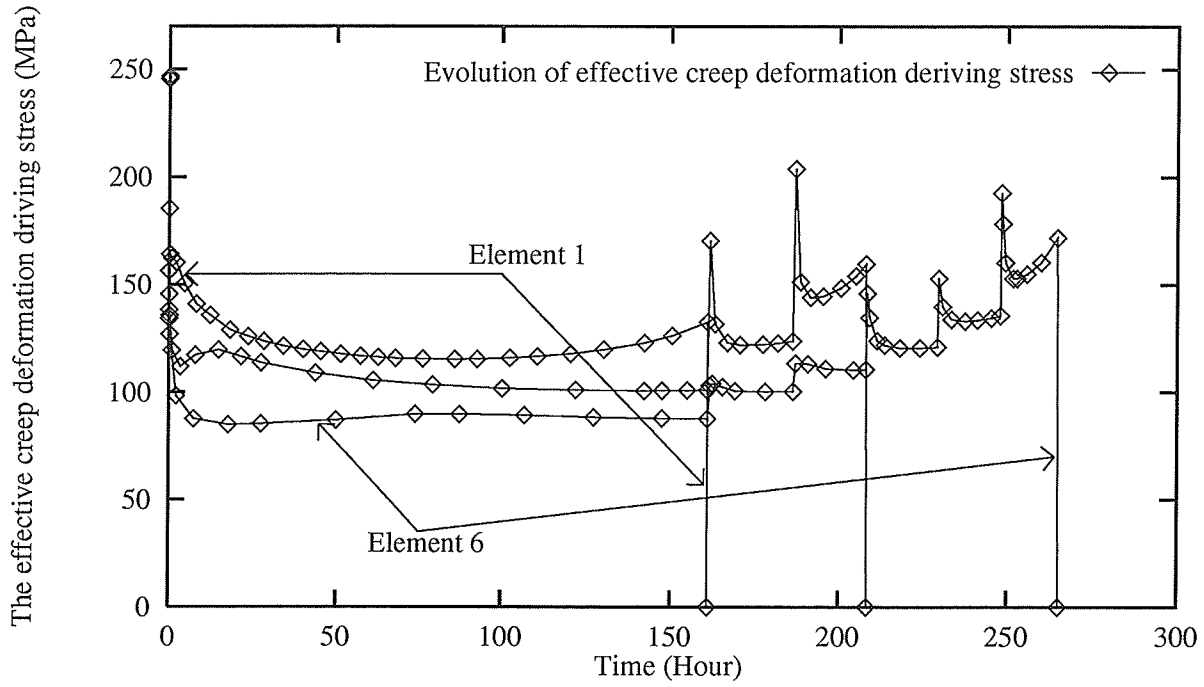

Figure J.9: The evolution of the effective creep deformation driving stress $\frac{\tilde{\sigma}-\tilde{R}}{1-c_o D}$ in the crack tip area

Appendix K

Evolution of the variables in the sixth element

This appendix contains the figures which show the evolution of the variables in the sixth element. The sixth element is located approximately at 0.5 mm ahead of the initial crack tip.

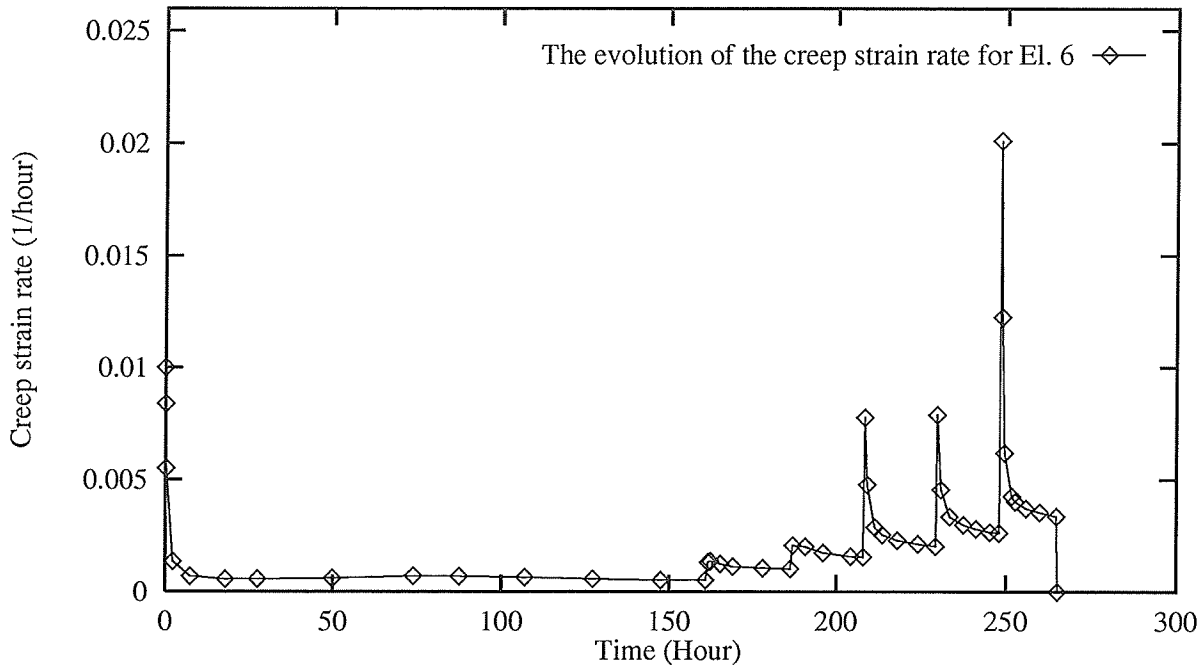

Figure K.1: The evolution of the creep strain rate in the sixth element

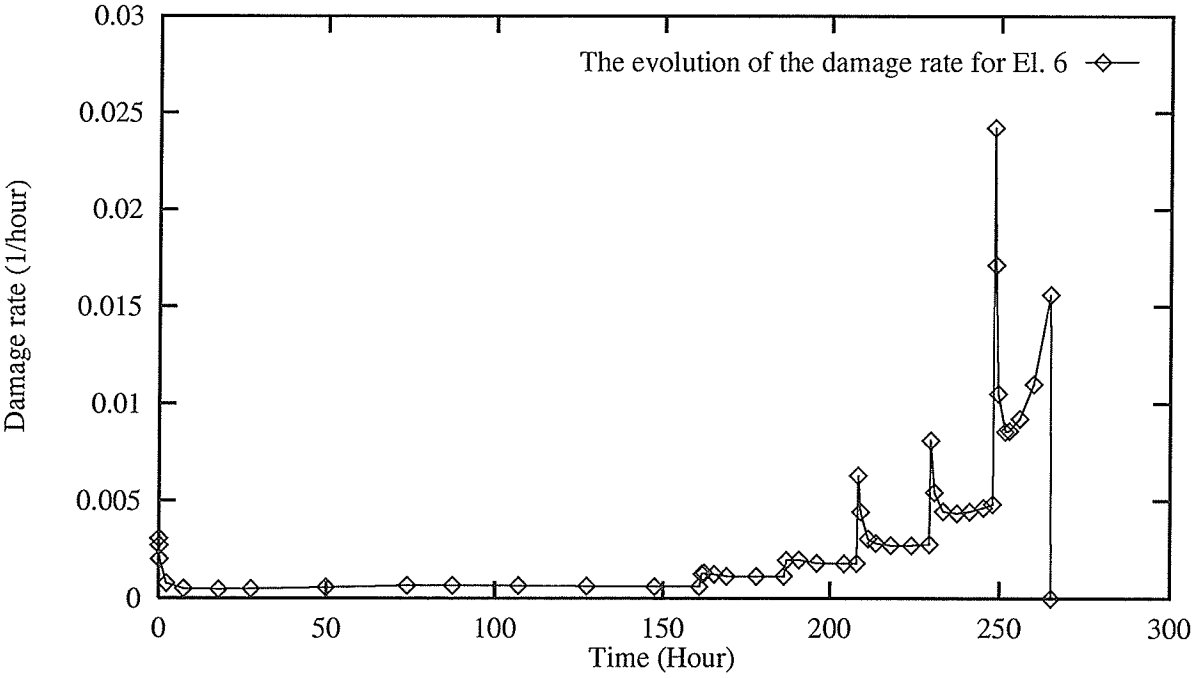

Figure K.2: The evolution of the damage rate in the sixth element

Appendix L

Evolution of the damage pattern in the crack tip area

This appendix contains the figures which show the evolution of the damage pattern of the crack tip area.

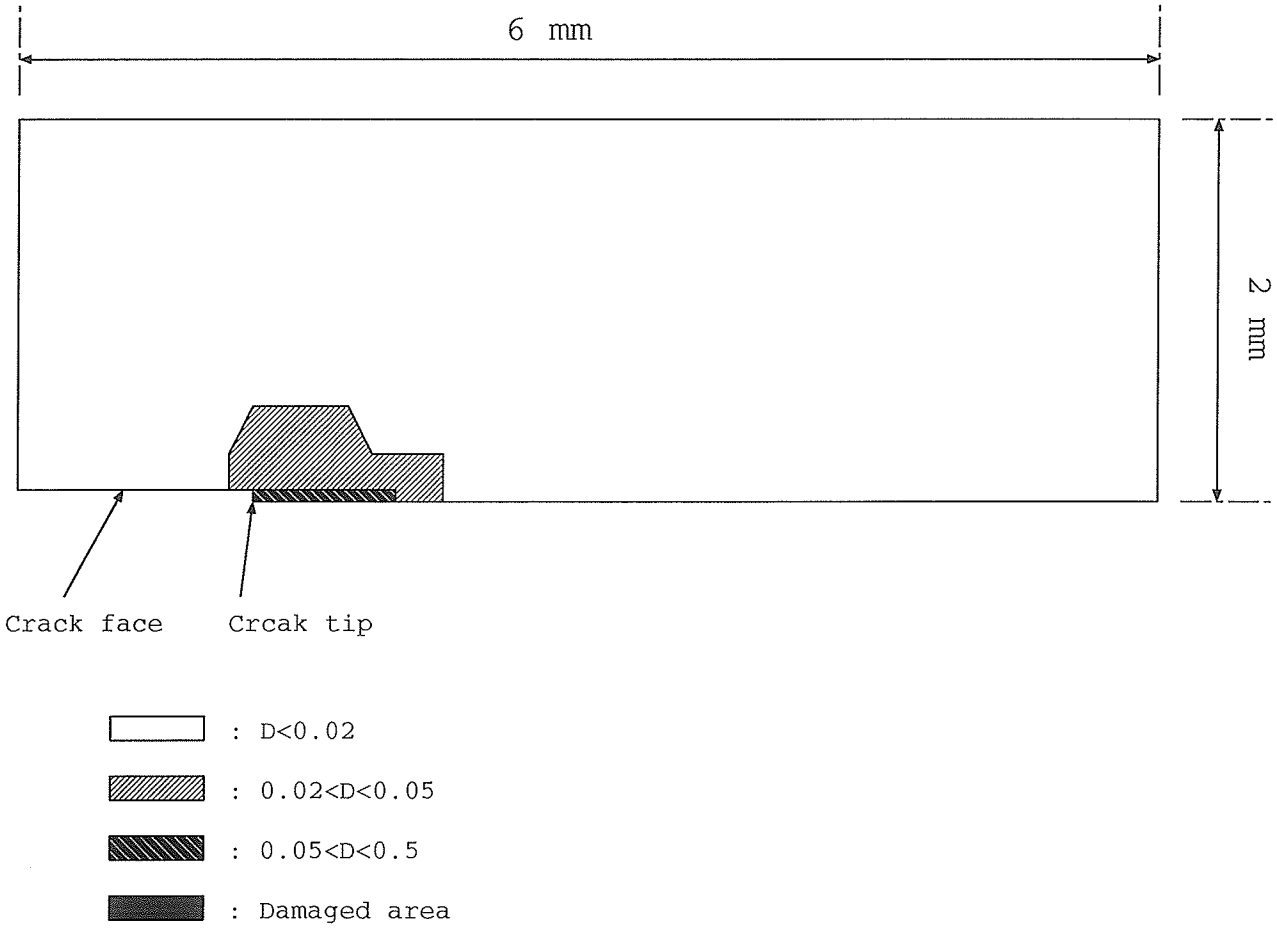

Figure L.1: The damage pattern of the crack tip area at the creep time of 87 Hours

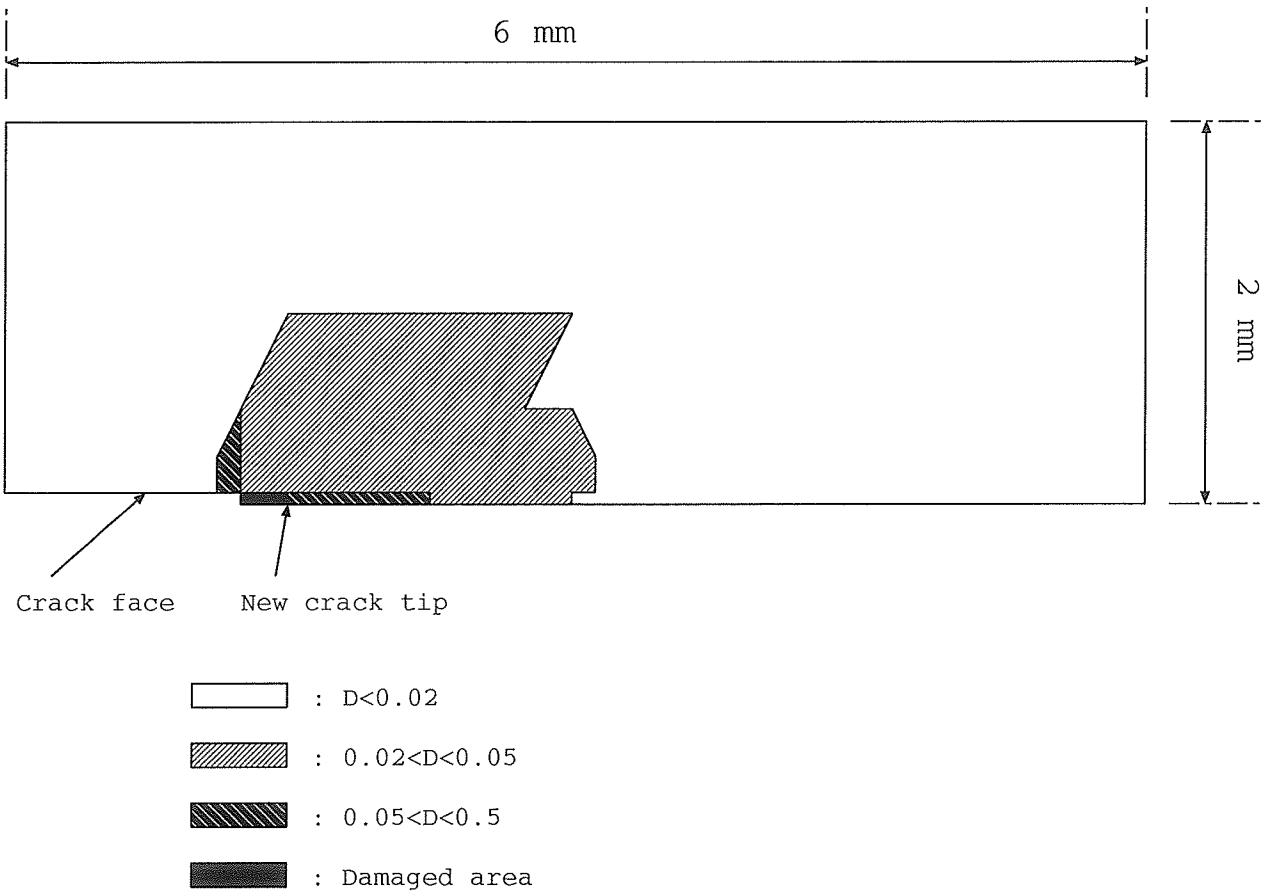

Figure L.2: The damage pattern of the crack tip area just after the second element is broken

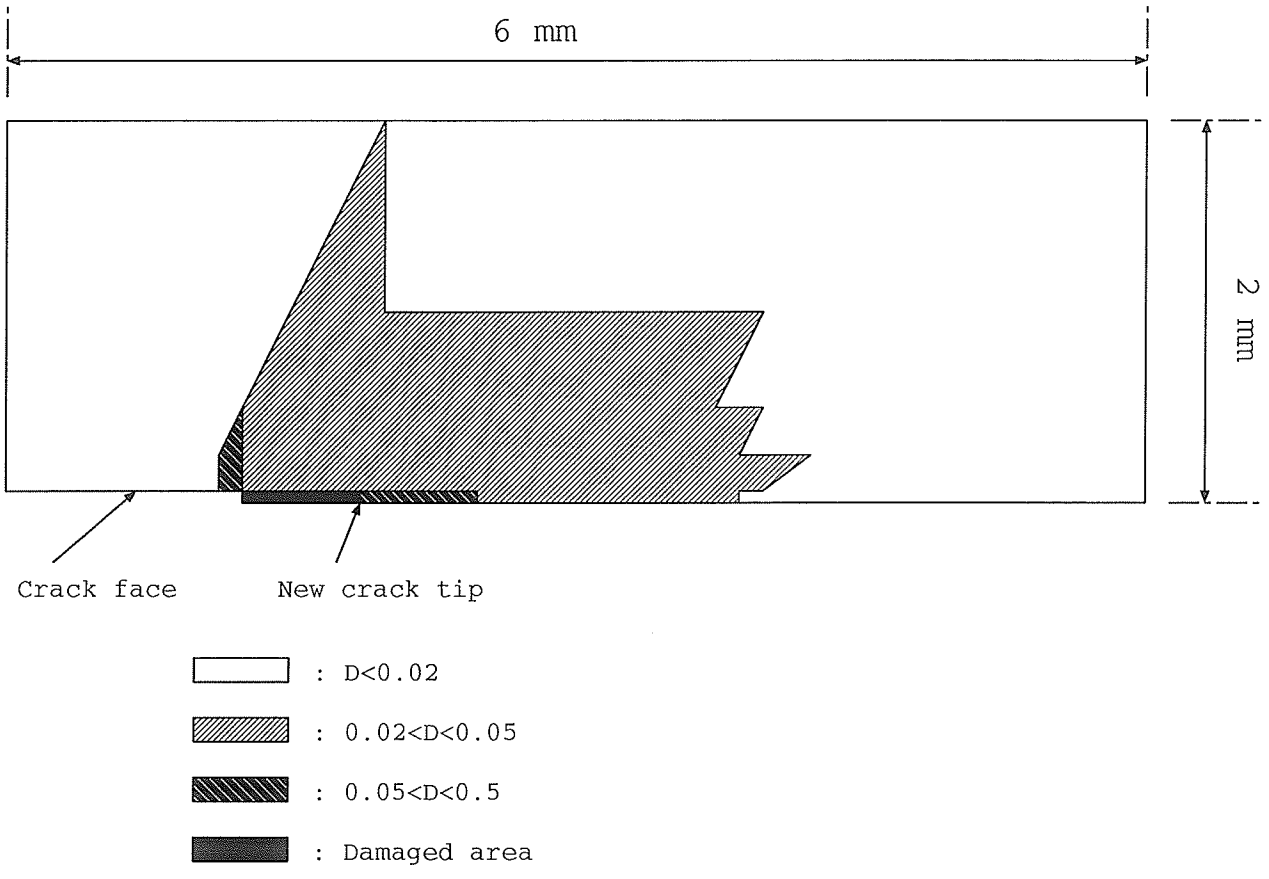

Figure L.3: The damage pattern of the crack tip area just after the fifth element is broken

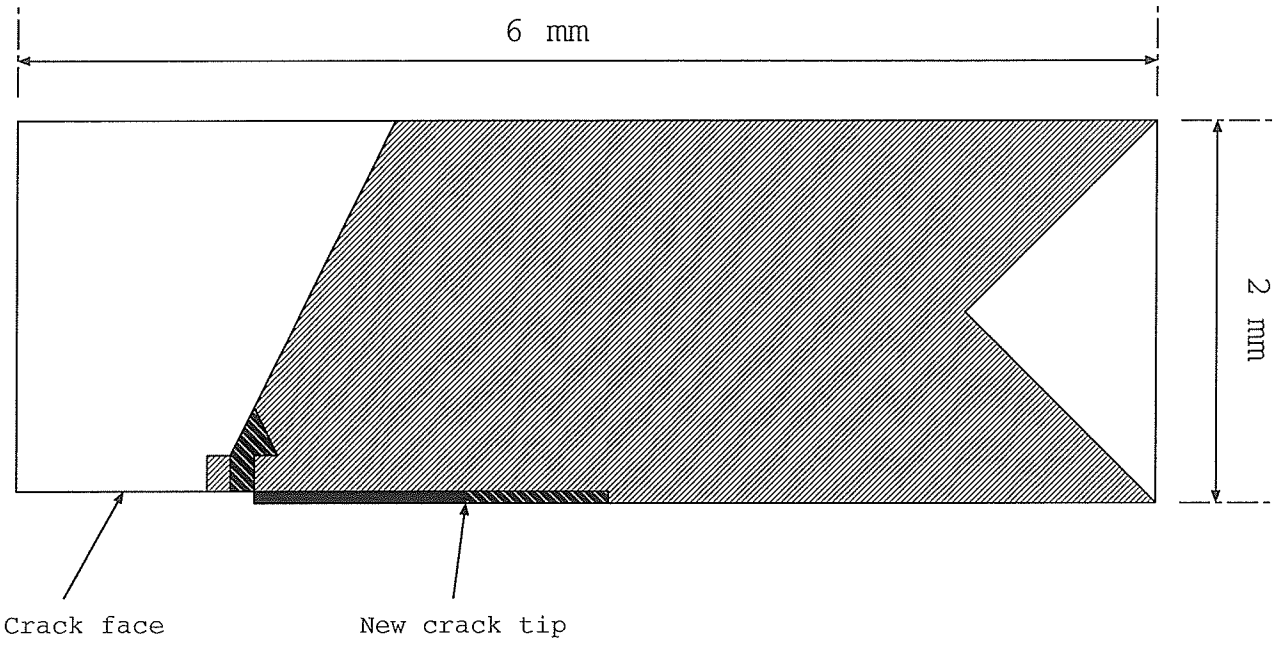

Figure L.4: The damage pattern of the crack tip area just after the ninth element is broken

Appendix M

Load cycling effect on the distribution of crack tip variables

This appendix contains the figures which show the importance of load cycling effect on creep response of the central cracked panel.

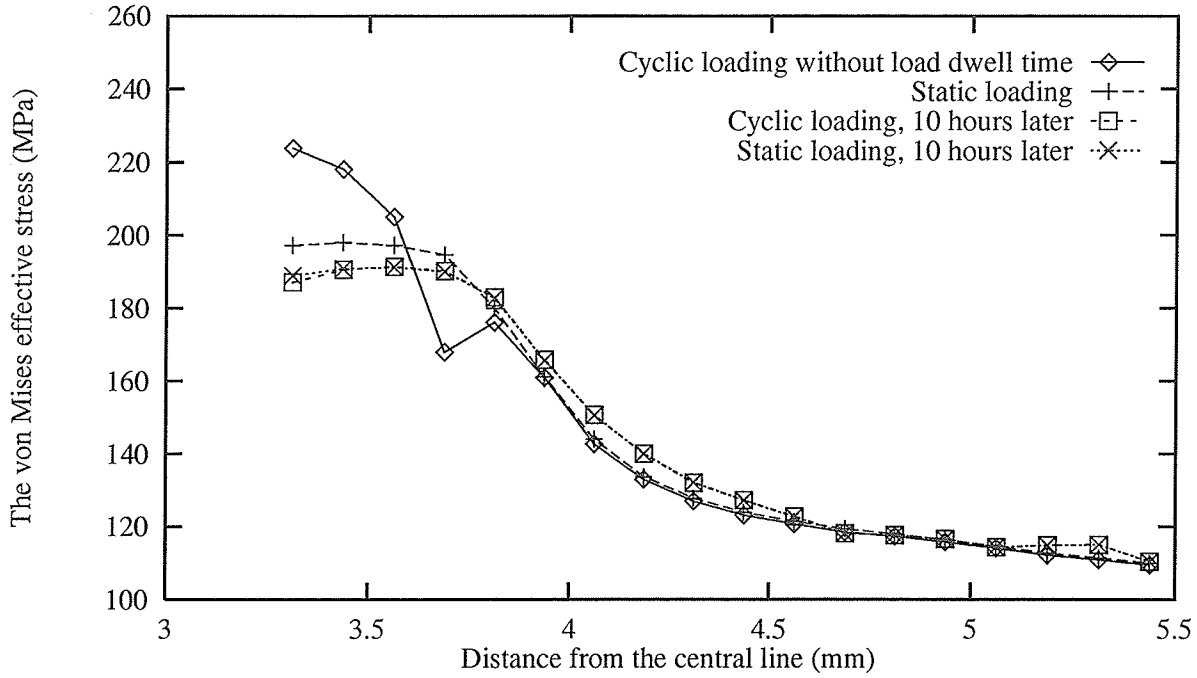

Figure M.1: The distribution of the von Mises effective stress in the crack tip area after one load cycling event without load dwell time and 10 hours later in comparison with the static loading results. The load cycling happens when creep time is 30 hours

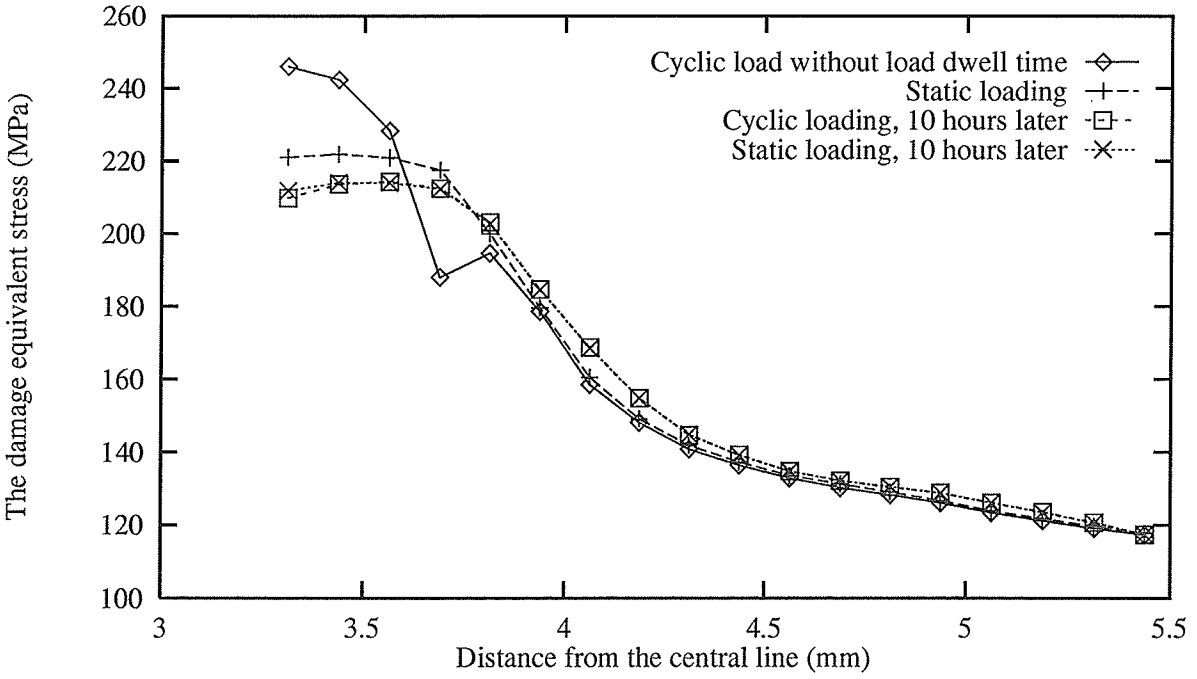

Figure M.2: The distribution of the damage equivalent stress in the crack tip area after one load cycling event without load dwell time and 10 hours later in comparison with the static loading results. The load cycling happens when creep time is 30 hours

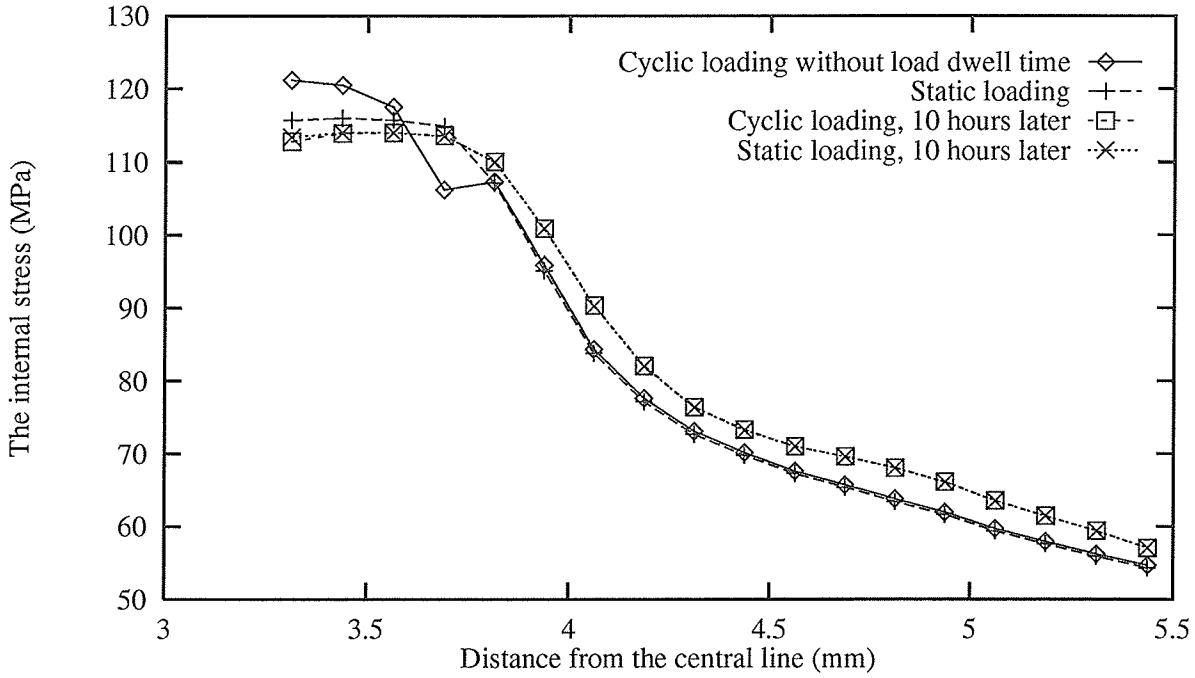

Figure M.3: The distribution of the internal stress in the crack tip area after one load cycling event without load dwell time and 10 hours later in comparison with the static loading results. The load cycling happens when creep time is 30 hours

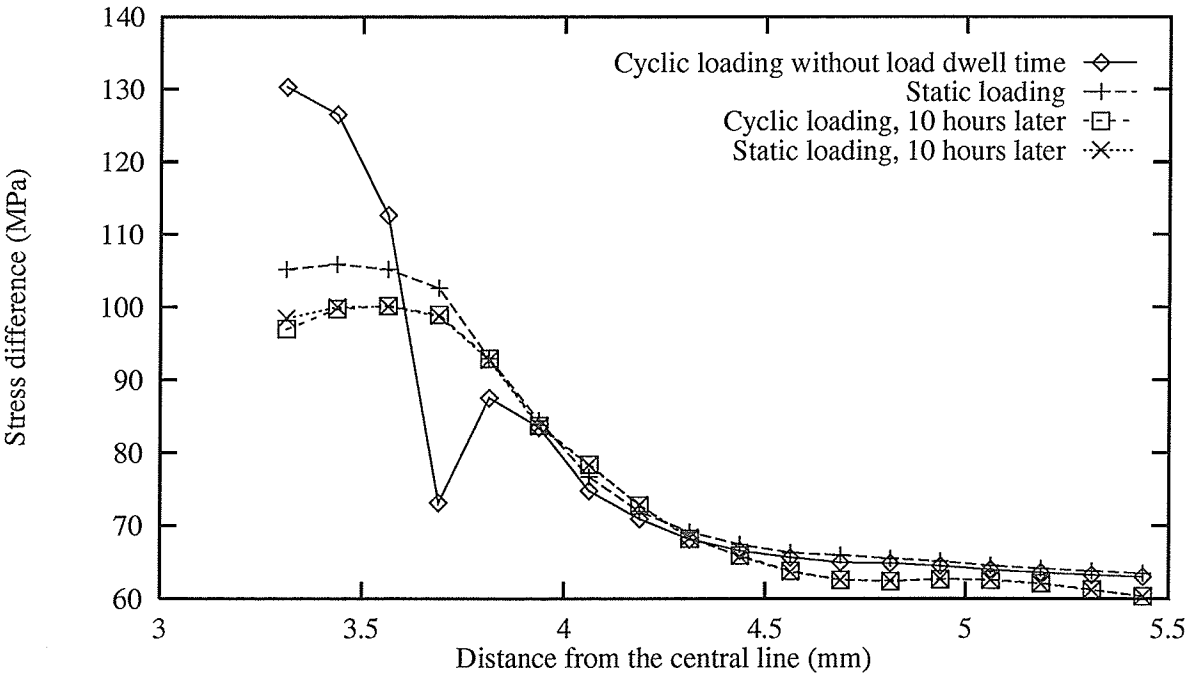

Figure M.4: The distribution of the difference between the damage equivalent stress and the internal stress $(\tilde{\sigma} - \bar{R})$ in the crack tip area after one load cycling event without load dwell time and 10 hours later in comparison with the static loading results. The load cycling happens when creep time is 30 hours

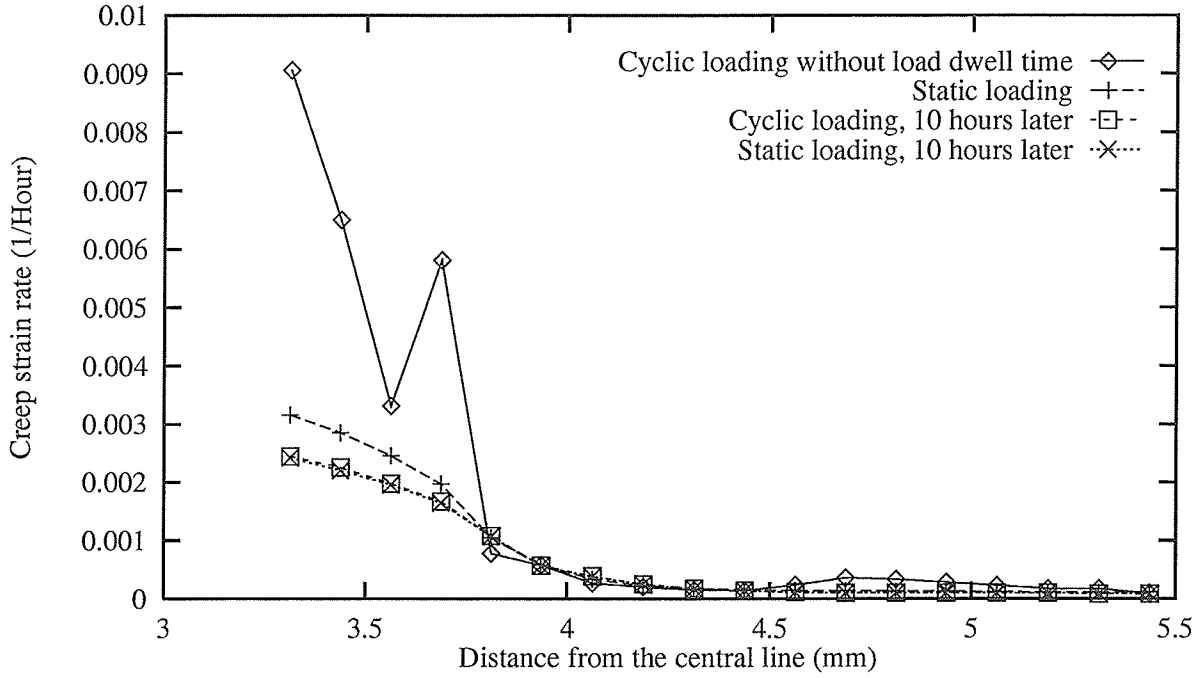

Figure M.5: The distribution of the creep strain rate in the crack tip area after one load cycling event without load dwell time and 10 hours later in comparison with the static loading results. The load cycling happens when creep time is 30 hours

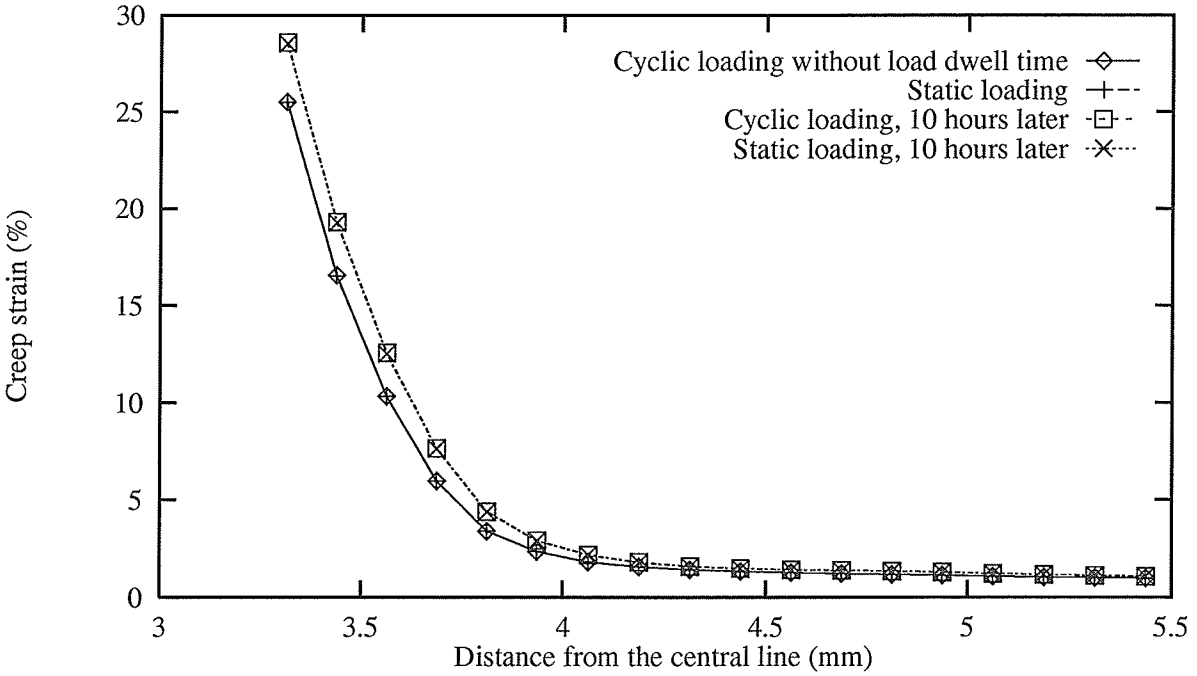

Figure M.6: The distribution of the creep strain in the crack tip area after one load cycling event without load dwell time and 10 hours later in comparison with the static loading results. The load cycling happens when creep time is 30 hours

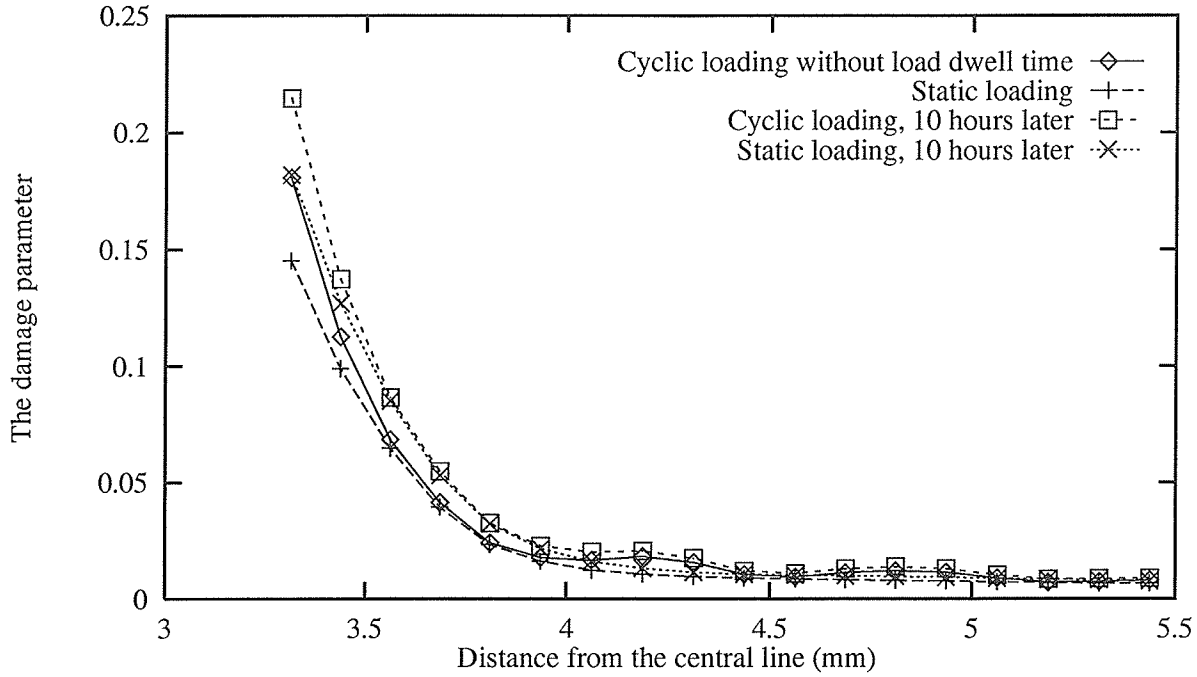

Figure M.7: The distribution of the damage in the crack tip area after one load cycling event without load dwell time and 10 hours later in comparison with the static loading results. The load cycling happens when creep time is 30 hours

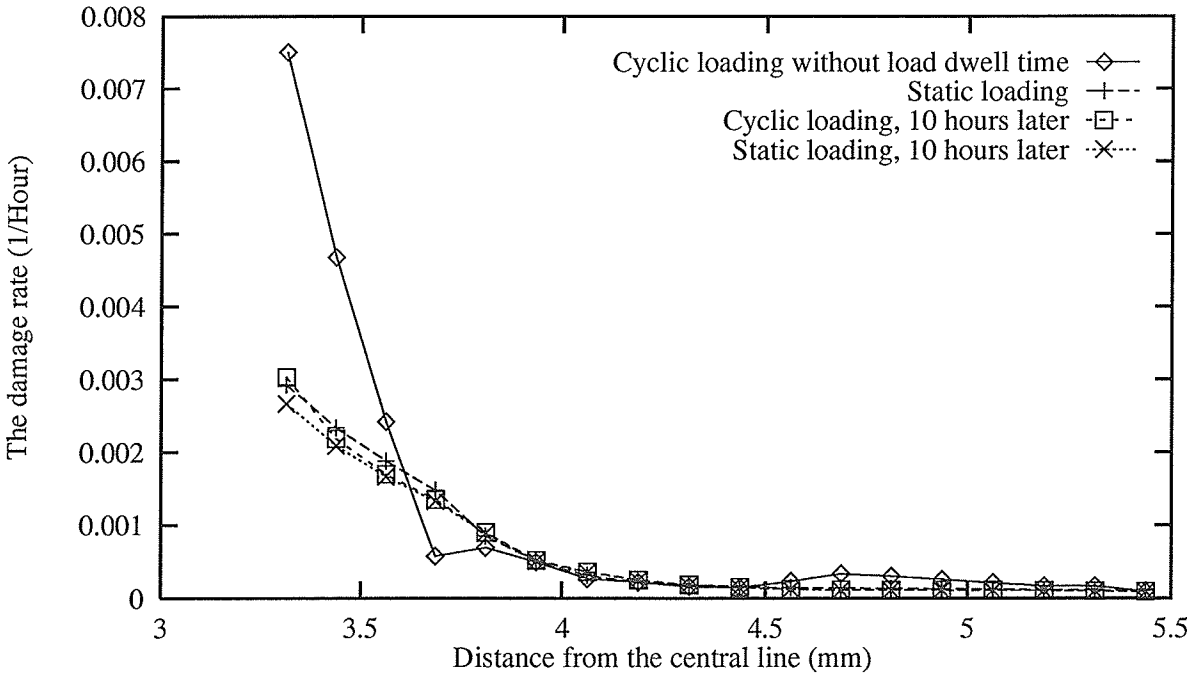

Figure M.8: The distribution of the damage rate in the crack tip area after one load cycling event without load dwell time and 10 hours later in comparison with the static loading results. The load cycling happens when creep time is 30 hours

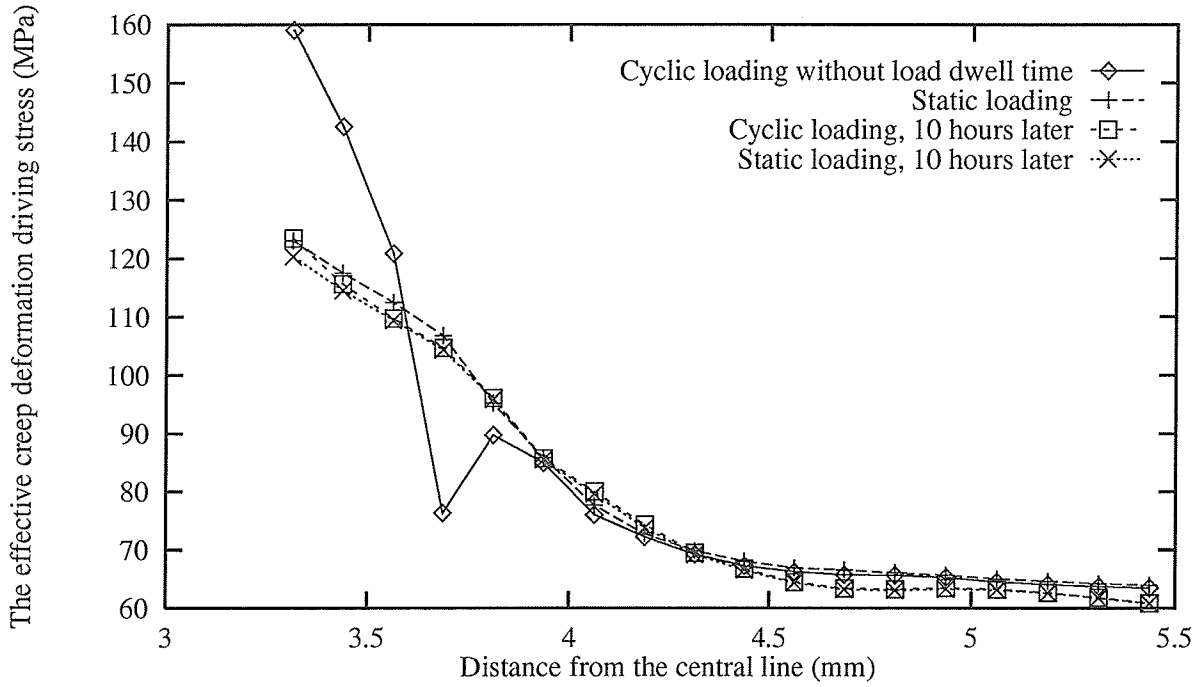

Figure M.9: The distribution of the effective creep deformation driving stress $\frac{\tilde{\sigma}-\bar{R}}{1-c_o D}$ in the crack tip area after one load cycling event without load dwell time and 10 hours later in comparison with the static loading results. The load cycling happens when creep time is 30 hours

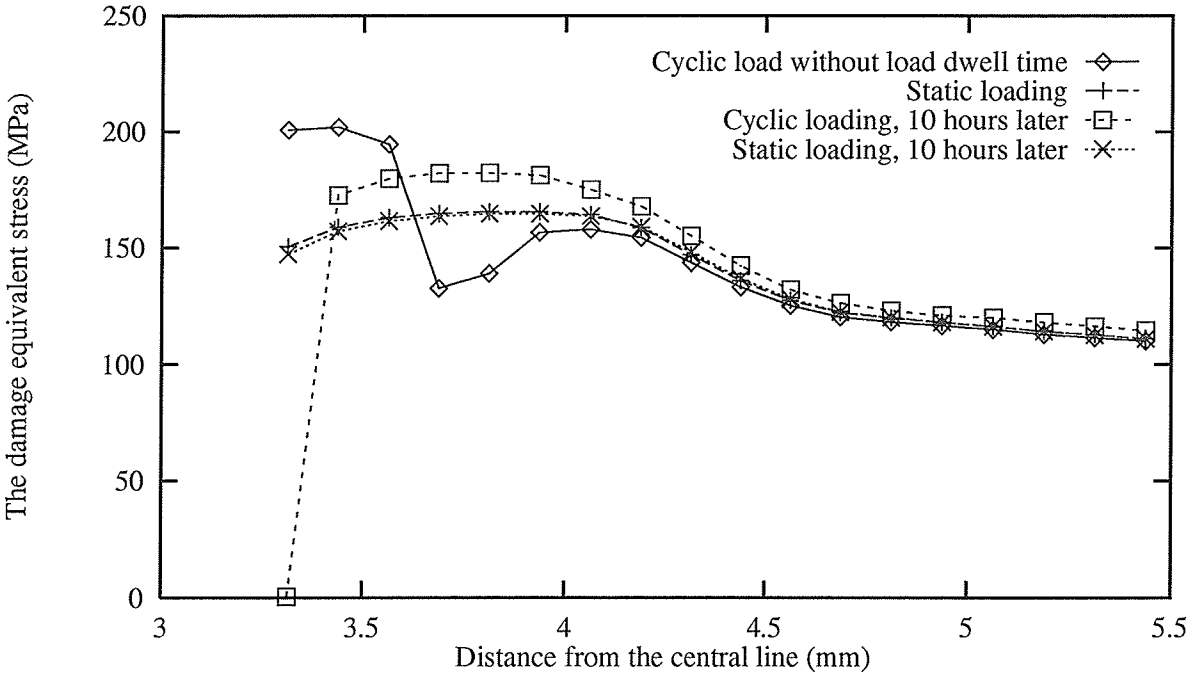

Figure M.10: The distribution of the von Mises effective stress in the crack tip area after one load cycling event without load dwell time and 10 hours later in comparison with the static loading results. The load cycling happens when creep time is 150 hours

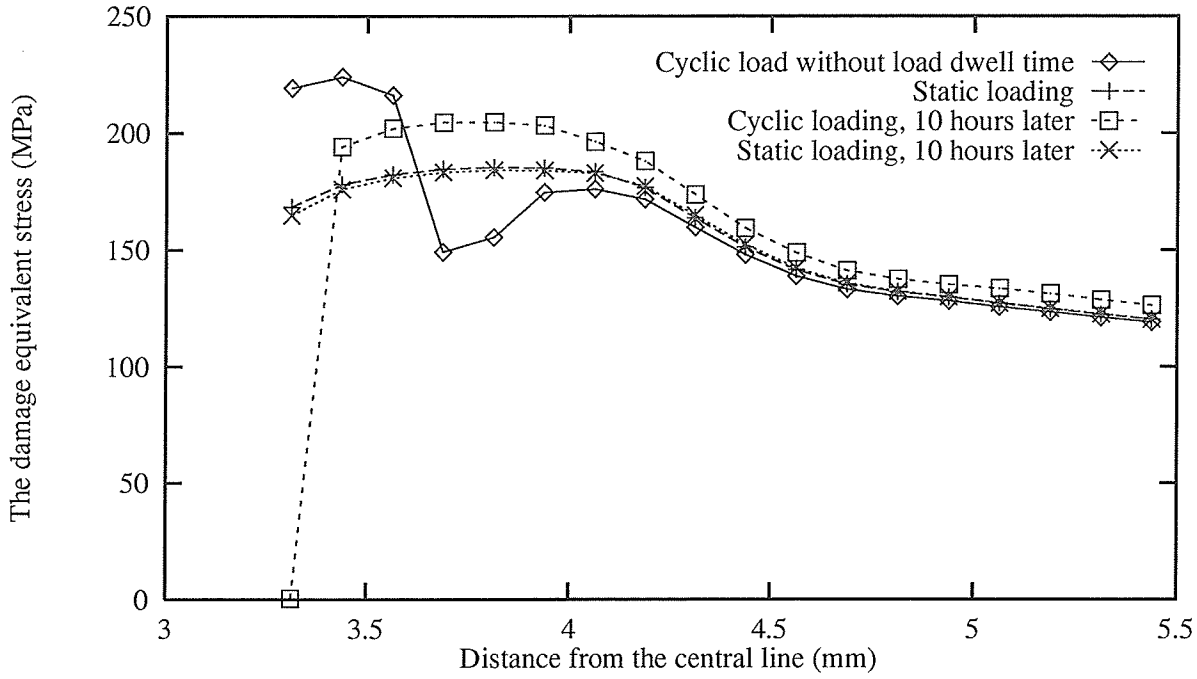

Figure M.11: The distribution of the damage equivalent stress in the crack tip area after one load cycling event without load dwell time and 10 hours later in comparison with the static loading results. The load cycling happens when creep time is 150 hours

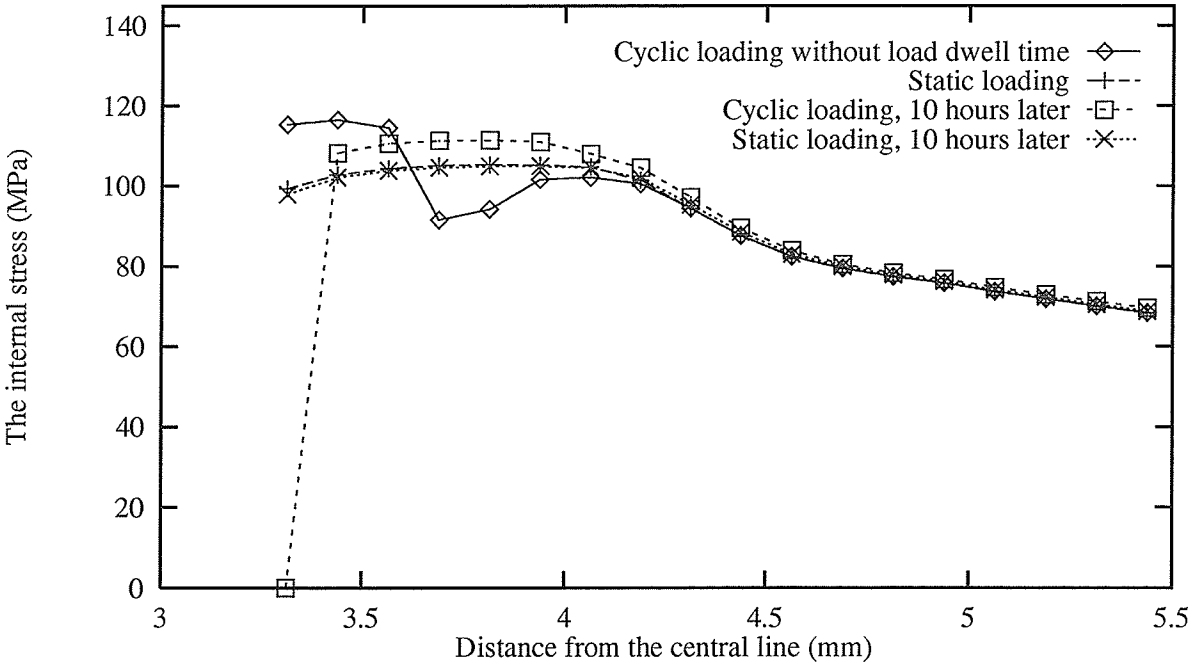

Figure M.12: The distribution of the internal stress in the crack tip area after one load cycling event without load dwell time and 10 hours later in comparison with the static loading results. The load cycling happens when creep time is 150 hours

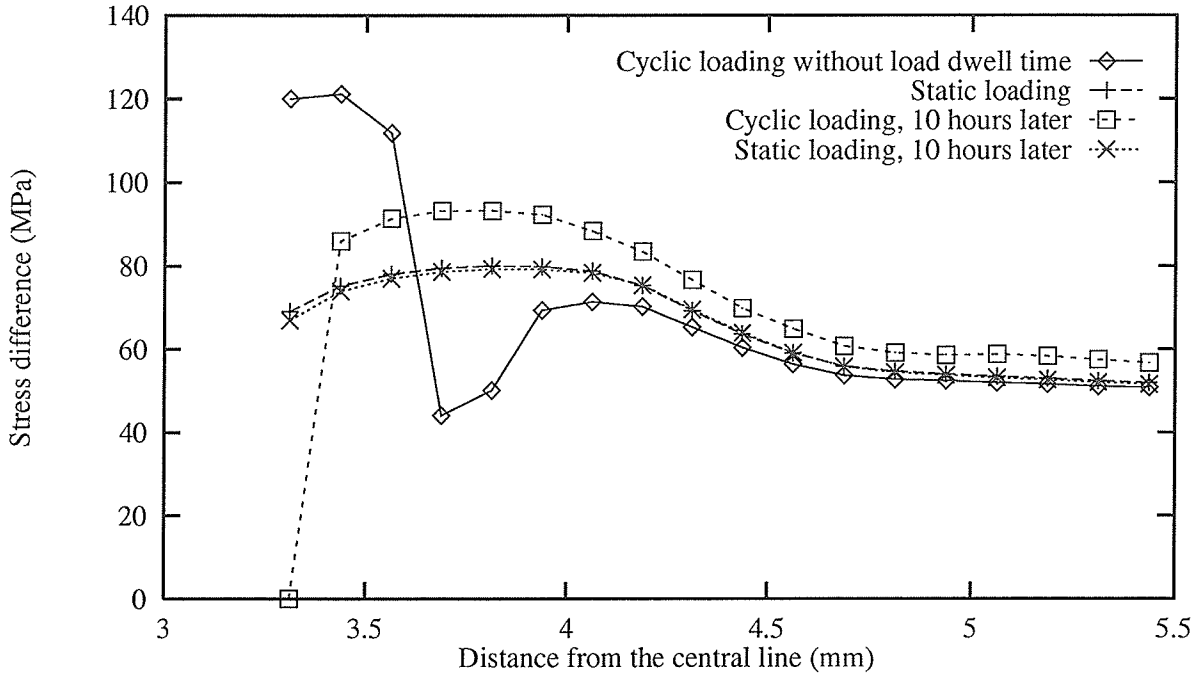

Figure M.13: The distribution of the difference between the damage equivalent stress and the internal stress $(\tilde{\sigma} - \bar{R})$ in the crack tip area after one load cycling event without load dwell time and 10 hours later in comparison with the static loading results. The load cycling happens when creep time is 150 hours

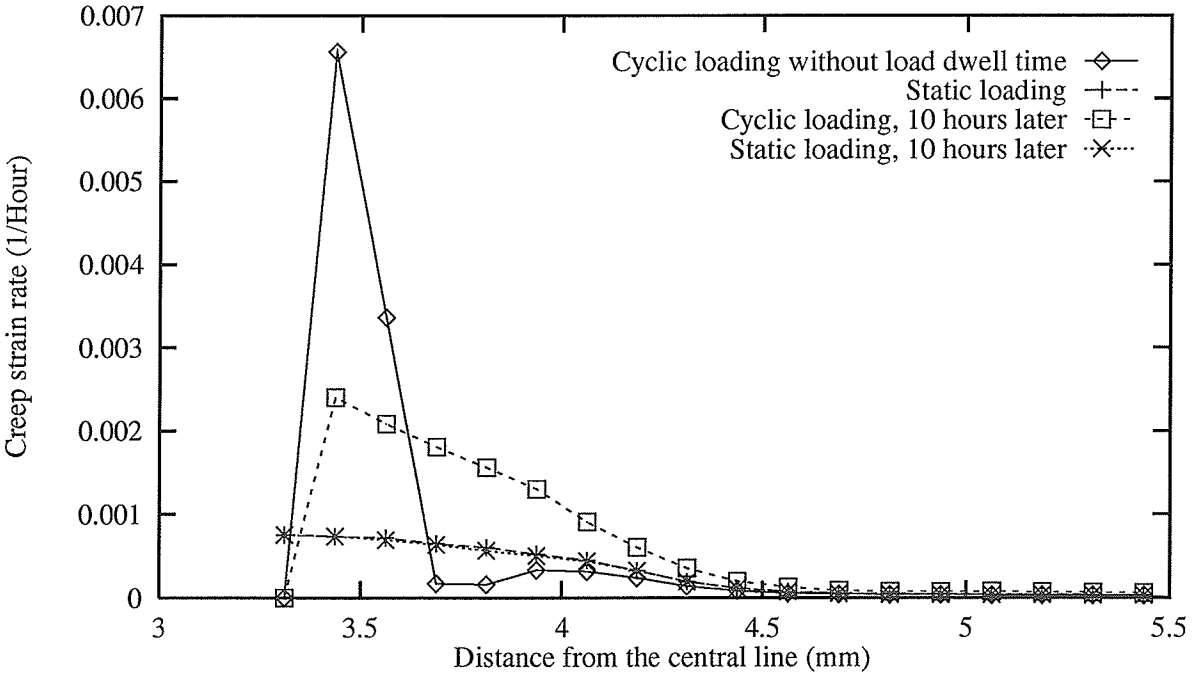

Figure M.14: The distribution of the creep strain rate in the crack tip area after one load cycling event without load dwell time and 10 hours later in comparison with the static loading results. The load cycling happens when creep time is 150 hours

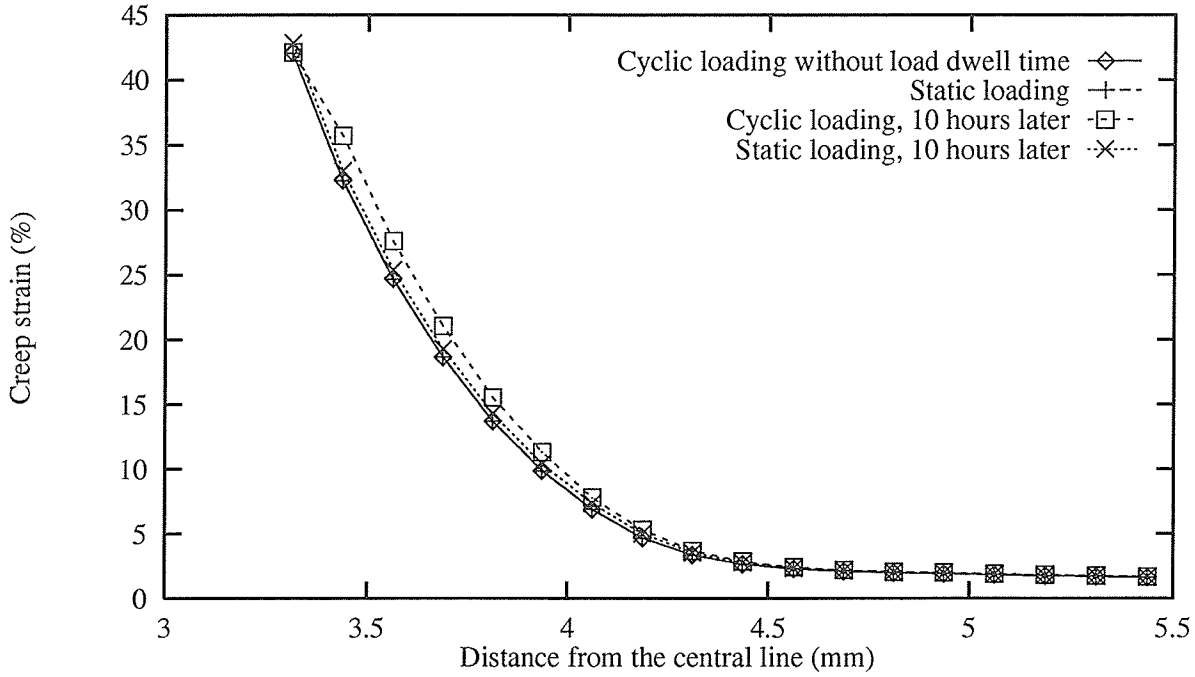

Figure M.15: The distribution of the creep strain in the crack tip area after one load cycling event without load dwell time and 10 hours later in comparison with the static loading results. The load cycling happens when creep time is 150 hours

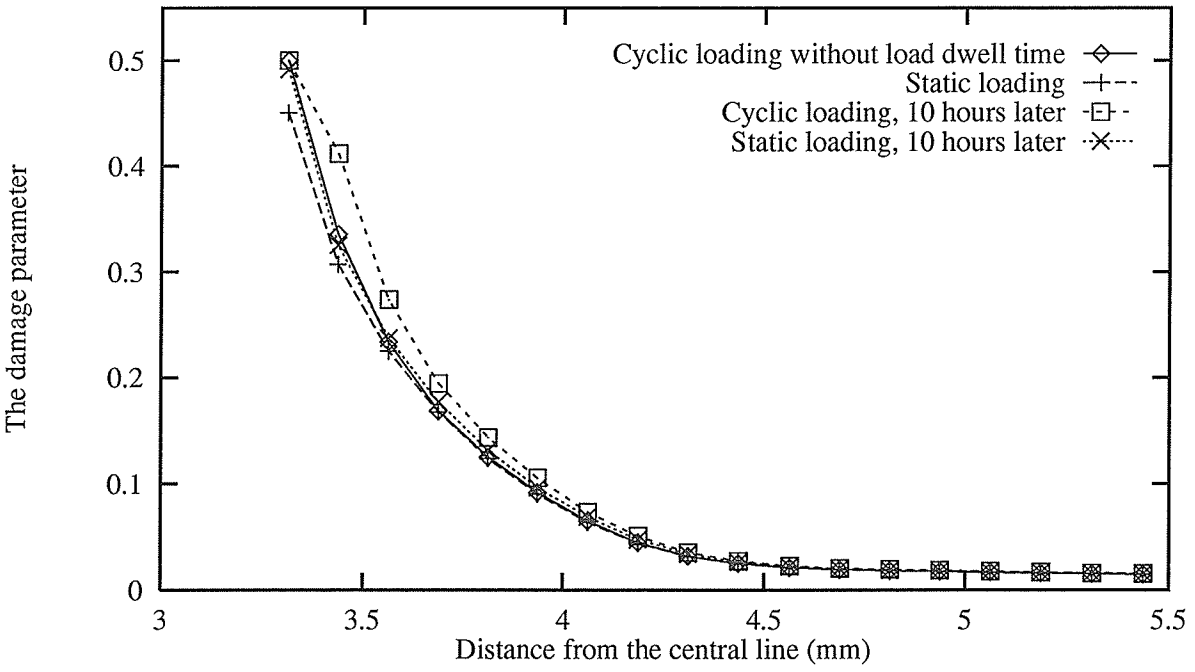

Figure M.16: The distribution of the damage in the crack tip area after one load cycling event without load dwell time and 10 hours later in comparison with the static loading results. The load cycling happens when creep time is 150 hours

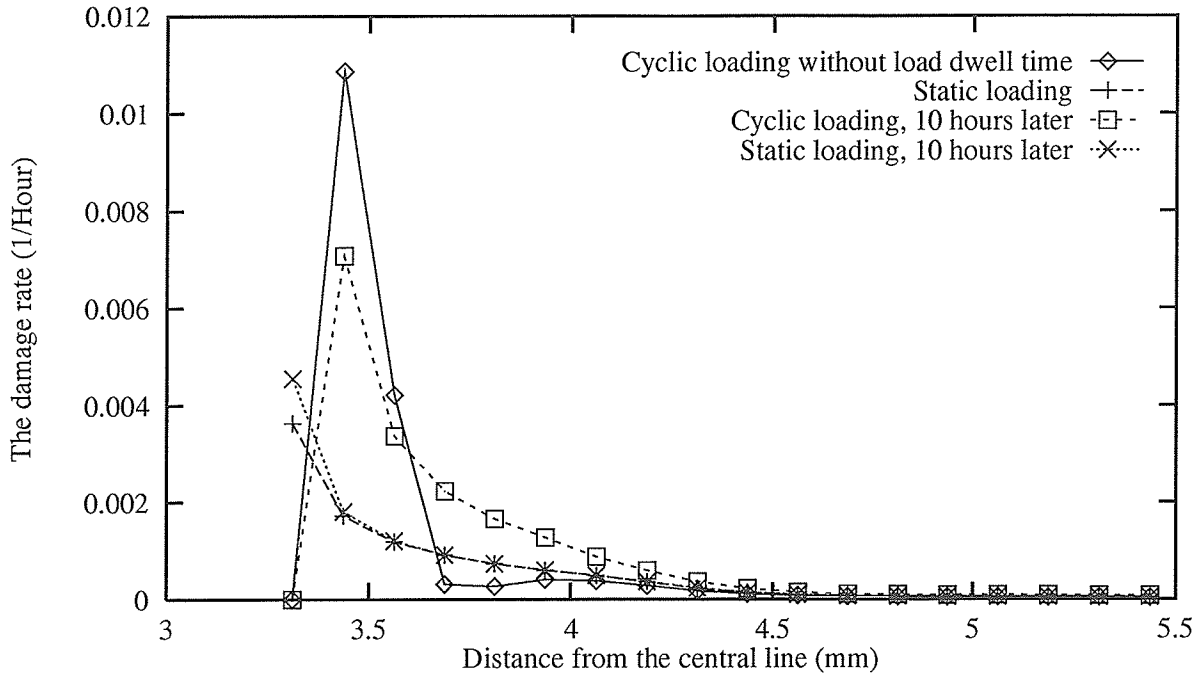

Figure M.17: The distribution of the damage rate in the crack tip area after one load cycling event without load dwell time and 10 hours later in comparison with the static loading results. The load cycling happens when creep time is 150 hours

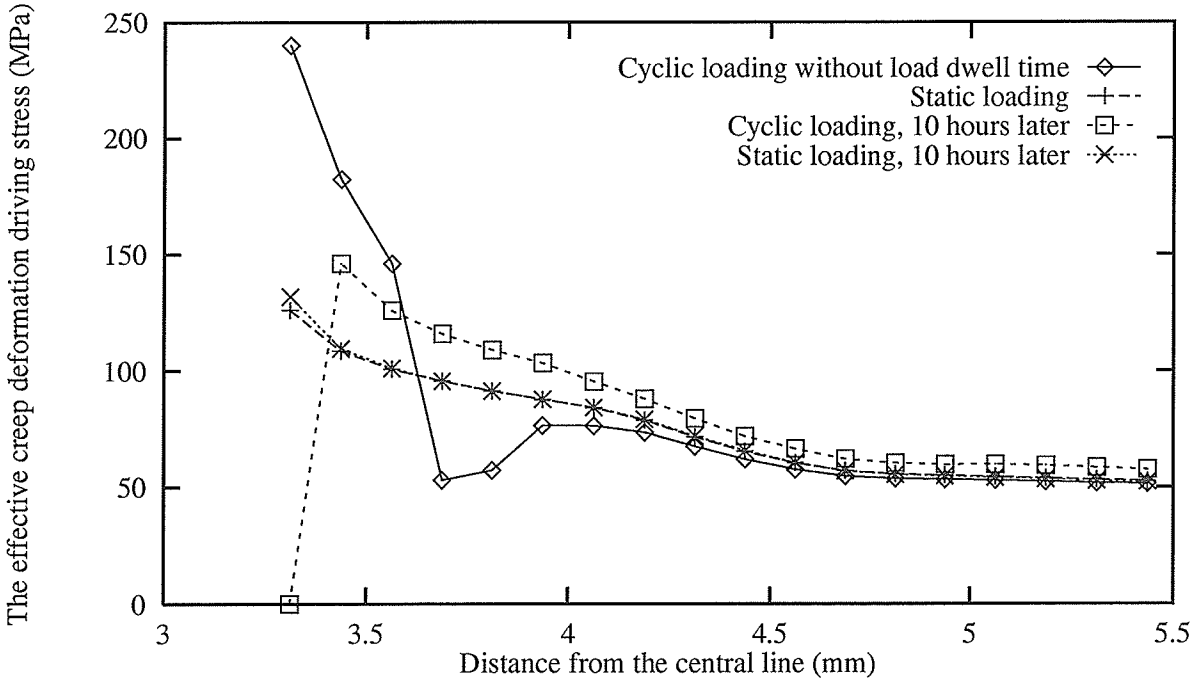

Figure M.18: The distribution of the effective creep deformation driving stress $\frac{\tilde{\sigma}-\bar{R}}{1-c_o D}$ in the crack tip area after one load cycling event without load dwell time and 10 hours later in comparison with the static loading results. The load cycling happens when creep time is 150 hours

Appendix N

Stress distribution in the load cycling process

This appendix contains the figures which show the stress distribution in the crack tip area of the central cracked panel before and after a load cycling event in the creep deformation process. The coordinate system is that as used in Fig. 5.7.

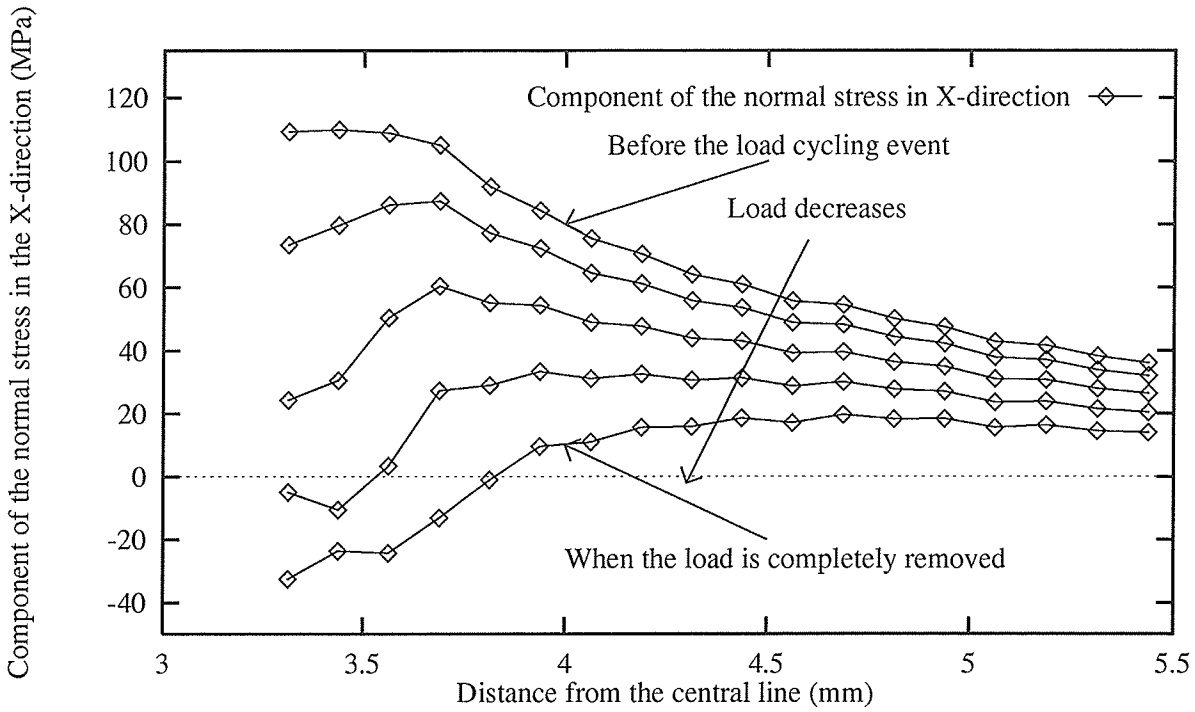

Figure N.1: The distribution of the component of the normal stress in the X-direction during the unloading process. The load cycling happens when the creep time is 30 hours

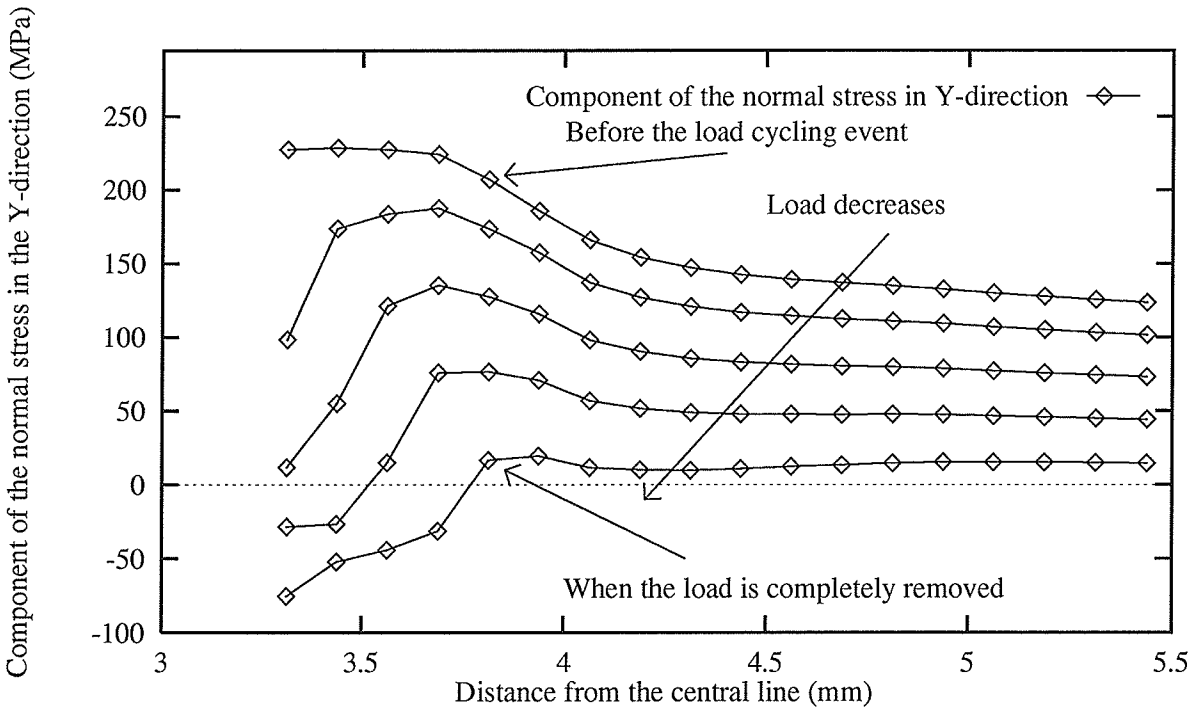

Figure N.2: The distribution of the component of the normal stress in the Y-direction during the unloading process. The load cycling happens when the creep time is 30 hours

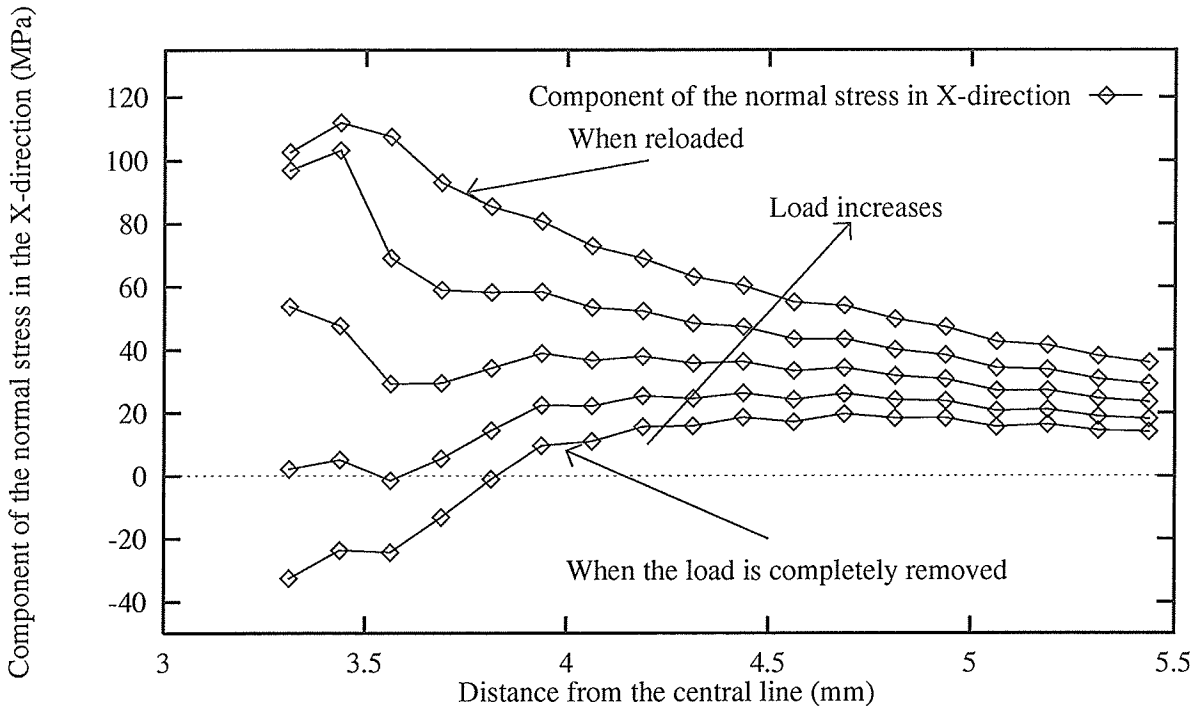

Figure N.3: The distribution of the component of the normal stress in the X-direction during the reloading process. The load cycling happens when the creep time is 30 hours

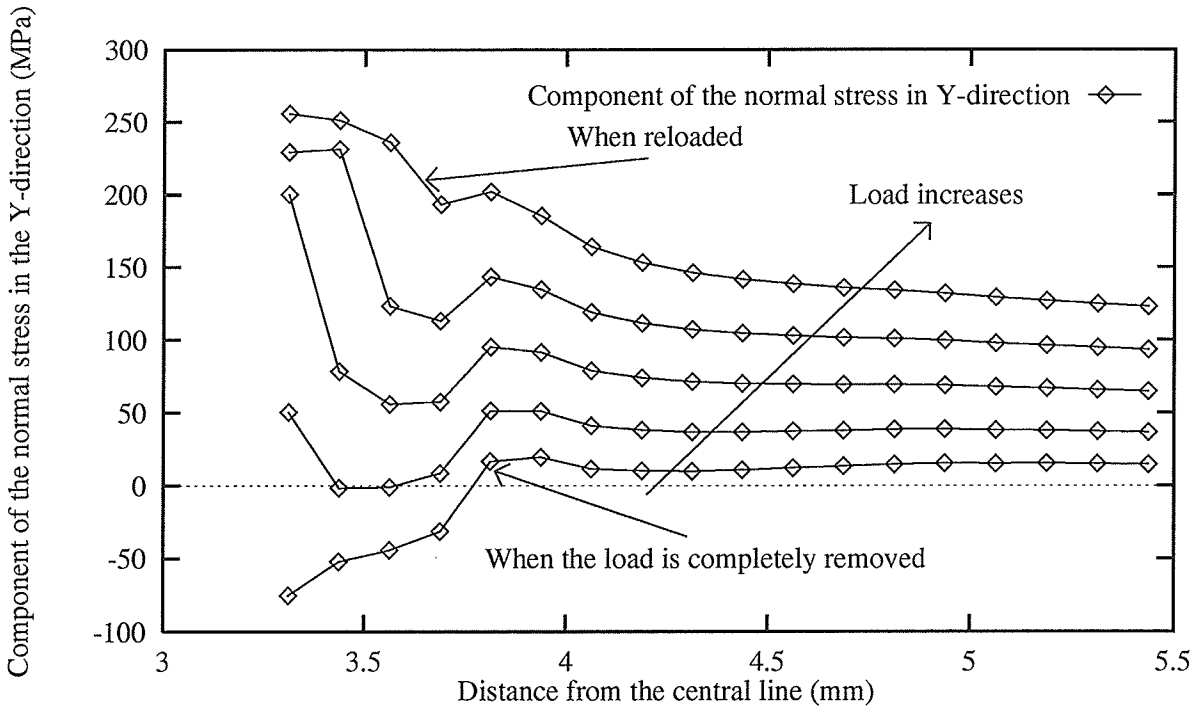

Figure N.4: The distribution of the component of the normal stress in the Y-direction during the reloading process. The load cycling happens when the creep time is 30 hours

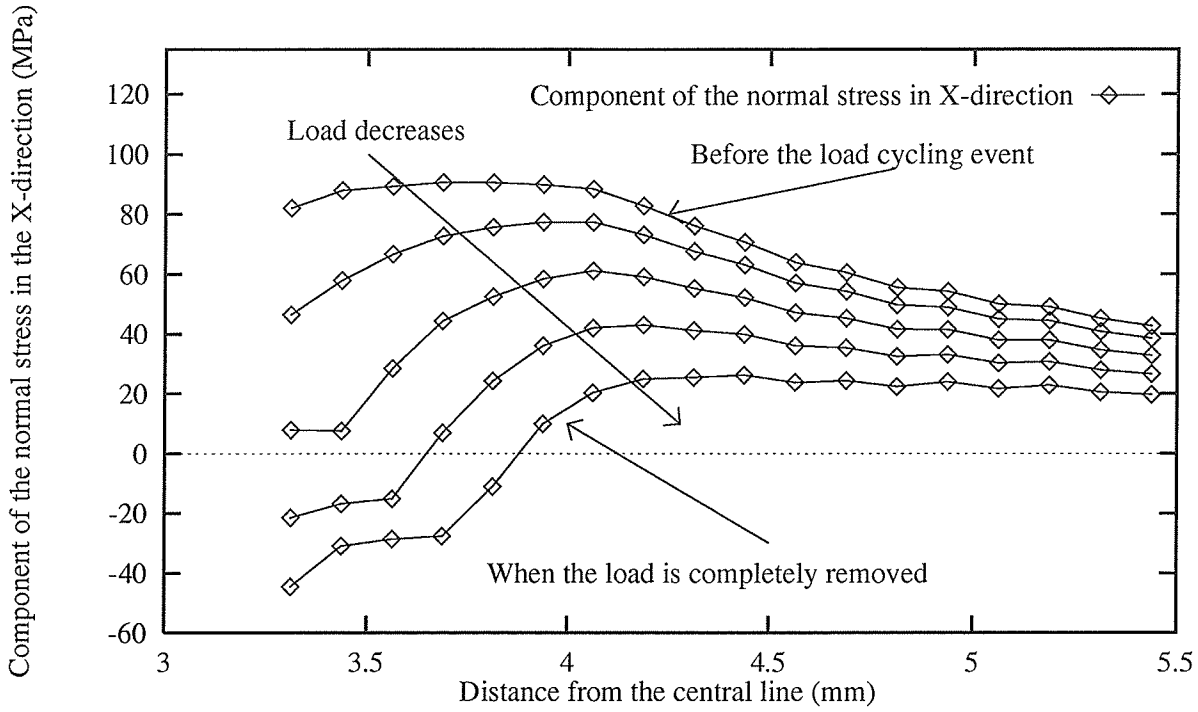

Figure N.5: The distribution of the component of the normal stress in the X-direction during the unloading process. The load cycling happens when the creep time is 150 hours

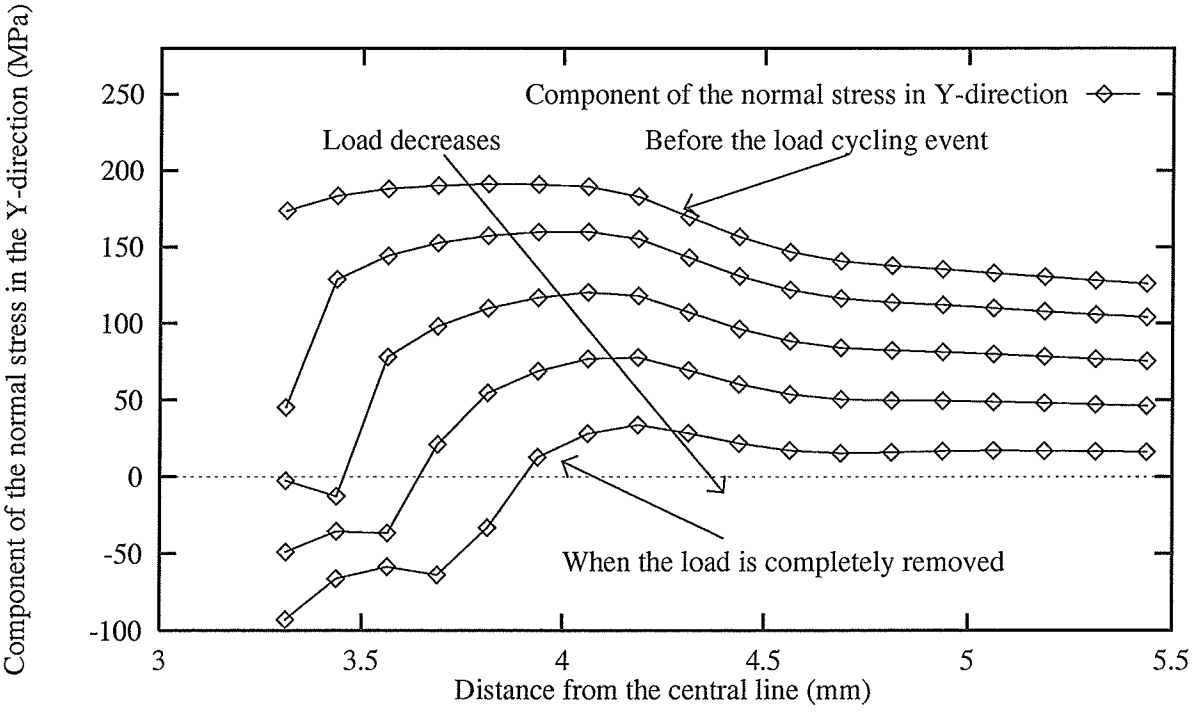

Figure N.6: The distribution of the component of the normal stress in the Y-direction during the unloading process. The load cycling happens when the creep time is 150 hours

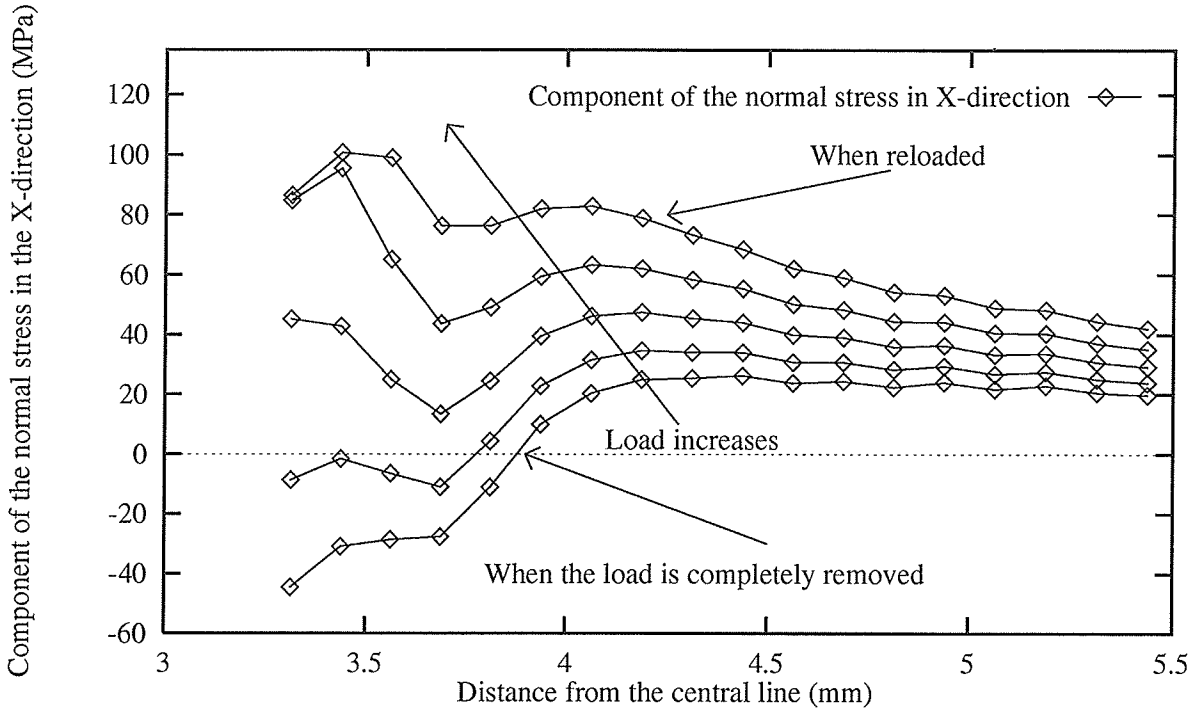

Figure N.7: The distribution of the component of the normal stress in the X-direction during the reloading process. The load cycling happens when the creep time is 150 hours

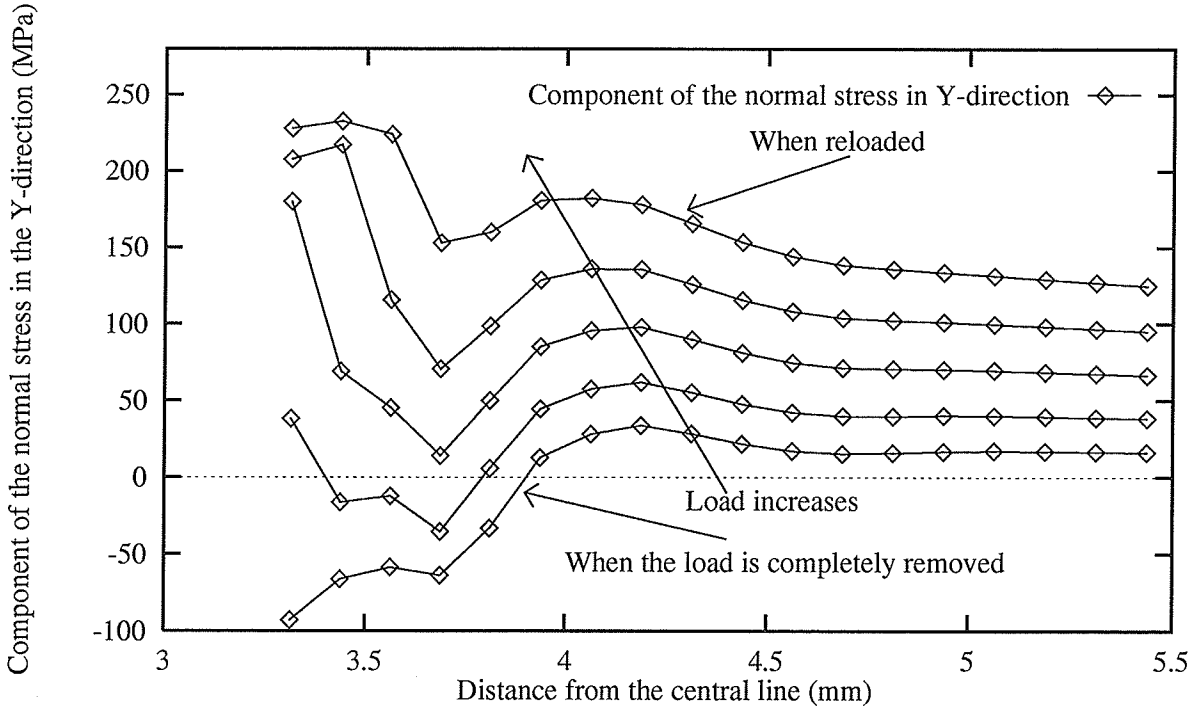

Figure N.8: The distribution of the component of the normal stress in the Y-direction during the reloading process. The load cycling happens when the creep time is 150 hours

Appendix O

Load dwell time effect on the distribution of crack tip variables

This appendix contains the figures which show the importance of the load dwell time effect on creep response of the central cracked panel.

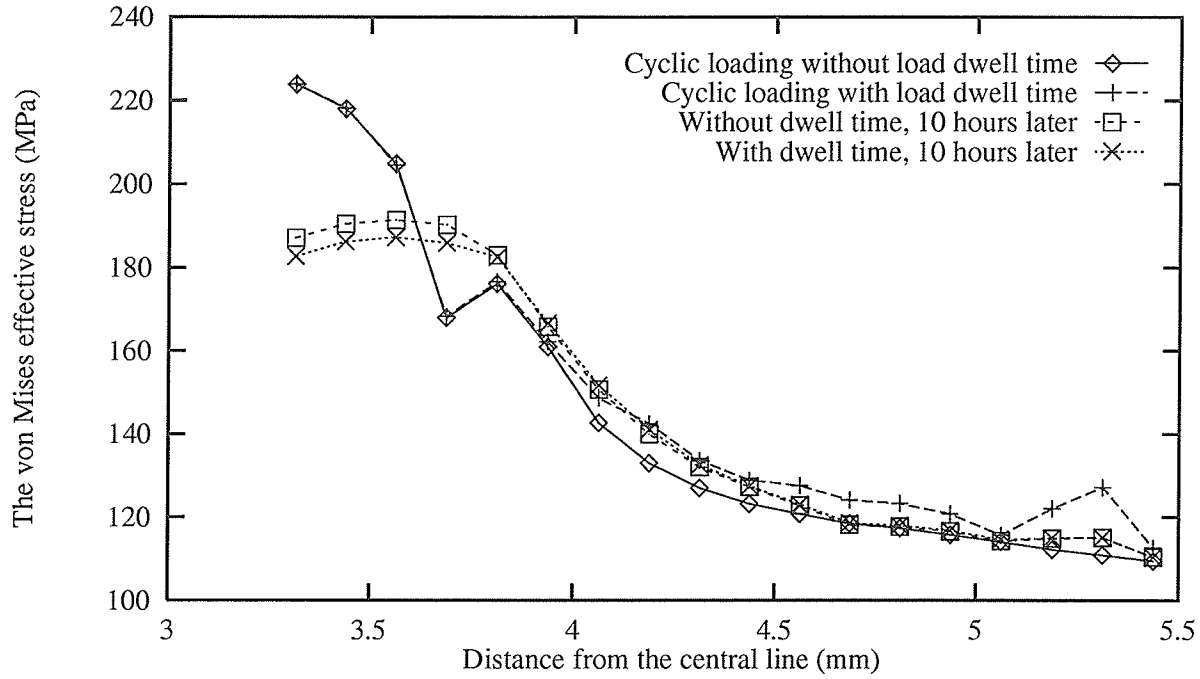

Figure O.1: Comparison of the distributions of the von Mises effective stress in the crack tip area after one load cycling event with and without load dwell time and 10 hours later. The load cycling happens when the creep time is 30 hours

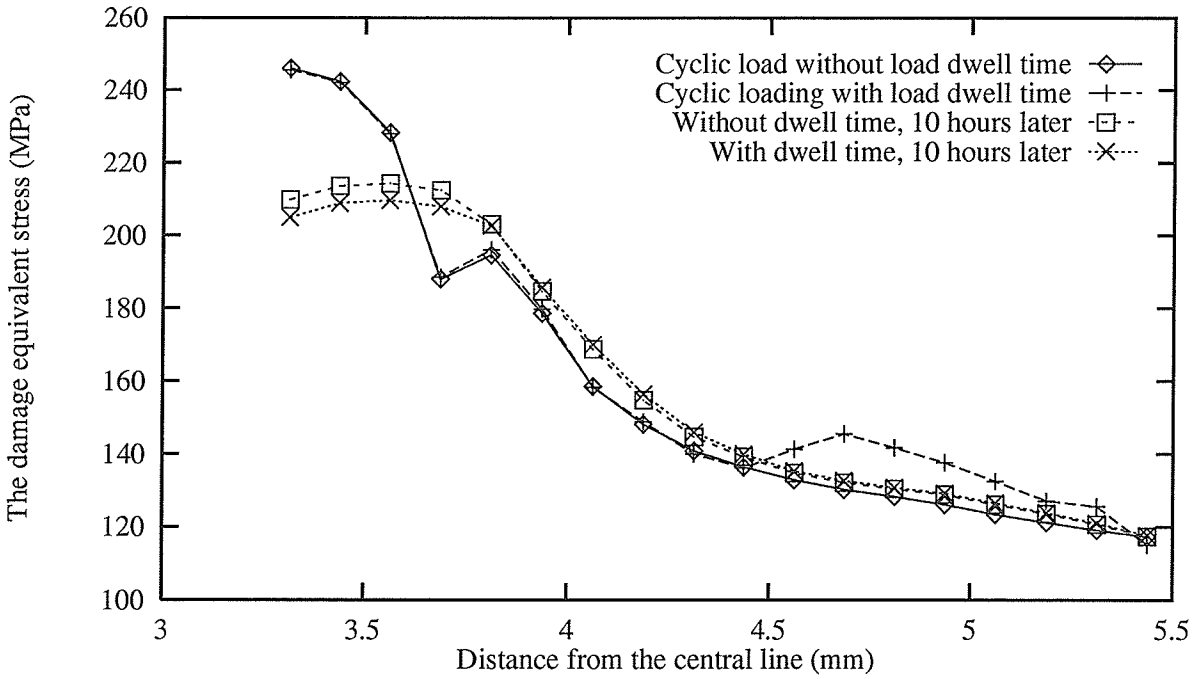

Figure O.2: Comparison of the distributions of the damage equivalent stress in the crack tip area after one load cycling event with and without load dwell time and 10 hours later. The load cycling happens when the creep time is 30 hours

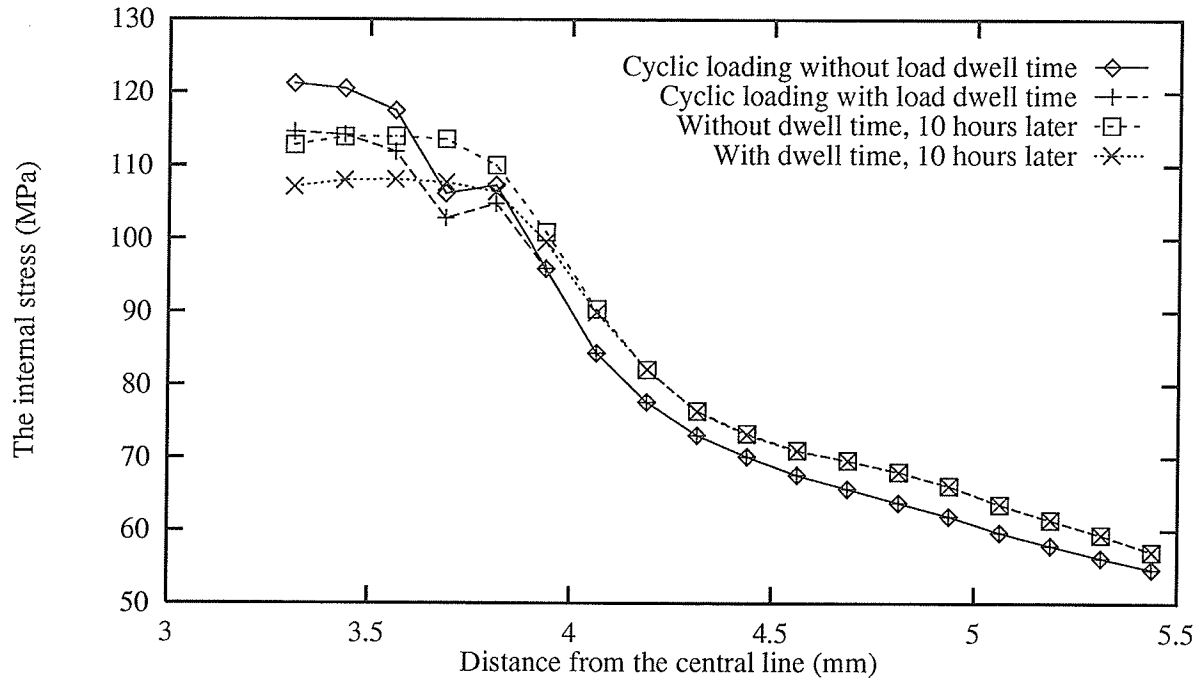

Figure O.3: Comparison of the distributions of the internal stress in the crack tip area after one load cycling event with and without load dwell time and 10 hours later. The load cycling happens when the creep time is 30 hours

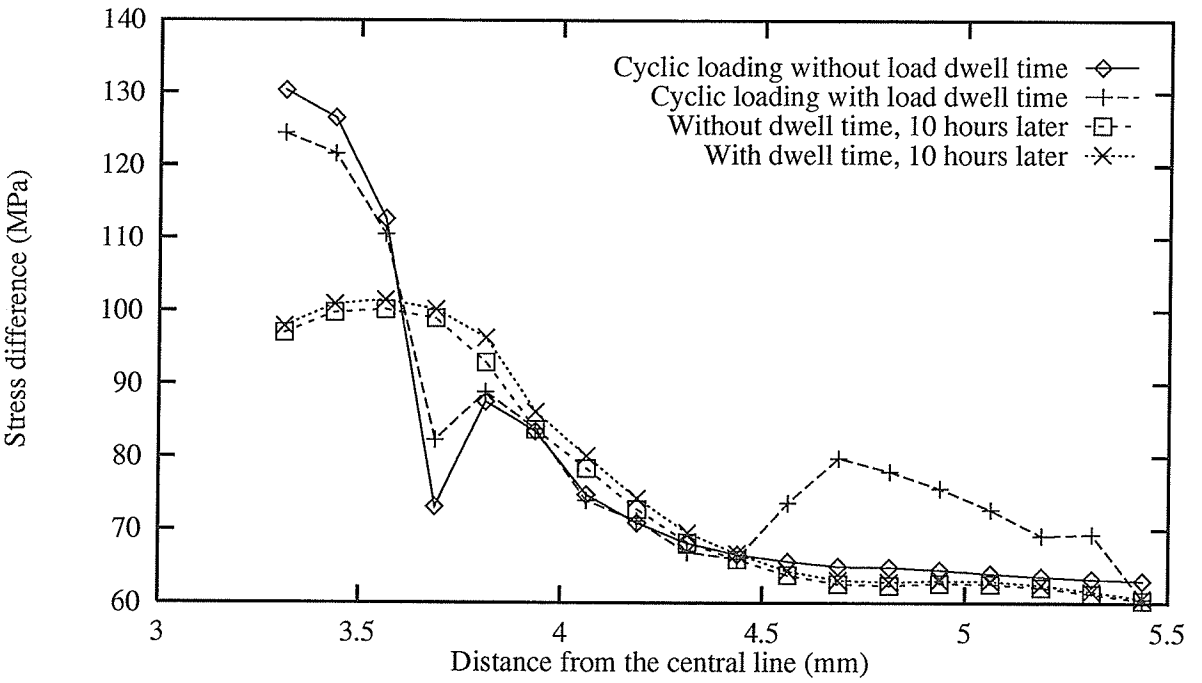

Figure O.4: Comparison of the distributions of the difference between the damage equivalent stress and the internal stress ($\tilde{\sigma} - \bar{R}$) in the crack tip area after one load cycling event with and without load dwell time and 10 hours later. The load cycling happens when the creep time is 30 hours

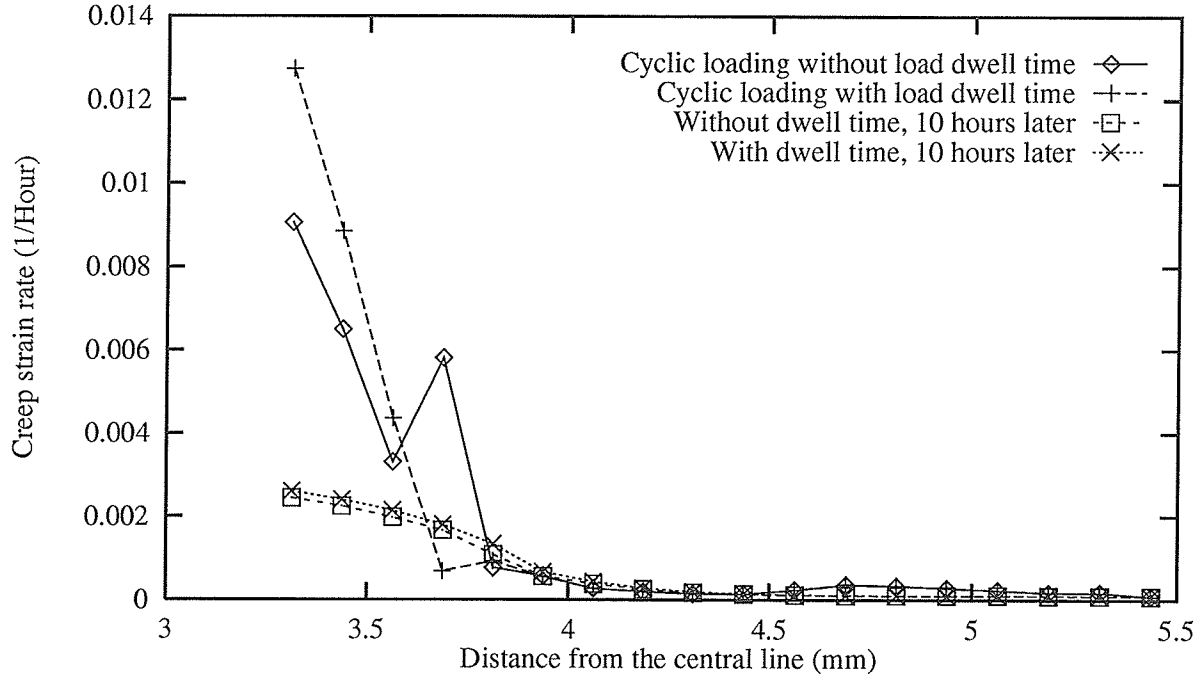

Figure O.5: Comparison of the distributions of the creep strain rate in the crack tip area after one load cycling event with and without load dwell time and 10 hours later. The load cycling happens when the creep time is 30 hours

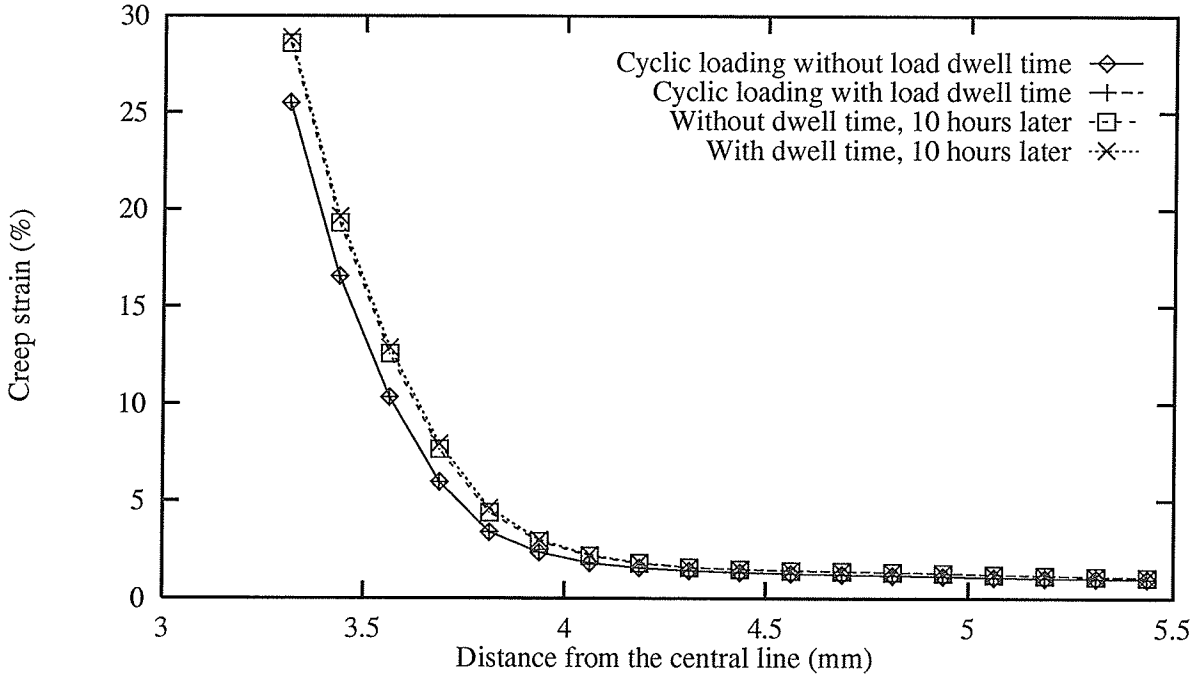

Figure O.6: Comparison of the distributions of the creep strain in the crack tip area after one load cycling event with and without load dwell time and 10 hours later. The load cycling happens when the creep time is 30 hours

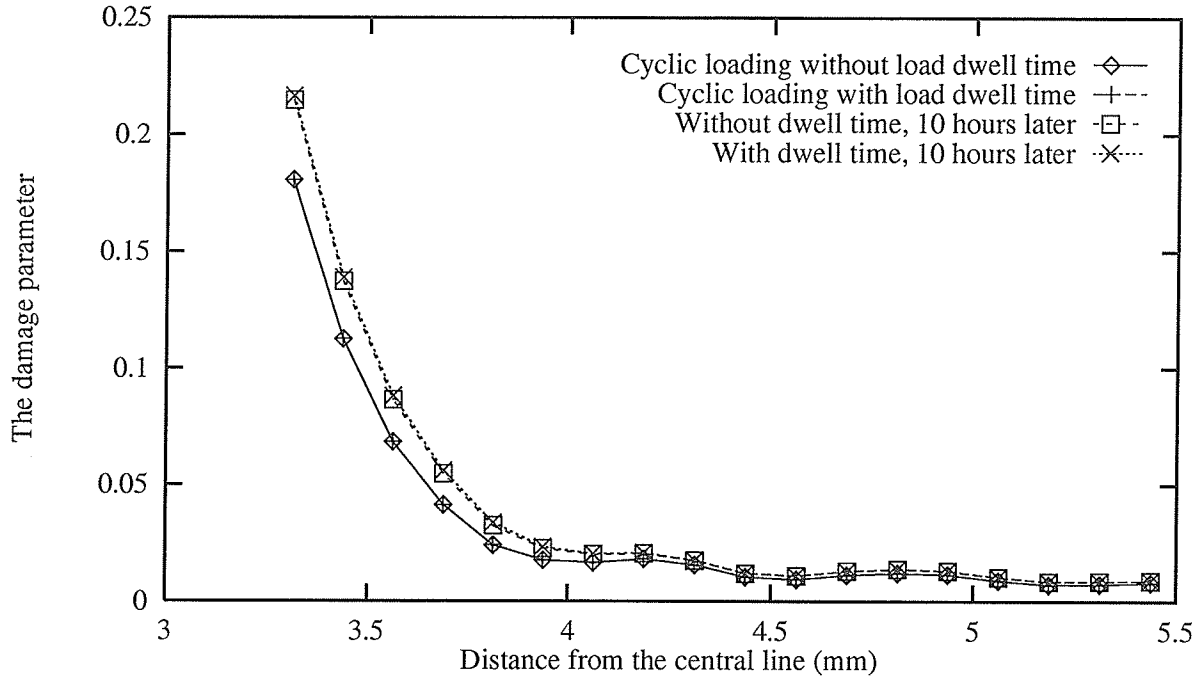

Figure O.7: Comparison of the distributions of the damage in the crack tip area after one load cycling event with and without load dwell time and 10 hours later. The load cycling happens when the creep time is 30 hours

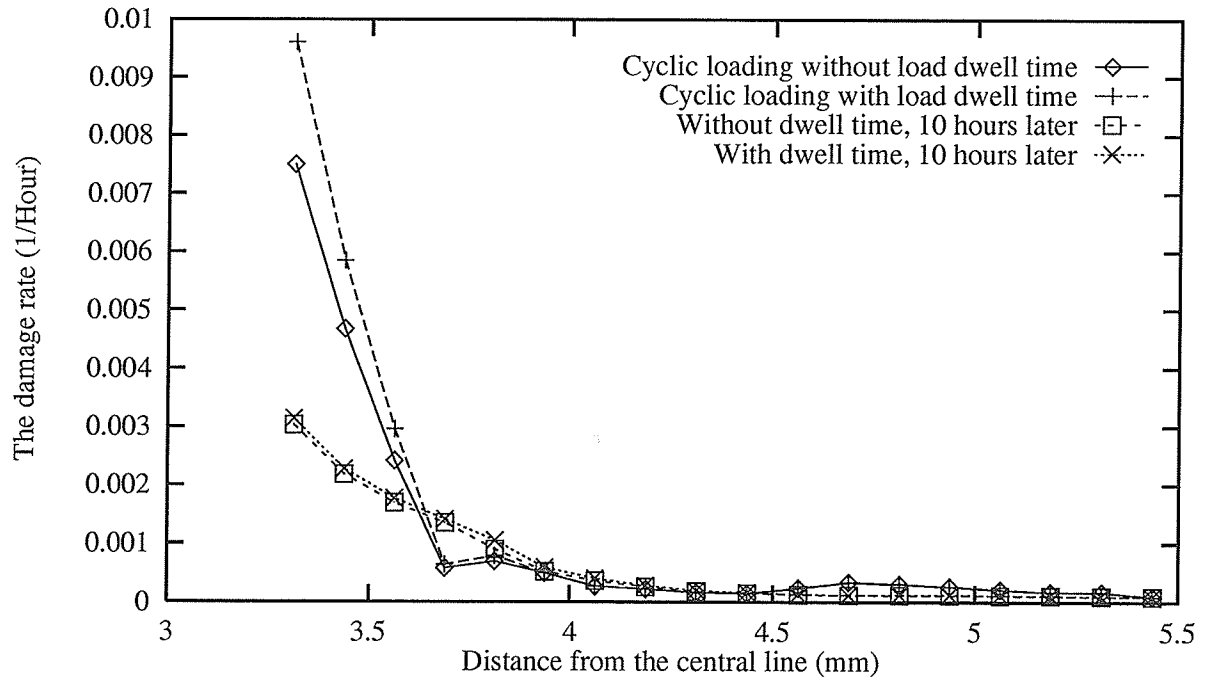

Figure O.8: Comparison of the distributions of the damage rate in the crack tip area after one load cycling event with and without load dwell time and 10 hours later. The load cycling happens when the creep time is 30 hours

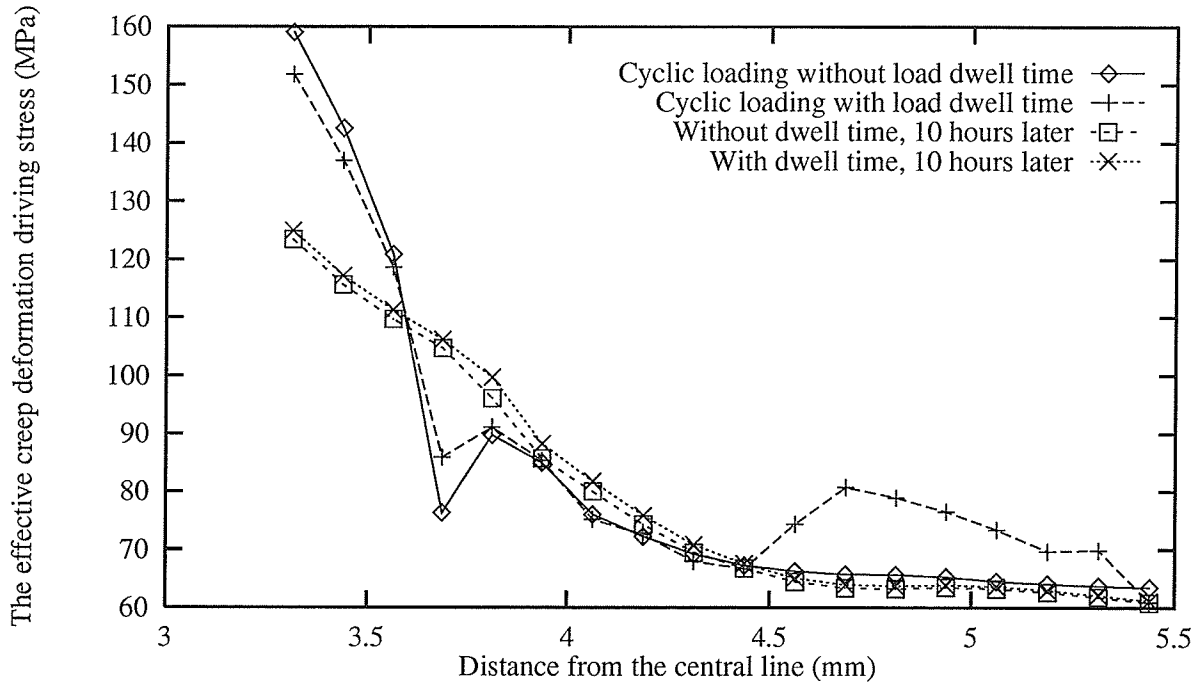

Figure O.9: Comparison of the distributions of the effective creep deformation driving stress $\frac{\tilde{\sigma}-\bar{R}}{1-c_o D}$ in the crack tip area after one load cycling event with and without load dwell time and 10 hours later. The load cycling happens when the creep time is 30 hours

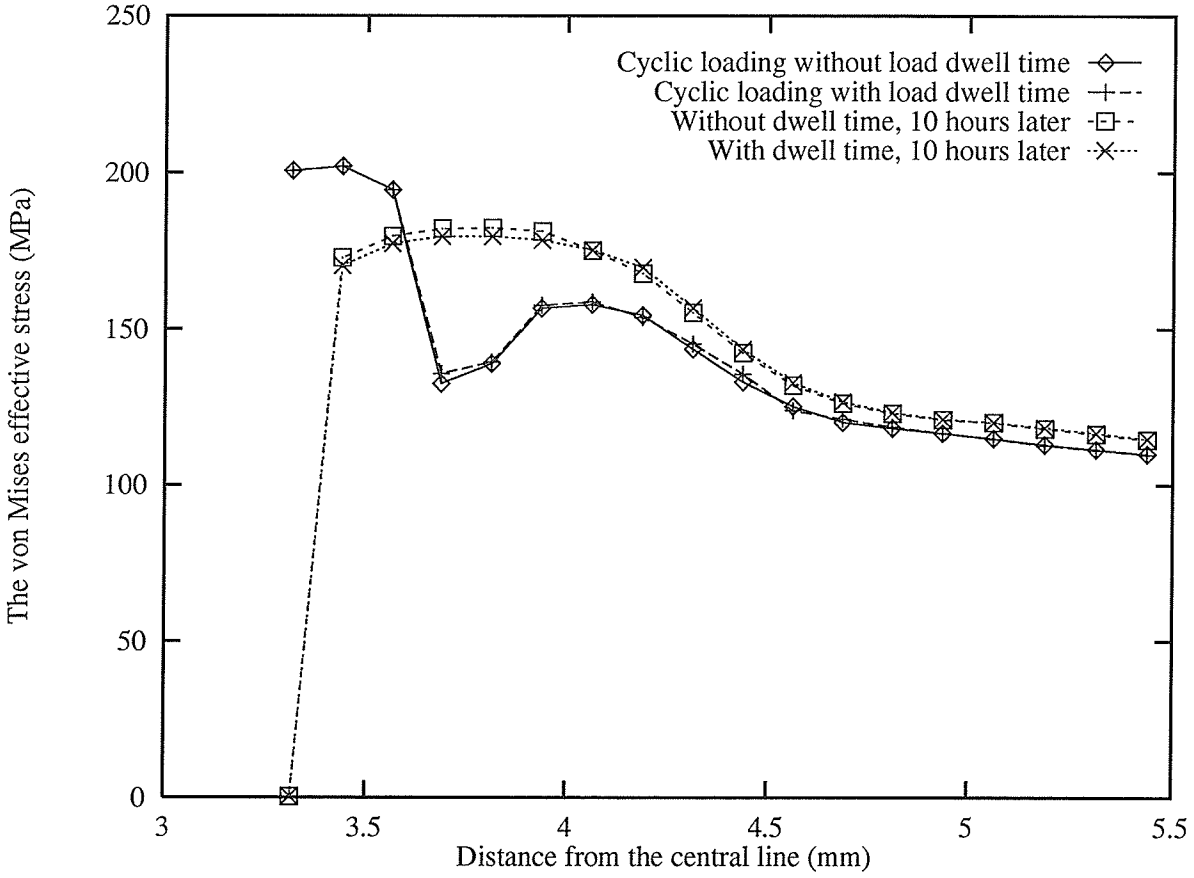

Figure O.10: Comparison of the distributions of the von Mises effective stress in the crack tip area after one load cycling event with and without load dwell time and 10 hours later. The load cycling happens when the creep time is 150 hours

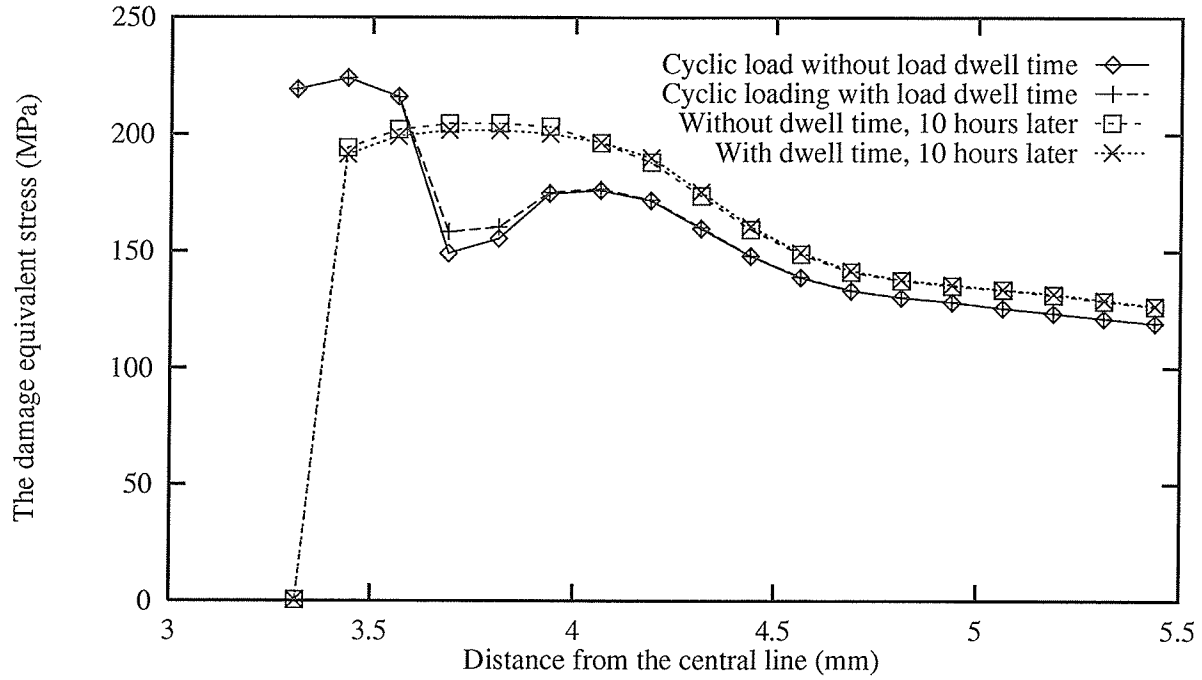

Figure O.11: Comparison of the distributions of the damage equivalent stress in the crack tip area after one load cycling event with and without load dwell time and 10 hours later. The load cycling happens when the creep time is 150 hours

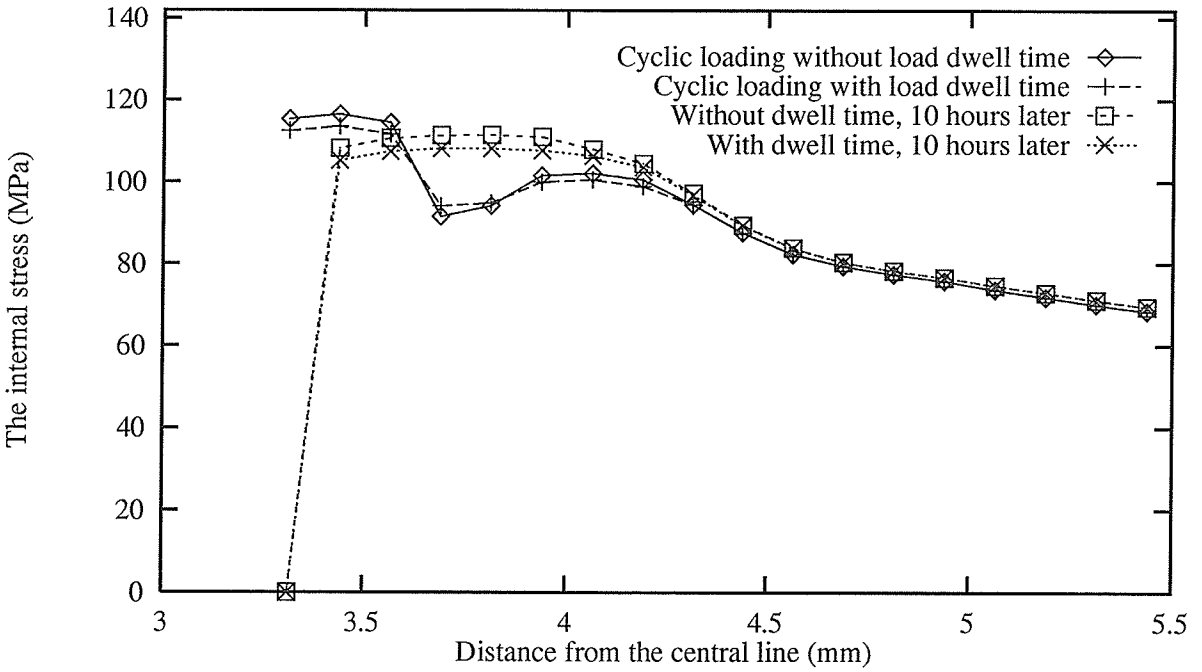

Figure O.12: Comparison of the distributions of the internal stress in the crack tip area after one load cycling event with and without load dwell time and 10 hours later. The load cycling happens when the creep time is 150 hours

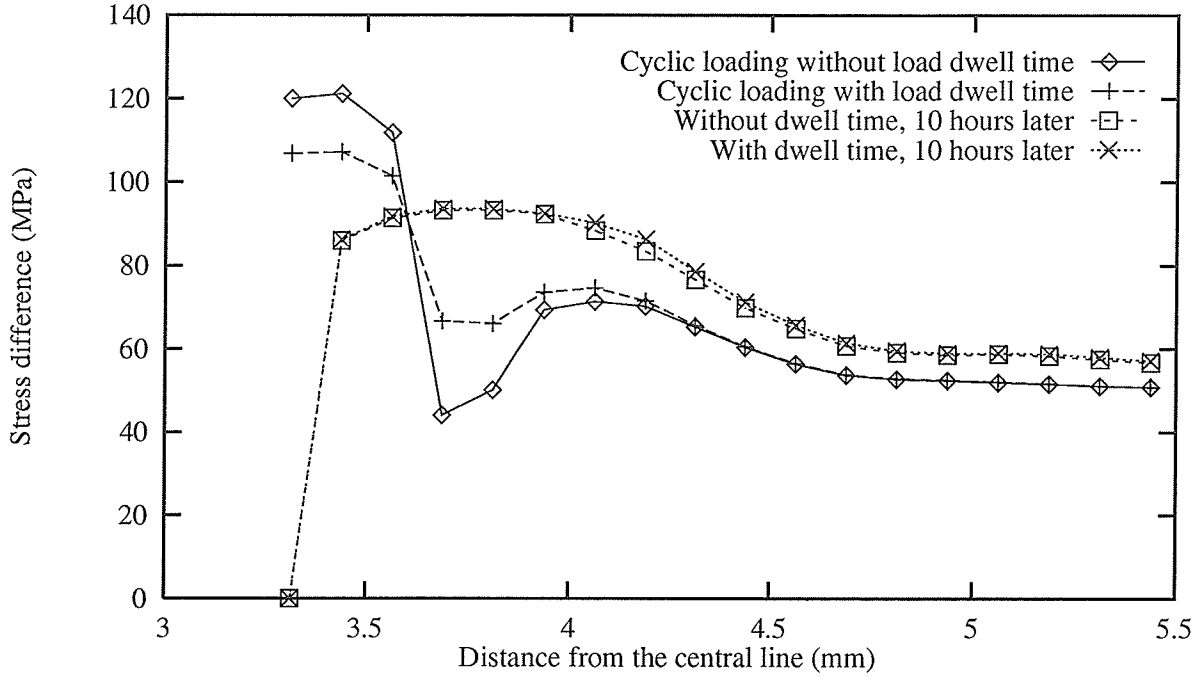

Figure O.13: Comparison of the distributions of the difference between the damage equivalent stress and the internal stress $(\tilde{\sigma} - \bar{R})$ in the crack tip area after one load cycling event with and without load dwell time and 10 hours later. The load cycling happens when the creep time is 150 hours

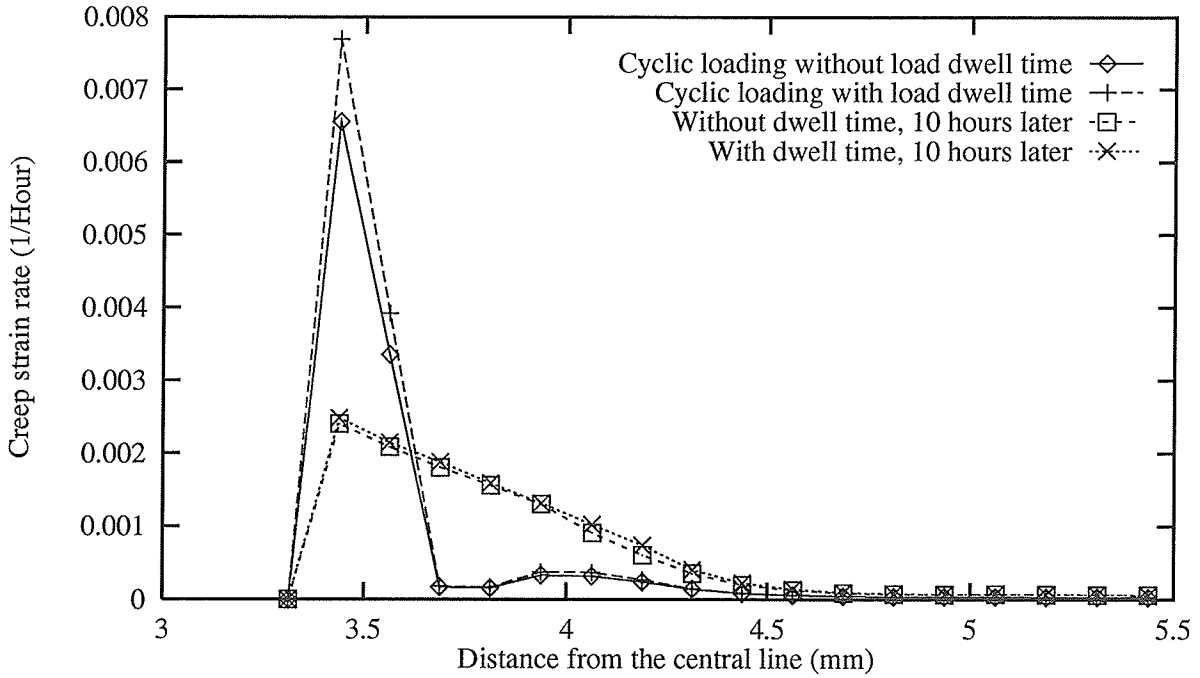

Figure O.14: Comparison of the distributions of the creep strain rate in the crack tip area after one load cycling event with and without load dwell time and 10 hours later. The load cycling happens when the creep time is 150 hours

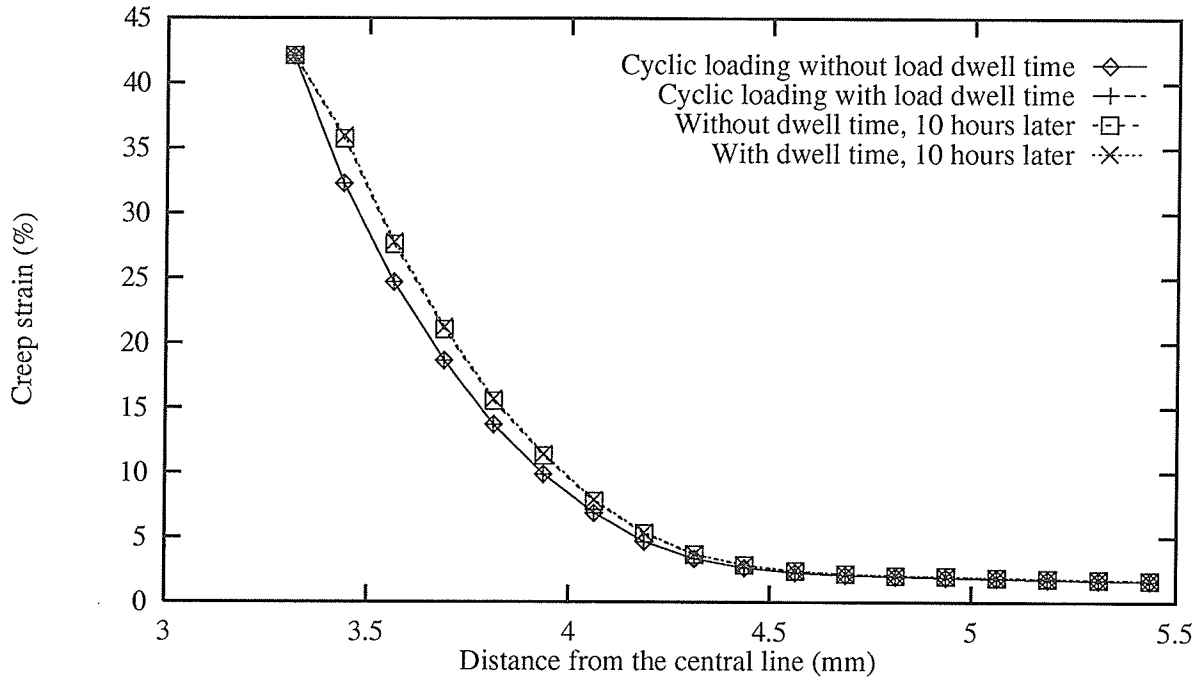

Figure O.15: Comparison of the distributions of the creep strain in the crack tip area after one load cycling event with and without load dwell time and 10 hours later. The load cycling happens when the creep time is 150 hours

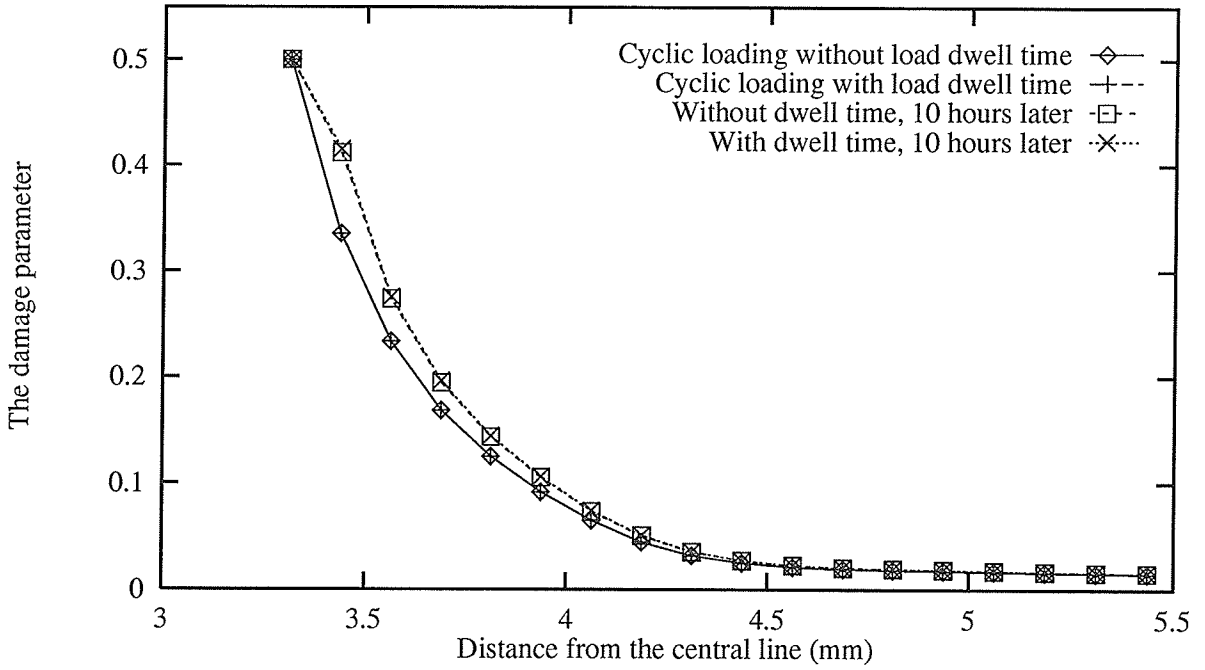

Figure O.16: Comparison of the distributions of the damage in the crack tip area after one load cycling event with and without load dwell time and 10 hours later. The load cycling happens when the creep time is 150 hours

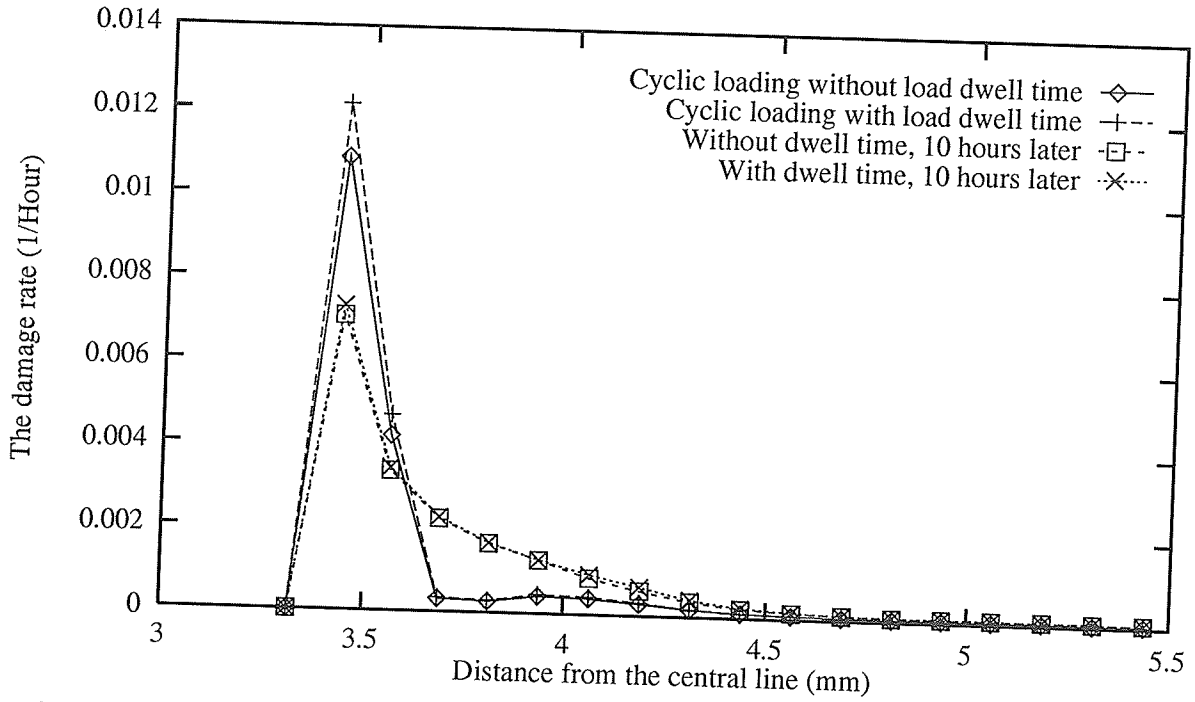

Figure O.17: Comparison of the distributions of the damage rate in the crack tip area after one load cycling event with and without load dwell time and 10 hours later. The load cycling happens when the creep time is 150 hours

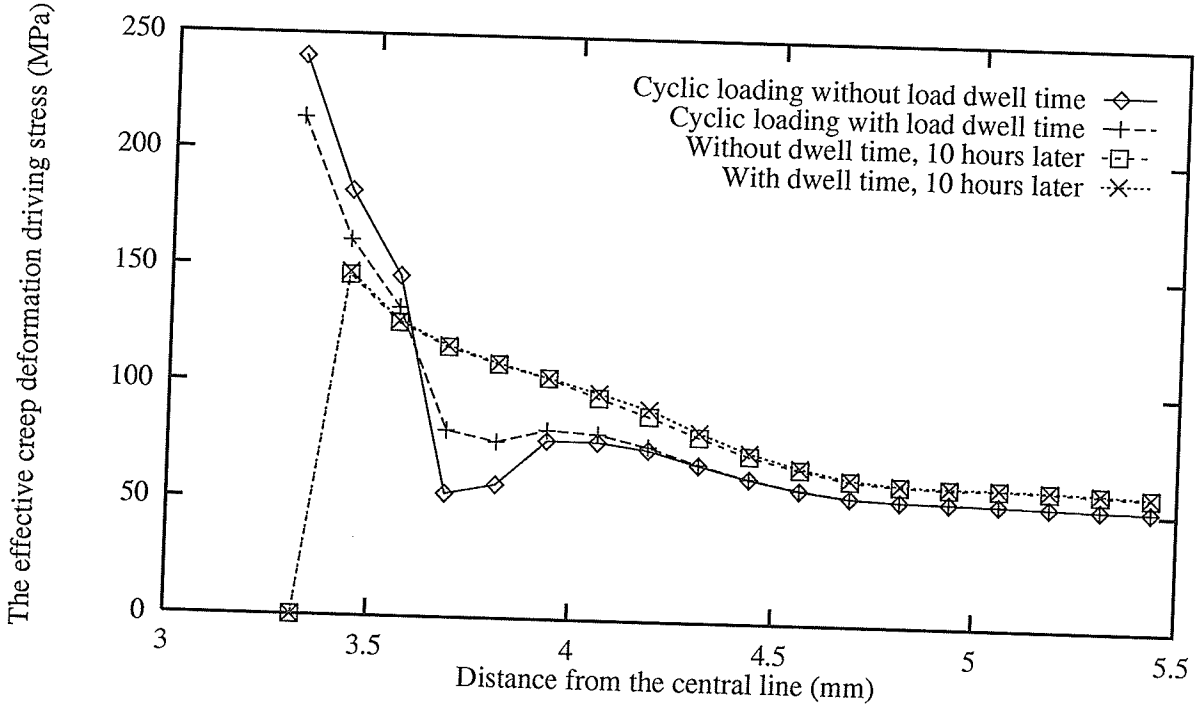

Figure O.18: Comparison of the distributions of the effective creep deformation driving stress $\frac{\tilde{\sigma}-\bar{R}}{1-c_o D}$ in the crack tip area after one load cycling event with and without load dwell time and 10 hours later. The load cycling happens when the creep time is 150 hours

Appendix P

Effect of interaction between creep/HTLCF damage on distribution of crack tip variables

This appendix contains the figures which show the importance of the interaction between creep damage and HTLCF damage on creep response of the central cracked panel.

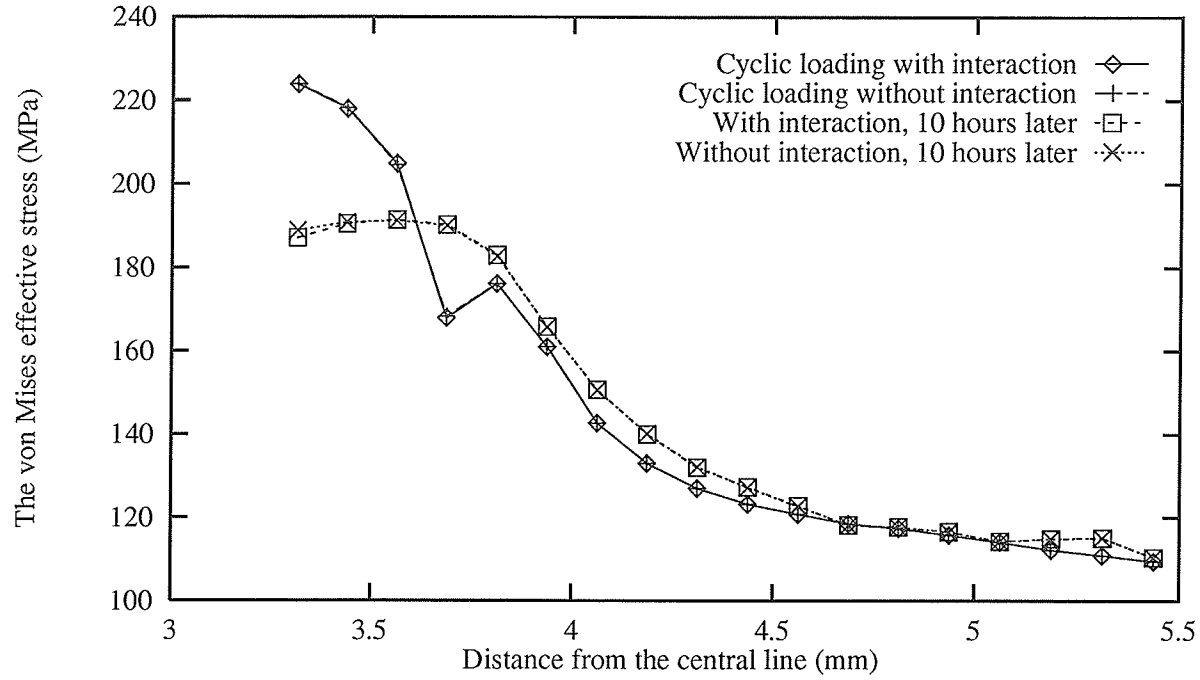

Figure P.1: Comparison of the distributions of the von Mises effective stress in the crack tip area after one load cycling event and 10 hours later with and without consideration of the interaction between creep damage and the HTLCF damage. The load cycling happens when the creep time is 30 hours

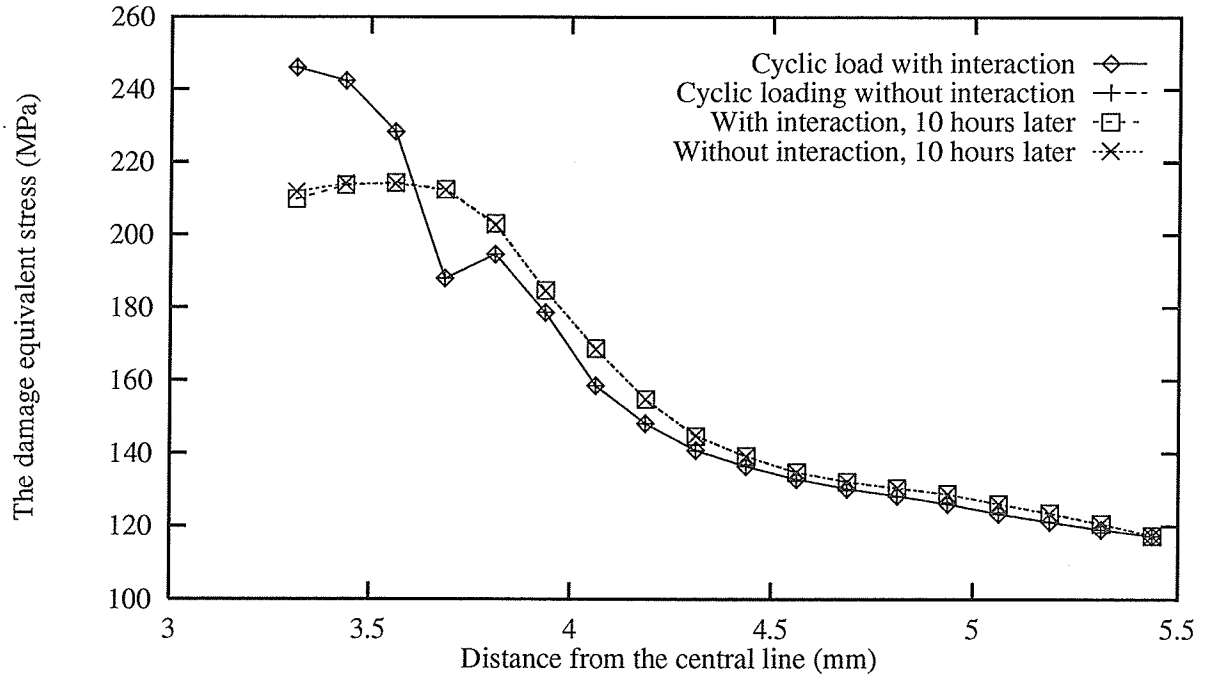

Figure P.2: Comparison of the distributions of the damage equivalent stress in the crack tip area after one load cycling event and 10 hours later with and without consideration of the interaction between creep damage and the HTLCF damage. The load cycling happens when the creep time is 30 hours

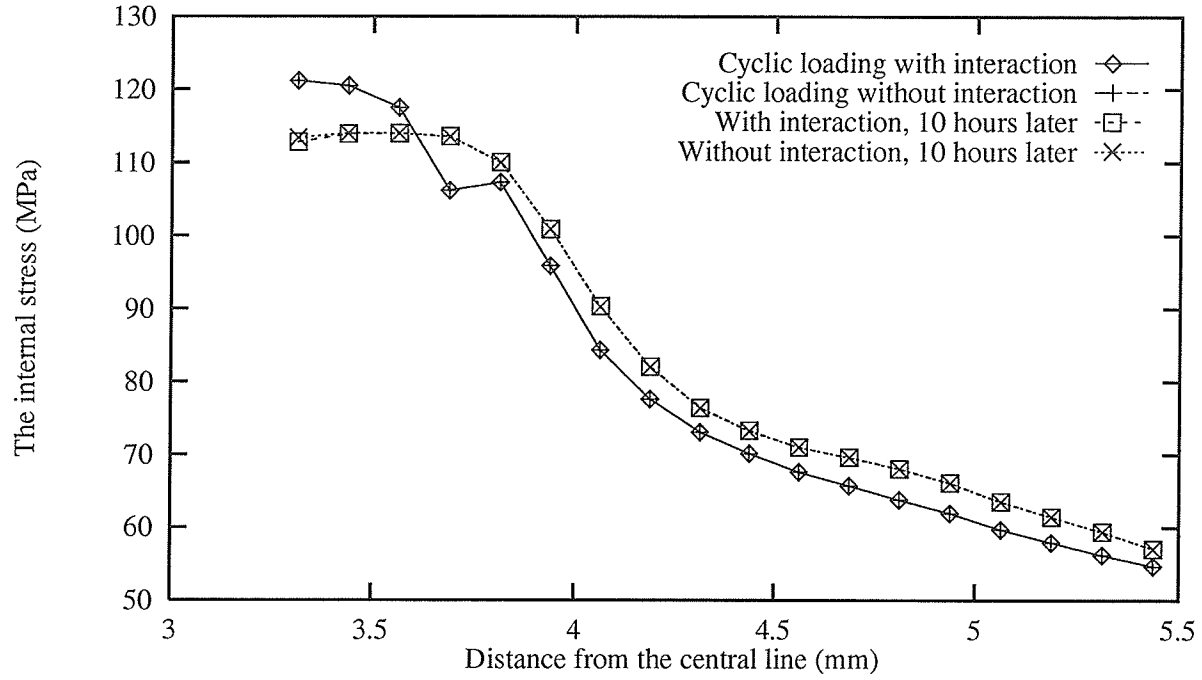

Figure P.3: Comparison of the distributions of the internal stress in the crack tip area after one load cycling event and 10 hours later with and without consideration of the interaction between creep damage and the HTLCF damage. The load cycling happens when the creep time is 30 hours

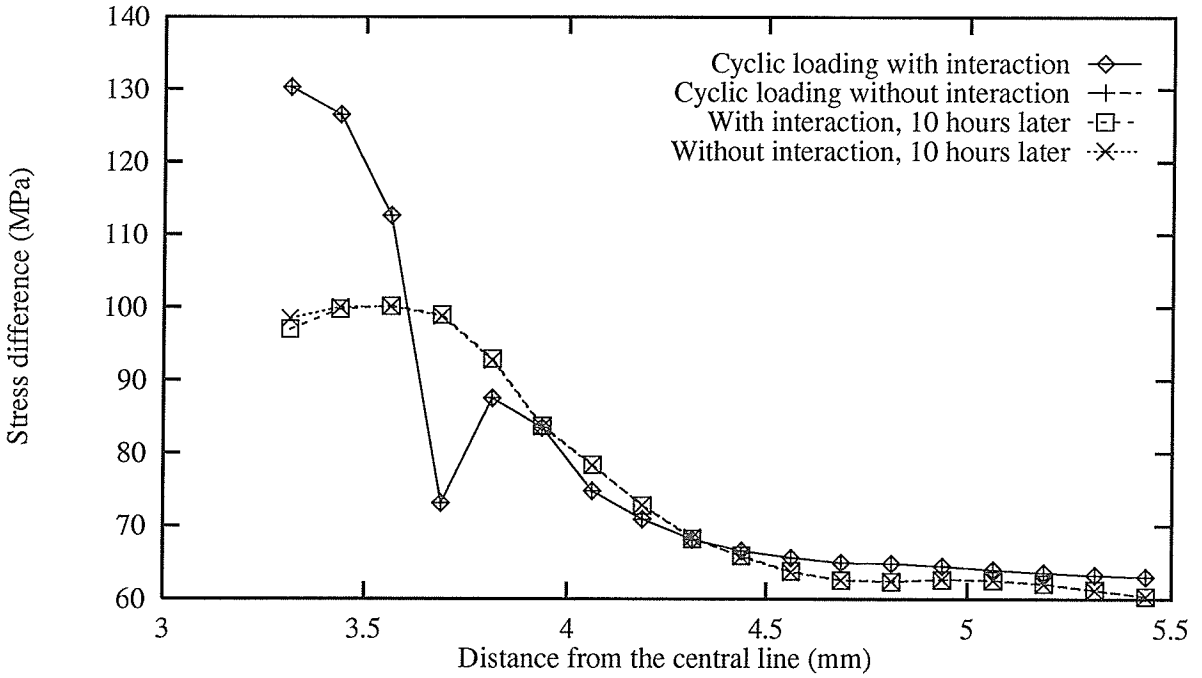

Figure P.4: Comparison of the distributions of the difference between the damage equivalent stress and the internal stress $(\tilde{\sigma} - \bar{R})$ in the crack tip area after one load cycling event and 10 hours later with and without consideration of the interaction between creep damage and the HTLCF damage. The load cycling happens when the creep time is 30 hours

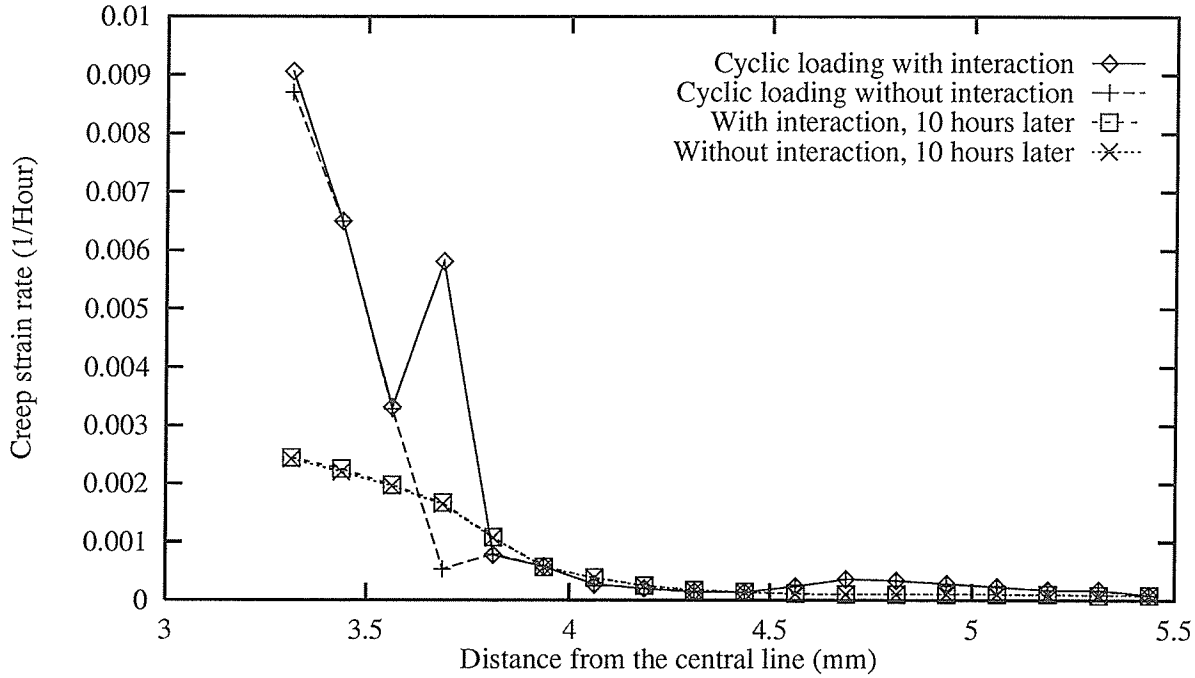

Figure P.5: Comparison of the distributions of the creep strain rate in the crack tip area after one load cycling event and 10 hours later with and without consideration of the interaction between creep damage and the HTLCF damage. The load cycling happens when the creep time is 30 hours

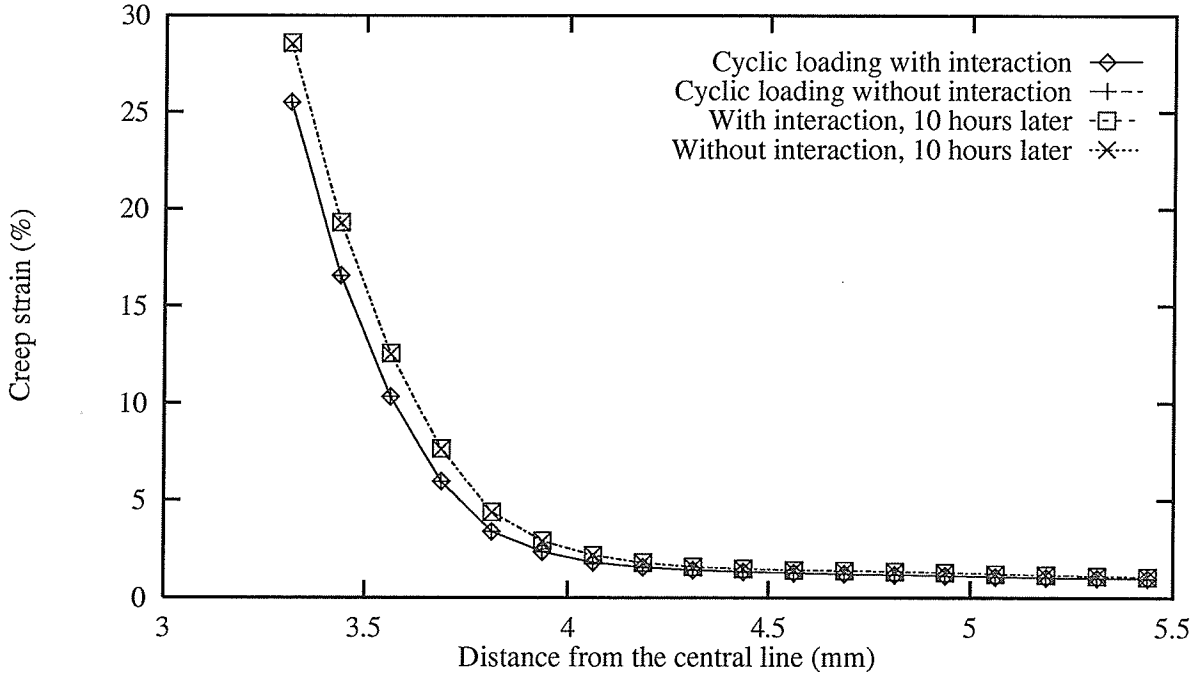

Figure P.6: Comparison of the distributions of the creep strain in the crack tip area after one load cycling event and 10 hours later with and without consideration of the interaction between creep damage and the HTLCF damage. The load cycling happens when the creep time is 30 hours

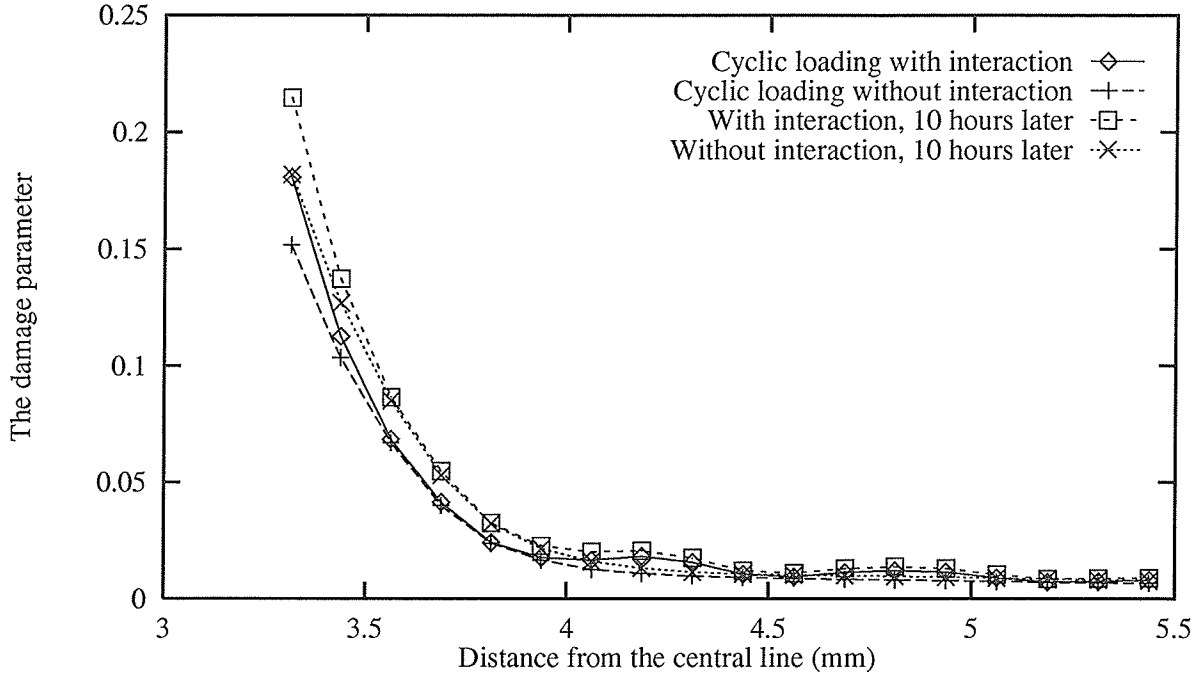

Figure P.7: Comparison of the distributions of the damage in the crack tip area after one load cycling event and 10 hours later with and without consideration of the interaction between creep damage and the HTLCF damage. The load cycling happens when the creep time is 30 hours

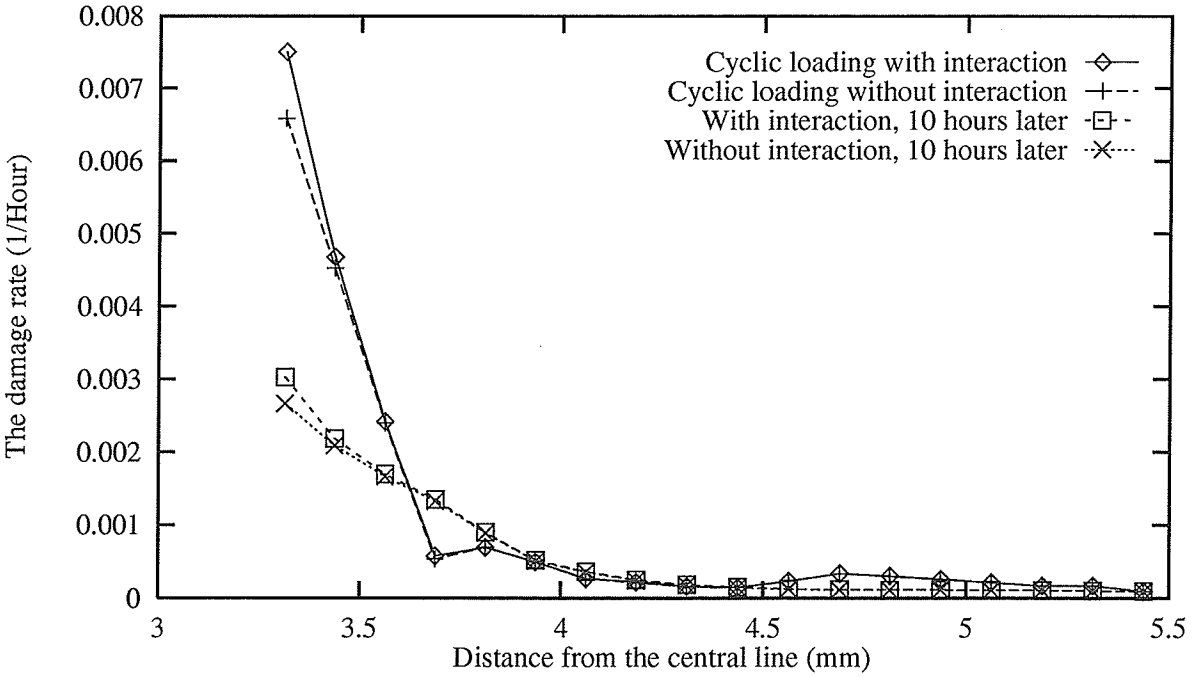

Figure P.8: Comparison of the distributions of the damage rate in the crack tip area after one load cycling event and 10 hours later with and without consideration of the interaction between creep damage and the HTLCF damage. The load cycling happens when the creep time is 30 hours

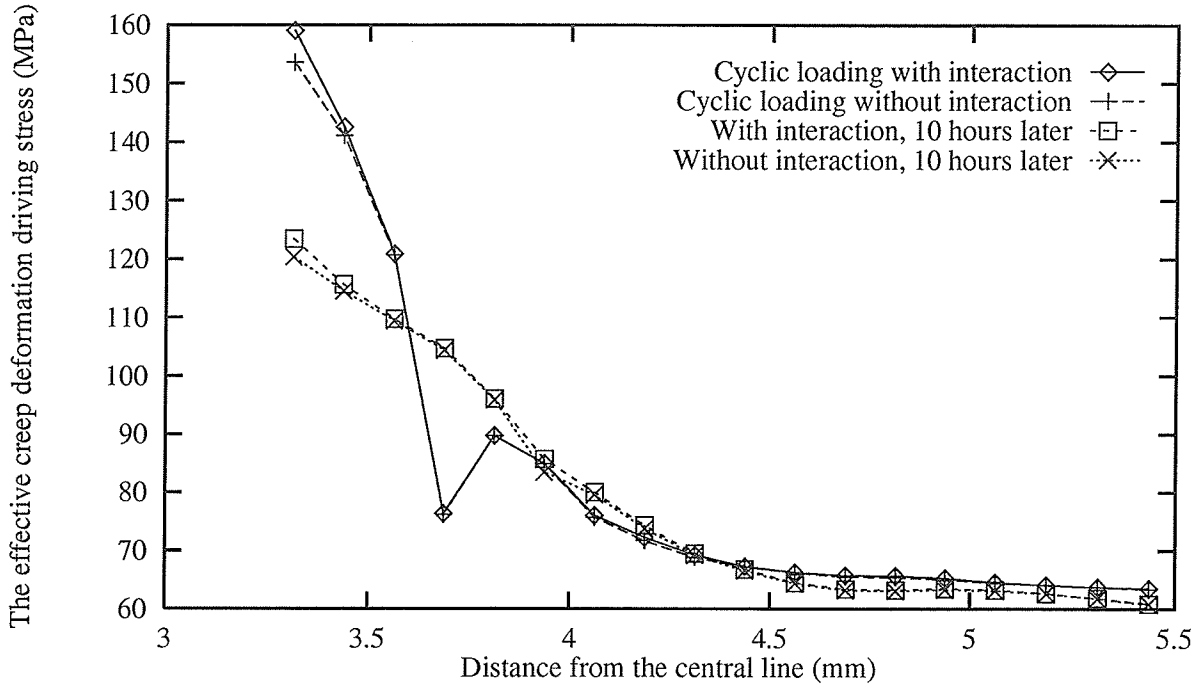

Figure P.9: Comparison of the distributions of the effective creep deformation driving stress $\frac{\tilde{\sigma}-\bar{R}}{1-c_o D}$ in the crack tip area after one load cycling event and 10 hours later with and without consideration of the interaction between creep damage and the HTLCF damage. The load cycling happens when the creep time is 30 hours

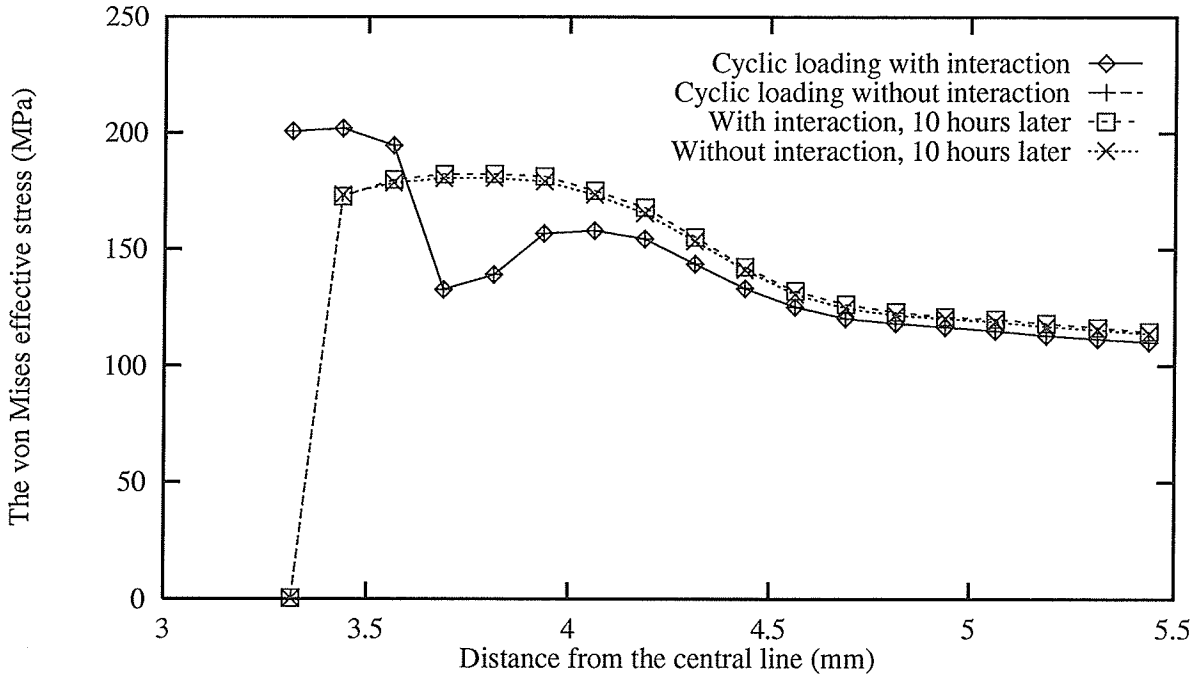

Figure P.10: Comparison of the distributions of the von Mises effective stress in the crack tip area after one load cycling event and 10 hours later with and without consideration of the interaction between creep damage and the HTLCF damage. The load cycling happens when the creep time is 150 hours

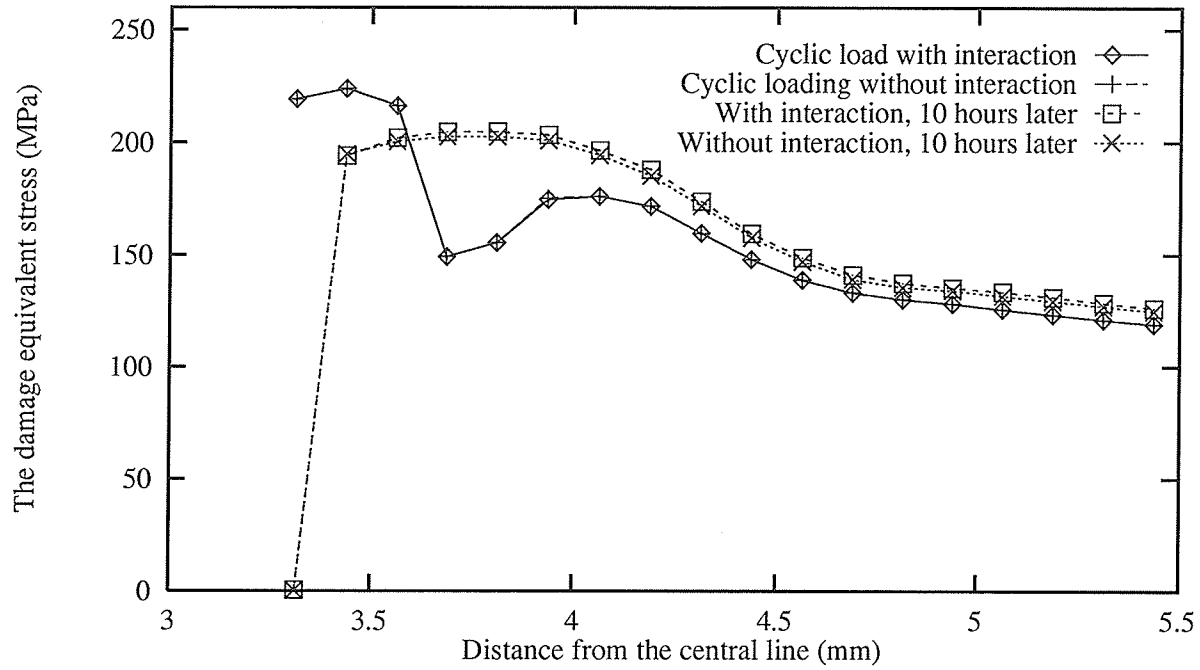

Figure P.11: Comparison of the distributions of the damage equivalent stress in the crack tip area after one load cycling event and 10 hours later with and without consideration of the interaction between creep damage and the HTLCF damage. The load cycling happens when the creep time is 150 hours

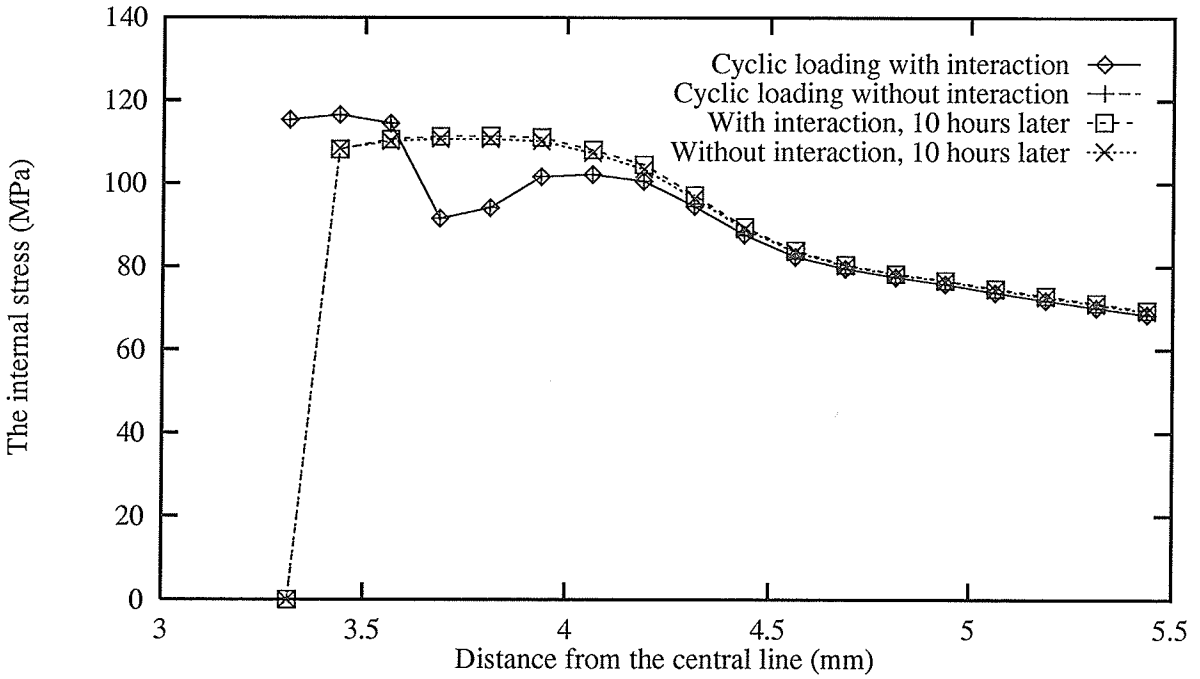

Figure P.12: Comparison of the distributions of the internal stress in the crack tip area after one load cycling event and 10 hours later with and without consideration of the interaction between creep damage and the HTLCF damage. The load cycling happens when the creep time is 150 hours

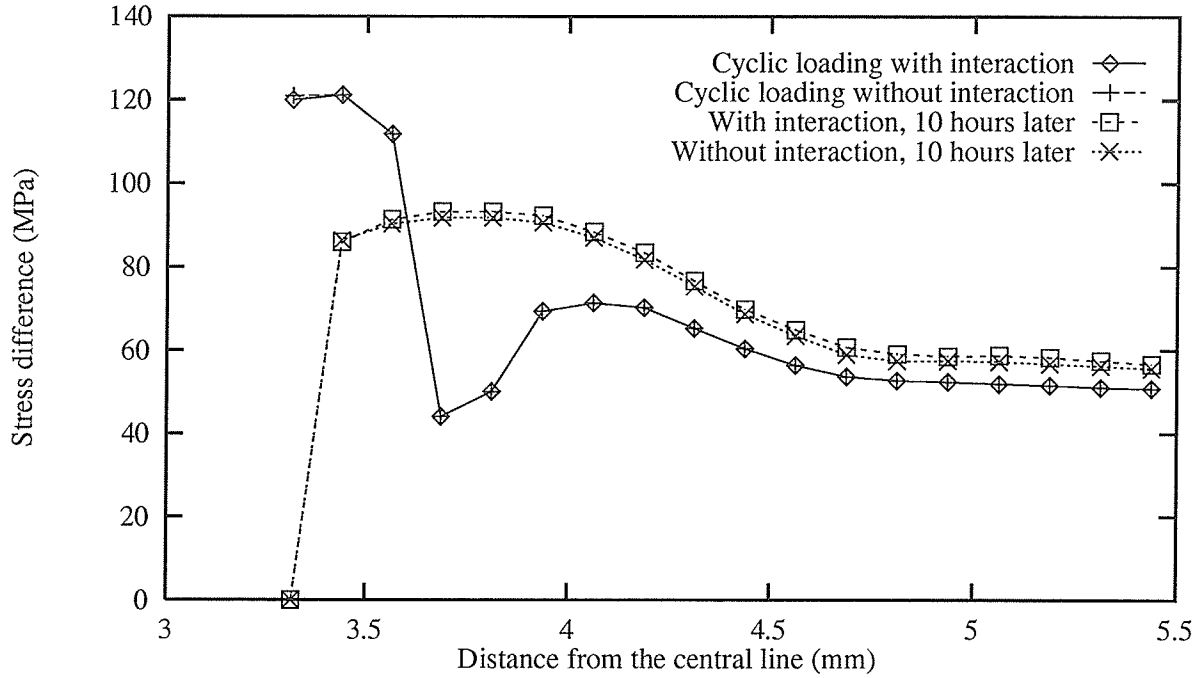

Figure P.13: Comparison of the distributions of the difference between the damage equivalent stress and the internal stress $(\tilde{\sigma} - \bar{R})$ in the crack tip area after one load cycling event and 10 hours later with and without consideration of the interaction between creep damage and the HTLCF damage. The load cycling happens when the creep time is 150 hours

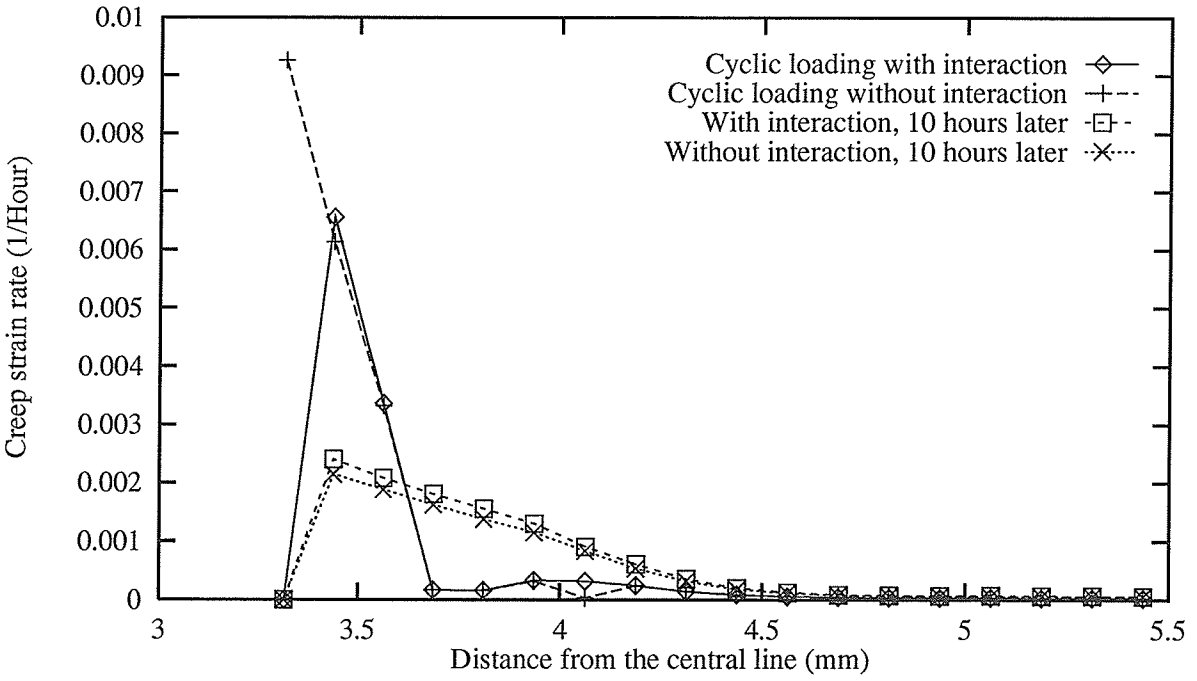

Figure P.14: Comparison of the distributions of the creep strain rate in the crack tip area after one load cycling event and 10 hours later with and without consideration of the interaction between creep damage and the HTLCF damage. The load cycling happens when the creep time is 150 hours

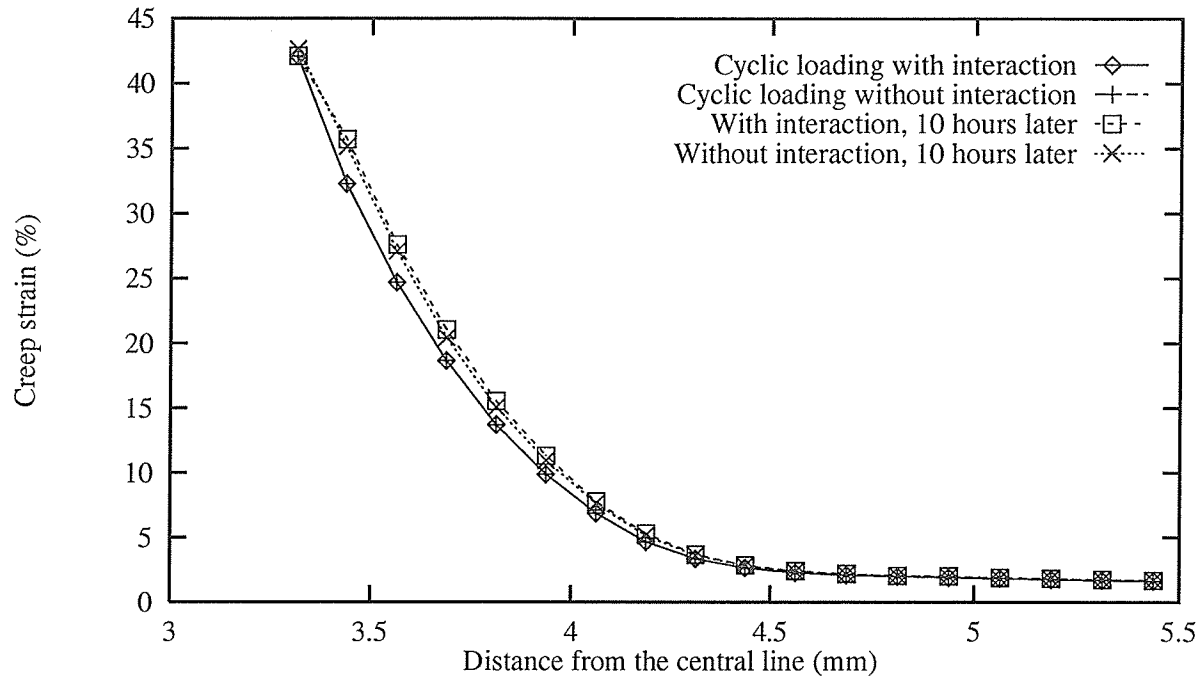

Figure P.15: Comparison of the distributions of the creep strain in the crack tip area after one load cycling event and 10 hours later with and without consideration of the interaction between creep damage and the HTLCF damage. The load cycling happens when the creep time is 150 hours

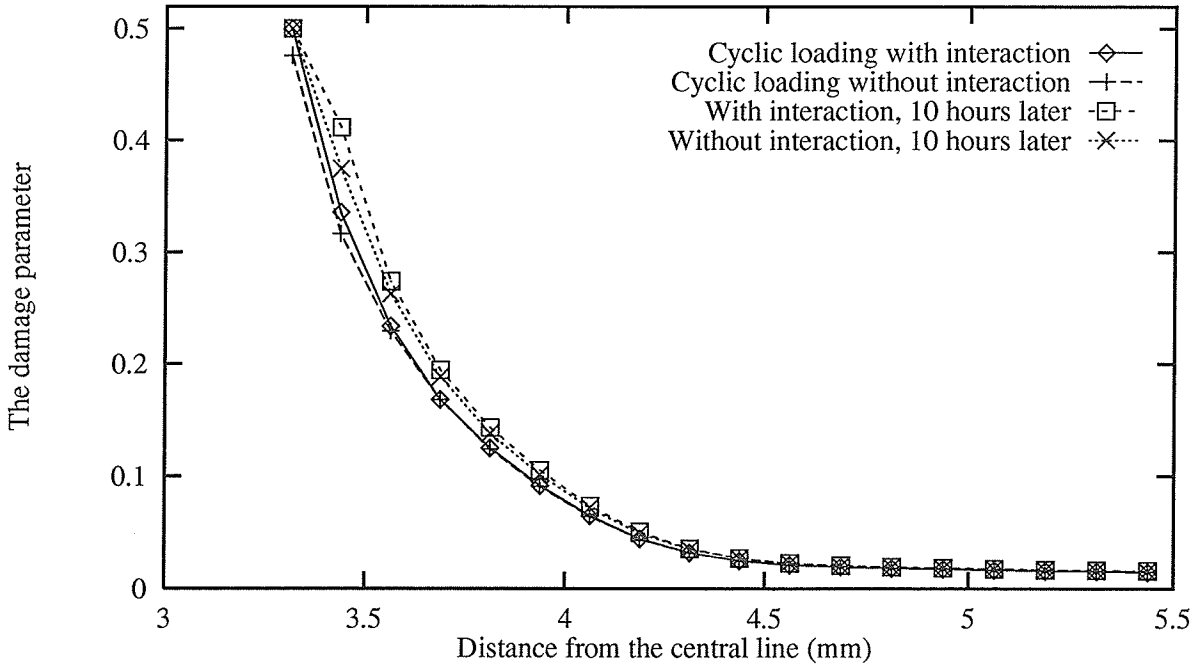

Figure P.16: Comparison of the distributions of the damage in the crack tip area after one load cycling event and 10 hours later with and without consideration of the interaction between creep damage and the HTLCF damage. The load cycling happens when the creep time is 150 hours

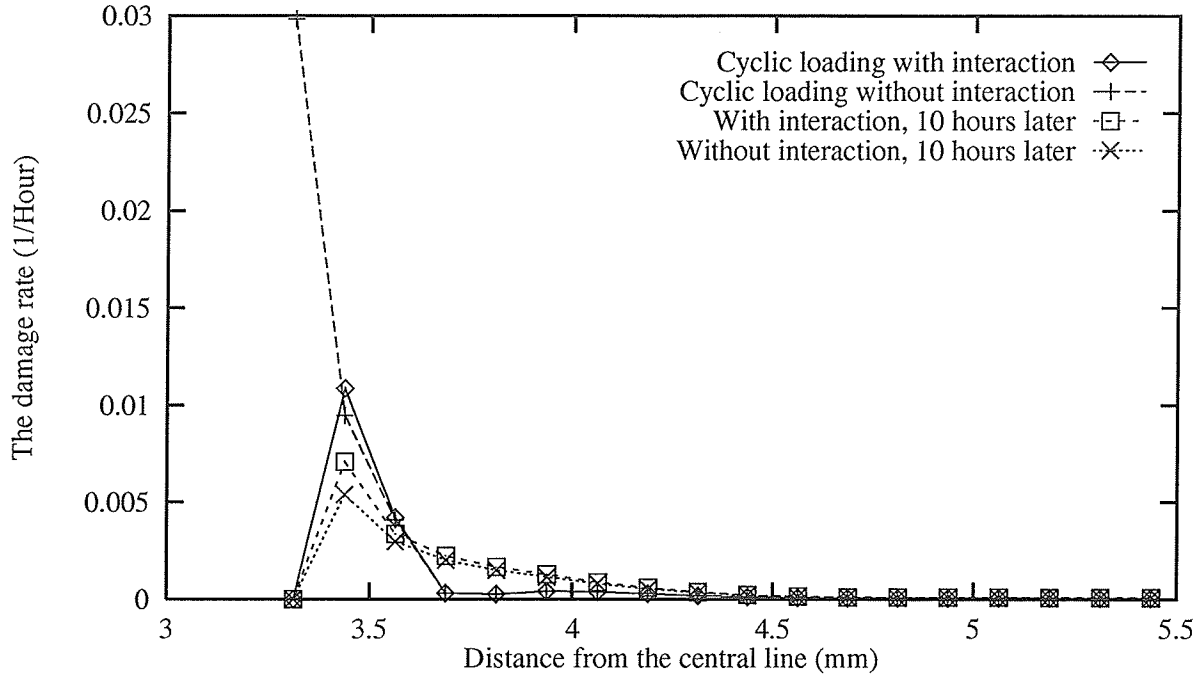

Figure P.17: Comparison of the distributions of the damage rate in the crack tip area after one load cycling event and 10 hours later with and without consideration of the interaction between creep damage and the HTLCF damage. The load cycling happens when the creep time is 150 hours

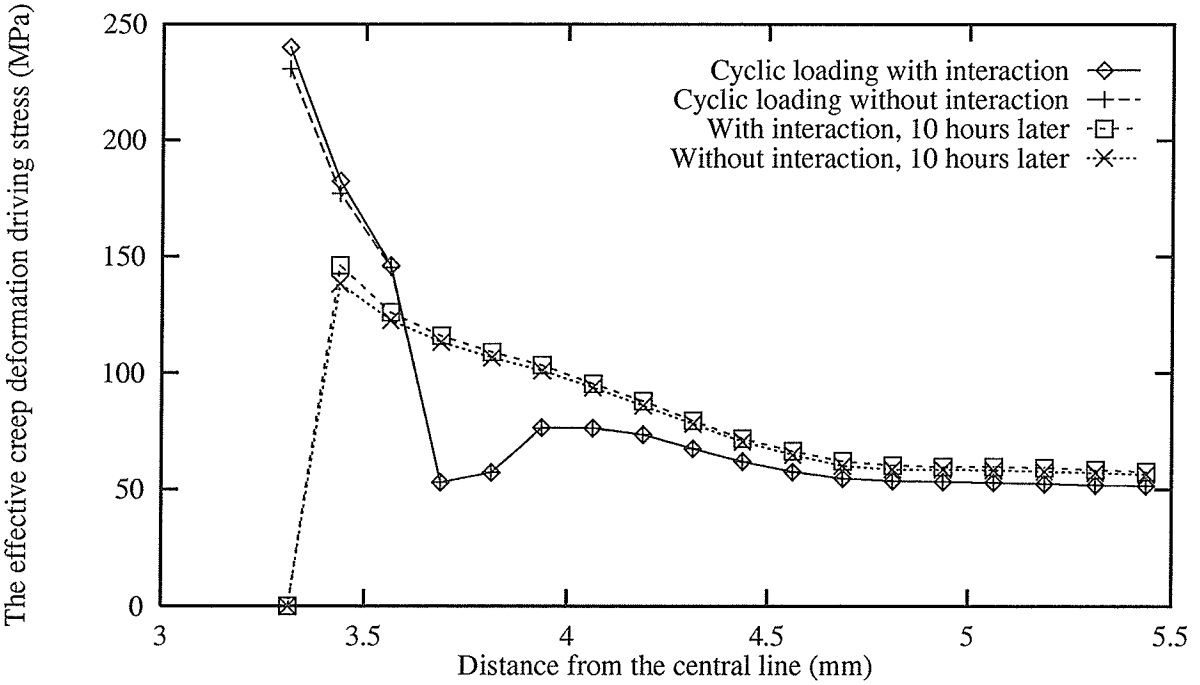

Figure P.18: Comparison of the distributions of the effective creep deformation driving stress $\frac{\tilde{\sigma}-\tilde{R}}{1-c_o D}$ in the crack tip area after one load cycling event and 10 hours later with and without consideration of the interaction between creep damage and the HTLCF damage. The load cycling happens when the creep time is 150 hours

Appendix Q

Distribution of the crack tip variables before the first element is broken

This appendix contains the figures which show the distribution of the crack tip variables immediately before the first element is broken. Curves corresponding to different loading histories are plotted together for comparison.

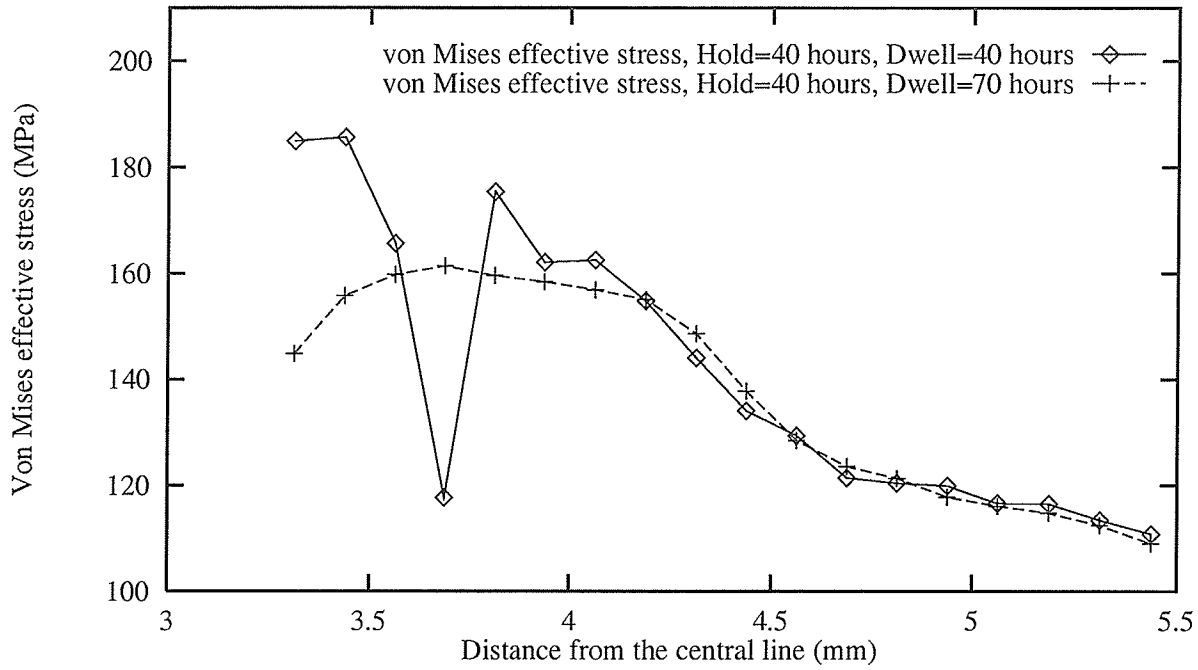

Figure Q.1: Distributions of the von Mises effective stress in the crack tip area just before the first element is broken. The loading is cyclic with 40 hours of holding time and 40 and 70 hours of dwell time

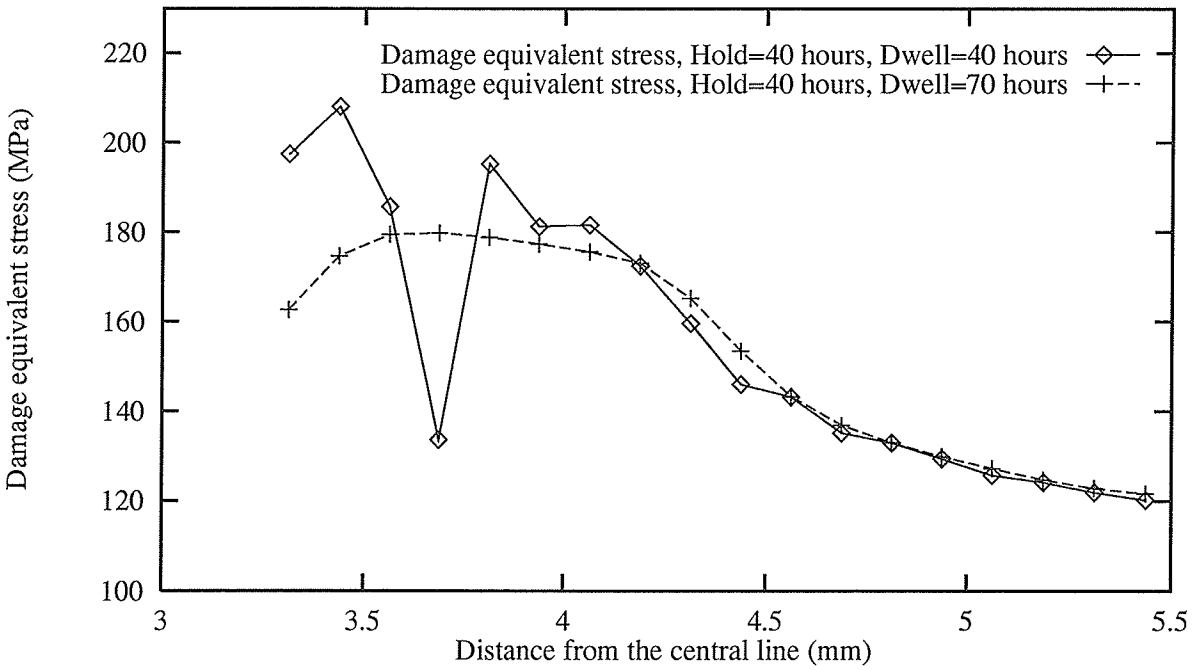

Figure Q.2: Distributions of the damage equivalent stress in the crack tip area just before the first element is broken. The loading is cyclic with 40 hours of holding time and 40 and 70 hours of dwell time

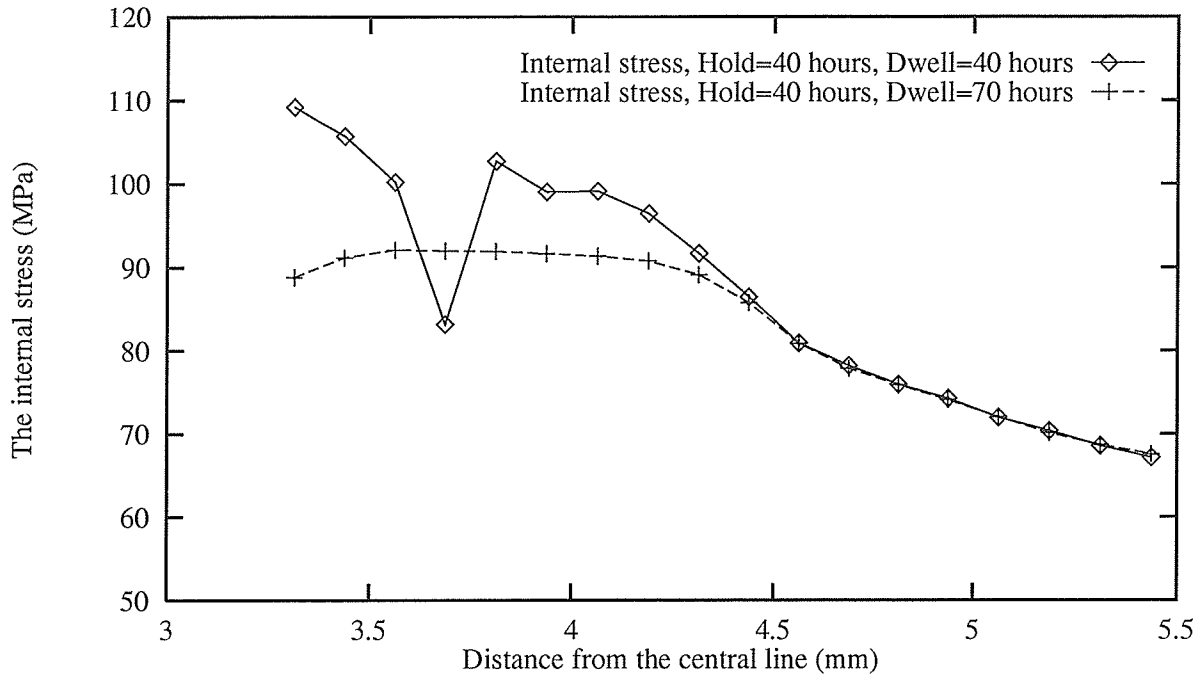

Figure Q.3: Distributions of the internal stress in the crack tip area just before the first element is broken. The loading is cyclic with 40 hours of holding time and 40 and 70 hours of dwell time

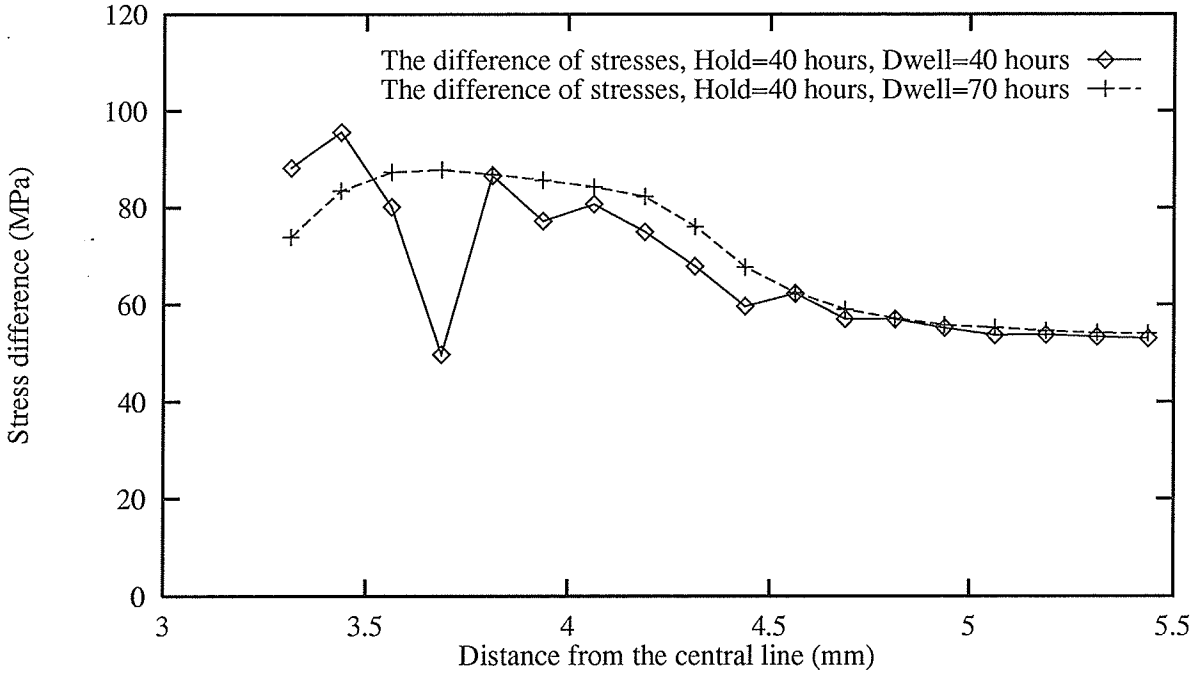

Figure Q.4: Distributions of the difference between the damage equivalent stress and the internal stress ($\tilde{\sigma} - \bar{R}$) in the crack tip area just before the first element is broken. The loading is cyclic with 40 hours of holding time and 40 and 70 hours of dwell time

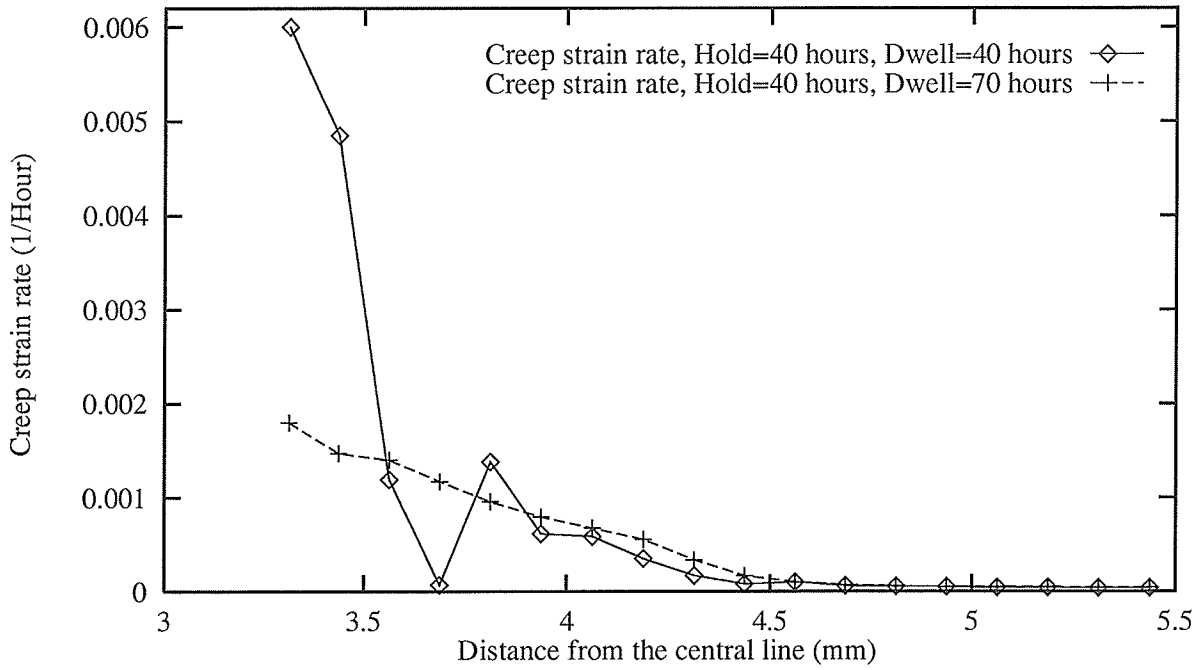

Figure Q.5: Distributions of the creep strain rate in the crack tip area just before the first element is broken. The loading is cyclic with 40 hours of holding time and 40 and 70 hours of dwell time

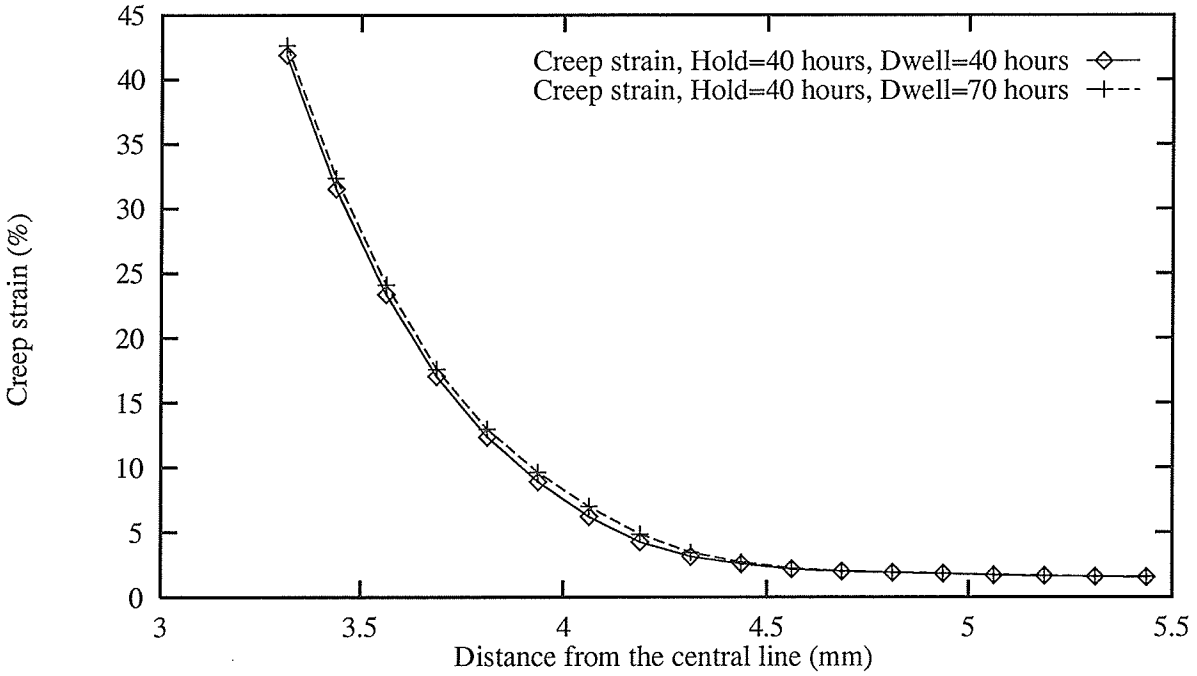

Figure Q.6: Distributions of the creep strain in the crack tip area just before the first element is broken. The loading is cyclic with 40 hours of holding time and 40 and 70 hours of dwell time

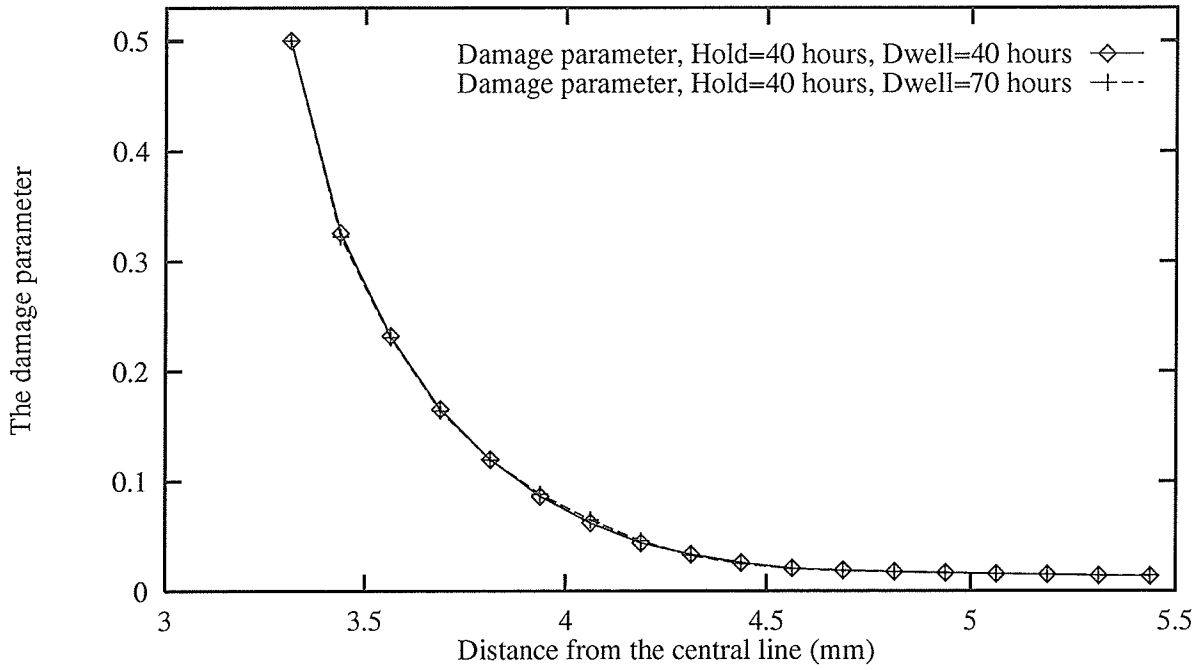

Figure Q.7: Distributions of the damage parameter in the crack tip area just before the first element is broken. The loading is cyclic with 40 hours of holding time and 40 and 70 hours of dwell time

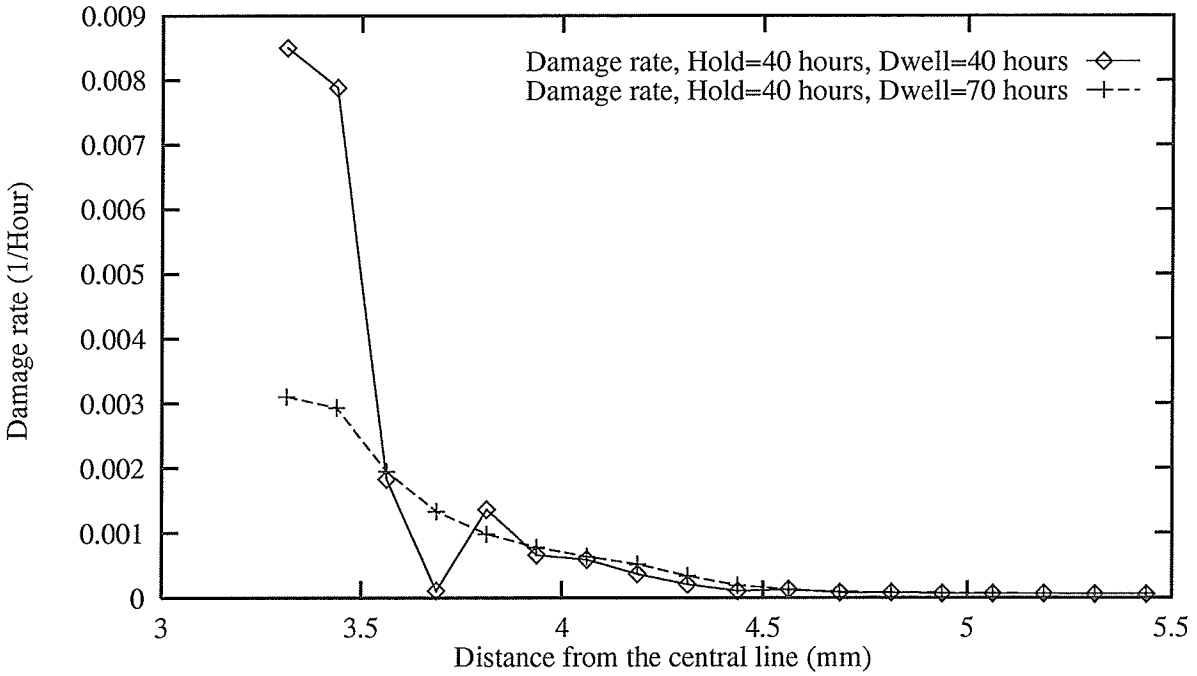

Figure Q.8: Distributions of the damage rate in the crack tip area just before the first element is broken. The loading is cyclic with 40 hours of holding time and 40 and 70 hours of dwell time

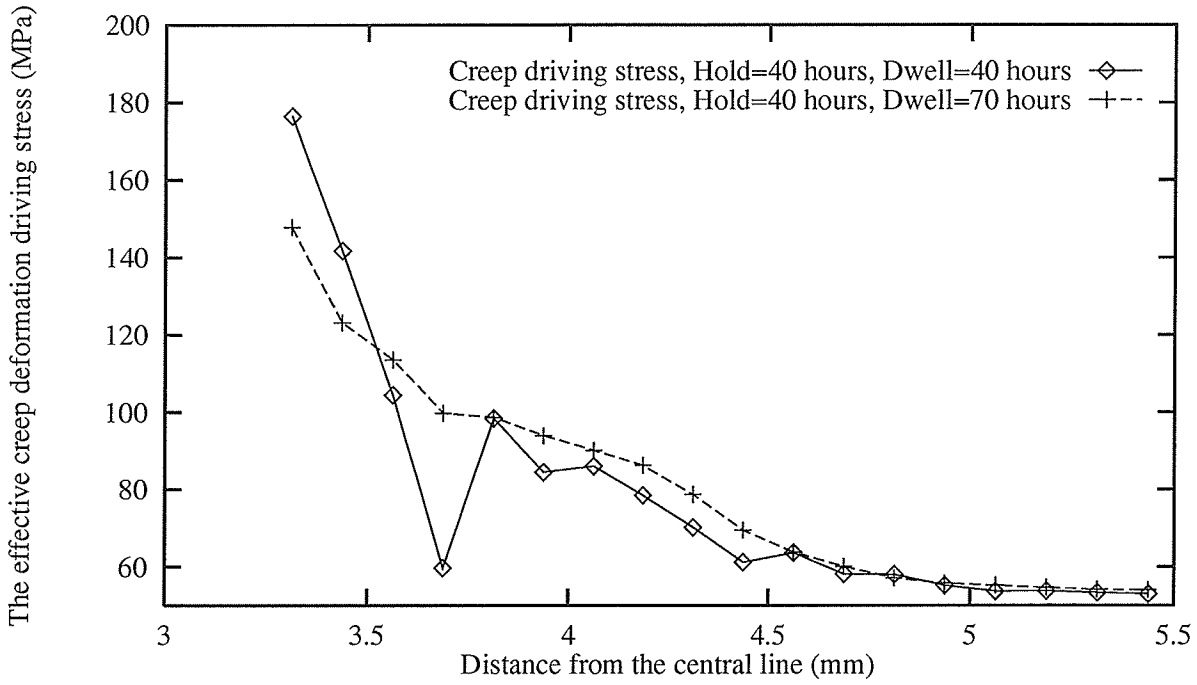

Figure Q.9: Distributions of the effective creep deformation driving stress $\frac{\tilde{\sigma}-\tilde{R}}{1-c_o D}$ in the crack tip area just before the first element is broken. The loading is cyclic with 40 hours of holding time and 40 and 70 hours of dwell time

Appendix R

Distribution of the crack tip variables after the first element is broken

This appendix contains the figures which show the distribution of the crack tip variables just after the first element is broken. Curves corresponding to different loading histories are plotted together for comparison.

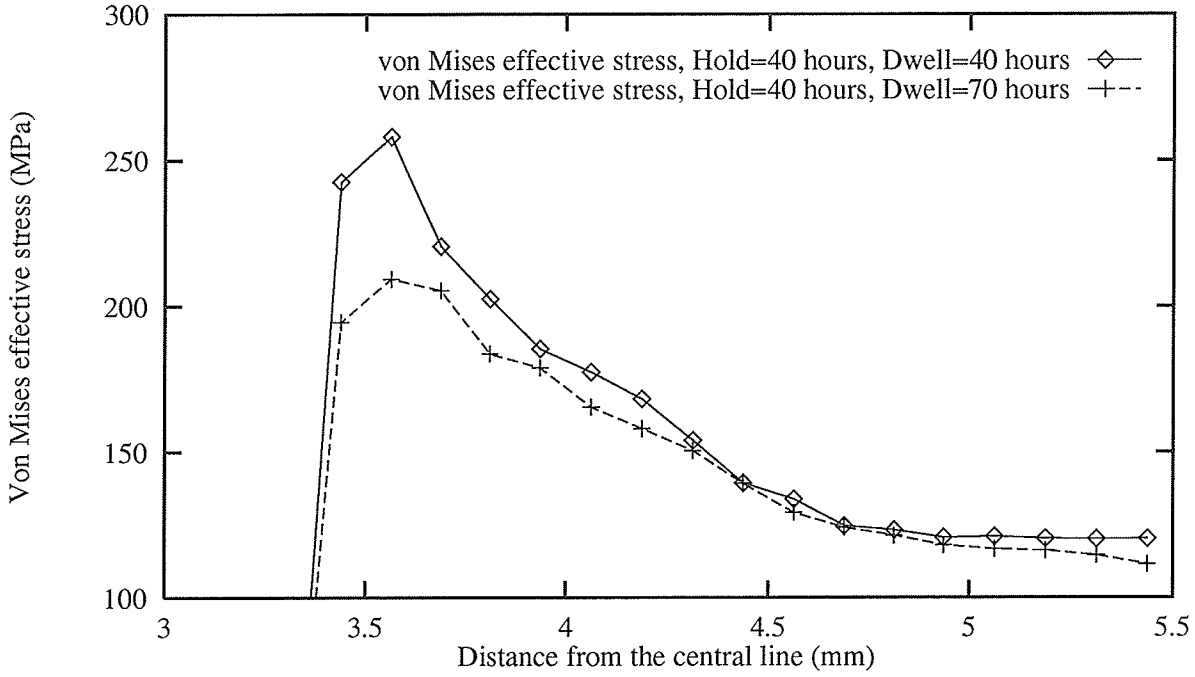

Figure R.1: Distributions of the von Mises effective stress in the crack tip area just after the first element is broken. The loading is cyclic with 40 hours of holding time and 40 and 70 hours of dwell time

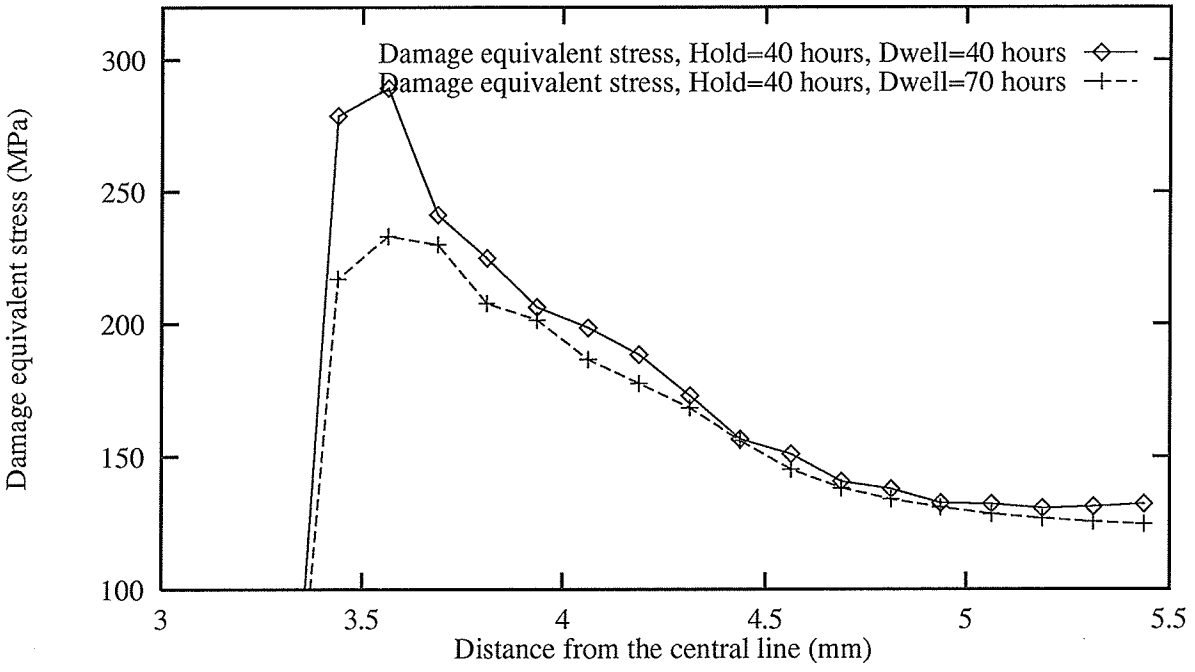

Figure R.2: Distributions of the damage equivalent stress in the crack tip area just after the first element is broken. The loading is cyclic with 40 hours of holding time and 40 and 70 hours of dwell time

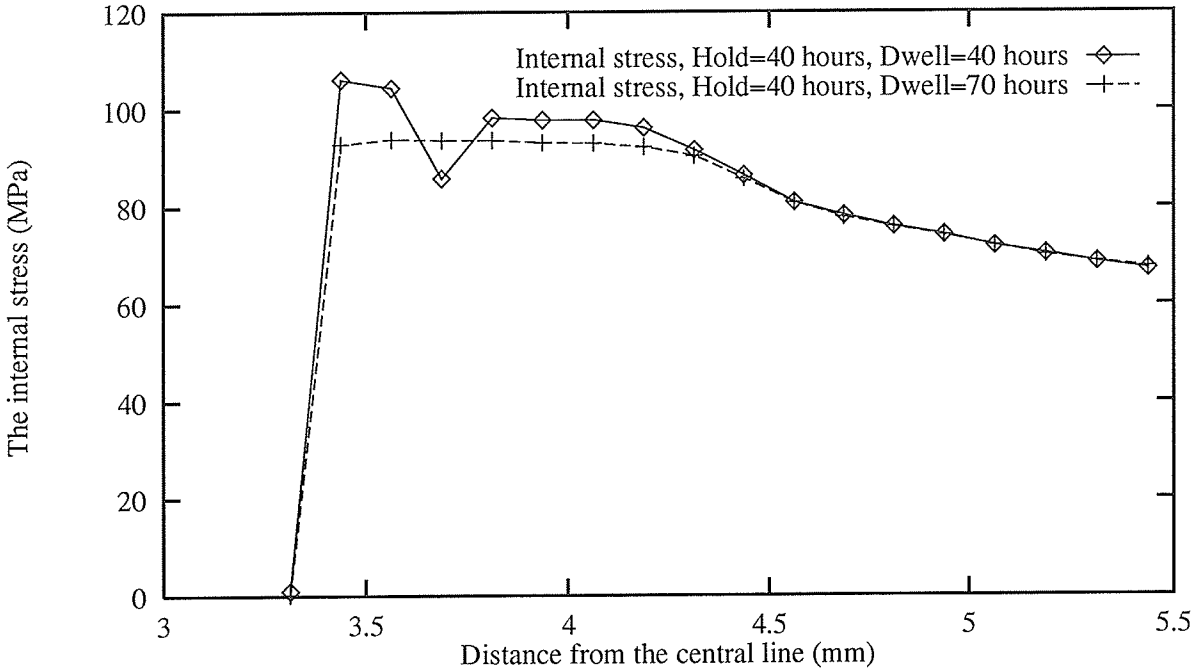

Figure R.3: Distributions of the internal stress in the crack tip area just after the first element is broken. The loading is cyclic with 40 hours of holding time and 40 and 70 hours of dwell time

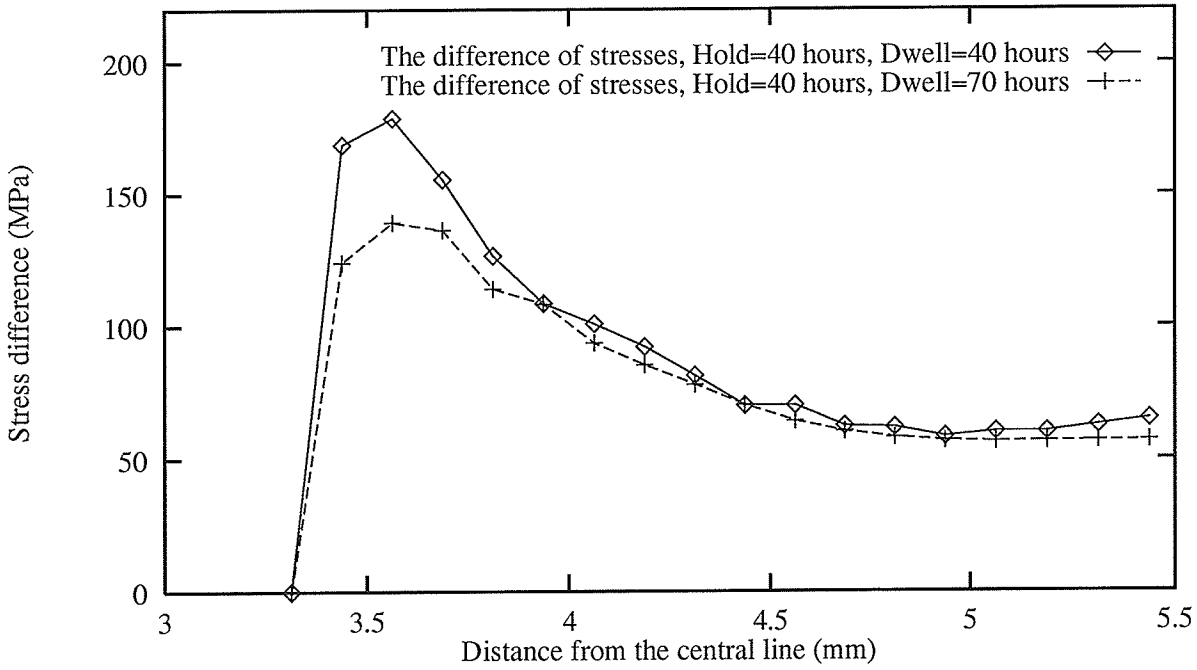

Figure R.4: Distributions of the difference between the damage equivalent stress and the internal stress $(\tilde{\sigma} - \bar{R})$ in the crack tip area just after the first element is broken. The loading is cyclic with 40 hours of holding time and 40 and 70 hours of dwell time

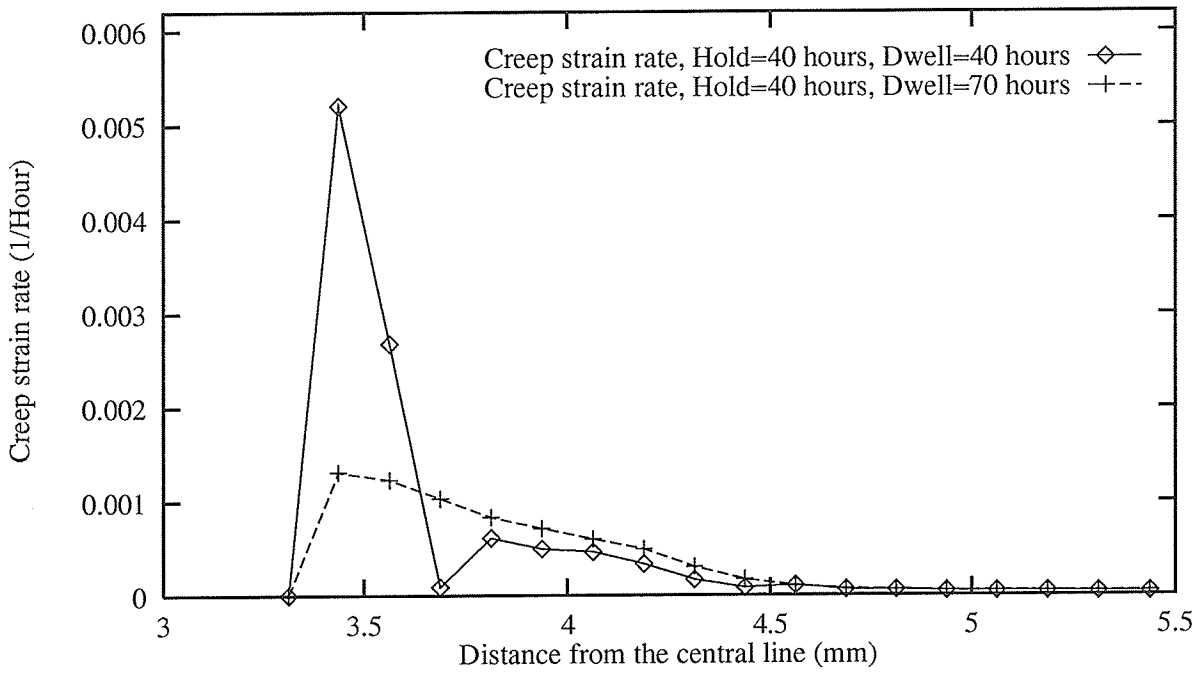

Figure R.5: Distributions of the creep strain rate in the crack tip area just after the first element is broken. The loading is cyclic with 40 hours of holding time and 40 and 70 hours of dwell time

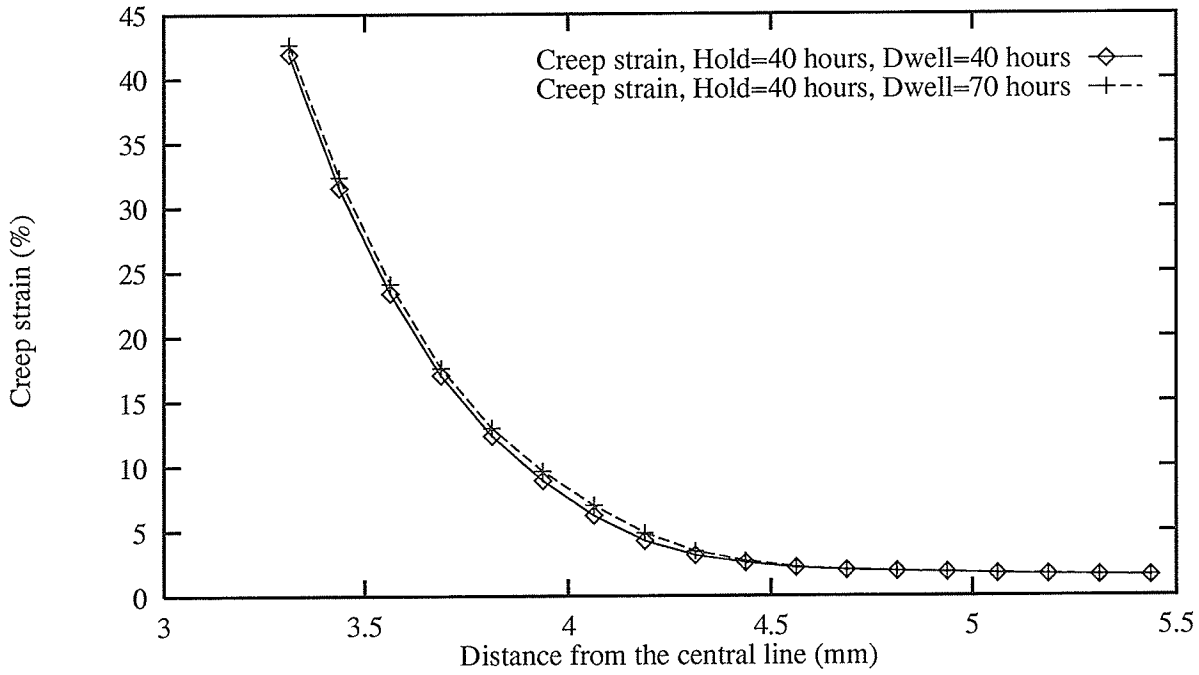

Figure R.6: Distributions of the creep strain in the crack tip area just after the first element is broken. The loading is cyclic with 40 hours of holding time and 40 and 70 hours of dwell time

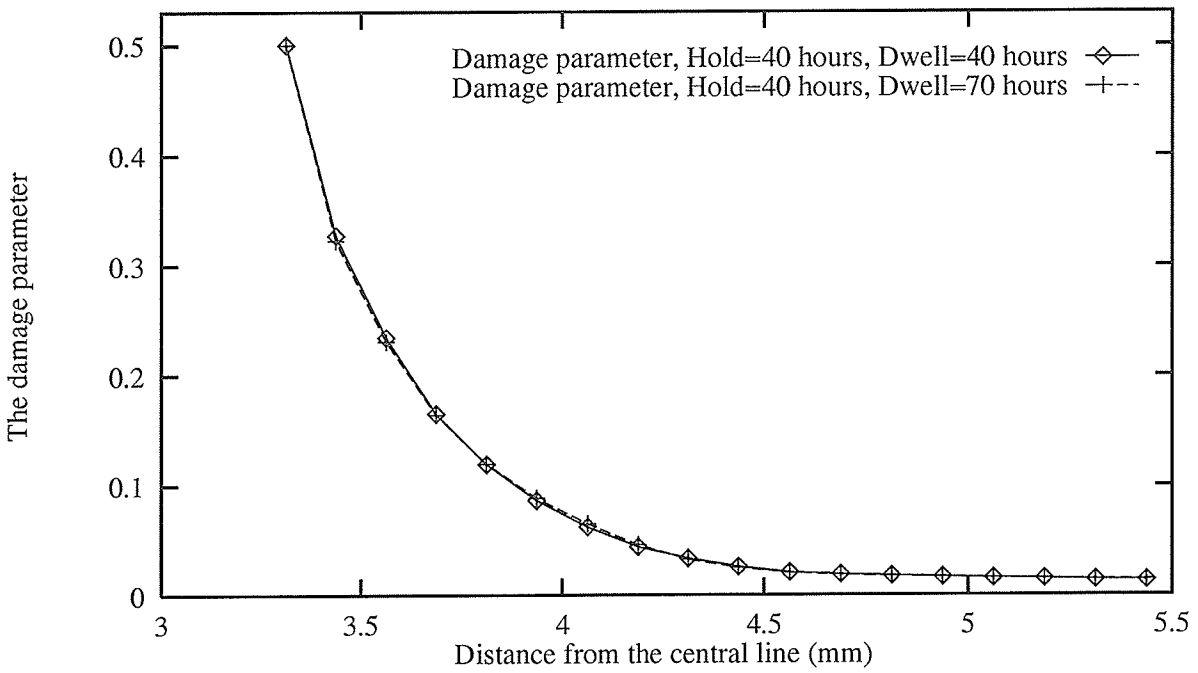

Figure R.7: Distributions of the damage parameter in the crack tip area just after the first element is broken. The loading is cyclic with 40 hours of holding time and 40 and 70 hours of dwell time

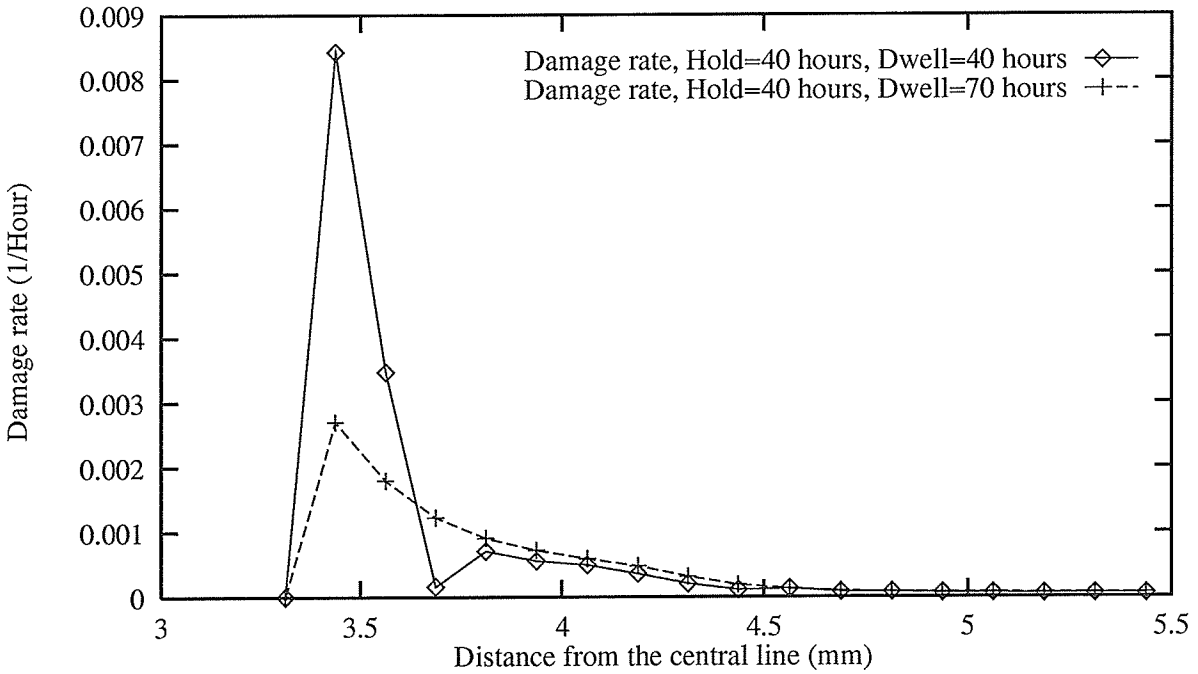

Figure R.8: Distributions of the damage rate in the crack tip area just after the first element is broken. The loading is cyclic with 40 hours of holding time and 40 and 70 hours of dwell time

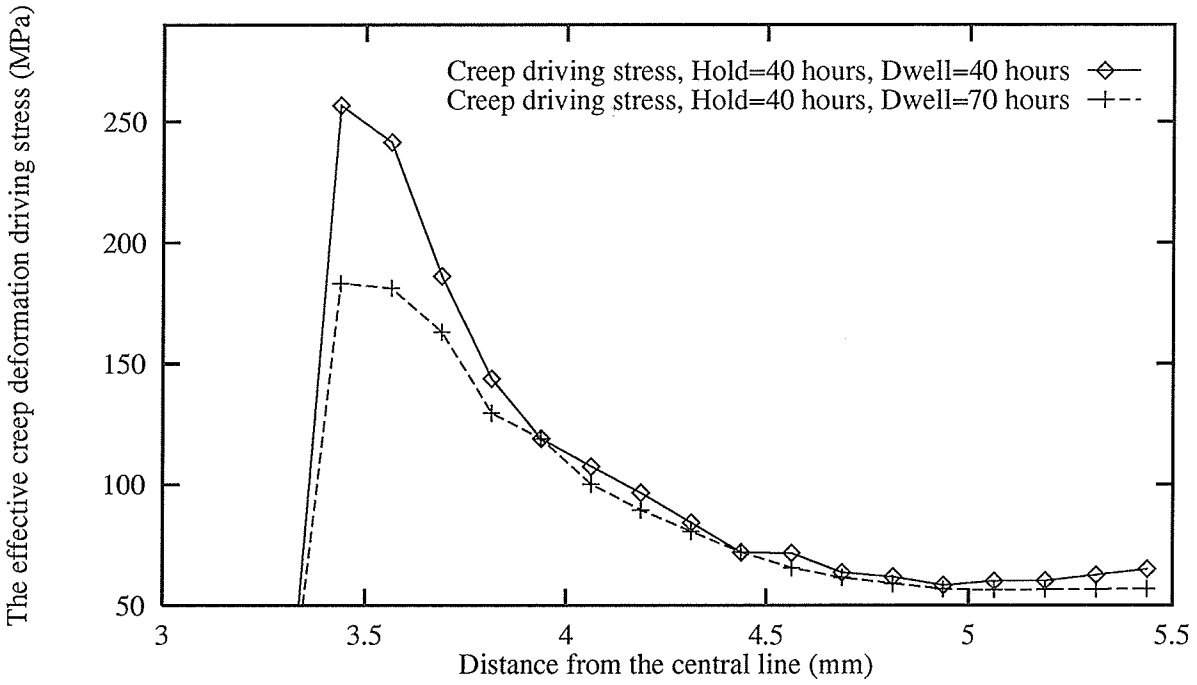

Figure R.9: Distributions of the effective creep deformation driving stress $\frac{\tilde{\sigma}-\bar{R}}{1-c_o D}$ in the crack tip area just after the first element is broken. The loading is cyclic with 40 hours of holding time and 40 and 70 hours of dwell time

Appendix S

Material state after the first element is broken

This appendix contains the figures which describe the material state just after the first element is broken. Curves corresponding to different loading histories are plotted together for comparison.

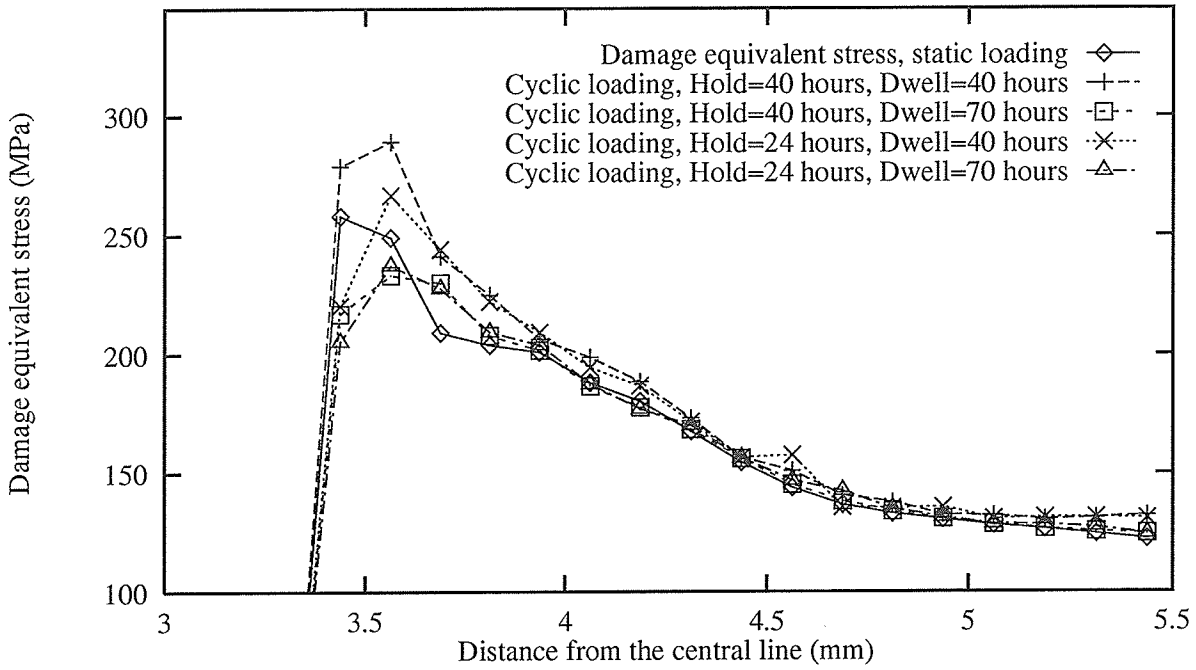

Figure S.1: Distributions of the damage equivalent stress in the crack tip area just after the first element is broken. The loading patterns are listed in Fig. 6.1

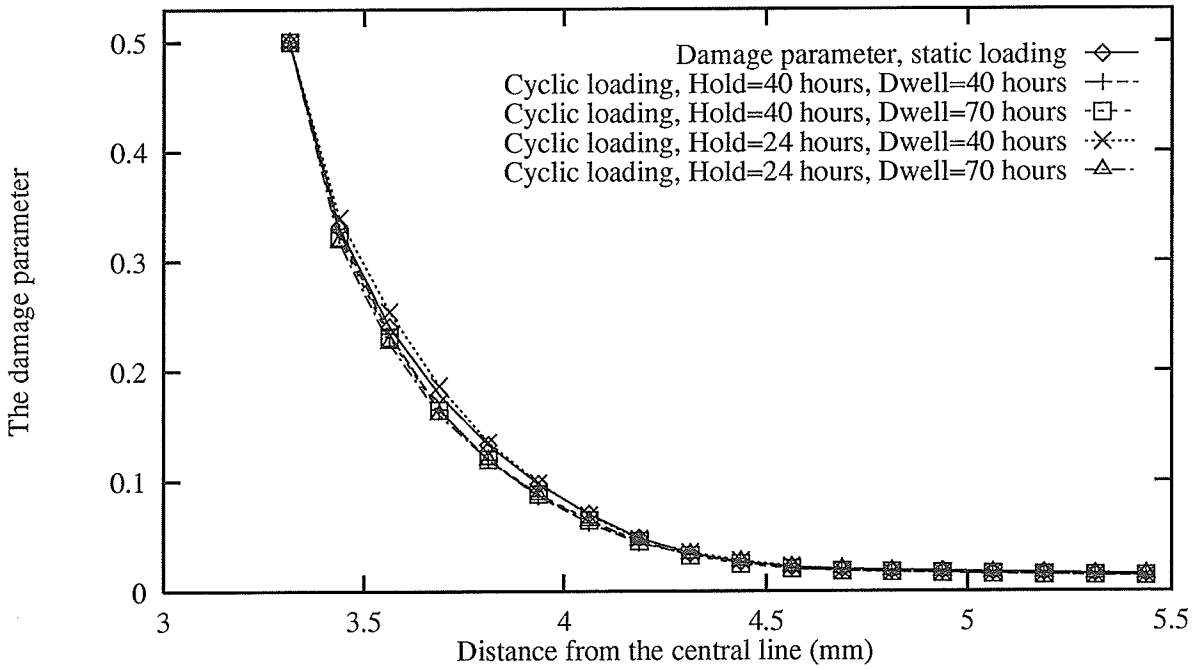

Figure S.2: Distributions of the damage parameter in the crack tip area just after the first element is broken. The loading patterns are listed in Fig. 6.1